Endocranial structures of Chiroptera (Mammalia) : contribution from fossils

Jacob Maugoust

THÈSE POUR OBTENIR LE GRADE DE DOCTEUR DE L'UNIVERSITÉ DE MONTPELLIER

Spécialité : Écologie, Evolution, Ressources Génétique, Paléobiologie

Discipline : Paléobiologie

École doctorale GAIA

Institut des Sciences de l'Evolution de Montpellier

Évolution des structures endocrâniennes des Chiroptera (Mammalia), apports des formes fossiles

Présentée par Jacob MAUGOUST

Le 10 décembre 2021

Sous la direction de Maëva ORLIAC

Devant le jury composé de

Mme. Suzanne HAND, Professeur, University of New South Wales, Sydney (AU)	Rapportrice
M. Guillaume BILLET, Maître de Conférences, Muséum National d'Histoire Naturelle, Paris (FR)	Rapporteur
M. Thomas MACRINI, Professeur, Saint Mary's University, San Antonio (USA)	Examinateur
M. John WIBLE, Chef de la Section des Mammifères, Carnegie Museum, Pittsburgh (USA)	Examinateur
M. Emmanuel DOUZERY, Professeur, Université de Montpellier (FR)	Examinateur, Président du jury
Mme. Maëva ORLIAC, Chargée de Recherche CNRS, Université de Montpellier (FR)	Directrice de thèse

UNIVERSITÉ DE MONTPELLIER

Résumé étendu

Organe central de l'organisme, le cerveau est un cas d'école pour décrypter l'histoire évolutive des traits fonctionnels (voire écologiques). Son étude est particulièrement pertinente chez les chauves-souris, un groupe de mammifères qui a développé deux traits hautement spécialisés : le vol actif et l'écholocalisation. Dans le cadre systématique actuel de l'ordre des chiroptères, on peut se demander si l'écholocalisation a été acquise pour l'ensemble de l'ordre et perdue dans la seule famille non-écholocatrice (les Pteropodidae), ou si elle a été acquise de manière convergente dans le groupe paraphylétique des "microchiroptères" écholocateurs (dans les deux clades Rhinolophoidea et Yangochiroptera). Il reste également à déterminer ce qui, de l'écholocation ou du vol actif, est apparu en premier, ou encore si l'un a effectivement précédé l'autre. Suivre l'évolution des caractéristiques du cerveau peut fournir des indices clés pour répondre à ces questions importantes ; cependant, peu de travaux ont traité de l'histoire évolutive du cerveau chez les chauves-souris.

Les "cerveaux fossiles" des chauves-souris ont été parmi les premiers à être étudiés au cours du XXe siècle. Si leur étude, à cette époque, n'a pas soulevé de nouveaux points en particulier, elle n'a pas bénéficié des avancées méthodologiques de la neurobiologie comparative depuis la fin du XXe siècle. En particulier, les études qualitatives de l'anatomie des "cerveaux fossiles" de chauves-souris se sont essoufflées au cours des années 1970, et seuls quelques travaux de neurobiologie comparée ont été entrepris depuis. Beaucoup plus d'efforts ont été consacrés à l'interprétation de la variation des volumes du cerveau (et des régions du cerveau) chez les espèces de chauves-souris actuelles. La masse cérébrale relative a été corrélée avec l'écologie, mais certains travaux ont démontré que cette corrélation était approximative, et que des sous-unités de fonctionnalités différentes pouvaient interagir. Seule la taille des bulbes olfactifs semble être un bon indicateur de l'acuité olfactive. Seule la masse cérébrale relative a (quelques peu) été explicitement étudiée dans un cadre temporel, sur la base de taxons actuels exclusivement. Les conclusions étaient que la masse cérébrale relative diminuait généralement au cours du temps, mais certains travaux plus récents ont mis en avant un scénario plus complexe, notamment en incluant des fossiles. L'objectif général de cette thèse est de fournir les premières étapes vers une étude moderne et actualisée du moulage endocrânien des chauves-souris.

En guise de travail préliminaire (Partie Un), le potentiel et les limites des connaissances actuelles en paléoneurologie des chauves-souris sont évalués. Pour ce faire, je décris quelques moulages endocrâniens appartenant à une famille de chauves-souris, les Hipposideridae, qui constituent une étude de cas pour commencer à étudier les moulages endocrâniens fossiles de chauves-souris. Je présente d'abord une nomenclature largement révisée de l'anatomie des moulages endocrâniens des chauves-souris, basée sur les observations faites sur l'échantillon fossile. Cette nomenclature mérite évidemment d'autres comparaisons et un échantillonnage plus large pour être généralisable à l'échelle des chiroptères, mais elle constitue un premier pas vers un recouplage entre paléoneurologie, neurobiologie comparée, et anatomie comparée chez les chauves-souris. En outre, elle confirme que l'organisation externe des tissus mous de l'endocrâne (principalement le cerveau) se reflète sur la surface interne de la boîte crânienne. En utilisant cette nomenclature, je décris et compare les moulages endocrâniens des quatre espèces fossiles échantillonnées (Fig. 1), et je compare également ces taxons fossiles à la seule illustration du cerveau d'un hipposidéridé moderne disponible dans la littérature (Baron et al. 1996).

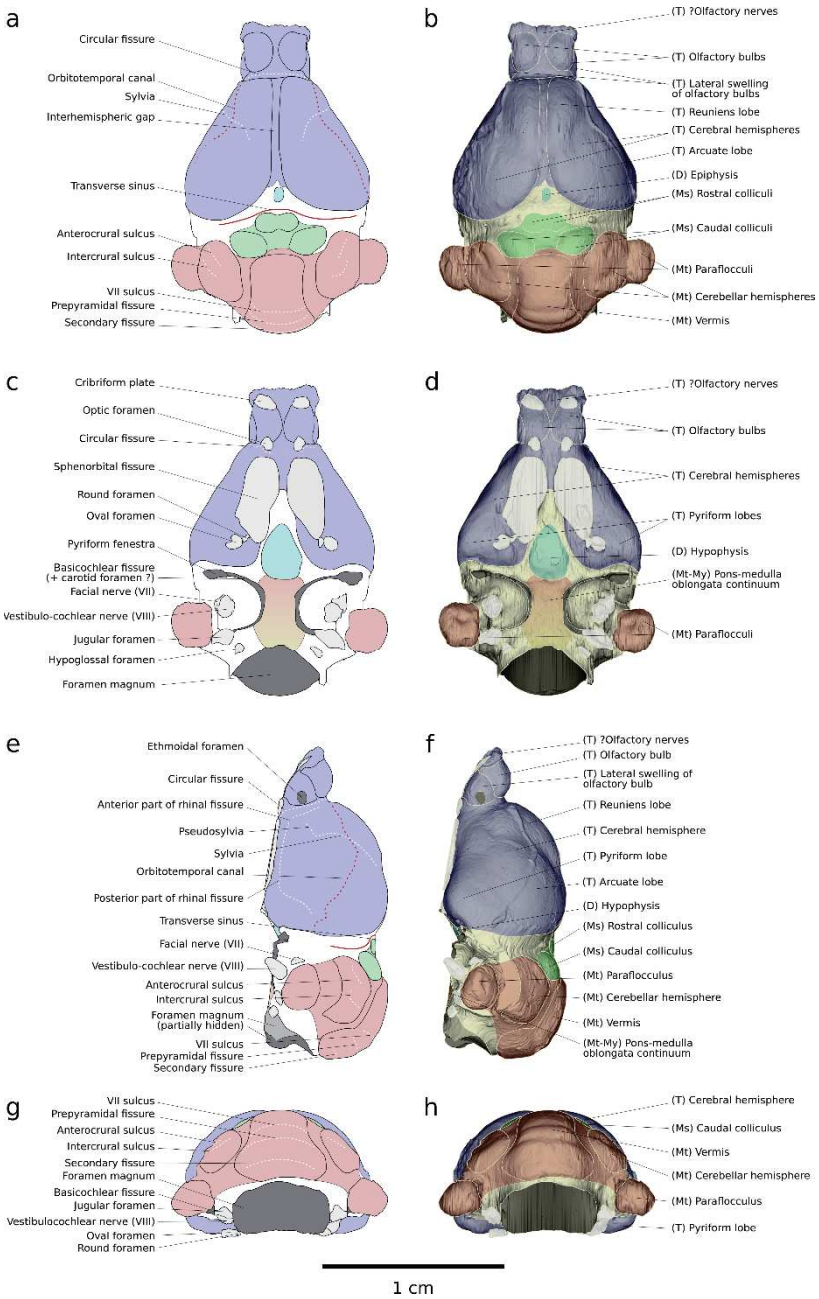

Figure 1 : Moulage endocrânien de *Palaeophyllophora oltina* datant de l'Eocène supérieur (NMB QP784) en vues dorsale (a-b), ventrale (c-d), latérale droite en vue miroir (e-f), et occipitale (g-h). Les figures de droite (b,d,f,h) illustrent le moulage endocrânien avec les principales subdivisions du cerveau (bleu/T-télencéphale, bleu clair/D-diencéphale, vert/Ms-mésencéphale, rouge/Mt-métencéphale, jaune/My-myélencéphale). Les figures de gauche (a,c,e,g) illustrent les différentes empreintes (vaisseaux sanguins, en rouge) et des sillons (sulci et fissures, en blanc) de ces aires, ainsi que les empreintes des sorties de nerfs crâniens (blanc clair) et d'autres foramens crâniens (gris foncé). D'après Maugoust & Orliac (2021): Figure 4.

Ce travail anatomique fournit les premiers indices sur la variation morphologique présente au sein d'une famille, et permet de discuter des tendances évolutives et temporelles potentielles. En particulier, la morphologie semble être homogène chez les Hipposideridae, ce qui peut être lié à une écologie conservée dans cette famille. Cependant, des comparaisons approfondies mettent en évidence des différences au niveau générique qui peuvent être expliquées soit par la phylogénie, soit par le temps (i.e., des "grades évolutifs"). J'utilise également des mesures classiques de volumes endocrâniens pour décrire l'évolution quantitative du cerveau, afin de pouvoir comparer les moulages endocrâniens que je décris à d'autres études. Je constate en particulier qu'il n'y a pas de changements apparents dans l'encéphalisation (calculée à l'aide du quotient d'encéphalisation) au fil du temps dans cette famille, ce qui contredit les études néontologiques précédentes (e.g., Niven 2005, Safi et al. 2005) et soutient la seule étude paléontologique publiée, bien que seulement quantitative (Yao et al. 2012). Je constate également

que les hipposidéridés fossiles se situent dans ou à proximité de l'espace morphologique de leurs proches parents actuels dans les régressions des logarithmes des bulbes olfactifs et des masses des paraflocculi par rapport au logarithme de la masse cérébrale. Dans l'ensemble, les résultats quantitatifs suggèrent qu'il n'y a pas de divergence fonctionnelle/écologique majeure entre les taxons d'hipposidéridés fossiles et actuels, ce qui confirme la monotonie relative des principales caractéristiques du cerveau dans cette famille. Si l'on considère à la fois la morphologie et les mesures du cerveau, peu de changements semblent s'être produits au cours de l'histoire évolutive des hipposidéridés. Certaines variations morphologiques plus fines sont cependant importantes à noter et à approfondir. Je mets également en avant le rôle des fossiles dans la description de l'évolution du cerveau dans un clade donné, car les fossiles sont des jalons essentiels pour contraindre les scénarios évolutifs.

Ce tout premier travail incite à résoudre les lacunes méthodologiques qui persistent et qui entravent l'étude de l'évolution du cerveau. Plusieurs limites de la paléoneurologie moderne restent à considérer et à traiter. Cette Partie Deux est donc une partie intermédiaire : j'y expose les raisonnements que j'utilise et y fais le bilan de la littérature exploitable, avant d'appliquer toutes les méthodes décrites à des études de cas de chauves-souris.

La première limite que j'essaie d'aborder concerne le fossé existant actuellement entre nos connaissances en paléoneurologie des chauves-souris, en neurobiologie comparée et en anatomie comparée. En effet, les études paléoneurologiques qualitatives chez les chauves-souris se sont arrêtées dans les années 1970 (Dechaseaux 1970, 1973) et n'ont jamais décrit de manière exhaustive et précise les moulages endocrâniens naturels des chauves-souris ; l'interprétation des corrélats (issus des moulages endocrâniens) des vraies structures cérébrales n'a pas été discuté. La neurobiologie comparée des chauves-souris, d'autre part, s'est clairement développée à la fin du XXème siècle, mais sans intégration plus large de la morphologie cérébrale, et sans comparaison détaillée avec d'autres groupes de mammifères (ce qui est particulièrement important pour évaluer les homologies des quelques plis néopalliaux présents chez diverses chauves-souris). Enfin, l'anatomie comparée du crâne des chauves-souris (pour les tissus mous non neuraux ou les os) a été très peu étudiée, même si les derniers travaux sur les structures osseuses sont riches et ont permis de discuter des homologies de structures (par exemple, Wible & Davis 2000, Giannini et al. 2006). Je tente donc de réviser et d'étendre le travail de nomenclature que j'ai effectué dans le cas des moulages endocrâniens d'hipposidéridés (Fig. 2, Partie Un). Cela vise à s'appliquer à l'ensemble de l'ordre des chiroptères, avec donc plusieurs hypothèses et homologies proposées afin qu'elles soient généralisables à toutes les chauves-souris.

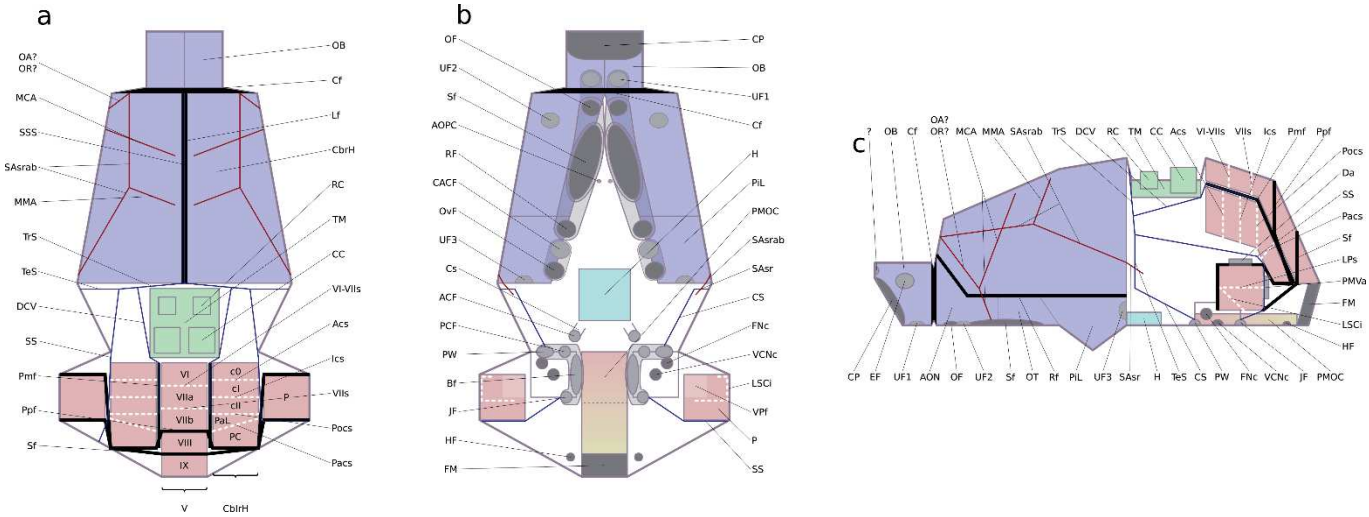

Figure 2 : Schéma simplifié des structures retrouvées sur un moulage endocrânien de chiroptère, à l'exception des sulci néopalliaux, en vues dorsale (a), ventrale (b), et latérale (c). Abréviations des structures cérébrales génériques : AON : Noyau Olfactif Antérieur / CblrH : Hémisphère Cérébelleux / CbrH : Hémisphere Cérébral / CC : Colliculus Caudal / Cf : fissure Circulaire / FNc : empreinte du Nerf Facial / H : Hypophyse / Lf : fissure Longitudinale / OB : Bulbe Olfactif / OT : Tubercule Olfactif / P : Paraflocculus / PiL : Lobe Piriforme / PMOC : Continuum Pons-Medulla Oblongata / RC : Colliculus Rostral / Rf : fissure Rhinale / TM : Tectum du Mésencephale / V : Vermis / VCNc : empreinte du nerf Vestibulo-Cochléaire. Abréviations des lobules et plissements cérébelleux : Acs : sulcus Antérocrural / c0 : crus 0 / cI : crus I / cII : crus II / PC : Copule Pyramidale / Ics : sulcus Intercrural / IX : Lobule IX = Uvula / LPs : sulcus Paraflocculaire Latéral / LSCi : impression du Canal Semicirculaire Latéral / Pacs : sulcus Paracrural / PaL : Lobule Paramédian / Pmf : fissure Paramédiane / Pocs : sulcus Postérocrural / Ppf : fissure Prépyramidale / Sf : fissure Secondaire / VI : Lobule VI = Déclive / VIIa : Lobule VIIa = Tuber Vermis / VIIb : Lobule VIIb = Folium Vermis / VIII : Lobule VIII = Pyramis / VIIs : sulcus VII / VI-VIIs : sulcus VI-VII / VPf : fosse Paraflocculaire Ventrale. Abréviations des structures vasculaires : CS : Sinus Communicant / DCV : veine Cérébellaire Dorsale / MCA : Artère Cérébrale Moyenne / MMA : Artère Méningée Moyenne / OA?OR? : peut être l'empreinte de l'Artère Ophthalmique ou du Ramus Orbital de l'artère maxillaire / SAsr : Artère Stapédienne - ramus supérieur / SAsrab : Artère Stapédienne - ramus supérieur - branche antérieure / SS : Sinus Sigmoïde / SSS : Sinus Sagittal Supérieur / TeS : Sinus Temporal / TrS : Sinus Transverse. Abréviations des ouvertures endocrâniennes : ? : ouverture inconnue / ACF : Foramen Carotide Antérieur / Bf : fissure Basicochléaire / CACF : Foramen Caudal du Canal Alisphénoïde / CP : Plaque Criblée de l'ethmoïde / Cs : sulcus Carotide / Da : ouverture Dorsale sur le paraflocculus / EF : Foramen Ethmoïde / FM : Foramen Magnum / HF : Foramen Hypoglosse / JF : Foramen Jugulaire / OF : Foramen Optique / OvF : Foramen Oval / PCF : Foramen Carotide Postérieur / PMVa : ouverture PostéroMédioVentrale sur le paraflocculus / POPC : Ouverture Postérieur du Canal Ptérygoïde / PW : Fenêtre Pyriforme / RF : Foramen Rond / SF : Fissure Sphénorbitaire / UF1 : Foramen Inconnu #1 / UF2 : Foramen Inconnu #2 / UF3 : Foramen Inconnu #3.

Le second grand souci de la paléoneurologie moderne concerne les métriques utilisées pour décrire l'évolution quantitative des "cerveaux fossiles" et leur traitement statistique. Je discute d'abord du bienfondé des métriques traditionnelles, et des erreurs potentielles commises par certains des travaux précédents. En particulier, le quotient d'encéphalisation est biaisé, et nul ne devrait effectuer de traitement statistique en utilisant des ratios ou des résidus de régression. Je propose donc de travailler directement avec des masses neuronales absolues, et d'utiliser un traitement statistique permettant de les exprimer par rapport à d'autres masses (i.e., comparer la masse du cerveau à la masse corporelle, et comparer la masse des parties du cerveau à la masse du cerveau). Je discute également des méthodes comparatives phylogénétiques (MCP) actuellement existantes, et j'essaie de mettre en évidence leurs avantages et leurs inconvénients. L'inclusion des espèces fossiles est cruciale, c'est pourquoi je décris et compare les implémentations actuellement disponibles de ces différentes méthodes. J'ai finalement choisi une méthode statistique (la régression d'arête phylogénétique, Castiglione et al. 2018) construite pour inclure des occurrences fossiles, qui ne repose ni sur la parcimonie (stricte) ni sur l'optimalité, mais qui vise plutôt à reconstruire l'évolution des traits au niveau des branches, en plaçant l'incertitude (inhérente) de la reconstruction au niveau phylogénétique le plus bas possible. En utilisant cette méthode et sa mise en œuvre, j'expose également le traitement statistique que j'effectue et ses objectifs, tant sur les données qualitatives que quantitatives. Ce traitement statistique me permet d'évaluer la pertinence phylogénétique et l'évolution des caractères anatomiques, de reconstruire et de discuter l'évolution morphologique à travers les clades, et enfin de décrire et de comparer l'évolution des masses neurales

relatives (tant leur valeur que leur variation).

Le premier cas concerne un clade majeur (le sous-ordre des Yinpterochiroptera) dont les sous-clades sont parmi les plus contrastés parmi tous les ordres de mammifères : la superfamille “microchiroptère” Rhinolophoidea, et la famille des “mégachiroptères” Pteropodidae. La Partie Un ne visait qu'à décrypter le potentiel et les limites et à donner une idée de la tâche à accomplir pour aborder de manière adéquate l'évolution endocrânienne chez les chauves-souris ; dans la Partie Trois, j’ai une visée plus large et j'augmente substantiellement l'effort d'échantillonnage. Pour les Yinpterochiroptera, je rassemble un échantillon d'espèces existantes représentant un huitième de la diversité spécifique actuelle, avec une résolution inter-tribale à intra-générique (selon la systématique des familles). J'inclus les quatre taxons fossiles d'hipposideridés décrits précédemment, et j'ajoute quatre autres espèces fossiles qui aident à mieux comprendre l'évolution endocrânienne chez les Hipposideridae et dans leur famille sœur, les Rhinonycteridae. Il n'y a pas d'occurrences fossiles dans les autres familles considérées, mais cela est dû à un manque de restes crâniens connus. Je considère donc toujours le sous-ordre des Yinpterochiroptera, les nœuds les plus profonds étant (au moins partiellement) contraints par les seules occurrences fossiles actuellement disponibles pour l'ensemble du sous-ordre. Je définis 73 caractères anatomiques inédits (en utilisant la nomenclature anatomique établie dans la Partie Deux) pour décrire la variation endocrânienne depuis le niveau subordinal (c'est-à-dire en comparant les rhinolophoïdes entiers aux ptéropodidés) jusqu'au niveau intrafamilial (au moins). Je suis le protocole statistique décrit dans la Partie Deux, en y ajoutant deux parties. La première concerne la variation impliquée par les topologies données, la place du genre hipposidéridé *Palaeophyllophora* restant incertaine dans cette famille. La seconde vise à comparer les analyses "néontologiques" (i.e., sans les formes fossiles) et "paléontologiques" concernant les traits neuraux quantitatifs (les seuls traits neuraux dont l'évolution a été décrite dans la littérature).

La distribution des états de caractères anatomiques montre un large éventail sur la topologie considérée, avec des modèles variant considérablement. Les caractères ont généralement un signal phylogénétique substantiel, mais varient beaucoup ; il faut cependant noter que cette variation ne dépend pas des structures générales (i.e., parties du cerveau, ouvertures crâniennes, marques des structures vasculaires etc). Certains caractères semblent également évoluer sous l'effet de la sélection, avec des cas de stase et des cas d'évolution temporelle vers un optimum. Le suivi de l'évolution de l'exposition dorsale du mésencéphale est également intéressant dans le clade des Yinpterochiroptera, qui oppose des chauves-souris écholocatrices et non écholocatrices. Les états du caractère traduisant le degré d’exposition générale du mésencéphale suivent la phylogénie, et le degré d'exposition diminue avec le temps, ce qui confirme des travaux antérieurs (e.g., Dechaseaux 1956). La distribution des autres caractères décrivant la morphologie mésencéphalique est cependant plus difficile à interpréter. Les distributions des autres états de caractères qui concernent les structures dont l'homologie a été provisoirement proposée dans la Partie Deux confirment l'homologie dans certains cas, et suggèrent des convergences dans d'autres. De manière générale, ces homologies doivent évidemment être approfondies. Je reconstruis également l'évolution de la morphologie endocrânienne parmi les principaux taxons de yinptérochiroptères (reconstructions ancestrales des familles et autres clades suprafamiliaux ; Fig. 3). Les ptéropodidés sont évidemment très divergents des rhinolophoïdes, mais il existe également des conformations familiales de la morphologie endocrâniennechez les rhinolophoïdes.

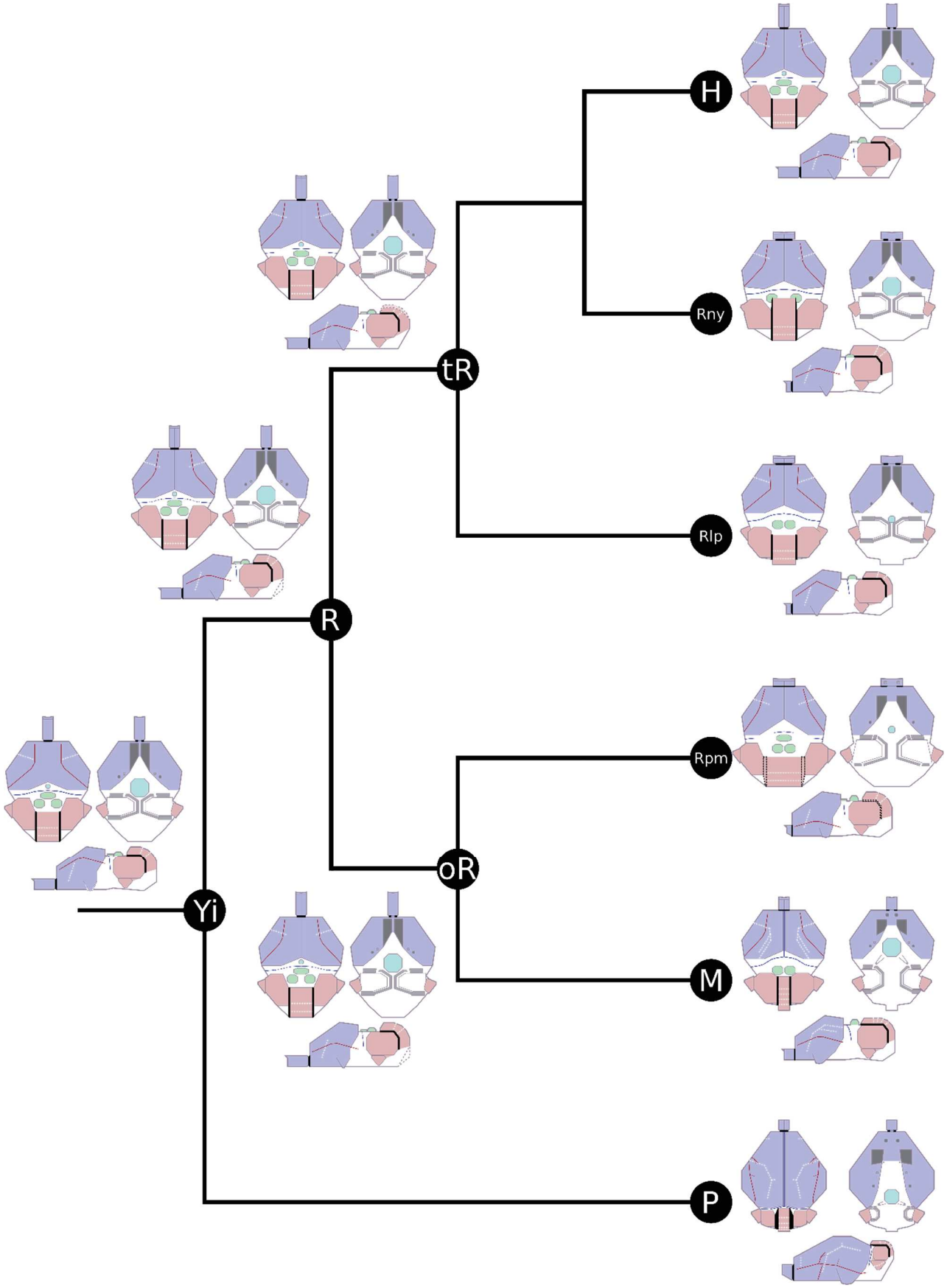

Figure 3 : phylogénie simplifiée des Yinpterochiroptera avec les moulages endocrâniens ancestraux théoriques pour les “noeufs profonds” étudiés ici en vues dorsale (haut gauche), ventrale (haut droite), et latérale (bas). Du plus basal au plus apical, les noeux sont ceux des Yinpterochiroptera (‘Yi’), ensuite des Rhinolophoidea (‘R’), puis des Rhinolophoidea “vrais” et “faux” (‘tR’ et ‘oR’), puis des familles échantillonnées qui sont les Hipposideridae (‘H’), les Rhinonycteridae (‘Rny’), les Rhinolophidae (‘Rlp’), les Rhinopomatidae (‘Rpm’), les Megadermatidae (‘M’), et les Pteropodidae (‘P’).

Les résultats concernant les masses neurales relatives incluant les fossiles contredisent généralement les travaux "néontologiques" précédents. Tout d'abord, il y a une augmentation dans le temps de la masse cérébrale relative, et la plupart des valeurs des nœuds familiaux sont supérieures à celle du nœud des Yinpterochiroptera. Cela contredit les travaux néontologiques précédents qui suggéraient une diminution dans le temps (Safi et al. 2005, Thiagavel et al. 2018). De manière générale, il existe des différences majeures en considérant ou non les taxons fossiles, principalement au niveau des tendances temporelles de l'évolution des masses neurales relatives. Ceci est d'une importance capitale, car les conclusions diffèrent radicalement avec ou sans fossiles. Les masses relatives des bulbes olfactifs et des paraflocculi diminuent avec le temps, avec donc une tendance générale opposée à celle de la masse relative du cerveau. Une tendance intéressante est une covariation apparente des taux absolus d'évolution des masses relatives du cerveau et des bulbes olfactifs : lorsque la masse relative du cerveau change, la masse relative des bulbes olfactifs change également. Cependant, la direction des changements n'est pas liée, et tous les cas possibles de concordance et de divergence sont retrouvés. Les corrélations avec des écologies qui ont été proposées dans la littérature (et parfois, plutôt considérées comme des causes) se retrouvent peu dans les résultats obtenus ici. Ceci est particulièrement vrai en ce qui concerne la masse cérébrale relative, proposée comme covariant avec les types de chauves-souris animalivores et comme constamment élevée chez les chauves-souris frugivores (c'est-à-dire les ptéropodes dans le contexte des Yinpterochiroptera). Ceci n'est pas retrouvé ici. D'autre part, il semble que la masse relative des bulbes olfactifs covarie mieux avec les types de régime alimentaire.

Le second cas d'étude concerne l'ensemble de l'ordre des chiroptères (Partie Quatre). Cet élargissement de l'échelle phylogénétique d'étude diminue la résolution de l'échantillonnage ; je ne décris donc les tendances de l'évolution cérébrale que des clades suprafamiliaux. Avec les valeurs ancestrales reconstruites pour les familles de yinpterochiroptères dans la Partie Trois, les analyses effectuées dans la Partie Quatre bénéficient de l'inclusion du moulage endocrânien d'un taxon éochiroptère. Pour la première fois, la morphologie interne de la boîte crânienne est décrite pour une espèce de chauve-souris n'appartenant pas au groupe couronne des chiroptères. Le fait marquant de ce moulage endocrânien est qu'il ressemble typiquement à celui d'une chauve-souris moderne (Fig. 4). En particulier, le tectum mésencéphalique est largement exposé, avec des colliculi caudaux saillants, signe distinctif de l'écholocalisation. Ce moulage endocrânien soutient donc l'hypothèse d'une acquisition de l'écholocalisation chez les chiroptères puis d'une perte secondaire chez les Pteropodidae.

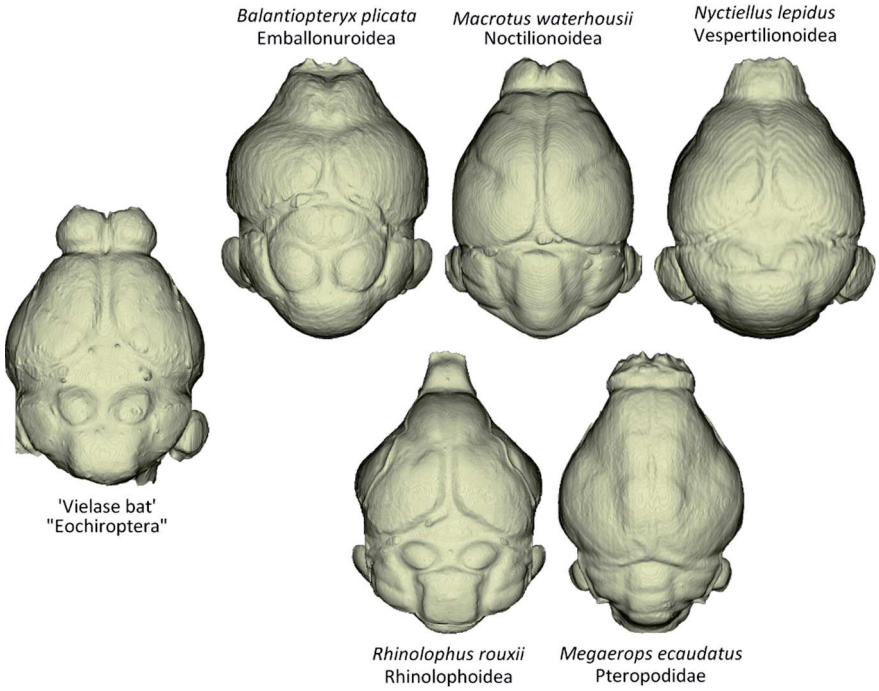

Figure 4 : Diversité de la morphologie du moulage endocrânien (en vue dorsale) chez les chiroptères, comparant un taxon hors du groupe couronne (la 'Vielase bat') et une espèce par clade principal du groupe couronne.

Les distributions des caractères anatomiques sont moins congruentes avec les relations phylogénétiques qu'elles ne l'étaient pour les analyses réalisées à l'échelle des Yinpterochiroptera. Ceci est probablement dû à la stratégie d'échantillonnage : la topologie est principalement composée de longues branches en direction des familles, permettant à la MCP utilisée de reconstruire de nombreux changements convergents sur une longue période plutôt que peu de changements sur une courte période. Néanmoins, certains nœuds se distinguent par la présence de plusieurs changements morphologiques, ce qui indique que le signal phylogénétique des caractères anatomiques est probablement fort. C'est notamment le cas de la superfamille des Noctilionoidea, et des nœuds successifs de cette superfamille jusqu'au niveau de la famille. A l'échelle des chiroptères et en considérant la morphologie d'un taxon éochiroptère, l'exposition du tectum mésencéphalique semble se réduire avec le temps, et les tendances varient beaucoup plus tant au niveau de la morphologie des structures mésencéphaliques que des structures censées recouvrir progressivement le tectum mésencéphalique. Ceci confirme les observations précédentes à l'échelle des Yinpterochiroptera, et met en évidence une évolution complexe du mésencéphale chez les chauves-souris.

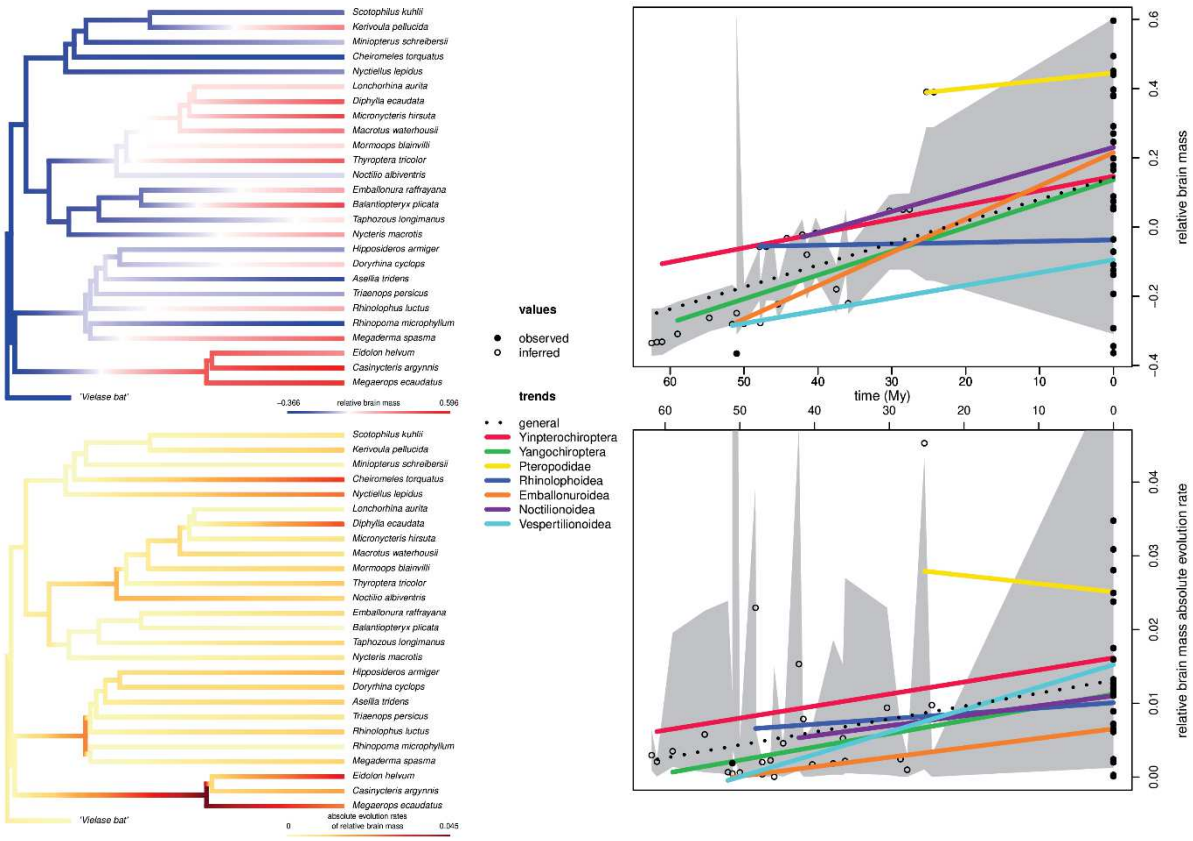

Figure 5 : Evolution de la masse relative du cerveau chez les chiroptères. Gauche: distributions sur la phylogénie des chiroptères réduite à l'échantillonnage utilisé. Droite: tendances temporelles, le fond gris illustrant une variation simulée sous un régime de mouvement Brownien. Haut: masse relative du cerveau. Bas: taux d'évolution absolus de la masse relative du cerveau.

Les tendances dans l'évolution de la masse cérébrale relative issues des travaux néontologiques, déjà remises en cause par un travail incluant des fossiles (Yao et al. 2012), sont en outre battues en brèche par les résultats des Parties Un et Trois. Toutes ces études ont cependant été réalisées à un niveau familial (Yao et al. 2012, Partie Un) ou subordinal (Partie Trois), et en ne considérant que les représentants actuels des clades couronnes. Ici, en étudiant l'ensemble de l'ordre des chiroptères plus un taxon éochiroptère, je soutiens les hypothèses précédentes selon lesquelles 1) les taxons fossiles sont cruciaux pour reconstruire l'histoire évolutive de la masse cérébrale relative car 2) elle a, de manière générale, augmenté au fil du temps à l'échelle des chauves-souris (Fig. 5). Comme chez les Yinpterochiroptera (Partie Trois), on observe une diminution dans le temps des masses relatives des bulbes olfactifs et des paraflocculi, et la proportionnalité inverse entre les tendances temporelles de la masse cérébrale relative et des masses relatives des bulbes olfactifs et des paraflocculi reste à étudier. La covariation des changements entre les masses relatives du cerveau et des bulbes olfactifs trouvée chez les Yinpterochiroptera (Partie Trois) n'est pas retrouvée à l'échelle des Chiroptera, et persiste faiblement dans le sous-ordre cité en considérant l'ordre entier. Des tendances dans les superfamilles de yangochiroptères apparaissent également : les emballonuroïdes ont connu les changements les plus drastiques dans le temps (pour toutes les masses relatives), tandis que les noctilionoïdes ont une masse cérébrale relative très élevée et ont maintenu une masse relative des paraflocculis élevée. Les clades de Yangochiropterans méritent donc une attention particulière concernant l'évolution de leur endocrâne.

Une première voie qui reste à tracer concerne la correspondance entre les tissus mous et les empreintes qu'ils laissent sur la surface interne de la boîte crânienne. J'essaie ici de reconnaître autant de structures que possible, mais je suis limité par la rareté des travaux traitant des homologies osseuses, de la macromorphologie cérébrale et de l'identification des structures vasculaires. Les techniques modernes telles que le diceCT (Clement et al. 2015, Anderson & Maga 2015, Gignac et al. 2016) permettent par exemple une meilleure numérisation des structures anatomiques : non seulement l'os mais aussi les tissus mous peuvent être contrastés et reconstruits ensemble. Un premier objectif à atteindre, qui fait cruellement défaut, utilisant ces méthodes non invasives, serait de clarifier la structure des tissus osseux et mous du crâne chez les chauves-souris. Cela impliquerait de comparer des espèces très différentes et d'extraire à la fois le moulage endocrânien et les structures des tissus mous, afin d'obtenir des informations sur les correspondances qualitatives (c'est-à-dire les structures qui peuvent être identifiées ou non) et les biais quantitatifs (c'est-à-dire les volumes réels par rapport aux volumes estimés du cerveau et de ses régions).

La façon dont la morphologie endocrânienne est appréhendée dans ce travail est une méthode pionnière et préliminaire qui vise à mieux décrire l'évolution morphologique dans le temps et dans un cadre évolutif. La décision de discrétiser la morphologie endocrânienne à l'aide de caractères et d'états, et de les supposer continus dans une MCP (la régression d'arête phylogénétique) conçue pour des traits quantitatifs est discutable. Il existe d'autres méthodes, telles que les méthodes de morphométrie géométrique (MMG) qui visent à tenir compte de la variation morphologique en utilisant une discrétisation quantitative de la morphologie et des traitements statistiques subséquents. Les MMG commencent à s'appliquer aux moulages endocrâniens et certaines études ont déjà fourni des résultats intéressants (e.g., Ahrens 2014, Segall et al. 2021, Weisbecker et al. 2021). Les deux approches diffèrent par leur raison d'être, la manière dont elles sont réalisées et leurs limites. Les deux devraient en fait être tentées, et peuvent ensuite être comparées. Le point que je veux soulever est que le traitement de l'information morphologique sur l'endocrâne de chauve-souris entrepris ici n'est qu'une manière possible d'investigation. Cela représente une première étape dans l'étude statistique de l'évolution de la morphologie de l'endocrâne.

La MCP utilisée ici est adaptée aux caractères quantitatifs, et à cet égard, la façon dont l'évolution des masses neurales relatives est abordée ici est moins "expérimentale" que l'est l'évolution de la morphologie endocrânienne. Il existe déjà des résultats prometteurs concernant la variation de la taille du cerveau dans le temps et dans les phylogénies chez les cétacés (Serio et al. 2019, McCurry et al. 2021) et chez les primates (Sansalone et al. 2020). Ces traits ont également été beaucoup plus étudiés chez les chauves-souris que la morphologie (puisqu'il n'existe pas de travaux équivalents pour la morphologie). Des investigations complémentaires devraient alors se concentrer sur les corrélations entre traits écologiques et neuronaux, souvent trop hâtives, proposées dans la littérature. En effet, les résultats retrouvés par plusieurs études chez les chauves-souris (avec des liens entre régime alimentaire et/ou complexité de l'habitat et taille relative du cerveau et des bulbes olfactifs) ne semblent pas se retrouver dans les résultats de cette thèse. Des travaux anatomiques, fonctionnels et éthologiques sont nécessaires avant d'évaluer ces causalités. Ces travaux sont indispensables pour étudier l'évolution des traits écologiques et/ou pour proposer des inférences paléobiologiques à partir des traits neuronaux.

Les fossiles apparaissent comme essentiels pour contraindre les hypothèses d'évolution des traits. Ceci est encore plus clair dans le cas des chauves-souris et des traits neuraux : les résultats incluant les fossiles obtenus ici sont catégoriques, et les résultats obtenus en ne considérant que les chauves-souris extantes sont susceptibles de conduire à des conclusions erronées. Le fait que la MCP utilisée ici ne se base que sur la longueur des branches est un avantage car elle s'émancipe des critères de parcimonie et d'optimalité et ne nécessite pas de modèle évolutif a-priori. Ce point peut s'avérer être un inconvénient : les changements sont plus susceptibles de se produire sur les longues branches d'une phylogénie que sur les plus courtes, et cela peut conduire à un nombre élevé de changements convergents s'il y a plusieurs longues branches. La principale amélioration du travail et des analyses présentés ici, si l'on utilise la même méthodologie, serait ainsi d'ajouter des taxons existants ou des occurrences fossiles (des crânes de taxons fossiles sont documentés dans les Emballonuroidea et les Vespertilionoidea). Changer le niveau systématique d'étude peut également aider à mieux contraindre l'évolution du cerveau pour l'ensemble de l'ordre des chiroptères. Ceci est démontré ici pour les Yinpterochiroptera, mais cela vaudrait sûrement aussi pour les Yangochiroptera, ou même au niveau superfamilial dans ces groupes.

Table of Contents

Introduction 1
I) The brain in paleontology 2
II) Generalities about the order Chiroptera and its evolutionary history 6
III) Comparative neurobiology and paleoneurology of bats 9
IV) Goals and work axes of this thesis 16
Materials & Methods 19
I) 3D Data acquisition 20
II) Cerebral volumes measured 22
Part One - Endocranial cast anatomy of the extinct hipposiderid bats *Palaeophyllophora* and *Hipposideros* (*Pseudorhinolophus*) (Mammalia: Chiroptera) 24
Part Two - Widening the frame of bats endocranial evolution: sampling characters and methodology 53
I) Introduction 54
II) Nomenclature and homologies of the chiropteran endocranial cast 56
1) Emendatum to: Major components of the chiropteran brain observed on endocasts (Fig. II-1) 57
2) General remarks on the folding and their origin of the cerebrum cast in bats 61
3) Emendatum to: Neopallial foldings and lobes (Fig. II-5) 63
4) Addendum to: Cerebellar foldings (Fig. II-1) 67
5) Addendum to: Casts of braincase openings (Fig. II-1) 70
6) Major vascular structures crossing the endocranial cavity (Fig. II-28) 77
A) Arteries 78
B) Veins 80
7) Vascular imprints (Fig. II-1) (replacing and completing the The orbitotemporal canal section) 83
III) Biological inferences: Limitations, pitfalls and solutions 88
IV) Into the evolutionary history of variables: methodological choices for phylogenetical mapping 92
1) Short review of Phylogenetic Comparative Methods (PCM) 92
2) Methods allowing branch-level heterogeneity 95
3) Details on the RRphylo functions used 96
V) Statistical treatment 100
1) General remarks 101
2) Qualitative data treatment (Table II-1) 103
A) Morphological characters: description, phylogenetic relevance, and evolution 104
B) Taxa descriptions and comparisons, and deep node reconstructions 105
C) Quantitative data treatment (Table II-2) 107
Part Three - Endocranial evolution in the disparate suborder Yinpterochiroptera 109
I) Introduction 110
II) Material & Methods 113
1) Evolutionary framework 113
A) Phylogenetic context of Yinpterochiroptera and sampling strategy of extant taxa 113
a) The “true” rhinolophoids clade 113
b) The “other” rhinolophoids clade 116
c) The Pteropodidae clade 117
B) Yinpterochiropteran fossil record and sampling strategy of extinct taxa 118
C) Fossil ages and nodes dating 119
2) 3D Data acquisition 121
3) Anatomical characters 122
A) Overall shape of the endocranial cast 125
B) Telencephalon 126
C) Diencephalon 127

D) Mesencephalon 128
E) Metencephalon 129
F) Pons-Medulla Oblongata Continuum 131
G) Neopallial foldings 132
H) Vascular structure casts 133
I) Cranial openings 135
4) Body mass estimates of fossil taxa 138
5) Statistical treatment 140
III) Morphological evolution 141
1) Results 141
A) Phylogenies 141
a) Consistency and Retention Indexes 141
b) Ancestral reconstructed states of characters (a.k.a. “aces”) 141
c) Morphological changes 141
B) Characters and morphological complexes 142
a) Distribution and support to the phylogenies 142
b) Evolution and rates of evolution 148
c) Covariation with size 151
C) Taxa and deep nodes 153
a) Sum of morphological changes and rates of evolution 153
b) Deep nodes rate evolution 154
c) Deep nodes ancestral character estimates 156
2) Discussion 160
A) Variation due to phylogenetical uncertainty 160
B) Character distribution, phylogenetic relevance, evolution 160
C) The case of the exposed mesencephalic tectum 162
D) Testing secondary homologies 165
E) General morphological evolution across taxa (Figs. III-23,26) 170
a) Early steps of evolution of the endocast: root and rhinolophoids (all, “true”, and “other”) 170
b) Megabat endocranial morphology, with the particular case of the highly derived pteropodines 172
c) Contrasting the “other” rhinolophoids: endocranial morphology of megadermatids and rhinopomatids 173
d) Endocranial morphology of rhinolophids: the genus Rhinolophus 174
e) The contrasted endocranial morphology evolution among rhinonycterid “lineages” 175
f) Hipposiderid endocranial morphology evolution 176
IV) Quantitative evolution 178
1) Bias of the numeric segmentation vs physical extraction 178
2) Total brain mass (Figs. III-35-37) 179
A) Relative brain mass evolution 179
B) Absolute rates evolution 181
C) Group by group evolution 183
D) Comparison with “neontological” works 186
3) Olfactory bulbs mass (Figs. III-38-40) 189
A) Relative olfactory bulbs mass evolution 189
B) Absolute rates evolution 191
C) Group by group evolution 193
D) Comparison with “neontological” works 196
4) Paraflocculi mass (Figs. III-41-43) 197
A) Relative paraflocculi mass evolution 197

B) Absolute rates evolution 199
C) Group by group evolution 201
5) Cross traits comparison 206
6) Contrasting evolutionary patterns with and without fossil taxa 209
A) Traits evolution without fossils 209
a) Brain mass (Figs. III-44-46) 209
b) Olfactory bulbs mass (Figs. III-47-49) 211
c) Paraflocculi mass (Figs. III-50-52) 214
B) Reconstruction parameters comparisons 217
C) Discussion 223
V) Conclusions 226
Part Four - A stem bat endocast helps addressing endocranial evolution in Chiroptera 228
I) Introduction 229
II) Material & Methods 230
1) Taxa and specimens 230
2) 3D Data acquisition 231
3) Phylogenetic framework 231
4) Anatomical characters 234
5) Quantitative data 236
6) Statistical treatment 237
III) Description of the endocranial cast of the 'Vielase bat' 238
1) Overall shape 238
2) Telencephalon 240
3) Diencephalon 241
4) Mesencephalon 241
5) Metencephalon 241
6) Cranial nerve exit casts (Fig. IV-3-c,d) 242
7) Other braincase opening casts (Fig. IV-3-c,d) 243
8) Vascular imprints 243
IV) Morphological evolution 245
1) Character support to the topology, evolution, and sampling implications 245
A) Consistency and Retention Indexes (Fig. IV-4) 245
B) Number of changes (Fig. IV-5) 246
C) Discussion on the phylogenetical relevance of endocranial characters at the Chiroptera scale 247
D) Characters temporal trends and interpretation of absolute rate trends sign 249
2) Evolution of endocranial morphology in Chiroptera 251
A) General overview of morphological variation 251
B) Evolution of the exposure of the mesencephalic tectum 252
C) Morphological evolution at main deep nodes of Chiroptera 254
D) Contrasting stem and crown bats (Fig. IV-11) 258
V) Quantitative evolution 260
1) Bias of the numeric segmentation vs physical extraction at the Chiroptera scale (Fig. IV-12) 260
2) Total brain mass (Fig. IV-13) 261
3) Olfactory bulbs mass (Fig. IV-13) 264
4) Paraflocculi mass (Fig. IV-14) 266
5) Cross traits comparison 269
VI) Conclusions 271
General conclusions and perspectives 273
I) Conclusions 274
II) Perspectives 278

Introduction

I) The brain in paleontology

The nervous system of an animal occupies a preponderant place: this system provides the control of the organism, and its immediate behavioral response to its external environment. A nervous system is found in all eumetazoans, with a differentiation between a central and a peripheral nervous system (Holland et al. 2013, Wenger & Galliot 2013). The central nervous system "centralizes" both the "integrating" and the "executive" centers of the organism. The peripheral nervous system, on the other hand, is a relay between the central nervous systems and both the sensory organs (for afferent, i.e., sensory signals) and the "executive" organs (for efferent, i.e., motor signals). The central nervous system therefore fully "drives" the whole body: it is the "anatomical substratum of the animal dynamism" (Anthony 1928:5). There are controversies about the homologous nature of such an organization among bilaterians, since ambulacrarians (hemichordates and echinoderms) are distinguished by having different organizations of their nervous system (see Holland et al. 2013 for a review). Protostomes and deuterostome chordates therefore share a similar organization (with a single nerve cord) that may be convergent, and the main difference between these two clades is the position of the nervous system (ventral in protostomes, dorsal in chordates). Among chordates, vertebrates further differ from other taxa (i.e., urochordates and cephalochordates) in the development of their central nervous system (see Holland 2015 and Schlosser 2017): vertebrates share a differentiated telencephalon (the fifth and anteriormost ventricle of the central nervous system), and they have neural crest cells (multipotent cells originating from the neural plate) and placodes (ectodermal region giving rise to sense organs). During the differentiation of vertebrate groups, cartilaginous to osseous tissues further develop around the central nervous system; the skeleton anteroposteriorly dichotomizes in a cranium and a vertebral column (Kardong 2012), and so does the central nervous system, dichotomizing in a brain and a spinal cord. Brain and skull are tightly linked to each other, starting with the fact that the brain is (partially to totally) surrounded and protected by the skull (with the chondrocranium, but also the dermatocranium in Osteichthyes; e.g., Kardong 2012): brain and skull changes can be tracked together along both the phylogenesis and the ontogenesis (Richtsmeier & Flaherty 2013).

The study of the nervous system is fundamental to understand the way organisms function, both regarding intrinsic and extrinsic aspects. The clinical science studying the nervous system is neurology, and the main study subject is the species neurologists belong to: the human species. If biological proximity is a main argument regarding the choice of a study subject (ultimately, neurologists could study themselves), there is a main proportional drawback: the human central nervous system is highly complex, and therefore highly difficult to understand. Many advances in our understanding of brain function arose from clinical cases and pathologies (Getz 2014). Neurology is often considered as synonymous to neuropathology, but there are also researchers studying the normal (i.e., "non-pathological") morpho-anatomy of the nervous system, which is the field of neuroanatomy (Barone & Bortolami 2004). Neuroanatomy does not only focus on humans; it also includes other animals, mainly domestic ones (e.g., Langley 1883, Anthony & de Grzybowski 1930, 1934, Barone & Bortolami 2004). By comparing neuroanatomical traits between species, and especially by trying to put these comparisons into an evolutionary framework, several researchers and especially Ludwig Edinger (Kreft 1997, Northcutt 2001) set the basis of the modern comparative neurobiology during the end of the XIXth century. Many comparative neurologists of the first half of the XXth century only aimed to place the groups they studied along a hierarchical "complexity scale" of life, for instance from insectivorans to humans among mammals (Dechaseaux 1970). During these times, some other researchers tried to keep a temporal perspective

while comparing taxa. To do this, they especially made comparisons of fresh and *fossil* brains. Nervous structures are made of soft tissues that obviously do not persist over geological times. However, the central nervous system of osseous vertebrates is enclosed, surrounded, by tissues that do preserve through time, whereas the peripheral nervous system only consists of nerves and nervous ganglia that are impossible to observe (even indirectly) in fossils. Brain and skull are highly interdependent (Richtsmeier & Flaherty 2013), and this especially allows for reconstructing fossil brains using fossil skulls (but see the following lines). Fossil spinal cords are more rarely studied: the spinal cord is enclosed by vertebrae, but the vertebral column often dissociates, whereas it is more frequent to retrieve skulls. Fossil spinal cord studies therefore frequently consist of measurements of the vertebral canal (e.g., Giffin 1990, MacLarnon 1996).

More can be said regarding fossil brains than for fossil spinal cords, therefore I focus on the former. The interaction between the brain and the skull takes place at the interface between the external surface of the brain and the internal surface of the skull (of its braincase). The brain is ontogenetically and phylogenetically "older" than the skull (Butler 2000, Kardong 2012), and the latter forms around the former: the inner surface of the braincase adapts to the external surface of the brain (actually, of the tissues present in the braincase, not only the brain; Richtsmeier & Flaherty 2013). Therefore, the inner surface of the braincase would reflect the external surface of the brain. These molds, or casts, of the inner braincase that putatively reflect the gross morphology of the brain are frequently named "endocranial casts", or more simply "endocasts". The first discoveries of such casts were finds of "natural" endocranial casts: for a given skull, the sediment fills the braincase and is therefore shaped by the internal surface of it, then the bone partially to totally break off and what remains is the internal mold of the braincase. Such description and definition of an endocast was provided by Georges Cuvier while presenting the endocast of the mammalian artiodactyl *Anoplotherium* (Cuvier 1822:44, Figure 1), but Lorenz Oken holds the first mention of an endocranial cast, describing two hemispheres ("zwey Hirnhälften", Oken 1819:1794) of a pterodactyl brain. After numerous mentions and short descriptions following these first works, with the discovery of more and more endocranial casts, and with an expanding comparative neurobiology knowledge, Tilly Edinger set the foundations of a new field of neurology: paleoneurology or paleoneurobiology (Edinger 1929, 1949). A prerequisite of paleoneurology is to know the correspondence between the true external brain shape and the internal braincase shape; in that respect, paleoneurology highly depends on comparative neurobiology and on comparative anatomy of the other tissues that surround a brain (e.g., vascular tissues). The differences between paleoneurology and comparative neurobiology, as stated by Edinger (1949) and Dechaseaux (1970) are i) the temporal perspective given by comparing extant and fossil species and ii) the fact that paleoneurologists do not try to place species on a biological hierarchy but rather to interpret the evolution of brain macromorphology.

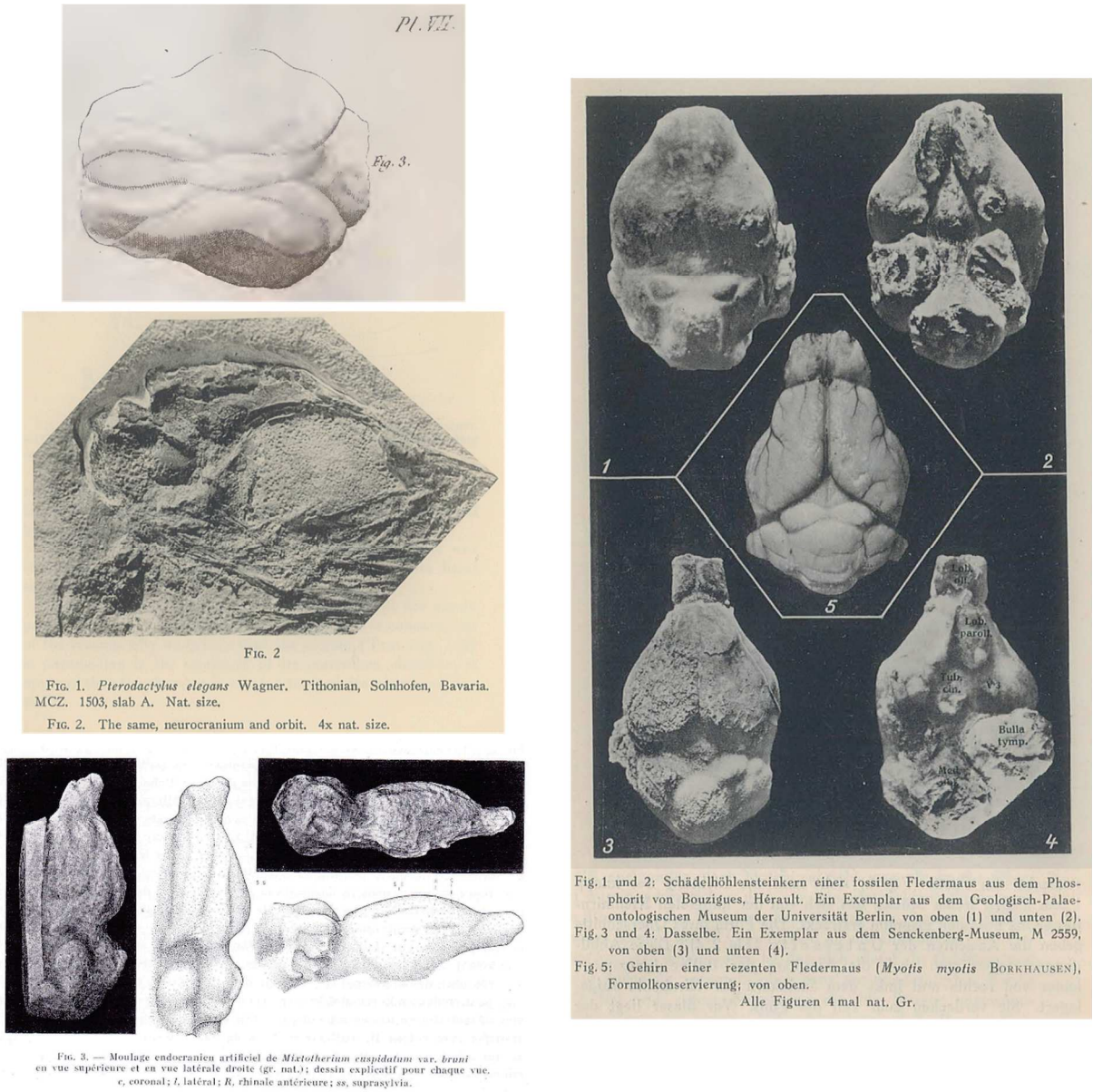

Figure 1: Historic illustrations of natural endocranial casts. Top left: Cuvier (1822), *Anoplotherium*. Center left: Edinger (1941), *Pterodactylus elegans*. Bottom left: Dechaseaux (1973), *Mixtotherium cuspidatum*. Right: Edinger (1926), various bat species.

Starting from these points, paleoneurological studies became more frequent through the XXth century, and the frequency of works followed technical innovations. A first one was the ability to create physical endocasts using synthetic materials (e.g., Murrill & Wallace 1971 for a protocol), enabling the access to endocasts of preserved skulls without natural endocast. A second one was the ability to create endocasts without risking damage to the specimen, using X-rays. This technique, X-ray computer tomography scan (or CT-scan), is formerly a clinical radiological imaging technique. It has been adapted to other species than humans and domestic animals, and to other objects than living organisms. Several advances led to the development of microtomography, or µCT-scanning, allowing studies at a higher resolution than medical imagery. These advances in imaging techniques led to a burst of studies dealing with biological internal structures (not only for vertebrates, also in botany), and especially with an increasingly easy access to the endocranial cavity of vertebrates. Nowadays, paleoneurological studies also focus on sensory organs: describing the inner ear through the study of its cast, the bony labyrinth, has become a widespread topic (e.g., Spoor & Zonneveld 1998, Luo et al. 2011, Ekdale 2013, Mourlam & Orliac 2017), but there are also studies regarding the nasal turbinals (e.g., Lundeen & Kirk 2019), and even more rarely the eyes (Young 2008, Lee et al. 2011, Strausfeld et al. 2016). “Fossil brains” are now less

studied than “fossil inner ears”, mainly because the petrosal bone housing the bony labyrinth is a single, strong, bone whereas the skull is more or less fragile and composed of several bones. Studies of “fossil brains” are still frequent in mammals for many orders (e.g., Macrini et al. 2007 and Rowe et al. 2011 for early mammals, Benoit et al. 2013 for proboscideans, Orliac & Gilissen 2012 for artiodactyls, Lyras 2009 for carnivorans, Orliac et al. 2014 for primates, Bertrand et al. 2021 for rodents), but also in reptiles and birds (e.g., Watanabe et al. 2021 for birds, Witmer et al. 2008 and Balanoff et al. 2010 for other archosaurs, Cuthbertson et al. 2015 for lepidosaurs, Voeten et al. 2018 for sauropterygians).

More researchers now work on more specimens able to provide a view on the external shape of the brain (and of its associated structures). The first comparative neurobiologists and paleoneurologists (such as Ludwig and Tilly Edinger) aimed at working in an evolutionary framework; this can now be better considered while addressing endocranial evolution, and ultimately brain evolution. But despite the progresses in the availability of specimens and in methodological concepts, there are still major limitations. The first one is the disparity of the taxonomic effort, which is due to a popularity effect (there are discrepancies in the “popularity” of vertebrate groups with iconic taxa such as primates, cetaceans, or theropods) but also to the fossil preservation bias (delicate skulls are less frequently retrieved undamaged). The second one is a weathering of the link between paleoneurology and comparative neurobiology. It is crucial to assess with the highest accuracy possible what an endocranial cast really reflects (Balanoff & Bever 2017). However, only few studies have addressed this problem, and in highly contrasted groups: the only works are in non-avian reptiles (Fabbri et al. 2017, Watanabe et al. 2019), birds (Early et al. 2020), and hominins (Kobayashi et al. 2018, Alatorre Warren 2019, Dumoncel et al. 2020). The third issue concerns the statistical treatment and the way the quantification of the brain is interpreted. A widely used measure is the encephalization quotient (EQ), a ratio between the observed and an expected (given allometry) brain masses, that serves as a proxy for intelligence (Jerison 1973:5). This measure and its derivatives (Jerison 1973, Eisenberg & Wilson 1978, Martin 1990 for EQ formulas, van Dongen 1998 for the ‘MEQ’ that accounts for metabolism, Ni et al. 2019 for the ‘PEQ’ that grossly accounts for phylogenetic covariation) actually correspond to the exponential residuals of a regression between the log brain and body masses, which skews the differences (this point is detailed in the Part Two). Additionally, statistical treatments on ratios or residuals are frequent in paleoneurology and in comparative neurobiology (e.g., Baron et al. 1996, Ratcliffe et al. 2006, Bertrand et al. 2018, Herculano-Houzel et al. 2020), but they turn out to lead to biased results (Freckleton 2002, 2009). The fourth limit regards the oversimplistic and/or premature conclusions drawn from studies with neural traits. This is again not limited to paleoneurological studies: there are studies that explain gross neural by ecological traits only by means of significant correlations (e.g., Safi et al. 2005) and others that propose evolutionary trends without using the full strength of the available statistical methods (e.g., Bertrand et al. 2021). Understanding how the brain evolves necessarily involves considering fossil taxa, even if they are scarce and bring limited data. But, in order to consider fossils, one needs to first assess the correspondences between the involved organs and their proxy (i.e., brain and associated structures vs. braincase endocranial cast), to use proper and thoughtful methods, and to adapt the significance of the conclusions to the limits implied by fossil proxies.

II) Generalities about the order Chiroptera and its evolutionary history

The bats, or order Chiroptera (as defined by Blumenbach 1779:58), group among the most spectacular animals. Indeed, these curious mammals are able to fly actively (with a skin patagium stretched between the fingers) and some are able to detect their environment and their food by means of echolocation (i.e., by sending and interpreting back sonar signals). Such a combination of ecological specializations (see also Figure 2) is unique among mammals, and even at the vertebrate scale: the only other species sharing an active flight are birds (pterosaurs also did but went extinct), and the only large taxon able to use high frequency echolocation is the Odontoceti suborder. Contrary to birds and to odontocete cetaceans, there are no "intermediate" link between "common" mammals and bats, and it remains mysterious how these mammals achieved such a specialization. There are numerous hypotheses regarding the progressive development of active flight, the more consensual one being a transition from being arboreal to gliding to flight, with various further sophistication. Echolocation is also retrieved punctually across mammals, by subterranean mammals (e.g., the mole rat, Kimchi et al. 2005), tenrecs (Gould 1965), shrews (Gould et al. 1964, Buchler 1976, Tomasi 1979, Chai et al. 2020), and some rodents (He et al. 2021), but there are also evidences of echolocation in a fossil condylarthran mammal (*Hyopsodus lepidus*, Orliac et al. 2012, Ravel & Orliac 2015). Echolocation therefore appeared more than once in mammals; being potentially less "difficult" to develop for ancient mammals, it may have been selected to navigate in the dark and/or to catch insects (what insectivorous nocturnal bats do), or it may have been an exaptation of a preexisting feature.

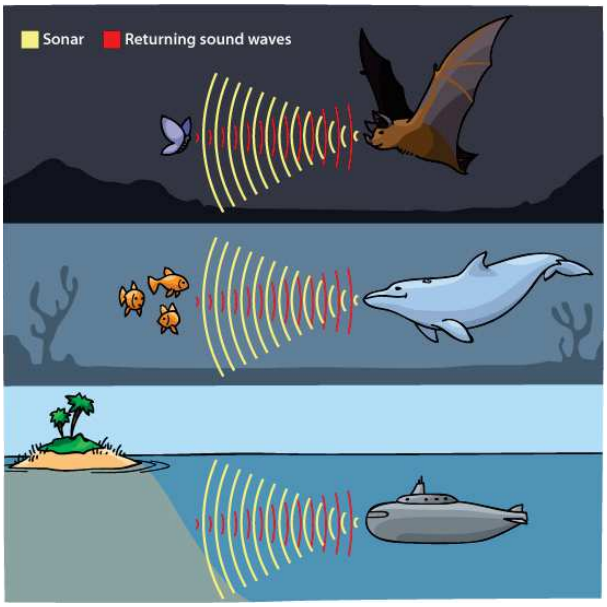

Figure 2: Simple illustration of the echolocation principle, also showing the ability of bats to fly. © Arizona State University.

In addition to their ecological singularity, bats form the second most diversified order of living mammals (Burgin et al. 2018), with more than 1300 species (~20% of the total mammal diversity). Bats were traditionally divided in two suborders: the Megachiroptera (large-sized, non-echolocating, phytophagous bats) and Microchiroptera (small-sized, echolocating, and mostly animalivorous bats). This distinction relied on numerous morpho-ecological differences, to such an extent that bats were proposed to be diphyletic by some authors (e.g., Pettigrew et al. 1989, see also Simmons 2000 for a review). They propose that the megabats were closer to the archontan taxa (primates, treeshrews, and colugos), and microbats being closer to Insectivora. The monophyly of bats is nowadays strongly supported by a cohort of both morpho-anatomical and molecular characters (e.g., Simmons 2000). With the rise of phylogenetic

studies using molecular data, the order Chiroptera is surprisingly split in two other suborders: Yinpterochiroptera and Yangochiroptera (Teeling et al. 2002). In this configuration, the megabats are still a monophyletic taxon as the family Pteropodidae, but the "microbats" become paraphyletic. Indeed, the Pteropodidae turn out to have as sister-clade the superfamily Rhinolophoidea, that encompasses six "microbat" families. Both Pteropodidae and Rhinolophoidea (formerly "Yinochiroptera" in the "Microchiroptera") now contribute to name this suborder Yinpterochiroptera. The other suborder, the Yangochiroptera, is hence only composed of three other "microbats" superfamilies.

In search of the oldest and/or most plesiomorphic bat taxa, several species were found to belong neither to megabats nor to microbats (and therefore neither to yinpterochiropterans nor to yangochiropterans). These findings initially led Dobson (1875) to gather them into a taxon he named Palaeochiroptera. Several subsequent works described very ancient bats, also placed by Smith (1976) into Palaeochiroptera. Later, Van Valen (1979) defined the basal bat suborder Eochiroptera, and further works (see Simmons & Geisler [1998] for a review) assessed that the "palaeochiropteran" bats belong to this newly defined group. Shortly before the new Yinpterochiroptera/Yangochiroptera division proposed by Teeling et al. (2002), Simmons & Geisler (1998) tried to address the phylogenetical position of some of the most iconic eochiropteran taxa (*Icaronycteris*, *Palaeochiropteryx*, *Hassianycteris*, and *Archaeonycteris*). They placed them as a stem group of microchiropteran bats, rather than stem bats to the whole chiropteran crown clade, therefore contradicting the hypothesis of a monophyletic suborder Eochiroptera basal to all other bats. However, molecular works broke the previous consensual basal dichotomy in bats; Simmons et al. (2008), constraining their analysis for extant bat relationships, found the four iconic eochiropteran taxa previously tested plus the newly described *Onychonycteris* as a stem group to the crown bat clade, still invalidating the Eochiroptera suborder. Later works (e.g., Smith et al. 2012) confirmed the paraphyletical nature of the Eochiroptera taxon, classifying the various ancient bat families as "eochiropterans" or "Eocene fossil bats", only meaning that they are "ancestral" to the two modern suborders.

Several eochiropteran taxa (especially the five previously quoted ones) are documented by fully 2D preserved skeletons, allowing to hypothesize about their paleobiology. In all cases, the postcranial skeleton indicates that these species were able to fly actively (e.g., Simmons & Geisler 1998, Amador et al. 2019), even though there were also specificities indicating that the flight was not their only locomotory mode (e.g., the basalmost *Onychonycteris* retains claws, Simmons et al. 2008). It is however more difficult to conclude about the echolocating abilities of these early bat taxa. Simmons & Geisler (1998) and Simmons et al. (2008), using the width of the cochlea (relative to the basicranial width) to discriminate echolocating and non-echolocating bats, found that eochiropteran taxa they tested (*Icaronycteris*, *Archaeonycteris*, *Palaeochiropteryx*, *Hassianycteris*) fall near non-echolocating bats, but still in the morphospace of echolocating bats. These eochiropteran taxa are therefore considered to be able to echolocate. Simmons et al. (2008) however found that the basalmost eochiropteran *Onychonycteris* has cochlear dimensions of non-echolocating bats, and that this taxon was unable to echolocate. This statement is however controversial: Veselka et al. (2010) proposed, based on anatomical basis (connection between the auditory bulla and the stylohyal bone), that *Onychonycteris* was actually able to echolocate, and Simmons et al. (2010) answered that this anatomical connection may be due to the preservation of the skeleton (which is flattened in two dimensions). Two main debates still concern the evolution of flight and echolocation in bats: one regards the scenario of the acquisition of echolocation in bats, and another one aims to know in which order active flight and echolocation were acquired.

The first debate arose when Teeling et al. (2002) shattered the Megachiroptera/Microchiroptera dichotomy and instead proposed a paraphyletic Microchiroptera, with some of them (the superfamily Rhinolophoidea) as the sister-taxon to Pteropodidae (i.e., former Megachiroptera). Indeed, with "microbats" as a clade, there was no doubt that echolocation was acquired before the "microbat" theoretical ancestor. With a paraphyly of "microbats", the question arises whether echolocation was acquired before the common ancestor of crown bats and lost before the common ancestor of crown pteropodids, or if it was acquired in a convergent way before the common ancestors of rhinolophoids and of yangochiropterans (Figure 3). Before the "molecular systematics" of bats, eochiropteran taxa were considered as a stem group of "microbats" (e.g., Simmons & Geisler 1998); with the current basal dichotomy in Chiroptera, they are now considered as a stem group of all bats (Simmons et al. 2008). In this evolutionary framework, echolocation evidence found in eochiropteran taxa (with *Onychonycteris* aside) suggests a common acquisition for bats, and a secondary loss in megabats. The anatomical basis (Simmons & Geisler 1998, Simmons et al. 2008) used to assess echolocation ability is however suboptimal. In that way, Davies et al. (2013) showed that 1) the length of the cochlear basilar membrane and its number of turns are correlated to echolocation abilities, but 2) there is a great cochlear variation across echolocating bats, and 3) echolocating bats furthermore only differ from mammals regarding the number of cochlear turn, not by the length of their cochlear basilar membrane. Whereas using cochlear parameters to discriminate echolocating and non-echolocating bats makes sense, it is however more difficult to discriminate echolocating bats from non-echolocating mammals. Due to the quite ancient age of eochiropteran taxa and because they represent the most "other mammalian" condition for bats, cochlear width appears as a weaker basis than expected to assess the echolocation ability of such old and basal taxon. Reinforcing potential doubts, a work dealing with the ontogeny of the hearing apparatus of bats (Nojiri et al. 2021) concluded that echolocation was acquired convergently in rhinolophoids and yangochiropterans. Eventually, and though there seem to be still indirect evidences for echolocation in eochiropteran bats, this point remains to be clarified once for all.

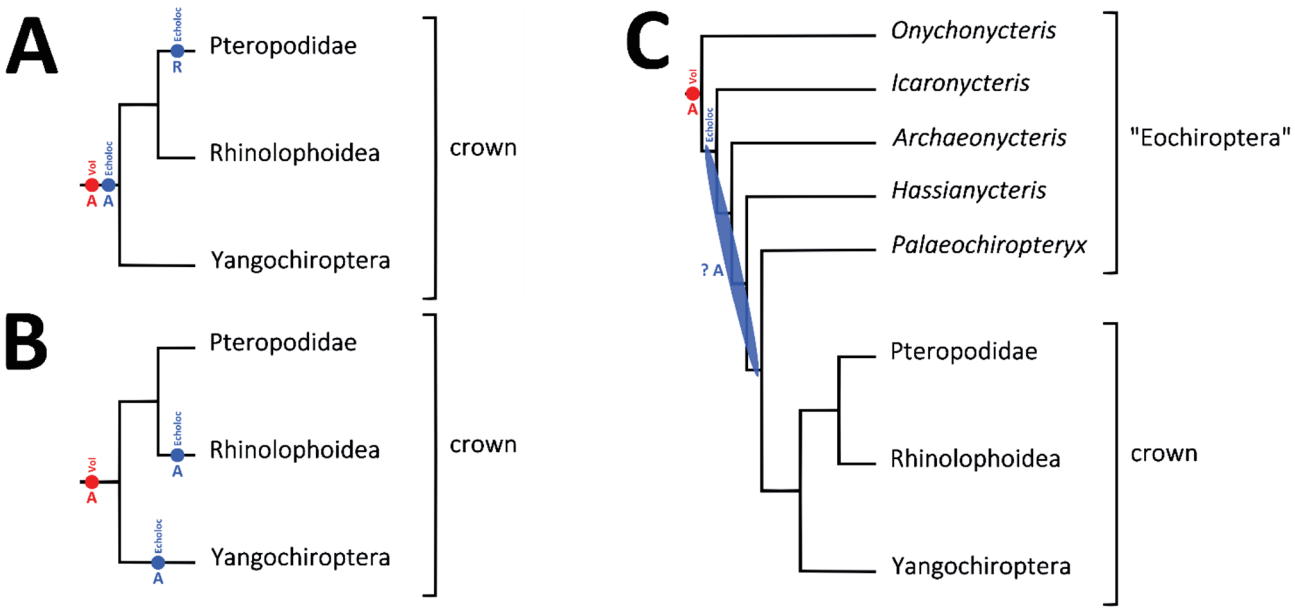

Figure 3: Hypothesis about flight and echolocation acquisition during bat evolutionary history. Left: the two equiparsimonious hypotheses considering only extant taxa. Right: considering eochiropteran taxa. A: acquisition. R: reversion. After Simmons et al. (2008).

Assuming a common origin for echolocation in bats, another debate regards whether flight appeared before echolocation or conversely (e.g., Anderson & Ruxton 2020). Since echolocating abilities appeared punctually across mammals (e.g., shrews, tenrecs, mole rat, rodents; see previous lines), the explanations to why and how echolocation appeared and developed in bats generally fit to the proposed hypothesis. In the "echolocation-first" hypothesis, arboreal and already nocturnal "pre-bats" used echolocation to catch insect preys, then echolocation became increasingly sophisticated, forelimbs extended with interdigital membrane to capture insects with an increasing efficiency, and then gliding and flight further developed. In the "flight-first" hypothesis, "pre-bats" were also arboreal and nocturnal, but they then became gliders and developed flight, before developing echolocation. Simmons et al. (2008) found that *Onychonycteris* was only able to fly, not to echolocate, which would give credit to the "flight-first" hypothesis. Both hypothesis have points and counterpoints, and there are also less popular hypothesis (tandem development, diurnal frugivory); Anderson & Ruxton (2019) summarized all these points and proposed another hypothesis (interdigital webbing), but there are today no evidences to clearly favor one of these hypotheses.

III) Comparative neurobiology and paleoneurology of bats

By understanding how the brain functions and how to interpret its characteristics, one is able to infer body characteristics, and to extrapolate eco-functional characteristics of that body. Brain comprehension is especially achievable by comparing species. For instance, if two species differ in brain characteristics but share common morphological points, either the apparent differences hide common points or there are different ways to achieve the same function. In the same way, for two species with similar brain characteristics but differences in functionality, one has either to seek if there are underlying differences that would explain functional differences, or to determine if there are multifunctional structures. Once brain and external characteristics are safely linked, one is therefore able to deal with extinct species and interpret brain characteristics as paleobiological proxies. This whole approach encompasses several fields of neurology, from neuroanatomy to comparative neurobiology and to paleoneurology. As previously exposed (first section of the Introduction), there have been several advances allowing interpreting "fossil brains": methodological ways of obtaining endocranial casts and of treating their characteristics have continuously improved, and endocranial cast studies became increasingly common. There are still methodological and conceptual issues, but they are not frozen limits that could not be overcome. The evolutionary history of the main traits of a unique mammalian group, bats, is still debated. In this case, the discussed point concerns the setting up of the abilities to fly actively and to echolocate. These behaviors obviously involve the brain: auditory information needs to be quickly and efficiently processed to provide real-time interpretation of sound signal, as well as other sensory information such as balance, somatosensation, and proprioception in addition to adequate motor responses regarding active flight. A sound hypothesis is therefore that such important eco-functional adaptations necessarily transform the brain to some extent, and that brain parts and characteristics follow the whole body in its functional specializations. Studying the evolution of the brain of bats is therefore of crucial interest: inferences based on the central organ of the body are likely to provide additional clues while addressing general evolutionary history of bats.

First, the brain shape of bats (and especially of echolocating bats) is quite unique among mammals (see Figure 4). It is not as highly derived and complex as in humans and human relatives or in cetaceans, but it has noteworthy features. As a general rule, the vertebrate brain is composed of ventricles that anteroposteriorly distinguish during ontogeny, with five final main brain parts (e.g., Nieuwenhuys 1998): from anterior to posterior are the telencephalon (with the cerebral hemispheres and the olfactory bulbs), the diencephalon (with the epiphysis and the hypophysis), the mesencephalon (with the tectum and its two pairs of colliculi), the metencephalon (with the cerebellum), and the myelencephalon (that, together with metencephalic and mesencephalic parts, forms the cerebral stem). What makes echolocating bat brains different from other mammals is the exposure of the mesencephalic tectum, and especially of their caudal colliculi (e.g., Dechaseaux 1956, Baron et al. 1996). These structures are associated with auditory information processing, and they even appear to be an obligatory step during sound information treatment in echolocating bats, which is unique in mammals (Reep & Bhatnagar 2000). The prominence of these structures in most echolocating bats and their covering in non-echolocating bats, together with somes neuroanatomical evidence, strongly suggest that dorsally exposed caudal colliculi are directly linked to echolocation (e.g., Edinger 1926, Dechaseaux 1973). Such exposure of dorsal mesencephalic structures is not observed in other mammals; some species do (see first section of the Introduction) but these are punctual cases, not high-level mammalian clades. Bats also show a well-developed cerebellum, involved in motor coordination but also in auditory information processing (e.g., Paulin 1993); this brain part is therefore directly concerned with both abilities to fly and to echolocate. The cerebral hemispheres of bats also appear as weakly complex, and smooth on their surface (e.g., Dechaseaux 1956, Baron et al. 1996). Most mammals have a more complex surface of their cerebral hemispheres: in addition to bats, only “insectivorans” and rodents generally have smooth (‘lissencephalic brain’) cerebral hemispheres, whereas they are more complex and folded (‘gyrencephalic brain’) in other mammalian orders (e.g., Herculano-Houzel 2012). Other external features of bat brains vary in their size and their degree of protrusion. The brain of an echolocating bat is therefore rather straightforward to identify: smooth cerebral hemispheres, exposed caudal colliculi, and well-developed cerebellum (Dechaseaux 1956). Non-echolocating bat brains mainly differ by the absence of exposed caudal colliculi and by bigger cerebral hemispheres that can be a little bit more folded; otherwise, they share with echolocating bats a highly developed cerebellum and a still lissencephalic brain (e.g., Dechaseaux 1956, Baron et al. 1996).

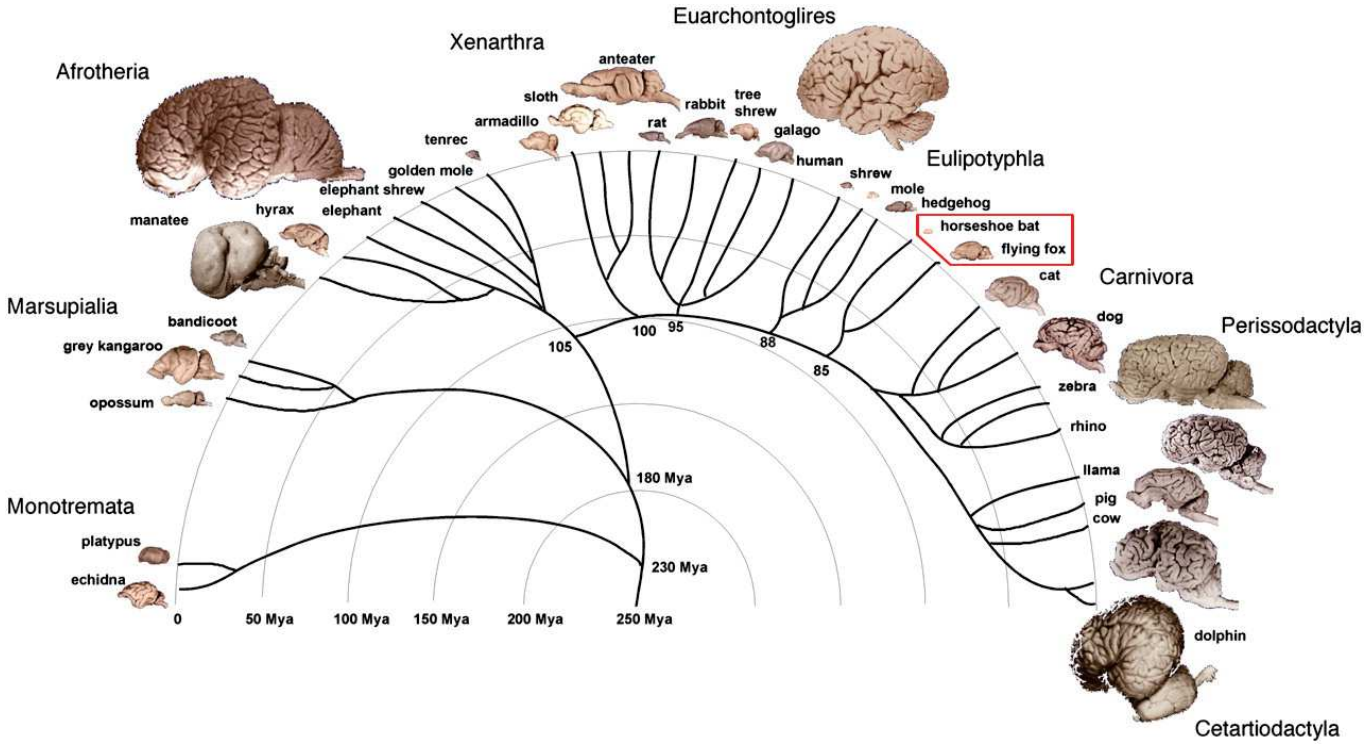

Figure 4: Overview of the morphological disparity of the brain across mammals. After Herculano-Houzel (2012): Figure 1.

Historically, fossil brains of bats have been among the first mammalian orders to be studied after paleoneurology basics were proposed by Edinger (1929, 1949). Tilly Edinger especially mentions a partly preserved Paleocene natural endocast, and refers it to bats due to the presence of inflated caudal colliculi. Yet, the attribution of this specimen remains controversial (no bats are known from the Paleocene, e.g., Brown et al. 2019), and it is known as the "Tilly-bat" (e.g., Buchholtz & Seyfarth 2001). Other works followed describing bat natural endocranial casts in the first half of the XXth century, mainly by Tilly Edinger (Edinger 1926, 1929, 1961, 1964a,b) and by Colette Dechaseaux (1956, 1962, 1970, 1973). These natural endocasts all document fossil representatives of extant bat families and all come from Quercy Phosphorites deposits. This formation is located in southwestern France, and consists in karstic infillings (a highly favorable preservation context for bats according to Brown et al. 2019), with more than 200 localities continuously ranging from the middle Eocene to the late Oligocene (38 to 25 My, e.g., Weppe et al. 2021). Quercy Phosphorites yielded almost 20% of the extinct bat diversity, and is the richest geological formation in fossil bats, with more than 50% of the known specimens of extinct species, and almost 20% of the total number of known bat fossils according to Brown et al. (2019). With the knowledge of their time regarding comparative neurobiology, Edinger and Dechaseaux briefly discussed the evolution of bat brain characteristics. They especially found that brains of bats changed only little in extant families (Dechaseaux 1956, 1962, Edinger 1964a), with trends towards a decrease of the exposed area of the mesencephalon and increases in the cerebral hemisphere size and neopallial surface (Dechaseaux 1956). Theses conclusions imply that ancient representatives of extant families were able to fly actively and to echolocate, but no finer inferences have been drawn.

Some works only dealing with extant bats described the general morphology of the brain and its variation across extant taxa (Schneider 1957, 1966, McDaniel 1976, Hackethal 1981). These works are however either only pure comparisons and anatomical descriptions, or deal very little with evolutionary hypotheses. For the latter case, and like the previous works on bat "fossil brains", the authors only aim to distinguish "primitive" and "derived" taxa. Some general reviews further came out in the literature (Henson 1970, Neuweiler 2000) and the last massive contribution to bat comparative neurobiology is the highly documented atlas of Baron et al. (1996). In this work, the authors describe both the macromorphology and the micromorphology of the brain in the bat families recognized at that time, but they do not put their observations into a more sophisticated evolutionary framework than previous works did. Therefore, there is a substantial corpus of qualitative data in comparative neurobiology for bats, some old works on natural endocasts, but little evolutionary considerations. Especially, the advances made in comparative neurobiology did not update our knowledge of bat paleoneurology, and this lack impeded integrating paleoneurological traits while discussing the evolutionary history of main bat traits.

A large part of the discussed data on bat general neural traits actually regard volumes, either of the whole brain or of sub-regions of it. For more than 50 years, several "waves" of works dealt with brain or brain region masses. The very first studies are from Guillermo Mann, dealing with the accessory olfactory bulb (Mann 1961) and with the relative proportions of several brain regions (Mann 1963). At that time, paleoneurological and comparative neurobiological works in Chiroptera were still tightly linked. Therefore, following the viewpoint of Edinger (1964a) and contrary to that of Dechaseaux (1956), Mann considered the pteropodid bats as pleisomorphic, the other "microchiropteran bats" (i.e., Yangochiroptera + Rhinolophoidea) exhibiting a secondarily derived "simple" condition, with less developed neocortex and olfactory bulbs and of an exposed mesencephalic tectum.

Then, several researchers (especially Paul Pirlot and Heinz Stephan; e.g., Stephan & Pirlot 1970, Pirlot & Stephan 1970, Stephan et al. 1981) pursued similar studies, comparing brain regions with an increasing sampling effort, being joined by Eisenberg & Wilson (1978), who proposed an alternative formula to calculate Jerison's (1973) Encephalization Quotient. These more strictly neurobiological studies generally attempted to establish "grades" in the quantified brain evolution among bats, with a hierarchy going from insectivorous bats (further split in "aerial insectivores" and "foliage gleaners") to carnivorous ones (with especially fish-hunting and blood-eating bats), to frugivorous ones (with a distinction between nectar/pollen and fruit-eating bats). In this hierarchy, insectivorous bats are the least encephalized (i.e., with the smallest brain mass), with the least developed neocortex and olfactory bulbs, whereas frugivorous bats are the most encephalized (i.e., with the largest brain mass), with the most developed neocortex and olfactory bulbs. In this viewpoint, insectivorous bats are considered as primitive, likely to represent the ancestral bat condition. The link between the feeding habits and brain (and other parts) size was, according to these authors, reinforced by the fact that microchiropteran frugivorous bats (groups of the family Phyllostomidae) also show enlarged brain and olfactory bulbs. Bhatnagar & Kallen (1974) contributed by assessing that the olfactory bulbs are linked to olfactory acuity, but they also demonstrated that olfactory bulbs and neocortical development are not correlated (though they should be if both increase and decrease according to the feeding habits).

Further works tried to observe the covariations between brain structures. Pierre Jolicoeur especially contributed to this (e.g., Pirlot & Jolicoeur 1982, Jolicoeur et al. 1984) and highlighted some major points. First, he found no significant negative covariations between brain regions (Pirlot & Jolicoeur 1982), with no compensatory effects; he explained this saying that compensations are probably present but take

place at a lower scale, not decipherable by considering large brain regions (and only qualitative studies could highlight these trade-offs). Second, he found some interesting covariations between brain regions (Pirlot & Jolicoeur 1982). Some of them were not surprising (neocortex and diencephalon: neocortical areas treat complex informations, and the diencephalic hippocampus is associated with spatial memory, both involved in foraging in complex environments, but see following sentences) and others were (especially one between the mesencephalon and the paleocortex). Jolicoeur et al. (1984) also found a correlation between olfactory bulbs and neocortex volumes (contra Bhatnagar & Kallen 1974), but interpreted it to be likely fortuitous and to result from the global adaptation to dietary habits of the brain in bats. Insectivorous species have smaller neocortex and olfactory bulbs, while frugivorous species have bigger ones, but maybe because both are independently associated with these diets. Latest works of the XXth century mainly concentrated on a hypothesis of a trade-off between echolocation in insectivorous bats and vision associated with olfaction in frugivorous bats (Barton et al. 1995). Baron et al. (1996), together with numerous qualitative data, mostly provided quantitative data reused in further studies. At the end of the XXth century, bats were still divided in two very contrasted clades (megachiropteran and "microchiropteran" bats), and the main hypotheses regarding bat brain evolution were that there was a dietary cause to the variation of the brain (and of its brain parts) across bats, rather than a phylogenetic/systematic signal. None of these studies included fossil taxa, though the quantification of cerebral cavity instead of fresh brains have been already proposed, tested, and approved in bats (Eisenberg & Wilson 1978, Stephan et al. 1981), and though endocasts were used in other mammlian groups (e.g., Jerison 1973, Radinsky 1978).

With the XXIth century, the new phylogenetic systematic context split bats in two "molecular" suborders (Teeling et al. 2002). Data previously accumulated also became increasingly easier to share and to use, and several studies further tried to explain the evolution of the brain in bats in the light of the new phylogenetic framework. Phylogenetic comparative methods were also increasingly used and refined, facilitating a better reconstructed evolutionary history of traits rather than simple value-to-value comparisons between extant species. The first studies did not bring revolutionary hypotheses and tested the phylogenetic and dietary effects. For instance, Hutcheon et al. (2002) found that the differences in brain size and in brain region sizes better correlated to ecology, with bigger brains and olfactory bulbs in frugivorous bats, and with a trade-off underwent by pteropodids between body size and echolocation (echolocation implying a small size). Jones & MacLarnon (2004) also found a difference in relative brain mass between fruit-eating bats (pteropodids and a phyllostomid group) and non fruit-eating bats (other ex-"microchiropteran" bats). The dietary correlation hypothesis was then further enhanced by the works of Safi & Dechmann (2005) and of Safi et al. (2005). They found a correlation between habitat complexity and wing area and between wing area and brain and brain region sizes, therefore correlating habitat complexity to brain and brain region sizes. They further explained the "dietary correlation" as being actually dependent from the cognitive and sensory demands associated with the type of diet. As "phytophagous" (i.e., plant, fruit, and nectar-eating) bats forage in open habitats, they need to memorize spatial information related to food availability (with a larger hippocampus), which would imply consistently high neuronal requirements such as vision (with a high relative brain size) and olfaction (with large olfactory bulbs). On the other hand, "animalivorous" (i.e., insects, fish, other animals, and blood-eating) bats rather have to process immediate habitat complexity and prey location using echolocation (with large auditory structures, and a wide range of neuronal requirements). Dechmann & Safi (2009) further summarized these results (Figure 5) together with other studies finding correlations between brain size and various ecological traits, such as testes size and mating strategy (Pitnick et al. 2006),

behavioral complexity (Ratcliffe et al. 2006), or migratory vs sedentary behaviors (McGuire & Ratcliffe 2009). Dechmann & Safi (2009) emphasized that phylogeny accounts for a quite high part of the variance explained in the brain-body size relationship, and that correlations could be only caused by the "animalivorous" bats. They also concluded that traits can be misleadingly found to covariate with relative brain size, their variation being actually caused by other traits that covary with relative brain size.

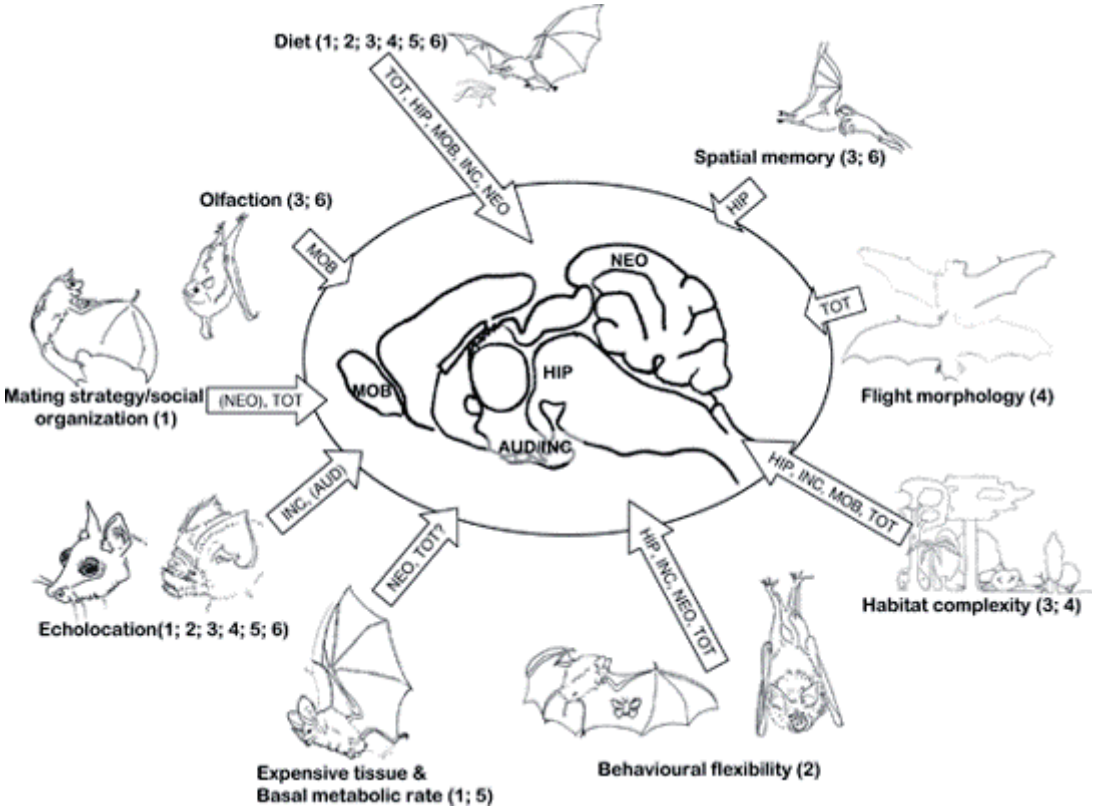

Figure 5: Overview of the putative ecological correlates of the corresponding neural traits. Parentheses of the abbreviations indicate non-significant correlations. Neural variables are the masses of: total brain (TOT), hippocampus (HIP), neocortex (NEO), main olfactory bulbs (MOB), inferior colliculus (INC), auditory nuclei (AUD). References: 1-Pitnick et al. (2006); 2-Ratcliffe et al. (2006); 3-Safi & Dechmann (2005); 4- Safi et al. (2005); Jones & MacLarnon (2004); 6-Hutcheon et al. (2002). After Dechmann & Safi (2009): Figure 1.

A first summary can be drawn: much effort has been put to explain brain neural masses by ecological traits, but there are actually few clear links. I want to emphasize two crucial points. The first is that, apart the work of Bhatnagar & Kallen (1974), there are no studies precisely explaining the causality between functions (sensitive and/or cognitive) and gross brain region size. Some structures are likely to be consistent in their function, which is for instance the case of caudal colliculi and of auditory nuclei, both related to audition. However, the work of Safi & Dechmann (2005) found different covariation patterns for both these structures, which may imply that their role could differ. Only olfactory bulb size has been quite strongly linked to olfactory acuity (Bhatnagar & Kallen 1974), and seems to be related to diet, contrasting "phytophagous" and "animalivorous" bats across studies. Otherwise, recalling in a sense the conclusions of Pirlot & Jolicoeur (1982), there is a crucial need to establish causality links between structure size and sensory or cognitive functions using anatomy at first; considering large brain regions, trade-offs can be present but not visible. The second point I would raise regards the general evolutionary context of these studies: groups of extant species only have been compared, considering phylogeny for the most recent quoted studies, but without real temporal context. However, one may find it a bit suspicious to assess that some traits are correlated to diet (or to any ecological trait) without temporal framework: in the case of feeding traits, diet regimes could also have a part of phylogenetic signal, all the more in a speciose order where there is a clearly dominant diet (i.e., insectivory).

Safi et al. (2005) also reconstructed values for some traits (brain and body size, wing area) for the "ancestor of bats"; they found that this "ancestor" would have had intermediate values for all traits, suggesting an "intermediate" bat between phytophagous and animalivorous extant bats. Safi et al. (2005) and Niven (2005, using the former's dataset) then found some increases or reductions of relative brain size in some families, with especially numerous decreases of relative brain mass (a rare thing during mammalian evolutionary history). These studies proposed that brain size reductions would be due to lower neurological demands and would occur in animalivorous bats, whereas brain size increases would be due to higher neural processing in phytophagous bats. Yao et al. (2012) further looked at a peculiar family, the rhinolophoid Hipposideridae, and showed that, by adding fossil taxa, the evolution of relative brain mass was completely changed (Figure 6). Indeed, while Safi et al. (2005) and Niven (2005) predicted a decrease from the chiropteran "ancestor", Yao et al. (2012) showed a first short decrease followed by an increase. Evolution of relative brain size thus looked more complicated by including fossil values, and Yao et al. (2012) especially questioned the scope of the conclusions that can be drawn using extant taxa only. Though, Thiagavel et al. (2018), while reconstructing the evolution of vision and of echolocation across bats, only gathered extant taxa. They show that phytophagous bats have a higher relative brain mass than animalivorous bats, with an enlargement of the neocortex, of the hippocampus, and of the olfactory bulbs. They also reconstructed the ancestral condition for bats and, like Safi et al. (2005), they found "intermediate" values, the bat "ancestor" having a relative brain mass equal to higher than some animalivorous extant lineages.

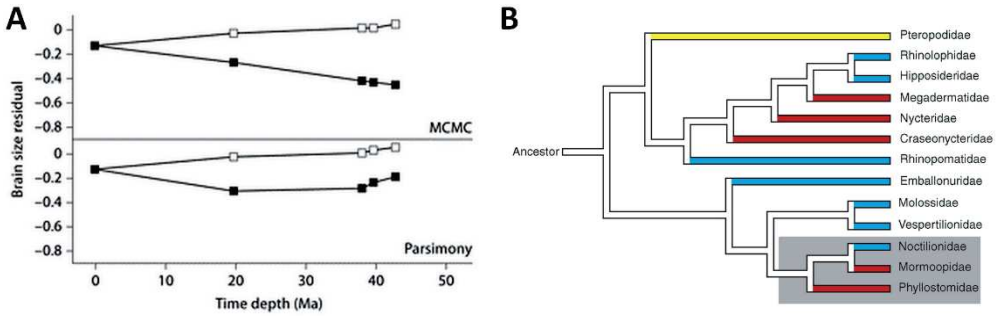

Figure 6: Comparisons of the relative brain mass evolution scenarii proposed by (A) Yao et al. (2012) including fossils (filled squares) or not (empty squares) in the family Hipposideridae and (B) Niven (2005) on all bats. Notice that the relative brain mass of hipposiderids decreases since the "chiropteran" ancestor according to Niven (2005), whereas it increases with a more or less complex scenario according to Yao et al. (2012). After Yao et al. (2012): Figure 5 and Niven (2005): Figure 1.

Smaers et al. (2012, 2021) recently looked at the brain/body relationship evolution in bats. However, their aim was to address how this relationship evolves in bats, rather than looking at how the deviations from the relationship evolve. By looking at both variables separately and then recalling results from both, they found interesting results partially questioning the results of previous works (i.e., Safi et al. 2005, Niven 2005, Thiagavel et al. 2018). They found a link between body size and both brain and relative brain masses evolvability in bats: the brain size value and variance decrease less than those of body size (and conversely). This implies that, when body mass decreases, relative brain mass increases (as brain size decreases less than does body size) as well as the independence from the brain/body size allometric relationship (as brain size variance decreases less than does that of body size). They explain these patterns by the fact that size might imply increasing energetic constraints (with thus less available variation of relative brain size), whereas physiological costs decrease with body size, allowing more variation of the brain size. They however do not discuss the relative brain size value itself, but their conclusions would contradict the statement that animalivorous bats have a lower relative brain mass than phytophagous one (as proposed by Safi et al. 2005 and previous other works).

IV) Goals and work axes of this thesis

Central organ of the organism, the brain is a case study for deciphering the evolutionary history of functional (to ecological) traits. It is especially of importance in bats, a mammalian group that developed two highly specialized traits: the active flight and the echolocation. In the current systematic framework of the Chiroptera order, it remains debated if echolocation has been acquired for the whole order and lost in a family (the Pteropodidae), or if it has been acquired in a convergent manner in paraphyletic echolocating "microbats" (found in the two clades Rhinolophoidea and Yangochiroptera). It also remains to be seen whether echolocation or active flight appeared first, if one indeed preceded the other. Tracking the evolution of brain characteristics may bring critical clues to help answer these important questions; though, few works dealt with the evolutionary history of the brain, and they were unable to bring new arguments. "Fossil brains" of bats have been among the first to be studied during the XXth century; if their study, at that time, did not raised new points, it did not benefit from the methodological advances of comparative neurobiology since the end of the XXth century.

This starts by a first overview of the chiropteran endocast in fossil species, and addresses a major question: which conclusions and perspectives can be drawn by studying bat "fossil brains" with XXIth century techniques? I use fossil endocranial casts of three hipposiderids species from the Quercy Phosphorites (southwestern France) plus a Miocene hipposiderid species from the Bouzigues Formation (southern France). Hipposiderids are striking among extant bat families regarding the number of fossilized skull, and especially of preserved braincases. This is also a diversified family nowadays, with quite clear relationships between extant groups. This makes this family a case study to begin a study of the chiropteran endocast. The first part aims to give a general idea of the current gap between paleoneurology and comparative neurobiology in bats, both on qualitative and on quantitative aspects. This part also aims to give a fresher idea of the morphological variation using current knowledge of the bat brain, and therefore to show the potential of proper analyses of the endocranial cast morphology. After considering the morphology, common quantitative traits of bat "fossil brains" are quickly described, in order to give a very first idea of the adequacy of neontological (i.e., arising from comparative neurobiological studies) scenarios by including fossils, and if fossil taxa stand out compared with their extant relatives.

After giving an idea of the benefits and of the perspectives when studying thoroughly the chiropteran endocasts in hipposiderids, I aim to develop a methodology for studying the endocranial cast at the scale of Chiroptera. Working with some hipposiderid species allows for proposing (in Part One) the first bases of further work that needs to be generalized, especially regarding the comparisons between an endocranial cast and the soft tissues present in the animal braincase. This phase implies a thorough survey of the available literature regarding comparative anatomy of the skull and/or of soft tissues in bats. It also implies, sometimes, to propose homologies of structures that have not been described in Chiroptera so far. Additionally, I expose the methodology to analyze the evolution of brain characteristics using a statistical method built to include fossils, whereas numerous mainstream methods can only deal with extant taxa. I divide the "brain characteristics" into qualitative and quantitative data. Qualitative data are anatomical characters, first established at the Yinpterochiroptera scale, and quantitative data are relative neural masses commonly used, but that I aim to *properly* analyze. Once all the methodological basics are set up, my aim is to broaden the phylogenetic picture. First observations have been provided regarding fossil hipposiderids, but a more thorough and extensive work can be done at a larger scale.

I first chose the case of the suborder Yinpterochiroptera. Indeed, this clade is composed of two extremely divergent clades: the “microbat” rhinolophoids and the megabats, or pteropodids. How does the brain evolve in this suborder? Is this evolution contrasted between rhinolophoids and pteropodids and, if so, to which extent? How does the brain evolve across rhinolophoids? What are the differences between the families? I aim to provide first clues to all these questions using a sample that in its phylogenetical resolution is to the inter-tribal to inter-specific level (depending on the families), and that documents approximately one eighth of the extant specific diversity and integrates eight additional fossil species belonging to two families. The anatomical characters have been previously (i.e., in Part Two) established at the Yinpterochiroptera scale: it probably is the clade with the most contrast between its two daughter taxa, so the characters established in this clade are likely to be valid at the scale of Chiroptera. I score these anatomical characters for this yinpterochiropteran sample, and measure the volumes of three commonly used neural traits (brain, olfactory bulbs, and paraflocculi masses). Using the previously described statistical treatment, my aim is multiple on both qualitative and quantitative traits. Regarding anatomical characters, I try to address multiple questions: are these characters phylogenetically relevant? Does their evolution make any biological sense? Can we suspect some state variation due to allometry? Are the previously established homologies still valid after phylogenetic testing? How does the mesencephalic tectum evolve, the only discussed feature in the literature? What are the ancestral endocranial morphologies of the yinpterochiropteran main clades? How to interpret the evolution of endocranial morphology between and within clades? Regarding the quantitative traits, I have two major goals. The first one is to discuss the evolution of relative brain, olfactory bulbs, and paraflocculi masses in the light of the few previously published works. How do these traits evolve? How do they interact? Does the proposed covariation with some ecological traits still stand? The second goal is to to assess the importance of the inclusion of fossil occurrences at a broader scale than hipposiderid bats by comparing reconstructions with and without fossils. How many inferences differ with the inclusion of fossils? Does this change the conclusions that can be drawn? What is the impact regarding the conclusions of the previous rare neontological works?

The second phylogenetical frame of study is broader: after showing some worthy directions with hipposiderids, after adapting the observations made at the hipposiderid scale to the Chiroptera scale, and after testing a precise and thorough methodology in a highly contrasting clade, I aim to investigate the potential trends of endocranial evolution at the Chiroptera scale. By widening the scale, resolution diminishes: while I aim to be able to distinguish inter-tribal to intra-generic differences at the Yinpterochiroptera scale, I now aim to decipher trends down to the family level at the Chiroptera scale. This allows a step back from the previously defined methodology and trading of resolution for phylogenetic scale. This Chiroptera-scale work is of particular interest as I integrate the first (and, yet, only) known eochiropteran endocranial cast. New eochiropteran material from the Eocene Quercy locality of Vielase provides an incredibly well-preserved cranium, allowing to easily extract and reconstruct the endocranial cast. After describing this endocast, I apply the same methodology as that used for Yinpterochiroptera. With a family-level sample, I therefore revise and score the previously established anatomical characters and I gather the commonly used volumetric data. Similarly, I divide the analytical work into qualitative and quantitative parts. Some questions are similar to those raised at the Yinpterochiroptera scale, and allow for comparing the results with similar methodology but different sampling and scale. Again, the main questions are: does the phylogenetic relevance of the anatomical characters change by considering the whole order? Are there elements to interpret biological evolution of them? How does the mesencephalic morphology evolve by considering a stem bat species, and what

are the implications for the evolution of echolocation? What are the ancestral endocranial morphologies of the main Chiroptera clades? Regarding quantitative traits, after having emphasized the importance of fossils, I only focus on the discussion and the interpretation of the relative neural masses evolution: are the results similar to those found at a lower scale? Are they similar to neontological works? How main bat clades evolve? Are there discrepancies, or similarities, or noteworthy patterns?

Materials & Methods

I) 3D Data acquisition

All virtual reconstructions of endocasts (i.e., the 'segmentation') have been performed using Avizo® 9.3.0 and Avizo® 2019.1 (Thermo Fisher Scientific-FEI). The segmentation protocol was as follows:

- the (original) image stack was initially reoriented using the skull mesh (obtained using the 'Threshold' tool), in order to have three meaningful orthogonal axes (with the floor of the braincase used as the reference for an horizontal plane), resulting in new, reoriented (named 'final') image stack

- if the final image stack was too heavy (i.e., in general, width, height and depth at the 10^4 level), the image stack was binned (halving the height, width, and depth of the image stack) using the software ImageJ © (Schneider et al. 2012, v1.48), resulting in a eight times lighter image stack (with width, height, and depth at the 10^3 level)

- the endocranial segmentation was then performed using the left-right axis (i.e., using para-sagittal slices), and depending on the specimen preservation:

  - if the braincase was empty (i.e., in extant specimens or in particularly well-preserved fossil ones), a threshold was chosen to distinguish the bone from the empty space, then all foramina were closed slice by slice using the 'Lasso' tool with this threshold (including the potential skull crushing), then the braincase was filled slice by slice using the 'Magic Wand' tool (with the 'Same Material Only' option checked) with the same threshold

  - if the braincase was filled (i.e., generally by sediment in fossil specimens), all the sediment surface in contact with bone was selected slice by slice using the 'Brush' tool, sometimes with a thresholding when applicable, while the exposed endocranial surface (if there was) was selecting using the 'Brush' tool using a thresholding

  - in particular cases with a mix of the two previously described cases, the first way was applied, then the second for filled portions of the braincase

- the endocast mesh reconstruction was done using the 'Generate Surface' tool, always with a value of 3 of 'Unconstrained Smoothing'; for heavy surfaces, the number of faces was reduced to 2 million of faces

- the mesh was then exported in .ply format ('Polygon File Format') and visualized using the freeware MorphoDig © (Lebrun 2018) for further anatomical visual analyses.

Anatomical plates and schemes were prompted using Inkscape © (Inkscape Project 2018, v0.92.3)

The complete list of the specimens used, with the curation places and the µCT-scanning details are provided in the Table 1 (see also Appendix 1 for more details on this table). Of these specimens, several scans (42) have been downloaded from the Morphosource (Boyer et al. 2017) repository of Shi et al. (2018), and the scans of the other specimens (35) were performed using the µ-CT facilities of the MRI platform in the ISEM. I performed the segmentation of all specimens with the exception of most of that of Palaeophyllophora quercyi.

Inventory number	Taxonomy		Temporal, geological, and geographical settings				µCT stack resolution (µm)
	Family	Binom	Age	Locality	Formation/Area	Country	
UMMZ 102659	Emballonuridae	*Balantiopteryx plicata*	Holocene				20
AMNH M-101939	Emballonuridae	*Emballonura raffrayana*	Holocene				20
AMNH M-103824	Emballonuridae	*Taphozous longimanus*	Holocene				20
UM 054 012 N	Hipposideridae	*Asellia tridens*	Holocene				35,72
AMNH M-159388	Hipposideridae	*Aselliscus tricuspidatus*	Holocene				20
MNHN CG-1983-1994	Hipposideridae	*Coelops frithii*	Holocene				17,86
NMB G 2369	Hipposideridae	*H. (Pseudorhinolophus) bouziguensis*	MN2a	Bouzigues	Hérault, Occitanie	France	23,8
NMB QV370	Hipposideridae	*H. (Pseudorhinolophus) schlosseri*	unknown	("ancient collections")	Quercy Phosphorites	France	35,72
UM 762 V	Hipposideridae	*Hipposideros armiger*	Holocene				18,08
AMNH M-161913	Hipposideridae	*Hipposideros caffer*	Holocene				40
AMNH M-239401	Hipposideridae	*Hipposideros cyclops*	Holocene				40
MNHN CG-1985-1420	Hipposideridae	*Hipposideros galeritus*	Holocene				17,86
AMNH M-236305	Hipposideridae	*Hipposideros gigas*	Holocene				40
MRAC RG 73-017-M-0241	Hipposideridae	*Hipposideros jonesi*	Holocene				17,86
AMNH M-57166	Hipposideridae	*Hipposideros pomona*	Holocene				40
NMB QP784	Hipposideridae	*Palaeophyllophora oltina*	MP18	Sainte-Néboule	Quercy Phosphorites	France	23,82
UM ACQ 6627	Hipposideridae	*Palaeophyllophora quercyi*	unknown	("ancient collections")	Quercy Phosphorites	France	18,08
UNSW AR22149	Hipposideridae	*Riversleigha williamsi*	~17Ma	Bitesantennary Site	Riversleigh	Australia	20
MRAC RG 5117	Megadermatidae	*Cardioderma cor*	Holocene				23,82
MRAC RG 12268	Megadermatidae	*Lavia frons*	Holocene				23,82
UMMZ 160294	Megadermatidae	*Megaderma spasma*	Holocene				40
UMMZ 156998	Miniopteridae	*Miniopterus schreibersii*	Holocene				20
AMNH M-247585	Molossidae	*Cheiromeles torquatus*	Holocene				40
AMNH M-271513	Mormoopidae	*Mormoops blainvilli*	Holocene				20
UMMZ 105767	Natalidae	*Nyctiellus lepidus*	Holocene				20
UMMZ 105827	Noctilionidae	*Noctilio albiventris*	Holocene				20
AMNH M-187705	Nycteridae	*Nycteris macrotis*	Holocene				20
UMMZ 99089	Phyllostomidae	*Diphylla ecaudata*	Holocene				20
AMNH M-269496	Phyllostomidae	*Lonchorhina aurita*	Holocene				20
UMMZ 95718	Phyllostomidae	*Macrotus waterhousii*	Holocene				20
UMMZ 125174	Phyllostomidae	*Micronycteris hirsuta*	Holocene				20
UMMZ 161197	Pteropodidae	*Acerodon jubatus*	Holocene				60
AMNH M-233970	Pteropodidae	*Balionycteris maculata*	Holocene				40
MRAC RG 33348	Pteropodidae	*Casinycteris argynnis*	Holocene				30,08
AMNH M-105177	Pteropodidae	*Dobsonia minor*	Holocene				40
AMNH M-48701	Pteropodidae	*Eidolon helvum*	Holocene				40
UMMZ 156952	Pteropodidae	*Eonycteris spelaea*	Holocene				40
UMMZ 162225	Pteropodidae	*Haplonycteris fischeri*	Holocene				40
AMNH M-86764	Pteropodidae	*Hypsignathus monstrosus*	Holocene				60
UMMZ 161346	Pteropodidae	*Macroglossus minimus*	Holocene				40
AMNH M-216753	Pteropodidae	*Megaerops ecaudatus*	Holocene				40
AMNH M-236289	Pteropodidae	*Megaloglossus woermanni*	Holocene				40
AMNH M-221419	Pteropodidae	*Nyctimene major*	Holocene				40
UMMZ 159632	Pteropodidae	*Penthetor lucasi*	Holocene				40
AMNH M-194275	Pteropodidae	*Pteropus capistratus*	Holocene				60
AMNH M-240006	Pteropodidae	*Pteropus lylei*	Holocene				60
AMNH M-105285	Pteropodidae	*Pteropus neohibernicus*	Holocene				60
UMMZ 162253	Pteropodidae	*Pteropus pumilus*	Holocene				40
AMNH M-154582	Pteropodidae	*Pteropus scapulatus*	Holocene				60
UMMZ 91079	Pteropodidae	*Pteropus vampyrus*	Holocene				60
UMMZ 161026	Pteropodidae	*Rousettus aegyptiacus*	Holocene				40
MRAC RG 81-052-M-28	Pteropodidae	*Rousettus obliviosus*	Holocene				30,08
AMNH M-274330	Pteropodidae	*Sphaerias blanfordi*	Holocene				40
MNHN CG-1985-894	Rhinolophidae	*Rhinolophus blasii*	Holocene				17,86
MRAC RG 97-077-M-3160	Rhinolophidae	*Rhinolophus denti*	Holocene				17,86
MNHN CG-2004-1195	Rhinolophidae	*Rhinolophus euryale*	Holocene				17,86
UM HM 11-091	Rhinolophidae	*Rhinolophus ferrumequinum*	Holocene				36,16
MRAC RG 73-015-M-0697	Rhinolophidae	*Rhinolophus fumigatus*	Holocene				17,86
UM CHI 052-007	Rhinolophidae	*Rhinolophus hipposideros*	Holocene				35,76
MRAC RG 73-015-M-0617	Rhinolophidae	*Rhinolophus landeri*	Holocene				17,86
MNHN CG-2006-87	Rhinolophidae	*Rhinolophus luctus*	Holocene				23,82
MNHN CG-1985-1500	Rhinolophidae	*Rhinolophus pearsoni*	Holocene				17,86
MNHN CG-1985-1978	Rhinolophidae	*Rhinolophus rouxii*	Holocene				17,86
MNHN CG-1983-1938	Rhinolophidae	*Rhinolophus shameli*	Holocene				17,86
MNHN CG-1985-1522	Rhinolophidae	*Rhinolophus simulator*	Holocene				17,86
UNSW AR22151	Rhinonycteridae	*Archerops annectens*	~14-15 Ma	AL90 Site	Riversleigh	Australia	20
MRAC RG 29244	Rhinonycteridae	*Cloeotis percivali*	Holocene				35,72
UNSW AR22376	Rhinonycteridae	*Rhinonycteris aurantia*	Holocene	un-named cave	Riversleigh	Australia	30
UNSW AR22375	Rhinonycteridae	*Rhinonycteris tedfordi*	~17Ma	Bitesantennary Site	Riversleigh	Australia	16,848
MRAC RG 38552	Rhinonycteridae	*Triaenops persicus*	Holocene				35,72
UNSW AR22150	Rhinonycteridae	*Xenorhinos halli*	~17Ma	Bitesantennary Site	Riversleigh	Australia	20
MRAC RG M31166	Rhinopomatidae	*Rhinopoma hardwickei*	Holocene				35,72
MRAC RG 73-017-M-134	Rhinopomatidae	*Rhinopoma microphyllum*	Holocene				35,72
UMMZ 53240	Thyropteridae	*Thyroptera tricolor*	Holocene				20
UMMZ 161396	Vespertilionidae	*Kerivoula pellucida*	Holocene				20
UMMZ 157013	Vespertilionidae	*Scotophilus kuhlii*	Holocene				20
UM VIE 250	Yet to define	*Vielasia sigei*	MP10/11	Vielase	Quercy Phosphorites	France	17,86

Table 1: List of all specimens scanned with their taxonomical and spatio-temporal details, and the resolution at which their endocast has been segmented.

II) Cerebral volumes measured

Three numeric measurements of the endocranial cast can approximate corresponding measurements of the brain: i) the general volume of the endocranial cast, that can approximate the general volume of the brain, ii) the volume of the olfactory bulbs chamber, that can approximate the general volume of the main olfactory bulbs, and iii) the volume of the subarcuate fossa of the petrosal, that can approximate the volume of the paraflocculi (see Maugoust & Orliac 2021). There are, for each approximation, some caveats that I tried to address as much as possible.

The volume of the whole endocranial cast does not only encompass the brain, but also that of the meninges, and of vascular structures. Some structures leave an imprint on the internal surface of the cranial cavity and can be identified. It is not possible to remove that bias, but I tried to keep that bias as homogeneous as possible throughout my sample. The course of cranial nerves and of the spinal cord (through the foramen magnum) can also affect the whole endocast volume, even more if they are segmented outside the cranial cavity; I chose to cut them at their skull exit in the sagittal plane, taking a straight line between their edges. This also stands for non-neural exits, in order to limit homogeneously the amount of non-neural structures. Finally, some skulls were crushed, with for some a little break in the cranial cavity (for extant species mostly), and for others up to half of the skull not preserved (for fossil species mostly). In general, if there were bone breaks in only one half of the skull, I chose to duplicate the values obtained from the other half only: this concerns some extant species and the poorly preserved fossil ones. When not possible, mostly in extant species, there were generally small breaks, and I decided to keep original global values. Finally, for several species, the petrosal bone is not preserved in situ and there is a large aperture in place of it. I decided to treat this like an aperture and to virtually cut it at its edges in the sagittal plane. Of all approximations, the latter is by far (to my sense) the most significant. I have in particular one specimen (documenting *Asellia tridens*) which is well-preserved with the exception of a petrosal on one side, which allowed me to roughly estimate the impact of the presence/absence of that bone; the volumetric difference between the two sides is 3.7mm^3, which represent 1.8-1.9% of the whole volume. I did not apply any correction from this percentage as it has been taken on a single specimen in which the petrosal is quite large (and therefore may not be representative of my whole sample); this measure gives an idea of the bias induced by the lack of a petrosal.

The olfactory bulbs chamber houses the exposed part of the main olfactory bulbs, but there are two main limitations. The first is that the olfactory bulbs also are partially internal to the main brain cavity, and that there are not only neural tissue in the olfactory bulbs chamber. The second limitation, as for the whole endocast, is however less subject to variation: there are not many vascular structures and the main cranial opening is the cribriform plate of the ethmoid, which has been segmented here as all other foramina (by taking a straight line between its edges in the sagittal plane). The main source of variation can be the posterior limit of this chamber, i.e., relative to the rest of the brain: I choose here to proceed as for foramina, taking a straight line between what I interpreted as the circular fissure. This does not mime the reality, because the circular fissure is not a plane, but since the real internal limit cannot be known with precision with endocasts only, I consider this approach as minimizing (and standardizing) the bias between an endocast and a brain.

The subarcuate fossa is largely thought to house the paraflocculi, but there are several counter-examples showing that the whole paraflocculi is not contained in that fossa (e.g., primates, see Gannon et al. 1988, or cetaceans, see O'Leary 2010). It has been however demonstrated that, in bats, the whole parafloccullus fills the subarcuate fossa and that there are no other structures (Schneider 1957). The only bias possible is thus a measurement bias. As also discussed in the Nomenclature section, there can be other bony apertures to that linking the parafloccullus to the rest of the cerebellum. For the latter, I decided to do as for other foramina, and to take a straight line between the edges of that aperture, but in the frontal plane. For the other apertures, I also took a straight line, not between the edges of the bone (where would likely lie cartilage) but a little bit "before", in the subarcuate fossa, in order to mime as good as possible the limits of the neural structure.

Part One

Endocranial cast anatomy of the extinct hipposiderid bats *Palaeophyllophora* and *Hipposideros* (*Pseudorhinolophus*) (Mammalia: Chiroptera)

Journal of Mammalian Evolution
https://doi.org/10.1007/s10914-020-09522-9

ORIGINAL PAPER

Endocranial Cast Anatomy of the Extinct Hipposiderid Bats *Palaeophyllophora* and *Hipposideros* (*Pseudorhinolophus*) (Mammalia: Chiroptera)

Jacob Maugoust[1] · Maeva J. Orliac[1]

Accepted: 4 October 2020

Abstract

Bat fossil endocasts have been little studied in the literature (nine published works, only one in the XXIth century), and macromorphology of the brain of extant bats has only been characterized at the family-level. We describe here in detail the endocranial casts of four fossil hipposiderid species based on μCT-scans data and propose a revised nomenclature of the hipposiderid brain structures that leave their imprint on endocranial casts. Exhaustive comparisons of the external morphology of our fossil cranial endocast sample allow us to discuss the distribution of both qualitative and quantitative features in this family for different epochs. A conservatism of the brain is considered to be the rule during bats evolution. Indeed, we found that encephalization did not increase since the Eocene in hipposiderid bats (contrary to other mammals) and that macromorphology of the brain is close between Paleogene, Miocene, and extant hipposiderid species. However, subtler but promising fine anatomical characters might allow distinguishing genera and species. Eventually, expanding the fossil sample and/or adding extant species could shake the paradigm of temporal homogeneity and bring new light on the morpho-anatomical evolutionary history of Hipposideridae.

Keywords Endocast · Hipposideridae · Paleogene · Brain · μCT-scan

Introduction

In the middle of the last century, Tilly Edinger stated that paleoneurology could be regarded as the "little-known child of paleontology and neurobiology" (Edinger 1949:1). Indeed, study of internal structures of fossils, a fortiori endocranial cast, was then limited by the destructive nature of internal investigation of fossil skulls. Generalization of non-invasive techniques (especially μCT-scanning) now allows for enhanced access to endocranial structures and has led to an increased knowledge of mammal fossil endocasts. These techniques increasingly allow for discussing the evolutionary history of the brain, which may reflect both phylogenetic history and ecological constraints, through the external morphology of cranial cavity casts. Among mammals, bats are a remarkable group by their crucial contribution to extant mammal diversity (second most diverse order, e.g., Teeling 2009) and by their unique ecological specializations towards sustained flight combined with the ability to echolocate (e.g., Teeling et al. 2000). The specificity of their ecology is reflected by their brain anatomy, which has been documented for several extant species (e.g., Larsell and Dow 1935; Eisenberg and Wilson 1978; Jolicoeur et al. 1984; Baron et al. 1996; Safi et al. 2005; Bhatnagar et al. 2016). However, surprisingly, the evolutionary history of the brain characteristics of Chiroptera has barely been discussed. Our knowledge of the brain morphology of extinct bats so far relies on a small number of short descriptions performed in the second half of the XXth century on natural endocranial casts belonging to the families Hipposideridae, Emballonuridae, and Vespertilionidae (Edinger 1926, 1929, 1961, 1964a, b; Dechaseaux 1956, 1962, 1970, 1973). These works briefly compare the fossil endocasts with one another and with some extant representatives of the order. They show that, just like extant representatives, fossil bats had a low complexity of the telencephalon with a moderately expanded

Supplementary Information The online version of this article (https://doi.org/10.1007/s10914-020-09522-9) contains supplementary material, which is available to authorized users.

✉ Jacob Maugoust
jacob.maugoust@umontpellier.fr

[1] Institut des Sciences de l'Evolution de Montpellier, UMR 5554 Université de Montpellier, CNRS, IRD, EPHE, place Eugène Bataillon, 34095 Montpellier cedex 5, France

Published online: 08 January 2021

neopallium bearing no or few sulci and an exposed mesencephalon. These traits are described as "primitive" features that would have been maintained through time (Edinger 1964a, b). More recently, Yao et al. (2012) included fossil data in their study on the evolution of the relative brain size in Hipposideridae, but provided no morphological description. To date, there is no formal description of a fossil bat endocast, no formal thorough/extensive comparison between extant and fossil species, and no integrative (i.e., qualitative and quantitative) discussion of the evolutionary history of the bat brain.

Regarding Chiroptera diversity, according to Amador et al. (2018), there are today 21 families and more than 1200 recognized species split into two suborders (ESM1: Fig. SI. 1), Yangochiroptera (with three superfamilies of echolocating "microbats": Emballonuroidea, Noctilionoidea, and Vespertilionoidea), and Yinpterochiroptera (gathering the echolocating "microbat" superfamily Rhinolophoidea and the non-echolocating "megabat" family Pteropodidae). The phylogenetic relationships supporting this rather recent systematic framework of Chiroptera raise questions about the evolutionary history of the whole group, especially regarding the acquisition of flight and of sophisticated echolocation of the paraphyletic "microbats" (e.g., Teeling et al. 2002). The fossil record of the order remains however fragmentary (Eiting and Gunnell 2009); Brown et al. (2019) identified 167 fossil genera and 441 fossil species, adding eight additional extinct families to the extant ones. They also highlighted the pretty low osteological preservation for bats, related to their very light skeleton adapted to flight. Regarding the brittleness of their cranium, a three-dimensional preservation of the braincase is therefore quite exceptional in the fossil record. Yet, a few fossil bats crania and natural endocasts provide an opportunity to investigate in detail the endocranial structures of chiropterans using µCT scanner imaging techniques. Cave deposits are most favorable for the preservation of bat skeletons (Brown et al. 2019); Quercy Phosphorites (SW France) are karstic infillings that yielded a tremendous amount of fossil bat material (17.6% of the world fossil bat record according to Brown et al. 2019), with a high taxonomic diversity (six families including three extinct, 11 genera and 46 species according to Brown et al. 2019), and ranging from the middle Eocene to the early Miocene (Maitre 2014). The few endocasts described by Dechaseaux (1956, 1962, 1970, 1973) and Edinger (1926, 1929, 1961, 1964a, b) mainly come from this geological formation where numerous natural endocasts and skulls have been collected (e.g., Maitre 2014).

Among extant bat families, Hipposideridae occupy the second rank in terms of specific diversity in the whole fossil record of the order (Brown et al. 2019) and the richest in the Quercy Phosphorites fossil record (Maitre 2014). These bats are commonly known as the "Old World leaf-nosed bats" and belong to the superfamily Rhinolophoidea. They appear in the fossil record in the middle Eocene of Europe (Maitre 2014; Brown et al. 2019)

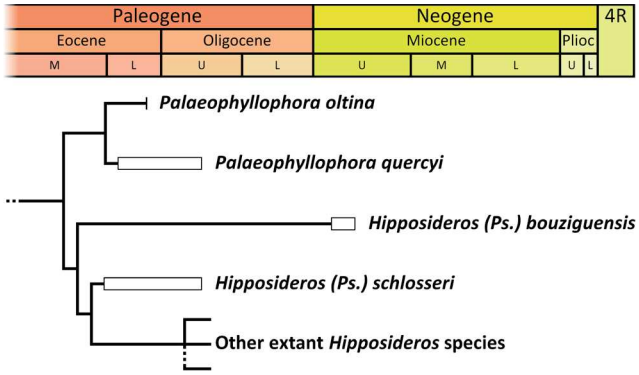

Fig. 1 Phylogenetic relationships and temporal occurrences over the last 45 Ma of the four fossil species studied here. Ages of *Pa. quercyi*, *Pa. oltina*, and *H. (Ps.) schlosseri* after Maitre (2014). Age of *H. (Ps.) bouziguensis* after Sigé (1968). Age of "extant *Hipposideros* species" node after Foley et al. (2015, 2017)

and nowadays include ten living genera and around 80 species, 70 of which are comprised in the widespread genus *Hipposideros* (Simmons 2005; Foley et al. 2017). This family is the sixth most diverse bat family (Shi and Rabosky 2015; Amador et al. 2018), just after the Rhinolophidae. They represent together the major part of the rhinolophoid superfamily (81 hipposiderid and 83 rhinolophid species of the 183 rhinolophoid species according to Amador et al. (2018)). The brain of modern Hipposideridae has been briefly described in the literature (Baron et al. 1996) and endocasts of extinct Hipposideridae are so far known through very succinct descriptions only (Edinger 1926; Dechaseaux 1956, 1962). However, cranial remains of fossil Hipposideridae are often well preserved (and particularly braincases; Brown et al. 2019). This makes this family a good candidate to investigate their brain evolution through endocasts and to set the basis for future studies on bat endocranial casts.

We propose here the first nomenclature of the external morphological features of the bat's brain, and we describe and compare in detail endocranial casts of extinct hipposiderid bats based on four species (Fig. 1): *Palaeophyllophora oltina*, *Palaeophyllophora quercyi*, *Hipposideros* (*Pseudorhinolophus*) *bouzigensis*, and *Hipposideros* (*Pseudorhinolophus*) *schlosseri*. We discuss general and detailed brain macromorphology of hipposiderid bats, together with common measurements of endocasts (EQ, olfactory bulb volume, paraflocculi volume). We finally propose the first hypotheses on the evolutionary history of the hipposiderid brain.

Material and Methods

Taxa and Specimens

We investigate and describe the external features of the brain through the reconstruction of the cranial endocasts of four fossil species belonging to two genera of the family

Hipposideridae. Each species is represented by a single specimen housed in the University of Montpellier (UM, France) or in the Naturhistoriches Museum Basel (NMBS, Switzerland):

- *Palaeophyllophora oltina* is documented by a partial cranium with braincase almost complete (NMBS QP784), which comes from the locality of Sainte-Néboule (Quercy, Lot, SW France) of Mammalian Paleogene standard level 18 ("MP18"; i.e., biostratigraphic assemblage zones in the stratigraphic record of the Paleogene period of Europe; Schmidt-Kittler 1987) age (upper Eocene; Maitre 2014);
- *Palaeophyllophora quercyi* is documented by a partial cranium with braincase almost complete (UM ACQ 6627), which comes from ancient Quercy collections of indeterminate age and precise provenance (except Quercy area, SW France);
- *Hipposideros (Pseudorhinolophus) schlosseri* is documented by a natural cranial cast (NMBS QV370) from ancient Quercy collections, also with indeterminate age and precise provenance;
- *Hipposideros (Pseudorhinolophus) bouziguensis* is documented by a natural cranial cast (NMBS G2369) from the locality of Bouzigues (S France) of Mammalian Neogene unit 2a ("MN2a"; Mein 1975) age (lower Miocene; Sigé 1968).

We compared these four fossil species to the extant *Hipposideros diadema*, whose figures (Baron et al. 1996: figs. 8, 24 and 40) are, to our knowledge, the only illustrations in the literature (for bats) with a sufficient quality to investigate brain external morphology. Specimens of *H. (Ps.) schlosseri* and *H. (Ps.) bouziguensis* have been figured in Yao et al. (2012) but not described. We quickly mention them in the description of the corresponding taxa.

Taxonomic Framework

A huge work of systematic paleontology has been done by Maitre (2014) who greatly clarified taxonomy of extinct bat species from Quercy deposits; we follow her work for the attribution of our three Quercy specimens (that are *Pa. oltina*, *Pa. quercyi* and *H. (Ps.) schlosseri*), which were already attributed to valid species names. Regarding *H. (Ps.) bouziguensis*, no work has been done since the works of Sigé (1968), Legendre (1982), and Sigé et al. (1997); we thus trust the former attribution of our Bouzigues specimen.

Within Hipposideridae, relationships of extant species are getting resolved (Foley et al. 2015, 2017), but phylogenetic relationships of extinct species are poorly studied and diverge depending on the analyses (see Hand and Kirsch 2003; Ravel et al. 2016; Wilson et al. 2016). We rather follow the results of Ravel et al. (2016) because they aim to decipher relationships between extinct species rather than placing them within a constrained extant species framework; besides, their matrix included both craniodental and postcranial characters. A pruned topology of Ravel et al. (2016) including the species of our sample is presented in Fig. 1.

Data Acquisition

Three dimensional data acquisitions of the four specimens were performed using the μCT facilities in the University of Montpellier (MRI; ISEM): *Pa. quercyi* was scanned using a Skyscan 1076 μCT and the three other species were scanned using a EasyTom 150 μCT. The voxel resolution is 18.08 μm for *Pa. quercyi*, 23.82 μm for *Pa. oltina*, 35.72 μm for *H. (Ps.) schlosseri* and 23.81 μm for *H. (Ps.) bouziguensis*. Other details regarding the acquisition parameters are summarized in ESM2: Table SI. 1. Segmentation and volumetric measurements of each specimen were performed using Avizo ® 9.3 (Thermo Fisher Scientific-FEI) and visualization was done using MorphoDig © (Lebrun 2018). Figures illustrating the cranial endocasts were done using Inkscape © (Inkscape Project 2018, v0.92.3) and other figures were done using Photofiltre © (Da Cruz 2015, v7.2.1). Linear measures were taken on the outline of each structure using both Inkscape and Photofiltre. Sagittal angles were taken using MorphoDig and ImageJ (Schneider et al. 2012, v1.48).

Encephalization

Encephalization quotient of a species (EQ; Jerison 1973) is the ratio between the observed mass of the brain of this species (E) over the expected mass of the brain of this species (E_e) given its body mass (M). The value of the ratio gives then an idea of the "encephalization" of the species: if the ratio is over one, the brain is "larger" than expected, and vice versa. The tricky point concerns the calculation of the expected mass of the brain. The original formula of Jerison (1973) is $EQ_{Jerison} = \frac{E}{0.12 \times M^{\frac{2}{3}}}$. However, Eisenberg and Wilson (1978) noted that Jerison (1973) defined this formula based on a mammalian-scale sample underrepresenting bats. They proposed another formula, including more mammals and especially more bat species: $EQ_{Eisenberg} = \frac{E}{0.055 \times M^{0.74}}$. We calculated EQ for our four fossil bat species using these two formulas, but mainly discussed EQ based on the equation of Eisenberg and Wilson (1978).

In order to compare EQ values of various mammal species through time, we gathered body and brain masses of several fossil and extant mammal species from the literature (Silcox et al. 2010; Shultz and Dunbar 2010; Orliac and Gilissen 2012; Ramdarshan and Orliac 2016; Bertrand et al. 2018a, b). Bats are absent from these datasets, so we added the extant bat data from Baron et al. (1996) and Bhatnagar et al. (2016)

(ESM2: Table SI. 2). For *H. (Ps.) schlosseri*, we used the brain mass value provided by Yao et al. (2012) because of the partial preservation of the specimen described here. Moreover, the temporal extension of the latter species covers both the Eocene and Oligocene epochs; as we do not know its precise age, we duplicated this value with an Eocene and an Oligocene age for each duplicate.

Maitre (2014) provided body mass estimates for each chiropteran species from Quercy, in each MP, based on the area of the first lower molar. We used the body mass estimate value of Maitre (2014) for *Pa. oltina* as this species is found only in the MP18 site of Ste-Néboule, from which the endocast described here derives. We considered the mean value of the different body masses through time for *Pa. quercyi* and for *H. (Ps.) schlosseri* because the precise provenance – and therefore precise age – of these specimens is unknown. We calculated the body mass of *H. (Ps.) bouziguensis* by taking the mean values of length and width of the first lower molars provided by Sigé (1968) and using the equation of Maitre (2014).

Statistical treatment of the EQ data was done using R (R Core Team 2018, v3.5.0) and its interface RStudio (RStudio Team 2016, v1.1.453) using package FSA (Ogle et al. 2019) in addition to built-in packages. EQ values for mammals are visually compared through Cenozoic epochs by plotting boxplots. We use a Shapiro-Wilk test (Shapiro and Wilk 1965; Royston 1995; shapiro.test function) of normality to know (at a 5% risk) if the various samples used are normally distributed. To know (at a 5% risk) if there is an homogeneity or not in the EQ values of a group through Cenozoic epochs, we use either a Kruskal-Wallis test (Kruskal and Wallis 1952; Hollander and Wolfe 1973; kruskal.test), also known as a "non-parametric ANOVA," if the sample was not normally distributed, or both a Kruskal-Wallis test and a Fisher test (Fisher 1970; Chambers and Hastie 1991; anova and lm functions) if the sample was normally distributed; in most cases, samples were not normally distributed so we kept Kruskal-Wallis even if it was the case. When there was a difference (i.e., a significant p-value), we used either non parametric Dunn's pairwise tests (Dunn 1964; dunnTest function of FSA package) or both parametric Tukey HSD (Tukey 1949; TukeyHSD function) tests and non-parametric Dunn's pairwise tests to know (at a 5% risk) which pair(s) were different.

As an additional graphical representation of the EQ formulas, we plotted the log brain masses against the log body masses (using natural logarithms) and we added to the plot the regression lines derived from the EQ formulas of Eisenberg and Wilson (1978) and Jerison (1973). Indeed, the expected brain mass for a given body mass is a $a.X^b$ relationship; the expected log brain mass for a given log body mass is thus $b.\log(X) + \log(a)$. Eisenberg and Wilson (1978) proposed an expected brain mass formula which is 0.055 x $M^{0.74}$; the expected log brain mass is thus 0.74 x log(M) + log(0.055); the regression line used here is therefore y = 0.74 x log(x) + log(0.055). In a similar way, regarding the expected brain mass formula of Jerison (1973), the regression line is y = 2/3 x log(x) + log(0.12).

The use of EQ values to compare encephalization between extinct taxa has received some criticism, notably regarding the uncertainty related to body mass estimates (e.g., Smith 2002; Alba 2010; Millien and Bovy 2010; Gingerich 2016; Ramdarshan and Orliac 2016). Moreover, brain masses are estimated based on partially preserved material for two of our four fossil species. We therefore remain cautious concerning the use of EQ values to qualify/quantify brain evolution through time.

Other Endocast Measurements

A common measurement on endocasts is the telencephalic flexure, or "cranial base angle" (Ramdarshan and Orliac 2016). However, the term "telencephalic" flexure is used to describe a bending of the telencephalon (and only it) that occurs during ontogeny. This angle between the ventral planes of the telencephalon and rhombencephalon in general rather corresponds to the definition of the cephalic flexure (Nieuwenhuys 1998). Another flexure that can be measured on endocasts is the cervical flexure (Nieuwenhuys 1998), a bending between the rhombencephalon and the spinal cord. This flexure can be measured by adding 90° (considering the major axis of the foramen magnum perpendicular to the orientation of its opening) to the angle between the ventral plane of rhombencephalon and the major axis of the foramen magnum (a line whose extremities are the most dorsal and the most ventral points of the foramen magnum in lateral view).

We also calculated volumes of "individualizable parts" of the brain, which are that of the olfactory bulbs (e.g., Jerison 1973; Orliac and Gilissen 2012; Benoit et al. 2013; Ramdarshan and Orliac 2016) and of the paraflocculi (e.g., Bertrand et al. 2018a, b, 2019). The volumes of these structures are inferred from the volumes of their containing cavities. The real volume of the olfactory bulbs and paraflocculi may differ from our measurement (e.g., if bulbs are partly covered by the cerebrum or if the subarcuate fossa encloses additional structures to the paraflocculi). One should therefore remain cautious regarding interpretations on these measures. Regarding olfactory bulbs volume, we used the datasets of Baron et al. (1996) and of Bhatnagar et al. (2016), which include more than 270 extant species, and we added values for our fossil species (ESM2: Table SI. 3). Regarding parafloccular volume, no substantial dataset is available for bats in the literature; we therefore compared our fossil sample to the small sample of mammals – including some bat species – provided by Ferreira-Cardoso et al. (2017) to which we

added the values of some extant and extinct rodents from Bertrand et al. (2018a, b) (ESM2: Table SI. 4).

As these measurements likely are affected by allometry, we plotted log-volumes (to avoid allometric bias) of each against that of the whole brain (using natural logarithms). Our goal is not to characterize evolution of olfactory bulb relative volume or paraflocculus relative volume through bat lineages (for the former) or mammalian lineages (for the latter), but simply to visualize where fossil bats lie compared to extant ones. Thus, we do not apply any PCM (Phylogenetic Comparative Method), such as PIC (Phylogenetic Independent Contrasts; Felsenstein 1985) or PGLS (Phylogenetic General Least Squares; Grafen 1989) regressions.

Data Availability

Fossil material is housed in the UM (University of Montpellier, Montpellier, France) and NMBS (Naturhistorisches Museum Basel, Basel, Switzerland). μCT-data and 3D surfaces are available upon reasonable request. Datasets (μCT-data acquisition parameters, brain and body volumes, EQ's, olfactory bulb volumes, paraflocculi volumes and test results) are provided in ESM2 (Tables SI. 1–5). The R code written and used for analyses in this paper is available in ESM3; see ESM4, 5, 6 for the raw datasets used in the code.

Nomenclature and Homologies of the Chiropteran Brain Structures

To date, no detailed study of chiropteran endocasts has been performed. Therefore, prior to describing the endocranial casts of extinct bat species from Quercy deposits, we need to properly identify and name the different observed structures. Various terms have been used across descriptions of endocast in other mammalian order, and, most of the time, discrepancies exist between paleoneurological and/or neurobiological studies. Consequently, we assess primary homologies of the chiropteran endocast structures and we choose and list the anatomical terms to use in future bat cranial cast descriptions. Unless otherwise discussed, we use anglicized terms derived from the terminology of the 6th edition of the Nomina Anatomica Veterinaria (NAV 2017).

Major Components of the Chiropteran Brain Observed on Endocasts (Fig. 2)

The vertebrate brain is composed of: i) the prosencephalon, anteriorly (the "forebrain"), which is divided in a **telencephalon** and a **diencephalon**, ii) the **mesencephalon,** medially (the "midbrain"), and iii) the rhombencephalon, posteriorly (the "hindbrain"), which is divided in a **metencephalon** and a **myelencephalon** (e.g., Barone and Bortolami 2004).

The telencephalon represents a major part of the brain (Fig. 2) and is composed of the **paleopallium** ventrally (with the **olfactory bulbs** at the anterior extremity and the **piriform lobes** posteriorly) and of the **neopallium** dorsally (a specific feature of mammals; Rowe et al. 2011). The paleopallium and the neopallium are separated by the **rhinal fissure** (Smith 1902a; Dechaseaux 1962; see below). The olfactory bulbs protrude anteriorly and are separated from the cerebral hemispheres (or "cerebrum," which contains the other telencephalic structures) by the **circular fissure**.

Regarding the diencephalon, the only parts visible on endocasts (Fig. 2) are the **epiphysis** dorsally and the **hypophysis** ventrally, also called the pineal gland and pituitary gland, respectively, in the NAV. We use the terms epi−/hypophysis because of their common root, which reflects their common general origin.

As for the mesencephalon, only the tectum mesencephali (or "**tectum**") is exposed (Fig. 2a) and the main recognizable structures are the corpora quadrigemina, or colliculi. These colliculi are disposed in two pairs which are the **rostral** (also called "superior" or "anterior") and **caudal** (also called "inferior" or "posterior") **colliculi** (according to the NAV).

The metencephalon is, dorsally, only represented by the **cerebellum** (Fig. 2a). Following the NAV, the cerebellum is medio-laterally composed of a **vermis** (or median vermis) in a median position, two **cerebellar hemispheres** lateral to the vermis, and two **paraflocculi** varying in position relative to the hemispheres (from ventral to lateral). In bats, the flocculi are small compared to the paraflocculi, and overshadowed during cerebellar ontogeny (Larsell and Dow 1935); it is unlikely that they can be observed on bat endocasts. The exposed part of the vermis is antero-posteriorly subdivided in a maximum of five lobules: the **declive** (lobule VI), the **folium vermis** (lobule VII A), the **tuber vermis** (lobule VII B), the **pyramis** (lobule VIII), and the **uvula** (lobule IX) (Dow 1942; Horikawa and Suga 1986; NAV 2017). The lobule X, or nodula, of the vermis is here not considered as a potential exposed part of the vermis because, in all bats, the cerebellum is bent and the nodula is fully internal. The cerebellar hemispheres ontogenetically develop from the tuber vermis and the folium vermis (Larsell and Dow 1935), forming two (**anterior** and **posterior**) **crura**. The declive, anterior to the two latter lobules, is also exposed. Larsell and Dow (1935) did not recognize a contribution from the declive to the cerebellar hemispheres in the species they studied (*Corynorhinus* sp.). However, in the case of an anterior expansion of the cerebellum, i.e., with an elongated vermis and elongated hemispheres, the declive could expand laterally and contribute to the hemispheres together with the tuber and folium vermis (Dow 1942). This anteriormost lobe of the cerebellar hemisphere is here named the **crus 0**. In ventral view (Fig. 2b),

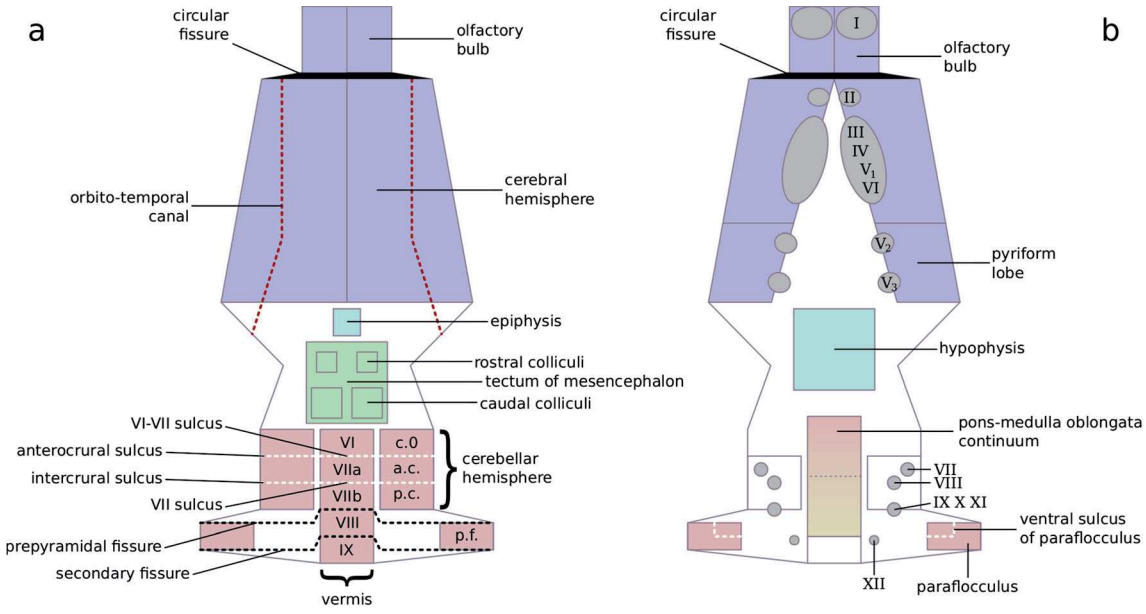

Fig. 2 Illustration of the nomenclature of a theoretical chiropteran endocast in dorsal (**a**) and ventral (**b**) views. The main subdivisions of the brain are in blue (telencephalon), light blue (diencephalon), green (mesencephalon), red (metencephalon) and yellow (myelencephalon). The color gradient from red to yellow of the pons-medulla oblongata continuum and the dashed mid-line indicate that both structures cannot be macromorphologically distinguished. Roman numbers indicate the corresponding cranial nerve exits. Abbreviations are: **c.0**-crus 0 of the cerebellar hemisphere; **a.c**.-anterior crus of the cerebellar hemisphere; **p.c**.-posterior crus of the cerebellar hemisphere; **p.f**.-paraflocculus

another part of the metencephalon is visible: the **pons**, located between the cochleae, posterior to the hypophysis.

Immediately posterior to the pons, the myelencephalon is visible as the **medulla oblongata** (Fig. 2b). A potential difficulty when studying endocasts is to separate these two contiguous structures. In Chiroptera, as illustrated by Baron et al. (1996) through sagittal sections, depending on taxa, there is no or very subtle separation on the brain (when a separation is present, it is a slight groove). Moreover, their relative position varies among bats: they can be both exposed ventrally (as for *Pteropus lylei* or *Dobsonia praedatrix*, Baron et al. 1996: figs. 51–52), or the pons can be positioned dorsal to the hypophysis and therefore not exposed ventrally (as for *Rhinolophus hipposideros* or *Mormoops megalophylla*, Baron et al. 1996: figs. 53–54). For these two reasons, on endocasts the region between the (cast of the) hypophysis and the foramen magnum will be called a "**pons-medulla oblongata continuum.**"

General Remarks on the Exposed "Foldings" of the Brain

The telencephalon and the metencephalon are more or less folded in mammals, depending on the orders. Depending on the authors, these foldings are either called "fissures" or "sulci." Here, we rather follow Smith (1902a) than the NAV in calling a "fissure" any groove that obviously separates a structure from another (such as the "rhinal fissure" of the telencephalon, separating the paleopallium and the neopallium, or the secondary fissure (fissura secunda) of the metencephalon, separating lobules VIII and IX throughout the cerebellum) and a "sulcus" any groove on the surface of a structure (such as, in an endocast description, any groove visible at the surface of the neopallium). For instance, the NAV refers to the rhinal fissure as the sulcus rhinalis and to the pseudosylvia and suprasylvia as the fissura pseudosylvia and the sulcus suprasylvius respectively; yet, the pseudosylvia and the suprasylvia are both foldings on the neopallium, while the rhinal fissure separates different entities of the telencephalon, the paleopallium and the neopallium. Here, we therefore use the terms pseudosylvian sulcus, suprasylvian sulcus, and rhinal fissure.

Neopallial Foldings and Lobes (Fig. 3)

We follow Smith (1902a) for the definition of the main sulcus on the neopallium (Fig. 3a): from the rhinal fissure originates the pseudosylvia (or pseudosylvian sulcus, 'Ps.s' in Fig. 3a), directed dorsally. The primary organization of mammalian brain foldings is a concentric organization of sulci around the pseudosylvia due to a flexion of the telencephalon (the telencephalic flexure per se), with the ectosylvian ('E.s' in Fig. 3a), the suprasylvian ('S.s' in Fig. 3a), and the lateral sulci ('L' in Fig. 3a; Smith 1902a: fig. 2; Dechaseaux 1962). The lateral sulcus is posteriorly followed by the postlateral sulcus ('Po.L' in Fig. 3a) and preceded anteriorly by the coronal sulcus ('Co' in Fig. 3a); the coronal and the lateral can merge to form a coronolateral sulcus (Dechaseaux 1962). The

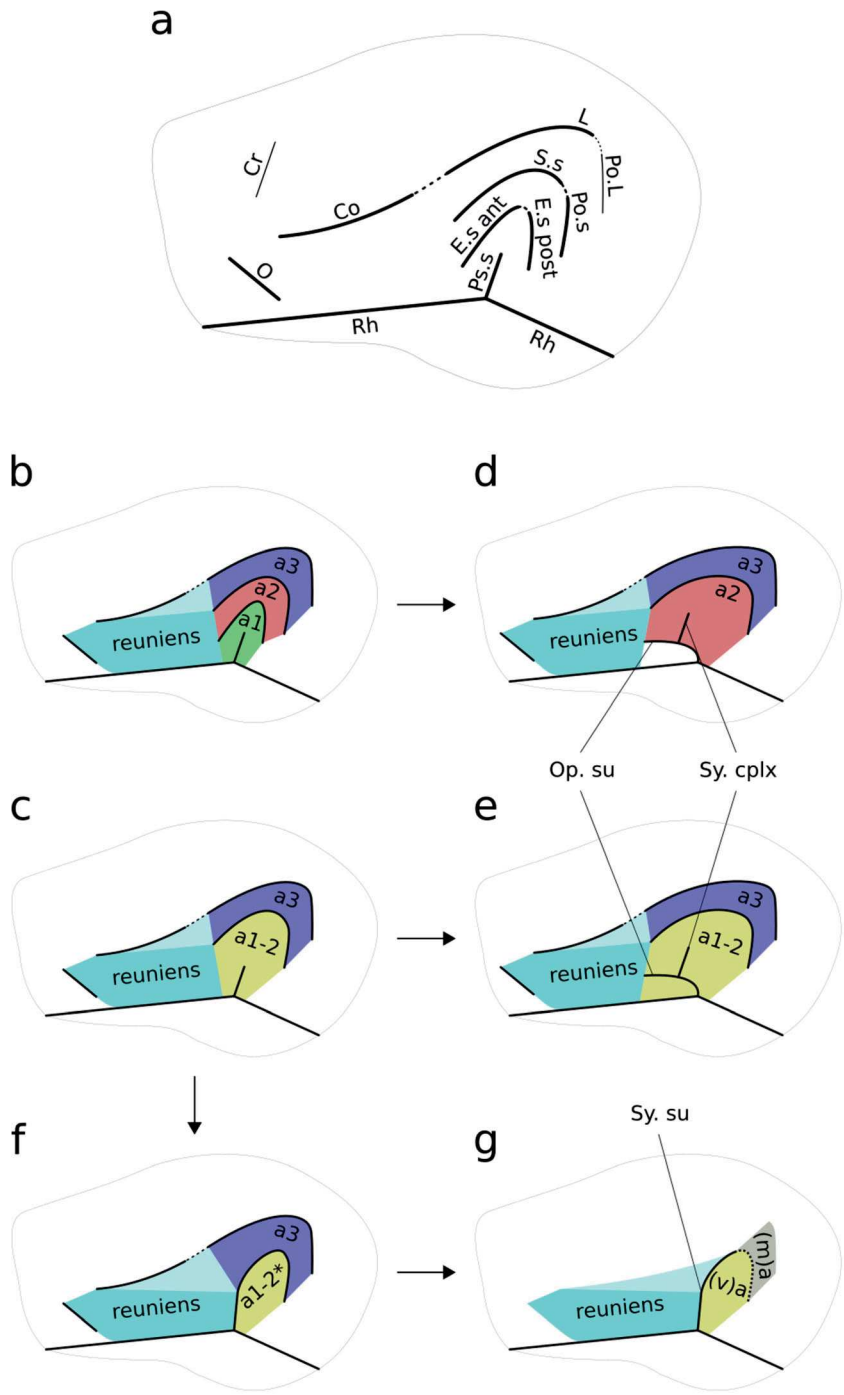

Fig. 3 Illustration of the nomenclature of primary sulci (**a**) and areas (**b-c**) of a theoretical brain and of primary changes of brain morphology (**d-g**) mainly following the hypotheses of Dechaseaux (1962). Arrows from b to d and from c to e show the operculization of the arcuate gyrus 1 by the arcuate gyrus 2 (b to d) or of the arcuate gyrus 2 by itself (c to e). The arrow from c to f indicates the formation of the sylvia by merging the posterior end of the pseudosylvia and the anterior end of the suprasylvia. The arrow from f to g indicates the transition from a "sylvian sulcus" theoretical condition to a "hipposiderid bat" theoretical condition, with the absence of orbital, coronal and lateral sulci and by the disparate presence or absence of the posterior extension of the suprasylvia, which therefore separates (or not when absent) the arcuate lobe ("a") in the ventral and medial arcuate lobes ("(v) a" and "(m) a"). Sulci abbreviations: **Co**-coronal (sulcus), **Cr**-cruciate (sulcus), **E.s ant**-anterior part of ectosylvia(n sulcus), **E.s post**-posterior part of ectosylvia(n sulcus), **L**-lateral (sulcus), **O**-orbital (sulcus), **Op. su**-operculization sulcus, **Po.L**-postlateral (sulcus), **Po.s**-postsylvia(n sulcus), **Ps.s**-pseudosylvia(n sulcus), **Rh**-rhinal fissure, **S.s**-suprasylvia(n sulcus), **Sy. Cplx**-sylvian complex, **Sy. Su**-sylvia(n sulcus). Areas abbreviations: **a1**-arcuate gyrus 1, **a2**-arcuate gyrus 2, **a3**-arcuate gyrus 3, **a1–2**-arcuate gyrus 1–2, **a1–2***-posterior arm of arcuate gyrus 1–2, **(v)a** and **(d)a**-(ventral) and (dorsal) arcuate lobe respectively

suprasylvia is posteriorly followed by the postsylvia ('Po.s' in Fig. 3a); the suprasylvia and the postsylvia can also merge together, but in most cases, there is a marked angle between the two so they can be distinguished. Dechaseaux (1962) also recognized a presylvia, directed anterodorsally and anterior to the pseudosylvia, extended even more anteriorly than the coronal sulcus. Smith (1902a) called this structure the orbital sulcus ('O' in Fig. 3a); this term is also used by Baron et al. (1996) in their review of the bat brain, and we therefore use it here too. Smith (1902a) also recognized a cruciate sulcus ('Cr' in Fig. 3a), which is located rather anteriorly (at the level of the coronal and orbital ones), medial to the lateral sulcus and rather in a transverse orientation (as for the postlateral and the orbital ones).

The ectosylvia can be divided into an anterior part (between the suprasylvia and the pseudosylvia; 'E.s ant' in Fig. 3a) and a posterior part (between the pseudosylvia and the postsylvia; 'E.s post' in Fig. 3a), which could merge (Dechaseaux 1962: fig. 12) or not (Friant 1932: fig. 1). However, the ectosylvia is rather a carnivoran feature (Smith

1902a); it is sometimes also referred to in other groups such as ruminants (Anthony and Grzybowski 1934) or manatees (Friant 1954), but results from the operculization of the two first arcuate gyri (cf. below; see arrows Fig. 3b-d and Fig. 3c-e), rather than being a "true" ectosylvian sulcus (as defined in carnivorans by Smith 1902a). What is mentioned as an "ectosylvian sulcus" in non-carnivorans by Anthony and Grzybowski (1934) and Friant (1954) is the operculization sulcus ('Op.su' in Fig. 3d-e), a long sulcus bent anteriorwards resulting from the operculization. According to Smith (1902a), the only "true" sylvian sulcus is a fusion of the pseudosylvia and the suprasylvia, and is a "complex of two sulci" (see arrow Fig. 3c-f). Dechaseaux (1962) shared the same global sulcal scheme but rather defined a "sylvian complex," which results from an operculization that covers (and then hides) the pseudosylvia. These two structures are thus distinct and can be distinguished as follows: i) the "sylvian sulcus" ('Sy.su' in Fig. 3f-g) of Smith (1902a) is a single sulcus anteriorly connected to the rhinal fissure and bent posteriorwards, and ii) the "sylvian complex" ('Sy.cplx' in Fig. 3d-e) of Dechaseaux (1962), mainly bent dorsally, joins the rhinal fissure ventrally through the operculization sulcus.

In addition to those sulci, Dechaseaux (1962) names primary convolutions (Fig. 3b): i) the arcuate gyrus 1 between the rhinal fissure and the ectosylvia (around the pseudosylvia), ii) the arcuate gyrus 2 between the ectosylvia and the suprasylvia, iii) the arcuate gyrus 3 between the suprasylvia and the lateral sulcus, and iv) the reuniens gyrus between the orbital sulcus and the anterior portions of the arcuate gyri 1 and 2. When there is a "sylvian complex" (Fig. 3d-e), the arcuate gyrus 1 is operculized (i.e., covered by the arcuate gyrus 2) and not visible (Dechaseaux 1962). When there is no operculization or ectosylvia (Fig. 3c), the arcuate gyri 1 and 2 are not separated by the ectosylvia and form therefore one arcuate gyrus 1–2, and the reuniens gyrus is located between the orbital sulcus and the anterior arm of this arcuate gyrus 1–2. When there is a "sylvian sulcus" (Fig. 3f), there is no gap anymore between the pseudosylvia and the suprasylvia, and no more between the suprasylvia and the rhinal fissure, but there is still a gap between the postsylvia (or posterior part of suprasylvia) and the rhinal fissure; only remains the posterior portion of the arcuate gyrus 1–2. The reuniens gyrus is therefore located between the orbital sulcus and the "sylvian sulcus." The chiropteran brain is considered to lack gyri strictu senso (their brain is lissencephalic; Baron et al. 1996) and the term "lobe" is preferred to name surfaces between sulci. Moreover, among the sulci defining the different lobes, the single recognizable one in our fossil sample is the sylvian sulcus, or sylvia (Fig. 3g). We therefore use the term of reuniens lobe for the surface anterior to the sylvia, the term arcuate lobe for the surface posterior to the sylvia if the suprasylvia is not extended posteriorly (if it is the case, no distinction could be made between the posterior arm of the arcuate gyrus 1–2 and the arcuate gyrus 3), or the terms ventral and medial arcuate lobes for the surfaces posterior to the sylvia and respectively ventral and medial to the posterior extension of the suprasylvia (the ventral arcuate lobe is close in its morphological definition to the posterior portion of the arcuate gyrus 1–2, as is the lateral arcuate lobe to the posterior portion of the arcuate gyrus 3).

Cerebellar Foldings (Fig. 2)

The five dorsally exposed cerebellar lobules of the metencephalon are separated by a minimum of four grooves, likely to be present on the exposed vermis (Fig. 2a). The first two have not been named and they separate lobules of the vermis restrictively, so they are here recognized as the VI-VII sulcus (separating lobules VI and VII) and the VII sulcus (separating lobules VII A and VII B). Barone and Bortolami (2004) named the VI-VII sulcus the fissura preansiformis as it separates lobules VI and VII, both in the vermis and in the cerebellar hemispheres. However, such a continuity is not obvious in bat brains (Horikawa and Suga 1986), and as the epithet of the fissure rather characterizes the cerebellar hemispheres, it will not be used here for a sulcus on the vermis surface. Barone and Bortolami (2004) also described a continuity between the vermis and the hemispheres and separated the folium vermis and the anterior crus from the tuber vermis and the posterior crus by the fissura intercruralis. The continuity between the vermis and the hemispheres has not been highlighted in bats (Larsell and Dow 1935) and in mammals in general (Dow 1942), so unless such a continuity is seen, the sulcus separating tuber and folium vermis of the vermis is called here the sulcus VII. Posteriorly is the prepyramidal fissure (fissura prepyramidalis in Barone and Bortolami 2004; Fig. 2a). This fissure is referred to as the sulcus prepyramidalis by Dow (1942), separating lobules VII and VIII, but it expands laterally (Horikawa and Suga 1986) and is in fact continuous with the fissura paraflocularis (Larsell and Dow 1935; Dow 1942); we therefore recognize this structure as a "fissure" (as do Barone and Bortolami 2004). The posterior-most groove is the secondary fissure (fissura secunda, the only cerebellar groove recognized by Baron et al. 1996): it separates the lobules VIII and IX but it also expands laterally (to where lie, anteriorly, the cerebellar hemispheres; Fig. 2a) (Horikawa and Suga 1986) and even inside the paraflocculi (Smith 1902b; NAV 2017), formed from parts of the lobules VIII and IX (Larsell and Dow 1935; Dow 1942). There can be additional sulci within each lobules when cerebellum complexifies (as seen in Baron et al. 1996: figs. 51–56).

The anterior and posterior crura of the cerebellar hemispheres are separated by the intercrural sulcus (Larsell and Dow 1935; Dow 1942), which is not continuous with the VII sulcus (Fig. 2a). If there is a crus 0 of these hemispheres,

an additional sulcus is expected, anterior to the intercrural sulcus, and is therefore named the anterocrural sulcus, because it separates the two crura (1–2) from the crus 0. It would be equivalent to the VI-VII sulcus, but not necessarily in its continuity, as for the intercrural sulcus and the VII sulcus.

Not much attention has been paid to the parafloccular morphology. Larsell and Dow (1935) recognized a lateral sulcus of the paraflocculus on its lateral aspect but it could simply correspond to the lateral expansion of the secondary fissure, which would be congruent with Smith (1902b). Nothing more is known about potential grooves on the surface of these structures. In hipposiderid bats described here, there is a ventral groove. Without any other reference, it will be called a ventral sulcus of the paraflocculus (Fig. 2b).

Casts of Braincase Openings

The mesencephalon, the pons (from metencephalon), and the medulla oblongata (from myelencephalon) together form a functional unit which is the brainstem (Barone and Bortolami 2004). From this structure, 12 "cranial nerves" exit. These nerves exit the braincase through foramina visible in ventral view for most of them (Fig. 2b). Other cranial foramina are pathways for other fundamental structures and also need to be identified. Skull foramina in Chiroptera have only been recognized for the genus *Pteropus* (Giannini et al. 2006). We rely on this work for most of the openings we describe in Hipposideridae. However, some of them deserve a bit more attention because they appear to vary among Chiroptera (at least, between pteropodids and hipposiderids). The first is the sphenorbital fissure, where at least exit the oculomotor (III), trochlear (IV), ophthalmic branch of trigeminal (V1), and abducens (VI) nerves, can be coalescent with the optic foramen and/or with the round foramen, therefore being also the exit of the optic (II) and maxillary branch of the trigeminal (V2) nerves. The second is the ethmoidal foramen, which in *Pteropus* is located in the frontal or between the frontal and the orbitosphenoid but which here, on endocasts, appears on the lateral aspect of the olfactory bulb cast.

The Orbitotemporal Canal

Finally, the orbitotemporal canal, which carries the anterior division of the superior ramus of the stapedial artery (Giannini et al. 2006; Orliac and O'Leary 2014) deserves special attention as it is largely thought to be a hallmark of the rhinal fissure position (e.g., Silcox et al. 2010; Bertrand and Silcox 2016; Ramdarshan and Orliac 2016). However, it is not always the case across mammals; for instance, the orbitotemporal canal can be in a more ventral position (Pantodonta, *Alcidedorbignya*, Muizon et al. 2015; Artiodactyla, *Homacodon*, Orliac and Gilissen 2012). In specimens described here, the orbitotemporal canal is visible (Fig. 2a): there is a marked longitudinal cast that runs parallel to the anterolateral side, it then reaches the posterolateral side of the telencephalon. In lateral view, it has in its first half a highly dorsal position, then it dives ventrally until it ends to a medial position, anterior and lateral to the petrosal bone. In the literature, the tissues surrounding the brain are removed during the preparation of fresh brains (see Baron et al. 1996); therefore, blood structures like the superior ramus of the stapedial artery are not reported on illustrations. Giannini et al. (2006) identified the orbitotemporal canal in *Pteropus*: it is a not-fully enclosed sulcus on the inner surface of the parietal and squamosal bones. We can identify the cast of this sulcus on endocasts, even if it is located in a more dorsal position than the rhinal fissure. However, these two structures join anteriorly. So, even if this canal is not a landmark of the rhinal fissure as a whole, its anterior extremity seems to be a good marker of the anterior location of the rhinal fissure.

Descriptions and Comparisons

Endocranial Cast of *Palaeophyllophora oltina*

Overall Shape

The cast of the braincase of *Pa. oltina* (Figs. 4 and 5, see also Fig. 6 and ESM1: Figs. SI. 2–6) was virtually reconstructed from a cranium of the Naturhistoriches Museum Basel collections (NMBS QP784). The endocranial cast largely fills the posterior

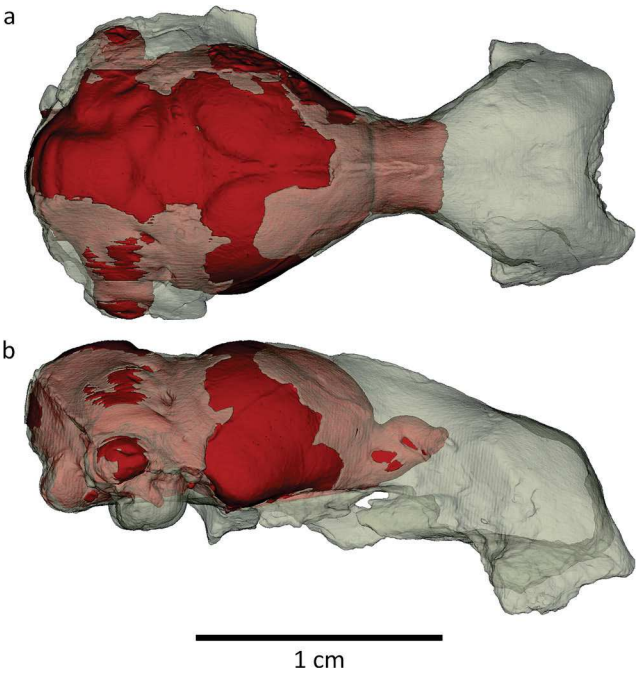

Fig. 4 Skull (transparent) and endocranial cast (red) of *Palaeophyllophora oltina* (NMBS QP784) in dorsal (**a**) and lateral right (**b**) views

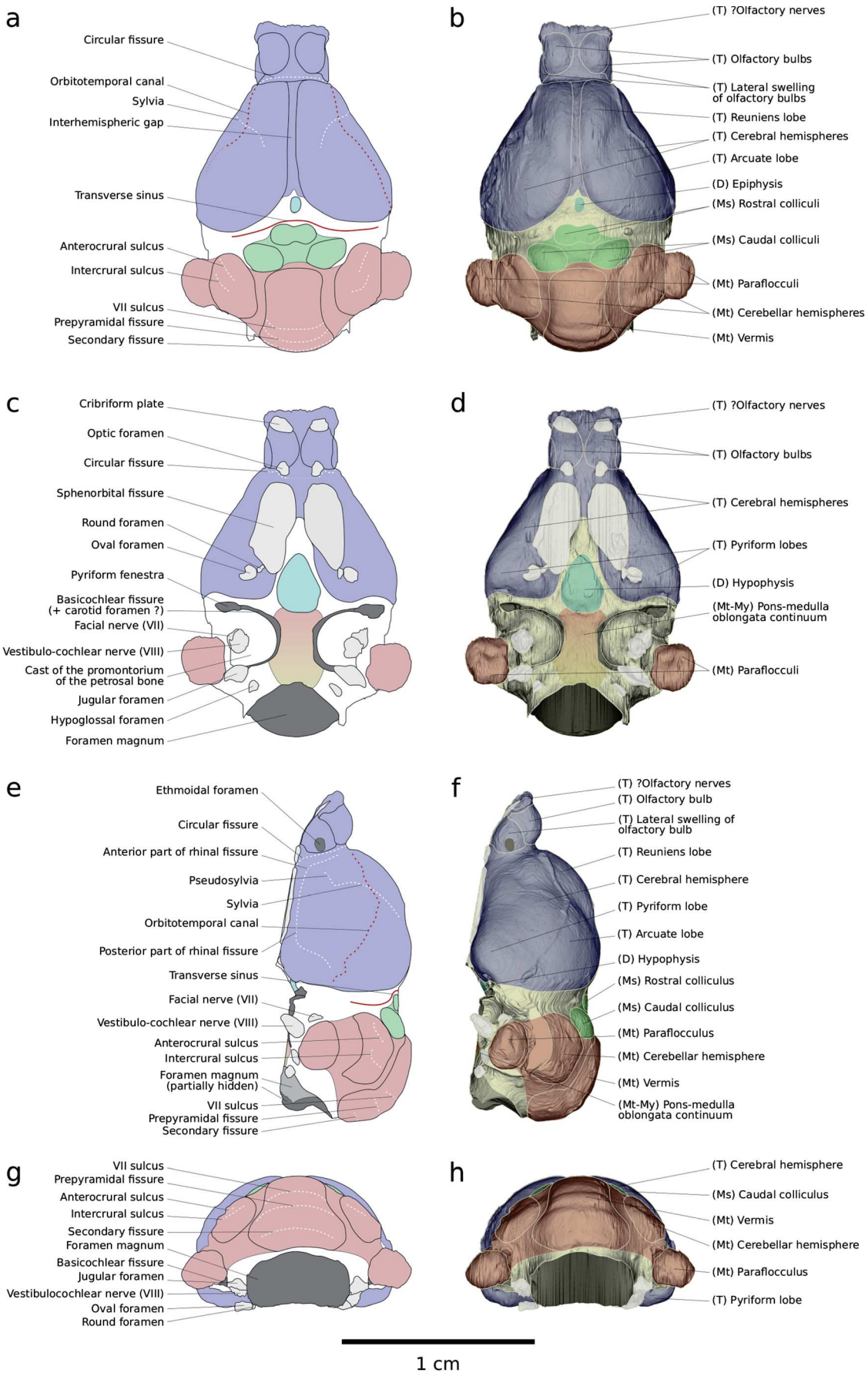

◀ **Fig. 5** Endocranial cast of *Palaeophyllophora oltina* (NMBS QP784) in dorsal (**a-b**), ventral (**c-d**), lateral right mirrored (**e-f**), and occipital (**g-h**) views. Right figures (b,d,f,h) illustrate the endocranial cast with the main subdvisions of the brain (blue/T-telencephalon, light blue/D-diencephalon, green/Ms-mesencephalon, yellow/Mt-metencephalon, red/My-myelencephalon). Left figures (a,c,e,g) illustrate the different casts (blood vessels, red) and grooves (sulci and fissures, white) of these areas, and the casts of cranial nerve exits (light white) and other cranial foramina (dark grey)

part of the cranium (Fig. 4); the cranial bones around the cranial cavity are very thin. The endocranial cavity extends anterior to the postorbital constriction, where lie the olfactory bulbs.

It has a total volume of 525.9 mm^3 (Tables 1 and 2). In dorsal view (Fig. 5a-b), its shape is hexagonal without the olfactory bulbs and the paraflocculi, and it is clearly longer than wide (Table 1). Only one sulcus is present on each side of the dorsal surface; this brain is thus regarded as lissencephalic. In ventral view (Fig. 5c-d), the two promontoria of the petrosal bones leave a huge depression on the endocranial cast: they occupy a large surface of the rhombencephalic surface (Table 1). In Chiroptera, the promontorium is very thin and the depression left by the promontorium on the endocast would approximate the imprint of the basal turn of the cochlear canal (see Fig. 5c-d). In *Pa. oltina*, the plane of the basal turn is slightly tilted dorsally relative to the median part of the rhombencephalon. In lateral view (Fig. 5e-f), the general shape of the endocast is rather elongated (especially relative to height, Table 1) with the different components almost aligned. There is only a very subtle angle between the ventral planes of telencephalon and metencephalon, with a cephalic flexure of 171° (Table 1). However, the foramen magnum is not aligned with the posterior part of the brain (it does not open strictly posteriorly), and is tilted ventrally with a cervical flexure of 150° (Table 1).

Telencephalon

In dorsal view (Fig. 5a-b), the olfactory bulbs are ovoid-shaped, antero-posteriorly elongated. They are distinct but still linked longitudinally on their whole length, and separated from the rest of the telencephalon by a short circular fissure of constant width. In lateral view (Fig. 5e-f), they show a lateral bulge distinct from the principal swelling, located posteroventrally. This postero-ventral bulge/swelling cannot be identified as the olfactory tubercle as its expected location would be more posterior to the olfactory bulbs. Overall, these olfactory structures represent 2.9% of the total volume of the endocast (Table 1). The circular fissure separates the olfactory bulbs from the cerebral hemispheres. It is a little bit tilted anteriorly (Fig. 5e-f and Table 1), and slightly visible in ventral view (Fig. 5c-d). These hemispheres have a pear shape in dorsal view (Fig. 5a-b), with a rounded anterior margin, and their maximal width is reached just before their posterior edge. They do not contact each other and are separated by a broad longitudinal fissure. Their posteromedial corners form obtuse angles. In lateral view (Fig. 5e-f), the posterior part is inflated, with a bigger height than the anterior part, and it occupies grossly the two-thirds of the surface. Such an inflation could correspond to a large hippocampus. The pyriform lobes are small and positioned posteriorly, at the same level as the highest point of the hemisphere (which reinforces the visual impression of a posterior inflation). If they are easy to locate, their dorsal margin is rather difficult to define.

In lateral view (Fig. 5e-f), the rhinal fissure is difficult to identify on its entire length. Its rostral part is rather clear: it starts anteriorly from a dorsal position, just posterior to the circular fissure, then it dives ventrally with a steep slope initially and then with a gentle slope. At its mid-length, it becomes difficult to spot: it passes dorsal to the pyriform lobe (see ESM1: Fig. SI. 5a) but, as they are difficult to delineate dorsally, it is impossible to determine if the rhinal fissure raises posteriorly or not. As the rhinal fissure is not clearly defined on its entire length, the neocortex/paleocortex limit cannot be accurately located, and the neocortical ratio cannot be calculated. The orbitotemporal canal is well visible in dorsal (Fig. 5a-b) and lateral (Fig. 5e-f) views. Its anterior extremity is as the same level as the anterior extremity of the rhinal fissure. It is located rather laterally (Fig. 5a-b) and opens just above the circular fissure (Fig. 5e-f). It has a marked angle in both views, with an anterior part a bit shorter than the posterior one: in dorsal view (Fig. 5a-b), both canals seem anteriorly parallel then posteriorly divergent (more than the borders of the telencephalon). There is a clearly visible sulcus on the neopalleal surface (Fig. 5a-b and e-f): it has a curved path, marked but not very deep. In dorsal view (Fig. 5a-b), the sulci converge posteriorly then start to be parallel. In lateral view (Fig. 5e-f), the curved shape of the path is parallel to the anterior border, and in fact it delineates the anterior border of the inflated posterior part of telencephalon. There is also, ventrally, a short and shallow ramus of this sulcus, with a diagonal orientation (toward the anteriormost and steep part of the rhinal fissure). The first short and shallow ramus is thought to be the pseudosylvia: it seems linked to the rhinal fissure and extends posterodorsally. The second larger sulcus is located more dorsomedially; it is a suprasylvia. Both sulci, linked continuously, form therefore a sylvia. The endocast lacks other sulci: there is no lateral sulcus (there are no sulcus medial to the sylvia) or coronal sulcus (no sulcus more anteriorly). However, the sylvia is marked enough to separate an anterior and a posterior part in the neopallium, which are identified as the reuniens lobe and the arcuate lobe, respectively. The reuniens lobe protrudes a bit, but is clearly shorter than the arcuate one (i.e., the sylvia has a very anterior position).

Diencephalon

Dorsally (Fig. 5a-b), the cast of the epiphysis is visible. It is close to the sagittal plane, located at the level of the posterior margin of the cerebral hemispheres, anterior to the transverse sinus. This cast is quite small in size.

Ventrally (Fig. 5c-d) is the cast of the hypophysis. It is clearly longer than wide (Table 1), with a subtriangular shape. It is located just anterior to the deep casts of the two promontoria, and its anterior margin is at the level of the posterior (narrowest) part of the sphenorbital fissure.

Mesencephalon

The tectum of the mesencephalon (Fig. 5a-b) is fully exposed, without overlap by the telencephalon and/or the metencephalon. The four corpora quadrigemina are exposed. The rostral colliculi, located posterior to the transverse sinus, are very low and hardly distinguishable. They are close to each other. The caudal colliculi are by far larger and prominent, located just posterior to the rostral ones. Contrary to the latter, they are widely separated. They are bulbous, ovoid in shape, and with their major axis almost medio-laterally oriented. In lateral view (Fig. 5e-f), the mesencephalon lies in a shallow valley between telencephalon and metencephalon.

Metencephalon

Dorsally (Fig. 5a-b), the metencephalon is the widest region of the braincase due to the lateral protrusion of the paraflocculi; even without these structures, the cerebellum is still nearly as wide as the cerebrum (Table 1). It is almost twice as wide as long (Table 1). The vermis (Fig. 5a-b and e-f) is almost twice longer than wide in this view, but it is nevertheless quite wide (Table 1). Its anterior part barely reaches the caudal colliculi and shows a small enlargement (Fig. 5a-b). Its posterior part bears three sulci (Fig. 5a-b and g-h), two deep and one shallower, and, contrary to the anterior end, it displays a sizable enlargement. It is difficult here to distinguish the lobules VI and VIIA: there only is a slightly flatter section; it is not a groove so it cannot be identified as a VI-VII sulcus, but these part seems to be distinguishable (even if it is not sure). Other parts, however, are more easy to separate: the most anterior groove is here identified as the VII sulcus, with anteriorly the folium vermis and posteriorly the tuber vermis, the median one should be the prepyramidal fissure with the pyramis posteriorly, and the posterior one should be the secondary fissure (even if it is the shallowest of the three), with the uvula posteriorly. Another possibility, relying on the depth of the grooves (Fig. 5e-h), could be to interpret the two deepest grooves (the anterior and median ones) as the prepyramidal and secondary fissures (as a fissure should be deeper than a sulcus) respectively, with therefore the uvula posteriorly and the tuber vermis anteriorly, and the posterior one as an "internal" sulcus of the uvula (which would be more logical as it is the shallowest of the three sulci). The slightly flatter part of the vermis located anterior to the pyramis could be the sulcus VI-VII, separating the lobules VI, VII, and VIII in parts of subequal length, or the sulcus VII. We consider that it is unlikely that a sulcus internal to a lobule is present when sulci separating lobules are absent; we therefore identify the three grooves on the vermis as the VII sulcus, the prepyramidal fissure, and the secondary fissure. The cerebellar hemispheres (Fig. 5a-b and e-f) are clearly separated from the vermis and are positioned more anteriorly relative to it (Table 1). Each of these hemispheres bears two sulci of close depth and length, one anteriorly located (the anterocrural sulcus) and one in a median position (the intercrural sulcus). The paraflocculi are best viewed in ventral view (Fig. 5c-d), where they have an irregular rounded shape (Table 1). They represent 2.3% of the total endocast volume (Table 1). They bear a groove delineating their anteromedial corner, the ventral sulcus of the paraflocculus, which is at its deepest in its central part (which is more or less the central point of the ventral face of the paraflocculi). In dorsal view (Fig. 5a-b), they are partially visible below the cerebellar hemisphere and they show a lateral, small but deep, depression.

The pons-medulla oblongata continuum is exposed in ventral view (Fig. 5c-d), being rather long and wide (Table 1), even if it looks narrow relative to the width of the cast of the promontoria of the petrosal bones (Fig. 5c-d).

Cranial Nerve Exit Casts

The anterior margin of the olfactory bulbs shows two potential exits for the olfactory nerve (I) (Fig. 5c-f). A bundle of nerves seems to exit at the anterodorsal extremity of the olfactory bulbs by a short and almost horizontal (antero-posterior) dorsal part, and there are smaller holes for olfactory nerves on the anteroventral surface of the olfactory bulbs (through the cribriform plate). The imprint of the latter is large, tilted anteriorly and has a quadrate/round shape. It occupies roughly the anterior third of the ventral surface of the olfactory bulbs.

The optical nerve (II) exits through the optic canal, whose anterior opening (the optic foramen) is located just posterior to the olfactory bulbs, anterior to the circular fissure (Fig. 5c-d). It is as large as the other single-nerve foramina, being just a bit smaller than the cribriform plate.

The oculomotor (III), trochlear (IV), and abducens (VI) nerves and the ophthalmic branch of the trigeminal nerve (V1) open together in the sphenorbital fissure while the optic and round foramina are individualized (Fig. 5c-d). The sphenorbital fissures are oblong-shaped, elongated antero-posteriorly (Table 1), and in a rather anterior position relative to the cerebrum: their anterior extremity is close to the circular fissure. They are clearly separated but anteriorly convergent,

with a slight diagonal orientation; the sphenorbital bridge (between them) is wider posteriorly.

The maxillary branch of the trigeminal nerve (V2) opens independently from the ophthalmic branch, because a round foramen is present. This foramen is located just near the posterolateral corner of the sphenorbital fissure, and is rather small compared to other single-nerve foramina.

The mandibular branch of the trigeminal nerve (V3) opens in a wide and oval-shaped oval foramen. This foramen is located just posterolateral to the round foramen: there is an alignment of the posterolateral corner of the sphenorbital fissure, the round foramen, and the oval foramen. The oval foramen is quite larger than the round foramen, and slightly larger than the optic foramen.

The facial (VII) and vestibulocochlear (VIII) nerves exit the endocranium through the internal auditory meatus of the petrosal bone. The facial nerve goes anterolaterally (Fig. 5c-d) and a bit ventrally (Fig. 5e-f), but the vestibulocochlear nerve goes clearly anteroventrally (Fig. 5e-f). The cochleae are so close to each other in ventral view (Fig. 5c-d) that the casts of these nerves are roughly on the same medio-lateral line as those of the mandibular branches of the trigeminal nerve (V3), which exit through the oval foramina.

The glossopharyngeal (IX), vagus (X), and accessory (XI) nerves exit through the jugular foramen (Fig. 5c-d). It is located just posterior to the two previous nerves, at the same medio-lateral level. This foramen is of large size, as three nerves pass through. It is coalescent with the basicochlear fissure, medially.

The hypoglossal nerve (XII) exits through the hypoglossal foramen. It is located a bit more medially than the previous foramina, at the medio-lateral level of the round foramen, and between the jugular foramen and the foramen magnum anteroposteriorly (it opens in the ventral condyloid fossa, comprised in the exoccipital). It is of medium size relative to other single-nerve foramina.

Other Braincase Opening Casts

The cast of the ethmoidal foramen (Fig. 5e-f) is present on both sides and is rather wide. It is located, on the endocast, on the lateral face of the olfactory bulb, in a posteroventral position. It is however difficult to spot this foramen without the skull (i.e., on a natural endocast) as it is shallow (ESM1: Fig. SI. 6a).

The casts of the pyriform (piriform) fenestra, of the carotid foramen, and of the basicochlear fissure are visible on the endocast (Fig. 5c-d), coalescent, and surrounding the petrosal bone anteriorly and medially. These three openings join the jugular foramen, posteromedial to the petrosal bone.

The foramen magnum (Fig. 5c-d and g-h) is rather wide (Table 1), almond-shaped. It is located just ventral to the posterior part of the cerebellum, its anterior margin lying posterior to the casts of the promontoria. This foramen is tilted ventrally (Table 1), opening posteroventrally.

Comparisons with Other Hipposiderid Fossil Endocasts

Overall Shape

The specimen of *Pa. quercyi* is a well-preserved cranium filled with clay matrix, only a small portion of its cranial vault is broken. Despite the presence of sediment in the braincase, the endocranial cast has been satisfactorily virtually extracted (Fig. 6b–i, and ESM1: Fig. SI. 2b and f, Fig. SI. 3b, f and i and Fig. SI. 4b, f and i) and has a total volume of 364.6 mm^3 (Table 1). The specimen of *H. (Ps.) schlosseri* is a natural endocranial cast partly embedded in a phosphatized clay matrix with dorsal and both lateral surfaces exposed (Fig. 6c and j, and ESM1: Fig. SI. 2c and g, Fig. SI. 3c and j and Fig. SI. 4c and j), but its ventral surface could not be virtually segmented; this aspect of the cranium therefore remains undescribed for this species, and the total volume of the braincase could not be estimated. This specimen is morphologically similar to those figured with very low details by Yao et al. (2012). The natural endocranial cast of *H. (Ps.) bouziguensis* is also partly embedded in the sediment and its ventral surface, not directly accessible, was extracted virtually (Fig. 6d–k, and ESM1: Fig. SI. 2d and h, Fig. SI. 3d, g and k and Fig. SI. 4d, g and k). Except for the petrosals, which are missing, the whole surface of the endocast of this taxon is well preserved and the volume of the braincase has been estimated of 435.2 mm^3 (Table 1). This specimen is also morphologically close to those figured by Yao et al. (2012), especially their specimen 3. Overall, specimens figured here are very similar to and of better quality than those of Yao et al. (2012); we thus do not include the latter in our comparisons. The four specimens show the same global shape (Fig. 6a-d): they are hexagonal, longer than wide (Table 1), with a single neocortical sulcus (shallower in *Pa. quercyi*, deeper in *H. (Ps.) bouziguensis*) and thus lissencephalic. In ventral view (Fig. 6e-g), endocasts of *Pa. quercyi* and of *H. (Ps.) bouziguensis* also resemble that of *Pa. oltina*, with petrosals occupying a large surface of the posterior part (Table 1), and with roughly the same pattern of basicranial foramina. In lateral view (Fig. 6h-k), the global scheme of all taxa described here is also very close. There are however some differences: (1) the telencephalon of *H. (Ps.) bouziguensis* is more inflated dorsally than the three others, (2) *Pa. quercyi* and *H. (Ps.) schlosseri* have a flatter reuniens lobe compared to *Pa. oltina* and *H. (Ps.) bouziguensis*, (3) the general position of the orbitotemporal canal cast on the telencephalon is clearly more ventral in *H. (Ps.) bouziguensis* than in the three others, and (4) the orientation and relative size of olfactory bulbs vary between taxa. The cephalic and cervical flexures are of a similar

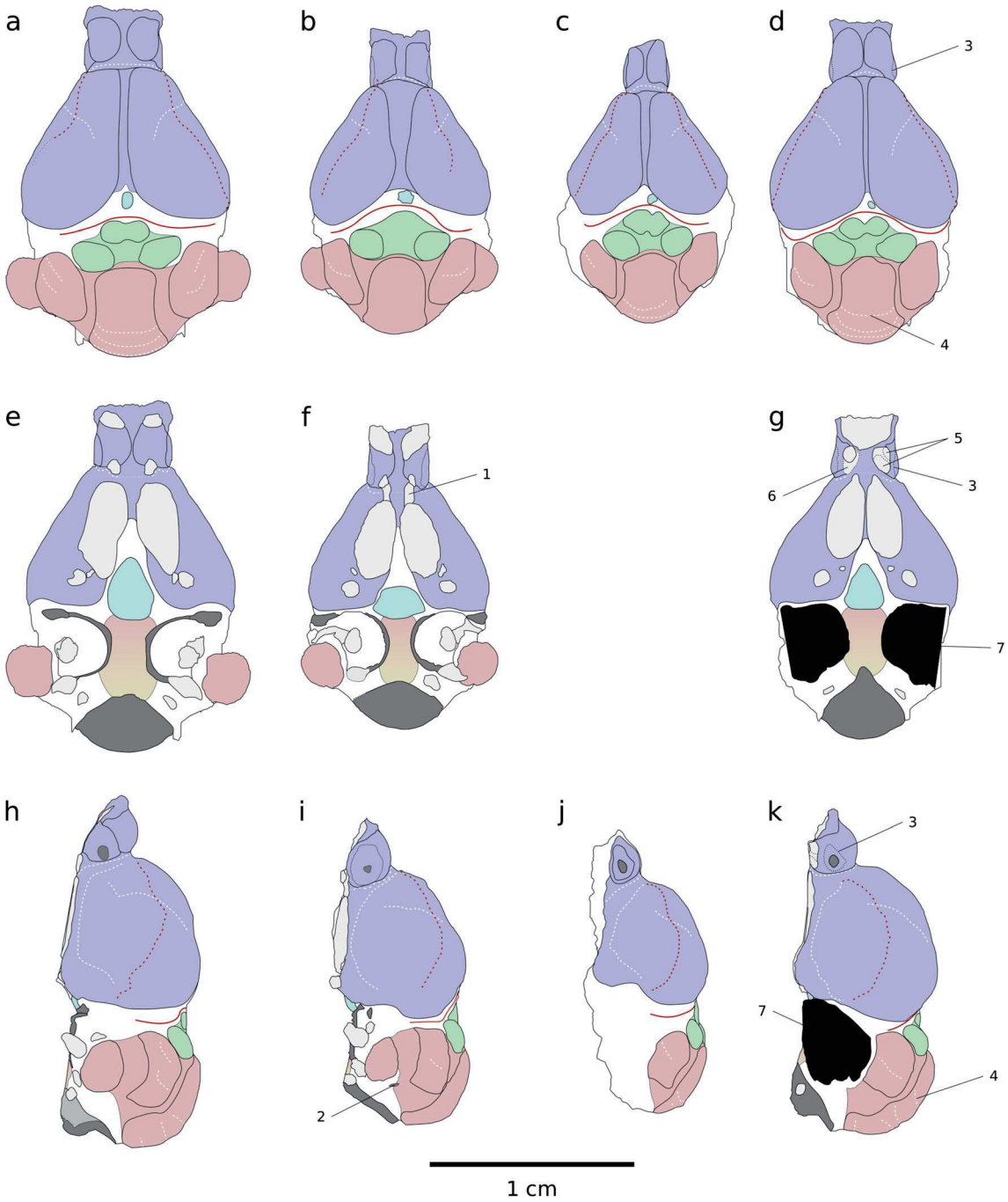

Fig. 6 Comparative schemes (as for Fig. 5a–g) of the fossil sample endocasts studied here in dorsal (**a-d**), ventral (**e-g**), and lateral (**h-k**) views. From left to right: *Palaeophyllophora oltina* (NMBS QP784; a,e,h), *Palaeophyllophora quercyi* (UM ACQ 6627; b,f,i), *Hipposideros (Pseudorhinolophus) schlosseri* (NMBS QV370; c,j) and *Hipposideros (Pseudorhinolophus) bouziguensis* (NMBS G2369; d,g,k). Numbers highlight absent structures in *Pa. oltina*: **1**-optic canal, **2**-mastoid foramen, **3**-shallow delineation of the lateral swelling of the olfactory bulb, **4**-VI-VII sulcus of the vermis, **5**-two "sub-foramina" of what is considered as the single left optic foramen in *H. (Ps.) bouziguensis*, **6**-potential posterior extent of the right optic foramen in *H. (Ps.) bouziguensis*, **7**-absence of petrosals

magnitude for all specimens (Table 1); the relative organization of brain sub-structures is the same across these taxa. The specimen of *H. (Ps.) bouziguensis*, compared to the three others, gives a visual impression of a slight antero-posterior compression (Fig. 6h-k), but has comparable height/length ratio for the endocast as a whole, for the cerebrum, and for the cerebellum relative to the other species (Table 1). Cephalic flexures vary a bit between the three species for which it could be measured: *Pa. oltina* has the largest value, *Pa. quercyi* an intermediate value, and *H. (Ps.) bouziguensis* has the acutest angle (Table 1). There are also differences in the angle between the circular fissure and the foramen magnum between

Table 1 Endocranial cast measurements of the fossil sample studied here

Measurement	*Pa. oltina*	*Pa. quercyi*	*H. (Ps.) schlosseri*	*H. (Ps.) bouziguensis*
endocast volume	525.9	364.6	–	435.2
olfactory bulbs volume	15.5	11.7	–	11.4
paraflocculi volume	11.9	6.5	–	–
endocast length (without olfactory bulbs)	14.2	12.1	11.3	13.1
endocast width (without paraflocculi)	10.2	8.9	–	9.2
width between the petrosal casts	2.0	1.2	–	1.5
endocast width at the level of the petrosal casts	9.7	8.3	–	8.3
endocast height	7.1	6.8	–	7.2
cerebrum height	6.8	6.3	5.7	7.0
cerebellum height	6.6	6.1	–	6.7
length of hypophysis	3.1	1.6	–	2.2
width of hypophysis	2.3	2.6	–	1.9
cerebrum width	10.2	8.9	–	9.2
cerebellum width	8.9	7.6	6.8	7.3
cerebellum length	5.7	4.7	4.5	5.0
vermis length	4.4	3.8	3.4	4.3
vermis width	2.9	2.9	2.4	2.6
left cerebellar hemisphere length	3.4	3.3	2.9	3.2
right cerebellar hemisphere length	3.8	3.3	2.9	3.4
left parafloccculus length	2.6	2.2	–	–
right parafloccculus length	2.5	2.3	–	–
left parafloccculus width	2.4	2.0	–	–
right parafloccculus width	2.3	2.1	–	–
pons-medulla oblongata continuum maximal length	3.6	3.0	–	2.8
pons-medulla oblongata continuum minimal width	1.6	1.0	–	1.5
sphenorbital fissures length	4.8	3.8	–	4.1
cerebrum length	7.9	6.8	6.0	7.5
foramen magnum length	2.9	2.4	–	3.5
foramen magnum width	4.8	4.4	–	4.1
cephalic flexure	171	162	–	156
cervical flexure	150	152	–	142
angle between the circular fissure and the ventral plane of the telencephalon	92	122	–	106
angle between the circular fissure and the foramen magnum	41	78	–	78
endocast (withtout olfactory bulbs and paraflocculi) length vs width	139	136	–	142
petrosal vs local whole width	79	86	–	82
endocast height vs length	50	56	–	55
cerebrum height vs length	86	93	95	93
cerebellum height vs length	116	130	–	134
olfactory bulbs volume relative to whole endocast	2.9	3.2	–	2.6
hypophysis length vs width	135	62	–	116
cerebrum vs cerebellum width	115	117	–	126
cerebellum width vs length	156	162	151	146
vermis length vs width	152	131	142	165
antero-posterior “overlap” between vermis and cerebellar hemispheres	44	51	40	54
left parafloccculus length vs width	108	110	–	–
right parafloccculus length vs width	109	110	–	–
paraflocculi volume relative to whole endocast	2.3	1.8	–	–
pons-medulla oblongata continuum length vs width	225	300	–	187
sphenorbital fissure vs telencephalon length	61	56	–	55

Table 1 (continued)

Measurement	*Pa. oltina*	*Pa. quercyi*	*H. (Ps.) schlosseri*	*H. (Ps.) bouziguensis*
foramen magnum length vs width	60	55	–	85

Volumes are in mm^3, linear measurements in mm, angles in °, and ratios in %. Missing values are indicated by a dash

species, *Pa. oltina* having the most acute one (Table 1). In fact, *Pa. quercyi* has a more ventrally tilted circular fissure than *Pa. oltina*, and *H. (Ps.) bouziguensis* has a much more ventrally tilted foramen magnum (Table 1).

Telencephalon

In dorsal view (Fig. 6a-d), the general shape of the olfactory bulbs is close for all fossil hipposiderid taxa but there are some subtle differences. The olfactory bulbs of *Pa. quercyi* and of *H. (Ps.) bouziguensis* are similar in shape and size to those of *Pa. oltina*, but they are closer to each other in *Pa. quercyi* and even more in *H. (Ps.) bouziguensis*. The olfactory bulbs of *H. (Ps.) schlosseri* are narrower than those of the three other taxa. In lateral view (Fig. 6h-k), each specimen differs from the other. Compared to *Pa. oltina*, the three other extinct hipposiderid taxa present olfactory bulbs that are pointing anteriorly, and not dorsally raised. *Palaeophyllophora quercyi* has the longest and biggest olfactory bulbs relatively to the whole endocast (3.2% of total volume; Table 1). Both specimens of *Hipposideros (Pseudorhinolophus)* have shorter and dorsoventrally larger olfactory bulbs, with a rounder shape, those of *H. (Ps.) schlosseri* being smaller than those of *H. (Ps.) bouziguensis*. The olfactory bulbs of the described species of *Hipposideros (Pseudorhinolophus)* are globally smaller than those of *Palaeophyllophora* (2.6% of total volume in *H. (Ps.) bouziguensis*). The lateral bulge observed in *Pa. oltina* is also present in the other three specimens but it is smaller. In *Pa. quercyi*, this swelling is weakly developed but present, while in *H. (Ps.) schlosseri*, it is well visible in spite of the smaller size of the olfactory bulbs. In *H. (Ps.) bouziguensis*, the lateral swelling has a large lateral extent similar to *Pa. oltina*, but its distinction relative to the main part of olfactory bulbs is smoother. The shape of the circular fissure of the two *Hipposideros (Pseudorhinolophus)* and of *Pa. quercyi* is similar to *Pa. oltina*. In dorsal view (Fig. 6a-d), the cerebral hemispheres of the fossil hipposiderids described here have the same pear-shape and a maximal width reached rather posteriorly. However, there are some differences in how they contact each other as well as on the shape of their posteromedial corner. In *H. (Ps.) bouziguensis*, the interhemispheric gap is the narrowest, the two cerebral hemispheres are closer to each other on a longer distance; their posteromedial corner is almost right, the least obtuse of all specimens. In other taxa described here, the interhemispheric gap is wider and the posteromedial corner is more opened. In *H. (Ps.) schlosseri*, the gap between cerebral hemispheres is a bit wider than in *Pa. oltina* but it is constant, while it is narrower anteriorly and widens posteriorly in *Pa. oltina*. This gap between cerebral hemispheres is even wider in *Pa. quercyi*: the interhemispheric gap, rather wide posteriorly (as *Pa. oltina* and *H. (Ps.) schlosseri*), is wider anteriorly. However, the medial margin of the reuniens lobe is blurry (maybe due to preservation) and the anterior width of the gap between the hemispheres is difficult to assess. Laterally (Fig. 6h-k), there are different degrees of inflation of the reuniens and arcuate lobes among species. Both lobes are much inflated in *H. (Ps.) bouziguensis*, a bit more than in *Pa. oltina*. In *Pa. quercyi* especially, but also in *H. (Ps.) schlosseri*, the reuniens lobe is less inflated. The cerebrum of *H. (Ps.) bouziguensis* appears to be more antero-posteriorly compressed; this could be a visual artefact due to its more dorsoventral global inflation. Laterally (Fig. 6h-k), the pyriform lobes are located a bit more posteriorly in *Palaeophyllophora* than in *Hipposideros (Pseudorhinolophus)*. They are located at, or just a bit posterior to, the summit of the arcuate lobe in the former, while they are a bit anterior to it in the latter. The development of the pyriform lobe follows that of the arcuate lobe (they are the most developed in *H. (Ps.) bouziguensis*), and they are a bit more salient in *H. (Ps.) schlosseri* than in *Palaeophyllophora* specimens. The ventral view (Fig. 6e-g) does not show any other difference of these lobes between taxa.

Laterally (Fig. 6h-k), on all specimens, the rhinal fissure is difficult to identify. Its anterior part is less visible in *Pa. quercyi* than in other specimens. Its posterior part is decipherable on the *Pa. quercyi* and *H. (Ps.) schlosseri* specimens: there is a subtle ridge delineating the dorsal margin of the pyriform lobe in anterior view (ESM1: Fig. SI. 5) that is continuous with the anterior part of the rhinal fissure observed in lateral view (Fig. 6h-k). This ridge could mark the location of the posterior part of the rhinal fissure, and it is also distinguishable in the other specimens (Fig. 6h-k; ESM1: Fig. SI. 5). This posterior part is best seen (through the ridge) in lateral view on the *Pa. quercyi* specimen (Fig. 6h-k). On its whole length, the course of the rhinal fissure is roughly the same in all specimens with its posterior third strongly dorsally tilted. The orbitotemporal canal, visible on all specimens, shows differences between taxa. In lateral view (Fig. 6h-k), it is located more ventrally in *H. (Ps.) bouziguensis*, especially its anterior

part, which is more ventrally flexed. In *Pa. quercyi*, the posterior part is difficult to track, but the dorsalmost angle of the canal is located more dorsally than in other specimens, suggesting a general more dorsal position. In *H. (Ps.) schlosseri*, the position of this canal is similar to *Pa. oltina*. In dorsal view (Fig. 6a-d), *H. (Ps.) bouziguensis*, again, differs markedly from the other hipposiderid taxa with a more lateral location of the orbitotemporal canal. Other specimens show a similar, more medial, position of the orbitotemporal canal. That of *Pa. oltina* is a little bit more lateral than the two others. The dorsal inflection of this canal is less acute in both *Hipposideros (Pseudorhinolophus)* taxa than in both *Palaeophyllophora* ones. The sylvia is visible on all specimens, roughly at the level of the second quarter (antero-posteriorly) of the cerebrum (Fig. 6a-d and h-k). In lateral view (Fig. 6h-k), it is shallow in *Pa. quercyi*, a bit deeper in *Pa. oltina* and in *H. (Ps.) schlosseri*, and it is the deepest in *H. (Ps.) bouziguensis*. The pseudosylvia seen in *Pa. oltina* is found only in *H. (Ps.) schlosseri* where it is very short. This sulcus is lacking in the other taxa of the sample. In dorsal view (Fig. 6a-d), the sylvia is shallow posteriorly for *Pa. oltina* and *H. (Ps.) schlosseri* (it is always shallow for *Pa. quercyi*). However, in *Pa. oltina*, there is a slight posterior extension of the sylvia (the posterior extension of the suprasylvia) marked by a terminal angle. In *H. (Ps.) bouziguensis*, the sylvia is deeper and its posterior extension is present, clearer than in *Pa. oltina*.

Diencephalon

In dorsal view (Fig. 6a-d), the delineation of the cast of the epiphysis of the fossil hipposiderid taxa described here is rather unclear. However, imprints of all expected structures on the dorsal surface between cerebrum and cerebellum (i.e., epiphysis cast, transverse sinus, rostral and caudal colliculi) in *Pa. oltina* allow us to identify and locate these different structures in all taxa. This cast is small and hardly distinguishable in both *Palaeophyllophora* species; it is even smaller in the *Hipposideros (Pseudorhinolophus)* ones.

In ventral view (Fig. 6e-g), the hypophysis is well preserved in all specimens (when ventral view is preserved). In *H. (Ps.) bouziguensis*, the hypophysis cast is similar to that of *Pa. oltina*: it is of subtriangular shape, longer than wide (Table 1), and in the same position. It is however a bit less protruding ventrally. In *Pa. quercyi*, it is wider than long (Table 1), ovoid in shape.

Mesencephalon

The tectum of the mesencephalon (Fig. 6a-d) is fully exposed in all specimens. The rostral colliculi are distinguishable in *Pa. oltina* and in the two *Hipposideros (Pseudorhinolophus)* specimens; their corresponding area is poorly preserved on the *Pa. quercyi* specimen. In *H. (Ps.) bouziguensis*, they have a shape similar to those of *Pa. oltina*. In *H. (Ps.) schlosseri*, there is rather a plateau, with the two little prominences of the rostral colliculi. These rostral colliculi are also a bit higher (Fig. 6h-k) than in *Pa. oltina*, but they are also more difficult to distinguish. The caudal colliculi are clearly visible: their major axis is diagonally oriented, and they are more elongated in *Pa. oltina* and *H. (Ps.) bouziguensis* than in *Pa. quercyi* and *H. (Ps.) schlosseri*. Moreover, they are more separated in *Pa. quercyi* than in other fossil hipposiderid taxa. Laterally (Fig. 6h-k), the tectum of the mesencephalon lies in a shallow valley between the cerebrum and the cerebellum. The two latter structures are, however, of different heights depending on the taxa. The cerebrum and cerebellum are the highest in *H. (Ps.) bouziguensis*, where the tectum lies in a clear depression; they are a bit lower and the tectum lies in a shallower depression in *Pa. oltina*, *Pa. quercyi*, and *H. (Ps.) schlosseri*. In *H. (Ps.) bouziguensis*, despite the fact that the mesencephalon is more depressed, the caudal colliculi are clearly the most protruding; those of other taxa are of a similar, less protruding, degree of prominence.

Metencephalon

In dorsal view (Fig. 6a-d), the metencephalon is the widest region of the braincase for *Pa. quercyi* and for *Pa. oltina*; the lack of preservation of the paraflocculi in the other taxa does not allow us to confirm this for *Hipposideros (Pseudorhinolophus)* specimens. Yet, in all specimens, the width of the cerebellum is twice its length, nearly as wide as the cerebrum (Table 1). The vermis is also quite wide (a bit larger in *Pa. oltina* than in others), but still longer than wide (the longest in *H. (Ps.) bouziguensis*, Table 1). In all specimens, as for *Pa. oltina*, it enlarges posteriorly and a bit anteriorly, almost reaching the caudal colliculi anteriorly. The anterior margin of the vermis is much more delineated in *Hipposideros (Pseudorhinolophus)* species than in *Palaeophyllophora*. In lateral view (Fig. 6h-k), the vermis is a bit higher in *Palaeophyllophora* species and in *H. (Ps.) bouziguensis* than in *H. (Ps.) schlosseri*. Moreover, the shape of the dorsal surface of the vermis in this view is more convex in *H. (Ps.) bouziguensis* than in *Palaeophyllophora* species and in *H. (Ps.) schlosseri*. The surface of the vermis of *Pa. quercyi* does not show any sulcus, but the preservation is poorer than in other specimens. There is a VII sulcus and a prepyramidal fissure in all three other species (Figs. 5g-h and 6a-d and h-k). There also is a secondary fissure on the occipital face of the vermis surface of *Pa. oltina* and *H. (Ps.) bouziguensis*. In the latter species, there even is a VI-VII sulcus: it is shallow but present, visible in both dorsal and lateral views (Fig. 6a-d and h-k). It divides the VI and VIIa lobules inequally, the declive (VI) being much longer (more than the half of the vermis length in dorsal view, Fig. 6a-d). The cerebellar hemispheres (Fig. 6a-d) of *H. (Ps.) schlosseri* are narrow, not protruding laterally, and the intercrural sulcus is hardly distinguishable, while the hemispheres have the same general shape and the intercrural sulcus is marked in other specimens. The

vermis is protruding posteriorly in *Pa. oltina* and in *H. (Ps.) schlosseri*, a bit less in *Pa. quercyi*, and it protrudes the least in *H. (Ps.) bouziguensis*. Concurrently, the cerebellar hemispheres are more anteriorly located relative to the vermis in the two former species; in dorsal view, they have a greater antero-posterior overlap between vermis and cerebellar hemispheres (Table 1). The paraflocculi have been only preserved in *Palaeophyllophora* specimens (Fig. 6e-g), where they are of close morphology, but they are a bit larger in *Pa. oltina* than in *Pa. quercyi* relatively to the whole endocast (2.3% vs 1.8% of the total volume; Table 1). In dorsal view (Fig. 6a-d), the paraflocculi of *Pa. oltina* are more visible than those of *Pa. quercyi*. In *Pa. quercyi*, the paraflocculi are located more medially: they protrude less laterally (Fig. 6a-d) and, in ventral view (ESM1: Fig. SI. 4e-g), "necks" of the paraflocculi (the part linking them to the rest of the metencephalon) are not visible (they are for *Pa. oltina*). The medial part of the parafloccculus (Fig. 6e-g) protrudes a bit posteriorly in *Pa. quercyi*, while the lateral one protrudes posteriorly in *Pa. oltina*. The ventral sulcus of parafloccculus is less marked in *Pa. oltina* than in *Pa. quercyi* (ESM1: Fig. SI. 4e-g), but it could also just be a matter of preservation. In lateral view (ESM1: Fig. SI. 4 h-k), the lateral depression present in *Pa. oltina* is absent in *Pa. quercyi*.

The pons-medulla oblongata continuum (Fig. 6e-g) is longer than wide in all specimens (Table 1), and relatively longer in *Pa. quercyi* than in the two other specimens. Otherwise, there are no clear differences between taxa.

Cranial Nerve Exit Casts

The olfactory nerve exit pattern is generally similar across specimens (Fig. 6e-k). Yet, some differences occur regarding the olfactory nerves exit (imprint of the cribriform plate + dorsal bundle of nerves). It varies in terms of orientation and of extension: it is more tilted anteriorly in *Pa. oltina* than in other taxa, and forms a large surface in *Pa. oltina* and *H. (Ps.) bouziguensis* while it is of intermediate dimensions in *Pa. quercyi* and consists of a small and rounded surface in *H. (Ps.) schlosseri* (Fig. 6e-g and ESM1: Fig. SI. 5). Optic foramina (Fig. 6e-g) are separated from the sphenorbital fissure in all specimens, but their position varies. They are at the posterior end of olfactory bulbs in *Palaeophyllophora* specimens (optic canals are even visible in *Pa. quercyi*), at the level of the circular fissure. Optic foramina are more anteriorly located in *H. (Ps.) bouziguensis*, being at the middle of the olfactory bulbs, just posterior to the imprint of cribriform plate. The structures identified here as optic foramina in *H. (Ps.) bouziguensis* are rather unusually located (ventral aspect of the olfactory bulbs) and very dissimilar on the left and right sides of the specimen. Their shape and size are roughly similar to those of *Pa. oltina* and they are a bit posteriorly located to the imprint of cribriform plate. Another possibility for optic foramina identification could be the small notches at the anterior end of each sphenorbital fissure; optic foramina would therefore be confluent with these fissures. In this case, compared to *Palaeophyllophora* specimens, the position of the optic foramina would be similar but their shape would be very different. The sphenorbital fissures (Fig. 6e-g) are similarly located ventral to the anterior part of cerebrum in all specimens. They are however located a bit more anteriorly in *H. (Ps.) bouziguensis* than in *Palaeophyllophora*, the former bearing a small anterior notch at the level of the circular fissure. They are also a little bit longer and a bit more apart in *Palaeophyllophora* specimens (Table 1). Otherwise, on the three specimens, the sphenorbital fissures are roughly oblong-shaped, rather large (especially relative to the gap between them), and converge anteriorly. Round and oval foramina are individualized on the three specimens. In all three specimens, the round foramen is clearly smaller than the oval one, which is rather large, round-shaped to oval-shaped. The position of the oval foramen is also similar, located posterolateral to the sphenorbital fissure. The position of the round foramen, however, varies: it is located between the sphenorbital fissure and the oval foramen in *Pa. oltina* (all three structures being juxtaposed and aligned), while it is lateral to the posteriormost part of the sphenorbital fissure in *Pa. quercyi* and posterior to it with a marked gap in *H. (Ps.) bouziguensis*. There are no differences regarding the exits of facial and vestibulocochlear nerves and the cast of the jugular foramen among the two *Palaeophyllophora* specimens (petrosal is not preserved in *H. (Ps.) bouziguensis*), in terms of size and orientation (Fig. 6e-k) for the two former, and in terms of size, shape, and location for the latter (Fig. 6e-g). The size, shape, and location of the hypoglossal foramen are similar across the three specimens where it is preserved; it lies in a slight more medial position in *Pa. quercyi* (Fig. 6e-g).

Other Braincase Opening Casts

The ethmoidal foramen is at the level of the lateral swelling of the olfactory bulbs in both *Palaeophyllophora* species (this is confirmed by cranial observation, ESM1: Fig. SI. 6a-b). This foramen is however tough to decipher without the skull (i.e., based on natural endocast); we thus consider that its location is similar in *Hipposideros (Pseudorhinolophus)* species (ESM1: Fig. SI. 6c-d), but this cannot be confirmed yet. Comparing apertures surrounding the petrosal imprint (Fig. 6e-g; i.e., pyriform fenestra, carotid foramen, and basicochlear fissure) of the *H. (Ps.) bouziguensis* specimen is difficult as only their lateral side is preserved (as for the jugular foramen). In both *Palaeophyllophora* specimens, the three previously mentioned structures plus the jugular foramen are confluent. The cast of the basicochlear fissure is thicker in *Pa. oltina*, and the pyriform fenestra cast is more lateral in *Pa. quercyi* (Fig. 6e-g). The foramen magnum is very similar in size, shape, and orientation between *Palaeophyllophora* specimens. In *H. (Ps.) bouziguensis*, the foramen magnum bears an anterior notch and opens more ventrally than in the three other taxa (Fig.

6h-k and Table 1). It therefore has a different shape and size in ventral view (Fig. 6e-g): its anterior outline is angular and its posterior one is curved.

Common Endocast Measurements

Encephalization Quotient

The encephalization quotient corresponds to the ratio between the observed brain mass of an organism and the expected brain mass of this organism given its body mass (Jerison 1973; van Dongen 1998). EQ values, brain and body masses of the described species are provided in Table 2, and the boxplots of EQ values of mammals through Tertiary epochs and of extant species are presented Fig. 7 and ESM1: Fig. SI. 7 (following Eisenberg and Wilson (1978) and Jerison (1973) formulas respectively). As previously described in the literature (e.g., Jerison 1973), a general increase of EQ values from Paleocene to Oligocene is observed in mammals; however, this is not true for hipposiderid bats, whose EQ values remain relatively constant through time. This is supported by Kruskal-Wallis tests of the EQ comparing these epochs: there is at least a difference between epochs in mammals (Table 3), especially around the Eocene/Oligocene boundary (Table 4 and ESM2: Table SI. 6), but not in bats (here only represented by hipposiderid for fossils species; Tables 5 and 6 and ESM2: Table SI. 6). In hipposiderids only, there is a slight significance of both Fisher and Kruskal-Wallis tests (Table 3 and ESM2: Table SI. 6) and there is a slight tendency to a difference between Eocene and extant hipposiderids (Table 6 and ESM2: Table SI. 6), but p-values are superior or close to the 5% alpha risk. Interestingly, extant bats, and especially extant hipposiderids, are in the lower part of mammal EQ values (overlapping the lower whisker of the general boxplot; Fig. 7 and ESM1: Fig. SI. 7), whereas EQ values of fossil hipposiderid bats were closer to central global mammalian values in the Eocene. This suggests that hipposiderid EQ apparently did not increase through time, contrary to non-bat mammals in general.

A complementary way to illustrate the EQ is to plot the log brain mass vs the log body mass with the regression lines

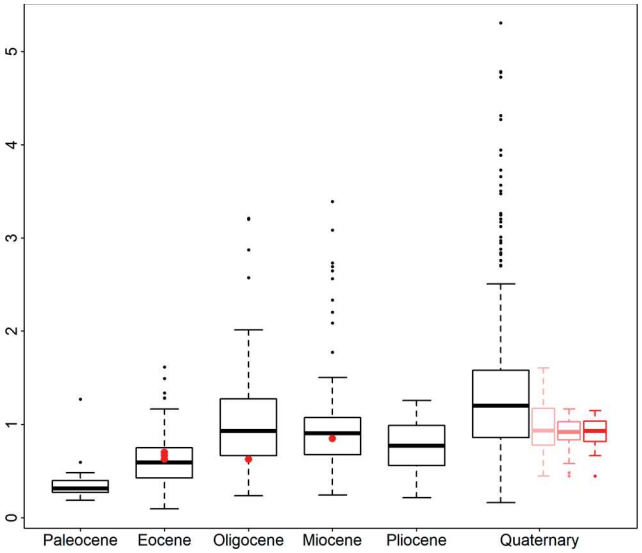

Fig. 7 Boxplot of EQ values (y-axis) following Eisenberg and Wilson's (1978) formula in mammals through cenozoic epochs (x-axis). Black boxplots: all mammals except bats. Light pink boxplot: bats. Pink boxplot: extant rhinolophoids. Red boxplot: extant hipposiderids. Red dots: extinct hipposiderids (with *H. (Ps.) schlosseri* represented in Eocene and in Oligocene)

derived from the EQ formulas of Eisenberg and Wilson (1978) and of Jerison (1973) for all mammals and for bats only (ESM1: Fig. SI. 8). As illustrated previously (Fig. 7) and statistically tested (Table 4 and ESM2: Table SI. 6), this figure (ESM1: Fig. SI. 8) shows a bump over the regression lines (i.e., in the encephalization) of the "other mammals" convex hull at the Eocene-Oligocene transition. Bats, on the other hand, are under the Jerison (1973) regression line and at the level of the Eisenberg and Wilson (1978) regression line, without clear difference between extant bats and Eocene to Miocene ranging bats (Tables 5 and 6 and ESM2: Table SI. 6).

Olfactory Bulbs and Paraflocculi Volumes Relative to Brain Volume

Olfactory bulbs and paraflocculi are quite prominent in bat brains (see Baron et al. 1996) and in fossil species described here (Figs. 3, 4, 5, and 6 and ESM1: Figs. SI. 2–4). The volume of

Table 2 Measurements and EQ values (following both Eisenberg and Wilson's and Jerison's formulas) for the fossil sample studied here

Taxon	*Pa. oltina*	*Pa. quercyi*	*H. (Ps.) schlosseri*	*H. (Ps.) bouziguensis*
Endocranial cast volume (mm^3)	525.9	364.6	233.3	435.2
Brain mass (g)	0.5448	0.3777	0.2417	0.4509
Body mass (g)	36.0615	23.6390	14.0306	21.5168
EQ (Eisenberg & Wilson 1978)	0.6977	0.6612	0.6225	0.8461
EQ (Jerison 1973)	0.4160	0.3822	0.3463	0.4857

Body masses after Maitre (2014) for *Pa. oltina*, *Pa. quercyi*, and *H. (Ps.) schlosseri*, and after Sigé (1968) and Maitre (2014) for *H. (Ps.) bouziguensis*. Brain mass of *H. (Ps.) schlosseri* after Yao et al. (2012)

Table 3 Results of the various tests performed on EQ values

Sample	EQ Formula	Test used	Statistic value	df	p-value
All mammals except bats	Eisenberg & Wilson (1978)	Shapiro-Wilk	$W = 0.85276$		$< 2.2 \times 10^{-16}$
		Kruskal-Wallis	$\chi = 188.79$	5	$< 2.2 \times 10^{-16}$
		Dunn (see pairwise tests Table 4 and Table SI. 2)			
	Jerison (1973)	Shapiro-Wilk	$W = 0.7496$		$< 2.2 \times 10^{-16}$
		Kruskal-Wallis	$\chi = 166.54$	5	$< 2.2 \times 10^{-16}$
		Dunn (see pairwise tests Table 4 and Table SI. 2)			
All bats	Eisenberg & Wilson (1978)	Shapiro-Wilk	$W = 0.97287$		4.108×10^{-6}
		Kruskal-Wallis	$\chi = 7.9626$	3	0.04679
		Dunn (see pairwise tests Table 5 and Table SI. 2)			
	Jerison (1973)	Shapiro-Wilk	$W = 0.9518$		2.982×10^{-9}
		Kruskal-Wallis	$\chi = 6.3104$	3	0.09745
		Dunn (see pairwise tests Table 5 and Table SI. 2)			
Hipposiderid bats	Eisenberg & Wilson (1978)	Shapiro-Wilk	$W = 0.97079$		0.4835
		Fisher	$F = 3.5815$	3, 30	0.0252
		Kruskal-Wallis	$\chi = 8.962$	3	0.0298
		Tukey HSD (see pairwise tests Table 6 and Table SI. 2)			
		Dunn (see pairwise tests Table 6 and Table SI. 2)			
	Jerison (1973)	Shapiro-Wilk	$W = 0.96755$		0.3972
		Fisher	$F = 3.7728$	3, 30	0.02075
		Kruskal-Wallis	$\chi = 8.1795$	3	0.04244
		Tukey HSD (see pairwise tests Table 6 and Table SI. 2)			
		Dunn (see pairwise tests Table 6 and Table SI. 2)			

Shapiro-Wilk test first performed to test the normal distribution of EQ values. Subsequent tests applied to determine if, through time, one pair (at least) of modalities (i.e., Cenozoic epochs) differ from the others (ANOVA through Fisher and/or Kruskal-Wallis tests)

these two structures relative to brain volume is commonly mentioned in the literature (e.g., Jerison 1973; Ramdarshan and Orliac 2016; Bertrand et al. 2018a, b, 2019). We plotted natural logarithms of each volume against the logarithm of brain volume, which allows to take into account the potential effect of allometry and to compare extreme points. Regarding olfactory bulbs, we compared our fossil hipposiderid species to bats in general, but also more specifically to other rhinolophoids and to other hipposiderids. In the biplot illustrating this relationship (Fig. 8a), our fossil sample falls roughly in the middle of all extant bats cloud of points. Pteropodids have the highest values, as they are generally bigger bats ("megabats"). Rhinolophoids and hipposiderids have a wide morphospace but also fall roughly in the middle of all "microchiropteran" bats (i.e., Yangochiroptera + Rhinolophoidea); fossil hipposiderid taxa fall in hipposiderids. Regarding parafloccular volume compared to endocranial volume (Fig. 8b), the morphospace of mammals is quite large, that of bats and of other laurasiatherians too. For

Table 4 Simplified results of the post-hoc (Dunn's) tests comparing 'time groups' of EQ values (Eisenberg and Wilson's, 'EW', or Jerison's, 'J') in non-bat mammals

Epoch	Paleocene		Eocene		Oligocene		Miocene		Pliocene		Quaternary	
	EW	J	EW	J	EW	J	EW	J	EW	J	EW	J
Eocene	NS	NS										
Oligocene	***	***	***	***								
Miocene	***	***	***	***	NS	NS						
Pliocene	*	***	NS	***	NS	NS	NS	NS				
Quaternary	***	***	***	***	***	***	***	***	***	*		

'NS' indicates a non-significance (no difference; p-value >0.1); '*' indicates a low significance (0.1 > p-value >0.05); '**' indicates a moderate significance (0.05 > p-value >0.01); '***' indicates a high significance (p-value <0.01)

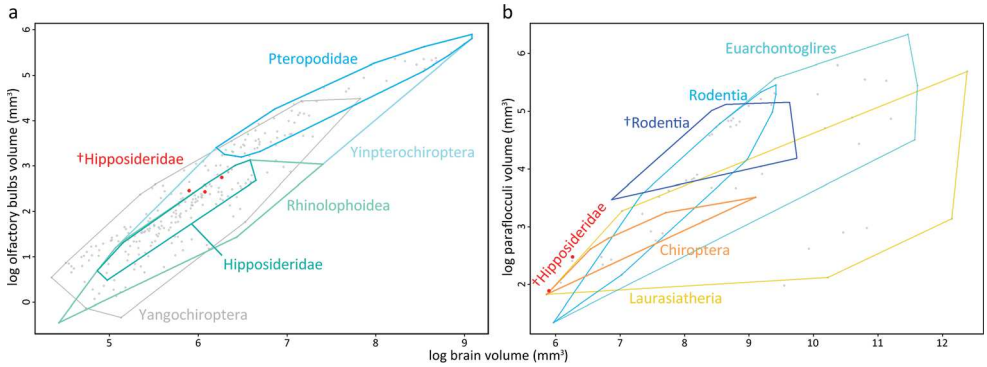

Fig. 8 Biplots of olfactory bulbs log-volume (**a**; y-axis) and paraflocculi log-volume (**b**; y-axis) relative to whole brain log-volume (x-axis). Biplot of olfactory bulb vs whole brain log-volumes (**a**) is at the Chiroptera scale, with the morphospaces of the two sub-orders (Yangochiroptera, Yinpterochiroptera), the two sub-clades of Yinpterochiroptera (Pteropodidae, Rhinolophoidea) and the extant family of the fossil sample in Rhinolophoidea (Hipposideridae). Biplot of paraflocculi vs whole brain log-volumes (**b**) is at the Mammalia scale, with the morphospaces of the super-order (Euarchontoglires and Laurasiatheria) and of the order (Rodentia and Chiroptera) of the other extinct mammals for which data is available (ischyromyid rodents, with enough points to draw another morphospace, and hipposiderid bats, with only two points)

rodents, both extinct and extant data are available: extinct species cluster together and overlap the morphospace of modern representatives. Concerning bats, the two fossil species are close to each other and to modern bat species (especially, *Pa. quercyi* falls very close to the rhinolophoid *Rhinolophus ferrumequinum*). "Microchiropteran" bats lie in the lower part of the biplot, which is expected given their smaller size; yet, they do not show extreme values compared to other mammals, despite of their particular locomotor behavior.

Discussion

Brain Vs Endocranial Cast External Morphology in Hipposideridae

Among mammals, some differences in the degree of similarity between the brain and the endocast are observed. For instance, Dechaseaux (1962) showed that, in sheep, the cranial endocast reflects well the morphology of the brain, which is not the case in cetacean and proboscideans, mostly due to the presence of meningeal tissues and/or blood vessels between the brain and the dorsal part of the braincase (e.g., dura mater, rete mirabile).

Table 5 Simplified results of the post-hoc (Dunn's) tests comparing 'time groups' of EQ values (Eisenberg and Wilson's, 'EW', or Jerison's, 'J') in bats

Epoch	Eocene		Oligocene		Miocene		Quaternary	
	EW	J	EW	J	EW	J	EW	J
Oligocene	NS	NS						
Miocene	NS	NS	NS	NS				
Quaternary	NS	NS	NS	NS	NS	NS		

See Table 4 for abbreviations

In the literature, "Insectivora", Chiroptera, and Carnivora are considered to show the highest correspondence between the endocranial cast and the external shape of the brain (Orlov 1961; Dechaseaux 1962; Kochetkova 1978). Paleoneurology is therefore promising, though limited and needs to be coupled with a detailed knowledge of the brain of extant species (Dechaseaux 1962; Neubauer 2014). This aspect is still patchy regarding bats, and especially Hipposideridae (see Baron et al. 1996 for the latest review at the Chiroptera scale), which makes morphological comparisons between extant and extinct species not straightforward. Only few hipposiderid brains have been macromorphologically described in the literature (one figure and a family-level general description in Baron et al. 1996) and no comparison of the external morphology of brain vs endocranial cast have never been realized for the family – or at the ordinal scale.

Another issue regarding the comparison between extinct and extant bat brains is that the phylogenetic relationships within Chiroptera has drastically evolved since the major works on extant bats of Baron et al. (1996) (e.g., bats placed

Table 6 Simplified results of the post-hoc (Dunn's, 'D', and Tukey's HSD, 'T') tests comparing 'time groups' of EQ values (Eisenberg and Wilson's, 'EW', or Jerison's, 'J') in hipposiderid bats

Epoch		Eocene		Oligocene		Miocene		Quaternary	
		EW	J	EW	J	EW	J	EW	J
Oligocene	D	NS	NS						
	T	NS	NS						
Miocene	D	NS	NS	NS	NS				
	T	NS	NS	NS	NS				
Quaternary	D	*	*	NS	NS	NS	NS		
	T	**	**	NS	NS	NS	NS		

See Table 4 for abbreviations

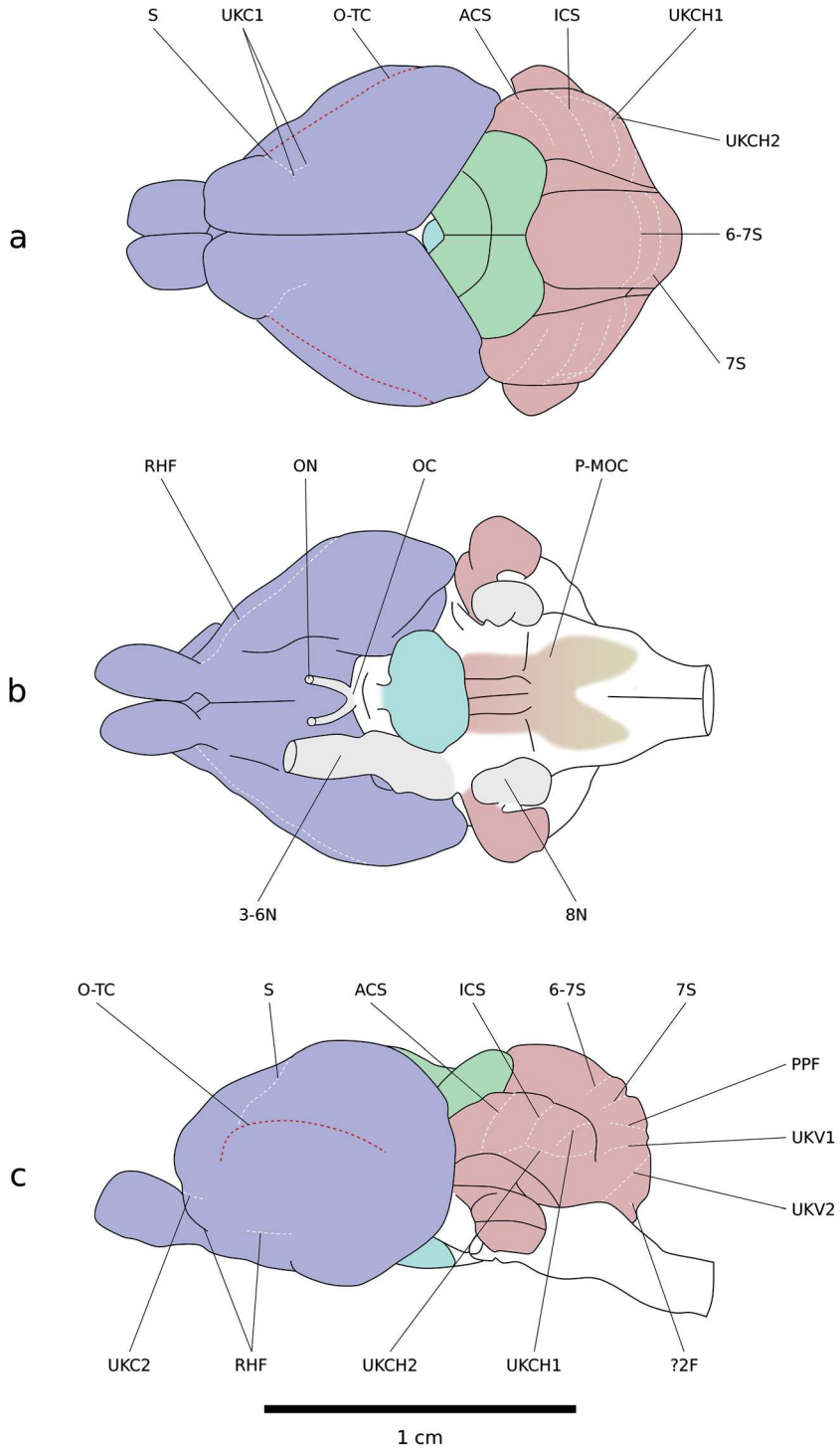

Fig. 9 Interpretation (following that of Figs. 5a–g and 6) of the illustration of the brain of *Hipposideros diadema* by Baron et al. (1996) in dorsal (**a**; Baron et al. 1996: fig. 8), ventral (**b**; Baron et al. 1996: fig. 40) and lateral (**c**; Baron et al. 1996: fig. 24) views. Except for the pons-medulla oblongata continuum (**P-MOC**), other captions indicates pathways:**?2F**-?secondary fissure, **3–6N**-bundle of cranial nerves III to VI, **6-7S**-VI-VII sulcus, **7S**-VII sulcus, **8N**-vestibulocochlear cranial nerve VIII, **ACS**-anterocrural sulcus, **ICS**-intercrural sulcus, **OC**-optic chiasm, **ON**-optic nerve, **O-TC**-orbitotemporal canal, **PPF**-prepyramidal fissure, **RHF**-rhinal fissure, **S**-sylvia, **UKC1**- and **UKC2**-unknown sulci of the cerebral hemispheres 1 and 2, **UKCH1**- and **UKCH2**-unknown sulci of the cerebellar hemispheres 1 and 2, **UKV1**- and **UKV2**-unknown sulci of the vermis 1 and 2

in Laurasiatheria rather than in Euarchontoglires, Mega−/Microchiroptera vs Yinptero-/Yangochiroptera; see Simmons and Geisler (1998), Simmons (2000), and Jones et al. (2005) for reviews) and brain characteristics proposed for different bat families have to be revised because of the changes in their taxonomic content. For instance, Baron et al. (1996) defined the general brain characteristics of Hippposideridae based on a taxonomic sample including species that are nowadays placed in a different family (*Triaenops persicus*, now placed in the Rhinonycteridae).

When compared to the brain of the modern *Hipposideros diadema* figured by Baron et al. (1996: figs. 8, 24, 40, and Fig. 9), the cranial endocasts of the present fossil sample (Fig. 6 and ESM1: Figs. SI. 3–4) appear to reflect well the external morphology of the brain of extant hipposiderid in dorsal and lateral views. The main differences concern: (1) the precision

of the folding of the cerebrum and the cerebellum (neocortical foldings are more marked on the brain; more foldings are visible on the vermis and on the cerebellar hemispheres on the brain); (2) the exact delineation of the midbrain region (there are imprecisions on an endocast regarding the posterior extent of the cerebral hemispheres and the anterior extent of cerebellar hemispheres); (3) the exposure of the mesencephalic colliculi (rostral colliculi are less visible and less delineated on an endocast); and (4) the presence of blood sinuses/vessels and other nervous structures that can obscure some brain parts and overestimate its size (e.g., Balanoff and Bever (2017) for a general review, and Benoit (2015) for how to account for this aspect in proboscideans).

In ventral view, there are major differences that mainly concern nerve pathways and exits. On endocasts, the cranial nerve pattern and blood vessel pathways can mainly be reconstructed via the foramina and fissures that pierce the different bones of the braincase (e.g., Muizon et al. 2015). This makes direct comparisons between endocranial cast and brain external morphology difficult. For instance, the shape of the olfactory bulb area differs between brain and endocasts because of the presence of the cribriform plate cast on the latter, making slight overestimation of olfactory bulb volume likely. The most striking difference concerns the optic nerve. On the cranial endocast of our hipposiderids, only the end of the intracranial course of the optic nerve is visible (either by the optic foramina or by the anterior part of the optic canal), and the location of the optic chiasma cannot be determined. On the brain illustrated by Baron et al. (1996), the optic chiasma reveals to be located more posteriorly than the exit of the optic nerve, close to the hypophysis. Another major difference apart from cranial nerve exits concerns the external morphology of the pons-medulla oblongata continuum: it is fully smooth on an endocast, whereas there are more details on the brain. However, these details do not guarantee to distinguish pons from medulla oblongata in other bat brains (Baron et al. 1996: figs. 51–56).

Cursory Glance at the Hipposiderid Brain Evolution

The general morphology of endocasts is similar in all four fossil hipposiderid species. They all show a similar morphology of the telencephalon in terms of neocortical fissuration and expansion, and of the general shape of the olfactory bulbs and pyriform lobes. They all exhibit protruding epiphysis and hypophysis, and a widely exposed mesencephalon with large, protruding caudal colliculi and subtle rostral colliculi. In all specimens, the metencephalon is wide, especially the cerebellum, which bears a wide and long vermis, a similar rough shape of cerebellar hemispheres, and large and protruding paraflocculi. The pattern of cranial nerve exits and basicranial foramina is also very conservative within the sample of fossil hipposiderid species described here, with a long sphenorbital fissure neither coalescent with the optic foramen nor with the round foramen. The external morphology of the brain of *H. diadema* as illustrated by Baron et al. (1996) indicates that this extant species also shares the same characteristics. Based on our observations, the general morphology therefore seems to be highly conservative within the hipposiderid family.

Concurrently with this general morphological conservatism through Cenozoic times, there is a stasis in EQ values in hipposiderid bats during the Paleogene/Neogene (Fig. 7 and ESM1: Figs. SI. 7–8). Since Eocene times, the EQ value of mammals generally increased with time (as postulated since Jerison (1973)), but it is apparently not the case in bats: the EQ of Eocene (or Oligocene for *H. (Ps.) schlosseri*) and Miocene hipposiderids is close to that of extant ones (Tables 3, 4, 5, and 6). EQ values of Eocene bats were closer to central values of other mammals, but this gap widened through time because of differential EQ evolution between bats and non-bat mammals. The global stasis in the EQ through time observed here in one chiropteran family may of course overlook mixed patterns of encephalization evolution across bat families. Be that as it may, this uncommon EQ stasis relative to other mammals, exemplified here by Hipposideridae, could be linked to the uncommon ecology of bats: their adaptations for flight and for echolocation (except for pteropodids) may have constrained the range of morpho-anatomo-functional variability of their brain (Safi et al. 2005).

The "principle/law of proper mass" defined by Jerison (1973:9) implies that "the relative masses of neural tissue (…) are related to the relative importance of the functions in the species." In fossil endocast studies, the relative volume of olfactory bulbs cast is generally linked to olfaction and to the importance of the sense of smell relative to other senses such as vision or audition (e.g., Jerison 1973; Takai et al. 2003; Silcox et al. 2009; Rowe et al. 2011; Gonzales et al. 2015; Bertrand et al. 2019). When olfactory bulb volume is plotted against brain volume (log-transformed data; Fig. 8a), the fossil hipposiderid bats fall within the morphospaces of extant bats (that of hipposiderids, rhinolophoids, and bats in general), suggesting a similar importance of olfaction in their behavior (and/or no difference through time). Regarding the paraflocculi, they are linked to the vestibuloocular reflex that stabilizes vision during movements (Ito 1982; Waespe et al. 1983; Paulin 1993; Rambold et al. 2002; Voogd and Wylie 2004). Recent studies used paraflocculi volumes (relying on the subarcuate fossa as a proxy) to discuss the degree of environment complexity during the evolution of sciuromorph rodents, assuming that a complex locomotor environment is related to gaze stabilization and thus large paraflocculi (Bertrand and Silcox 2016; Bertrand et al. 2018a, b). However, based on a sample of birds and mammals, Ferreira-Cardoso et al. (2017) did not find any correlation between parafloccular fossa volume and ecological traits, suggesting that this measure is not a reliable ecological proxy. This studies use a wide sample with

few representatives per group, but covers a broad range of ecological traits. Given the assumed role of paraflocculi in spatial movement, and following the principle of proper mass (Jerison 1973), large paraflocculi would be expected in bats given their complex locomotor behavior (3D and aerial environment). According to our results (Fig. 8b), there are no clear difference between bats and other mammals, or when comparing extant and fossil bats.

The general evolution of the macromorphology of our fossil endocasts is therefore congruent with the various measurements mentioned above, suggesting that the main characteristics of the hipposiderid brain are conserved through time. For instance, the prominence of the caudal colliculi clearly indicate a sophisticated echolocation as in extant bats (Baron et al. 1996; Voogd et al. 1998); the large cerebellum, similar to extant species, is also supposedly related to sophisticated echolocation and (at least) powered flight (Paulin 1993). This apparent general stasis in hipposiderid brain characteristics (previously proposed at the Chiroptera scale, but never tested; Dechaseaux 1956; Baron et al. 1996) is congruent with the paradigm that bats adapted very rapidly and very early during their evolutionary history (Simmons and Geisler 1998; Simmons et al. 2008) and then did not change much afterwards, except punctual new optima in some families, which is not the case of Hipposideridae (Amador et al. 2020). Furthermore, the lissencephalic telencephalon (with a limited expansion of the neocortex) and exposed mesencephalon made the brain of bats generally regarded as plesiomorphic within mammals (Dechaseaux 1956; Edinger 1963). However, these features could in fact be derived conditions (Edinger 1963; Kelava et al. 2013) that would have appeared early in Chiroptera evolution and would have been retained through time since at least the late Eocene given our detailed observations on fossil hipposiderid bats. This also raises questions about the ancestral morphology of bats brains and the very first steps of their evolutionary history.

Thorough Examination of the Hipposiderid Brain

Despite the general conservative morphology of the brain of hipposiderid bats described above, several differences are observed that can be interpreted in terms of phylogeny and/or evolutionary "grades" and/or allometry. Our sample is composed of two groups of two species: *Pa. oltina* and *Pa. quercyi* that belong to the genus *Palaeophyllophora* (Maitre 2014), sister taxon to the genus *Hipposideros* (Ravel et al. 2016; Fig. 1), and *H. (Ps.) schlosseri* and *H. (Ps.) bouziguensis* that belong to the same genus, *Hipposideros*, and to the same subgenus, *Pseudorhinolophus* (Maitre 2014). Differences observed between *Palaeophyllophora* and *Hipposideros* (*Pseudorhinolophus*) species are thus likely to be of phylogenetic interest. *Hipposideros (Pseudorhinolophus)* subgenus has been proposed to be a paraphyletic assemblage of stem species to the extant genus *Hipposideros*, with *H. (Ps.) bouziguensis* diverging earlier than *H. (Ps.) schlosseri* (Ravel et al. 2016; Fig. 1). Therefore, differences distinguishing *H. (Ps.) schlosseri* are also likely to be of phylogenetic interest. A further aspect is that *H. (Ps.) bouziguensis* is more recent than the three other species (i.e., early Miocene vs at least Paleogene, at most late Eocene; Fig. 1), but diverges earlier than *H. (Ps.) schlosseri* (Ravel et al. 2016). Thus, differences distinguishing *H. (Ps.) bouziguensis* from all other three species might be of temporal interest (i.e., "evolutionary grades"). Finally, size also varies a bit in this sample: *H. (Ps.) schlosseri* is the smallest species of our fossil sample, *Pa. oltina* is the largest, and *Pa. quercyi* and *H. (Ps.) bouziguensis* are of close intermediate size; such an ordination of differences is likely to be correlated to size and to be related to allometry.

Characters of Potential Phylogenetic Interest

Several characteristics differentiate *Palaeophyllophora* from *Hipposideros* (*Pseudorhinolophus*) and are likely to characterize both genera. These characters mainly concern the telencephalon area (Fig. 6a-d and 6h-k). *Hipposideros* (*Pseudorhinolophus*) has relatively smaller but also relatively higher and rounder olfactory bulbs, a wider angle of the orbitotemporal canal (Fig. 6h-k), a more marked sylvia but a less marked pseudosylvia, and more marked pyriform lobes; *Palaeophyllophora* species have more posteriorly located pyriform lobes. Regarding the diencephalon, the cast of the epiphysis (Fig. 6a-d) is also more marked in *Palaeophyllophora*. On the tectum of the mesencephalon, the shape and location of the rostral colliculi (Fig. 6a-d) make it possible to differentiate *Palaeophyllophora* species from *Hipposideros* fossil species described here: they are a little bit higher in *Hipposideros (Pseudorhinolophus)* and closer to each other and to the caudal colliculi (they are a bit more anterior in *Palaeophyllophora*, even closer to the epiphysis than to the caudal colliculi). The cerebellum (Fig. 6a-d) also allows one to distinguish the two genera: its anterior margin is more delineated in *Hipposideros* (*Pseudorhinolophus*), and the vermis and the cerebellar hemispheres are more aligned in this genus than in *Palaeophyllophora* (where the cerebellum is a bit more elongated and the cerebellar hemispheres are more anteriorly located relative to the vermis). Finally, cranial openings of the brain (Fig. 6e-g) also help to distinguish the two genera: (i) the optic foramina are much more anteriorly located in *H. (Ps.) bouziguensis* than in *Palaeophyllophora* species (this is tempered by the quite bizarre position of these foramina in *H. (Ps.) bouziguensis*), (ii) the sphenorbital fissures are closer to each other and more anteriorly located in *Hipposideros* (*Pseudorhinolophus*), they are also a bit shorter and bear a small anterior notch (which is absent in *Palaeophyllophora*), and (iii) the foramen magnum opens

more ventrally, whereas it opens more posteriorly in *Palaeophyllophora*. The telencephalic features observed in *H. (Ps.) bouziguensis* and *H. (Ps.) schlosseri* are also present in *H. diadema* (Fig. 9a and c). Other characteristics are difficult to compare finely between the brain of *H. diadema* and our endocast sample because the delineations of each part vary between an endocast and a brain, which is particularly true for exits of cranial nerves (see brain vs endocast comparisons above).

Potential Trends within Hipposideridae

The three Paleogene species and the Miocene species differ by some characters that might show a temporal pattern. Among these is the posterior extension of the suprasylvia (Fig. 6a-d), which is absent in *Pa. quercyi* and in *H. (Ps.) schlosseri*, only starts to elongate posteriorly in *Pa. oltina*, and elongates a bit more in *H. (Ps.) bouziguensis* and in *H. diadema*. The two latter, Neogene, taxa also have more protruding caudal colliculi and a more convex (Fig. 6h-k) and more folded vermis (especially with a VI-VII sulcus present additionally to the other sulci already present; Fig. 6a-d and 6h-k).

H. (Ps.) schlosseri is the smallest species of the four. It differs from other species by characters of the cerebellum: the vermis is shallower (Fig. 6h-k), the cerebellar hemispheres are narrower and less protruding, and the intercrual sulci are less marked (Fig. 6a-d). These differences could be related to allometry.

Congruency between Brain Morphology, the Temporal and the Phylogenetic Contexts

The phylogenetic context provided by Ravel et al. (2016) is rather robust: their matrix includes dental, cranial, and postcranial characters coded for a representative number of extinct hipposiderid taxa; their exact cladistic analysis retrieves a single parsimonious tree, and nodes have rather good support. However, of the four fossil species of our sample, two of them (*Pa. quercyi* and *H. (Ps.) schlosseri*) are only scored for dental characters and their phylogenetic position is therefore based on a single source of characters. On the other hand, the precise age of the specimens of these two species of our sample is unknown. Following Maitre (2014), *Pa. quercyi* is recorded from MP17a (early late Eocene, ~37 Mya) to MP22 (middle early Oligocene, ~31 Mya) and *H. (Ps.) schlosseri* is recorded from MP16 (late middle Eocene, ~38 Mya) to MP22. Given these uncertainties, other patterns of endocast morphological variation could be explained assuming different temporal and/or phylogenetic settings.

Regarding *H. (Ps.) schlosseri*, if swapping the relative positions of *H. (Ps.) schlosseri* and *H. (Ps.) bouziguensis* on the tree, all temporal characters distinguishing Paleogene vs Neogene fossil species would be regarded as phylogenetic characters (inducing a lot of changes at the *H. (Ps.) bouziguensis* – modern *Hipposideros* node).

In *Pa. quercyi*, several morphological characters distinguish this specimen from the others. For some characters, *Pa. quercyi* shows a morphological state and the three other species show another one: this pattern could be explained by a paraphyly of *Palaeophyllophora* with an early divergence of *Pa. quercyi*. These characters regard i) the olfactory bulbs (*Pa. quercyi* has the largest and longest of the sample; Table 1) and their lateral swelling (*Pa. quercyi* has the least developed of the sample; Fig. 6a-d); ii) the cerebrum, with a shallower anterior part of the rhinal fissure and a shallower sylvia (Fig. 6a-d and 6h-k), cerebral hemispheres much more separated, and less inflated lobes (reuniens, arcuate, and pyriform; Fig. 6h-k); and iii) the mesencephalon, which is the shallowest (tectum of mesencephalon is higher relative to cerebrum and cerebellum; Fig. 6h-k) and with caudal colliculi more rounded and farther from each other (Fig. 6a-d). For another character, *Pa. quercyi* shows a condition, while *Pa. oltina* and *H. (Ps.) schlosseri* show a second one, and *H. (Ps.) bouziguensis* shows a third one, reflecting a potential temporal pattern of morphological variation. This pattern is retrieved for the position of the orbitotemporal canal (more dorsally located in *Pa. quercyi*, a bit more lateral in *Pa. oltina* and *H. (Ps.) schlosseri*, and even more in *H. (Ps.) bouziguensis* and in *H. diadema*; Fig. 6a-d and 6h-k). The different hypotheses regarding these two morphological patterns are non-exclusive and could explain both patterns of morphological variation.

These various hypotheses are highly speculative but, given the uncertain temporal and phylogenetic context, such a set of morphological differences has to be taken into consideration and tentatively explained.

Conclusion

This work provides a revised nomenclature of the external structures of the Chiroptera brain and a detailed anatomical description of extinct hipposiderid bat endocranial casts. It constitutes the first thorough description of a chiropteran endocranial cast and sets the basis for future studies of this object at the ordinal scale. Generally, the new specimens described here greatly enhance our knowledge of brain macromorphology in fossil hipposiderid bats. Preliminary comparisons of extinct and extant hipposiderid bats brain external features indicate that, as previously proposed in the literature, endocranial casts are an accurate approximation of external features of the brain. Yet, some morphological traits such as cranial nerve pathways may not be fully reachable on endocranial cast. Based on our sample, the general morphology of the brain seems to be highly conservative within the hipposiderid family. Concurrently with this general morphological conservatism through Cenozoic times, there are no

noticeable changes for usual measurements of endocasts (EQ, olfactory bulb volume, paraflocculus volume). This apparent general homogeneity in hipposiderid brain characteristics is congruent with their general monotonous morphological diversity through time and may be linked to their conservative ecology. At a smaller scale, detailed comparisons further highlight several macromorphological features that could, for instance, separate *Palaeophyllophora* and *Hipposideros* genera. Fine anatomical characters, behind the global constant pattern and besides the reduced variation range induced by their ecological sophistication, could be of interest for tracking less apparent, maybe overlooked, but key morpho-anatomical evolution. These first results on fossil hipposiderid bat endocasts still rely on a small sample and a rather unclear phylogenetical context; future works at a wider scale and/or including extant species will allow for refining the different hypotheses proposed here.

Acknowledgements We thank L. Costeur (NMBS) for access to the collections. We are grateful to the MRI platform member of the national infrastructure France-BioImaging supported by the French National Research Agency (ANR-10-INBS-04, «Investments for the future»), the labex CEMEB (ANR-10-LABX-0004) and NUMEV (ANR-10-LABX-0020). We also acknowledge Nicolas Brualla for the segmentation of the *Pa. quercyi* endocast and Romain Weppe for fruitful comments on the figures. Finally, we acknowledge two anonymous reviewers for their fruitful comments. This is ISEM publication 2020-252.

Funding This work was, in part, financially supported by the ANR program DEADENDER (ANR-18-CE02–0003-01) headed by M. J. Orliac.

Compliance with Ethical Standards

Competing Interests The authors declare having no competing interests.

References

Alba DM (2010) Cognitive inferences in fossil apes (Primates, Hominoidea): does encephalization reflect intelligence? J Anthropol Sci 88:11–48

Amador LI, Almeida FC, Giannini NP (2020) Evolution of traditional aerodynamic variables in bats (Mammalia: Chiroptera) within a comprehensive phylogenetic framework. J Mammal Evol 27:549–561

Amador LI, Moyers Arévalo RL, Almeida FC, Catalano SA, Giannini NP (2018) Bat systematics in the light of unconstrained analyses of a comprehensive molecular supermatrix. J Mammal Evol 25:37–70. https://doi.org/10.1007/s10914-016-9363-8

Anthony R, Grzybowski J de (1934) Le Neopallium du Boeuf. Etude de son Développement et Interprétation de ses Plissements. J Anat 68: 558–70

Balanoff AM, Bever GS (2017) 1.10 The role of endocasts in the study of brain evolution. In: Kaas JH (ed) Evolution of Nervous Systems, 2nd ed. Academic Press, Oxford, pp 223–241

Baron G, Stephan H, Frahm HD (eds) (1996) Comparative Neurobiology in Chiroptera. Birkhäuser Verlag, Basel

Barone R, Bortolami R (eds) (2004) Anatomie comparée des mammifères domestiques : Tome 6, Neurologie I, Système nerveux central. Vigot, Paris

Benoit J (2015) A new method of estimating brain mass through cranial capacity in extinct proboscideans to account for the non-neural tissues surrounding their brain. J Vertebr Paleontol 35:e991021. https://doi.org/10.1080/02724634.2014.991021

Benoit J, Crumpton N, Mérigeaud S, Tabuce R (2013) A memory already like an elephant's? The advanced brain morphology of the last common ancestor of Afrotheria (Mammalia). Brain Behav Evol 81:154–169. https://doi.org/10.1159/000348481

Bertrand OC, Amador-Mughal F, Lang MM, Silcox MT (2018a) New virtual endocasts of Eocene Ischyromyidae and their relevance in evaluating neurological changes occurring through time in Rodentia. J Mammal Evol 26:345–371. https://doi.org/10.1007/s10914-017-9425-6

Bertrand OC, Amador-Mughal F, Lang MM, Silcox MT (2018b) Virtual endocasts of fossil Sciuroidea: brain size reduction in the evolution of fossoriality. Palaeontology 61:919–948. https://doi.org/10.1111/pala.12378

Bertrand OC, Shelley SL, Wible JR, Williamson TE, Holbrook LT, Chester SGB, Butler IB, Brusatte SL (2019) Virtual endocranial and inner ear endocasts of the Paleocene 'condylarth' *Chriacus* : new insight into the neurosensory system and evolution of early placental mammals. J Anat 236:21–49. https://doi.org/10.1111/joa.13084

Bertrand OC, Silcox MT (2016) First virtual endocasts of a fossil rodent: *Ischyromys typus* (Ischyromyidae, Oligocene) and brain evolution in rodents. J Vertebr Paleontol 36. https://doi.org/10.1080/02724634.2016.1095762

Bhatnagar KP, Smith TD, Rai SN, Frahm HD (2016) The chiropteran brain database: volumetric survey of the hypophysis in 165 species. Anat Rec 299:492–510. https://doi.org/10.1002/ar.23321

Brown EE, Cashmore DD, Simmons NB, Butler RJ (2019) Quantifying the completeness of the bat fossil record. Palaeontology 62:757–776. https://doi.org/10.1111/pala.12426

Chambers JM, Hastie TJ (eds) (1991) Statistical Models in S. Chapman & Hall/CRC, London

Da Cruz A (2015) Photofiltre 7 [Computer Software]. Retrieved from http://www.photofiltre.com/

Dechaseaux C (1956) L'encéphale des mammifères volants. Colloq Int Cent Natl Rech Sci 80:51–58

Dechaseaux C (1962) Cerveaux d'animaux disparus. Masson et Cie, Paris

Dechaseaux C (1970) Récents résultats en paléoneurologie. Bull Académie Société Lorraines des Sci 9:223–232

Dechaseaux C (1973) Essais de paléoneurologie. Ann Paléontol 59:8–132

Dow RS (1942) The evolution and anatomy of the cerebellum. Biol Rev 17:179–220. https://doi.org/10.1111/j.1469-185X.1942.tb00437.x

Dunn OJ (1964) Multiple comparisons using rank sums. Technometrics 6:241. https://doi.org/10.2307/1266041

Edinger T (1926) Fossile Fledermausgehirne. Senckenbergiana 8:1–16

Edinger T (1929) Die fossilen Gehirne. Ergeb Anat Entwicklungsgesch 28:1–249

Edinger T (1949) Paleoneurology vs comparative brain anatomy. Confin Neurol 9:5–24

Edinger T (1961) Fossil brains reflect specialized behavior. World Neurol 2:934–41

Edinger T (1963) Meanings of midbrain exposure, past and present. In: XVI International Congress of Zoology, pp 225–228

Edinger T (1964a) Midbrain exposure and overlap in mammals. Am Zool 4:5–19. https://doi.org/10.2307/3881308

Edinger T (1964b) Recent advances in paleoneurology. Prog Brain Res 6: 147–160. https://doi.org/10.1016/S0079-6123(08)63721-8

Eisenberg JF, Wilson DE (1978) Relative brain size and feeding strategies in the Chiroptera. Evolution 32:740–751. https://doi.org/10.2307/2407489

Eiting TP, Gunnell GF (2009) Global completeness of the bat fossil record. J Mammal Evol 16:151–173. https://doi.org/10.1007/s10914-009-9118-x

Felsenstein J (1985) Phylogenies and the comparative method. Am Nat 125:1–15

Ferreira-Cardoso S, Araújo R, Martins NE, Martins GG, Walsh S, Martins RMS, Kardjilov N, Manke I, Hilger A, Castanhinha R (2017) Floccular fossa size is not a reliable proxy of ecology and behaviour in vertebrates. Sci Rep 7:2005. https://doi.org/10.1038/s41598-017-01981-0

Fisher SRA (1970) Statistical Methods for Research Workers, 14th ed. Oliver and Boyd, Edinburgh

Foley NM, Goodman SM, Whelan CV, Puechmaille SJ, Teeling EC (2017) Towards navigating the Minotaur's labyrinth: cryptic diversity and taxonomic revision within the speciose genus *Hipposideros* (Hipposideridae). Acta Chiropterol 19:1–18. https://doi.org/10.3161/15081109ACC2017.19.1.001

Foley NM, Thong VD, Soisook P, Goodman SM, Armstrong KN, Jacobs DS, Puechmaille SJ, Teeling EC (2015) How and why overcome the impediments to resolution: lessons from rhinolophid and hipposiderid bats. Mol Biol Evol 32:313–333. https://doi.org/10.1093/molbev/msu329

Friant M (1932) L'influence de la taille sur la morphologie des dents chez les mammifères. La Terre la Vie 135–144

Friant M (1954) Le cerveau du Lamantin (*Manatus inunguis* Natterer). Vierteljahrsschrift der Naturforschenden Gesellschaft Zürich 99:129–135

Giannini NP, Wible JR, Simmons NB (2006) On the cranial osteology of Chiroptera. I. *Pteropus* (Megachiroptera: Pteropodidae). Bull Am Mus Nat Hist 295:1–134. https://doi.org/10.1206/0003-0090(2006)295[0001:OTCOOC]2.0.CO;2

Gingerich PD (2016) Body weight and relative brain size (encephalization) in Eocene Archaeoceti (Cetacea). J Mammal Evol 23:17–31. https://doi.org/10.1007/s10914-015-9304-y

Gonzales LA, Benefit BR, McCrossin ML, Spoor F (2015) Cerebral complexity preceded enlarged brain size and reduced olfactory bulbs in Old World monkeys. Nat Commun 6:7580. https://doi.org/10.1038/ncomms8580

Grafen A (1989) The phylogenetic regression. Philos Trans R Soc B Biol Sci 326:119–157. https://doi.org/10.1098/rstb.1989.0106

Hand SJ, Kirsch JAW (2003) *Archerops*, a new annectent hipposiderid genus (Mammalia : Microchiroptera) from the Australian Miocene. J Paleontol 77:1139–1151. https://doi.org/10.1666/0022-3360(2003)077<1139:AANAHG>2.0.CO;2

Hollander M, Wolfe DA (1973) Nonparametric Statistical Methods. John Wiley & Sons, New York

Horikawa J, Suga N (1986) Biosonar signals and cerebellar auditory neurons of the mustached bat. J Neurophysiol 55:1247–1267. https://doi.org/10.1152/jn.1986.55.6.1247

Inkscape Project (2018) Inkscape [Computer software]. Retrieved from https://inkscape.org/

Ito M (1982) Cerebellar control of the vestibulo-ocular reflex–around the flocculus hypothesis. Annu Rev Neurosci 5:275–297. https://doi.org/10.1146/annurev.ne.05.030182.001423

Jerison HJ (1973) Evolution of the Brain and Intelligence. Academic Press, New York

Jolicoeur P, Pirlot P, Baron G, Stephan H (1984) Brain structure and correlation patterns in Insectivora, Chiroptera, and Primates. Syst Biol 33:14–29. https://doi.org/10.1093/sysbio/33.1.14

Jones KE, Bininda-Emonds ORP, Gittleman JL (2005) Bats, clocks, and rocks: diversification patterns in Chiroptera. Evolution 59:2243–2255. https://doi.org/10.1554/04-635.1

Kelava I, Lewitus E, Huttner WB (2013) The secondary loss of gyrencephaly as an example of evolutionary phenotypical reversal. Front Neuroanat 7:1–9. https://doi.org/10.3389/fnana.2013.00016

Kochetkova VI (1978) The subject matter of paleoneurological studies. In: Kochetkova VI, Jerison HJ, Jerison I (eds) Paleoneurology. V. H. Winston & Sons, Washington, D.C., pp 17–45

Kruskal WH, Wallis WA (1952) Use of ranks in one-criterion variance analysis. J Am Stat Assoc 47:583–621. https://doi.org/10.1080/01621459.1952.10483441

Larsell O, Dow RS (1935) The development of the cerebellum in the bat (*Corynorhinus* sp.) and certain other mammals. J Comp Neurol 62:443–468. https://doi.org/10.1002/cne.900620210

Lebrun R (2018) MorphoDig, an open-source 3D freeware dedicated to biology

Legendre S (1982) Hipposideridae (Mammalia: Chiroptera) from the Mediterranean middle and late Neogene, and evolution of the genera *Hipposideros* and *Asellia*. J Vertebr Paleontol 2:372–385. https://doi.org/10.1080/02724634.1982.10011939

Maitre E (2014) Western European middle Eocene to early Oligocene Chiroptera: systematics, phylogeny and palaeoecology based on new material from the Quercy (France). Swiss J Palaeontol 133:141–242. https://doi.org/10.1007/s13358-014-0069-3

Mein P (1975) Résultats du groupe de travail des vertébrés: biozonation du Neogène méditerranéen à partir des mammifères. In: Senes J (ed) Report on Activity of the RCMNS (Regional Committee on Mediterranean Neogene Stratigraphy) Working Groups (1971–1975). Bratislava, pp 78–81

Millien V, Bovy H (2010) When teeth and bones disagree: body mass estimation of a giant extinct rodent. J Mammal 91:11–18. https://doi.org/10.1644/08-MAMM-A-347R1.1.Key

Muizon C de, Billet G, Argot C, Ladevèze S, Goussard F (2015) *Alcidedorbignya inopinata*, a basal pantodont (Placentalia, Mammalia) from the early Palaeocene of Bolivia: anatomy, phylogeny and palaeobiology. Geodiversitas 37:397–631. https://doi.org/10.5252/g2015n4a1

Neubauer S (2014) Endocasts: possibilities and limitations for the interpretation of human brain evolution. Brain Behav Evol 84:117–134. https://doi.org/10.1159/000365276

Nieuwenhuys R (1998) Morphogenesis and general structure. In: Nieuwenhuys R, ten Donkelaar HJ, Nicholson C (eds) The Central Nervous System of Vertebrates. Springer Berlin Heidelberg, Berlin, Heidelberg, pp 159–228

Nomina Anatomica Veterinaria (NAV) (2017) International Committee on Veterinary Gross Anatomical Nomenclature (I.C.V.G.A.N.), 6th edn. The Editorial Committee with permission of the World Association of Veterinary Anatomists (W.A.V.A.), Hanover (Germany), Ghent (Belgium), Columbia, MO (USA), Rio de Janeiro (Brazil)

Ogle DH, Wheeler P, Dinno A (2019) FSA: Fisheries Stock Analysis. R package version 0.8.30.9000, https://github.com/droglenc/FSA

Orliac MJ, Gilissen E (2012) Virtual endocranial cast of earliest Eocene *Diacodexis* (Artiodactyla, Mammalia) and morphological diversity of early artiodactyl brains. Proc R Soc B Biol Sci 279:3670–3677. https://doi.org/10.1098/rspb.2012.1156

Orliac MJ, O'Leary MA (2014) Comparative anatomy of the petrosal bone of dichobunoids, early members of Artiodactylamorpha (Mammalia). J Mammal Evol 21:299–320. https://doi.org/10.1007/s10914-014-9254-9

Orlov YA (ed) (1961) В мире древних животных (In the ancient animal kingdom). Publishing House of the Academy of Sciences of the USSR, Moscow

Paulin MG (1993) The role of the cerebellum in motor control and perception. Brain Behav Evol 41:39–50. https://doi.org/10.1159/000113822

R Core Team (2018) R: A Language and Environment for Statistical Computing. R Foundation for Statistical Computing, Vienna. https://www.r-project.org/

Rambold H, Churchland A, Selig Y, Jasmin L, Lisberger SG (2002) Partial ablations of the flocculus and ventral paraflocculus in monkeys cause linked deficits in smooth pursuit eye movements and adaptive modification of the VOR. J Neurophysiol 87:912–924. https://doi.org/10.1152/jn.00768.2000

Ramdarshan A, Orliac MJ (2016) Endocranial morphology of *Microchoerus erinaceus* (Euprimates, Tarsiiformes) and early evolution of the Euprimates brain. Am J Phys Anthropol 159:5–16. https://doi.org/10.1002/ajpa.22868

Ravel A, Adaci M, Bensalah M, Charruault AL, Essid EM, Ammar HK, Marzougui W, Mahboubi M, Mebrouk F, Merzeraud G, Vianey-Liaud M, Tabuce R, Marivaux L (2016) Origine et radiation initiale des chauves-souris modernes : nouvelles découvertes dans l'Éocène d'Afrique du Nord. Geodiversitas 38:355–434. https://doi.org/10.5252/g2016n3a3

Rowe TB, Macrini TE, Luo Z-X (2011) Fossil evidence on origin of the mammalian brain. Science 332:955–957. https://doi.org/10.1126/science.1203117

Royston P (1995) Remark AS R94: a remark on algorithm AS 181: the W-test for normality. Appl Stat 44:547. https://doi.org/10.2307/2986146

RStudio Team (2016) RStudio: Integrated Development Environment for R. RStudio, PBC, Boston. http://www.rstudio.com/

Safi K, Seid MA, Dechmann DKN (2005) Bigger is not always better: when brains get smaller. Biol Lett 1:283–286. https://doi.org/10.1098/rsbl.2005.0333

Schmidt-Kittler N (ed) (1987) International Symposium on Mammalian Biostratigraphy and Palaeoecology of the European Paleogene-Mainz, February 18th–21st 1987. Münchner Geowissenschaftliche Abhandlungen A 10:1–312

Schneider CA, Rasband WS, Eliceiri KW (2012) NIH Image to ImageJ: 25 years of image analysis. Nat Methods 9:671–675. https://doi.org/10.1038/nmeth.2089

Shapiro SS, Wilk MB (1965) An analysis of variance test for normality (complete samples). Biometrika 52:591–611. https://doi.org/10.1093/biomet/52.3-4.591

Shi JJ, Rabosky DL (2015) Speciation dynamics during the global radiation of extant bats. Evolution 69:1528–1545. https://doi.org/10.1111/evo.12681

Shultz S, Dunbar R (2010) Encephalization is not a universal macroevolutionary phenomenon in mammals but is associated with sociality. Proc Natl Acad Sci USA 107:21582–21586. https://doi.org/10.1073/pnas.1005246107

Sigé B (1968) Les Chiroptères du Miocène inférieur de Bouzigues. 1-Etude systématique. Palaeovertebrata 1:65–133. https://doi.org/10.18563/pv.1.3.65-133

Sigé B, Crochet J-Y, Sudre J, Aguilar JP, Escarguel G (1997) Nouveaux sites d'âges variés dans les remplissages karstiques du Miocène inférieur de Bouzigues (Hérault, Sud de la France). Geobios 30:477–483. https://doi.org/10.1016/S0016-6995(97)80054-X

Silcox MT, Benham AE, Bloch JI (2010) Endocasts of *Microsyops* (Microsyopidae, Primates) and the evolution of the brain in primitive primates. J Hum Evol 58:505–521. https://doi.org/10.1016/j.jhevol.2010.03.008

Silcox MT, Dalmyn CK, Bloch JI (2009) Virtual endocast of *Ignacius graybullianus* (Paromomyidae, Primates) and brain evolution in early primates. Proc Natl Acad Sci USA 106:10987–10992. https://doi.org/10.1073/pnas.0812140106

Simmons NB (2000) Bat phylogeny: an evolutionary context for comparative studies. In: Adams RA, Pedersen SC (eds) Ontogeny, Functional Ecology, and Evolution of Bats. Cambridge University Press, New-York, pp 9–58

Simmons NB (2005) Chiroptera. In: Rose KD, Archibald JD (eds) The Rise of Placental Mammals. John Hopkins University Press, Baltimore, pp 159–174

Simmons NB, Geisler JH (1998) Phylogenetic relationships of *Icaronycteris*, *Archaeonycteris*, *Hassianycteris*, and *Palaeochiropteryx* to extant bat lineages, with comments on the evolution of echolocation and foraging strategies in Microchiroptera. Bull Am Mus Nat Hist 235:1–182

Simmons NB, Seymour KL, Habersetzer J, Gunnell GF (2008) Primitive early Eocene bat from Wyoming and the evolution of flight and echolocation. Nature 451:818–821. https://doi.org/10.1038/nature06549

Smith GE (1902a) On the homologies of the cerebral sulci. J Anat Physiol 36:309–319

Smith GE (1902b) The primary subdivision of the mammalian cerebellum. J Anat Physiol 36:381–5

Smith RJ (2002) Estimation of body mass in paleontology. J Hum Evol 43:271–287. https://doi.org/10.1006/jhev.2002.0573

Takai M, Shigehara N, Egi N, Tsubamoto T (2003) Endocranial cast and morphology of the olfactory bulb of *Amphipithecus mogaungensis* (latest middle Eocene of Myanmar). Primates 44:137–144. https://doi.org/10.1007/s10329-002-0027-3

Teeling EC (2009) Bats (Chiroptera). In: Hedges SB, Kumar S (eds) The Timetree of Life. Oxford University Press, New York, pp 499–503

Teeling EC, Madsen O, Van Den Bussche RA, De Jong WW, Stanhope MJ, Springer MS (2002) Microbat paraphyly and the convergent evolution of a key innovation in Old World rhinolophoid microbats. Proc Natl Acad Sci USA 99:1431–1436. https://doi.org/10.1073/pnas.022477199

Teeling EC, Scally M, Kao DJ, Romagnoli ML, Springer MS, Stanhope MJ (2000) Molecular evidence regarding the origin of echolocation and flight in bats. Nature 403:188–192. https://doi.org/10.1038/35003188

Tukey JW (1949) Comparing individual means in the analysis of variance. Biometrics 5:99. https://doi.org/10.2307/3001913

van Dongen PAM (1998) Brain size in vertebrates. In: Nieuwenhuys R, ten Donkelaar HJ, Nicholson C (eds) The Central Nervous System of Vertebrates. Springer Berlin Heidelberg, Berlin, Heidelberg, pp 2099–2134

Voogd J, Nieuwenhuys R, van Dongen PAM, ten Donkelaar HJ (1998) Mammals. In: Nieuwenhuys R, ten Donkelaar HJ, Nicholson C (eds) The Central Nervous System of Vertebrates. Springer Berlin Heidelberg, Berlin, Heidelberg, pp 1637–2097

Voogd J, Wylie DRW (2004) Functional and anatomical organization of floccular zones: a preserved feature in vertebrates. J Comp Neurol 470:107–112. https://doi.org/10.1002/cne.11022

Waespe W, Cohen B, Raphan T (1983) Role of the flocculus and paraflocculus in optokinetic nystagmus and visual-vestibular interactions: effects of lesions. Exp Brain Res 50. https://doi.org/10.1007/BF00238229

Wilson LAB, Hand SJ, López-Aguirre C, Archer M, Black KH, Beck RMD, Armstrong KN, Wroe S (2016) Cranial shape variation and phylogenetic relationships of extinct and extant Old World leaf-nosed bats. Alcheringa An Australas J Palaeontol 40:509–524. https://doi.org/10.1080/03115518.2016.1196434

Yao L, Brown J-P, Stampanoni M, Marone F, Isler K, Martin RD (2012) Evolutionary change in the brain size of bats. Brain Behav Evol 80:15–25. https://doi.org/10.1159/000338324

Part Two

Widening the frame of bats endocranial evolution: sampling characters and methodology

I) Introduction

The work of Maugoust & Orliac (2021; Part One) illustrates the existing gap between our understanding of bat paleoneurology and of comparative neurobiology. They also analyze the evolution of the encephalization quotient (EQ) over time, a metric widely used to describe animal "intelligence" and cognition (Jerison 1973). Finally, they contrast the log mass of two brain parts (the olfactory bulbs and the paraflocculi) against the total log brain mass. Maugoust & Orliac (2021) find a general morphological homogeneity in the fossil hipposiderids they describe, but also in the only available extant species illustrated in the literature (Baron et al. 1996). They also find that the EQ did not vary through time in this family when considering fossil species, and the relative brain part masses of the studied fossil species fall within or near the morphospace of their extant representatives. These implications are interesting and support the results of Yao et al. (2012) on hipposiderids that contradict other neontological works proposing a generalized decrease of relative brain mass in bats (Safi et al. 2005, Thiagavel et al. 2018), and especially in hipposiderid bats (Niven 2005). Such implications are however limited to the family Hipposideridae. The aim of this thesis is to propose a general picture of brain evolution, at the ordinal scale. Therefore, after having set and used first methodological adjustments to be able to deal with bat endocasts, I intend to describe the methods I will use and to make them generalizable to the whole Chiroptera order. These methodological adjustments closely follow and try to correct two major limits of current paleoneurological studies (as exposed throughout the general Introduction).

The first limit concerns the obligatory dialog that has to exist between paleoneurology and comparative neurobiology: as already emphasized by Edinger (1949), paleoneurology highly relies on the advances made in comparative neurobiology. However, there have been no studies dealing with the external morpho-anatomy of the brain of fossil bats since the works of Dechaseaux in the 1970's (Dechaseaux 1970, 1973). The paleoneurological works until those quoted were tightly linked with the progress of bat comparative neurobiology (e.g., Dechaseaux 1970). However, bat comparative neurobiology knowledge continued to expand with time, with some works at general (Schneider 1957) or more focused taxonomic scales (Schneider 1966 in the pteropodid *Rousettus*, McDaniel 1976 in phyllostomids). The latest major work is the comparative neurobiology atlas of Baron et al. (1996). To update the knowledge of bat paleoneurology by taking into account the progresses of bat comparative neurobiology is thus a mandatory step. Solving this point is, however, insufficient. Indeed, if bats species have been compared with each other, there are little comparisons with other mammals (generally, there are mostly quantitative comparisons with insectivorans). This lack of broad integration of the cerebral morphology is particularly needed regarding the few neopallial foldings: apart from the short descriptions of Schneider (1957) and Baron et al. (1996), there is no discussion about the homology of neopallial sulci. Solving this point would complete the available knowledge in bat comparative neurobiology. Furthermore, endocranial structures are not only brain tissues; there are other soft-tissued structures, mostly of vascular nature. In this case, other works are needed regarding the comparative anatomy of the bat skull and head. There are, however, few works regarding that point. Some works regarding blood circulation in the head of bats are available, but date from the XIXth/XXth centuries' boundary (Tandler 1899, Grosser 1901); if there are no reasons why these works would be wrong, terms used evolved since these times, and some observations may be irrelevant, lacking, or erroneous due to the context of knowledge of these times. There are also only few works, though thoroughly discussed, that deal with the course of the internal carotid artery (Wible 1987), the identification of the homologies of bony structures in pteropodids (Giannini et al. 2006), and the chiropteran basicranium ontogeny (Wible & Davis

2000). In these works, some elements are useful while dealing with the endocranial morpho-anatomy, but this remains an incomplete corpus of knowledge for clearly summarizing the whole endocast anatomy at the whole Chiroptera scale. I therefore gather as much of the previous works I can (with works at the mammalian level, and also veterinary and medical works), and tentatively emend and expand the nomenclatural work I performed in the case of hipposiderids endocasts (Part One). The aim of this is double. A first goal is to propose first hypotheses and homologies for brain and endocranial structures. Second, and waiting corrections arising from the first point, this nomenclature aims to set a standard for morphological description of the endocast at the whole Chiroptera order level.

A second major limitiation in modern paleoneurology regards the general statistical treatment for describing brain evolution. In this limit, there are actually two major points that need improvements: the metrics used and their subsequent statistical treatment. The metrics used to describe the quantitative evolution of "fossil brains" concern the whole endocast (interpreting the endocranial volume as the brain mass) and the volumes of protruding parts, that are the olfactory bulbs and the paraflocculi in bats. The evolution of the brain mass is always expressed relatively to the whole body mass, in order to account for allometric scaling of the brain. There are many existing metrics, the most used being the encephalization quotient (EQ) of Jerison (1973) that is as the ratio of the observed brain mass over an expected (i.e., allometric) brain mass. The formulas for calculating this expected brain mass are multiples (e.g., Eisenberg & Wilson 1978, Martin 1990, van Dongen 1998, Ni et al. 2019) and aim to better take into account a confounding effect (sampling, particularity of a group, phylogenetic or metabolic effects etc). Recently, several authors instead used direct residuals of the regression of log brain mass against log body mass, and generally correlated them to ecological effects (e.g., Jones & MacLarnon 2004). This procedure is also used for brain part masses (i.e., residuals of log brain part mass vs log total brain mass), sometimes expressed as "progression indices", that are ratios of relative brain part mass of a given species over that of a reference species (e.g., Jolicoeur et al. 1984). Finally, there are also (non-chiropteran) works comparing the relative brain or brain part mass among species, without phylogenetic correction (e.g., Bertrand et al. 2018). The commonly used metrics and/or their common treatment is however statistically incorrect and is likely to lead to errors, both because of the metrics themselves (e.g., the EQ) or of the statistical treatment (e.g., statistical operations on ratios or on residuals). I therefore review the metrics available to quantitatively describe endocasts, and I discuss their limits. As the statistical treatment is generally poor, and often lacks phylogenetic correction, I simply show why it is important to use the powerful toolkits of phylogenetic comparative methods ('PCM'). However, many methods exist, with as many aims and goals; I quickly review the rationales and the way these methods are applied, considering their advantages and drawbacks. I then expose and explain a method I chose to follow, and the tools available with its implementation. Finally, I describe the statistical treatment I will follow using this PCM, explaining how the statistical points help answering to biological and/or methodological questions.

II) Nomenclature and homologies of the chiropteran endocranial cast

Maugoust & Orliac (2021) proposed a nomenclature of the endocranial cast structures in bats, at least at the Hipposideridae scale (see Part One, pp. 44-48). An updated and augmented version of this nomenclature is here provided, given the broader phylogenetic scale this nomenclature aims (i.e., the Chiroptera order).

Schneider (1957) describes the external aspect of the brain of several chiropteran species of various families (pteropodids, rhinolophids, phyllostomids, etc.) and summarizes its descriptions at the order scale, both regarding the brain macromorphology and the "cranio-cerebral topography" (which corresponds to the endocranial cast morphology in that work). Schneider (1966) also describes the brain of *Rousettus aegyptiacus* in detail and provides outstanding high quality representations and descriptions of the brain together with a three-dimensional stereotaxic atlas (in transversal plane, as in other stereotaxic atlases published since [Schneider 1966, Baron et al. 1996, Bhatnagar 2008, Scalia et al. 2013, Washington et al. 2018, Radtke-Schuller et al. 2020], but also in parasagittal and in horizontal planes). Schneider's descriptions and figures are a tremendous contribution and are indubitably helpful regarding brain external morphology and endocranial casts studies. Actually, studies establishing the correspondence between soft tissues of the cranial cavity and the soft tissues leaving an impression on the inner face of that cranial cavity are incredibly rare. Comparative neurobiology studies often study brain in "too much" details to be directly applied to paleoneurology; internal structures of the brain cannot be studied in paleoneurology. Works such as those of Schneider (1957, 1966) therefore bridge a gap between comparative neurobiology and comparative anatomy of endocranial casts.

Henson (1970) reviews previous works on bat brains, providing supplementary illustrations (with a megachiropteran bat, *Eidolon helvum*, and a microchiropteran one, *Macronycteris gigas*) and summarizing what is known of bat brains, both in terms of macro- and micromorphology. McDaniel (1976) also describes extensively the external morphology of the brain of phyllostomid bats - even if it concerns one particular group in my clade of interest, its methodology may stand. Hackethal (1981) reviews what has been done regarding the cerebral and cerebellar morphology in whole mammals, order by order; if its discussion about the cerebral morphology in bats is a summary and a discussion of the previous works, his work about cerebellar morphology is way more complete, with numerous figures and an impressive anatomical content discussed family by family. These works highly complete the review of Baron et al. (1996, the main work used for bats brain by Maugoust & Orliac [2021]), who compiled a large dataset of brain metrics and shortly discussed about the brain of bats in an evolutionary framework. Unfortunately, Baron et al. (1996) described the external morphology of the brain to a quite lesser extent compared to the previously cited references.

Thus, I take as a starting point the nomenclature of Maugoust & Orliac (2021) and I modify it following mainly Schneider (1957, 1966), Henson (1970) and Hackethal (1981) for the identification of the cerebral structures, and I use Anglicized terms of the Nomina Anatomica Veterinaria (NAV, 2017) or of the Latin terms of the previously cited articles if missing in the NAV.

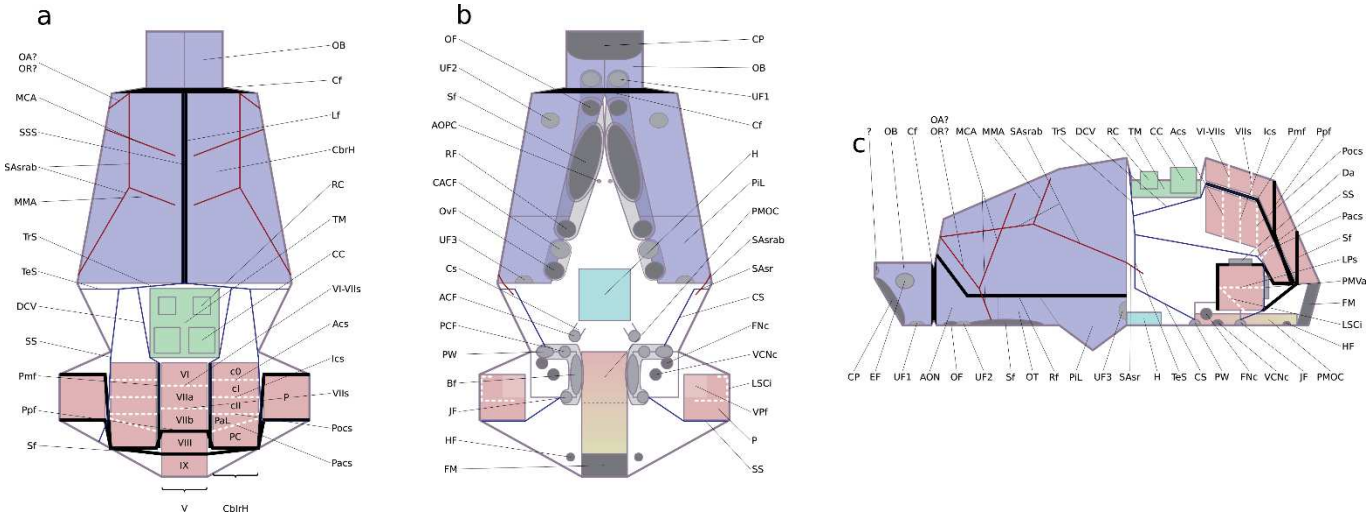

Figure II-1: Simplified scheme of the structures found on an chiropteran endocranial cast, excepting the neopallial sulci (see Fig. II-5) in dorsal (a), ventral (b) and lateral (c) views. Abbreviations of general various brain structures: AON: Anterior Olfactory Nuclei / CblrH: Cerebellar Hemisphere / CbrH: Cerebral Hemisphere / CC: Caudal Colliculi / Cf: Circular fissure / FNc: Facial Nerve cast / H: Hypophysis / Lf: Longitudinal fissure / OB: Olfactory Bulb / OT: Olfactory Tubercle / P: Paraflocculus / PiL: Piriform Lobe / PMOC: Pons-Medulla Oblongata Continuum / RC: Rostral Colliculi / Rf: Rhinal fissure / TM: Tectum of Mesencephalon / V: Vermis / VCNc: Vestibulo-Cochlear Nerve cast. Abbreviations of cerebellar lobules and foldings: Acs: Anterocrural sulcus / c0: crus 0 / cI: crus I / cII: crus II / PC: pyramidal copula / Ics: Intercrural sulcus / IX: Lobule IX = Uvula / LPs: Lateral Paraflocular sulcus / LSCi: Lateral Semicircular Canal impression / Pacs: Paracrural sulcus / PaL: Paramedian Lobule / Pmf: Paramedian fissure / Pocs: Posterocrural sulcus / Ppf: Prepyramidal fissure / Sf: Secondary fissure / VI: Lobule VI = Declive / VIIa: Lobule VIIa = Tuber Vermis / VIIb: Lobule VIIb = Folium Vermis / VIII: Lobule VIII = Pyramis / VIIs: VII sulcus / VI-VIIs: VI-VII sulcus / VPf: Ventral Paraflocular fossa. Abbreviations of vascular structures: CS: Communicant Sinus / DCV: Dorsal Cerebellar Vein / MCA: Middle Cerebral Artery / MMA: Middle Meningeal Artery / OA?OR?: may be cast of Ophthalmic Artery or Orbital Ramus of the maxillary artery / SAsr: Stapedial Artery - superior ramus / SAsrab: Stapedial Artery - superior ramus - anterior branch / SS: Sigmoid Sinus / SSS: Superior Sagittal Sinus / TeS: Temporal Sinus / TrS: Transverse Sinus. Abbreviations of endocranial apertures: ?: Unknown aperture / ACF: Anterior Carotid Foramen / Bf: Basicochlear fissure / CACF: Caudal Alisphenoid Canal Foramen / CP: Cribriform Plate of the ethmoid / Cs: Carotid sulcus / Da: Dorsal aperture on the paraflocculus / EF: Ethmoidal Foramen / FM: Foramen Magnum / HF: Hypoglossal Foramen / JF: Jugular Foramen / OF: Optic Foramen / OvF: Oval Foramen / PCF: Posterior Carotid Foramen / PMVa: PosteroMedioVentral aperture on the paraflocculus / POPC: Posterior Opening of the Pterygoid Canal / PW: Pyriform Window / RF: Round Foramen / SF: Sphenorbital Fissure / UF1: Unknown Foramen #1 / UF2: Unknown Foramen #2 / UF3: Unknown Foramen #3.

II.1) Emendatum to: Major components of the chiropteran brain observed on endocasts (Fig. II-1)

In the telencephalon, the paleopallium is composed of (e.g., Pigache 1970): the olfactory bulbs at the anterior extremity of the telencephalon; the anterior olfactory nuclei (“regio retrobulbaris” in Schneider [1966]) which are the visible part of the olfactory peduncles (Cleland & Linster 2019); the olfactory tubercles; the piriform lobes (“pseudotemporallappen” in Schneider [1966]). According to Schneider (1957), the rhinal fissure is only embodied by the circular fissure, and the imprint on the lateral aspect of the cerebral hemisphere often identified as the rhinal fissure is in fact a vascular impression. However, by looking carefully at Schneider’s transversal sections (Schneider 1957, 1966), one can notice that he spotted the rhinal fissure a bit dorsally to a slight impression, where there seems to be a change in the nature of the pallium. For this reason, I do not follow Schneider’s (1957) assumption (see also the Neopallial foldings section) and I assume that a rhinal fissure can be detected on endocasts by a depression.

In the diencephalon, taking into account the thorough descriptions and figures of Schneider (1957) for modern taxa, I consider by default that the epiphysis is very unlikely visible in Chiroptera. Baron et al. (1996) found a particularly exposed epiphysis in *Dobsonia* species and in *Rhinolophus luctus* and *Rhinolophus trifoliatus.* Here (Fig. II-2), *Dobsonia minor* endocast does not show an epiphysis, which may be covered by the confluence of the superior sagittal and transverse sinuses. *Rhinolophus luctus* endocast shows a bizarre pattern of structures between the cerebral hemispheres and the caudal colliculi; it is not obvious to locate the transverse sinus, whose identification is a key to identify the other (i.e., neural) structures. However, as the transverse sinus runs parallel and near to the posterior border of the cerebral hemispheres in other rhinolophids, I parsimoniously consider the same situation for *Rhinolophus luctus*. The epiphysis is thus not visible on the endocranial cast of this taxon. Regarding the hypophysis, following Schneider (1957), the safest way to identify this structure is to locate the dorsum sellae, the posterior border of the sella turcica (to where lies the hypophysis). Without clear imprint of dorsum sellae, other central, shallower, depressions may be erroneously interpreted as the hypophyseal fossa.

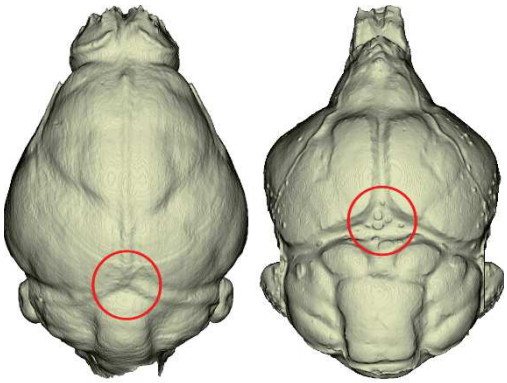

Figure II-2: Dorsal views of the endocasts of the pteropodid *Dobsonia minor* and the rhinolophid *Rhinolophus luctus* showing the area where the epiphysis cast should be seen (in red). Not to scale.

The tectum of the mesencephalon is variably covered by the cerebral hemispheres and the cerebellum (vermis and/or cerebellar hemispheres). As a result, the colliculi are more or less apparent on the external surface of the brain. The rostral colliculi may be visible but are less frequently observed than the caudal colliculi in my sample, as well as in the sample of Schneider (1957). An important note is that the variation in the morphology of the colliculi casts, especially regarding the caudal colliculi, is not necessarily the mirror of a variation in the morphology of those colliculi; it is rather a variation in their covering (by cerebral/cerebellar hemispheres; Schneider 1957, McDaniel 1976). Schneider (1957) also explains that the caudal colliculi are often inflated and that exposed colliculi of bats may be caused by inflated caudal colliculi rather than because of non-expanded cerebral and/or cerebellar structures, joining the conclusions of Edinger (1964a).

Regarding the visible elements of the cerebellum, following Larsell & Dow (1935), Maugoust & Orliac (2021) postulated that the flocculi is very unlikely to be visible on the external brain, and thus on an endocranial cast. However, Schneider (1966) labeled a part of what Maugoust & Orliac (2021) would have attributed to the paraflocculus as the flocculus. This flocculus is located medioventrally compared to the paraflocculus, which is consistent with what is illustrated by Larsell & Dow (1935). Moreover, cerebellar structure distinguishes from the paraflocculus on the frontal plane of the stereotaxic atlas of the *Rousettus aegyptiacus* brain (Schneider 1966: e.g., section 4-2-4). Hackethal (1981) also illustrates in most species a medioventral flocculus, of varying size. I now consider that the flocculus can be visible on the external aspect of the chiropteran brain. However, the delineation separating it from the paraflocculus is

not retrieved in my endocast sample (Fig. II-3), and only the paraflocculus is visible (see also the Cerebellar foldings section).

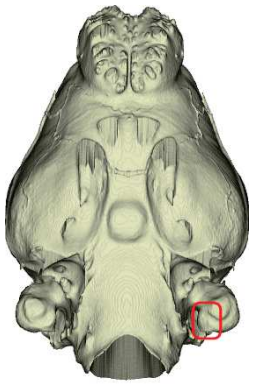

Rousettus aegyptiacus

Figure II-3: Ventral view of the endocast of the pteropodid *Rousettus aegyptiacus* showing the area where the flocculus should be seen (in red). Not to scale.

The exposed lobules of the cerebellar vermis on an endocranial cast as proposed by Maugoust & Orliac (2021) are congruent with the descriptions, schemes, and sagittal sections of Schneider (1957, 1966) and Hackethal (1981) and may fit, in fact, for the whole order: the anteriormost exposed lobule is the **declive (lobule VI)**, followed by the **tuber vermis (VIIa)**, the **folium vermis (VIIa)**, the **pyramis (VIII)**, and the posteriormost one is the **uvula (lobule IX)**. The sagittal sections of Schneider (1957, 1966) and Hackethal (1981) are, however, of great importance and help for the identification of cerebellar fissures and sulci on the vermis. Maugoust & Orliac (2021) proposed a third crus of the cerebellar hemispheres (the crus 0), ontogenetically developing from the declive (lobule VI), which is located anteriorly to the two other crura (the I and II, or anterior and posterior, crura), ontogenetically developing from the tuber and folium vermis respectively (Larsell & Dow 1935). In my chiropteran sample, the cerebellar hemispheres indeed may have more than a single groove, separating more than two sections (Fig. II-4). An issue is to identify them. Schneider (1957, 1966), Henson (1970) and Baron et al. (1996) do not compare the external anatomy of the cerebellar hemispheres; Schneider (1966) and Henson (1970) tentatively identify the crura of the hemispheres, but without such a thorough comparative work as for other brain structures (e.g., "olfactory brain", tectum of mesencephalon, vermis). On the other hand, Larsell & Dow (1935) pay more attention to the development of the whole cerebellum, its lobules and fissures/sulci, but in a single bat species. The only fully extensive work (i.e., regarding both the structure and the taxonomic group) is that of Hackethal (1981), so I mainly base my identifications on it. According to Hackethal (1981), the cerebellar hemispheres may be composed of up to five lobules. The three most anterior of the five are the (previously defined on endocasts by Maugoust & Orliac [2021]) **crura 0, I, and II**. The two posteriormost lobules are the **paramedian lobule**, extending from the folium vermis, and the **pyramidal copula** ("copula pyramidis"), extending from the pyramis. The two latter lobules are more variously present and of varying shape, size, and position relatively to the three crura; I therefore use the term "crus" for the three former to mark the fact that these lobules are less varying across species. I also do not name the crus 0 a "lobulus simplex" as in Hackethal (1981) or in the NAV (NAV, 2017) because it refers to an ancient lobule name of the vermis (e.g., see Larsell & Dow 1935), which I found both obsolete and confusing.

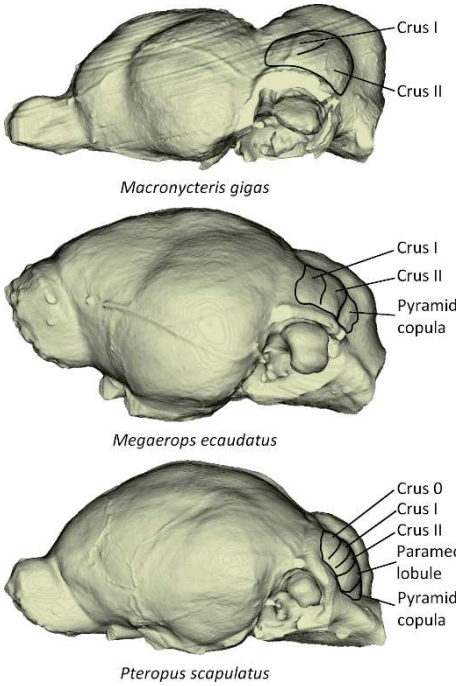

Figure II-4: Lateral views of the endocasts of the hipposiderid *Macronycteris gigas* and of the pteropodids *Megaerops ecaudatus* and *Pteropus scapulatus* showing the variation in the subdivision of the lobules of the cerebellar hemispheres. Not to scale.

It has to be pointed out that the subarcuate fossa (which houses the paraflocculus and the flocculus) may not be fully formed by bone: for instance, the figure 72b of Schneider (1957) clearly shows a fibrous membrane closing externally the subarcuate fossa. On an endocranial cast, fibrous tissues are not preserved; the subarcuate fossa would appear as laterally open, which is in fact not the case in the living animal. The figure 72b of Schneider (1957) is (to my knowledge) the only section of a bat skull showing the paraflocculus. An interesting fact is that it does not show other structures comprised in the subarcuate fossa than the paraflocculus and the flocculus, and Schneider did not mention that other structures than these (such as vascular structures) may be present in this fossa. Even though a single figure and the absence of anatomical note is not enough to propose rules at the infra-ordinal scale (by the way, regarding a species [*Pteronotus suapurensis*] not belonging to the considered infra-order), I at least propose that the interpretations based on subarcuate fossa cast morphology have to first consider that external apertures of that fossa (on the external wall of it) on skulls and fossils results from the decay of fibrous tissues rather than vascular pathways, unless clear vascular links can be demonstrated. Such external apertures are still retrieved, and named in the Casts of braincase openings section.

Regarding the ventral surface of the metencephalon, Schneider (1957, 1966) and Henson (1970) provide high-quality illustrations showing that many structures appear on the ventral surface of the brain; Baron et al. (1996) underlined the prominence of these structures on their illustrations and point out that the distinction between the pons and the medulla oblongata is not clear. Accordingly, the area where the pons and the medulla oblongata are located on a brain is smooth in my endocasts sample; I keep the term of pons-medulla oblongata continuum defined by Maugoust & Orliac (2021) and I address its morphology without more details.

II.2) General remarks on the folding and their origin of the cerebrum cast in bats

In his bat brain reviews, Schneider (1957, 1966) points out the fact that grooves on the brain surface can be erroneously referred to as pallial foldings, such as the rhinal fissure or neopallial sulci. He points out that an osseous crest and/or the imprint of a vascular structure are actually responsible of a sylvian-like groove. The studies of Schneider (1957, 1966) are the only studies (to my knowledge) to describe the inner surface of the bat braincase in details ("cranio-cerebral topography") and to compare it to the external surface of the brain. The review works of Henson (1970), Hackethal (1981) and Baron et al. (1996) thus follow Schneider's observations. The only deviation is from Baron et al. (1996), who schizophrenically identify a sylvian sulcus while clearly assessing that they follow Schneider's conclusions; the nuance may be in the fact that they say that impressions "appear" as neopallial sulci. In his study of the phyllostomid brain, McDaniel (1976) however observes more-than-just-an-imprint structures, which really are neopallial sulci: there is a "pseudocentral" sylvian-like (= central-like) sulcus that Schneider described as an inner osseous crest, and a more anterior sulcus that McDaniel did not name. Taking into account the review of Baron et al. (1996) (which takes into account the works of Schneider [1957, 1966]), Voogd et al. (1998) recognize on the external surface of the brain in some microchiropteran bats a rostral (= orbital) sulcus (which is probably that one that McDaniel did not name), a lateral sulcus "which might be homologous to the sylvian sulcus of primates" (as proposed by Maugoust & Orliac 2021) and a suprasylvian sulcus. They also retrieve that sylvian-like sulcus in megachiropteran bats.

Therefore, there is a mismatch in the terms used in the literature: the observations of Schneider (1957, 1966) have been later followed by works treating of brain morphology (Henson 1970, Hackethal 1981, Baron et al. 1996), whereas other interpretations have been proposed by Maugoust & Orliac (2021) based on endocasts, meeting to some extent the brain review of Voogd et al. (1998). Since the review of Baron et al. (1996), some high quality atlases became available, even though they generally document phyllostomid species (*Desmodus rotundus* in Bhatnagar 2008; *Carollia perspicillata* in Scalia et al. 2013; the mormoopid *Pteronotus parnellii* in Washington et al. 2018; *Phyllostomus discolor* in Radtke-Schuller et al. 2020). All these forms, at least a species of the same genus, are also figured by Schneider (1957). These atlases, together with various works published regarding the brain-skull interaction, help in tackling Schneider's conclusions and to chose between the interpretations of Schneider (1957, 1966) or of Maugoust & Orliac (2021).

Schneider postulates that the rhinal fissure is not at the same location as a slight imprint, the latter not reflecting the former and being in fact induced by a vascular structure. However, on his histological figures locating the transition area between the paleopallium and the neopallium (Schneider 1957: figs. 47, 57, 63, 64), the distinction is difficult to see and, when visible, it may seems to be a bit lower than the arrow he uses to spot it, being at the level of a slight external imprint (Schneider 1957: figs. 57, 63) as well as on recent stereotaxic atlases. Every illustrated brain by Schneider (1957) exhibits some neopallial sulci, that would be caused by ridges on the inner surface of the braincase. Such ridges are also illustrated with histological sections (Schneider 1957: figs. 62-64) and are bony thickenings filled with marrow. However, the more recent stereotaxic atlases confirm that they are true sulci, as McDaniel (1976) observed in several phyllostomid species. Schneider also illustrates a similar bony ridge at the dorsal top of the braincase, filling the interhemispheric fissure. It is however straightforward that the corresponding groove visible on the brain is not only due to a bony thickening, but because there are two cerebral hemispheres with a morphologically visible separation. All in all, thorough observations of Schneider's work give the impression that there are some inaccuracies regarding that point, or at least that his

observations are questionable, and that counter-examples are to be found without difficulty. Henson (1970), Hackethal (1981) and Baron et al. (1996) follow Schneider's observations, without bringing new support to it; if one can raise doubts about Schneider's observations, then one can raise doubts about the following references building on these observations.

Schneider's main hypothesis about the pallial imprints is that the brain adapts to the skull by filling it, and then that pallial foldings only reflect the inner osseous crests of the brain. It is however tricky to find potential functional relevance of an inner bony thickening, if not "filling" the brain external surface. The superficial and medial portions of the temporal muscle insert on the skull on both sides of the location of this crest (see Czarneki & Kallen 1980: fig. 5 and Kallen & Gans 1972: fig. 4), but one would expect an external rather than an internal bony thickening for the attachment of muscles (e.g., the sagittal crest). On the other hand, Washburn (1947) experimentally removed the muscles of mastication in the rat and find modifications of the skull crests but not of the internal form of the braincase. In addition, from an ontogenetical point of view, there are now evidences that the brain shape adapts neither to the skull shape (Barron 1950; see also Welker 1990, Raghavan et al. 1997, Garcia et al. 2018) nor to softer structures such as meninges and vascular vessels (Welker 1990). This would be consistent with the idea that, during the ontogeny, the skulls wrap around the brain and fills the concavities of the external surface of the brain (concerning both the interhemispheric fissure and the pallial grooves), as proposed to be the case at the vertebrate scale by Richtsmeier & Flaherty (2013) and described in birds by Fabbri et al. (2017). Inner skull shape may thus be thought to represent external brain shape. Schneider's hypothesis is therefore not supported following both ontogenetical and functional evidences. According to Schneider's observations and figures (Schneider 1957: figs. 62-64), there is a bony thickening filled with marrow dorsally to the various dorsal to lateral concavities of the external surface of the brain. Refuting Schneider's hypothesis about the pallial imprints, and since a similar case is found for the interhemispheric fissure, one can propose that the externally visible grooves are not induced by the inner braincase morphology but are true pallial grooves.

Some studies tried to assess the relevance of using endocasts to discuss the brain morphology using modern techniques. They however did not consider so-called "basal" mammalian brains such as those of bats: Watanabe et al. (2019) studied birds and archosaurs, whose brain organization clearly differs from that of bats (especially regarding the neopallium, a mammalian feature), and Dumoncel et al. (2020) studied hominids, whose brain complexity (especially regarding the neopallium) is not representative of that of other mammals. To largely consider the brain/skull interaction, both in terms of anatomy (through histology or brain/endocast comparisons) and of development, is out of the scope of the present study. What I propose only relies on the available literature and obviously needs further studies focused on bats and using modern techniques (such as diceCT, e.g., Anderson & Murat 2015, Gignac et al. 2016, Hedrick et al. 2018). However, this enables for revising most of the (scarce) literature regarding in detail the macromorphology of the bat brain, and to consider that the external impressions on endocasts are real pallial foldings, including a rhinal fissure and neopallial sulci. Taking this into account, I follow and complete the sulcal pattern proposed by Voogd et al. (1998) and Maugoust & Orliac (2021).

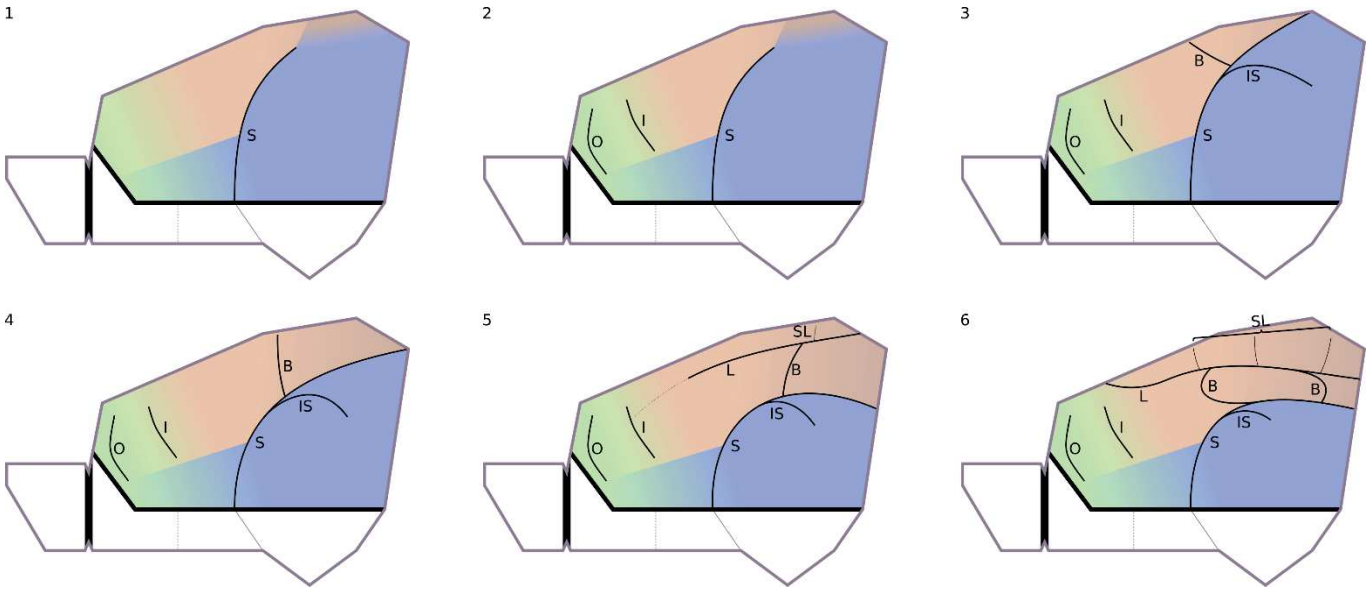

Figure II-5: Neopallial sulci (lines) and areas (colors) on theoretical chiropteran brains of increasing complexification (1 to 6). Abbreviations of neopallial sulci epithets: B- Bridge; I- Intermediate; IS- Infrasylvian; L- Lateral; O- Orbital; S- Sylvian; SL- Supralateral. Colors of neopallial areas: green- fronto-orbital; orange- parietal; brown- occipital; light blue- insular; blue- temporal. The color gradient areas indicate a putative transitional area between two defined ones without mark delineating them. Progressive cases: 1) is a case with a single sylvian sulcus, separating the temporal area from the fronto-orbito-parieto-orbital (FOPO) area, with a putative insular area in the anteroventral continuation of the temporal one; 2) is a case with an orbital sulcus separating the fronto-orbital cortex anteriorly from the other areas posteriorly, with two transitional areas between that area and the parietal and insular areas respectively; 3) to 6) are cases of increasing complexity of the sylvian area, with appearance of a bridge sulcus at stage 3), its posterior bending at stage 4), the appearance of a lateral sulcus at stage 5), and the complex configuration of the sylvio-lateral area in stage 6) with up to three bridge and supralateral sulci.

II.3) Emendatum to: Neopallial foldings and lobes (Fig. II-5)

The present definition of the main neopallial sulci relies on Maugoust & Orliac (2021), who adapted a general "primitive" mammalian scheme to the bats they describe, that are, hipposiderids. However, a substantial rider (Fig. II-5) must be provided given the much broader phylogenetical framework considered here, that is, all chiropteran bats.

Almost every chiropteran specimen studied here shows, at least, one neopallial sulcus. As in previously described fossil hipposiderids (Maugoust & Orliac 2021), it is here referred to as the sylvian sulcus. This sulcus, formed by the pseudosylvia and the suprasylvia, arises from the rhinal fissure with a dorsolateral orientation (in lateral view) and then bends more and more posteriorwards. Of this course, the dorsoventral-most part (even bended a bit anteriorly in some cases), linked to the rhinal fissure, is the pseudosylvian part, while the posteriorly bended part is the suprasylvian part. Among the specimens of my sample (Fig. II-6), it is not rare to see a sylvian sulcus isolated from the rhinal fissure, and that is already bended posteriorwards. I identify this part as the suprasylvian part of the sylvian sulcus.

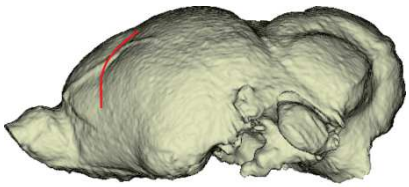

Rhinolophus ferrumequinum

Figure II-6: Lateral view of the endocast of the rhinolophid *Rhinolophus ferrumequinum* showing the dorsal position and the curvature of the sylvian sulcus (in red). Not to scale.

Chiropterans exhibit various degrees of complexity of sulcation pattern, from very simple ones (e.g., rhinopomatids, with a single, short, and shallow sylvian sulcus) to more complex ones (e.g., *Pteropus* species, with more than five sulci). The sylvian sulcus is the most frequently retrieved. On most complex endocasts, a lateral sulcus is also present: it is parallel to the sylvian sulcus, and dorsomedially located relative to it. Depending on the cases (Fig. II-7), there can be either (1) a single straight sulcus linking the lateral and sylvian sulci, perpendicular to both of them and roughly at the level of the dorsal convexity of the sylvian sulcus, or (2) up to three more oblique and curved sulci linking the lateral and sylvian sulci (sometimes even seeming to extend from one or the other sulcus). This or these sulci are called bridge sulci, as they "bridge" the lateral and sylvian sulci. In pteropodids without lateral sulcus (excepting *Casinycteris argynnis*), there is always a short and straight sulcus located dorsomedially, arising grossly perpendicular from the sylvian sulcus. Depending on the cases, it may point anteriorly (being oblique) or dorsally (being perpendicular to the sylvian sulcus). The latter, dorsally pointing, isolated sulcus is very close in its shape and location to the perpendicular bridge sulcus; I propose a homology between these two sulci. The bridge sulcus can thus be oblique or perpendicular, straight or curved, and it can be linked to the sylvian sulcus or to the the sylvian and lateral sulci.

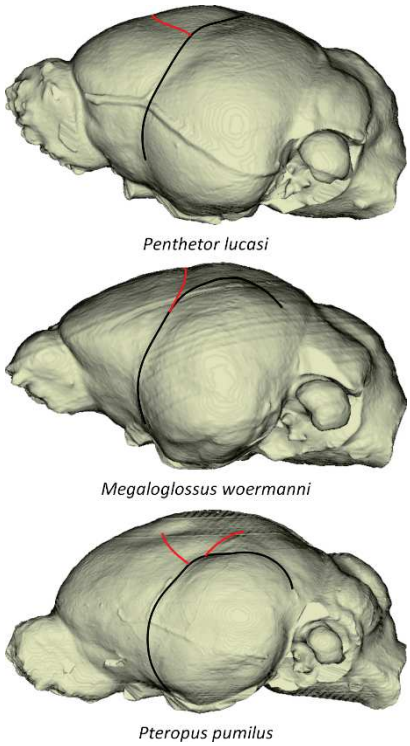

Figure II-7: Lateral views of the endocast of the pteropodids *Penthetor lucasi*, *Megaloglossus woermanni*, and *Pteropus pumilus* showing the variation in the shape, orientation, and number of the bridge sulcus (in red). The sylvian sulcus is in black. Not to scale.

In some taxa (Fig. II-8), a sulcus arises from the sylvian sulcus more anteroventrally than the bridge sulcus. This sulcus generally points posteriorly or posteroventrally, and it can be flat or dorsally convex. Due to its position, I name it the infrasylvian sulcus: it arises from the sylvian sulcus and connects only it, and it is more ventrally located than the suprasylvian sulcus.

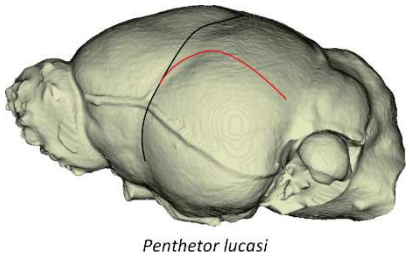

Figure II-8: Lateral view of the endocast of the pteropodid *Penthtor lucasi* showing the position of the infrasylvian sulcus (in red) relative to the sylvian sulcus (in black). Not to scale.

On most complex endocasts (Fig. II-9), there can also be one to several sulci located medially to the lateral sulcus, being perpendicular to it. Due to their varying number, I do not propose an identification for each and call them supralateral sulci.

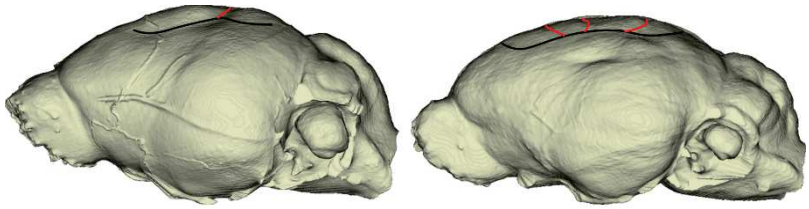

Rousettus aegyptiacus *Pteropus capistratus*

Figure II-9: Lateral views of the endocast of the pteropodids *Rousettus aegyptiacus* and *Pteropus capistratus* showing the variation in the number of supralateral sulci (in red) relative to the lateral sulcus (in black). Not to scale.

An anteriorly located sulcus, not connected with the sylvian sulcus, is often retrieved (Fig. II-10). It parallels to some extent the circular fissure in lateral view, being more dorsally located than the latter. This sulcus is referred to as an orbital sulcus (Smith 1902a, Smith 1903), as previously described by Baron et al. (1996) and Voogd et al. (1998).

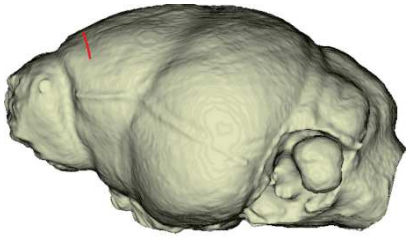

Balionycteris maculata

Figure II-10: Lateral view of the endocast of the pteropodid *Balionycteris maculata* showing the position and the shape of the orbital sulcus (in red). Not to scale.

A sulcus is sometimes found (Fig. II-11) between the orbital sulcus and the area of sulcal complexification, grossly parallel to and of similar extent that the orbital sulcus. I name it intermediate sulcus. No clear homology can be found with a classical pattern (see the basal pattern figured by Maugoust & Orliac [2021]) and it is of varying position and connections; it is potentially not homologous between chiropteran species.

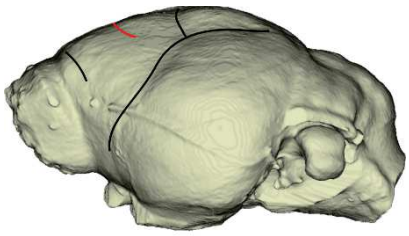

Megaerops ecaudatus

Figure II-11: Lateral view of the endocast of the pteropodid *Megaerops ecaudatus* showing the position of the intermediate sulcus (in red) relative to the other surrounding sulci (orbital, sylvia, bridge, in black). Not to scale.

I decide to leave the gyral terminology of Dechaseaux (1962) adapted to hipposiderid bats by Maugoust & Orliac (2021) out because: (1) the epithet of the terms may correspond to a primitive and/or carnivoran gyral pattern but not to a chiropteran gyral pattern, which is not convoluted (or not convoluted centrifugally), and (2) this nomenclature appears to be incomplete compared to that of some recent studies. In their stereotaxic atlas of *Phyllostoma discolor*, Radtke-Schuller et al. (2020) name the structural and functional areas of the brain of that species, even though they did not name the neopallial sulci. However, the correspondence between the brain of that species and the brain of some chiropteran species is not difficult to establish and may be applicable, at least regarding the major areas that are grossly surrounded by similar sulci to those named here (Fig. II-5).

The frontal and dorsolateral-orbital cortexes are anteriorly located: the frontal cortex is posteriorly bounded by the orbital sulcus, and the dorsolateral-orbital cortex is in its ventrolateral continuity. However, both areas are not separated by a sulcus (even though the frontal part seems to be the only of the two that is bounded posteriorly by the frontal sulcus), so I group them here and name this area the fronto-orbital cortex. Posteriorly to the orbital sulcus and dorsomedially to the sylvian sulcus is the parietal cortex, posteriorly followed by the occipital cortex. Again, it is tricky to separate the parietal cortex from the occipital one, as the limit between them is not a sulcus: according to Radtke-Schuller et al. (2020), they are located on each side of the dorsal convexity of the sylvian sulcus (the parietal and occipital cortexes being anterior and posterior to it, respectively). As they cannot be clearly separated, I will refer to them together as the parieto-occipital cortex. Below the sylvian sulcus are the insular and temporal (sometimes also called auditory cortex [e.g., Washington et al. 2018] as it includes auditory nuclei) cortexes. As previously, no clear sulcus separates them; the only way to distinguish them is that the temporal cortex is the most inflated part of the two. Moreover, the insular cortex generally refers to the insula, an area located near the rhinal fissure and where forms the basis of the sylvian sulcus, the pseudosylvia; it is thus the most ventral area of the two. I will refer to both area as the insulo-temporal cortex. It has to be noted that this insulo-temporal cortex resembles to some extent to the reuniens and arcuate areas of Maugoust & Orliac (2021), even though the insular cortex seems to encompass the ventral basis of the sylvian sulcus.

There are therefore three main neopallial areas: the fronto-orbital cortex anteriorly, the parieto-occipital cortex dorsally and the insulo-temporal cortex ventrally. In each, slight distinctions without clear limit can sometimes be inferred depending on the boundaries of each. The sulci separating these three areas are the orbital sulcus (regarding the fronto-orbital and the parieto-occipital cortexes) and the sylvian sulcus with its posterior extent (regarding the parieto-occipital and the insulo-temporal cortexes). If the orbital sulcus is absent and thus the fronto-orbital and parieto-occipital cortexes cannot be distinguished, I will refer to this area as the fronto-orbito-parieto-occipital (FOPO) cortex.

II.4) Addendum to: Cerebellar foldings (Fig. II-1)

Hipposiderid bat endocasts have a somewhat simpler cerebellum than other chiropteran bats. In that way, the nomenclature of Maugoust & Orliac (2021) is still valid regarding the fissuration and the cutting of the vermis because there are no more than five exposed lobules in Chiroptera according to Hackethal (1981).

However, the cerebellar hemispheres may be more complex in other chiropteran bats than in hipposiderids. Hackethal (1981) clearly confirms the lateral non-linearity of the lobules in bats proposed by Larsell & Dow [1935]. He also confirms that the declive may contribute laterally to the cerebellar hemispheres through the crus 0 of Maugoust & Orliac (2021). Depending on the taxa (Fig. II-4), there can also be a supplementary contribution of the tuber vermis to the cerebellar hemispheres as the paramedian lobule and of the pyramis as the pyramidal copula. One can thus expect more than two sulci separating the lobules of the cerebellar hemispheres. Dow (1942) did not provide any name for the sulci anterior and posterior to the paramedian lobule. Without other references, I name (1) posterocrural sulcus the sulcus separating the crus II from the following lobule (which can be either the paramedian lobule or the pyramidal copula) and (2) paracrural sulcus the sulcus separating the paramedian lobule from the pyramidal copula, which is of varying position (either posteriorly to the previous lobules, or posteroventrally to them).

The vermis and the cerebellar hemispheres may be separated by a groove of variable depth, the paramedian fissure. I consider this groove as a fissure because it separates two main units of the cerebellum (i.e., the vermis and the considered cerebellar hemisphere). The paramedian fissure can be a varying width (Fig. II-12): I consider it narrow when a clear distinction can be made; sometimes, there is a very shallow and gentle transition between the two structures, indicating a wider fissure (on endocasts). Moreover, this fissure does not necessarily separate the vermis and the considered cerebellar hemisphere on their whole length; for instance, in the brain of *Rousettus aegyptiacus* figured by Schneider (1966), there is a clear discontinuity between vermian and hemispheric parts of the lobules VIIA, VIIB, and VIII but a clear lateral continuity of the lobule VI, so I expect this pattern to be likely found on endocasts.

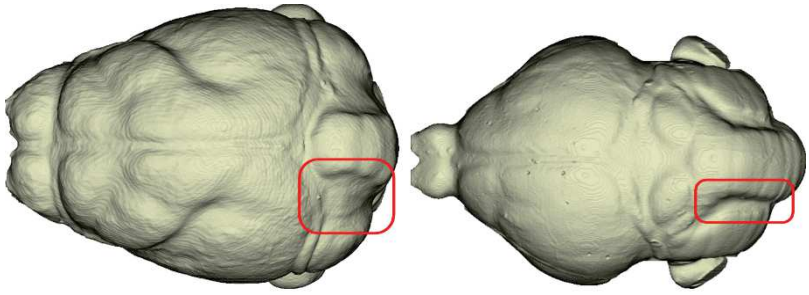

Figure II-12: Dorsal views of the endocasts of the phyllostomid *DIphylla ecaudata* and of the megadermatid *Lavia frons* showing the variation in depth and width of the paramedian fissure. Not to scale.

The uvula, or lobule IX, expands laterally: it is thought to contribute to the paraflocculus (Larsell & Dow 1935, Dow 1942) and it forms the flocculus (Dow 1942) on its lateral extremity. However, there is also a posterior lateral inflation of the vermis, mainly caused by the inflation of the vermian part of the uvula. Moreover, Dow (1942) and Hackethal (1981) demonstrate that there is no additional hemispheric lobule formed by the uvula. Thus, a lateral expansion of the posteriormost lobule of the vermis on my endocasts (Fig. II-13) sample will be interpreted as a lateral inflation of the uvula.

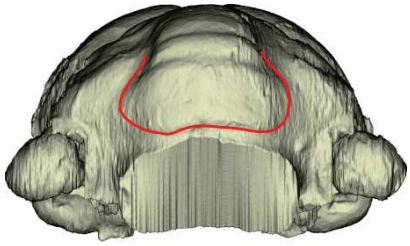

Figure II-13: Occipital view of the endocast of the fossil hipposiderid *Palaeophyllophora oltina* showing the width of the ventralmost part of the lobule IX (uvula) of the cerebellum. Not to scale.

Schneider (1957, 1966) and Hackethal (1981) demonstrated that a flocculus can be ventrally exposed in bats. A posterolateral fissure may thus be visible on the ventral aspect of both the flocculus and the paraflocculus. However, on endocranial casts, such a delineation is not observed and the flocculus is even not decipherable at all throughout my chiropteran sample; only visible is the paraflocculus, without posterolateral fissure (e.g., Fig. II-3). On the ventral aspect of the paraflocculus, a depression is frequently retrieved throughout my sample with associated sulci surrounding it with more variation (Fig. II-14). Thus, rather than defining a single sulcus associated with this as did Maugoust & Orliac (2021), I propose to define this structure as the ventral parafloccular fossa. The variation around this structure is too high to propose other identifications; the fossa itself can be a delineated fossa, or a broad sulcus deepening locally etc.

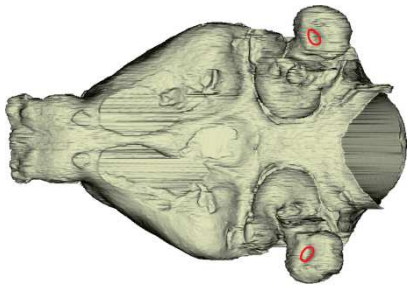

Figure II-14: Ventral view of the endocast of the fossil hipposiderid *Palaeophyllopora oltina* showing the position and size of the ventral parafloccular fossa. Not to scale.

A delicate groove can also occur anteroventrally or ventrally (Fig. II-15), delineating a small platform; this groove is the imprint of the lateral semicircular canal. The ventral parafloccular fossa lies (antero) medially to this imprint. Some artificial openings are sometimes visible on the dorsolateral aspect of the paraflocculus, but they are more probably non-osseous walls of the subarcuate fossa (see Major components of the chiropteran brain observed on endocasts and Casts of braincase openings sections).

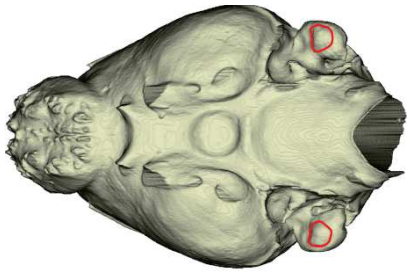

Dobsonia minor

Figure II-15: Ventral view of the endocast of the pteropodid *Dobsonia minor* showing the position of the imprint of the lateral semicircular canal on the paraflocculus (in red). Not to scale.

On the lateral aspect of the paraflocculus, a sulcus may occur (especially in pteropodids; Fig. II-16): this sulcus is grossly anteroposteriorly oriented, but it is often bent at its anterior and posterior extremities. This sulcus is very close in its shape and location to the sulcus separating the dorsal and ventral paraflocculus illustrated by Schneider (1966). Larsell & Dow (1935) named it the lateral sulcus of the paraflocculus, but I simplify this here and name it the lateral parafloccular sulcus. Following the illustrations of Larsell & Dow (1935) and Hackethal (1981), it appears clear to me that the secondary fissure extends laterally but not up to the paraflocculus, and the lateral sulcus of the paraflocculus is not a lateral extension of the secondary fissure, as proposed by Smith (1902b) that Maugoust & Orliac (2021) followed. Indeed, this lateral sulcus is not oriented in the same way (anteroposteriorly, or diagonally in the anterodorsal-posteroventral axis for the lateral sulcus; mediolaterally for the secondary fissure) and the lack of continuity between the two structures is clear in adults (Hackethal 1981: text-figs. I-X) and even more obvious during the ontogeny (Larsell & Dow 1935: figs. 15-17).

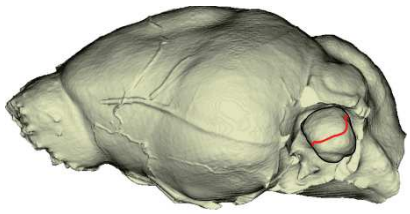

Rousettus aegyptiacus

Figure II-16: Lateral view of the endocast of the pteropodid *Rousettus aegyptiacus* showing the position of the lateral parafloccular sulcus (in red) relative to the whole paraflocculus (in black). Not to scale.

II.5) Addendum to: Casts of braincase openings (Fig. II-1)

As proposed by Maugoust & Orliac (2021), I rely on the skull foramina recognition by Giannini et al. (2006) for the genus *Pteropus*.

There is however some variation across Chiroptera regarding the spheno-ethmo-orbital region (i.e., regarding the foramina of the anterior half of the ventral endocranial surface). The expected pattern is retrieved consistently regarding the exit of the nerves I to VI, with anteroposteriorly the cribriform plate of the ethmoid, the optic foramen (the optic chiasm is also sometimes visible), the sphenorbital fissure, the round foramen, the oval foramen, and, sometimes, an alisphenoid canal in between the round and oval foramina. However, a coalescence of some of these foramina is frequent (Fig. II-17). For instance, the sphenorbital fissure is sometimes coalescent with the optic foramen and/or the round foramen. When present, the rostral (anterior) opening of the alisphenoid canal is coalescent with the sphenorbital fissure and the alisphenoid canal does not have a "canal structure", and only its caudal (posterior) opening is individualized as the caudal alisphenoid canal foramen (e.g., *Megaderma lyra* in Wible & Davis 2000). In some cases, there is a single, large, foramen following posteriorly, with a respectable gap, a short sphenorbital fissure; as do Giannini et al. (2006), I interpret this case as a coalescence of the posterior opening of the alisphenoid canal (= caudal alar foramen) with the oval foramen (causing a longer foramen than expected for the oval one only). If the round foramen is coalescent with the sphenorbital fissure and the posterior opening of the alisphenoid canal is individualized (as in *Megaderma lyra*, Wible & Davis 2000), then the latter can be mistakenly identified as the former looking at an endocranial cast only. The only way to address this is to also consider the skull regarding extant species and, regarding natural endocranial casts or poorly preserved skulls, to systematically consider isolated reversions of a coalescence of the round foramen with the sphenorbital fissure as being in fact a posterior opening of an alisphenoid canal. There is, to my knowledge, no cases where the four (five if the alisphenoid canal is present) apertures coalesce.

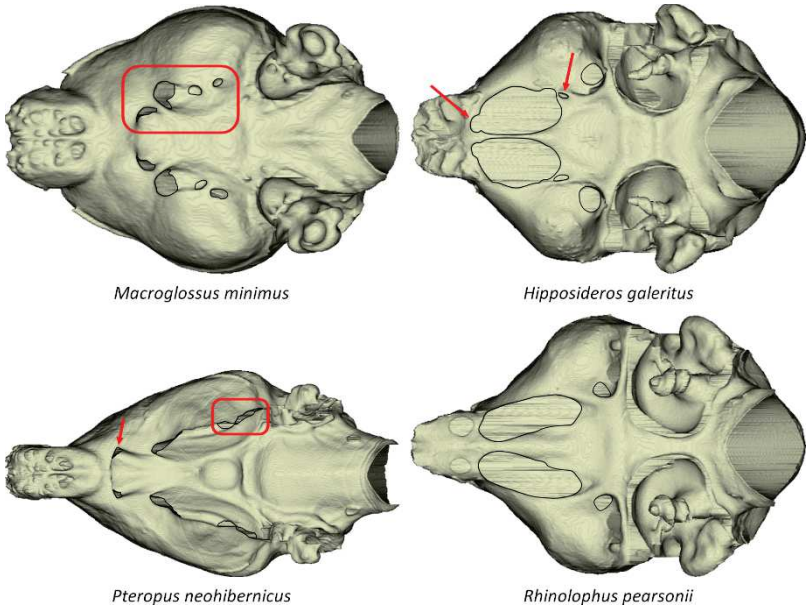

Figure II-17: Ventral view of the endocasts of the pteropodid *Macroglossus minimus*, of the hipposiderid *Hipposideros galeritus*, of the pteropodid *Pteropus neohibernicus*, and of the rhinolophid *Rhinolophus pearsonii* showing the variation in the coalescence of various sphenoidal apertures (optic foramen, sphenorbital fissure, caudal alisphenoid canal foramen, oval foramen). Top left: independence of all four apertures. Top right: optic foramen confluent the sphenorbital fissure (left arrow), caudal alisphenoid canal foramen individualized (right arrow). Bottom left: optic foramen individualized (left arrow), caudal alisphenoid canal foramen coalescent with oval foramen (right arrow). Bottom right: only oval foramen individualized from sphenorbital fissure. Not to scale.

In some taxa, the sphenorbital fissure narrows mediolaterally and can be visually subdivided (Fig. II-

18). This is particularly true in some pteropodids, as already illustrated in *Rousettus aegyptiacus* (Schneider 1966: fig. D). Distinguishing which component of the nerve bundle (i.e., with nerves III, IV, V1 and VI) goes across one or the other aperture is tedious as there is little literature about the cranial nerve pathways in non-human mammals. As do Giannini et al. (2006), I follow what is known in the dog (Evans & Lahunta 2012: fig. 19-8): the abducent (VI) nerve has the medialmost course, the ophthalmic branch of the trigeminal nerve (V1) has the lateralmost one, the trochlear (IV) nerve seems to be lateral too, while it is unclear for the oculomotor (III) nerve, even though it is more medial than IV and V1. In the studied species, the lateral subdivision of the sphenorbital fissure is generally wider than the medial one. I can confidently propose that the V1 branch exits through the lateral subsection of the sphenorbital fissure while the VI nerve exits through the medial one; I also propose that the IV nerve exits through the lateral subsection (as it is still somewhat lateral) while the III nerve exits through the medial one (together with the VI nerve, as they are both ocular motor nerve).

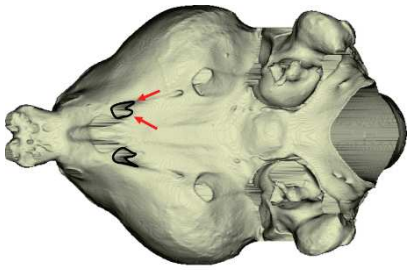

Cardioderma cor

Figure II-18: Ventral view of the endocast of the megadermatid *Cardioderma cor* showing (red arrows) the mediolateral subdivision of the sphenorbital fissure. Not to scale.

A small foramen sometimes lies just medially to the sphenorbital fissure, in general at the middle of the sphenorbital fissure length in the anteroposterior axis (or at mid-distance between the anterior extremity of the sphenorbital fissure and the round foramen when the latter is individualized), and it opens posteriorly in the palatine region. Such an aperture is found by Giannini et al. (2006) in *Pteropus*, Wible (2011) in *Ptilocercus* (Scandentia), and Muizon et al. (2015) in *Alcidedorbignya* (Pantodonta) for instance. It is related to the pterygoid (or "vidian") canal, through which run the pterygoid branch of the maxillary artery (or "vidian" artery) and the pterygoid nerve (or "vidian" nerve, which is the uniting of the greater petrosal nerve, that arises from the facial nerve, and the deep petrosal nerve). This foramen corresponds to the **anterior opening of the pterygoid canal**. This foramen is elongated and clearly smaller than the posterior opening of the alisphenoid canal; they can be differentiated by the fact that the former is more medially located (on the medial side of the sphenorbital fissure) while the latter is more laterally located (laterally to the sphenorbital fissure).

An aperture is frequently found anterodorsal to the cribriform plate, rather thin but generally continuous mediolaterally on the whole olfactory bulbs width (Fig. II-19). I do not know which structure could be transmitted via this aperture: Maugoust & Orliac (2021) interpreted it as transmitting olfactory nerves as the cribriform plate does in fossil bats, but this is very unlikely as in some extant species, it forms sort of a canal which opens on the dorsal surface of the nasal bone. As already described by Maugoust & Orliac (2021), an ethmoid foramen is also present on the lateral wall of the olfactory bulbs but it is difficult to delineate on endocranial casts.

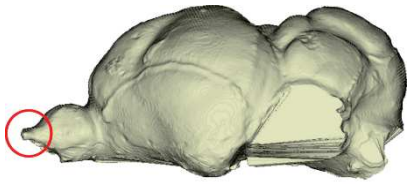

Hipposideros (Pseudorhinolophus) bouziguensis

Figure II-19: Lateral view of the endocast of the fossil hipposiderid *Hipposideros* (*Pseudorhinolophus*) *bouziguensis* showing the indeterminate structure anterior to the olfactory bulbs. Not to scale.

In the sphenoidal area, up to four additional foramina are also retrieved in a consistent way: there is no case with all additional foramina present, but each one is found in several species.

The first one (unknown foramen #1; Fig. II-20) is located posteriorly on the ventral aspect of the olfactory bulbs (i.e., just anteriorly to the circular fissure) and can be sometimes (erroneously, to my sense) identified as an optic foramen; its position is much more anterior than expected for an optic foramen, and in some cases, a "true" optic foramen is retrieved together with this unknown foramen #1. This foramen can be coalescent with the sphenorbital fissure; in that case, I consider that the optic foramen is also coalescent with the sphenorbital fissure as it would be located between the unknown foramen #1 and the sphenorbital fissure. It is variable in size: it can be large (as the oval foramen for instance) or small. This foramen may correspond to the suboptic foramen (Cartmill & MacPhee 1980) which "carries an [interorbital] vein connecting the ophthalmic veins" and is located "immediately posterior[ly] to the olfactory chamber" (Butler 1948).

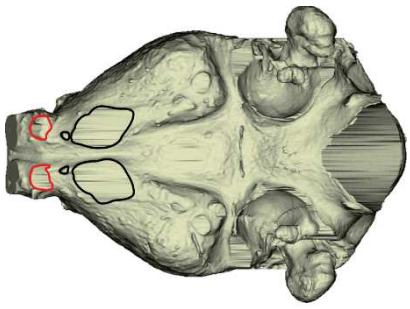

Hipposideros armiger

Figure II-20: Ventral view of the endocast of the hipposiderid *Hipposideros armiger*, showing the position of the unknown foramen #1 (in red) relative to the optic foramen and the sphenorbital fissure (in black). Not to scale.

The second one (unknown foramen #2; Fig. II-21) is located just anterolaterally to the sphenorbital fissure, anteroposteriorly between the unknown foramen #1 (when present) or the optic foramen (when individualized) and the sphenorbital fissure. When present, it is generally large (as large as the oval foramen, for instance). No nervous structure could be expected to need an additional foramen in this area and there is no documentation about an additional branch of a cranial nerve. This foramen may transmit a vascular structure, and its location may indicate that it could transmit the orbital ramus and/or the ophthalmic artery and/or the superior ophthalmic vein (see the Major vascular structures crossing the endocranial cavity section), which classically enter the orbit to join the meningo-lacrimal artery and vein through the optic foramen.

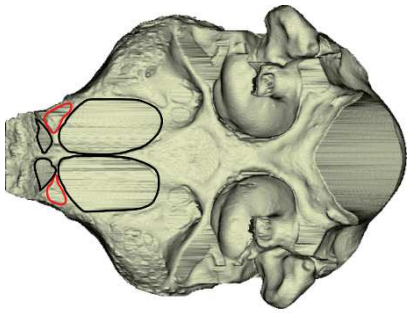

Hipposideros jonesi

Figure II-21: Ventral view of the endocast of the hipposiderid *Hipposideros jonesi* showing the position of the unknown foramen #2 (in red) relative to an ?unknown foramen#1 and the sphenorbital fissure (in black). Not to scale.

The third one (unknown foramen #3; Fig. II-22) is also frequently retrieved laterally to the oval foramen, and opens posteriorwards. This aperture is big, as large to larger than the oval foramen. It opens in the bony wall that constitutes the posterior wall of the piriform lobes (and, more generally, of the cerebral hemispheres), above the pyriform window. Such an aperture has not been reported in the literature to my knowledge, and I cannot identify it. As it concerns a bony wall limiting a part of the brain, it could also be an artefact caused by a softer tissue than bone, as for the lateral wall of the subarcuate fossa (see Major components of the chiropteran brain observed on endocasts and Casts of braincase openings sections and Schneider 1957). However, even on well-preserved skulls (i.e., with still some delicate and/or cartilaginous structures) used to virtually extract their endocast, this aperture is well-defined and does not seem to be an artefact.

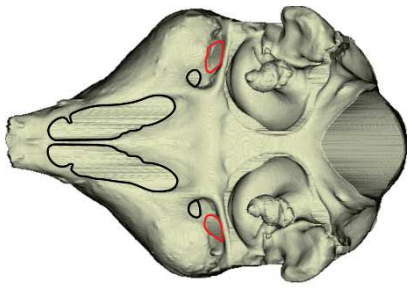

Rhinolophus rouxii

Figure II-22: Ventral view of the endocast of the rhinolophid *Rhinolophus rouxii* showing the position of the unknown foramen #3 (in red) relative to the sphenorbital fissure and the oval foramen (in black). Not to scale.

A similar aperture is sometimes found lateral to the unknown foramen #3 (Fig. II-23), sharing otherwise all its other properties. I name it the unknown foramen #3 bis.

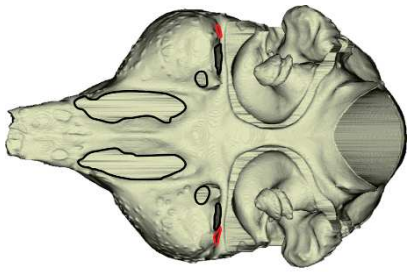

Rhinolophus luctus

Figure II-23: Ventral view of the endocast of the rhinolophid *Rhinolophus luctus* showing the position of the unknown foramen #3bis (in red) relative to the sphenorbital fissure, the oval foramen, and the unknown foramen #3 (in black). Not to scale.

Regarding the cast of the foramina opening in the posterior half of the ventral surface of the endocranial cast, there is much more morphological consistency across taxa. The only varying structures are the apertures surrounding medially the petrosal, that are, the **pyriform window**, the **carotid foramen**, the **basicochlear fissure**, and the **jugular foramen** (Giannini et al. 2006). These structures can be coalescent or individualized, depending on the taxa, and vary in width. Of all, the pyriform window varies the most in shape (being sometimes V-shaped). According to my sample, it has to be pointed out that, if they coalesce, each aperture is still distinguishable from the other with the exception of the carotid foramen (see following lines).

In pteropodids and megadermatids, there are also some manifestations of the entrance of the internal carotid artery. This vessel enters the braincase through the carotid foramen (see the Major vascular structures crossing the endocranial cavity section), but there is some variation regarding that structure across chiropterans. No literature is available regarding that point, so I only rely on the observations I made on my sample. In megadermatids and some pteropodids (Fig. II-24), there is an aperture located anterolaterally to the hypophysis opening posterolaterally and which is followed anteromedially by the cast of a groove. In other pteropodids, there is a groove anterolaterally to the carotid foramen. I interpret both manifestations to be marks of the internal carotid pathway. In pteropodids where there only is a groove, it clearly starts from the carotid foramen, so the interpretation of that mark is straightforward: it is interpreted and named as a **carotid sulcus**.

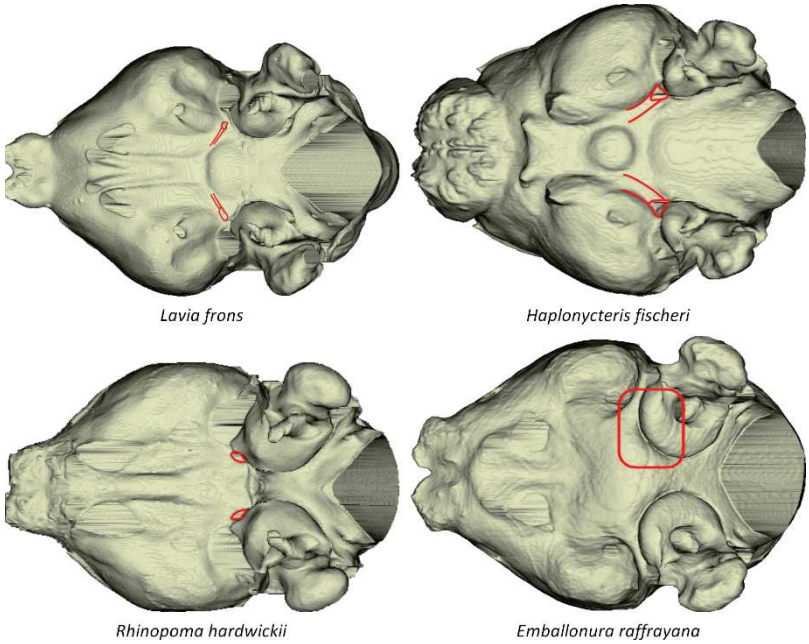

Figure II-24: Ventral view of the endocasts of the megadermatid *Lavia frons*, the pteropodid *Haplonycteris fischeri*, the rhinopomatid *Rhinopoma hardwickii*, and the emballonurid *Emballonura raffrayana* showing the various presence of an (anterior or posterior) carotid foramen and of the carotid sulcus (in red). Top left: anterior carotid foramen with carotid sulcus. Top right: posterior carotid foramen with carotid sulcus. Bottom left: only posterior carotid foramen. Bottom right: no clear carotid foramen. Not to scale.

In other pteropodids and in megadermatids where there is a slight cast finishing in an aperture, it seems from further observations (Fig. II-25) on the skull that there is canal between the carotid canal and that aperture. This canal would be a **carotid canal**; the carotid foramen would simply be a **posterior carotid foramen**, and the endocranial aperture of that canal would be the **anterior carotid foramen**.

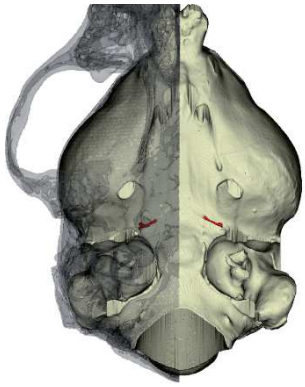

Figure II-25: Ventral view of the endocast and of the right half of the cranium of the megadermatid *Cardioderma cor* showing the position of one form of carotid canal (in red) above the endocast (right) and within cranial bones (left). Here, the carotid canal opens on an anterior carotid foramen located medially to the cerebral hemispheres and anterolaterally to the hypophysis. Not to scale.

In some other species (Fig. II-26), the pterygoid bones extend far posteriorly, and their posterior extremity is an opening located just anterolaterally to the contact point between the petrosal and the basisphenoid. An endocranially visible aperture, located just posteriorly to the oval foramen, opens in the pterygoid shortly before the pterygoid itself opens over the petrosal/basisphenoid junction. I can propose that the channel between the posterior opening of the pterygoid and that aperture is also a carotid canal. This aperture would also be an anterior carotid foramen, and the classical, posterior, carotid foramen would be fully external to the braincase.

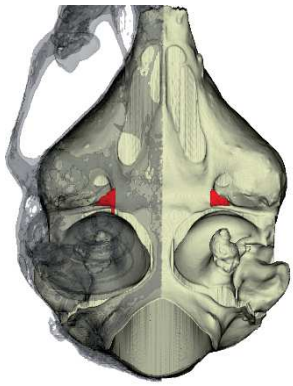

Rhinolophus rouxii

Figure II-26: Ventral view of the endocast and of the right half of the cranium of the rhinolophid *Rhinolophus rouxii* showing the position of another (cf. Fig. II-25) form of carotid canal (in red) above the endocast (right) and within cranial bones (left). Here, the carotid canal opens just posteriorly to the oval foramen. Not to scale.

Finally, there can be some aperture-like structures on the paraflocculi casts, that probably are cartilaginous closings that withered (see Major components of the chiropteran brain observed on endocasts section and Schneider 1957). There generally are up to two apertures: one is located on the posteromedioventral aspect of the paraflocculus, and the other on its dorsal aspect. Both apertures can greatly vary in size, and generally connect with the sigmoid sinus cast dorsally and posteriorly. Due to the varying position of the petrosal (and then of the subarcuate fossa housing the paraflocculus) with respect to the skull, the **dorsal aperture** can open dorsomedially to dorsolaterally, always toward the sigmoid sinus cast. From another point of view, the direction of the opening of this structure informs about the rotation of the petrosal relative to the skull. The **posteromedioventral aperture**, on the other hand, quite less varies in its position and in the direction of the opening. Both apertures can be seen in lateral views, but both are best seen using 3D models (Fig. II-27): the dorsal aperture can be invisible in lateral view if it opens lateromedially, and the posteromedioventral aperture has a more strict medial direction and is therefore still difficult to spot in lateral view.

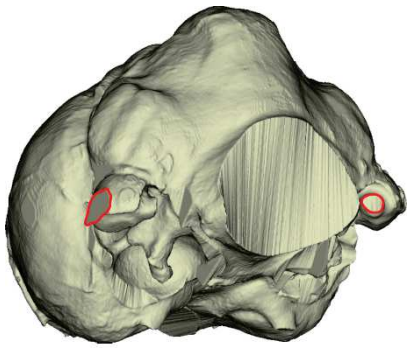

Noctilio albiventris

Figure II-27: Posterolateroventral hybrid view of the endocast of the noctilionid *Noctilio albiventris* showing the position of the lateral (left red outline) and of the posteromedioventral (right red outline) apertures on the paraflocculus. Not to scale.

II.6) Major vascular structures crossing the endocranial cavity (Fig. II-28)

Several vascular structures enter and/or exit the braincase and may leave a mark on the bony walls of the braincase. These marks can be either grooves along the vascular pathway or foramina pierced into/between bones. I do not attempt to define or generalize the cranial vascular system of bats, which is largely beyond the scope of this section; I rather summarize works about the mammalian (chiropteran when available) cranial circulation. This summary is illustrated in Figure II-28 that stands for the whole section.

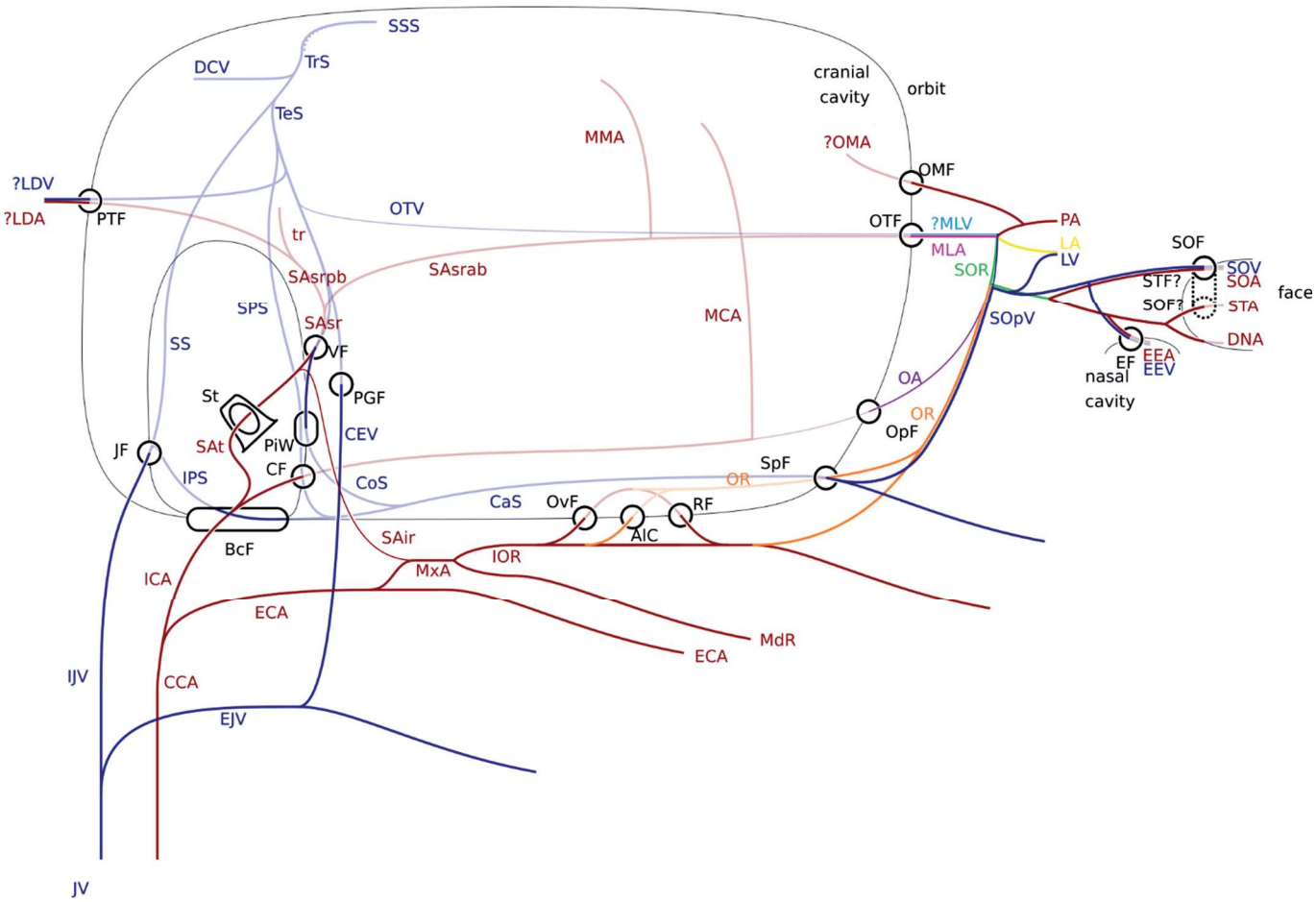

Figure II-28: Simplified scheme of the main vascular structures crossing the braincase in bats, after Bugge (1974), Wible (1987, 1993), Diamond (1991a,b, 1992), Wible & Davis (2000), Giannini et al. (2006), Evans & Lahunta (2012), Palermo (2013), Muizon et al. (2015), Standring (2016). Shaded lines indicate an intracranial course, and plain lines indicate an extracranial course. Arteries are in red and veins in blue. Segments in other colors and question marks indicate more debated segments (i.e., features only reported in humans, multiple possible courses, etc). Abbreviations of arterial structures: CCA: Common Carotid Artery / DNA: Dorsal-Nasal Artery / ECA: External Carotid Artery / EEA: External Ethmoidal Artery / ICA: Internal Carotid Artery / IOR: Infra-Orbital Ramus (of the Maxillary Artery) / LA: Lacrimal Artery / LDA: Large Diploic Artery / MCA: Middle Cerebral Artery / MdR: Mandibular Ramus (of the Maxillary Artery) / MLA: Meningo-Lacrimal Artery / MMA: Middle Meningeal Artery / MxA: Maxillary Artery / OA: (Internal) Ophthalmic Artery / OMA: Orbito-Meningeal Artery / OR: Orbital Ramus (of the Intra-Orbital Ramus of the Maxillary Artery) / PA: Periorbital Artery / SAir: Stapedial Artery, inferior ramus / SAsr: Stapedial Artery, superior ramus / SAsrab: Stapedial Artery, superior ramus, anterior branch / SAsrpb: Stapedial Artery, superior ramus, posterior branch / SAt: Stapedial Artery, trunk / SOA: Supra-Orbital Artery / SOR: Supra-Orbital Ramus (i.e., anastomotic ramus between the Meningo-Lacrimal Artery, the Ophthalmic Artery and the Orbital Ramus; sometimes called "External Ophthalmic Artery") / STA: Supra-Trochlear Artery / tr: temporal ramus. Abbreviations of venous structures: CaS: Cavernous Sinus / CEV: Capsuloparietal Emissary Vein / CoS: Communicant Sinus / DCV: Dorsal Cerebellar Vein / EEV: External Ethmoidal Vein / EJV: External Jugular Vein / IJV: Internal Jugular Vein / IPS: Inferior Petrosal Sinus / JV: Jugular Vein / LDV: Large Diploic Vein / LV: Lacrimal Vein / OTV: Orbito-Temporal Vein / MLV: Meningo-Lacrimal Vein / SOpV: Superior Ophthalmic Vein / SOV: Supra-Orbital Vein / SPS: Superior Petrosal Sinus / SS: Sigmoid Sinus / SSS: Superior Sagittal Sinus / TeS: Temporal Sinus / TrS: Transverse Sinus. Abbreviations of bony apertures: AlC: Alisphenoid Canal / BcF: Basicochlear Fissure / CF: Carotid Foramen / EF: Ethmoidal Foramen / JF: Jugular Foramen / OMF: Orbito-Meningeal Foramen / OpF: Optic Foramen / OvF: Oval Foramen / OTF: Orbito-Temporal Foramen / PGF: Post-Glenoid Foramen / PiW: Pyriform Window / PTF: Post-Temporal Foramen / RF: Round Foramen / SOF: Supra-Orbital Foramen / SpF: Sphenorbital Fissure / St: Stapes / STF: Supra-Trochlear Foramen / VF: Varying Foramen

II.6.A) Arteries

The main artery that supplies the head and the neck in mammals is the common carotid artery (e.g., Wible & Davis 2000, Barone & Bortolami 2004, Standring 2016). At the basis of the head, it divides into the internal and external carotid arteries (e.g., Wible & Davis 2000, Barone & Bortolami 2004, Standring 2016), which are of varying relative importance across mammals (Barone & Bortolami 2004). The internal carotid artery is my main focus because, as its name means, it supplies the internal part of the cranium, including the brain (e.g., Wible & Davis 2000, Standring 2016). Among other branches, the internal carotid artery sends off a branch known as the stapedial artery (e.g., Wible 1987, Dilenge & Ascherl 1980), which is secondarily lost during the ontogeny in several mammalian groups where its subsequent branches are annexed by other arteries (for instance, see Wible [1987] at the mammalian scale and Hitier et al. [2013] regarding humans); in bats, the stapedial artery is present in adults and thicker than the rest of the internal carotid artery after passed this dichotomy (Wible & Davis 2000).

The stapedial artery then passes through the obturator foramen of the stapes (e.g., Wible & Davis 2000), and then dichotomizes in two rami: a superior and an inferior one, the latter being thinner (if not absent) than the former in bats (Wible & Davis 2000).

The superior ramus of the stapedial artery is of interest because it then enters the braincase (e.g., Giannini et al. 2006), through various apertures in bats (e.g., through a foramen in the tegmen tympani of the petrosal in *Megaderma lyra* [Wible & Davis 2000], or in an unnamed space between the parietal and the squamosal in *Pteropus livingstonii* [Giannini et al. 2006]). This superior ramus then also ramifies in two branches: an anterior and a posterior one. The posterior branch gives off several temporal rami (Wible 1987, Wible & Davis 2000, Giannini et al. 2006) and then becomes the large diploic artery ("arteria diploëtica magna") which runs along the posttemporal canal ("parietosquamosal canal" in Diamond [1992]) and exits the braincase through a posttemporal foramen ("parietosquamosal foramen" in Diamond [1992]) (Wible 1987, 2012). It is unclear whether this artery is present in bats (as discussed by Buchanan & Arata [1969] in the phyllostomid *Artibeus lituratus* and Diamond [1992] in the phyllostomid *Carollia perspicillata*) or not (Wible & Davis 2000). The anterior branch is bigger and runs anteriorly along the braincase (Wible 1987, Wible & Davis 2000) in the orbito-temporal canal (Giannini et al. 2006; also called "cranio-orbital sulcus" e.g., Wible 1987, Diamond 1991a, Diamond 1992). During its course, it gives off several meningeal rami including a major one, the middle meningeal artery; Wible (1987) expresses doubts about the homology between this "human structure" as it could be only partially composed of a main meningeal ramus of the superior ramus, but to my sense several works support this hypothesis (e.g., Tandler 1899, Bugge 1974, Diamond 1991b, Wible 1993, Silbergleit et al. 2000, Coleman & Boyer 2011). It exits the skull through the orbito-temporal foramen (Giannini et al. 2006; also called "cranio-orbital foramen" e.g., Wible 1987, Diamond 1991a, Diamond 1992) and becomes the meningo-lacrimal artery (Diamond 1991b; also referred to as the "external ophthalmic artery" in the medical and veterinary literature).

The inferior ramus of the stapedial artery, on the contrary, stays outside the braincase (Wible 1987 in a sense; Wible & Davis 2000, Giannini et al. 2006) and goes anteroventrally, finally joining a branch of the external carotid artery to form the maxillary artery (Wible 1987). The maxillary artery then dichotomizes, giving off a mandibular ramus (going more ventrally) and an infraorbital ramus, which remains on the external ventral surface of the braincase (Wible 1987). In bats, the infraorbital ramus, which can have an intracranial course, sends off a branch, the orbital ramus (Wible 1987). This intracranial course varies across bats: in some taxa, the infraorbital ramus enters through the oval foramen, sends off the orbital ramus, and exits through the round foramen (in "chiropterans" in general; Wible 1987); in other bat species, the orbital ramus is sent off before it enters the braincase through the alisphenoid canal (in *Megaderma lyra*; Wible & Davis 2000); in others, the infraorbital ramus does not enter at all in the braincase and the orbital ramus individualizes more anteriorly (in *Rhinolophus* [Grosser 1901, Kallen 1977] and *Desmodus* [Kallen 1977]); in others, there is both an intracranial and an extracranial course (in *Artibeus lituratus*; Buchanan & Arata 1969). If the orbital ramus travels through the braincase, it exits from it to the orbit through the sphenorbital fissure. It then goes anteriorly, along the posterior surface of the orbit, sending off several minor branches to the inferior and superior optic muscles (Tandler 1899).

The rest of the internal carotid artery (i.e., after sending off the stapedial artery) then enters the braincase through the carotid foramen (Wible & Davis 2000, Giannini et al. 2006). It crosses the cavernous sinus ("cavernous part" of its course) in the dural roof of the skull and sends off several small branches during its course, supplying various structures (such as the hypophysis and the trigeminal ganglion) (e.g., Barone & Bortolami 2004, Standring 2016). It then (anteriorly) pierces the dura matter ("intracranial part" of its course) and turns back dorsally. While it bends, it sends off the ophthalmic artery (e.g., Barone & Bortolami 2004, Standring 2016), which travels to the orbit through the optic foramen and then anastomoses with the meningo-lacrimal artery and the orbital ramus to form the supra-orbital ramus (Diamond 1991b). The remaining internal carotid artery sends off other small branches, then two branches connecting to the circle of Willis (the posterior communicating artery and the anterior cerebral artery) and then remains as the middle cerebral artery (e.g., Barone & Bortolami 2004, Standring 2016). The latter is of interest here because it sometimes marks the internal surface of the braincase, and it was also called "sylvian fossa artery" (Robertson 1828, Barone & Bortolami 2004) due to its location close to the sylvian neopallial sulcus.

An anastomosis of three arteries (i.e., the ophthalmic and meningo-lacrimal arteries and the orbital ramus) has been found so far in guinea pigs (Kuchinka 2018) and it appears that the relative contributions from the stapedial ("meningeal") and "ophthalmic" (to designate the part from the internal carotid artery) parts vary greatly in humans (Hayreh & Dass 1962). Regarding bats, I have to generalize the relationships between vessels from the available literature at the mammalian scale. In "extant mammals", and especially "in megachiropterans and some microchiropterans", Wible (1987) highlights that the meningo-lacrimal artery exits the braincase to the orbit and anastomoses with the orbital ramus. In bats, according to Tandler (1899), this anastomosis also comprises the (internal) ophthalmic artery, the last branch to be sent off by the internal carotid artery; however, Tandler (1899) emphasizes that the contribution of the ophthalmic artery is minor (to absent) compared to those of the orbital ramus and of the meningo-lacrimal artery (for instance, as previously said, it is the orbital ramus that irrigates the optic muscles). In humans, Diamond (1991b) homologizes and defines the supra-orbital ramus as being the anastomotic part between these three components: it is the transition between the meningo-lacrimal artery, the orbital ramus, and the ophthalmic artery posteriorly and two bundles of arteries anteriorly that irrigate the eye, the nasal cavity and the face.

One of these two bundles is closer to the meningo-lacrimal artery (i.e., more dorsal), and it quickly splits into the lacrimal artery and the periorbital artery in humans (Diamond 1991b, Narayan & Ghosh 2021). The latter may give off an orbito-meningeal artery which travels back in the braincase through an additional orbito-meningeal foramen, but this configuration seems to be limited to humans or, at least, hominids (Diamond 1991b). The periorbital artery, described in humans by Diamond (1991b), may correspond to the short posterior ciliary artery of Palermo (2013) or to palpebral arteries (Standring 2016). But Steven (1964), for instance, did not find another artery than the lacrimal one in the ox. I chose to keep the term "periorbital" given the fact that it is not clearly known which structures are irrigated, keeping in mind that this part of this bundle may be absent in bats as well.

The second group of arteries also dichotomizes in two main branches (Diamond 1991b, Standring 2016, Narayan & Ghosh 2021): one is the supraorbital artery, going to the top of the skull by crossing the supraorbital foramen, and the other one gives off the ethmoidal artery during its course (Tandler 1899, Giannini et al. 2006), traveling to the nasal cavity through the ethmoidal foramen, then dichotomizing in the supratrochlear artery (which parallels the supraorbital artery, crossing an adjacent supratrochlear foramen in humans [e.g., Diamond 1991b, Standring 2016, Narayan & Ghosh 2021] which is absent in bats; I may suppose that both arteries cross the same supraorbital foramen) and the dorsalnasal artery (irrigating the face).

II.6.B) Veins

A main vein, the **jugular vein**, drains the blood from the head and the neck. This vein follows the pathway of the carotid artery: it is single ventrally to the head, and divides in the neck in the (superficial) **external** and (deep) **internal jugular veins** (e.g., Hegedus & Shackelford 1965, Evans & Lahunta 2012). A human feature is that there are also anterior and posterior jugular veins (e.g., Standring 2016) which are not retrieved in other mammals (e.g., Hegedus & Shackelford 1965). Moreover, across mammals, the relative predominance of the external or internal jugular vein is variable (Hegedus & Shackelford 1965). In bats, according to Grosser (1901), the external jugular vein is predominant. As previously done regarding head arteries, the internal jugular vein is my focus here as it drains the blood from the braincase (e.g., Hegedus & Shackelford 1965, Evans & Lahunta 2012, Standring 2016). The internal jugular vein exits the skull through the jugular foramen (e.g., Hegedus & Shackelford 1965); just before exiting it, it receives two major sinuses located around the petrosal: the sigmoid sinus (dorsally and posteriorly) and the inferior petrosal sinus (ventrally) (Barone & Bortolami 2004, Giannini et al. 2006, Evans & Lahunta 2012). The sigmoid sinus is a branch of an early dichotomy of the transverse sinus (Diamond 1992, Barone & Bortolami 2004, Giannini et al. 2006, Evans & Lahunta 2012); the other one is the temporal sinus (Diamond 1992). I keep the term temporal sinus because it is used in descriptions of veins in the dog (Reinhard et al. 1962, Evans & Lahunta 2012) and in other domestic mammals (Barone & Bortolami 2004); using this term marks a difference between the part of this sinus having or having not received its tributaries, as Diamond (1992) who calls it "petrosquamous sinus". The transverse sinus, oriented mediolaterally and located usually between the cerebrum and the cerebellum, drains the superior sagittal sinus, oriented anteroposteriorly and located between the cerebral hemispheres (e.g., Barone & Bortolami 2004, Giannini et al. 2006, Evans & Lahunta 2012, Standring 2016). The sister branch of the sigmoid sinus, the temporal sinus, then drains several branches.

A first vein (not a sinus) is drained by the transverse sinus: the dorsal cerebellar vein, which is located between the vermis of the cerebellum and the cerebellar hemispheres (Barone & Bortolami 2004), filling the paramedian fissure.

Two venous branches accompany endocranial arteries: a large diploic vein ("vena diploëtica magna"; "parietosquamosal vein" in Diamond [1992]) joins and parallels the large diploic artery, and another joins and parallels the anterior branch of the superior ramus of the stapedial artery (Diamond 1992). The latter branch is sometimes named "cranio-orbital sinus", referring to the bony structure housing it, the cranio-orbital sulcus; it is here named orbito-temporal canal, so I call this venous branch the orbito-temporal vein (following Wible 2010, Muizon et al. 2015, Martinez et al. 2019). It is unclear if these two veins are present in bats: it is already unclear if there is a large diploic artery (see previously), and when considered present, the venous contribution may be quite smaller to absent (Diamond 1992, Wible 1993); regarding the orbito-temporal vein, it seems that the orbito-temporal canal is largely, if not fully, filled by the anterior branch of the superior ramus of the stapedial artery (Diamond 1992).

Two other branches, definitely present in bats (Diamond 1992, Giannini et al. 2006), connect to the temporal sinus: the superior petrosal sinus, which goes on the anterior aspect of the petrosal (e.g., Diamond 1992, Wible 1993, Barone & Bortolami 2004, Giannini et al. 2006), and the capsulo-parietal emissary vein. This vein is also called "retromandibular vein", "postglenoid vein", or "parietosquamosal vein"; I keep the term "capsulo-parietal emissary vein" because it is the ontogenetically original structure giving rise to this vein according to Diamond (1992), and because it better accounts for the function of this vein (i.e., connecting extracranial and intracranial veins. The capsulo-parietal emissary vein then exits the skull through the postglenoid foramen (e.g., Diamond 1992, Wible 1993, Barone & Bortolami 2004, Giannini et al. 2006). This vein may also drain a tributary communicating with the cavernous sinus, the communicant sinus (Diamond 1992), which is accompanied intracranially by the inferior ramus of the stapedial artery. In *Megaderma lyra* (Wible & Davis 2000), the communicant sinus exits the braincase by the aperture crossed by the superior ramus of stapedial artery (which is, in this species, a foramen in the tegmen tympani of the petrosal) and then goes back in it through the pyriform window, joining the cavernous sinus. There is no mention if the inferior ramus of the stapedial artery accompanies the communicant sinus or not. Diamond (1992) did not find a communicant sinus in the phyllostomid *Carollia perspicillata*; this sinus may be variably present in bats.

The branching pattern of these veins and sinuses drained by the temporal sinus is subject do debate as it varies across mammals: in the phyllostomid *Carollia perspicillata* (Diamond 1992) and in the megachiropteran *Pteropus* (Giannini et al. 2006), this is not specified; in the primitive primate scheme of Diamond (1992), the superior petrosal sinus and the large diploic vein are not figured, and the orbito-temporal vein, the capsulo-parietal emissary vein and the communicant sinus all exit through the postglenoid foramen; in the colugo *Cynocephalus volans* (Wible 1993), the superior petrosal sinus diverges at the same time than the sigmoid and temporal sinuses and the latter sends off a large diploic vein before continuing as the communicant sinus (there is no capsulo-parietal emissary vein as defined here; the "capsulo-parietal emissary vein" of this article would correspond, in its definition, to my "temporal sinus"); in the primitive eutherian scheme of Wible (1993), the superior petrosal sinus diverges first from the temporal sinus, then is a trichotomy between the large diploic vein, the capsulo-parietal emissary vein and the orbito-temporal vein; in the tree shrew *Ptilocercus lowii* (Wible & Zeller 1994), the superior petrosal sinus is firstly differentiated, but there is no information about the level at which the orbito-temporal vein connects to the temporal sinus, and there is no mention of the large diploic vein; in

the nine-banded armadillo *Dasypus novemcinctus* (Wible 2010), the sigmoid sinus, the orbito-temporal vein, the capsulo-parietal emissary vein and the large diploic vein all branch together at the same level; in the pantodont *Alcidedorbignya inopinata* (Muizon et al. 2015), the superior petrosal sinus individualizes from the sigmoid sinus, and along the temporal sinus, the large diploic vein is first connected, then is the orbito-temporal vein. Regarding bats, what I can interpret from this noisy summary is that the superior petrosal sinus seems to differentiate early, and rather from the temporal sinus; regarding the large diploic vein and the orbito-temporal vein, only Muizon et al. (2015) in the pantodont *Alcidedorbignya inopinata* propose that the large diploic vein diverge earlier. I retained these hypothesis in my scheme for bats, but with a low confidence.

The inferior petrosal sinus, located on the ventral aspect of the petrosal, remains inside the braincase in bats (even if it variously fills the basicochlear fissure; Giannini et al. 2006). Anteroventrally to the petrosal, it drains together with the superior petrosal sinus the cavernous sinus (e.g., Wible 1993, Muizon et al. 2015, Standring 2016). The communicant sinus also drains the cavernous sinus, joining it anteriorly to the inferior/superior petrosal sinuses dichotomy (Wible 1993, Wible & Davis 2000).

In mammals in general, this cavernous sinus, of anastomotic aspect, is located on the ventral surface of the braincase: it surrounds the hypophysis and several structures cross it, of vascular (such as the internal carotid artery) or neural (such as the cranial nerves III to VI) natures (e.g., Wible 2011, Evans & Lahunta 2012, Standring 2016). The cavernous sinus drains other venous structures outside the braincase; they join at the level of the sphenorbital fissure to form this cavernous sinus (e.g., Diamond 1992, Wible 1993, Wible 2011, Evans & Lahunta 2012). Of the various structures forming it is the superior (in humans; e.g., Diamond 1992, Cheung & McNab 2003, Standring 2016) or external (in the dog; e.g., Evans & Lahunta 2012) ophthalmic vein (e.g., Wible & Zeller 1994, Cheung & McNab 2003, Palermo 2013).

The orbito-temporal vein extends anteriorly to the orbit through the orbito-temporal foramen as do the anterior branch of the superior ramus of the stapedial artery. While trying to propose homologies of human veins for other mammals, Diamond (1992) names this segment the periorbital vein; in a purpose of homogenization based on relative location of vascular segments, I call it a **meningo-lacrimal vein**. This vein anastomoses with the superior ophthalmic artery in the back of the orbit (Diamond 1992). However, the orbito-temporal vein may be tiny in bats according to Diamond (1992), so I consider that the orbital venous anastomosis mostly relies on the contribution of the superior ophthalmic artery.

This orbital venous anastomosis drains several veins that grossly (i.e., to a lesser extent than in general, and with substantial inter-individuals variation, according to Cheung & McNab [2003] in humans) parallel the orbital arteries (Cheung & McNab 2003, Standring 2016). To refer to the previously described orbital arteries only, it first drains a lacrimal vein then a supraorbital vein (paralleling the supraorbital artery, it comes from the upper part of the face, draining the frontal diploic vein, to the orbit through the supraorbital foramen) which receives during its course the ethmoidal vein (traveling from the nasal cavity through the ethmoidal foramen; as for the arteries, there are two, anterior and posterior, ethmoidal veins in the human, but I may suppose that there is a single one in bats, as for the corresponding artery) (e.g., Cheung & McNab 2003, Evans & Lahunta 2012, Standring 2016).

II.7) Vascular imprints (Fig. II-1) (replacing and completing the The orbitotemporal canal section)

A main structure found on bat endocranial casts is the orbito-temporal canal, in which lies the anterior branch of the superior ramus of the stapedial artery and the orbito-temporal vein. The latter is likely to be absent from the orbito-temporal canal (Diamond 1992), so I assume in Figure II-1 that the anterior branch of the superior ramus is the only of the two vascular structures that lies in it. I here discuss about the "orbito-temporal canal", because this is the name of the structure seen on an endocast, but I illustrate and label it as the "anterior branch of the superior ramus of the stapedial artery" on the Figure II-1 to mark its connections with other arterial structures.

It is clear that the orbito-temporal canal does not mark the position of the rhinal fissure in bats (Schneider 1957, 1966, Maugoust & Orliac 2021). It is however of varying morphology across chiropterans, depending on the skull organization and especially of the angle between the braincase and the rostrum (Fig. II-29). However, the orbito-temporal canal is not necessarily the only vascular structure that can mark the skull and be retrieved on an endocranial cast. According to the previous section, several vascular structures run through the braincase.

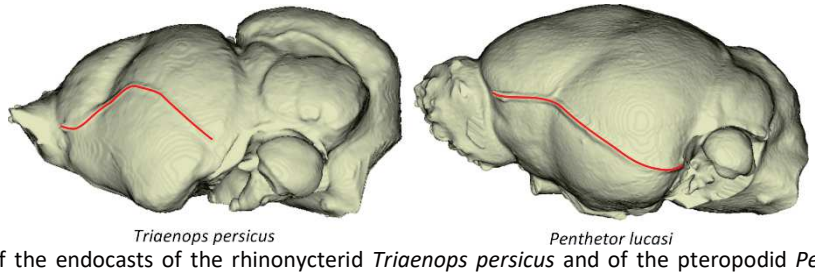

Figure II-29: Lateral view of the endocasts of the rhinonycterid *Triaenops persicus* and of the pteropodid *Penthetor lucasi* showing the variation in the shape of the anterior branch of the superior ramus of the stapedial artery (in red). Not to scale.

The stapedial artery and its following rami and branches received a peculiar attention, because of its phylogenetic interest (e.g., Wible 1983, 1987) but also because it leaves several marks on the petrosal bone (e.g., Butler 1948, Cartmill & MacPhee 1980, Rougier et al. 1992, Wible 2010, Wible 2011). These marks are however not only on the endocranial face of that bone, and some branches of the stapedial artery sometimes pierce it. Of the stapedial artery, the superior ramus has an intracranial course (entering through various foramen or fissure); the inferior ramus may also have an intracranial course in the sphenoid region. The trunk of the superior ramus of the stapedial artery may be visible on the posterior wall of the piriform lobes cast (Fig. II-30), forming distally an angle with the proximal end of its anterior branch (see following). The anterior branch of the superior ramus obviously marks the inner surface of the braincase, lying in the orbito-temporal canal (e.g., Wible 1987, Diamond 1991a, Maugoust & Orliac 2021).

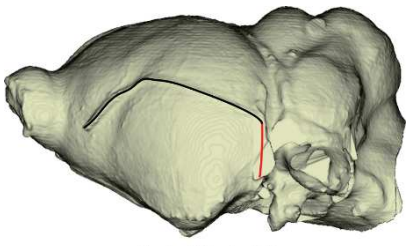

Figure II-30: Lateral view of the endocast of the vespertilionid *Scotophilus kuhlii* showing the position of a potential trunk of the superior ramus of the stapedial artery (in red) relative to its anterior branch (in black). Not to scale.

Its meningeal rami also may be visible (Fig. II-31): I propose that the middle meningeal artery, the main temporal ramus of this anterior branch, is the first that can be recognized (being the main one of the temporal rami), but it is also the only that can be homologized throughout species (e.g., Wible 1987, Diamond 1991a), and I will simply label as "temporal rami" the other branches arising from the anterior branch of the superior ramus. On the contrary, the posterior branch usually runs in the posttemporal canal (e.g., Wible 1993, Muizon et al. 2015), which is located between the petrosal and the squamosal, an area which I did not reconstruct because it is not a "brain area". The large diploic artery is therefore not visible on an endocranial cast (in addition, following previous section, it is variably present in bats) as well as the temporal ramus arising from it. The inferior ramus of the stapedial artery can have an intracranial course through its infra-orbital ramus (between the oval and round foramina) and/or its orbital ramus (between some point between the oval and round foramina or the alisphenoid canal, and the sphenorbital fissure). However, the whole sphenoid region is filled in the dura mater by the cavernous sinus, with several structures crossing it. I cannot expect the infra-orbital and/or orbital rami, whose course is intracranial, to leave an imprint on the bone; the only manifestation of this structure would be the presence of a distinct anterior opening of the alisphenoid canal.

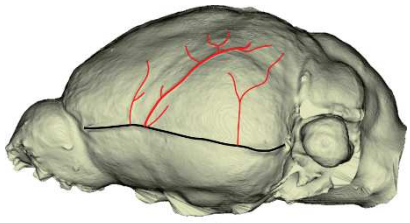

Rousettus obliviosus

Figure II-31: Lateral view of the endocast of the pteropodid *Rousettus obliviosus* showing the dense vascular structure casts sometimes retrieved on an endocast, with the middle meningeal artery (thick red line) and several temporal rami (thin red lines) relative to the anterior branch of the superior ramus of the stapedial artery (in black). Not to scale.

A little aside seems necessary. Wible & Davis (2000) propose that a major feature distinguishing microchiropteran bats from megachiropteran bats is the disappearance of the stapedial artery during the ontological development, its branches being annexed by the external carotid artery. This seems, to me, a too definitive conclusion: my sample clearly highlights that there is a well-defined and marked orbito-temporal canal in non-pteropodine megachiropteran bats (Fig. II-32). There would be at least an anterior branch of the superior ramus of the stapedial artery, which seems not to be annexed by the external carotid artery given the quite posterior location of its posterior extremity (which is similar to that of other bats). I cannot answer to that problem using endocasts only (my aim is, in this section, to provide as much terms as possible that can be used without osteological context), so I will assume that the organization of the stapedial artery is retained in megabats, contra Wible & Davis (2000), and a perspective would be to test if secondary modifications characterize this taxon among pteropodids.

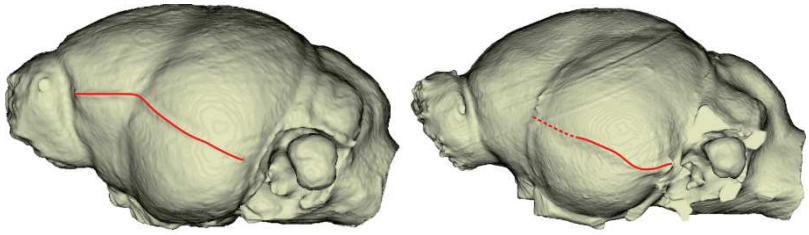

Balionycteris maculata *Hypsignathus monstrosus*

Figure II-32: Lateral view of the endocast of the pteropodids *Balionycteris maculata* and *Hypsignathus monstrosus* showing the variation in the anterior extension of the anterior branch of the superior ramus of the stapedial artery (in red), and especially that even though it varies in its form, this branch is present in megabats. Not to scale.

The rest of the internal carotid artery, after (i.e., anteriorly to) sending off the stapedial artery, is considered to be a reduced structure in bats (Wible & Davis 2000); that would imply less and/or less marked endocranial imprints. After entering the braincase through the carotid foramen, the internal carotid artery crosses the cavernous sinus, in the dura mater; I do not expect a peculiar mark for the internal carotid artery, but maybe a larger groove for the whole structures involved (including cranial nerves III, IV, V1, and VI). During the (following) intracranial course of this artery, several other small branches are sent off, leaving terminally the internal carotid artery as the large (relative to the other branches already sent) middle cerebral artery, also called "sylvian fossa artery" because of its location. Across my sample, the only mark that could be attributed to the internal carotid artery is that of the middle cerebral artery, an anteriorly convex mark at the anterior third of the cerebrum whose ventral part sometimes extends to the sphenorbital fissure (Fig. II-33). The ophthalmic artery would exit through the optic foramen, but it may also exit through the unknown foramen #2 when present. However, there is several times the cast of a channel branching to the ventral (i.e., proximal) part of the middle cerebral artery that goes anterodorsally and joins the anterior extremity of the anterior branch of the ramus superior of the stapedial artery; such a vessel would fully correspond in its definition (based on vessel connexions) to the ophthalmic artery, but with an unexpected fully intracranial course.

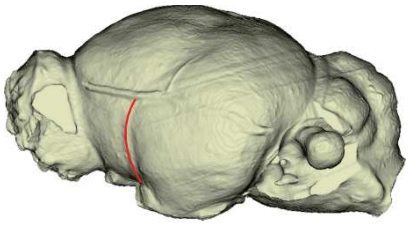

Figure II-33: Lateral view of the endocast of the pteropodid *Nyctimene major* showing the position of the cast of the middle cerebral artery (in red). Not to scale.

In the optic network of arteries, some structures exiting the orbit can be retrieved on an endocranial cast. First is the orbito-meningeal artery; it seems however to be a human or hominid feature (Diamond 1991b). Second is the external ethmoidal artery, which travels back to the nasal cavity through the olfactory bulbs fossa, entering through the ethmoidal foramen that is located at the level of the lateral walls of the olfactory bulbs. Other arteries stay in the orbit or travel to the face, being therefore not present on an endocranial cast.

Several venous sinuses also clearly mark the inner surface of the braincase and surround the petrosal bone, with thus, as for the stapedial artery, further branches and several works dealing with the identification of these structures (e.g., Butler 1948, Cartmill & MacPhee 1980, Rougier et al. 1992, Wible 2010, Wible 2011). The superior sagittal sinus is sometimes visible as a cast between the two cerebral hemispheres, and more consistently is retrieved a wide transverse sinus, delineating the posterior limit of the cerebral hemispheres (Fig. II-34). Its medial part may be tricky to identify, as it passes near/over the rostral colliculi and the epiphysis according to Maugoust & Orliac (2021). I however now consider very unlikely the epiphysis to be visible.

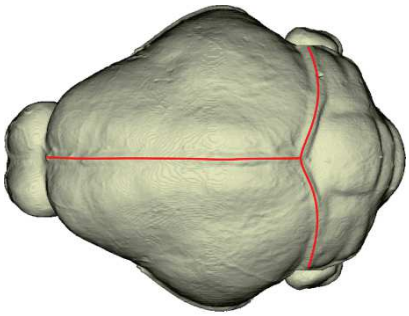

Casinycteris argynnis

Figure II-34: Dorsal view of the endocast of the pteropodid *Casinycteris argynnis* showing the position, development and connection between the longitudinal and tranverse sinuses (in red). Not to scale.

Evidences in several taxa of my sample (Fig. II-35) show that the medial course of the transverse sinus is anterior to the location of the rostral colliculi, clearly paralleling the posterior border of the cerebral hemispheres. This sinus extends far laterally, along the anterior side of the cerebellar hemispheres.

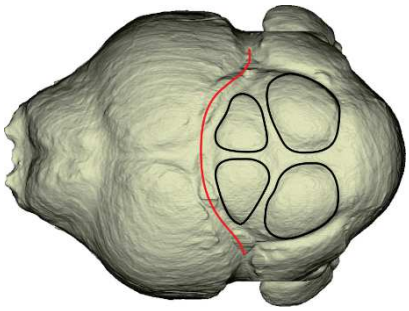

Balantiopteryx plicata

Figure II-35: Dorsal view of the endocast of the emballonurid *Balantiopteryx plicata*showing the pathway of the transverse sinus (in red) relative to the position of the rostral and caudal colliculi (in black). Not to scale.

During its course, the transverse sinus receives proximally the dorsal cerebellar vein, which leaves an imprint in some taxa (Fig. II-36). It then splits in a perpendicular and posteriorly located sigmoid sinus, which surrounds the petrosal dorsally and posteriorly, and the temporal sinus on its continuation.

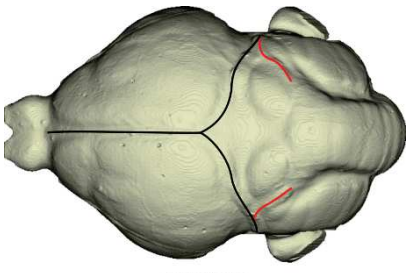

Lavia frons

Figure II-36: Dorsal view of the endocast of the megadermatid *Lavia frons* showing the dorsal cerebellar veins (in red) and their position and connection relative to the longitudinal and transverse sinuses (in black). Not to scale.

The temporal sinus shortly enters a canal which is variously closed among taxa (Fig. II-37): grossly, it is still visible on the surface of the posterior wall of the piriform lobes in megachiropterans, while it is less visible to not visible at all in most other bats. In pteropodids, its most proximal part is even interrupted between a short time: there is not a clear continuation between the transverse sinus and that canal cast. This canal is subtle and, when present, often joins the pyriform window ventrally, crossing the cast of the posterior end of the anterior branch or the trunk of the ramus superior of the stapedial artery. While it is quite safe to attribute the ventral part of this cast (i.e., after crossing the superior ramus) to the communicant sinus (even though that imply no extracranial course), it is quite harder to found the ramification point of the other branches as they are not clearly distinct. The orbito-temporal vein may individualize and follow the anterior branch of the superior ramus, but if so, it happens at the crossing point of the venous and arterial structures. The superior petrosal sinus, the large diploic vein and the capsulo-parietal emissary vein and their branching point to the temporal sinus are not visible.

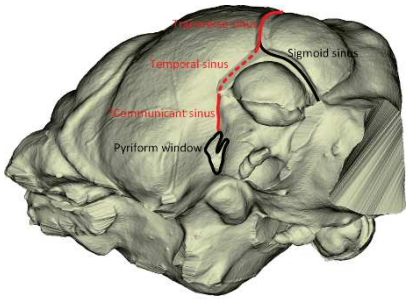

Diphylla ecaudata

Figure II-37: Posterolateroventral hybrid view of the endocast of the phyllostomid *Diphylla ecaudata* showing the various venous sinuses arising from the temporal sinus (in red), with especially its two direct branches, the sigmoid sinus (in black) and the temporal sinus (in dotted red line), and the continuation of the temporal sinus hypothesized as the communicant sinus (in red) until the pyriform window (in black). Not to scale.

Noticeable is that the sigmoid sinus is continuous with the posterior side of the cerebellar hemisphere: there is often a groove delineating each structure, but both are still continuous (Fig. II-38). Posteriorly, it is also often (but irregularly) continuous with the jugular foramen, where it exits and forms the internal jugular vein with the inferior petrosal sinus. The latter is thought to variably fill the basicochlear fissure. Here, as the latter aperture is confluent with the jugular foramen, one can propose that the inferior petrosal sinus variably fills the whole confluence. However, this confluence also implies the carotid foramen and the pyriform window, though the coalescence may be very thin between the concerned structures. Moreover, there is no peculiar “break” at the anterior apex of the basicochlear fissure cast. With all these facts in mind, the cast of the confluence might represent a blend of venous structures, not the inferior petrosal sinus only; I thus cannot deal with its morphology.

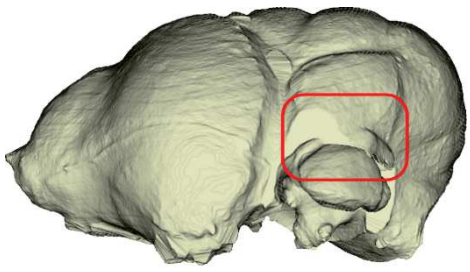

Balantiopteryx plicata

Figure II-38: Lateral view of the endocast of the emballonurid *Balantiopteryx plicata* showing the absence of a clear lateral limit between the cerebellar hemisphere and the sigmoid sinus. Not to scale.

The cavernous sinus, anteriorly, is drained by the inferior and superior petrosal sinuses and by the communicant sinus. The three former are not depictable here, while the latter has been previously discussed. The cavernous sinus, through which the nerves III to V cross, is moreover impossible to delineate, as well as the cavernous part of the internal carotid artery (which probably parallels the cranial nerves III, IV, V1, VI and potentially V2 until the sphenorbital fissure). The superior ophthalmic vein, which is drained by the cavernous sinus, follows a parallel pathway to that of the orbital ramus; the hypotheses for the latter (i.e., a probably not visible intracranial course between the sphenorbital fissure and either the round, oval, or caudal alisphenoid canal foramina) also stand for the former, as well as for the external ethmoidal vein that follows the external ethmoidal artery (i.e., exiting the braincase to the orbit by the ethmoidal foramen, on the lateral walls of the olfactory bulbs chamber).

III) Biological inferences: Limitations, pitfalls and solutions

Three primary quantitative variables are used here and have been used by Maugoust & Orliac (2021), which are the masses of the whole brain, of the olfactory bulbs, and of the paraflocculi. They are, however, not usable as they are. They need to be scaled to provide secondary, biologically meaningful variables: one measures the encephalization, involving the brain and body masses, and two are allegedly related to sensitive function, that are the relative mass of olfactory bulbs (linked to olfaction) and of paraflocculi (linked to balance).

The first of the three biological measures is the encephalization. According to Jerison (1973), the brain size is correlated with "the total number of neurons and glial cells in the brains of living mammals" (Jerison 1973: p.3), being a proxy of the "behavorial capacity" of Lashley (1949). The latter defines that "behavorial capacity" as being the "index of cephalization" of Dubois (1897), a ratio of observed over expected (given an allometric relationship) brain mass, and that "seems to represent the amount of brain tissue in excess" (Lashley 1949: p.33). Following Jerison (1973: p.55), brain size is related "to two factors, (a) body size and bodily functions, and (b) the "encephalization" of psychic functions": one part is explained by allometry, and the other ("in excess" according to Lashley 1949) is explained by the "encephalization" of psychic, cognitive functions. Jerison (1973) defines his own index of cephalization, that he names "Encephalization Quotient" (EQ), as being the ratio of the observed brain mass over the expected brain mass, whose formula is $0.12 \times BM^{2/3}$ (Jerison 1973: p. 61), with BM being the body mass in the same unit as the brain mass. Assuming an allometric relationship $Y = a \times X^b$ to estimate the expected brain mass given the body mass, these values (a and b) are obtained by regressing the natural logarithm of brain mass against that of body mass: the relationships becomes $\log(Y) = b \times \log(X) + \log(a)$; the slope is the allometric power of the function and the exponential of the intercept is the multiplicative factor. The EQ has no unit, but its value informs about the "encephalization" of the considered species: with a ratio over 1, there is an excess of brain tissue, and more or less "encephalization of psychic function". If the term "encephalization" has formerly a sense of development of specific functions in rostral part of the brains along a phylogenetic scale (Jerison 1973: p.8), it has become a common practice to use the term "encephalization" to describe those indexes of cephalization as the EQ of Jerison (1973), and talk about "encephalization" as it is, in fact, an expression of brain size relative to the brain mass (i.e., a relative brain size).

The EQ is widely used especially in studies dealing with endocranial casts (e.g., Radinsky 1978, Benoit et al. 2013, Orliac & Gilissen 2012, Bertrand et al. 2016, Maugoust & Orliac 2021), because the brain size is one of the rare brain measures to be possible with "fossil brains". Since the original definition or Jerison for all mammals (Jerison 1973), there were successive alternative definitions for mammals including bats, a clade not included in the dataset of Jerison (1973) (Eisenberg & Wilson 1978), but also for rodents (Pilleri et al. 1984) or for primates (Martin 1990). These alternative EQs, especially those not dealing with all mammals but with a single mammalian order, regress logarithms of brain and body masses for that group only and derivate the allometric parameters from that sample. This allows to better take into account the peculiarities of each group. However, with the progresses of Phylogenetic Comparative Methods (or PCM, see next section) to take into account the phylogenetical effects, some recent works established "phylogenetic EQ" (or pEQ), with a slope not obtained through an Ordinary Least Squares (OLS) regression (as for the XXth's studies defining EQ formulas) but through a Phylogenetic Generalized Least Squares (PGLS) regression (Ni et al. 2019 for anthropoids, Bertrand et al. 2021 for rodents).

There is, however, a critical issue to the use of the EQ that arises from a statistical point of view. This is due to the back and forth between natural and logarithmic scales. The encephalization quotient of a species is nothing more than the exponential of the residual of the log-log regression of brain and body mass for that species. The transformation of biological measurements to the logarithmic scale allows for direct comparisons of species without having to consider their size. Thus, the residuals of a log-log regression make sense in logarithmic units; by back-transforming them using the exponential, slight differences will be flattened while huge differences will be outstretched, deforming the scale of differences. This problem has been raised by Smith (1993): the residuals of an OLS have to be normally distributed (with a mean of zero and a given variance), but detransformed to natural values using the exponential, their distribution becomes log-normal (with a mean of one and an exponential variance proportional to the variance of the residuals), skewed toward high values. Thus, comparisons of encephalization should only remain at the logarithmic scale, not at the natural value scale.

The two other biological measures are the relative sizes of olfactory bulbs and of paraflocculi. Similar to the relative brain size (either named as "index of cephalization", "encephalization quotient" or "encephalization"), the goal is to express them against a predictor value in order to be able to compare species. Jerison (1973) stated that the size of a brain part is proportional to the function of this part compared to the other in his "principle of proper mass" (Jerison 1973: p.8). This principle has been extensively used in paleoneurology, not only with quantitative considerations, as it allows using endocast structures as paleobiological proxies. Several studies simply compared these "brain part" relative developments, but there also quickly were quantitative comparisons. I would emphasize the fact that, if one wants to follow the principle of proper mass, the sole and only variable to compare a brain part size is the brain size. Some studies recently compared these brain part sizes to the whole body mass (e.g., Bertrand et al. 2017; my goal here is only to provide some instances of that methodology, but not to target the authors). There is a critical issue to this methodology, as there also is another relationship between the brain mass and the body mass; the relationship that can be highlighted between a brain part mass and the body mass would encompass the encephalization relationship.

What I want to emphasize here with this little mathematical aside is that the brain part mass / body mass relationship is fully predictable using the encephalization and principle of proper mass relationships. This is rather straightforward, and the real message is that it does not mean that the terms are individually predictable (they only can be estimated, and only using other estimates…), but the whole relationship is predictable without using a new term. No biological sense that would not have been already detected using the encephalization and principle of proper mass relationships can be obtained by regressing a brain part mass against the body mass. There is no statistical interest to study this relationship, and the conclusions drawn from it can be biologically misleading as two biological relationships are actually considered. Here, the only predictor used for the olfactory bulbs and paraflocculi masses will hence be the brain mass.

Saying the BM is the body mass, BRM is the brain mass, and BPM is the brain part mass, applying the principle of proper mass would lead to define the equation (1) $\ln(\mathrm{BRM}) = a + b\ln(\mathrm{BM})$ and applying the "encephalization principle" would lead to define the equation (2) $\ln(\mathrm{BPM}) = a' + b'\ln(\mathrm{BRM})$. Starting with the simplest linear equation form, if one wants to explore the relationship (3) $\ln(\mathrm{BPM}) = \alpha + \beta\ln(\mathrm{BM})$, one can recall the equations (1) and (2) and find that $\ln(\mathrm{BPM}) = a' + b'\ln(\mathrm{BRM}) = a' + b'(a + b\ln(\mathrm{BM}))$ and $\ln(\mathrm{BPM}) = a' + ab' + bb'\ln(\mathrm{BM})$ (4); comparing this to the equation $\ln(\mathrm{BPM}) = \alpha + \beta\ln(\mathrm{BM})$, it is straightforward to find that (5) $\beta = bb'$ and (6) $\alpha = a' + ab'$.

By adding a bit of complexity to these equations, one can propose that the three previous equations are not fully true because some autocorrelation in the residuals may be expected, because of the phylogeny and/or of the ecology. If we add these incompressible residuals (r, r', and ρ) in the equations, we obtain (7) $\ln(\mathrm{BRM}) = a + b\ln(\mathrm{BM}) + r$ for the encephalization, (8) $\ln(\mathrm{BPM}) = a' + b'\ln(\mathrm{BRM}) + r'$ for the principle of proper mass, and one then wants to investigate the (9) $\ln(\mathrm{BPM}) = \alpha + \beta\ln(\mathrm{BM}) + \rho$ relationship. Again, recalling the two first equations, we have $\ln(\mathrm{BPM}) = a' + b'(a + b\ln(\mathrm{BM}) + r) + r'$ that is (10) $\ln(\mathrm{BPM}) = a' + ab' + bb'\ln(\mathrm{BM}) + r' + rb'$. Contrasting this to the third equation, it is straightforward to find that (11) $\beta = bb'$ (as in the previous equation) and that (12) $\alpha + \rho = a' + ab' + r' + rb'$. The latter term only is a "y-axis adjustment" of the regression line and both components α and ρ are theoretically not distinguishable, but one still may propose that (13) $\alpha = a' + ab'$ as previously (keeping only the single-valued elements) and that (14) $\rho = r' + rb'$ (keeping only the multiple-valued elements). Empirically, this is true only if the residuals are perfectly distributed around the regression line (i.e., if their mean is zero): the expectation of the whole formulas (equations (7), (8), and (9)) returns to the first set of formulas (equations (1), (2), and (3)), without residuals. Otherwise (as it can be expected in such a biological case), it is empirically impossible to randomly find these two equations (i.e., (13) and (14)) because the empirical estimates of the three parameters will only *estimate* them. The whole equation (10), however, remains valid and can be calculated because the errors between the estimates and the known parameters they estimate compensate each other.

Adding the complexity inherent to the estimation of those parameters (noted with a hat), that are the estimation errors (noted e) of each parameter (i.e., in a biological and *real* case), one in fact has the equation (15) $\ln(\mathrm{BRM}) = (\hat{a} + e_1) + (\hat{b} + e_2)\ln(\mathrm{BM}) + (\hat{r} + e_3)$ for the encephalization, the equation (16) $\ln(\mathrm{BPM}) = (\hat{a}' + e'_1) + (\hat{b}' + e'_2)\ln(\mathrm{BRM}) + (\hat{r}' + e'_3)$ for the principle of proper mass, and one wants to investigate the equation (17) $\ln(\mathrm{BPM}) = (\hat{\alpha} + \epsilon_1) + (\hat{\beta} + \epsilon_2)\ln(\mathrm{BM}) + (\hat{\rho} + \epsilon_3)$. Though not resolvable with a

sample (with n individuals) of the population (of N individuals), one is still able to find that $\ln(BPM)=(\hat{a}'+e'_1)+(\hat{b}'+e'_2)(((\hat{a}+e_1)+(\hat{b}+e_2)\ln(BM)+(\hat{r}+e_3))+(\hat{r}'+e'_3)$ that develops in (18) $\ln(BPM)=\hat{a}'+e'_1+\hat{a}(\hat{b}'+e'_2)+e_1(\hat{b}'+e'_2)+(\hat{b}'+e'_2)(\hat{b}+e_2)\ln(BM)+\hat{r}'+\hat{r}(\hat{b}'+e'_2)+e'_3+e_3(\hat{b}'+e'_2)$.

Recalling the equation (17), one can find that $\hat{\beta}+\epsilon_2=(\hat{b}+e_2)(\hat{b}'+e'_2)$ that develops in (19) $\hat{\beta}+\epsilon_2=\hat{b}\hat{b}'+\hat{b}e'_2+\hat{b}'e_2+e_2e'_2$; in the latter equation, two terms are unequivocally contributing to $\hat{\beta}$ and ϵ_2 that are $\hat{b}\hat{b}'$ and $e_2e'_2$ respectively, but there are also two terms contributing to both that are $\hat{b}e'_2$ and $\hat{b}'e_2$, explaining the previous discrepancy in β estimation using $\hat{b}$ and $\hat{b}'$ even if the real value of β is known. Similarly, recalling the equation (17), on can also find that (20) $\hat{\alpha}+\epsilon_1+\hat{\rho}+\epsilon_3=\hat{a}'+\hat{a}(\hat{b}'+e'_2)+e'_1+e_1(\hat{b}'+e'_2)+\hat{r}'+\hat{r}(\hat{b}'+e'_2)+e'_3+e_3(\hat{b}'+e'_2)$; intuitively, one can propose that $\hat{\alpha}=\hat{a}'+\hat{a}(\hat{b}'+e'_2)=\hat{a}'+\hat{a}\hat{b}'+\hat{a}e'_2$, that $\epsilon_1=e'_1+e_1(\hat{b}'+e'_2)=e'_1+e_1\hat{b}'+e_1e'_2$, that $\hat{\rho}=\hat{r}'+\hat{r}(\hat{b}'+e'_2)=\hat{r}'+\hat{r}\hat{b}'+\hat{r}e'_2$, and that $\epsilon_3=e'_3+e_3(\hat{b}'+e'_2)=e'_3+e_3\hat{b}'+e_3e'_2$. Similar to the case of the slope, there are in all these four equations terms that unequivocally link to the parameter estimates but also to their estimation error, such as none is computable without knowing at least the true value of another parameter. However, knowing the true value of these parameters, the equations (18), (19) and (20) still stand. It can also be showed that, as n tends towards N (i.e., as the sample widens and approaches the population), the parameter estimates tend to be closer to the true value of the parameters, the error terms near zero, and the equations (15) to (20) tend to the equations (7) to (12).

It is worth noting that the deviations observed in the parameter estimates in these three relationships are only due to the fact of sampling a population, even by considering autocorrelated and incompressible residuals. These deviations only are deviations between the slope, the intercept, the residuals, and their estimates. Absolutely no biological sense can be made out of the considered quantitative data in noting that the equations (5)/(11), (6)/(13), or (14) are not verified by replacing the parameters by their estimates in the calculations, as the further equations (19) and (20) showed that local estimates of the parameters cannot equal the true parameter values.

Finally, there is a general issue regarding the statistical use of residuals, in natural or logarithmic scale. With the recent burst of available Phylogenetic Comparative Methods that allow for discussing the evolution of traits, it is not rare to go beyond the values of the variable itself but to use them in further statistical treatments, which often involves linear regression. Using residuals is in fact misleading, and Freckleton (2002, 2009) demonstrated that this leads to bias in the regression parameter estimates; he rather encourages to perform a multiple linear model, with both the variable of interest (here, the brain mass) and its predictor (here, the body mass). In the phylogenetic method used here (see next section), the brain mass, olfactory bulbs mass, and paraflocculi mass will be regressed to the phylogeny but also to, respectively, the body mass, the brain mass, and the brain mass as additional predictors (following the multiple regression advised by Freckleton [2002, 2009]).

IV) Into the evolutionary history of variables: methodological choices for phylogenetical mapping

IV.1) Short review of Phylogenetic Comparative Methods (PCM)

My aim is to discuss the evolution of the qualitative and quantitative variables presented above based on a time-calibrated phylogeny. Several statistical methods (knowns as "PCM", for "Phylogenetic Comparative Methods") allow mapping variables on a phylogeny. Every PCM has underlying assumptions about the evolution of the variable. Some PCM are particularly common, but their underlying assumptions may not be.

The first principal method considers a number of changes as low as possible along phylogenetic branches. First called a "method of minimum evolution" (Cavalli-Sforza & Edwards 1967), it has later on been referred to as a "maximum parsimony" method (e.g., Maddison 1990, 1991, Martins & Hansen 1996, Steel & Penny 2000). The original sense of a "minimum" evolution can however also be interpreted as being an "optimality", and not necessarily "minimal number of transformation involved"; the original "minimum evolution" being "a computational approximation for ML [maximum likelihood]" in a context of continuous character evolution (Steel & Penny 2000: p.1). Implementations of maximum parsimony for the reconstruction of the evolution of characters have been further proposed, with a dichotomy between linear and squared-change parsimony (e.g., Swofford & Maddison 1987, Maddison 1990, 1991, Martins & Hansen 1996). Linear parsimony in fact applies Wagner parsimony (tolerating reversible changes; e.g., Felsenstein 1983) and aims to minimize the sum of all changes, while squared-change parsimony aims to minimize the sum of all squared changes (e.g., Maddison 1991, Martins & Hansen 1996 and references therein). Both techniques can be applied on continuous traits, but also on discrete ones if the state changes are linearly ordered. For unordered discrete variables, other algorithms are used (see Fitch 1971 and Narushima & Hanazawa 1997). Though quite intuitive, the parsimony criterion in fact relies on some assumptions about the evolution of the mapped trait: rates of evolution are assumed to be slow (the fewer the changes, the lower the rates), equal and symmetric (Felsenstein 1983, Martins & Hansen 1996, Cunningham et al. 1998, Omland 1999, Steel & Penny 2000, Joy et al. 2016), the full equality of evolutionary rates implying to ignore branch lengths (Martins & Hansen 1996, Omland 1999, Currie & Meade 2014, Joy et al. 2016).

Adjustments have been proposed to face these assumptions, resulting in modified techniques. Regarding linear parsimony, a recently developed technique takes into accounts branch lengths and does not consider a symmetry in evolution rates (Csűrös 2008, Didier 2017); it outputs an array of ancestral reconstruction estimates depending on the degree of asymmetry. A later work (Didier et al. 2019) implements an algorithm to detect the nodes of the tree where a shift in the trend of trait evolution would reduce the overall evolutionary cost of the tree (i.e., with lower evolutionary costs than with no shift). The branch lengths and the symmetry of rates are a critical problem of parsimony approaches (Cunningham et al. 1998, Omland 1999), and the implementations of Didier (2017) and Didier et al. (2019) are a critical advance in linear parsimonious reconstructions. Regarding squared change parsimony, a method allows to take branch lengths in count by penalizing the sum of squared change by the branch lengths (Maddison 1991). A main advantage of parsimony methods is that there are no explicit model of evolution, but only implicit assumptions, that do not need to be estimated a priori (regarding speed and variation of rate of evolution), or that cannot be estimated differently in any PCM (regarding branch lengths). Regarding evolutionary rates, the main drawback of parsimony methods is that the assumptions still exist, are not rarely violated (e.g., Felsenstein 1983, Cunningham et al. 1998, Joy et al. 2016, Holland

et al. 2020), and cannot be discussed a posteriori.

Explicit a priori evolutionary models (i.e., with explicit a priori parameters) are the second main group of PCM techniques. Several techniques have been proposed that rely on a fixed model (generally a Brownian motion or a derivative, like the "arithmetic brownian motion" and the "Ornstein-Uhlenbeck" models, see Royer-Carenzi & Didier [2016] for a review), whose parameters are estimated together with the nodal reconstructions. The most used are the "phylogenetic independant contrasts" ("PIC"; Felsenstein 1985), "maximum likelihood" ("ML"; Schluter et al. 1997), "restricted maximum likelihood" ("REML"; Paradis et al. 2004), and the "phylogenetic generalized least squares" ("PGLS"; Grafen 1989) (see Martins & Hansen 1996, Rohlf 2001, and Royer-Carenzi & Didier 2016 for reviews). Some links have been demonstrated between these techniques, some being particular cases of others; especially, under a strict Brownian motion, PIC, ML and PGLS but also (weighted) squared-change parsimony may reconstruct same ancestral states (see Webster & Purvis 2002 and Royer-Carenzi & Didier 2016). Dedicated models for discrete traits have also been proposed, especially the Mk (for Markov) model (Lewis 2001), generalizing the heterogeneous substitution models established for nucleotides to other discrete traits. While initially used for phylogenetic inferences, this model has then also been used in the PCM framework (e.g., Ekman et al. 2008, Boyko & Beaulieu 2021).

These techniques rely (explicitly or not) on a maximum likelihood method, that is an estimation of the "best fitting" scenario. This method estimates the probabilities of all possible reconstructions and returns the value with the highest probability (e.g., Cunningham et al. 1998, Folinsbee et al. 2015); it is proportional to the probability of having the (given) data as a result of a (given) evolutionary model, one of whose parameter being the (given) phylogenetic relationships (e.g., Folinsbee et al. 2015, Joy et al. 2016). A different reconstruction can thus be found compared to parsimony methods, being not as short (i.e., in terms of numbers of evolutionary steps) but more likely (e.g., Cunningham et al. 1998). It is not rare for authors (for examples of the applied process see Hunt et al. 2008, Slater et al. 2010, Sansalone et al. 2015, Beaulieu & O'Meara 2016, Martinez et al. 2020) to apply one or several of the previously quoted techniques (most often PGLS) with multiple models, to get the most likely reconstruction for each, compare them, and then to retain the best-fitted but also lowest-parametrized model by the use of decision criterion like the AIC ("Akaike Information Criterion", see Akaike 1973, 1974, Anderson et al. 1998, Pennell et al. 2015). The parsimony still stands in its ontological concept (see Cutcliffe & Harder 2009 and Folinsbee et al. 2015 for a comparison of concepts of parsimony), but in a different form, not retaining the single shortest path but the single most likely (or the "simplest model", that explains the best while staying as simple as possible). A noticeable extension of the Mk model is the BiSSE model (for "Binary-State Speciation and Extinction"; Maddison et al. 2007, but see also Holland et al. 2020) that incorporates supplemental parameters that are the speciation and extinction rates for all states of a trait.

Further development of the probabilistic approach, both in phylogenetic reconstruction and in PCM, is the Bayesian inference, or Bayesian likelihood method: the rationale is to compute the posterior probability of having a given topology (in the case of phylogenetic inference) or ancestral values (for instance, in the case of PCM) given prior probabilities about the tree, the data, and the data given the tree (i.e., what is estimate in the maximum likelihood method) (e.g., Folinsbee et al. 2015 and references therein). The likelihood is no more a result but becomes a parameter, allowing knowing the posterior probabilities for an array of values all at once. In the PCM framework, the output is therefore not a maximal probability for a single value, but a distribution of maximal probabilities for an array of values. This also allows the investigator to go back to the parameters of the evolutionary model provided as a

prior, in order to discuss the optimal values of the parameters and/or adjust their prior range before another analysis. Bayesian likelihood method is not different from maximum likelihood method in relying on explicit evolutionary models; they both only differ in the way to get the "simplest" model.

Therefore, the two mains types of PCM techniques rely on different interpretations of the parsimony concept. According to Cutcliffe & Harder 2009 and Folinsbee et al. 2015, "traditional" parsimony applying this concept in an 'epistemological' (i.e., literal) way by searching the single **shortest** path, and model-based techniques applying parsimony in an 'ontological' (i.e., more figurative) way by searching the **simplest** path (with all what 'simple' implies). This conceptual difference however don't prevent finding similar results while applying a rationale from a different mindset that, in the end, match: using the simplest evolutionary model (the brownian motion) with all its implicit assumptions and a time-calibrated phylogeny, both parsimony (i.e., weighted square-change parsimony) and model-based methods (i.e., ML and PGLS) will reconstruct the same ancestral values (Martins & Hansen 1997, Webster & Purvis 2002, Royer-Carenzi & Didier 2016), and other methods such as PIC will reconstruct similar value, and especially an identical root value (Royer-Carenzi & Didier 2016). A problem arises when considering the assumptions of the brownian motion, which implies a general consistency of evolutionary rates through time; at a global level, this model quickly become unrealistic and its assumptions are more and more likely to be violated (e.g., Harvey & Purvis 1991, Smaers & Mongle 2017). Only model-based methods can consider this and adjust the reconstruction algorithms: this yields adjusted models of increasing complexity (e.g., Diaz-Uriarte & Garland 1996, Hansen 1997; see also Pennell & Harmon 2013 and Pennell et al. 2015) needing criterion (like the AIC) to choose between (that choice remaining arbitrary and, moreover, empirical). Moreover, the successive adjustments of these models are only attempts to find a less non-fitted model to the tested data, but remain far from ideal (Pennell et al. 2015, Smaers & Mongle 2017, Blomberg et al. 2020). Especially, evolutionary rates remain homogeneous and defined at the whole tree level, while it is not unreasonable to expect discrepancies between clades depending on the initial question (see Chira & Thomas 2016). Some studies tried to implement models that tolerate rate heterogeneity and estimate this heterogeneity and/or the evolutionary rates for subtrees (e.g., Garland 1992, O'Meara et al. 2006, Eastman et al. 2011, Beaulieu & O'Meara 2016). However, these techniques are still under development, and they run the risk to "overfit" the model to the data (O'Meara et al. 2006, Eastman et al. 2011).

Most of the previous recently developed methods (i.e., Bayesian likelihood approaches-based methods) rely on exploratory Monte-Carlo Markov Chain (MCMC) search, involving a parametrized prior evolutionary model, that posteriorly reconstruct ancestral states and evolutionary rates. This involves a large amount of parameters that are estimated a posteriori, and as written by Smaers et al. (2016): p79, "the interpretation of what precisely is explained by the application of these methods is, however, not as straightforward as it may seem". In addition, and without intending to denigrate this method, I would just like to highlight that, by specifying an a priori model that is tested through the analysis, this methodology "only" aims to determine if the data is linked to the biological process underlying the prior evolutionary model or not, or at least to reconstruct the evolution of the data under the evolutionary model considered. Instead of discussing the phylogenetic reconstruction methods, Goloboff et al. (2018, 2019) explained that, dealing with discrete traits, the performance of methods relying on an explicit a priori evolutionary model is better than for parsimony-based (and more naive) methods, and this is assessed by contrasting their results to simulations realized using those a priori evolutionary models (an ultimately tautological rationale, that said). These authors however showed that model-based methods are less efficient (sometimes even worse than parsimony-based methods) when using real, empirical, datasets,

and Sansom et al. (2018) retrieved a weaker stratigraphic congruence of bayesian than parsimony phylogenies.

Another approach is to go back to the simplest possible model, that is the Brownian motion, and to put a maximal effort on the tolerance of heterogeneity across the tree. This is the rationale of two recent developed techniques that aim to work as much as possible with "the available phenotypic and phylogenetic information" (Smaers et al. 2016: p79), in order "to reconstruct ancestral character states of continuous characters when no definite assumptions can be made about the type of evolutionary process, or when the assumption of a model for phenotypic evolution is not appropriate at all" (Kratsch & McHardy 2014: p.i528). The latter assertion is particularly interesting in a case of exploratory analyses. Both techniques work at the branch level - the most focused level - and use a Brownian motion regime - the simplest evolutionary model. The Brownian motion regime assumptions may be often violated while working at the whole tree level; however, working at the single node level, it would be unrealistic (and "unparsimonious") to assume a priori another regime than the Brownian motion, especially without 'intermediate' information. These techniques are the "multiple variance Brownian motion" (or "mvBM"; Smaers et al. 2016, Smaers & Mongle 2017) and the "phylogenetic ridge regression" (or "RRphylo"; Kratsch & McHardy 2014, Castiglione et al. 2018).

IV.2) Methods allowing branch-level heterogeneity

The mvBM aims to rescale a time-calibrated phylogeny given the phenotypic variation that allows to estimate the variance parameter of a Brownian motion regime branch-wise and then adjust a multiple variance BM model with these variance estimates. The phylogenetic ridge regression rather regresses the phenotypic data against a time-calibrated phylogeny (and a covariate and/or a predictor if desired) and applies a ridge regression (a statistical method that regularizes the overfit of a linear regression, which is particularly likely while dealing with phylogenetically-correlated data) branch-wise, the slope being the local evolutionary rate. I use here the latter method for two main reasons. The first one is methodological: the first step of this method works at the smallest possible level of a tree and is fully deterministic, only relying on the phenotypic and phylogenetic data, but then mvBM still aims to fit the data (even though the phylogenetic information is rescaled) to a Brownian motion evolutionary model. On the other hand, the phylogenetic ridge regression is fully deterministic by only working with the inputted phenotypic and phylogenetic data. The second reason is practical: the phylogenetic ridge regression methods has been implemented (with a R package) and subsequently developed, allowing to test questions **after** reconstructing ancestral estimates and evolutionary rates (see next paragraphs for the references).

As explained by Kratsch & McHardy (2014) and then by Castiglione et al. (2018), one can consider the difference between a tip value and the root value as the result of all contributions during the evolutionary history that happened between these two points. The interest is that there can be a variation for each branch that are between these two points, and each "local" variation only depends on the length of the considered branch (under a Brownian motion regime) and on the speed of the process for that very branch (i.e., the evolutionary rate of the branch). Predicted tip values thus only depend on the length of the various branches between them and the root (a matrix of patristic distances) and on the evolutionary rates applying on each of these branches (the slopes to estimate). To find these slopes, in an ordinary least squares (OLS) regression, the goal is to minimize the sum of squared residuals to the slope that include the inputted phylogenetic information (relationships and distances). With an OLS regression, the bias of the model (i.e., the misfit between the regression and the data) would be minimized, while its variance (i.e., the variance of the range of predictions from this model) would be greatly increased. This

property would result in a potential overfit of the model, and it would be annoying to have a low confidence in the inferences one may want to make regarding the node (i.e., ancestral) values. This issue is particularly likely to occur in phylogenetic inferences because the phylogenetic tree will be necessarily a non exhaustive sample of the whole diversity of the considered group: the fossil record is scarce by default (and a sampling of the *real* fossil diversity is inevitable), and most studies cannot sample the whole extant diversity of the considered group. In order to avoid an overfit of that regression, a regularization technique is applied, the ridge regression: not only the sum of squared residuals have to be minimized, but also a term that penalizes high slope values by multiplying the squared slope value by a regularization weight λ. Knowing that weight, there is a textbook solution to this optimization problem, the slopes (i.e., the evolutionary rate of each branch) can be known, and the node values can be retrieved using these slopes.

Kratsch & McHardy (2014) and Castiglione et al. (2018) rely on this principle, but differ in the exact way to compute the penalization term. First, they differ on the method to estimate the λ parameter: Kratsch & McHardy (2014) perform a leave-one-out iteration over all tip values and select the λ value with the lowest leave-one-out error, while Castiglione et al. (2018) use a maximum likelihood λ value that minimizes the slopes, which is more conservative but also takes more in consideration the phenotypic and phylogenetic data involved in the estimation of these slopes. Second, Kratsch & McHardy (2014) apply a quadratic (L2 norm) penalization of the slope, while Castiglione et al. (2018) apply an absolute (L1 norm) penalization; as Kratsch & McHardy (2014) say, the latter technique drives the slope values towards zero (that choice by Castiglione et al. [2018] being consistent with their conservative choice of most likely λ value), which would result in "a phylogeny with many phenotypic rates at zero and only few branches with rates of high absolute values, describing a rather implausible model of phenotypic evolution" (Kratsch & McHardy 2014: p.i529). I agree with the methodology of Castiglione et al. (2018), again for two main reasons. The first is conceptual: attracting evolutionary rates towards zero makes sense, as a "conservative" way approaches a "parsimonious"/"simple" one, and as the goal of that technique is actually to better take rate heterogeneity across the tree into account. The second is practical, as already said: Castiglione et al. (2018) further developed their method with a R package and functions (detailed hereafter) dedicated to evolutionary questions.

IV.3) Details on the RRphylo functions used

Castiglione et al. (2018) implemented the phylogenetic ridge regression technique in the R package `RRphylo`. The main function of this package, also named `RRphylo`, serves as a basis for the other functions they further developed: taking as input at least a phylogenetic tree and a trait dataset, it notably outputs the evolutionary rates for each tip and node and the estimated trait data values for the nodes. This allows performing analyses on these data after estimating them. Additionally, a predictor can be provided, and it is added to the distance matrix (of tips vs tips and nodes) that represents the phylogeny.

A main interest of phylogenetic ridge regression is that it reconstructs evolutionary rates at the branch level of the tree. The latter property is particularly interesting compared to numerous other PCM techniques that try to fit a model with whole tree-scaled parameters, though there can be variation(s) of evolutionary rates and/or of evolutionary rate regimes on some nodes of the tree, i.e., in the tempo of the evolution of the considered trait. This is the initial reason why Castiglione et al. (2018) developed this technique: they were interested in providing a technique able to locate evolutionary rate shifts on a tree. They implemented the latter technique in the `RRphylo` package through the `search.shift` function. The latter function only takes as mandatory input the fitted object arising from the `RRphylo` function. Several

options are available, and one is here of interest: `search.shift` is able to search if clades of the tree evolve at a different rate regime than the rest of the tree. This option gathers the absolute values of the evolutionary rates (as it aims to seek a shift, no matter its direction) and, for each clade smaller than half of the tree (otherwise, the regime of that clade is the majority evolutionary regime), it compares all evolutionary rates within the given clade to all the evolutionary rates outside that clade. The significance of this difference is assessed by a comparison with randomized differences: absolute evolutionary rates of the whole tree are mixed and randomly attributed to points pertaining or not to the considered clade, the difference between points within vs outside the clade is calculated, and the procedure is repeated. By doing this, the goal is to have an empiric distribution of random differences (i.e., when there are no shifts); then, that allows calculating an empiric p-value for the previously calculated value of the difference between the absolute evolutionary rates within vs outside the considered clade. It is important to note that, if there is a shift (i.e., a change of tempo), the difference may be either positive or negative: if the rates are significantly larger in the clade compared to outside the clade, that means that the absolute evolutionary rates on the branches of that clade are higher than outside it, and that the trait values for the nodes and tips in that clade will change more (no matter the direction of that change, rates can be highly positive, highly negative, or both), there is an increase of trait versatility in the clade; in the opposite, if the difference is negative, then rates will less change in the considered clade, and there will be a conservatism. The comparison of the difference within vs outside to the empiric null distribution is therefore two-tailed; the taken α risk is here of 5%, meaning that there will be a significant lower difference if the p-value is lower than 2.5%, and a significant higher difference if the p-value is higher than 97.5%. The `search.shift` function not only calculates these differences and their significance: it also considers that, if a clade changes in rate regime, it is likely that several branches of that clade may all be significant in the same way. To handle this, after computing all significant differences, if some are phylogenetically linked (i.e., if several successive branches are significant), the function only keeps the node with the lowest/largest (depending on the significance) difference. I apply this function, but I gather all differences and I describe and discuss all significant differences. This allows for highlighting the phylogenetic area (i.e., between which and which nodes) there would have been a shift of rate regime rather than keeping a single node. The aim is to 1) detect area of the tree where there are changes in the evolutionary rate regime, 2) describe the change of regime for each (i.e., versatility or conservatism), and 3) discuss the rate values (i.e., in the case of versatility, if the rates are highly positive, negative, or both).

Besides accounting for the tempo of the evolution of the given trait, another function reports the mode of its evolution. The further developed function `search.trend` (Castiglione et al. 2019) looks at the pattern of the evolution of both the evolutionary rates and the trait values through time. This function takes as mandatory inputs the fitted object from the `RRphylo` function and the trait values.

The first goal of this technique is to compare the general 'phenotypic' (for the trait value, often a phenotypic trait) and rate trends (by mean of a linear regression of one of the two previous against the time) to brownian simulations of each. The function simulates trait values following a Brownian motion regime (that are, due to the function, in a 0-1 range of values) and performs a phylogenetic ridge regression of this "Brownian trait": this allows calculating the evolutionary rates and then the node values of that trait, and the function then calculates the slope of evolutionary rates and of that of the Brownian trait values against the time. By repeating this procedure several times, this allows having an empiric distribution of the rate and 'phenotypic' slopes under a brownian motion regime. As previously done with shifts, this randomization technique providing an empiric distribution under a "null" assumption (which is, here, a Brownian motion regime) serves to assess the significance of the slope values of the evolutionary rates and of the actual values of the considered trait (the slopes being noted `slope` and these empiric p-values being noted `p.random` in the function output). The function also outputs a more classical p-value regarding the nullity of the slope of the considered trait (noted `p.real`). Another way to compare the observed trends to a Brownian motion is to compare the parameters of both trends. In the 'phenotypic' regression, a metric is calculated to evaluate the deviation from a Brownian motion (which can be interpreted as a drift from a Brownian motion, the "arithmetic Brownian motion" of Royer-Carenzi & Didier 2016). This metric, called `deviation`, is the amounts of standard deviations of the actual 'phenotypic' trend (the mean of that simulated under a Brownian motion regime being zero). Similarly, in the rate regression, a metric is calculated to evaluate the difference in variance spread over time (a reduced variance can be interpreted as marking the effect of a selection, a trend). This metric, called `spread`, is the ratio between the relative increase in variance over time (calculated as the ratio of the variance at half time over the extant one) for the actual trait over that simulated under a Brownian motion regime.

The second goal of this technique is to work at a more focused level, contrasting clades with each other. By adding nodes to compare as arguments to the function, besides the previously described outputs at a whole tree scale, it is possible to have part of these results for each node, and even to compare nodes. For each node, regarding the 'phenotypic' regression, the function outputs the slope of that node (noted `slope`) and its significance compared to Brownian motion regime simulations (noted `p.slope`). In a similar way, regarding the rate regression, the function outputs its slope (noted `slope`) and its significance compared to that of the rest of the tree (noted `slope.difference`), the goal here being to know if the evolutionary regime of a clade is peculiar in the tree. Both general metrics (deviation and spread) are not computed for each node, but instead are provided the estimated marginal means (means of groups removing the weight of the number of individuals, i.e., species) and their significance compared to the rest of the tree for both the 'phenotypic' and the rate regression (both being noted `emm.difference` and `p.emm`). These estimated marginal means (or "emmeans") are particularly useful as they give an idea of the displacement of the global trend of a given group compared to the rest of the tree; the slope alone can be not significant, but if there is an initial shift, the estimated marginal means will reveal it. The comparison between groups only works properly if the groups species do not overlap (i.e., not possible for a clade and one of its subclades); similarly, for the 'phenotypic' trend and for the rate regression, the function returns the slope difference of the trend (noted `slope.difference`), its significance (`p.slope`), the difference in estimated marginal means (`emm.difference`), and its significance (`p.emm`).

Finally, another function used here tests the robustness of the found results by randomly removing a defined proportion of tips, randomly swaps a defined proportion of the remaining tips, and randomly changes node ages (between that of its parent node and those of its daughter nodes/tips). Through randomization, this function, named `overfitRR` (Serio et al. 2019), aims to check whether the significant results robust to sampling effects and to potential phylogenetic errors (through phylogenetic rearrangements). By inputting the same arguments than the other functions and by specifying which functions to test, the outputs depend on these function. By default are some results regarding the most basic function, `RRphylo`, which are a 95% confidence interval for the ancestral root estimate (`rootCI`), the regression parameters between the ancestral node estimates obtained after resampling a phylogenetic rearrangements against those obtained with the full data (`ace.regressions`). If using the `search.shift` function, the results (in the `shift.results` element) are the proportion of significant 'positive' (i.e., toward high values) and 'negative' (i.e., toward low values) of shifts in absolute evolutionary rates obtained using search.shift (`p.shift+` and `p.shift-`). If using the `search.trend` function, the results (in the `trend.results` element) for the whole tree (in the `tree` sub-element) are the proportion of slopes that are significantly above (`p.slope+`) or under (`p.slope-`) the simulated Brownian slopes, and the results if specifying clades to test are provided (in the node sub-element) are the proportion of significant slopes above (`p.slope+`) or under (`p.slope-`) Brownian motion regime (for 'phenotypic regression') or the rest of the tree (for rate regression), the proportion of significant estimated marginal means above (`p.emm+`) or under (`p.emm-`) the rest of the tree (for both regressions), and the pairwise comparisons between clades.

So far, the phylogenetic ridge regression has only be explicitly implemented for continuous traits; regarding the quantitative data used here. I use this PCM with the previously explained functions. Regarding the qualitative data (that is, the anatomical characters), I will also use this PCM. Considering the previous PCM descriptions, I consider the phylogenetic ridge regression the best technique (with the least preconditions) to reconstruct the evolutionary history of a trait. I think the best is to the smallest level of evolution (i.e., at the branch level) in order to better figure out the variation in the evolution of a character. I think that what stands for a continuous character will also stand for a discrete one. However, there are some issues and assumptions by treating a discrete trait like a continuous one that I list, explain, and try to address below.

The first issue is that a discrete trait can only take discrete values, not intermediate (i.e., non integer) ones. The solution I propose is to consider a posteriori rounded values regarding the ancestral reconstructions and only it. Rounding values while reconstructing the evolutionary history of a character would undesirably drop a significant amount of doubt in the reconstruction; this is even not possible using phylogenetic ridge regression, as only rates are estimated, and ancestral estimates are only calculated a posteriori from the rates. Work only on rounded values and, for instance, re-calculate rates given these values would also drop the uncertainty in the reconstruction. Other methods using the Mk model or the BiSSE method will output probabilities for each state; this may seem a better option, but it can be misleading if one only retains the state of maximal probability: a mean of the states weighted by their probability (which may be not an integer value) may lead to a different rounding, better taking into account these probabilities. Non-integer reconstructed values actually make sense because they give an idea of the uncertainty. The only drawback of getting only the non-integer reconstructed value is to not know the weight of that uncertainty, which can be appreciated with probabilities; however, since phylogenetic ridge regression does not deal with a probabilistic model, there would be no way to get them, even with a discrete-suited implementation.

The second issue regards the assumptions relative to that discrete trait: by considering it as a continuous (linear) variable, I see three main assumptions: (1) the character has to be ordered, and the transition costs are (2) symmetric and (3) homogeneous (there is the same weight by going from a state 0 to a state 1 than from a state 1 to a state 0 but also than from a state 1 to a state 2). I would emphasize that, among the three previous assumptions, the homogeneity of transition costs between states are not supposed to be the same across the whole tree, they vary on each branch. All these three assumptions are relaxed in model-based methods, but in these case they need a priori distributions and are estimated a posteriori given these distributions, while this is not the case here. These assumptions thus force the user to set characters that may match (or, at least, that does not mismatch a priori) these assumptions. Regarding my anatomical characters, only the character 20 (delineation of rostral colliculi) has more than two states and is not ordered, mostly because I doubt on the degree of difference between the states. However, this is a personal opinion and, given its states, it could be ordered; in the further analyses, this character is treated as ordered, but I want to warn about the potential distribution and interpretations arising from this character.

As of little but noticeable practical interest, I would like to add that only RRphylo is able to run an analysis on a phylogenetic tree containing fossil species; none of the (so far) mainstream and best-performing methods (Mk model in a model-based method; BiSSE method) that are implemented in R (in the package `diversitree`, FitzJohn 2012) can.

V) Statistical treatment

The morphological variation of the endocranial cast appears to be subtle in hipposiderid fossil taxa, but is present (Maugoust & Orliac 2021), and the monotony of the endocranial morphology may only be apparent. Considering a larger sample at a larger taxonomic scale, a larger morphological variation is therefore expected. The approach developed here consists in establishing discrete anatomical characters for the sample tested, and to study them through phylogenetic ridge regression (Castiglione et al. 2018). As already emphasized in the previous section, this involves major hypotheses, but I aim to provide a first step towards the statistical treatment of endocranial morphology in bats. Phylogenetic ridge regression allows to describe the phylogenetic signal of the defined anatomical characters, to detect if some appear to be driven by selection (looking at the temporal trends of the states and of their absolute evolutionary rates can bring clues indicating a selection), to discuss the evolution of some particular features of the endocranial morphology, but also to reconstruct and describe the morphological evolution between major taxa. Other main questions regard the variation over time and in a phylogenetic framework of the three relative neural masses (i.e., of the brain, the olfactory bulbs, and the paraflocculi). By using the encephalization quotient as a measure of the relative brain mass, Maugoust & Orliac (2021) supported earlier results (Yao et al. 2012) suggesting that the relative brain mass actually did not decrease in bats, at least not in hipposiderids. These works emphasize the role of fossils and highlight more complex scenarios than a simple increase or decrease since the “ancestor of bats”, that are based on “neontological” works (Niven 2005, Safi et al. 2005, Thiagavel et al. 2018). Similarly, the relative masses of olfactory bulbs and of paraflocculi are thought to be linked to eco-functionalities: olfaction acuity has been linked to olfactory bulbs mass (Bhatnagar & Kallen 1974), and ecological correlates are sometimes found for paraflocculi mass (e.g., Bertrand et al. 2018, 2021). However, the latter may be erroneous (Ferreira-Cardoso et al. 2017). Phylogenetic ridge regression allows for testing the effect of both the phylogeny and of the predictor mass (i.e., body or brain mass) on the tested mass (i.e., one of the three measured here), and therefore looks directly at the evolution of the relative neural mass. For the three

variables, my aim is to describe and discuss the evolution of each relative neural mass (both their value and their absolute evolutionary rates) in a phylogenetic framework, and to compare their patterns, which is surprisingly rarely done in recent works (Jolicoeur et al. 1984 being the latest comprehensive reference).

V.1) General remarks

The statistical treatment has been performed using R (R Core Team 2020) and its interface RStudio (RStudio Team, 2016). All scripts used for the statistical treatment are provided in the Appendixes III-1 and IV-1. I used the packages ape (Paradis & Schliep 2019), `phytools` (Revell 2012), and `RRphylo` (Castiglione et al. 2018, 2019, Serio et al. 2019) for the phylogenetic comparative treatment, plus a function of the package `geiger` (Pennell et al. 2014) embedded in a function of the package `RRphylo`. I used the package `FSA` (Ogle et al. 2019) for statistical tests; the package `openxlsx` (Schauberger & Walker 2020) to write the Tables arising from the statistical treatment, the package `RColorBrewer` (Neuwirth 2014) for graphical purposes, and the package `ULT` (Maugoust 2021) for miscellaneous tasks (phylogenetic assemblage, graphical purposes, simple statistical tests).

In general, I choose to use non-parametric tests as they are more robust and do not rely on normality assumptions. I do not expect biological variables considered in a phylogenetic framework to be normally distributed, and a significant normality of the data could only be found by chance. Moreover, even if a variable is distributed normally in my sample for an unknown reason, treating it with non-parametric test will not violate any assumption (since there are none), while treating clearly non normal variables with parametric test would violate assumptions and may need data transformation. Since I would like to avoid case-to-case transformations and be able to propose a generalizable data treatment, I prefer using non parametric tests as far as possible. In the following lines, unless particular cases, I will always describe tests a little, then cite the quote that establishes the test, and the quote that implemented the test in R together with its package. Tests of normality are sometimes used here, but not to verify normality assumptions before using a parametric test (see third point of part V.2.A); the used test is the Shapiro-Wilk test (Shapiro & Wilk 1965 for the statistical test, Royston 1995 for its implementation in the base package `stats`). The other non-parametric tests are: i) the Wilcoxon or Mann-Whitney test (Wilcoxon 1945, Mann & Whitney 1947, Bauer 1972, Hollander et al. 2015 for the statistical test, R Core Team 2020 for its implementation as the function `wilcox.test` in the base package `stats`) that applies to two samples and whose null hypothesis is that these sampled are distributed similarly and that the ranks of the values are equal (no matter the shape of the distribution) by summing the data ranks (it is a "rank sum test") (it is the non-parametric counterpart of the parametric Student t-test); ii) the Kruskal-Wallis test (Kruskal & Wallis 1952, Hollander et al. 2015 for the statistical test ,R Core Team 2020 for its implementation as the function `kruskal.test` in the base package `stats`) that generalizes the Wilcoxon test to n samples (it is the non-parametric counterpart of the parametric one-way ANOVA); iii) the Dunn test (Dunn 1964 for the statistical test, Dinno 2017 and Ogle et al. 2019 for its implementation as the function `dunnTest` in the package `FSA`) that contrasts each modalities of a factorial group if there is a general heterogeneity between groups as found by the Kruskal-Wallis test (it is the non-parametric counterpart of the parametric Tukey HSD post-hoc test); iv) the Kendall τ test (Kendall & Gibbons 1990, Hollander et al. 2015 for the statistical test, R Core Team 2020 for its implementation as the option `method="kendall"` in the function `cor.test` of the base package `stats`) which is a correlation test based on data ranks and that is more robust than the Spearman r_s test (Croux & Dehon 2010) (both tests are the non-parametric counterpart of the parametric Pearson r_p test). The only assumptions for all these

non-parametric tests are the independence between data values. Since all these tests are performed on results of the various `RRphylo` functions, the phylogenetic autocorrelation is supposed to be removed, and only may remain a correlation between characters, which is difficult (to impossible) to exactly quantify, or even to decipher. The only asserted dependence between characters regards the characterization of structures that may be present or absent; however, since taxa with absent structures are removed while treating other characters dealing with properties of that structure, there cannot be any autocorrelation.

I use parametric tests in two particular cases. The **first case** is the brain/endocast measurement bias: I use a linear model to contrast endocast vs brain measurements in order to unbias the measurements made on endocasts, and thus have a relative brain mass as close to the reality as possible. In that way, I use Student t-tests (Student 1908, Welch 1947, Fisher 1970 for the statistical test, R Core Team 2020 for its implementation as the function `t.test` in the base package `stats`) to assess the non-nullity of the regression slope and intercept, and I calculate the adjusted R squared that expresses the part of variance in the data explained by the regression taking into account the number of parameters. The **second case** is a regression of character states against body mass ranks in order to detect a potential allometry in the given character. If there is an allometry, there is a change of shape (and thus, of character state) that parallels the change of size; therefore, by regressing the character states against the size, a significant regression would indicate a correlation between shape and size, which may be explained by an allometry. There is no a priori particular shape of the relationship: it can be linear, exponential, logarithmic, lognormal etc. To test this, I used two tests and a metric. The first test is the previously quoted Kendall τ test: it works on ranks, and this is independant of the shape of the relationship between the character states and the size. The second is the Pearson r_p test (Bravais 1846, Galton 1877, Pearson 1895 for the statistical test, R Core Team 2020 for its implementation as the option `method="pearson"` in the function `cor.test` of the base package `stats`); this parametric test measures the proportion of global variance of the two given variables explained by the covariance between these variables. Since one of the two variables can be considered to be already expressed as ranks (the character states, with equal ranks for the taxa with an equal state), I also express the body mass as ranks, in order to test a linear relationship between two ranked variables. This procedure is thus a bit intermediate, using a parametric test on de-parametrized variables. The metric is the adjusted R squared (or adjusted coefficient of determination; Wright 1921, Smith 1925, 1926, Ezekiel 1929 for the statistical test, R Core Team 2020 for its implementation as an element of the function `summary.lm` in the base package `stats`) of the regression of the character states against the body mass ranks. This is a complementary way to express the proportion of total variance explained by the interaction between the two variables. It does not correspond here to the covariance as for the Pearson test, but to the sum of squared estimate of errors, because it takes into accounts the number of parameters and it gives a clear idea of the strength of the regression (though it does not have a significance level).

V.2) Qualitative data treatment (Table II-1)

In the qualitative data (i.e., taxon/character matrix) treatment, the matrix is imported and transformed in order to apply the same procedure to each character independently. The first phase of the procedure is the acquisition of the results arising from the previously described functions of the package `RRphylo`. It has to be pointed out that these function cannot deal with missing values. Therefore, for each character, taxa with inapplicable or unknown states have been removed and the phylogenetic tree used have been pruned, keeping only coded taxa. For the qualitative data, only the functions `RRphylo` and `search.trend` have been used, but not those of the `search.shift` function (see below, third part, second point). Some taxonomically meaningful "deep nodes" are also established in order to contrast the evolution of each character in these groups; here, these "deep nodes" are at least family-level and biologically meaning clades. These nine clades are considered as "deep nodes", and they are used with the `search.trend` function in order to have the temporal trends of the "phenotype" (i.e., the given character) and of its rates of evolution. The second phase of the procedure is a treatment of these first, rough, results, to obtain finer results on which hypotheses can be further tested. These finer results are : 1) the matrices of morphological changes and of evolutionary rates (with, for each, one matrix, with characters/rates respectively and nodes + tips as entries), that yield to reduced datasets such as the global number of morphological changes and the evolutionary rates (both natural and absolute) for each taxon and given all characters; 2) the various mappings on the phylogeny of the character states (in a continuous and in a discrete, rounded, manner) and of the evolutionary rates (with natural and absolute values for each character) for each character on the phylogeny; 3) the trend parameters, regarding both the whole tree and each "deep node", for each character on the phylogeny; 4) the discretized ancestral character estimates for each character and for each "deep node".

Focus	Problematic	Approach / metric(s)	All points			Grouping			Data used	
			Type of plot used	Test problematic	Test used	Type of plot used	Test problematic	Test used	Original data	Transformation
Characters	Phylogenetic relevance	Consistency and Retention indexes (CI/RI)	Histogram of each index			Boxplot of each index	Homogeneity	Kruskal-Wallis test + Dunn test if no homogeneity		
		Number and location (nodes vs. tips) of morphological changes	Biplot of number of changes at nodes against at tips	Interaction	Kendall correlation test	Biplot of number of changes at nodes against at tips	Interaction	Kendall correlation test	RRphylo ancestral estimates	Computation of number of state changes for each taxon
						Boxplots of number of changes at nodes, at tips, and at nodes and tips	Homogeneity	Kruskal-Wallis test + Dunn test if no homogeneity		
	Evolution through time	Slopes of temporal trends of traits and of trait rates	Histogram of each slope type (i.e., trait and trait rate trends)	Normality	Shapiro-Wilk test	Boxplot of each (i.e., trait and trait rate trends)	Homogeneity	Kruskal-Wallis test + Dunn test if no homogeneity		
							Null average	Wilcoxon test	search.trend trend slopes	
			Biplot of slopes of trait against those of trait rates	Interaction	Kendall correlation test					
	Potential allometry	Covariation of character states with brain size	Biplot of character states against brain size ranks	Interaction on natural values	Kendall correlation test				Character matrix + brain mass dataset	
				Linear interaction on ranks	Pearson correlation test + adjusted R squared					
Taxa	Morphological evolution	Graphical reconstruction of ancestral estimates				Topology pruned to the main nodes + graphical reconstruction			RRphylo ancestral estimates	
	Evolution along the phylogeny	Sum of number of morphological changes	Mapping on the phylogeny							Computation and sum of number of character changes for each taxon
		Average absolute rates over all characters							RRphylo rates	Averaging absolute rates for each taxon
	Variation in evolution rates	Slopes and averages ('emmeans') of temporal trends of trait rates				Boxplot of each variable	Homogeneity	Kruskal-Wallis test + Dunn test if no homogeneity	search.trend trend slopes and emmeans	

Table II-1: Simplified representation of the workflow for qualitative statistical treatment.

V.2.A) Morphological characters: description, phylogenetic relevance, and evolution

A second part of the statistical treatment aims to describe the characters, how they support the phylogeny, and how they evolve along the branches of the trees. In that part, characters are both treated one by one (i.e., considering each character and summarizing the information for all characters) and by morphological complex (defined as being the headings of the Anatomical characters section, considering each character and summarizing the information for each general structure). Five approaches are used and explained hereafter.

First, I use two commonly metrics used to describe both the tree and each characters using parsimony: the consistency index ("CI") and the retention index ("RI") (Kluge & Farris 1969, Farris 1989a, b). Their formulas are $CI=\frac{m}{s}$ and $RI=\frac{g-s}{g-m}$, with m the minimal number of steps of a character (i.e., the number of steps going from an extreme state to the other one via all other states, i.e., the number of states minus one), s the effective number of changes of that character on the given phylogeny, and g the maximal number of steps of that character on the given phylogeny (i.e., the sum of autapomorphic changes for all states with the exception of the most common state). The values m, s, and g are here calculable with the reconstructed distribution of the characters, given the fact that I computed the number of changes for each character. Thus, although these indexes are commonly used in a fully parsimonious framework, I believe that they can express the degrees of homoplasy and homology of each character in the present framework. Still, it is worth noting that, since the distribution of character states has not been reconstructed following a parsimony method, there can be more state changes on the tree than the maximal expected number of state changes under a parsimony method (i.e., cases with $s > g$). This does not impact the score of the CI, but if this case happens, the RI becomes negative. It however remains impossible to have less changes than the minimal number of changes. Thus, the CI still has a [0;1] distribution interval and the RI has a $[-\infty;1]$ distribution interval; values close to 1 still highlight a highly non homoplasic or homologous character, while low values (close to 0 for the CI, or even below for the RI) indicate the reverse. To have an idea of the general behavior of each characters, I plot a histogram showing the general distribution of the CI and RI of each character. This allows giving a general idea of the phylogenetic consistency of the characters. Then, CI and RI are summed up by general structure, and plotted using boxplots in order to better illustrate their distributions in each group. The significance of the heterogeneity in CI or RI between general structures is assessed using a Kruskal-Wallis test and, if significant, Dunn post-hoc pairwise tests are performed in order to see which general structures significantly differ.

Second, I use the number of morphological changes for each character that can occur at nodes and/or tips. I first contrast the number of changes at nodes and tips (by ordering the number of changes at nodes, and keeping the same order for the number of changes at tips) both considering all characters and general structures; this leads to graphical x-y plots and to Kendall correlation tests to assess the significance of these correlations. Then, regarding the global heterogeneity and the potential differences in the number of changes between global structures, a similar procedure than for the CI and RI is applied: boxplots of the number of morphological changes at nodes, at tips, and at both are used to contrast each global structure distribution, and Kruskal-Wallis and Dunn tests are used to assess significances at the whole and at the modality levels respectively.

Third, regarding the temporal evolution of these characters, the slopes of temporal trends of the trait and trait rates are gathered from the previously refined datasets for each character. Using this, a Shapiro-Wilk test is used on all trait and trait rates temporal trend slopes in order to assess the homogeneity of the whole endocast through time. Using these datasets, it is also possible to see the trend slopes that significantly differ from 0, and to contrast trait to trait rates trend slopes using a Kendall correlation test. The various metrics outputted by the `search.trend` function that compare the behavior of the variable against a Brownian motion are not used here: to see if there is a temporal trend or not is, to me, enough given the fact that this rely on non-integer values for the nodal estimations. Contrasting this to Brownian motion simulations that are rather suited for quantitative data would be going too far, and it would be better to contrast this to simulations suited for qualitative data (that exist in the literature, but are not implemented yet in `RRphylo`).

Fourth, as previously done, it is also possible to have an idea about the heterogeneity between global structures in their trait and trait rates trend slopes using Kruskal-Wallis and Dunn tests. In addition, I test if the trait and the trait rates temporal trend slopes are different from zero by considering global structures: to do so, I calculate the average slopes for all characters of each global structure (which gives a rough idea of the central tendency of that structure), and I perform a Wilcoxon test on all slope values of that global structure to assess the potential offset of the slopes distribution compared to zero.

Fifth, I compare the distribution of the states of each character to that of the body mass, in order to detect a potential covariation between the two variables. This is done by following the previously described procedure (with the Kendall and Pearson correlation tests and the adjusted R squared), by outputting the x-y plot of the character states against the ranked body mass, by superimposing to that plot the linear regression line, and by graphically indicating if this relationship is supported by the Pearson (thicker line) and/or by the Kendall (colored line) correlation tests.

V.2.B) Taxa descriptions and comparisons, and deep node reconstructions

A second part aims to describe the taxa and to compare them: the goal is to observe the amount of morphological changes at the different nodes, etc. This is done using three approaches that I describe as follows.

First, I output the average absolute rates variations along the phylogeny, together with the total number of morphological changes. Averaging the evolutionary rates across characters is totally meaningful here. These rates are computed as being the slopes of change through time, and their variation only depends on the trait variation and on the time variation. Given that rates are computed for each character on the same phylogeny, the time variation is exactly similar between all rates. In a case of qualitative traits that has been converted to continuous ones, with same gaps between states, the trait variation is also totally comparable between all characters because the scale is the same for each character and only depends on the number of states. The underlying assumption is that all state changes have the same cost no matter the character; for two characters with respectively two and three states, the cost is the same by going from the first to the second state in each character. This is a heavy assumption that can be objected: for instance, some may normalize change costs depending on the number of states, but recalling the previous examples, this would mean that a state change in a three-state character would cost half a state change in a two-states character. I prefer to rely on the assumption that all costs are similar; this is the simplest hypothesis, though probably wrong. My rationale is to deal with the simplest possible assumptions, since I just cannot verify more complex hypotheses. I however try not to make too firm conclusions following that point, given the heavy assumption chosen. I also

consider only absolute rate values than natural rate values because averaging natural values may artificially output a value meaning a “neutral” evolution: if a node has rates of values -x and x, the average of the natural values will give 0, while there are things happening at that node, but by considering the average of the absolute values, the output will be x. This is the same rationale used by the `search.shift` function to detect shifts in evolutionary rate regimes; this function then look at the sign of the rate value to inform that the shift is negative or positive. Here, I only consider the absolute values and I limit my discussion on the location of rate variation, not on the sign of that variation. Looking at the sign would require to look at the distribution of rate values at taxa where there is a high variation, in order to know 1) if there are characters evolving slower or faster, 2) depending on the previous, what are the proportions for each, and 3) depending on the previous, know the characters that vary the most and in which direction. My purpose is not to give a precise picture of each varying taxa, but to inform about the general trends at the considered scale and to raise potential questions about taxa that would open to more focused studies. I limit my remarks on absolute rate variation. This is also the reason why I do not use the `search.shift` function, though its rationale parallels mine in some points: this function works character by character, while I aim to describe general patterns. I deprive my remarks of the significance of the rate variation that `search.shift` outputs, but this significance cannot be established using already reviewed techniques, or it would need a specific methodological part. Thus, as a part of the information the `search.shift` function would yield can be appreciated using a simple and meaningful calculation, I do not use this function for qualitative traits. Indicating, together with this, the number of morphological changes for each taxa also informs about the general behavior of characters and of nodes, such as the taxonomic level(s) at which the anatomical characters are relevant, but also which taxa evolve very differently from the others. This is a complementary information to the average absolute evolution rate provided for each taxon, thus I output these two sources of information together.

Second, I describe the evolution of the “deep nodes” using the rate temporal trends, recalling refined datasets. I do not use the trait temporal trends because the trait evolution has been already treated, and is better figured out by directly looking at the structures rather than at numbers (see next point). Very simply, as done for the character groups (that are the general structures), I plot the distributions of rate temporal trend slopes in each “deep node” using boxplots, and I assess the heterogeneity and the discrepancies between “deep nodes” using Kruskal-Wallis and Dunn tests respectively. The `search.trend` function also outputs estimated marginal means that compare the average rate for the considered clade to that of the rest of the tree, in order to see if a clade may evolve at different rates. As for the slopes, I thus output the distribution of estimated marginal means of rates for the various “deep nodes” using boxplots, and I assess the heterogeneity and the discrepancies between “deep nodes” using Kruskal-Wallis and Dunn tests respectively.

Third, I output the ancestral character estimates for the “deep nodes”, keeping uncertainty when there is, and I graphically schematize the endocasts of these “deep nodes”. This allows further comparisons of morphological evolution between these “deep nodes”, but also with the other, more apical, taxa using all previous mappings and sources of information.

V.2.C) Quantitative data treatment (Table II-2)

All endocasts prepared here have been extracted following the same strict protocol, minimizing potential bias between specimens. However, there could be a discrepancy between endocasts volumes measured from µCT data and fresh brains masses. This bias is of importance, especially regarding the relative brain mass. The first step is therefore to perform an unbiasing procedure by contrasting estimations of neural mass (i.e., brain or olfactory bulbs mass) after numeric segmentation to real measures done by Baron et al. (1996). The procedure is however dependent of the sample, the correction is empirical, and this has to be performed for each case of study.

Then, I treat each of these log masses as relative log masses: the log brain mass is expressed relatively to the log body mass (i.e., to account for the general encephalization of the brain), and both the olfactory bulbs and paraflocculi log masses are expressed relatively to the log brain mass (i.e., to follow the principle of proper mass). In each case, the statistical treatment is similar; I detail here this procedure using the example of the log brain mass, but it stands for all three relative masses (replacing the log structure mass and the log mass on which it biologically would depend). Like in the Qualitative data treatment section above, I look both at the whole tree level and at some specific, "deep nodes". The goal is also to give a general picture of the evolution of these variables on that tree. As previously, there are two initial phases that allow obtaining rough results from `RRphylo` functions then refining these results to be used in my statistical treatment. Some important graphical outputs are also obtained at that time.

Problematic	Approach / metric(s)	All points			Grouping			Data used	
		Type of plot used	Test problematic	Test used	Type of plot used	Test problematic	Test used	Original data	Transformation
Trait value evolution	Trait values	Mapping on the phylogeny						Tips: values of used variables (X and Y for X expressed relative to Y) for tips; nodes: RRphylo ancestral estimates for each variable	Residuals of linear regression of the two variables (considering tips + nodes values)
	Trends through time	Biplot of trait given time with general trend line	Fit to Brownian motion regime	Randomization test (performed by the search.trend function)	Group trend lines superimposed to the general plot	Fit of group slopes to a Brownian motion regime Chosen pairwise comparisons of group slopes Group emmeans difference vs the rest of the tree	Randomization test (performed by the search.trend function)	search.trend trend slopes and emmeans (values, difference values, and significance)	Slightly modified version of the search.trend plot output
Trait absolute rates evolution	Absolute rates values	Mapping on the phylogeny						Absolute rates of the RRphylo of the X trait with Y as a predictor	
	Trends through time	Biplot of trait absolute rates given time with general trend line	Fit to Brownian motion regime	Randomization test (performed by the search.trend function)	Group trend lines superimposed to the general plot	Difference of group slope to the rest of the tree Chosen pairwise comparisons of group slopes Group emmeans difference vs the rest of the tree	Randomization test (performed by the search.trend function)	search.trend trend slopes and emmeans (values, difference values, and significance)	Slightly modified version of the search.trend plot output
	Shifts in rate regime		Shift in absolute rates (i.e., difference between average absolute rates) within and outside a given clade	Randomization test (performed by the search.shift function)				search.shift shift values and significance	Original search.shift plot not used; renamed rows of main groups tested by their systematic or vernacular name instead of "NXX"

Table II-2: Simplified representation of the workflow for quantitative statistical treatment.

The first phase only involves the `RRphylo` function on reduced datasets and pruned trees for the three 'log masses of interest' (i.e., brain, olfactory bulbs, and paraflocculi log masses) and for the log body mass; here, only the phylogenetic tree and the variable are specified. This allows producing the first graphical output, which is a mapping of the relative log brain mass: I reconstruct ancestral estimations using `RRphylo` independently for each variable (i.e., log brain mass and log body mass), then I regress one against the other (using the tip values plus the nodal estimates `RRphylo` produced) using a standard ordinary least squares (OLS) procedure, and I extract the residuals that I map on the phylogeny. An OLS is used here as the goal is precisely to see the potential phylogenetic autocorrelation in the residuals on the phylogeny, not to remove it. This procedure strictly follows that of Serio et al. (2019) in cetaceans, for

instance. This mapping provides a first idea of the evolution of the relative log brain mass, such as the increases or decreases through time along some phylogenetic branches of interest, and to discuss the impact of the inclusion of fossils on the results.

In the example of the statistical treatment of the log brain mass, the second phase re-uses the `RRphylo` function on the log brain mass, but specifying the log body mass (and its reconstructed ancestral states during the first time) as an additional predictor to the phylogeny, which modifies the reconstructed evolutionary rates. Following this, a second graphical output is printed, this time mapping the evolutionary rates of log brain mass (with log body mass as additional predictor) on the phylogeny. Next in the second phase is the use of the `search.trend` and `search.shift` functions. In both cases, two cases are contrasted depending on if the sample includes fossil taxa or not. In the case of the `search.shift` function, all clades (i.e., all taxa with at least two units) are tested: as previously explained, the goal is to compare the average absolute rates within the considered clade to those outside that clade, and to assess the significance of that difference using repetitions of such differences after shuffling the evolutionary rates. In the case of the `search.trend` function, the "deep nodes" of interest are indicated in order to get the trait (i.e., log brain mass) and its evolutionary rates trends through time for the general case and for each "deep node", but also to have the estimated marginal means of the "phenotype" and of the rates, and also to compare some deep nodes between them (in this function, it is possible to compare nodes if they do not share any taxon, thus some pairwise comparisons have been done). Finally, at the end of the second phase, the plots of the trait and trait rates trends through time are outputted, showing the general trend and that of each "deep node".

A little aside regarding the `search.trend` function has to be mentioned. The whole `RRphylo` package and this function in particular are made with the aim to benefit from the inclusion of fossil taxa (e.g., Castiglione et al. 2019). Without fossils, the only observed values are at the present day; in the case of reconstructing trends through time, knowing only values at time zero and relying only on estimations for older times makes quite less sense. For this reason, it is not normally possible to apply this function to datasets with less than 10% of fossil species, and it is a specific will from the authors of this package (Raia pers. comm.). Here, I managed to bypass this condition in order to contrast the with fossils vs without fossils evolutionary reconstructions; this little hack only aims to not stop the function after detecting that there are less than 10% of fossil species in the sample, and let the function go ahead. However, just like the authors of this function, I obviously do not recommend doing that if one does not want to assess the change implied by fossil values.

After obtaining the "rough" results, the refining process is a bit shorter than for the qualitative data: there are less variables, and I do not intend to summarize them altogether, but to treat them separately. This allows me relying much more on the direct outputs of the `RRphylo` package functions. The refining process consists in reorganizing the results arising from the `search.shift` and `search.trend` functions that are almost directly outputted as tables.

Part Three

Endocranial evolution in the disparate suborder Yinpterochiroptera

I) Introduction

The conquest of the aerial environment by bats, the second most diversified mammalian order (e.g., Teeling et al. 2009, Burgin et al. 2018), implies among the most spectacular morpho-anatomical modifications of mammalian evolutionary history. Bats notably present deep changes of organs responsible for perception and for sensory integration in relation to their lifestyle and to the aerial environment constraints (balance linked to sustained flight and echolocation system; e.g., Teeling et al. 2000). Bats can straightforwardly be split in two main groups: "megabats", with the family Pteropodidae, that are fruit-eating, large-sized bats that mostly rely on vision, and "microbats", with four bat superfamilies, that are mostly insectivorous (though there also are groups eating fruits, fish, little vertebrates, and blood), small-sized bats that are capable of laryngeal echolocation (e.g., Freeman 2000, Teeling 2009). This morpho-ecological dichotomy has long been the rule of bats systematics until more recent studies establishing phylogenetical relationships using genetic sequences. These studies showed that bats are divided in two counter-intuitive suborders: Yangochiroptera, with three "microbat" superfamilies, and Yinpterochiroptera, associating the fourth "microbat" superfamily (Rhinolophoidea, also formerly called Yinochiroptera) and the "megabats", the Pteropodidae family (e.g., Teeling et al. 2000, van den Bussche & Lack 2013, Anderson & Ruxton 2020). The suborder Yinpterochiroptera is only (but strongly and consistently) supported by molecular phylogenies, and implies numerous questions about the general evolutionary history of bats. Among others, as the pteropodid bats do not echolocate while the rhinolophoids do, a main interrogation is to determine whether echolocation is plesiomorphic for all bats and has been lost in pteropodids or if it is a convergent acquisition between Yangochiroptera and Rhinolophoidea (e.g., Teeling et al. 2012, Nojiri et al. 2021). The integration of sensory signals and of motor control are of primary importance in bats given their unique ecology. Treating both types of information, the brain is then a key organ in this group: the specificity of bats ecology reflects on brain anatomy (e.g., Baron et al. 1996) and only starts to be properly studied in an evolutionary (i.e., temporal) framework (Yao et al. 2012, Maugoust & Orliac 2021, Smaers et al. 2021). The contribution of brain morphology to bats systematics has not been tackled yet; the brain has mostly been studied using volumes of it and of its sub-regions (e.g., Pirlot & Jolicoeur 1982, Safi et al. 2005, Dechmann & Safi 2009). Using fossil taxa, my goal is to combine these approaches and put them in an evolutionary framework, using the particular Yinpterochiroptera context. Indeed, both Pteropodidae and Rhinolophoidea are highly contrasted groups; addressing the initial steps of yinpterochiropteran brain evolution and proposing first hypotheses regarding how the brain evolved before and after the onset of such different taxa is crucial for understanding better both the brain and Yinpterochiroptera evolution. The phylogenetic comparative method used here, the phylogenetic ridge regression (Castiglione et al. 2018), is particularly well suited to studies dealing with fossil taxa as it reconstructs trait evolution by highly taking into account fossil information. This is also quite well studied for a clade in which families have long branches between their origin and their crown diversification, generally occurring in the last 30 My for all families, whereas fossils are found back to the middle Eocene (~ 35-40 Mya).

From a historical point of view, brain evolution in bats has first been tackled by comparing extant forms (Dräseke 1903) and shortly thereafter using endocranial casts, or "fossilized brains", of bats (e.g., Edinger 1926, Dechaseaux 1962). Highly represented in the fossil record (Brown et al. 2019), hipposiderid endocasts are among the most frequently studied and compared, to other endocasts and to extant representatives. These studies however very briefly describe and compared in the literature, with comparisons to the external brain morphology of these yinpterochiropteran bats, the main conclusions being that 1) these bats were similar in their brain morphology to their extant relatives and then 2) that

they were both capable of flight and of echolocation 30-40 Mya. Not very much has been provided since regarding the study of fossil bat "brains" until very recently, again regarding hipposiderids (Maugoust & Orliac 2021); especially, the evolution of brain morphology has not been formerly addressed, and the phylogenetical context of Yinpterochiroptera offers a duality of particularly interestingly contrasted groups. Evolution of endocranial morphology in this group can be interpreted from three points of view. First, dealing with endocranial characters implies to assess generally the endocranial morphology in Yinpterochiroptera. However, endocranial morphology is only partially documented among bats (see Giannini et al. 2006 and Maugoust & Orliac 2021), and even more the variability of the endocranial morphology. To study endocranial morphological variation at the Yinpterochiroptera scale allows me to propose primary homology hypotheses encompassing two groups of contrasted skull morphology, and to test them in a phylogenetical framework, especially regarding structures that are not shared by all groups. Moreover, some external structures of the brain also have been studied and compared in both fossil and extant bats: the caudal colliculi. The external exposure of these structures has frequently been associated with the ability to echolocate (e.g., Dechaseaux 1956, 1973), and are putatively characteristic structures of "microbats"; properly addressing their evolution in Rhinolophoidea and in Yinpterochiroptera (i.e., with the contrast of pteropodid "megabats") may also bring new information and at least better understand the variation of the exposure of these structures. Second, these anatomical characters are aimed to be used as phylogenetic characters. The degree of systematic relevance of the endocast morphology has rarely been studied in mammals, and never in bats; it is important to know to what extent endocast morphology is relevant to characterize phylogenetic groups and to identify fossil species based on endocasts. Third, these anatomical characters used as phylogenetic characters are built to approach the global endocranial evolution in Yinpterochiroptera, as a clade, and with its sub-clades. Deciphering the evolution of brain morphology during the earlier yinpterochiropteran groups differentiation is especially interesting to better understand how two groups evolved that differently. It is also crucial to address the evolution of morphological variability of the brain before and within rhinolophoid families: there is a standard opposition between "microbats" and "megabats" regarding their brain, but there have been only few studies investigating "microbats" diversity, and generally with non-representative samples (e.g., Schneider 1957). By using a balanced sample and an evolutionary context, proper comparisons between clades will be possible from the infra-ordinal to the infra-familial level. The first part of this study thus deals with the evolution of the endocranial morphology in Yinpterochiroptera. I rely on the identification of the homologous structures across the whole order (Part Two). Based on this nomenclature, I propose phylogenetic characters based on endocranial morphology and I establish a taxon/character matrix comprising 60 taxa and 73 anatomical characters. I use phylogenetic ridge regression method to track the evolution of each anatomical character on the phylogeny. Given the uncertainty of the phylogenetic position of some fossil species, there are as many evolutionary scenarios as possible phylogenies, and I first discuss the variation due to this uncertainty. I then discuss the distribution of characters, their phylogenetic relevance, and their evolution. As a long discussed structure, I also describe and interpret the repartition of the characters linked to the mesencephalic tectum across rhinolophoids (as being absent in all pteropodids). I also discuss the secondary homologies of some morphological structures, which are either unknown or defined here. I finally address the general evolution of the endocranial morphology in the Yinpterochiroptera, down to the family level.

Several subsequent waves of quantitative studies occurred after this first morphological overview of the bat brain. Brains and brain region volumes have been compared between extant taxa (e.g., Mann 1963, Stephan & Pirlot 1970) to find that there is a duality between phytophagous and animalivorous bats, with some works regarding brain region covariations (e.g., Pirlot & Jolicoeur 1982). Then was a period with works correlating numerous ecological traits with brain mass (e.g., Jones & MacLarnon 2004, Pitnick et al. 2006), with also the first phylogenetic corrections (e.g., Safi et al. 2005). Finally, some works tried to address more explicitly the evolution of brain mass rather than comparing extant values (Yao et al. 2012, Smaers et al. 2012, 2021). Temporal characterization has been thus rarely tried, and only regard relative brain mass (e.g., Safi et al. 2005, Niven 2005, Smaers et al. 2021). Apparently, there are numerous covariations between relative brain and brain region masses and ecological traits, but some may be fortuitous and not independent (Dechmann & Safi 2009); among these, only the olfactory bulbs mass has been somewhat proven to be a good proxy for olfactory acuity (Bhatnagar & Kallen 1974), but there generally is too much variation in other gross brain regions to confidently link them to precise functions (Pirlot & Jolicoeur 1982). Brain region covariations have little been examined (only the works of Pirlot & Jolicoeur 1982 and Jolicoeur et al. 1984). Finally, the overwhelming majority of these studies include only extant species. Three studies dealt with fossils. First, Smaers et al. (2012) apparently included values for some eochiropteran bats, but these values are doubtful as they are impossible to find elsewhere in the literature. Second, Yao et al. (2012) examined some hipposiderid brains and contradicted a "neontological" scenario of brain mass decrease in hipposiderids (proposed by Safi et al. 2005 and Niven 2005). More recently, Maugoust & Orliac (2021) also described hipposiderid endocasts and studied the evolution of the encephalization in fossil hipposiderids, supporting the results of Yao et al. (2012). Inclusion of fossils thus seems to challenge results based on extant taxa only and to provide new insights into the evolution of brain and brain region masses. Considering Yinpterochiroptera and previous works, their brain and brain regions masses evolution are expected to be opposed, with clear trends. The second part of this study will then treat brain quantitative variables; inclusion of fossils allows to better constrain the evolution of brain traits, but also prevents use of the volumes of internal regions. Thus, only two brain parts are considered: the olfactory bulbs (housed in the olfactory bulb chamber) and the paraflocculi (housed in the petrosal subarcuate fossa). Together with the brain volume, I will deal with three traits: brain, olfactory bulbs, and paraflocculi masses (converted from volumes). The phylogenetic ridge regression technique provides direct access to each branch evolutionary rate, and allows to better assess the temporal evolution of traits. Using this technique, I aim to better visualize brain and brain region masses evolution through time. This allows to follow the evolutionary trends before and within (i.e., along the tree edges leading to and following the root of) clades; this is the first time these two levels of the evolutionary history of a clade are contrasted and discussed in bats, apart from comparing pteropodids to other bats. This further allows me to describe and to discuss each trait, but also to compare them. Finally, adding fossils to the evolutionary picture allows me to compare the reconstructed evolutions with or without them, and to have a precise idea of the bias of inferring trait evolution based on extant taxa only.

II) Material & Methods

II.1) Evolutionary framework

The yinpterochiropteran sample comprises 60 species, including eight fossil and 52 extant species, documenting six of the seven yinpterochiropteran families. The phylogenetic relationships regarding extant species are well-known thanks to numerous recent studies, which permits me to construct a composite phylogeny, to add to it the fossil species, and to reconstruct the evolution of the endocast at the suborder scale in bats.

II.1.A) Phylogenetic context of Yinpterochiroptera and sampling strategy of extant taxa

At the suprafamilial level, the suborder Yinpterochiroptera dichotomizes in the family Pteropodidae and the superfamily Rhinolophoidea (e.g., Simmons 2005, Teeling et al. 2012). That superfamily also dichotomizes into two clades each comprising three families: one encompasses the families Hipposideridae, Rhinolophidae, and Rhinonycteridae, and the other comprises the families Craseonycteridae (absent in my sample), Rhinopomatidae, and Megadermatidae (e.g., Teeling et al. 2005, Meredith et al. 2011, Amador et al. 2018). The first clade, that will be referred to as "true" rhinolophoids ("Rhinolophoidea sensu stricto" in Benda 2019), is highly diversified nowadays (206 species for the three families, but 109 and 65 species in the particularly rich genera *Rhinolophus* and *Hipposideros*; Wilson & Mittermeier 2019). The second clade has a lower diversity (one single species *Craseonycteris thonglongyai* in the family Craseonycteridae, six species in the rhinopomatids, and six species in the megadermatids; Burgin et al. 2018, Wilson & Mittermeier 2019); this clade will be here referred to as "other" rhinolophoids.

II.1.A.a) The "true" rhinolophoids clade

The "true" rhinolophoids clade contains three recently recognized families; the whole clade was originally referred to as one single family Rhinolophidae, with two subfamilies later raised at the familial level (Rhinolophidae and Hipposideridae) (e.g., Simmons & Geisler 1998, Simmons 2005), but Foley et al. (2015) raised a hipposiderid tribe to the familial rank, adding the Rhinonycteridae to the two other families. Even though Amador et al. (2018) found a closer relationship between Rhinolophidae and non-rhinonycterine Hipposideridae, with the Rhinonycteridae as the sister-taxon of the two others, several studies place the Rhinonycteridae either as basal paraphyletic assemblage (Shi & Rabosky 2015) or as a sister-taxon (Foley et al. 2015, 2017) to Hipposideridae. It is important to note that the analyzes of Foley et al. (2015, 2017) focused on the rhinolophid/rhinonycterid/hipposiderid relationships, while the analyzes of Shi & Rabosky (2015) and Amador et al. (2018) focused on the whole order, with thus less resolution. I therefore follow the phylogenies of Foley et al. (2015, 2017) regarding the internal relationships of the "true" rhinolophoids clade, with Rhinolophidae sister-taxon to a clade comprising Rhinonycteridae and Hipposideridae.

Rhinolophidae is a monogeneric family comprising 100 to 110 species (102 species according to Burgin et al. 2018; 109 species according to Csorba et al. 2019; 106 according to Demos et al. 2019) with several "geographical clades" of African or Asian species, European species being in one clade or the other (see Fig. III-1). The most recent and extensive studies about rhinolophid phylogeny (Dool et al. 2016, Demos et al. 2019) recover and define four major groups: an afro(-palearctic) clade, an Asian clade, and two groups comprising few species that are the "*hipposideros* group" (with the European *Rhinolphus hipposideros*) and the "*trifoliatus* group" (with the Asian *Rhinolophus luctus* and *Rhinolophus trifoliatus*). Such groups are also found in studies dealing with the phylogeny either at the Rhinolophoidea scale (Foley

et al. 2015) or at the Chiroptera scale (Shi & Rabosky 2015, Amador et al. 2018). However, all these studies disagree regarding the relationships between these four groups (Fig. III-1); for instance, each group is once proposed as being the sister-taxon to all other (the Asian clade, being moreover paraphyletic, by Shi & Rabosky 2015; the "*trifoliatus* group" by Dool et al. 2016; the Afro-palearctic clade by Amador et al. 2018; the "*hipposideros* group" by Demos et al. 2019). Such uncertainty may be due to an initial explosive radiation of rhinolophids, and therefore very short branches between all these groups, as proposed by Dool et al. (2016). Here, I choose to follow the phylogeny of Dool et al. (2016) because (1) it is a rhinolophid-focused study, (2) they associated divergence times to their topology (while Demos et al. 2019 did not), and (3) they used Bayesian techniques on nuclear introns (both outperforming maximum-likelihood technique on mitochondrial DNA that Amador et al. 2018 used). My aim is to sample rhinolophids in order to document all the major deep nodes of the rhinolophid phylogeny. My sample includes 12 rhinolophid species, documenting every major rhinolophid "groups" recovered by Dool et al. 2016 (that also have been recovered by Demos et al. 2019), except for the "*maclaudi* group" (with *Rhinolophus ruwenzorii* and *Rhinolophus willardi*) of Demos et al. (2019). This allows my rhinolophid sample to document the nodes A-I, K, and U of Dool et al. (2016): Fig. S5, and I use the age estimates of these nodes in my pruned rhinolophid phylogeny.

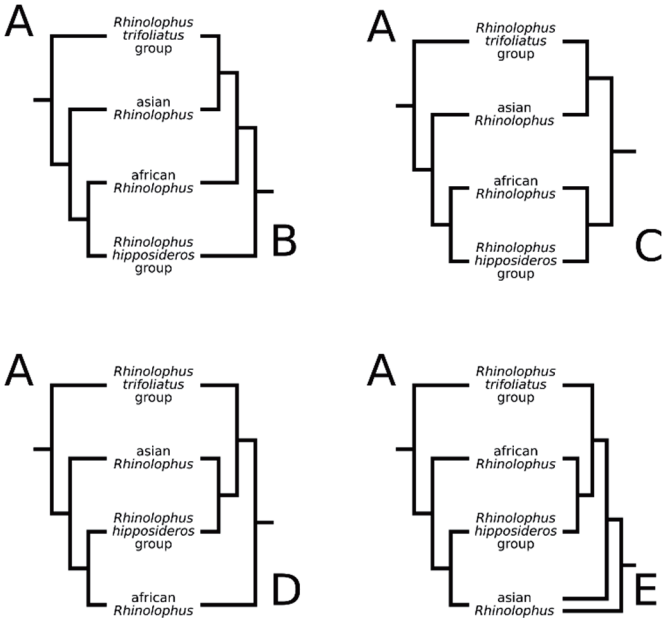

Figure III-1: Phylogenetic relationships used in this work (A- Dool et al. 2016) compared with the other main phylogenetic hypotheses (B- Demos et al. 2019; C- Foley et al. 2015; D- Amador et al. 2018; E- Shi & Rabosky 2015).

Hipposideridae is close to that of Rhinolophidae in terms of specific richness (88 species; Monadjem et al. 2019), differing from this family by the number of extant genera (seven) whose phylogenetic relationships remain debated to some extent (Fig. III-2). The Hipposideridae family includes seven genera, among which one (*Hipposideros*) is particularly rich (65 species; Monadjem et al. 2019). Recent works agree to propose a close relationship between the genera *Aselliscus* and *Coelops* (Lavery et al. 2014, Shi & Rabosky 2015, Foley et al. 2015, Foley et al. 2017, Amador et al. 2018), between the genera *Macronycteris* and *Doryrhina* (formerly included in the genus *Hipposideros*; Foley et al. 2015, Foley et al. 2017), and between the genera *Anthops* and *Hipposideros* (Lavery et al. 2014). Phylogenetic relationships of order-scale studies yield confused results regarding hipposiderid phylogeny (Shi & Rabosky 2015, Amador et al. 2018). More focused studies at the familial scale (Foley et al. 2015, 2017, Patterson et al. 2020) generally retrieve a similar pattern of inter-generic relationships, with the successive divergences of *Asellia*, (*Aselliscus* + *Coelops*), and (*Anthops* + *Hipposideros*). Only the position of the (*Macronycteris* +

Doryrhina) clade varies, being either the first clade to diverge (Patterson et al. 2020), or the second one, being the sister-taxon to the (*Aselliscus* + *Coelops*) + (*Anthops* + *Hipposideros*) clade (Foley et al. 2017) or only to the (*Aselliscus* + *Coelops*) clade and both being the sister-taxon of the (*Anthops* + *Hipposideros*) clade (Foley et al. 2015). If they may disagree regarding inter-generic relationships, the results of Foley et al. (2015, 2017) and Patterson et al. (2020) are congruent regarding the inter-specific relationships within the genus *Hipposideros*. They both retrieve a paraphyletic assemblage of Asian species (with the African *Hipposideros jonesi* and *Hipposideros marisae* that interleave between one basal and several more derived Asian clades) and a monophyletic group of African species. I choose to use the phylogeny of Foley et al. (2017), as it is a more hipposiderid-focused study than that of Foley et al. (2015) and as it (1) uses nuclear DNA instead of mitochondrial DNA and (2) displays age nodes while Patterson et al. (2020) don't. I first aimed to document the generic diversity of that family; my hipposiderid sample documents six of the seven extant genera (*Anthops* is absent). With the exception of the richly diversified genus *Hipposideros*, each genus is represented by one species as their diversity is low. For *Hipposideros*, I sampled one species per major clade, following Foley et al. 2017: Fig. 3. My sample contains one species of the most basal, Asian, clade (*Hipposideros armiger*), two intermediate, more derived, species (*Hipposideros jonesi* and *Hipposideros galeritus*), and one of each of the most derived African and Asian clades (*Hipposideros caffer* and *Hipposideros Pomona*, respectively).

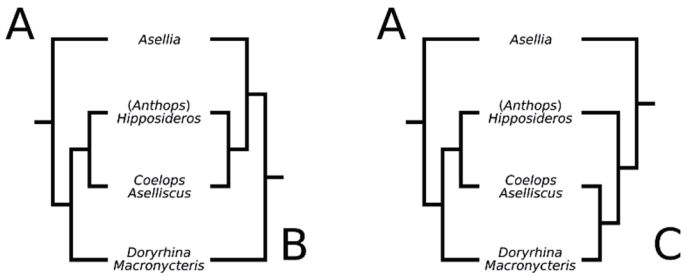

Figure III-2: Phylogenetic relationships used in this work (A- Foley et al. 2017) compared with the other main phylogenetic hypotheses (B- Patterson et al. 2020; C- Foley et al. 2015).

Rhinonycteridae is a family of poorer specific diversity compared to Rhinolophidae and Hipposideridae, and was considered as part of the Hipposideridae family until recently (Foley et al. 2015). In its current conception, this family comprises four genera and nine species. The phylogeny of this poorly diversified family is quite well assessed (Foley et al. 2015): the genus *Paratriaenops* diverged first, then diverges the monospecific genus *Rhinonicteris*, and then are the genera *Triaenops* and *Cloeotis*. My sample includes one species of each of the three more derived genera of this family.

II.1.A.b) The "other" rhinolophoids clade

The "other" rhinolophoids clade monophyly has been challenged by Agnarsson et al. (2011), but other studies (e.g., Shi & Rabosky 2015, Amador et al. 2018) confirmed it. Relationships between families remain, however, unclear. Using a total-evidence approach at the Chiroptera scale, Simmons & Geisler (1998) found Craseonycteridae and Rhinopomatidae as sister-taxa, forming the superfamily Rhinopomatoidea. Some molecular phylogenies further agreed with this hypothesis (Agnarsson et al. 2011, Shi & Rabosky 2015), with paraphyletic or monophyletic (respectively) megadermatids as the sister-taxon of the superfamily, while others found a closer relationship between megadermatids and craseonycterids (Teeling et al. 2005, Meredith et al. 2011, Teeling et al. 2012, Foley et al. 2015, Amador et al. 2018). I rely on the latter hypothesis because of its stronger support; anyway, having no craseonycterid endocast in my sample, this problem does not impact my phylogeny.

The family **Rhinopomatidae** comprises six species (Hulva et al. 2007, Benda et al. 2019) and dichotomizes in two groups of three species that would have split at least 28.1 Mya (Hulva et al. 2007): the first group comprises *Rhinopoma muscatellum*, *Rhinopoma hadramauticum*, and *Rhinopoma microphyllum* and the second one comprises *Rhinopoma hardwickii*, *Rhinopoma cystops*, and likely *Rhinopoma mcinnesi* (Horacek 2019). My sample comprises the species *Rhinopoma microphyllum* and *Rhinopoma hardwickii*, documenting both rhinopomatid groups that diverged during the early Oligocene.

The family **Megadermatidae** also comprises six species which are, contrary to the rhinopomatids, distributed in six genera (Soisook et al. 2015, Francis 2019), and whose phylogenetic affinities are still debated (Fig. III-3). Recent studies propose a close relationship between *Macroderma gigas* and *Cardioderma cor* (Kanuch et al. 2015, Shi & Rabosky 2015) and between *Lavia frons* and *Lyroderma lyra* (Kanuch et al. 2015). Several studies retrieved these two groups as sister-taxa (Kanuch et al. 2015, Shi & Rabosky 2015, Amador et al. 2018), but the new species *Eudiscoderma thongareeae* Soisook et al. 2015 founds its place between the *Cardioderma cor*+*Megaderma spasma* clade and *Lyroderma lyra*, flipping around the previously proposed relationships. I keep the "*Megaderma spasma* diverges first" hypothesis as it is has been retrieved in the most recent analyses. Only Amador et al. (2018) provided age estimates for each node of the megadermatid family; I rely on their estimates. My sample documents the three main "groups" of megadermatids, with *Cardioderma cor*, *Lavia frons*, and *Megaderma spasma*. According to Amador et al. (2018), the split between *Macroderma gigas* and *Lyroderma lyra* is dated at 15.55 Mya, so I keep this value for the split between *Cardioderma cor* (the sister-taxon to *Macroderma gigas*) and *Lavia frons* (the sister-taxon to *Lyroderma lyra*), and the split between these two clades and *Megaderma spasma* is dated at 23.16 Mya.

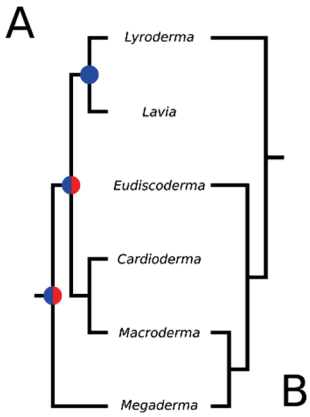

Figure III-3: Phylogenetic relationships used in this work (A- Kanuch et al. 2015, with also the nodes retrieved in the reduced megadermatid phylogenies of Shi & Rabosky 2015 in blue and Amador et al. 2018 in red) compared with the other main phylogenetic hypothesis (B- Soisook et al. 2015).

II.1.A.c) The Pteropodidae clade

The second large Yinpterochiroptera clade is the highly diversified family Pteropodidae, comprising 45 or 46 genera (according to Giannini et al. [2019] or Almeida et al. [2020]) and 191 species (Giannini et al. 2019). Phylogenetic relationships of this family are, as in rhinolophoid families, still blurry. Six major pteropodid groups can be established, roughly following the most recent classification of Almeida et al. (2020): the pteropodines (subfamily Pteropodinae), with especially the genus *Pteropus*; a "noto-nycti" group (subfamilies Notopterisinae and Nyctimeninae), with the genera *Notopteris*, *Paranyctimene*, and *Nyctimene*; the eidolines (subfamily Eidolinae), with the genus *Eidolon*; a "harpio-macro" group (subfamilies Harpionycterinae and Macroglossusinae); the rousettines (subfamily Rousettinae), a generic-rich subfamily; the cynopterines (subfamily Cynopterinae), another generic-rich subfamily. These six groups have been retrieved in all recent analyzes (except the "harpio-macro" group that is polyphyletic in Hassanin et al. [2020], though a single species documents each of its composing subfamilies); the relationships between them are, however, quite blurry (Fig. III-4). Eidolines and "noto-nycti" are frequently retrieved close to the pteropodines, either as a paraphyletic basal assemblage (eidolines being basal to a larger assemblage than these three groups, and "noto-nycti" being the sister-taxon of pteropodines in Almeida et al. 2011; "noto-nycti" being basal in Hassanin et al. 2020; eidolines being basal in Almeida et al. 2020) or as a monophyletic sister-taxon to pteropodines (Shi & Rabosky 2015, Amador et al. 2018). Rousettines and cynopterines are of more varying position: cynopterines are often retrieved as the sister-taxon to all other pteropodid groups (Almeida et al. 2011, Amador et al. 2018, Almeida et al. 2020), while rousettines are found almost everywhere in the family (sister-taxon to "harpio-macro" in Almeida et al. 2011 and in the ML phylogeny of Almeida et al. 2020; sister-taxon to cynopterines in Shi & Rabosky 2015; sister-taxon to all other pteropodid groups in Almeida et al. 2016; sister-taxon to all but cynopterines in Amador et al. 2018 and in the Bayesian phylogeny of Almeida et al. 2020; sister-taxon to pteropodines+eidolines+"noto-nycti" in Hassanin et al. 2020). I use here the Bayesian phylogeny of Almeida et al. 2020 because it (1) is the most comprehensive pteropodid-focused study to date, (2) relies on a Bayesian analysis, and (3) provides node ages. My pteropodid sample documents almost each subfamily (the Notopterisinae, as the sole genus *Notopteris*, is not documented in my sample) and most tribes (Melonycterini and Pteralopini in the Pteropodinae, Harpionycterini in the Harpionycterinae, and Plerotini [as the sole genus *Plerotes*] and Stenonycterini [as the sole genus *Stenonycteris*] in the Rousettinae are not documented). Though there are not as many tribes in Cynopterinae as in Rousettinae, there are numerous genera in that sub-family; a similar sampling effort has therefore been made for each sub-family. Finally, my pteropodid sample includes seven out of the eight subfamilies, nine out of the 14 tribes, and 16 out of the 46 genera. The genus *Pteropus* is particularly diversified (57 species according to Giannini et al. 2019); phylogenetic studies (Almeida et al. 2014, Shi & Rabosky 2015, Amador et al. 2018, Almeida et al. 2020) are more in accordance regarding intra-specific relationships of this genus than those exploring intrafamilial relationships, and they roughly retrieve similar relationships between species. The only phylogeny providing node ages between *Pteropus* species is that of Amador et al. (2018); though being a large scale phylogeny, it is very close to the more focused one of Almeida et al. (2020). Using six *Pteropus* species, I also account for the great specific richness of that genus so that most of the deep nodes of the genus are indirectly represented by distant-most taxa.

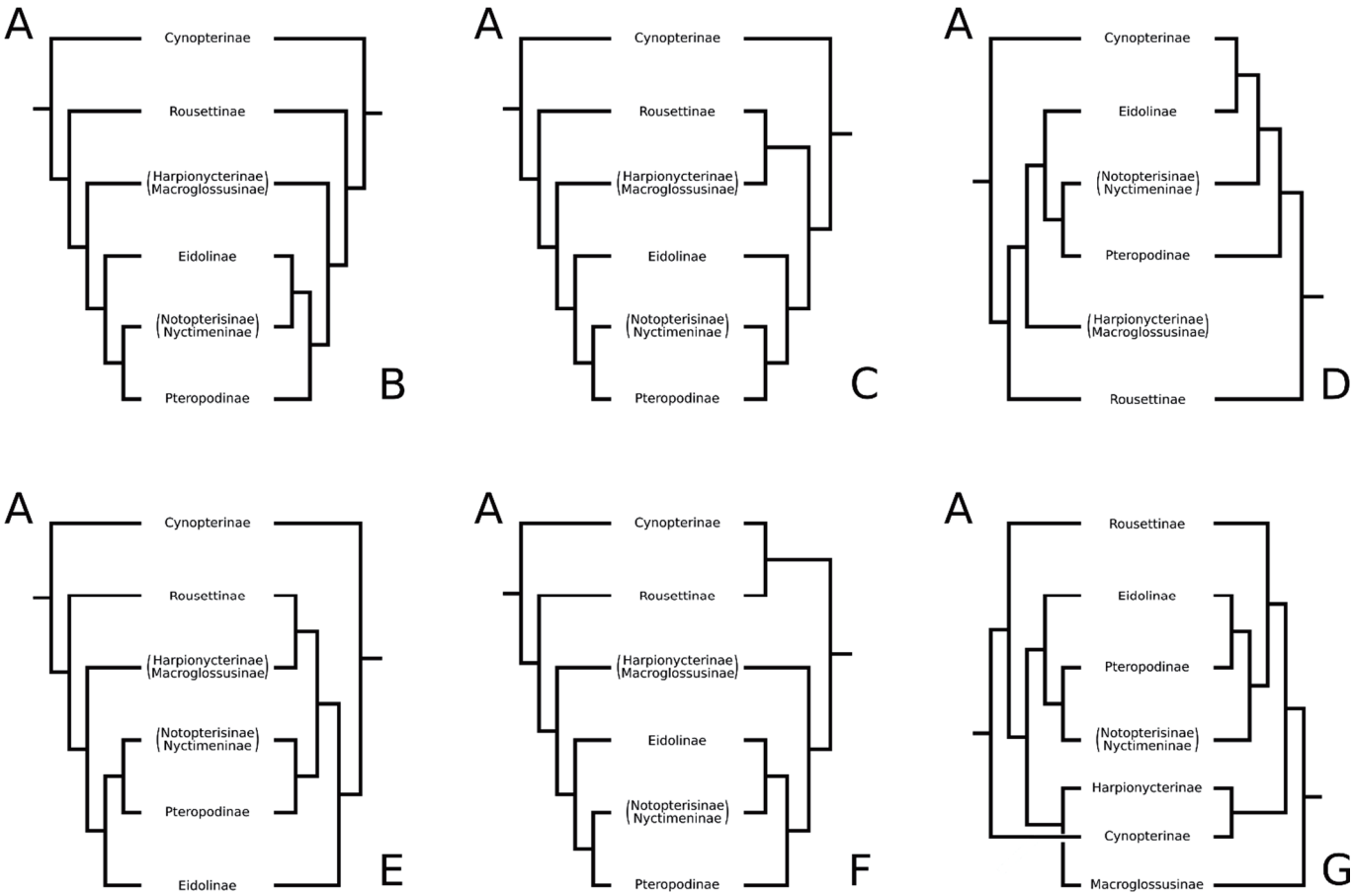

Figure III-4: Phylogenetic relationships used in this work (A- Bayesian phylogeny of Amador et al. 2020) compared with the other main phylogenetic hypotheses (B- Amador et al. 2018; C- maximum likelihood phylogeny of Amador et al. 2020; D- Almeida et al. 2016; E- Almeida et al. 2011; F- Shi & Rabosky 2015; G- Hassanin et al. 2020).

II.1.B) Yinpterochiropteran fossil record and sampling strategy of extinct taxa

The fossil record of this suborder documents almost every extant family. Four pteropodid monospecific genera are extinct, and six extinct species of the genera *Eidolon*, *Micropteropus*, and *Rousettus* have been found so far (Ducrocq et al. 1993, Brown et al. 2019). Two extinct monospecific genera document the rhinopomatids, together with a species attributed to the genus *Rhinopoma* (Brown et al. 2019). In megadermatids, a single monospecific genus is extinct but three of the six extant genera (*Cardioderma*, *Macroderma*, and *Megaderma*) are documented by fossil species (one, five, and 12 species, respectively) (Brown et al. 2019). A close relationship has also been proposed between megadermatids and the extinct Quercy genus *Necromantis*, but this hypothesis has been quite debated (Hand et al. 2012) and remains to be formally tested. Rhinolophids are documented by two extinct genera (Brown et al. 2019): an Asiatic one is monospecific (*Protorhinolophus shanghuangensis*), while a second, documented from Quercy Phosphorites formation, is rich in diversity (*Vaylatsia*, with eight species; Maitre 2014, Ravel et al. 2016, Brown et al. 2019). Otherwise, there are 24 extinct species attributed to the genus *Rhinolophus* (Brown et al. 2019). However, no cranial remains are known in the fossil record of these four families (Brown et al. 2019). Hipposiderids and rhinonycterids are each documented by three extinct genera (with only the hipposiderid extinct genus *Palaeophyllophora* being non-monospecific, with seven species; Maitre 2014, Brown et al. 2019), and with respectively 27 and three species documenting extant genera in each family (Maitre 2014, Brown et al. 2019). More importantly, cranial specimens have been retrieved for several species, some being of exceptional preservation (e.g., Revilliod 1917, Hand 1998a,b, Hand & Kirsch 2003). I document here five and three species for each family. Hipposiderids are documented by two species of the *Palaeophyllophora* genus (*Palaeophyllophora oltina* and

Palaeophyllophora quercyi) from the Quercy Phosphorites, two species of the *Hipposideros* (*Pseudorhinolophus*) subgenus (*Hipposideros* [*Pseudorhinolophus*] *schlosseri* from the Quercy Phosphorites, and *Hipposideros* [*Pseudorhinolophus*] *bouziguensis* from South France), and *Riversleigha williamsi* from the Riversleigh formation (Australia). Rhinonycterids are documented by *Rhinonicteris tedfordi*, *Archerops annectens*, and *Xenorhinos halli*, all from the Riversleigh Formation.

The phylogenetic position of the fossil taxa included in my sample has not been assessed with certainty. Among the fossil hipposiderid species, Ravel et al. (2016) found the subgenus *Hipposideros* (*Pseudorhinolophus*) at its expected phylogenetic position given its systematic attribution: basally to the crown genus *Hipposideros*. An interesting finding of Ravel et al. (2016) is that this subgenus may be paraphyletic, with the Miocene *Hipposideros* (*Pseudorhinolophus*) *bouziguensis* diverging earlier than the Paleogene *Hipposideros* (*Pseudorhinolophus*) *schlosseri*. Moreover, the fossil genus *Palaeophyllophora* is the sister-taxon of the whole genus *Hipposideros*, including its subgenus *Pseudorhinolophus*. However, the phylogenetic analysis of Ravel et al. (2016) does not include many extant hipposiderid genera, with only two representatives of the genus *Hipposideros*. While it would make sense to keep the subgenus *Pseudorhinolophus* close to the extant representatives of the genus *Hipposideros*, the position of the genus *Palaeophyllophora* relative to the other extant hipposiderid genera is not known. Without clear data regarding that point, I will consider different possible positions for that genus: i) as the sister-taxon of the *Hipposideros* genus, or deeper in the phylogeny, ii) as the sister taxon of the (*Hipposideros* + [*Coelops* + *Aselliscus*]) clade, iii) as the sister taxon of the previous clade + the (*Macronycteris* + *Doryrhina*) clade, and iv) as the most basal taxon of the family. Wilson et al. (2016), using the molecular scaffold of Foley et al. (2015), found a close affinity between *Riversleigha williamsi* and the (*Aselliscus* + *Coelops*) clade, so I keep this position for that species. Regarding rhinonycterid fossil species of my sample, *Xenorhinos halli* has been proposed to be the sister-taxon of the genus *Triaenops* and *Archerops annectens* the sister-taxon of the genus *Cloeotis* (Hand & Kirsch 2003, Wilson et al. 2016). *Rhinonicteris tedfordi* has been retrieved close to the extant species of the same genus, *Rhinonicteris aurantia* by Hand & Kirsch (2003), but not by Wilson et al. (2016); I decide to follow the former hypothesis, as *Rhinonicteris tedfordi* has been firstly attributed to the genus *Rhinonicteris*.

II.1.C) Fossil ages and nodes dating

Tips and node age estimates are needed in order to provide a picture of the evolution of the endocranial cast in Yinpterochiroptera as accurately as possible. I use the molecular ages of the various selected references regarding the clades that do not contain fossil species of my sample. For the other clades (Hipposideridae and Rhinonycteridae with fossil species; inter-familial nodes containing them), I use the recently-developed program DateFBD (Didier & Laurin 2020). This program implements a fossilized birth-death model (Heath et al. 2014) that uses a given topology whose tips are dated (by a single value for extant species or fossil species known from a locality with an absolute age and/or by a numerical range for fossil species known from a given biozone). This model estimates speciation, extinction, and fossilization rates, and finally outputs the ages of both the tree nodes and the terminal units whose age is uncertain. As there is some uncertainty regarding the phylogenetic position of the two *Palaeophyllophora* species (see previously), I run DateFBD on the four possible phylogenies. The inputted phylogenies do not contain all extant species sampled, as this specific richness may affect the fossilization rate; instead, I input pruned phylogenies to the oldest possible nodes, and I use the molecular ages for them (e.g., for the Pteropodidae, there only is one terminal unit whose age is that of the crown group of Pteropodidae estimated by Almeida et al. 2020). The fossil taxa used here and their biochronological and

numerical ages are given in the Table III-1: in each case, the given ages (biochronological and numerical) are those of the oldest site from which the given species is known. The resolution of the estimated ages (i.e., number of significant figures) can be given as an input to DateFBD; I choose here a precision of 0.1 Ma (to avoid any precision excess but but to still be precise enough) and I round the inputted more precise molecular age estimates to that resolution.

Species	Oldest locality known	Biochronological age	Numerical age range
Hipposideros (*Pseudorhinolophus*) *bouziguensis*	Bouzigues 1 locality (Sigé 1968, Sigé et al. 1997), Bouzigues site, southern France	Laugnac European fauna (Sigé 1968), MN2b biozone = early Miocene (Becker et al. 2010)	-20.5 to -20.0 Mya (Becker et al. 2010)
Hipposideros (*Pseudorhinolophus*) *schlosseri*	Le Bretou and Saint-Lizier localities (Maitre 2014), Quercy Phosphorites, southwestern France	European standard-level MP16 = late middle Eocene (Maitre 2014)	-38.2 to -37.9 Mya (Maitre 2014)
Palaeophyllophora quercyi	Le Bretou locality (Maitre 2014), Quercy Phosphorites, southwestern France	European standard-level MP16 = late middle Eocene (Maitre 2014)	-38.2 to -37.9 Mya (Maitre 2014)
Palaeophyllophora oltina	Sainte-Néboule locality (Maitre 2014), Quercy Phosphorites, southwestern France	European standard-level MP18 = late Eocene (Maitre 2014)	-35.2 to -34.9 Mya (Maitre 2014)
Riversleigha williamsi	Bitesantennary locality (Archer et al. 2006), Riversleigh Formation, northeastern Australia	Faunal zone B2 = early Miocene (Arena et al. 2016)	-17.4 to -16.8 Mya (Woodhead et al. 2016)
Archerops annectens	AL90 locality (Archer et al. 2006), Riversleigh Formation, northeastern Australia	Faunal zones C2-C3 = middle Miocene (Arena et al. 2016)	-15.1 to -14.2 Mya (Woodhead et al. 2016)
Xenorhinos halli	Bitesantennary locality (Archer et al. 2006), Riversleigh Formation, northeastern Australia	Faunal zone B2 = early Miocene (Arena et al. 2016)	-17.4 to -16.8 Mya (Woodhead et al. 2016)
Rhinonicteris tedfordi	White Hunter locality (Archer et al. 2006), Riversleigh Formation, northeastern Australia	Faunal zone A = late Oligocene (Arena et al. 2016)	-28.1 to -23.0 Mya (Woodhead et al. 2016)

Table III-1: fossil species used in the yinpterochiropteran sample with their first appearance (locality, biochronological, and numerical ages of it).

The other prior parameters of dateFBD are:

- regarding the estimated ages, the lower bound of the root age (here set at -60 Mya which is far older than other previous estimates of the root age for Yinpterochiroptera)

- regarding the speciation, extinction, and fossilization rates:

- the upper bound of the value range in which the MCMC (Monte-Carlo Markov Chain) samples, here set at 5 for all rates (the default values used by Didier & Laurin 2020)

- the width of the sliding windows used for sampling these rates, here set at 0.1, 0.1, and 0.01 respectively (the default values)

- the proportion of moves in the rates, here set at 0.25 (the default value)

- the relation proportion of moves in the speciation and in the extinction (and thus in the fossilization) rates, here set at 0.33 and 0.33 (the default values)

- regarding the MCMC:

  - the number of iterations of the burning stage, here set at 10,000 iterations (the default value)

  - the thinning parameter, here set at one over 300 iterations (the default value)

  - the number of required samples, here set at 20,000 (ten times the default value of 2000).

The commands to run these analyses and the direct output figures are given in Appendix III-0-1. The retained node ages are those of maximal posterior probability; the posterior distribution of values varies among nodes and there are nodes whose posterior distribution may be such to consider an age range rather than a single age. However, the used statistical method does not allow a varying age for the nodes, so I keep the most posteriorly probable node age for all nodes. One of the four time-calibrated phylogenies is given as example (Fig. III-5), the other being given in Appendix III-0-2.

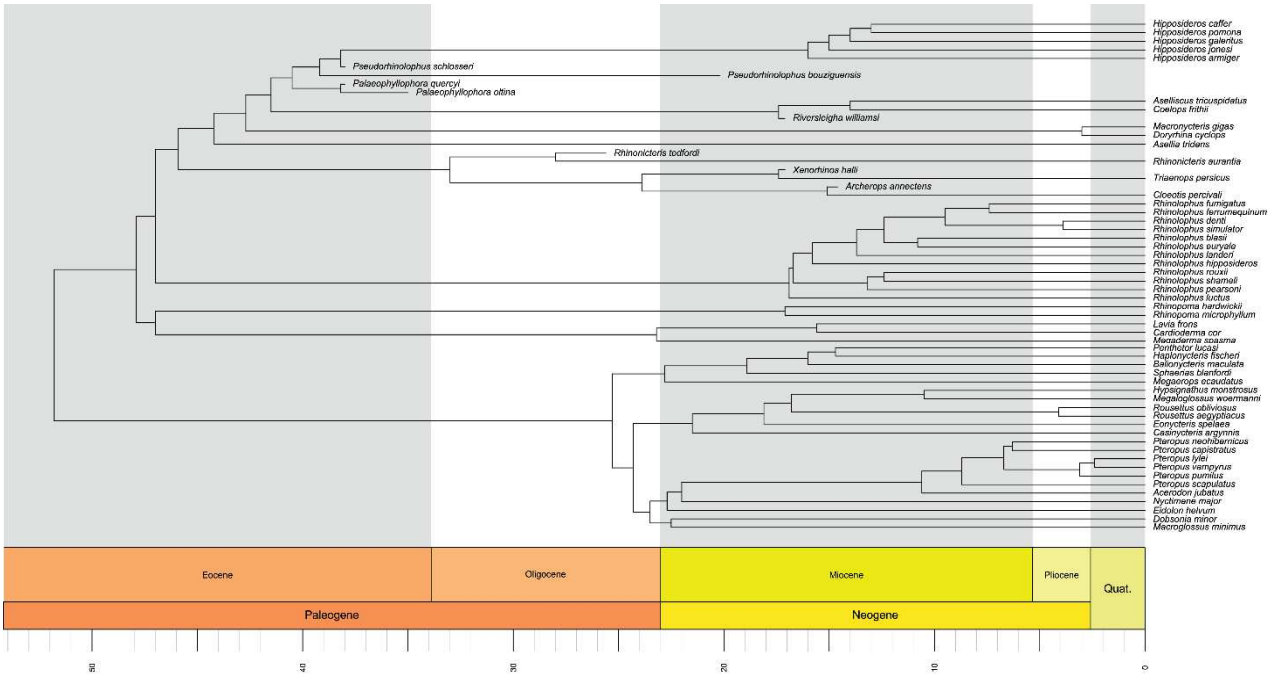

Figure III-5: Time-calibrated phylogeny of the yinpterochiropteran sample here. This stands for the phylogeny with *Palaeophyllophora* as sister-genus to *Hipposideros*. Other cases are figured in the Appendix III-0-2.

NB: a further improvement of DateFBD is yet to be published (Didier & Laurin 2021) implying an improvement of the DateFBD software. This occurred after I performed the time calibrations of my phylogenies; the function only changes in name but not in parameters, but there may be improvements in the reconstruction using the newer version of the software. The older version is thus not available anymore, but I can provide it upon request.

II.2) 3D Data acquisition

Each species is documented here by a single endocranial cast; Table 1 (general Material & Methods part) summarizes curation places and µCT-scan information, including the species used here. All species do not have a value for the three quantitative variables studied here: the endocast of the fossil hipposiderid species *Hipposideros* (*Pseudorhinolophus*) *schlosseri* is not well enough preserved to obtain confident measurements, and this species is pruned for the three variables; a fossil hipposiderid species (*Riversleigha williamsi*), the three fossil rhinonycterid species (*Rhinonicteris tedfordi*, *Xenorhinos halli*, and *Archerops annectens*) and an extant rhinonycterid species (*Rhinonicteris aurantia*) lack paraflocculi, and are removed from the analyses dealing with relative paraflocculi log mass.

II.3) Anatomical characters

Unless otherwise indicated, all anatomical characters have been scored using the plates illustrated by Figures III-6 to III-8.

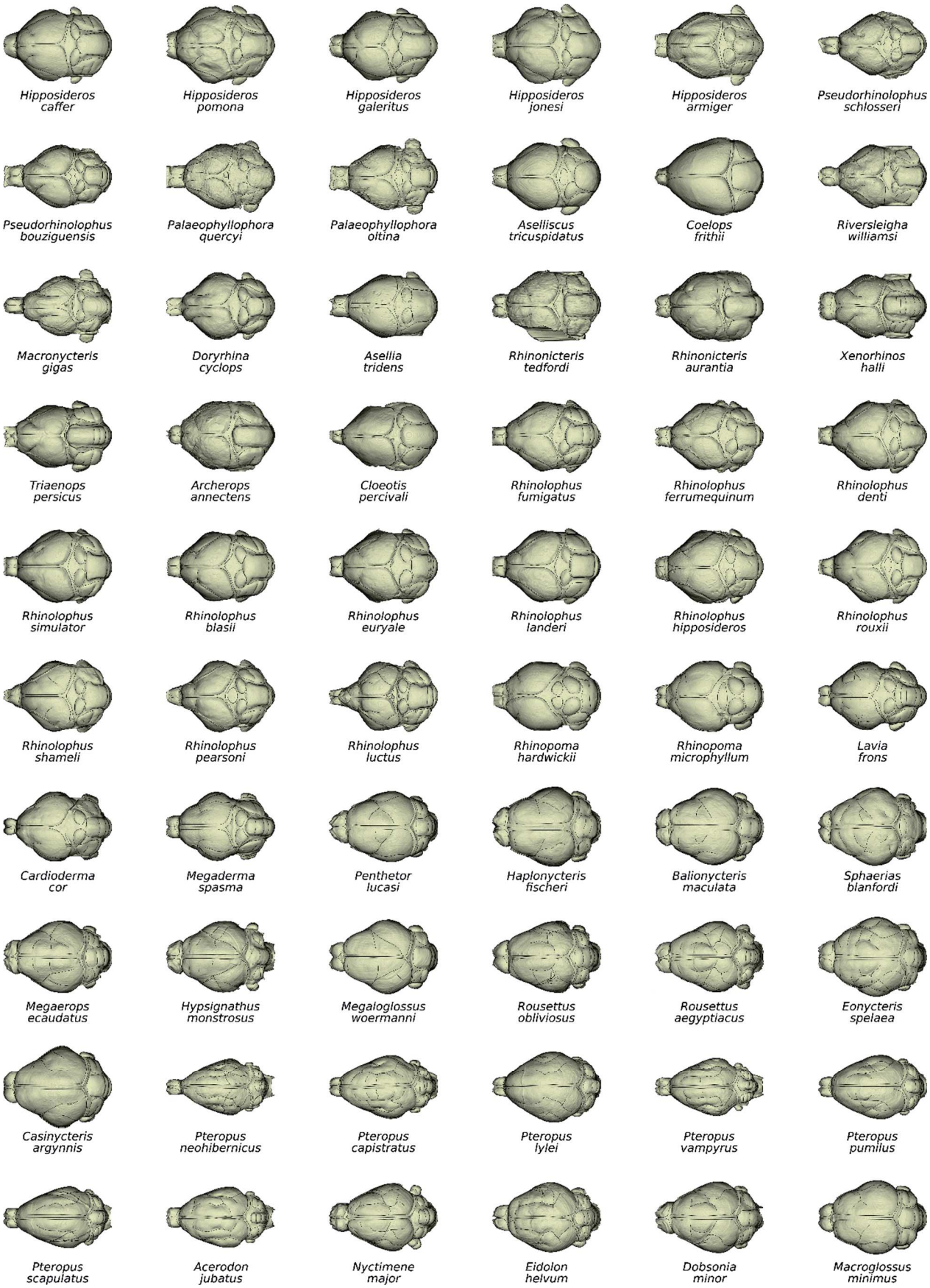

Figure III-6: illustration of the dorsal view of the 60 endocasts used here. Species are sorted in the same order as in Fig. 5. On all endocasts, the structures are outlined. Not to scale.

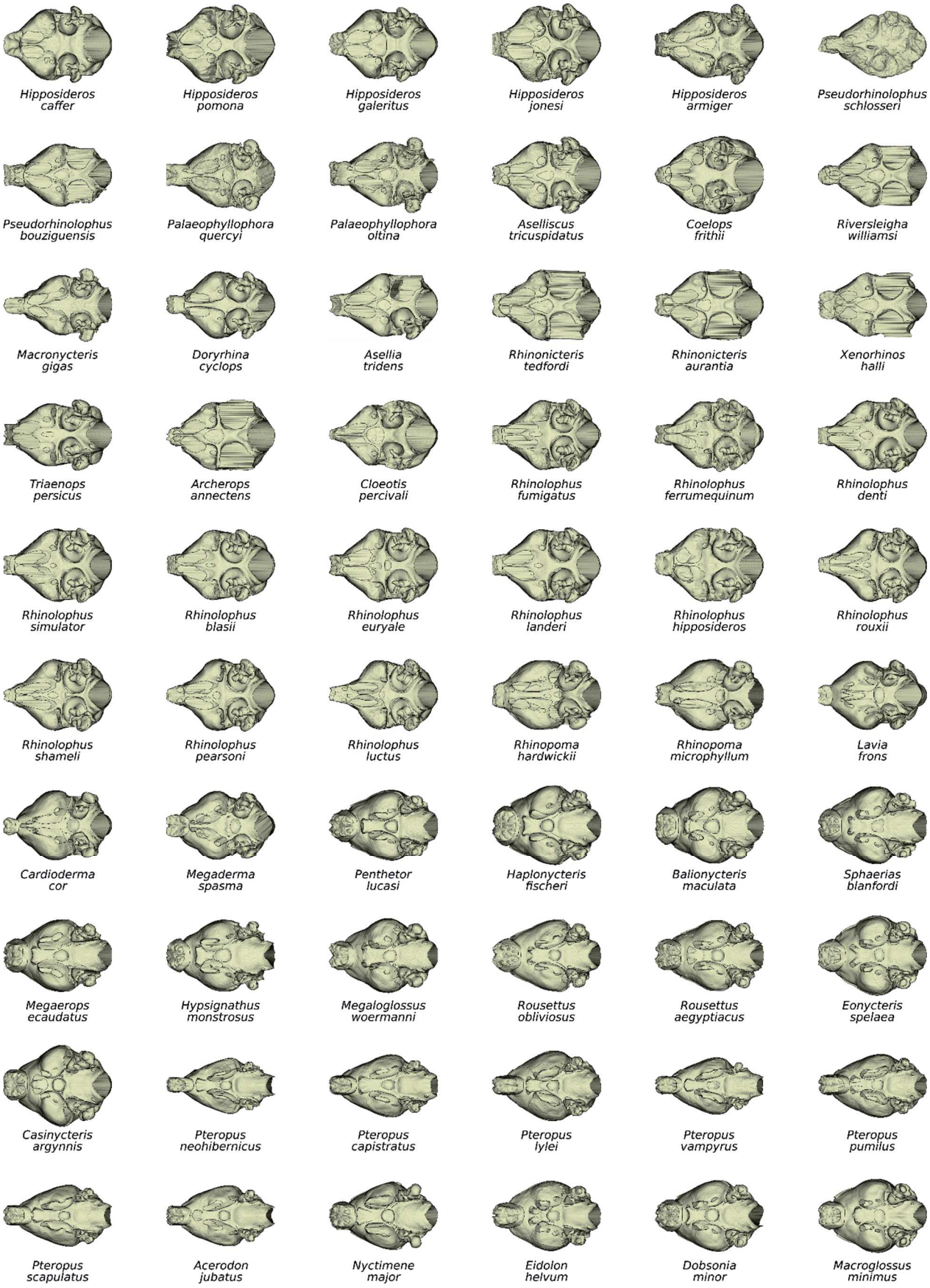

Figure III-7: illustration of the ventral view of the 60 endocasts used here. Species are sorted in the same order as in Fig. 5. On all endocasts, the structures are outlined. Not to scale.

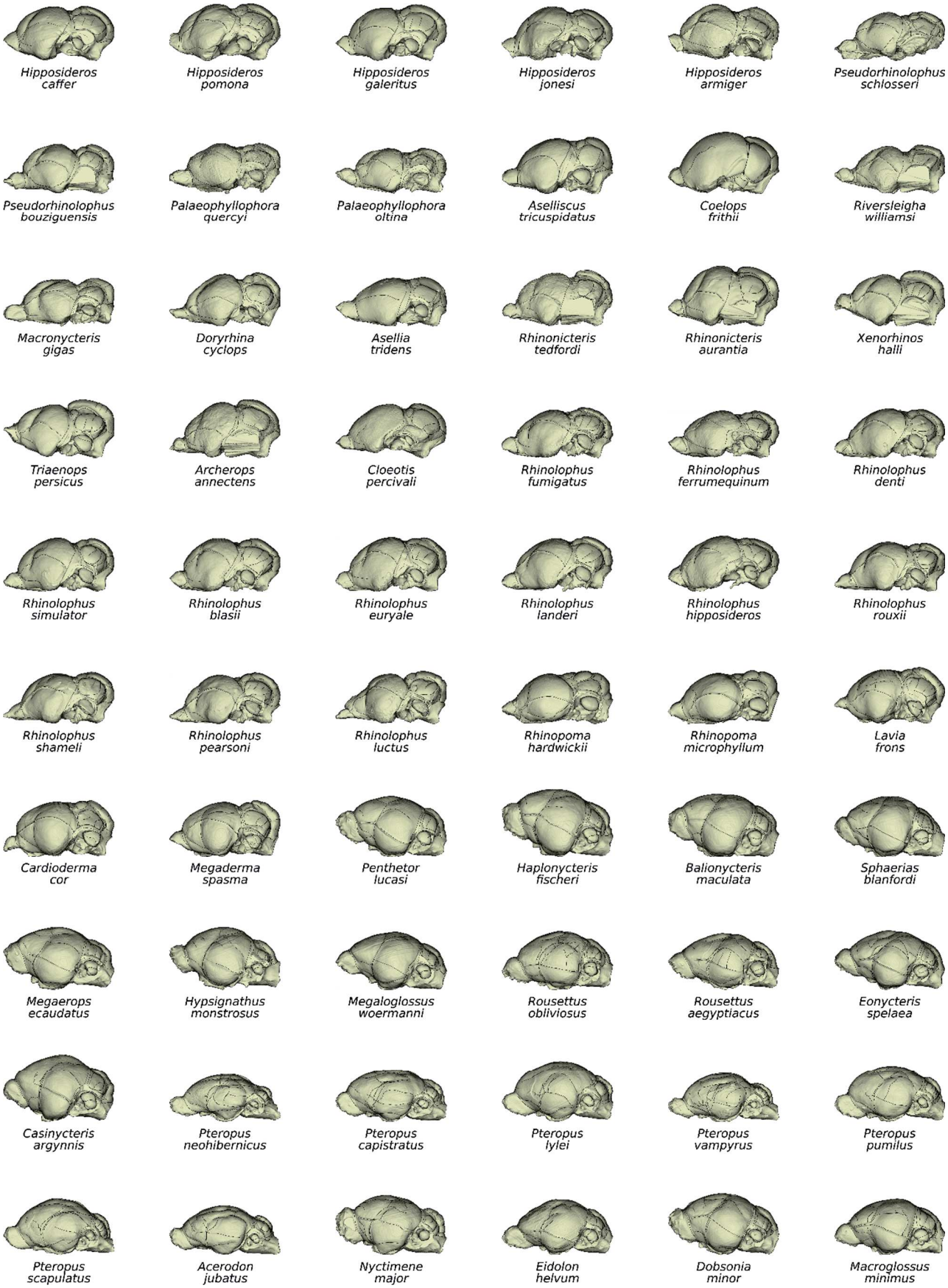

Figure III-8: illustration of the lateral left view of the 60 endocasts used here. Species are sorted in the same order as in Fig. 5. On all endocasts, the structures are outlined. Not to scale.

II.3.A) Overall shape of the endocranial cast

1. Angle of the cephalic flexure: under or equal to 180° (0); over 180° (1). The cephalic flexure (e.g., Nieuwenhuys 1998, Maugoust & Orliac 2021), sometimes called "mesencephalic" flexure, is the angle between the ventral planes of the prosencephalon (telencephalon + diencephalon) and the rhombencephalon (metencephalon + myelencephalon), on both sides of the hypophysis cast. It has been used especially in primates (e.g., Ross & Ravosa 1993, Ramdarshan & Orliac 2016, Profico et al. 2017) to measure the degree of globularity of the brain: the derived primate taxa (hominids for instance) would exhibit a very globular brain, while less derived mammals (insectivores for instance) would exhibit a more linear brain (e.g., Stephan & Bauchot 1959). Bats are not thought to exhibit a derived, globular, brain such as hominids; however, across my sample, there is a variation of the angle of that flexure (ranging from 156° in the pteropodid *Balionycteris maculata* to 209° in the rhinopomatid *Rhinopoma hardwickei*). I choose the threshold of a 180° angle, meaning that the brain is either very linear, the angle being a bit convex (under 180°) or starts to be globular, the angle being a bit concave (above 180°).

2. Angle of the cervical flexure: under or equal to 210° (0); over 210° (1). The cervical flexure (e.g., Nieuwenhuys 1998, Maugoust & Orliac 2021) is the angle between the ventral plane of the rhombencephalon and the spinal cord. It is calculated as being the angle between the ventral plane of the rhombencephalon and the major axis of the foramen magnum plus 90° (considering that the spinal cord exits the foramen magnum perpendicularly to it). Across my sample, there is a variation of that flexure (ranging from 188° in the pteropodid *Pteropus neohibernicus* to 231° in the megadermatid *Lavia frons*) and I choose the threshold of a 210° angle (corresponding to a 120° angle between the rhombencephalon and the major axis of the foramen magnum) meaning that the spinal cord exits the cranial cavity posteriorwards, in-line with the brain (under 210°), or posteroventralwards, with a marked bending following the brain (over 210°).

3. Relative rough proportions of cerebrum vs cerebellum: cerebrum close to or a bit larger than cerebellum (0); cerebrum way larger than cerebellum (1). In my sample, depending on the taxa, the cerebrum (i.e., cerebral hemispheres) can be similar to a bit bigger than the cerebellum (i.e., vermis and cerebellar hemispheres), especially in rhinolophoids, or much bigger than the cerebellum, especially in pteropodids. This character can be assessed by many ways: the relative lengths of each structure (the cerebrum being longer vs very much longer than the cerebellum), the shape of the dorsal outline of the endocast in lateral view as each structure forms a convexity in lateral view (with the two convexities of same inflation vs that of the cerebrum much higher and sometimes that of the cerebellum in its continuity), or the general shape of the endocast excluding the olfactory bulbs and the paraflocculi (hexagon shape if both are of comparable gross size vs lozenge shape if the cerebrum is much bigger).

4. Relative width of cerebrum vs cerebellum: cerebellum slightly wider to equal in width (0); cerebrum slightly wider (1); cerebrum wider (2); cerebrum much wider (3). In my sample, there are taxa where the cerebellum (considering the vermis and the cerebellar hemispheres only) is equal in width to a little bit wider in dorsal view than the cerebrum (e.g., the rhinonycterid *Cloeotis percivali*), and others where the cerebrum is clearly wider, but to different extent. Among them, there are numerous taxa where the cerebrum is only a bit wider, the cerebrum being less wide than the whole metencephalon (i.e., including the paraflocculi) (e.g., the hipposiderid *Aselliscus tricuspidatus*), some other where it is very much wider, the cerebrum being (by far) the widest structure of the endocast (e.g., the pteropodid *Pteropus lylei*), and some other in an intermediate case, the cerebrum being generally as wide to slightly wider than the whole metencephalon (e.g., the megadermatid *Cardioderma cor*). I do not split this character in "cerebellum or

cerebrum wider" then "extent to which the cerebrum is wider" and I order the four states of this character as it is a visual discretization of a continuous trend.

II.3.B) Telencephalon

5. Olfactory bulbs, independence relative to the cerebrum: full (0); partial (1). Depending on the taxa, it seems obvious that some of them exhibit olfactory bulbs that are very independent from the cerebrum (i.e., the cerebral hemispheres; e.g., the hipposiderids *Macronycteris gigas* or *Riversleigha williamsi* or the megadermatid *Cardioderma cor*) while in other species it is clear that the olfactory bulbs are partially embodied in the cerebrum (e.g., the hipposiderid *Hipposideros galeritus*, the megadermatid *Megaderma spasma* or the pteropodid *Sphaeris blanfordi*).

6. Olfactory bulbs, independence of each to the other: clear (0); unclear (1). Across my sample, the olfactory bulbs may be either clearly distinct one to the other (e.g., the megadermatid *Cardioderma cor*, the rhinopomatid *Rhinopoma microphyllum*, almost all pteropodids) or difficult to impossible to distinguish, and appear like a bundle (e.g., the hipposiderid *Asellia tridens*, the rhinonycterid *Triaenops persicus*).

7. Olfactory bulbs, angulation of their ventral surface (in lateral view): oblique, slightly ventrally raised (0); horizontal (1); oblique, slightly dorsally raised (2); rather vertical, very dorsally raised (3). Olfactory bulbs greatly vary in their angulation across our sample. Measuring this character is difficult because there is no clear homologous point to use to account for that angle. Here, I choose to consider the ventral plane of the olfactory bulbs as, when fully independent of the cerebrum, it seems to me the visually most immediate proxy to characterize the general angulation of these bulbs. As in the character 4, it is a discretized continuous gradient, so I choose to order the states of this character.

8. Olfactory bulbs, length vs width: wider than long (0); roughly as long as wide (1); clearly longer than wide (2). Considering the olfactory bulbs together, they greatly vary in their elongation: some are clearly short (e.g., the hipposiderid *Hipposideros pomona*, the rhinopomatid *Rhinopoma hardwickeii*), others are a bit more elongated (being roughly as long as wide; e.g., the hipposiderid *Hipposideros cyclops*, the rhinolophid *Rhinolophus luctus*) while others are very long (e.g., the hipposiderid *Macronycteris gigas*, the pteropodid *Pteropus neohibernicus)*. This character is best scored using both dorsal and ventral views in order to be independent of the olfactory bulbs orientation and position relative to the cerebrum. It is a continuous trend, so I order the states of this character.

9. Cerebral hemispheres, angulation of their posteromedial margin in dorsal view: rather mediolaterally oriented (0); a bit more oblique, in the medioanterior lateroposterior axis (1); very oblique, almost diagonal (2). The cerebral hemispheres, and especially the neopallium, are more or less posteriorly expanded across the sample. Considering each cerebral hemisphere outline, the angle between the anteromedial part of it (which is generally anteroposteriorly oriented) and the posteromedial part of it gives an indication about that development: the more a cerebral hemisphere is posteriorly expanded, the more mediolateral its posteromedial border will be (e.g., see the rhinopomatid *Rhinopoma microphyllum*, the megadermatid *Megaderma spasma* and the pteropodid *Haplonycteris fischeri* for each state). I consider this character as progressive and the character states are ordinated.

10. Cerebral hemispheres, shape of their posterior margin in dorsal view: rather flat (0); clearly convex (1). In a complementary way to the character 9, this character (partially) accounts for the posterior development of the cerebral hemispheres: the more the hemisphere is posteriorly expanded, the more convex is its posterior margin (e.g., see the hipposiderid *Coelops frithii* and the pteropodid *Pteropus*

capistratus for each state). To be scored as “convex”, the posterior margin has to be clearly convex in its middle.

11. Piriform lobes, anteroposterior position: in the posterior half of the cerebrum (0); close to the middle of the cerebrum (1); in the anterior half of the cerebrum (2). The piriform lobes of the cerebrum can be more or less anteriorly or posteriorly positioned across the sample. In some taxa, they are very posteriorly located (e.g., the hipposiderids *Hipposideros armiger* and *Palaeophyllophora quercyi*), or roughly at the middle of the cerebrum in the anteroposterior axis (e.g., the megadermatid *Lavia frons*, the hipposiderid *Hipposideros galeritus*) or clearly anterior (e.g., the hipposiderid *Coelops frithii*). This character can be difficult to code since the piriform lobes are of varying length. I consider here their position depending on the relative length of the spaces anterior and posterior to them: in the previously quoted species, there is either a large space anteriorly, or a similar space anteriorly and posteriorly, or a larger space posteriorly. This character is ordered because of its (discretized) gradual states.

12. Piriform lobes, shape in lateral view: slender and sharp (0); wide and blunt (1). As previously said, the piriform lobes are of varying width, and thus shape (e.g., see the hipposiderid *Hipposideros pomona* and the rhinopomatid *Rhinopoma microphyllum* for each state).

13. Piriform lobes, ventral protrusion: present (0); absent (1). In lateral view, one can align the base of the olfactory bulbs and the base of the foramen magnum; the base of the piriform lobes is sometimes grossly aligned with the two former (e.g., the hipposiderid *Asellia tridens*, the rhinolophid *Rhinolophus pearsoni*, the pteropodid *Pteropus pumilus*) or clearly extends ventrally beyond this virtual line (e.g., the pteropodid *Balionycteris maculata*, the rhinonycterid *Triaenops persicus*).

II.3.C) Diencephalon

14. Epiphysis, cast: visible (0); not visible (1). The epiphysis cast is primarily not expected to be visible on a yinpterochiropteran endocast (see Nomenclature section), but some fossil species (the hipposiderids *Palaeophyllophora quercyi*, *Palaeophyllophora oltina*, *Hipposideros* (*Pseudorhinolophus*) *bouziguensis* and *Hipposideros* (*Pseudorhinolophus*) *schlosseri*) exhibit a structure clearly resembling an epiphysis cast in its shape, size, and location, that is located too far anteriorly to be a mark of the transverse sinus.

15. Hypophysis, cast: visible (0); not visible (1). Most of the species of the current sample exhibit a cast of the hypophysis, but some species do not (the hipposiderids *Coelops frithii*, *Hipposideros caffer*, *Doryrhina cyclops*, and *Macronycteris gigas*).

16. Hypophysis, delineation: clear (0); unclear (1). The cast of the hypophysis, when present, can be either clearly delineated and very prominent (e.g., the pteropodid *Rousettus obliviosus* or the megadermatid *Lavia frons*) or not very well delineated and very shallow (e.g., the hipposiderid *Asellia tridens* or the rhinolophid *Rhinolophus hipposideros*).

17. Hypophysis, global size: small (0); large (1). Since the border of the hypophysis is not very clear for numerous taxa where this structure is present, one can only deal with the global size of this structure instead of its shape. Among the sample, there are numerous taxa where the hypophysis cast is large (e.g., the hipposiderid *Palaeophyllophora oltina*, the megadermatid *Cardioderma cor*, or the pteropodid *Hypsignathus monstrosus*) and others where it is quite small (e.g., the rhinolophid *Rhinolophus landeri* or the rhinopomatid *Rhinopoma hardwickii*). It has to be kept in mind that this character accounts for the ventral prominence of the hypophysis as an organ and thus its mark in the sphenoid bone rather than for the ‘true’ size of that organ.

18. Hypophysis, global position relative to the petrosal casts and to the cerebral hemispheres:

posterior, posteriorly to the cerebral hemispheres and mostly anteroposteriorly overlapping the petrosal casts (0); median, anteroposteriorly overlapping both the cerebral hemispheres and the petrosal casts (1); anterior, anteroposteriorly overlapping only the cerebral hemispheres (2). The hypophysis cast position greatly varies across the sample: it is very posteriorly located in some species, at the anteroposterior level of the petrosal casts (e.g., the megadermatid *Megaderma spasma*), or more anteriorly, being anteroposteriorly located between the cerebral hemispheres and the petrosal casts (e.g., the rhinopomatid *Rhinopoma hardwickii* or the hipposiderid *Hipposideros pomona*), or even more anteriorly, anteroposteriorly overlapping only the cerebral hemispheres (e.g., the pteropodid *Dobsonia minor* or the rhinolophid *Rhinolophus fumigatus*). This character is ordered, given the graduality between the states.

II.3.D) Mesencephalon

19. Tectum of the mesencephalon, general covering: none, with exposed anterior tectum and caudal colliculi (0); partial, with fully exposed caudal colliculi (1); advanced, with partially exposed caudal colliculi (2); full, without exposed tectum and/or caudal colliculi (3). The covering of the mesencephalon has been a major discussion topic in the early stages of mammalian paleoneurology (Edinger 1963, 1964a,b, Dechaseaux 1970, 1973): for instance, Edinger (1964a) considers that an exposed tectum of the mesencephalon in extant bats may be a derived maintainence of a putative primitive condition and is a hallmark of the echolocation (as also said by Dechaseaux 1970, 1973). In the current sample, various stages of covering of the mesencephalon are retrieved, from a full exposure (e.g., the rhinopomatid *Rhinopoma hardwickii*), then a covering of the anterior part of the tectum of the mesencephalon and a full exposure of the caudal colliculi only (e.g., the hipposiderid *Hipposideros galeritus*), then a wide covering of the tectum of the mesencephalon, covering partially the caudal colliculi (e.g., the rhinonycterid *Triaenops persicus*), to a fully covering of the tectum of the mesencephalon (e.g., the pteropodid *Casinycteris argynnis*). Regarding the distinction between the states 0 and 1, a state 1 (covering of the anterior part of the tectum of the mesencephalon) is considered when there only is a short space between the cerebral hemispheres and the caudal colliculi that could or is mostly covered by the transverse sinus. Regarding the distinction between the states 1 and 2, fully exposed colliculi have a circular to ovoid shape while partially covered colliculi have a more triangular shape. This character is ordered.

20. Rostral colliculi, delineation: clear (0); unclear (1); absent (2). In taxa where the tectum of the mesencephalon is fully exposed, the rostral colliculi can be fully and clearly delineated (in the rhinopomatid *Rhinopoma hardwickii*), or an area can be delineated where these colliculi are but without being able to distinguish one to the other (e.g., in the rhinopomatid *Rhinopoma microphyllum* or in the rhinolophid *Rhinolophus pearsoni*), or such an area cannot be distinguished, and there only is a “free space” between the transverse sinus and the caudal colliculi (e.g., in the hipposiderid *Asellia tridens*or in the rhinolophid *Rhinolophus blasii*). This character is not ordered here, as it regards structures that are rarely protruding on fresh brains and leaving a mark on the bone; such a fine degree of differences in their protrusion may indeed be impacted by the preservation of the skull. This character is applicable only for taxa with state 0 of character 19.

21. Caudal colliculi, inflation: low, visible but not protruding (0); moderate, protruding but not being that salient (1); high, very much protruding (2). The caudal colliculi are often exposed, especially in rhinolophoids. When visible, they can be either only delineated (e.g., in the hipposiderid *Asellia tridens*), or marked, protruding a bit (e.g., in the hipposiderid *Hipposideros caffer*, the rhinolophid *Rhinolophus*

ferrumequinum, or the megadermatid *Lavia frons*), or very much protruding (e.g., in the hipposiderid *Doryrhina cyclops*, the megadermatid *Cardioderma cor*, or the rhinopomatid *Rhinopoma hardwickii*). This character is here ordered, as it regards protruding structures that are functionally of great importance, and is best coded using the lateral views of the specimens. This character is not applicable for taxa with a state 3 of the character 19.

22. Caudal colliculi, distance between each one: small, (almost) in contact (0); medium, clearly separated but not very far from each other (1); high, with (almost) the vermis anteriorly protruding between them (2). When exposed, the caudal colliculi vary in their relative position and especially in the distance separating them. In some cases, they are very close to each other and (almost) in contact (e.g., the hipposiderid *Doryrhina cyclops* or the megadermatid *Megaderma spasma*), while in other cases they are a bit separated from each other (e.g., in the rhinolophid *Rhinolophus blasii* or in the hipposiderid *Aselliscus tricuspidatus*), and in other cases they are very much separated and the vermis may start to protrude between them (e.g., in the hipposiderid *Riversleigha williamsi* or in the rhinonycterid *Cloeotis percivali*). This character is ordered due to its gradual states. It is easy to code for specimens with fully exposed caudal colliculi; in species with partially covered caudal colliculi (especially rhinonycteres), it is very likely that these colliculi are covered by the vermis, which matches state 2 of the current character. This character is not applicable for taxa with state 3 of character 19.

II.3.E) Metencephalon

23. Width of the vermis: very wide (0); wide (1); narrow (2). By comparing (in dorsal view) the width of the vermis to that of each cerebellar hemisphere and to the whole cerebellum (i.e., without the paraflocculi), the current sample exhibits clear variation. Some taxa (the hipposiderids *Asellia tridens*, *Aselliscus tricupidatus*, and *Coelops frithii*, and the rhinopomatids) exhibit a very wide vermis, being much wider than the cerebellar hemispheres and visually roughly accounting for one half of the whole cerebellum. Some other taxa (e.g., the hipposiderid *Hipposideros caffer*, the rhinolophid *Rhinolophus denti*, or the pteropodid *Sphaerias blanfordi*) have a wide vermis without being as wide as the previous taxa, being visually similar in width to the cerebellar hemispheres, and accounting for a third of the whole cerebellar width. Other taxa (e.g., the hipposiderid *Hipposideros armiger*, the rhinonycterid *Triaenops persicus*, or the pteropodid *Pteropus neohibernicus*) exhibit a narrower vermis, that may even seem narrower than the cerebellar hemispheres, and that accounts for roughly one quarter of the whole cerebellar width. Being gradual, I order the states of this character.

24. Paramedian fissure, depth: shallow, difficult to delineate (0); deep, easy to delineate (1). The space between the vermis and the cerebellar hemispheres, the paramedian fissure, varies in terms of delineation and of depth: some taxa exhibit a very shallow and very gradual paramedian fissure (e.g., the hipposiderid *Asellia tridens*, the rhinonycterid *Cloeotis percivali*, or the rhinopomatid *Rhinopoma microphyllum*) while it is deeper and very easy to spot in other taxa (e.g., the hipposiderid *Doryrhina cyclops*, the rhinolophid *Rhonolophus blasii*, or the pteropodid *Acerodon jubatus*).

25. Paramedian fissure, width: narrow (0); wide (1). Depending on the taxa, when clearly marked, the paramedian fissure may be narrow, resembling a fissure (e.g., the hipposiderid *Hipposideros galeritus*, the rhinolophid *Rhinolophus luctus*, or the megadermatid *Lavia frons*), or it can be wider (e.g., the hipposiderid *Hipposideros armiger*, the pteropodid *Pteropus scapulatus*, or the rhinonycterid *Triaenops persicus*). This character is not applicable for taxa with state 0 of character 24.

26. Vermis, anterior protrusion: present (0); absent (1). The vermis can extend anteriorly beyond the

anteriormost level of the cerebellar hemispheres in some taxa (e.g., the pteropodid *Haplonycteris fischeri*), sometimes partially covering the caudal colliculi of the mesencephalon (e.g., the rhinonycterid *Rhinonycteris aurantia*), or the cerebellar hemispheres can be more anteriorly located than the vermis, extending more anteriorly than the latter (e.g., the hipposiderid *Hipposideros armiger*, the rhinolophid *Rhinolophus landeri*, or the megadermatid *Megaderma spasma*).

27. Vermis, posterior protrusion: present (0); absent (1). In some taxa, there is a posterior protrusion of the vermis: when the posterior outline of the cerebellum (in dorsal view) is not smoothly continuous, this can be due to a posterior protrusion of the vermis (it can also be due to a posterior protrusion of the cerebellar hemispheres, see after) (e.g., see the megadermatid *Megaderma spasma* and the rhinopomatid *Rhinopoma hardwickii* for each state).

28. Vermis, thickness in lateral view: low, being a thin layer (0); intermediate (1); thick (2). In lateral view, the vermis (and especially its anterior portion) is of varying thickness across taxa: in some species, the vermis is not very thick, with the aspect of a thin layer (e.g., the rhinonycterid *Cloeotis percivali*, the rhinolophid *Rhinolophus fumigatus*, or the pteropodid *Casinycteris argynnis*), or thicker, but not being disproportionate (e.g., the hipposiderid *Hipposideros galeritus*, the rhinolophid *Rhinolophus shameli*, or the pteropodid *Nyctimene major*), and in some cases, it seems particularly thick (e.g., in the rhinonycterid *Triaenops persicus*, or in the megadermatid *Megaderma spasma*). Representing a continuous trend, I order the states of this character.

29. Vermis, number of grooves: none (0); one or two (1); three or more (2). The nomenclature of vermian grooves has been discussed previously, and we expect some to appear before others as being fissures separating not only vermian lobules but also other metencephalic elements. In my sample, there is a rough three-mode pattern with some species having no vermian grooves (e.g., the hipposiderid *Asellia tridens*, the rhinonycterid *Archerops annectens*), numerous species having one or two grooves (e.g., the hipposiderid *Coelops frithii*, the rhinolophid *Rhinolophus landeri*, or the rhinopomatid *Rhinopoma hardwickii*), and several ones having numerous grooves (pteropodids in general, but also the megadermatid *Lavia frons* or the rhinonycterid *Triaenops persicus* for instance). I prefer coding the vermian complexity in a single character instead of establishing several characters for each groove because (1) it finally accounts in a similar way than overweighting the absence of several grooves in species with few to no groove, (2) the few grooves are generally the same to appear, and (3) when there are more than three grooves, it is not rare to have more than the four grooves separating the vermian lobules, with intra-lobulian sulci to identify (which is impossible with endocasts only). I order this character due to its progressive type.

30. Cerebellar hemispheres, anterior protrusion compared to the vermis: slight, being a bit more anterior (0); high, with almost half of the hemispheres being anterior to the vermis (1). In taxa with cerebellar hemispheres extending more anteriorly than the vermis, there is a rough duality: some taxa exhibit cerebellar hemispheres that are slightly more anteriorly located than the vermis (e.g., the hipposiderid *Hipposideros caffer*, the rhinolophid *Rhinolophus euryale*, or the megadermatid *Lavia frons*) and others where the cerebellar hemispheres are clearly anteriorly displaced relatively to the vermis (e.g., the rhinopomatid *Rhinopoma microphyllum* or the hipposiderid *Palaeophyllophora quercyi*). This character is not applicable for taxa with state 0 of character 26.

31. Cerebellar hemispheres, posterolateral protrusion: present (0); absent (1). Related to character 27, the posterior outline of the cerebellum in dorsal view may be irregular and not smooth. This can be due to a posterior protrusion of the vermis and/or to a posterolateral protrusion of the cerebellar

hemispheres. Indeed, in some cases the posterolateral aspect of the cerebellar hemispheres is angular, not very smooth, or even protruding, and associated with a posterior protrusion of the vermis (e.g., the pteropodid *Penthetor lucasi*) or not (e.g., the hipposiderid *Riversleigha williamsi*); in a reverse manner, there are cases where the posterolateral corner of the cerebellar hemisphere is smoother with a posterior protrusion of the vermis (e.g., the hipposiderid *Doryrhina cyclops*), or not, with a fully smooth posterior outline of the cerebellum (e.g., the rhinopomatid *Rhinopoma microphyllum*).

32. Paraflocculi, additional dorsal opening (i.e., forming a continuity with the rest of the endocast): present (0); absent (1). As previously discussed in the Nomenclature section, the paraflocculi may exhibit more than one opening that are likely to correspond to cartilaginous walls that are not preserved on skulls. An opening can be retrieved on the dorsal aspect of the paraflocculus, joining the cast of the sigmoid sinus dorsally. This aperture is present, for instance, in the hipposiderids *Aselliscus tricuspidatus*, *Hipposideros jonesi*, and *Hipposideros pomona*, or in the megadermatid *Cardioderma cor*. Two main remarks have to be pointed out. First, this character is quite difficult to score on plates of static views since these openings are on the medial side of the paraflocculi; it has to be scored using the 3D models. Second, in some cases these openings were fully segmented (i.e., visible connection on the 3D model) and in others they were cut (i.e., as a foramen); thus, the "none" condition was scored in taxa where paraflocculi were clearly smooth at the expected location of these openings.

33. Paraflocculi, additional posteromedioventral opening (i.e., forming a continuity with the rest of the endocast): present (0); absent (1). In a similar way to the previous (32) character, an opening may be found on the ventral aspect of the posteromedial side of the paraflocculus, joining the sigmoid sinus posteriorly (a bit before the sigmoid sinus joins the jugular foramen). This aperture is present, for instance, in the hipposiderid *Asellia tridens*, the pteropodid *Macroglossus minimus* or the rhinolophid *Rhinolophus blasii*. There are the same concerns for this posteromedioventral opening regarding its coding and segmentation as for the posteromediodorsal one (see character 32).

34. Paraflocculi, size of the additional openings: small (0); large (1). The previously described openings, when present and depending on the taxa, show a quite high variability of their width: in some cases they are very thin and narrow, at a point that they can be present on a single side of the endocast (e.g., the pteropodid *Macroglossus minimus* or the rhinonycterid *Cloeotis percivali*), or quite large, of a comparable width to (i.e., at least one quarter of the width of) the junction of the paraflocculus to the rest of the brain (i.e., through the lateral semicircular canal) (e.g., the hipposiderid *Coelops frithii*, the rhinolophid *Rhinolophus landeri* or the megadermatid *Lavia frons*). This character is not applicable for taxa with state 1 of characters 32 and 33.

35. Paraflocculi, lateral sulcus: present (0); absent (1). A lateral sulcus of the paraflocculus (see Nomenclature section) is retrieved in some taxa (the rhinonycterid *Triaenops persicus* and several pteropodids as *Acerodon jubatus*, *Casinycteris argynnis*, or *Macroglossus minimus*).

II.3.F) Pons-Medulla Oblongata Continuum

36. Pons-Medulla Oblongata Continuum, width relative to that of the petrosal casts: much lower (0); lower to subequal (1); higher (2). This character less accounts for the width of the pons-medulla oblongata continuum than for the width of the petrosal casts; however, that measure of this structure is, to me, the best way to account for it. There is a considerable variation of the space between these casts, and depending on the cases, I score the width of the P-MOC at its minimal width by comparing grossly it to either (1) the distance between the medialmost point of the petrosal cast outline and the VIIIth cranial

nerve root or (2) the whole petrosal cast width. Globally, rhinolophoids have big and close petrosals (first of the two methods in the previous sentence is used) while pteropodids have smaller and further petrosals (second of the two methods is used). In rhinolophoids, several taxa show very close petrosals, the width between them being lower to subequal to the first measure (e.g., the hipposiderid *Coelops frithii*, the rhinonycterid *Triaenops persicus* or the rhinolophid *Rhinolophus denti*), and others exhibit more distant petrosals, the gap between them being wider than the first measure and/or approaching the whole petrosal width (e.g., the hipposiderid *Hipposideros caffer* or the megadermatid *Lavia frons*). All pteropodids have petrosals much more distant from each other, with a gap wider than the whole petrosal width (e.g., *Dobsonia minor*, *Haplonycteris fischeri* or *Pteropus neohibernicus*). This character is ordered.

II.3.G) Neopallial foldings

37. Sylvia(n sulcus): present (0); absent (1). The sylvia, or sylvian sulcus, is formed of both the pseudosylvia(n sulcus) and the suprasylvia(n sulcus) as in primates (see Nomenclature section). It is present in most of the species studied here (e.g., the hipposiderid *Hipposideros armiger*, the rhinolophid *Rhinolophus fumigatus*, the megadermatid *Megaderma spasma* or the pteropodid *Hypsignathus monstrosus*) but some species lack this fundamental sulcus (the hipposiderids *Asellia tridens*, *Aselliscus tricuspidatus* and *Coelops frithii*). The presence of the sylvia represents the first stage of the neopallial sulcal complexification pattern previously discussed (see Nomenclature section).

38. Posterior extension of the suprasylvia(n sulcus): present (0); absent (1). Pteropodids and numerous rhinolophoid species exhibit a posterior extension of the suprasylvian part of the sylvia. In rhinolophoids, the sylvia can either be a mostly ventrodorsal sulcus a bit anteroposteriorly tilted, without posterior extension (e.g., the hipposiderid *Hipposideros caffer*, the rhinolophid *Rhinolophus landeri* or the rhinopomatid *Rhinopoma hardwickii*) or it can posteriorly bend and extend posteriorwards (e.g., the hipposiderid *Hipposideros armiger*, the rhinolophid *Rhinolophus luctus* or the megadermatid *Megaderma spasma*). The posterior elongation of the sylvia represents the second stage of the neopallial sulcal complexification pattern previously discussed (see Nomenclature section).

39. Bridge (sulcus): present (0); absent (1). The rhinolophoid species studied here (except the megadermatid *Lavia frons*) and the pteropodid *Casinycteris argynnis* only show, at most, an elongated sylvian sulcus; all other pteropodid species show an increased stage of neopallial sulcal complexification (see Nomenclature section) with the presence of a bridge sulcus.

40. Bridge (sulcus), shape: straight (0); curved (1). In all pteropodids except *Casinycteris argynnis*, the bridge sulcus can be either straight (in the third to fifth neopallial complexification stages, see Nomenclature section and Fig. II-5; e.g., *Balionycteris maculata* for the stage 3, *Haplonycteris fischeri* for the stage 4, and *Nyctimene major* for the stage 5) or curved (in the sixth and most complex stage; see Fig. II-5; e.g., *Pteropus vampyrus*).

41. Bridge (sulcus), orientation: anterodorsal (0); dorsal (1). In all pteropodids except *Casinycteris argynnis*, the bridge sulcus can be oriented either anterodorsally (in the third neopallial complexification stage, see Nomenclature section and Fig. II-5; e.g., *Penthetor lucasi*) or dorsally (in the fourth to sixth neopallial complexification stages; see Fig. II-5; e.g., *Hypsignathus monstrosus* for stage 4, *Rousettus aegyptiacus* for stage 5, and *Pteropus neohibernicus* for stage 6).

42. Lateral (sulcus): present (0); absent (1). In pteropodids with a complex neopallial sulci pattern, a lateral sulcus is also present dorsomedially to the sylvia, paralleling the suprasylvian part of the sylvia (in the fifth and sixth neopallial complexification stages, see Nomenclature section and Fig. II-5; e.g.,

Rousettus obliviosus for stage 5 and *Pteropus scapulatus* for the stage 6).

43. Infrasylvia(n sulcus): present (0); absent (1). In some pteropodid species (and in the megadermatids *Lavia frons* and *Megaderma spasma*), there also is an additional neopallial sulcus arising from the sylvia and located ventrolaterally to the suprasylvian part, the infrasylvia or infrasylvian sulcus. This sulcus is sometimes present in species with a moderate complexity of neopallial sulci, such as *Hypsignathus monstrosus*, but it can also be present (and shorter) in species with a lower (e.g., *Balionycteris maculata*) or higher (e.g., *Pteropus neohibernicus*) neopallial sulci complexity.

44. Orbital (sulcus): present (0); absent (1). In pteropodids except *Casinycteris argynnis*, an orbital sulcus, paralleling to some extent the anterior border of the cerebral hemisphere, is frequently found independent of the complexification stage (e.g., *Balionycteris maculata* or *Pteropus pumilus*).

45. Intermediate (sulcus): present (0); absent (1). As for the orbital sulcus, some pteropodid species with (at least) a bridge sulcus may also exhibit an intermediate sulcus, in a less frequent manner than the orbital sulcus, but also independent of the neopallial complexification stage (e.g., *Sphaeris blanfordi* or *Nyctimene major*).

II.3.H) Vascular structure casts

46. Orbitotemporal canal, general shape: convex (0); sigmoid (1); flat (2). The orbitotemporal canal is the cast of a canal carrying the anterior branch of the superior ramus of the stapedial artery ("SAsrab"; see Nomenclature section and Fig. II-28). This canal has a varied shape in my sample. In all rhinolophoids (except the rhinonycterid *Cloeotis percivali* where it does not appear), it is convex (e.g., the hipposiderid *Hipposideros armiger*, the rhinonycterid *Xenorhinos halli*, or the rhinopomatid *Rhinopoma hardwickii*). In pteropodids, on the other hand, it may be mostly of a convex shape as in rhinolophoids, but a bit more flattened, and with its proximal (i.e., posterior) part being concave, being sigmoid (e.g., *Balionycteris maculata* or *Eidolon helvum*). In some pteropodid species, it is even more flat, with numerous but tiny convexities and concavities (e.g., *Nyctimene major* or *Pteropus pumilus*). This character is ordered because, in the convex state, the canal is more or less flattened and the sigmoid then flat conditions seem to be in the continuity of this flattening trend (or, inversely, the most convex states seem to be in the continuity of an increasing convex condition).

47. Orbitotemporal canal, shape of the dorsal convexity: sharp (0); blunt (1). Most of the species studied here exhibit an orbitotemporal canal with a dorsal convexity during its course. This convexity varies in its shape, being a wide and blunt angle in several species (e.g., the hipposiderid *Aselliscus tricuspidatus*, the the megadermatid *Cardioderma cor*, or the pteropodid *Maccroglossus minimus*) while there is a more acute and sharp angle in some species (e.g., the rhinonycterid *Triaenops persicus* or the rhinolophid *Rhinolophus ferrumequinum*).

48. Orbitotemporal canal, general dorsoventral (in lateral view) position: rather dorsal (0); rather median (1); rather ventral (1). In some species, the orbito-temporal clearly parallels the dorsal outline of the cerebral hemispheres in lateral view, with a very dorsally displaced orbitotemporal canal (e.g., the hipposiderid *Palaeophyllophora quercyi* or the rhinolophid *Rhinolophus fumigatus*), while in others it lies clearly much more ventrally (e.g., in the rhinopomatid *Rhinopoma hardwickii* or the pteropodid *Sphaerias blanfordi*), and in others it is in a median position on the cerebral hemisphere (e.g., the hipposiderid *Hipposideros galeritus*, the rhinonycterid *Triaenops persicus*, or the megadermatid *Megaderma spasma*). Due to the varying shape of the orbitotemporal canal, this character may be difficult to score: it is particularily true for most pteropodids with a sigmoid-shaped canal, the anterior part being at a median

level while the posterior part is at a ventral level. I used the paraflocculi as a proxy to assess the character state in these taxa: if the posterior part of the orbitotemporal canal is at the level or ventral to the paraflocculi, the character is coded as state 1, while if this part only reaches the dorsalmost level of the paraflocculi, the character is coded as state 0. Due to its gradual type, this character is ordered.

49. Orbitotemporal canal, anteroposterior position of the anterior opening: close or anterior to the circular fissure (0); close to the middle cerebral artery cast (1). All rhinolophoids and some pteropodids show a "complete" orbitotemporal canal, extending anteriorly to the level of the circular fissure or to the the olfactory bulbs (e.g., the pteropodids *Balionycteris maculata* or *Macroglossus minimus*, the rhinonycterid *Rhinonycteris tedfordi*, or the megadermatid *Megaderma spasma*) while other pteropodids show a truncated orbitotemporal canal (e.g., *Hypsignathus monstrosus* or *Pteropus pumilus*), the SAsrab (see character 46, or Nomenclature section, or Fig. II-28) might be blending with the middle cerebral artery or another artery (as proposed, but at the whole pteropodid scale, by Wible & Davis 2000).

50. Complexity of the meningeal rami of the SAsrab: absent, only the SAsrab is present as the orbitotemporal canal (0); low, with only a supplementary middle meningeal artery (1); high, with more meningeal rami (2). The degree of complexity of the meningeal rami arising from the SAsrab greatly varies across my sample: in most rhinolophoids and in several pteropodids, there only is a SAsrab as an orbitotemporal canal (e.g., the hipposiderid *Hipposideros armiger*, the rhinolophid *Rhinolophus pearsoni*, or the pteropodid *Megaerops ecaudatus*), but in the pteropodid *Nyctimene major* and in the megadermatid *Lavia frons* there also (and only) is the presence of the cast of the middle meningeal artery, and in other pteropodids there also are supplementary meningeal rami to either the SAsrab or the middle meningeal artery (e.g., *Acerodon jubatus*, *Macroglossus minimus*, or *Rousettus aegyptiacus*). These character states are of increasing complexity, so I order this character.

51. Middle cerebral artery, cast: present (0); absent (1). Pteropodids exhibit the cast of the middle cerebral artery (e.g., *Balionycteris maculata*, *Nyctimene major*, or *Rousettus obliviosus*) while rhinolophoids do not.

52. Superior sagittal sinus, cast: present (0); absent (1). Pteropodids of this sample (e.g., *Casinycteris argynnis*, *Pteropus capistratus*, or *Megaloglossus woermanni*) and two of the three megadermatids (*Lavia frons* and *Megaderma spasma*) exhibit the cast of the superior sagittal sinus, while other rhinolophoids do not.

53. Transverse sinus, completeness of the cast: full (0); partial (1). The transverse sinus cast is mediolaterally complete in all pteropodids of this sample (e.g., *Eonycteris spelaea*, *Pteropus lylei*, or *Sphaerias blanfordi*) and in numerous rhinolophoids (e.g., the hipposiderid *Coelops frithii*, the rhinolophid *Rhinolophus simulator*, or the megadermatid *Lavia frons*) while the central part is not visible in several rhinolophoids (e.g., in the hipposiderid *Doryrhina cyclops*, the rhinonycterid *Cloeotis percivali*, or the rhinopomatid *Rhinopoma hardwickii*). The latter condition may be concurrent, to some extent, to the exposure of the anterior part of the tectum of the mesencephalon, which would cancel/blur a potential mark left by the transverse sinus in this area. However, this co-occurrence is not "perfect", as a full transverse sinus cast is present in species where an anterior tectum can be delineated (e.g., the hipposiderid *Aselliscus tricuspidatus*).

II.3.I) Cranial openings

54. Bundle-like aperture anterodorsal to the olfactory bulbs: present (0); absent (1). In all of the rhinolophoids sampled here (e.g., the hipposiderid *Asellia tridens*, the rhinonycteris *Triaenops persicus*, or the megadermatid *Cardioderma cor*), there is an indeterminate aperture anterodorsally to the bulbs (see Nomenclature section) that is not retrieved in pteropodids.

55. Optic foramen: distinct and individual (0); confluent with the sphenorbital fissure (1). The optic foramen is individualized from the sphenorbital fissure in pteropodids and some rhinolophoids (the three megadermatids *Cardioderma cor*, *Lavia frons*, and *Megaderma spasma* and three Hipposideridae, *Hipposideros armiger*, *Doryrhina cyclops*, and *Palaeophyllophora quercyi*), while it is not in the other rhinolophoids.

56. Anterior opening of the pterygoid canal: distinct and individual (0); confluent with the sphenorbital fissure (1). The megadermatid *Lavia frons* and several pteropodids (e.g., *Dobsonia minor*, *Eidolon helvum*, or *Pteropus vampyrus*) exhibit a small, individualized anterior opening of the pterygoid canal, while the other species have an anterior opening of that canal coalescent with the sphenorbital fissure.

57. Posterior opening of the alisphenoid canal: distinct and individual (0); confluent with the oval foramen (1). The posterior opening of the alisphenoid canal is individualized from the sphenorbital fissure in several hipposiderids (e.g., *Hipposideros armiger*, *Hipposideros galeritus* and *Hipposideros* (*Pseudorhinolophus*) *bouziguensis)*, the rhinolophid *Rhinolophus euryale*, all three megadermatids (*Cardioderma cor*, *Lavia frons*, and *Megaderma spasma*) and several pteropodids (e.g., *Balionycteris maculata*, *Eidolon helvum*, *Eonycteris spelaea*, and *Rousettus aegyptiacus*). When not individualized, I interpret this opening to be coalescent with the oval foramen (see Nomenclature section).

58. Sphenorbital fissure, global elongation: small, roughly as long as wide (0); moderate, longer than wide (1); high, much longer than wide (2). In most pteropodids (such as *Balionycteris maculata*, *Macroglossus minimus*, or *Pteropus pumilus*), megadermatids and some other rhinolophoids (*Hipposideros armiger*, *Macronycteris gigas*, *Xenorhinos halli*, *Rhinolophus hipposideros*), the sphenorbital fissure is not elongated, of similar length and width in ventral view; in pteropodids and megadermatids, this is probably due to a posterior bending of the cranial cavity relative to the rest of the head, the structures exiting the sphenorbital fissure less ventrally than in most rhinolophoids and more anteroventrally to anteriorly (as previously proposed for the oval foramen). In other rhinolophoids and some pteropodids, the sphenorbital fissure can be very much elongated (in rhinolophids except *Rhinolophus hipposideros*, in the rhinonycterid *Cloeotis percivali*, and in the hipposiderids *Asellia tridens*, *Aselliscus tricuspidatus*, *Palaeophyllophora oltina*, and *Palaeophyllophora quercyi*) or in an intermediate case, being a bit elongated but not as the previously cited taxa (in other hipposiderids, such as *Doryrhina cyclops* or *Riversleigha williamsi*, in other rhinonycterids, such as *Triaenops persicus* or *Archerops annectens*, in rhinopomatids, and in other pteropodids, such as *Acerodon jubatus*, or *Pteropus neohibernicus*).

59. Sphenorbital fissure, anterior extension: small, being clearly ventral to the cerebral hemisphere (0); high, close to the anteroposterior level of the circular fissure to the olfactory bulbs (1). Pteropodids and several rhinolophoids (megadermatids, rhinopomatids, the rhinonycterid *Xenorhinos halli*) exhibit a sphenorbital fissure of variable length but in all cases not extending very far anteriorly (to not far at all), while in several species (most hipposiderids such as *Aselliscus tricuspidatus* or *Hipposideros caffer*, the rhinonycterid *Rhinonycteris aurantia*, some rhinolophids such as *Rhinolophus luctus* or *Rhinolophus*

simulator) the sphenorbital fissure extends to the level of the circular fissure, and in other species (the hipposiderid *Asellia tridens*,most rhinonycterids such as *Cloeotis percivali* or *Rhinonycteris tedfordi*, most rhinolophids such as *Rhinolophus landeri* or *Rhinolophus rouxii*) it extends even more anteriorly, ventrally to the olfactory bulbs. I choose to group the two latter conditions in a single character state because the difference between both can simply rely on the individualization of the unknown foramen #1 (i.e., the sphenorbital fissure anteriorly reaching the level of the circular fissure) or on its coalescence with the sphenorbital fissure (i.e., the sphenorbital fissure extending anteriorly ventral to the olfactory bulbs). This is particularly well exemplified by the case of the rhinonycterid *Rhinonycteris tedfordi*, in which one of the two unknown foramina #1 is coalescent with the sphenorbital fissure while the other one is not.

60. Sphenorbital fissure, width of the gap between them (= of the sphenorbital bridge): very thin, sphenorbital fissures almost in contact (0); thin, sphenorbital fissures close but clearly not in contact (1); average, as wide as each fissure (2); wide, as wide as the hypophysis (3). The width of the gap between the sphenorbital fissures, corresponding to the bony sphenorbital bridge on the skull, greatly varies among the yinpterochiropteran species sampled here: in some, this gap is so narrow that it may be difficult to separate the sphenorbital fissures (e.g., the hipposiderid *Asellia tridens* or the rhinonycterid *Rhinonycteris tedfordi*), in others, the fissures can be distinguished easily but their gap is still narrow (e.g., the hipposiderid *Aselliscus tricuspidatus* or the rhinolophid *Rhinolophus pearsoni*), in others the gap is not very wide, being similar to the width of each fissure (e.g., the rhinopomatid *Rhinopoma microphyllum* or the megadermatid *Cardioderma cor*), and in others (pteropodids), the gap is wider than each fissure, similar to the width of the hypophysis. This character is ordered as it discretizes a continuous trend.

61. Oval foramen, shape: circular to ovoid (0); anteroposteriorly elongated (1). The oval foramen in several pteropodid species (e.g., *Pteropus scapulatus* or *Rousettus obliviosus*) appears very elongated, while it is more ovoid to circular in other pteropodids and in all rhinolophoids. Such a shape could indicate a confluence of two foramina, but an elongated oval foramen is retrieved in species where the posterior opening of the alisphenoid canal is individualized. That shape may be linked to the angle of the braincase relative to the rest of the head, the nerve pathway being less ventrally directed (as in species with an ovoid to circular oval foramen) and more anteroventrally to anteriorly directed.

62. Oval foramen, size: small (0); large (1). The oval foramen can be of great size in some species (e.g., the hipposiderid *Coelops frithii*, the rhinonycterid *Triaenops persicus*, or the pteropodid *Megaerops ecaudatus*) or of moderate to small size in others (e.g., the hipposiderid *Doryrhina cyclops*, the rhinolophid *Rhinolophus denti*, or the pteropodid *Macroglossus minimus*).

63. Oval foramen, position: fully comprised in the cerebral hemisphere (0); abuts the posterior wall of the cerebral hemisphere (1). Depending on the taxa, the oval foramen is variously located relative to the posterior wall of the cerebral hemispheres: in pteropodids and several rhinolophoids, it is fully inside the posterior part of the hemisphere without being at its posterior end (e.g., the hipposiderid *Palaeophyllophora quercyi*, the rhinonycterid *Triaenops persicus*, the megadermatid *Cardioderma cor*), while in numerous rhinolophoids it seems to form a part of the posterior border or the posteromedial border of the cerebral hemisphere (e.g., the hipposiderid *Coelops frithii*, the rhinonycterid *Rhinonycteris aurantia*, or the rhinolophid *Rhinolophus landeri*).

64. Unknown foramen #1: present (0); absent or coalescent with the sphenorbital fissure (1). An individualized unknown foramen #1 (see Nomenclature section) is frequently retrieved in various rhinolophoid species (e.g., the hipposiderid *Aselliscus tricuspidatus* or the rhinonycterid *Xenorhinos halli*) while it can be found to be coalescent with the sphenorbital fissure in others (see the case of the

rhinonycterid *Rhinonycteris tedfordi*). It is however impossible, using endocasts, to surely assess if the sphenorbital fissure "contains" an unknown foramen #1 because of its unidentification, thus I cannot establish a character regarding the coalescence of this foramen.

65. Unknown foramen #2: present (0); absent (1). An unknown foramen #2 (see Nomenclature section) is sometimes found in some rhinolophoid species (the hipposiderids *Aselliscus tricuspidatus*, *Hipposideros galeritus*, *Hipposideros jonesi*, and *Hipposideros pomona*, the rhinonycterid *Xenorhinos halli*, the rhinolophid *Rhinolophus blasii*, the megadermatid *Cardioderma cor* and the rhinopomatid *Rhinopoma hardwickii*), but is absent in others and in pteropodids.

66. Unknown foramen #3: present (0); absent (1). An unknown foramen #3 (see Nomenclature section) is present in some rhinolophoids (in the hipposiderid *Coelops frithii*, in the rhinonycterid *Triaenops persicus*, and in all rhinolophids) while it is absent in pteropodids.

67. Anterior carotid foramen: present (0); absent (1). An anterior carotid foramen is retrieved in several rhinolophoids (e.g., the hipposiderid *Hipposideros armiger*, the rhinolophid *Rhinolophus luctus*, or the megadermatid *Lavia frons*) and in some pteropodids (*Casinycteris argynnis*, *Macroglossus minimus*, *Megaloglossus woermanni*, and *Sphaerias blanfordi*).

68. Posterior carotid foramen: present (0); absent (1). A posterior carotid foramen is sometimes retrieved in pteropodids without anterior carotid foramen (e.g., *Dobsonia minor* or *Penthetor lucasi*). In rhinolophoids without anterior carotid foramen, the posterior carotid foramen can also be not decipherable: this implies that either there is an anterior carotid foramen that may be confluent with the oval foramen or that the posterior carotid foramen is confluent with either the pyriform window or the basicochlear fissure but without being decipherable on an endocast.

69. Carotid sulcus: present (0); absent (1). Associated with the anterior carotid foramen is a carotid canal joining the anterior and posterior carotid foramina, but this canal is obviously not visible on an endocast; in pteropodids without anterior carotid foramen, a carotid sulcus is however frequently found anteriorly to the (posterior) carotid foramen (e.g., *Balionycteris maculata* or *Nyctimene major*) but also in some species with an anterior carotid foramen (e.g., the megadermatid *Lavia frons* or the pteropodid *Casinycteris argynnis*). This character is not applicable for taxa with states 1 and 1 to characters 67 and 68.

70. Pyriform window: individualized (0); confluent with other aperture(s) (1). The pyriform window is present in every species, but is variably individualized (e.g., in the hipposiderid *Aselliscus tricuspidatus*, in the megadermatid *Cardioderma cor*, or in the pteropodid *Eonycteris spelaea*) or it can coalesce with the posterior carotid foramen when present (e.g., in the pteropodid *Pteropus scapulatus*) or with the basicochlear fissure (e.g., in the rhinolophid *Rhinolophus luctus*).

71. Basicochlear fissure and jugular foramen: individualized (0); confluent (1). The basicochlear fissure and the jugular foramen are also present in every species sampled here (except *Rhinolophus hipposideros* which seems to lack a basicochlear fissure). Both apertures can be individualized (e.g., in the hipposiderid *Doryrhina cyclops*, in the rhinonycterid *Cloeotis percivali*, or in the pteropodid *Acerodon jubatus*).

72. Posterior carotid foramen: individualized (0); confluent with another aperture (1). The posterior carotid foramen, when present, may either be coalescent with the pyriform window (e.g., in *Acerodon jubatus* or *Eidolon helvum*) or with the basicochlear fissure (e.g., in *Haplonycteris fischeri* or *Pteropus pumilus*). This character is not applicable for taxa with state 1 to characer 68.

73. Pyriform window, size relative to that of the jugular foramen: clearly smaller (0); comparable (1);

clearly higher (2). The pyriform window, always present in my sample, is however greatly varying in size: it can either be clearly small and quite smaller than the jugular foramen (e.g., in the hipposiderid *Coelops frithii* or in the pteropodid *Acerodon jubatus*), of grossly similar size (e.g., in the hipposiderid *Hipposideros caffer*, in the rhinolophid *Rhinolophus blasii*, or in the pteropodid *Dobsonia minor*), or clearly bigger (e.g., in the rhinolophid *Rhinolophus luctus*, in the rhinopomatid *Rhinopoma hardwickii*, or in the pteropodid *Casinycteris argynnis*). This character is ordered.

II.4) Body mass estimates of fossil taxa

Body mass data have been estimated for extinct taxa only. Gunnell et al. (2009) reviewed several methods to estimate chiropteran body mass, using either tooth areas (lower fourth premolar, lower first molar, upper first molar) or postcranial dimensions (humerus length and midshaft diameter). They recommended to use midshaft humerus diameter, as "tooth area in chiropterans is less highly correlated with body mass than in other small mammals" (Gunnell et al. 2009: 273). Giannini et al. (2012) further confirmed the high quality signal from the midshaft humerus diameter, but Maitre (2014) instead used dental equations derived from Legendre (1989) regarding Quercy fossil bats.

Here, I chose to also use dental equations instead of humeral ones, because teeth are more likely to be associated with confidence with skulls than humeri. Maitre (2014) chose the area of the first lower molar and used the equation of Legendre (1989) where log(BOM)=1.096*log(M/1)+0.770, with BOM being the body mass in grams and M/1 the product of the greatest length and width of the first lower molar in millimeters. In their comparisons, Gunnell et al. (2009) however found that the fit of the equation using the first lower molar was lower than those using either the fourth lower premolar or the first upper molar. Here, I decided to apply the four equations (that of Legendre [1989] used by Maitre [2014], and the three of Gunnell et al. [2009]) at the species level, using arithmetic means of dental measurements, in order to have body mass estimates.

I will only use the body mass as a predictor for the brain mass; for that reason, I will instead use the log (natural logarithm) body mass and average (with a geometric mean) the log body masses obtained through the four previously cited equations. It is recommended, in body mass estimations, to average the body masses obtained from log body mass equations using a geometric mean instead of an arithmetic mean (e.g., Smith 1993). Yet, averaging body masses with a geometric mean is strictly equal to average log body masses with an arithmetic mean; my initial rationale also satisfies this recommendation.

Maitre (2014) provided average dental measurements for each fossil Quercy bat species at the locality-level that allows me to obtain the body masses of three of the eight fossil species I document (*Palaeophyllophora quercyi*, *Palaeophyllophora oltina*, and *Hipposideros* (*Pseudorhinolophus*) *schlosseri*). My goal is to obtain mean log body masses at the species-level, as I consider the earliest occurrences without knowing the exact provenance for two of my three Quercy specimens. Therefore, I averaged log body masses at the species level, detailed at the level of locality-level and at the MP standard level-level for each species. I first kept that degree of precision to estimate the log body masses of each species of each MP standard level in each locality, then I averaged them at the MP level, and then I averaged the average log body mass for all MP standard levels for each species.

The dental measurements of both the upper and lower toothrows of *Hipposideros* (*Pseudorhinolophus*) *bouziguensis* have been provided by Sigé (1968). Especially, he also provides averages of each measurement, which I directly used for the four equations. However, regarding the two equations based on the dimensions of the first lower molar, only the widths of the trigonid and of the

talonid are provided, none of them equaling the general width of that tooth. These three dimensions are provided for Quercy bats by Maitre (2014); assuming two similar proportionalities between the width of that tooth and the width of both the widths of the trigonid and of the talonid across bats, I calculated the general width of that tooth. This way assumes a risked and unfounded hypothesis, but is the only way to allow me to calculate the log body masses using the two associated equations.

I also used this method regarding the Riversleigh species of my sample, the hipposiderid *Riversleigha williamsi* (described and measured by Hand 1998a), and the rhinonycterids *Rhinonicteris tedfordi* (Hand 1997), *Xenorhinos halli* (Hand 1998b), and *Archerops annectens* (Hand & Kirsch 2003). For the latter, no teeth measurements are provided, and its log body mass only relies on the measurements of the first upper molar I have been able to take on the illustrated skull in the dedicated article. In a similar way, regarding *Rhinonicteris tedfordi*, no lower teeth have been measured and only the dimensions of its first upper molar are provided; its log body mass only relies on the dimensions of that tooth.

For all fossil species, the body masses are provided in the Table III-2. I voluntarily let a high number of significant figures, in order to retrieve an as accurate as possible value of the log body mass for each species, which are the "real" data I am interested in.

Family	Binom	Body mass estimate (g) according to the reference and the proxy of the formula				Geometric mean of the body mass estimates (g)
		Maitre (2014)	Gunnell et al. (2009)			
		M/1	P/4	M/1	M1/	
Hipposideridae	*Hipposideros (Pseudorhinolophus) bouziguensis*	21,9617268	25,9080425	25,2629639	24,34614352	24,32225801
Rhinonycteridae	*Rhinonicteris tedfordi*	NA	NA	NA	8,925653506	8,925653506
Rhinonycteridae	*Xenorhinos halli*	11,90194138	16,63363188	14,08375716	13,01479515	13,80194173
Hipposideridae	*Riversleigha williamsi*	18,87194786	23,26569727	21,8612348	20,16493092	20,97495593
Rhinonycteridae	*Archerops annectens*	NA	NA	NA	7,529831477	7,529831477

Table III-2: Body mass estimates calculation for the corresponding fossil species with the references and the proxies used.

II.5) Statistical treatment

The scripts used for the statistical treatment of this part are provided in the Appendixes III-1.

In both the qualitative and quantitative data treatment, I consider as “deep nodes” to investigate the sampled families (Hipposideridae, Rhinonycteridae, Rhinolophidae, Rhinopomatidae, Megadermatidae, and Pteropodidae) and the suprafamilial clades that have a biological and/or vernacular sense (Rhinolophoidea, but also “true” and “other” Rhinolophoidea). The reconstructed general trends, on their side, account for the whole Yinpterochiroptera suborder evolution.

As explained above in the Phylogenetical framework section, four phylogenies have been considered depending on the position of the genus *Palaeophyllophora* relative to the other hipposiderid taxa. According to the outputs of the dateFBD software used to calibrate the topologies, the branch lengths and the node ages change very little depending on *Palaeophyllophora* positions. A supplementary part of the qualitative statistical treatment regards the impact of the variation between phylogenies on the characters, on the taxa, and on the whole tree description. In this part, I first look at both the number and the location of morphological changes. This gives information about the impact caused by the varying position of *Palaeophyllophora*, especially regarding the variation of ancestral character estimates at nodes and regarding the location of nodal morphological changes. I also use the number of morphological changes (minimal, maximal, and observed) and I calculate the RI and the CI for each tree. Comparing these indexes is equivalent to comparing the number of changes for each phylogeny, and it further allows for discussing the phylogenetic uncertainty implied by the genus *Palaeophyllophora*.

Regarding the statistical treatment of the quantitative variables, it has to be noted that most of the literature use samples of extant species only, whereas I also use fossil to better calibrate the evolution of these variables. A supplementary aspect in that section therefore aims to compare the reconstructions of evolution of these variables for samples with fossils vs without fossils. All the statistical procedure is thus applied to both cases. The difference in the treatment is that, in the “without fossils sample”, the fossil species are removed from the datasets and pruned from the phylogenetic tree, and only the extant species remain. However, I do not use a single phylogeny, but four: the topology (i.e., the phylogenetic relationships) are the same in all cases, but the branch lengths and nodes ages are not similar, which could be regarded as four hypotheses of time-calibration of nodes using fossils of uncertain position. In order to contrast differently the with vs without fossil reconstructions, I graphically compare the results of the `search.shift` and `search.trend` functions (ancestral reconstructions, shifts in evolutionary rates, and evolutionary trends through time) using x-y plots. First, I output the ancestral reconstructions for all nodes with vs without fossils, highlighting the “deep nodes”. Second, in the case of shifts, I output both all rate differences and their p-values, which allows seeing if the rate differences vary and if their significance vary. Third, in the case of trends, I output the slopes and emmeans differences and their respective p-values for both the trait and trait rates trends through time, assessing the changes the inclusion of fossils imply on the various evolutionary trends.

III) Morphological evolution

III.1) Results

III.1.A) Phylogenies

III.1.A.a) Consistency and Retention Indexes

Four alternative phylogenies are used here to map the morphological characters, and they induce few but noteworthy changes. These regard the ancestral character estimates of the phylogeny nodes, which lead to changes in the number of morphological changes along edges and in the values of the Retention and Consistency Indexes (RI and CI). There are not enough variation to drastically change the values for these two metrics at the tree scale: the general RI is of 0.58 (0.581 to 0.583) and the general CI is of 0.13 (0.129 to 0.130) (Appendix III-2, Table 1).

III.1.A.b) Ancestral reconstructed states of characters (a.k.a. “aces”)

Six out of the 73 characters show varying aces (Appendix III-4): depending if *Palaeophyllophora* is sister-genus to *Hipposideros* or not, the cervical flexure is estimated to be over 210° (character 2, state 1) or under 210° and the cast of the transverse sinus is estimated as being fully complete (character 53, state 0) or partial (state 1) at the rhinolophoids and the “other” rhinolophoids nodes, the shape of piriform lobes is estimated as being wide and blunt (character 12, state 1) or thin and sharp (state 0) at the root, the anterior carotid foramen is either absent (character 67, state 1) or present (state 0) and the pyriform window is estimated as being clearly larger than the jugular foramen (character 73, state 2) or of comparable size (state 1) at the (*Hipposideros pomona* + *Hipposideros caffer*) + *Hipposideros galeritus* node; depending on if *Palaeophyllophora* diverges the earliest in hipposiderids or not, the vermis is estimated as being of low, as a thin layer (character 28, state 0), or of average thickness (state 1) at the “true” rhinolophoids node, and the anterior carotid foramen is either present (character 67, state 0) or absent (state 1) at the *Hipposideros pomona* + *Hipposideros caffer* node; depending on if *Palaeophyllophora* diverges later than both *Asellia* and *Macronycteris*+*Doryrhina* or not (i.e., between them or the earliest), the vermis is reconstructed as being either thin (character 28, state 0) or of average thickness (state 1) at the hipposiderids+rhinonycterids node.

III.1.A.c) Morphological changes

Indeed, the same six characters show varying position (and, sometimes, number) of morphological changes (Appendix III-5). Character 2 (cervical flexure) varies at the rhinolophoid and “other” rhinolophoid nodes, implying a change at the “true” rhinolophoid node (which is of reconstructed state 0, while that of rhinolophoids is of state 1 if *Palaeophyllophora* diverges late) and either at the megadermatid or rhinopomatid node (both being of different reconstructed ancestral states; the change is on the megadermatid branch if *Palaeophyllophora* diverges late, or on the rhinopomatid branch otherwise). Character 12 (shape of the piriform lobes) varies at the root (see previously), which implies either a change at the rhinolophoid node (apicalmost position of *Palaeophyllophora*) or at the pteropodid node (other cases). Character 28 (thickness of the vermis in lateral view) either changes at the hipposiderid node (*Palaeophyllophora* more closely related to *Hipposideros* than the *Macronycteris*+*Doryrhina* clade), the hipposiderid+rhinonycterid node (*Palaeophyllophora* more apical than *Asellia* but more basal than the *Macronycteris*+*Doryrhina* clade), or the “true” rhinolophoid node, implying a supplemental change at the rhinolophid node (if *Palaeophyllophora* is more basal than *Asellia*). Character 53 (completeness of the transverse sinus cast) either changes in a convergent manner at the “true” rhinolophoid and rhinopomatid nodes (*Palaeophyllophora* sister-genus to *Hipposideros*) or it

changes at the rhinolophoid node and reverses at the megadermatid node (other cases). Character 67 (presence/absence of anterior carotid foramen) either changes at the (*Hipposideros pomona* + *Hipposideros caffer*) + *Hipposideros galeritus* node then reverses for *Hipposideros galeritus* (*Palaeophyllophora* as the sister-genus of *Hipposideros*), or it changes only at the *Hipposideros pomona* + *Hipposideros caffer* node (*Palaeophyllophora* being neither the most apical nor the most basal hipposiderid genus), or it changes in a convergent manner in *Hipposideros pomona* and *Hipposideros caffer* (*Palaeophyllophora* being the most basal hipposiderid genus). Finally, character 73 (size of the pyriform window relative to that of the jugular foramen) either changes at the *Hipposideros pomona* + *Hipposideros caffer* node (if *Palaeophyllophora* is the sister-genus of *Hipposideros*) or at the (*Hipposideros pomona* + *Hipposideros caffer*) + *Hipposideros galeritus* node and then reverses for *Hipposideros galeritus* (other cases).

One tip and two nodes do not vary in their overall number of morphological changes, but they do in which character changes depending on the phylogeny (Appendix III-5). While it keeps the same number of morphological changes, there is either a change of character 12 (apicalmost position of *Palaeophyllophora*) or of character 53 (other cases) at the rhinolophoid node. As well, for the (*Hipposideros caffer* + *Hipposideros pomona*) + *Hipposideros galeritus* node and *Hipposideros galeritus*, there is either of change of character 67 (apicalmost position of *Palaeophyllophora*) or of character 73 (other cases). There is a supplemental change at the "true" rhinolophoid node, either of character 53 (apicalmost position of *Palaeophyllophora*) or of character 28 (basalmost position of *Palaeophyllophora*).

Of these six characters that vary in their aces and in the distribution of their changes, three (characters 28, 67, and 73) vary in their number of morphological changes depending on the phylogeny, which leads to changes in the values of the RI and CI.

III.1.B) Characters and morphological complexes

III.1.B.a) Distribution and support to the phylogenies

The RI and CI for each character (Appendix III-2, Table 1) show quite different, opposed distributions (Fig. III-9). The RI distribution looks like an exponential, with few characters with RI < -0.2, and more than the half of the characters with RI > 0.5. On the opposite, CI looks like a negative exponential distribution, with very few characters with CI > 0.5 and most of the characters with CI < 0.2. Few characters have both high RI and CI, and most of the high RI characters have low CI. The distribution of RI for each morphological complex (Appendix III-2, Table 1; Fig. III-10) shows little (i.e., not significant; p-value around 0.35, Appendix III-2, Table 3) discrepancies across morphological complexes, even though the (single character of the) 'Pons-Medulla Oblongata Continuum' complex has a high RI, and the 'Mesencephalon', the 'Neopallial foldings', and the 'Cranial openings' complexes show a high variability of the RI of their characters. The distribution of CI for each morphological complex (Appendix III-2, Table 1; Fig III-11) significantly differs among morphological complexes (p-value near 0.02, Appendix III-2, Table 3), but no pairwise association has been retrieved as being significant (all p-values > 0.2 Appendix III-2, Table 4); the boxplots show a quite high variation for the 'Vascular structure casts' complex, while it is more moderate for other morphological complexes, and the previous three morphological complexes with apparently highly variable RI (i.e., 'Mesencephalon', 'Neopallial foldings', and 'Cranial openings') have a less variable and generally low CI.

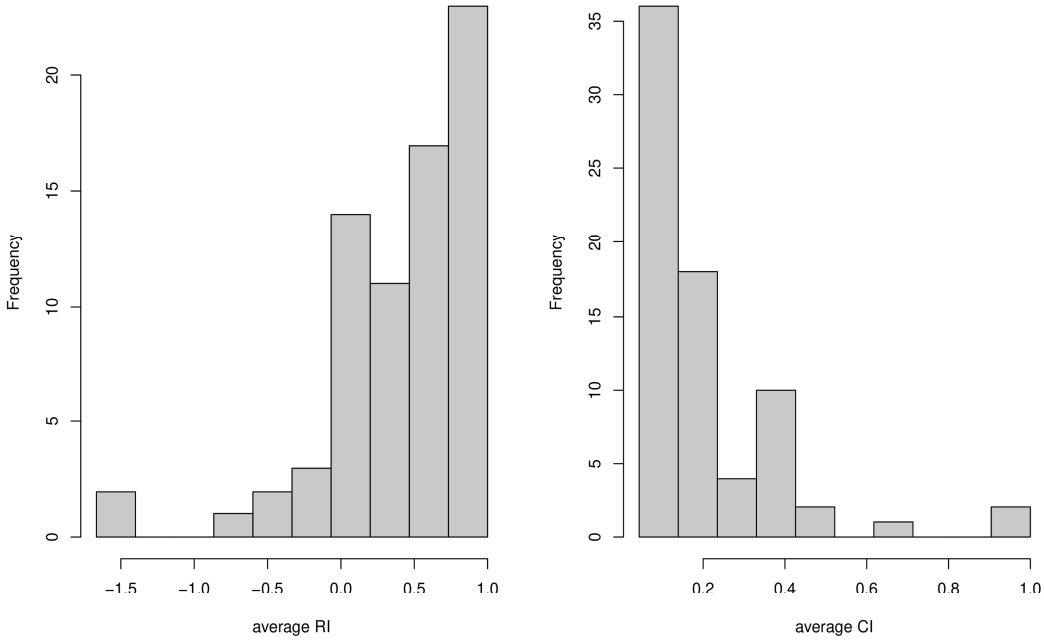

Figure III-9: Distribution of the RI (retention index) and CI (consistency index) of character averaged over all phylogenies.

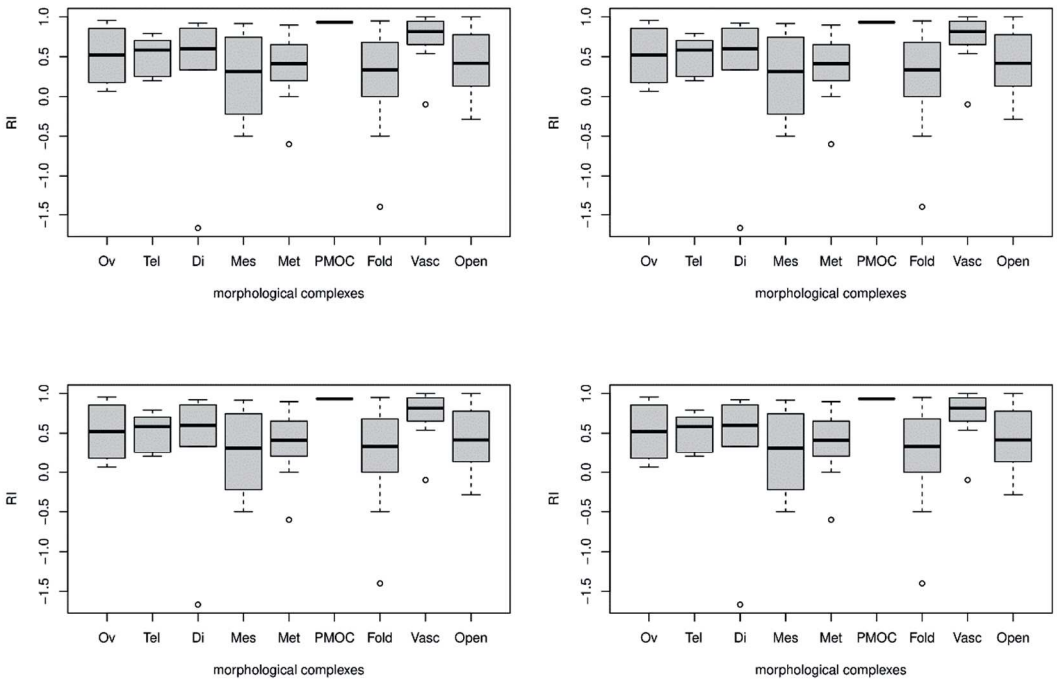

Figure III-10: Distribution of the RI (retention index) for each "global region" of the endocranial cast and for each phylogeny (*Palaeophyllophora* in most apical to most basal position going from left to right and from top to bottom). Abbreviations: Ov-Overall shape; Tel-Telencephalon; Di-Diencephalon; Mes-Mesencephalon; Met-Metencephalon; PMOC-Pons-Medulla Oblongata Continuum; Fold-Neopallial foldings; Vasc-Vascular structure casts; Open-Cranial openings.

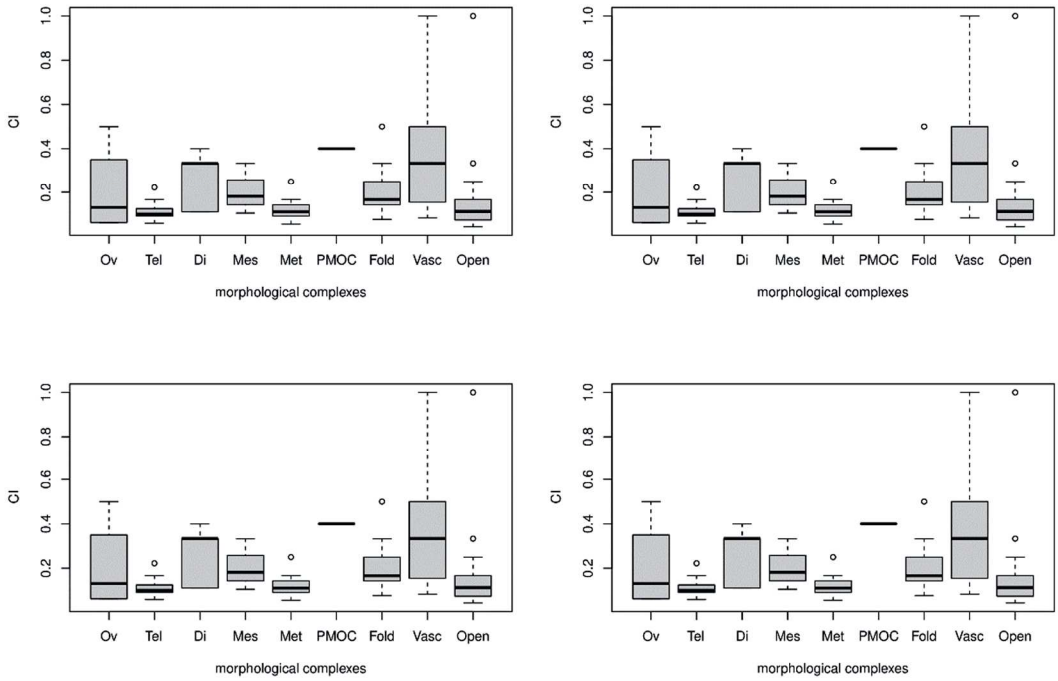

Figure III-11: Distribution of the CI (consistency index) for each "global region" of the endocranial cast and for each phylogeny (*Palaeophyllophora* in most apical to most basal position going from left to right and from top to bottom). Abbreviations: Ov-Overall shape; Tel-Telencephalon; Di-Diencephalon; Mes-Mesencephalon; Met-Metencephalon; PMOC-Pons-Medulla Oblongata Continuum; Fold-Neopallial foldings; Vasc-Vascular structure casts; Open-Cranial openings.

Across characters, if there is a consequent range in the number of changes at nodes (zero to 11), there is an even greater range in the number of changes at tips (zero to 17). Whereas a correlation is significant between these number of changes using Kendall's correlation test (p-values around 1.10^{-5}, Appendix III-2, Table 3), a pattern is still difficult to retrieve in the distribution of both these variables (Fig. III-12): characters with increasing changes at nodes seem to have increasing changes at tips and/or increasing variability in the number of changes at tips. This correlation between number of changes at nodes and at tips disappears by considering morphological complexes (p-values around 0.48, Appendix III-2, Table 3), and no graphical correlation can be described (Fig. III-13). There however is a significant heterogeneity between morphological complexes regarding the number of changes at nodes and tips (Fig. III-14; p-values between 7.10^{-4} and 8.10^{-4}, Appendix III-2, Table 3), nodes (Fig. III-15; p-values between 4.10^{-3} and 5.10^{-3}, Appendix III-2, Table 3), and tips (Fig. III-16; p-values around 0.02, Appendix III-2, Table 3), with significant differences between the 'Telencephalon' complex and both the 'Neopallial foldings' and the 'Vascular structure casts' complexes (p-values close to 0.04, Appendix III-2, Table 4) for both node and tip changes, between the 'Neopallial foldings' complex and both the 'Telencephalon' and the 'Mesencephalon' complexes (p-values close to 0.02, Appendix III-2, Table 4) for node changes, and none for tip changes (Appendix III-2, Table 4). There indeed is some variation between morphological complexes (Figs. III-14-16), with generally few changes for the 'Overall shape of the endocranial cast', 'Diencephalon', 'Pons-Medulla Oblongata Continuum', 'Neopallial foldings', and 'Vascular structure casts' complexes, and strikingly numerous changes for the 'Mesencephalon' complex regarding node changes and the 'Telencephalon', 'Metencephalon', and 'Cranial openings' complexes regarding tip changes (even though the latter trend is not confirmed by post-hoc pairwise tests).

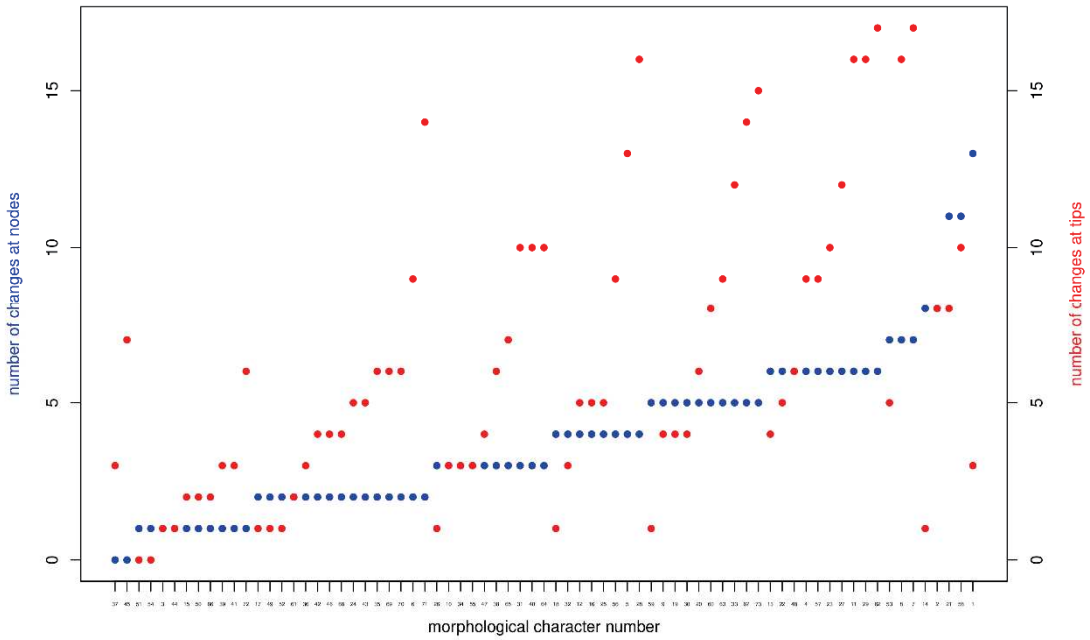

Figure III-12: Number of morphological changes at nodes and at tips for each morphological character. Characters are ordinated from lowest to highest number of changes at nodes to show if there is a link between the two variables. This stands for the phylogeny with *Palaeophyllophora* as sister-genus to *Hipposideros*. Other cases are figured in the Appendix III-6-1.

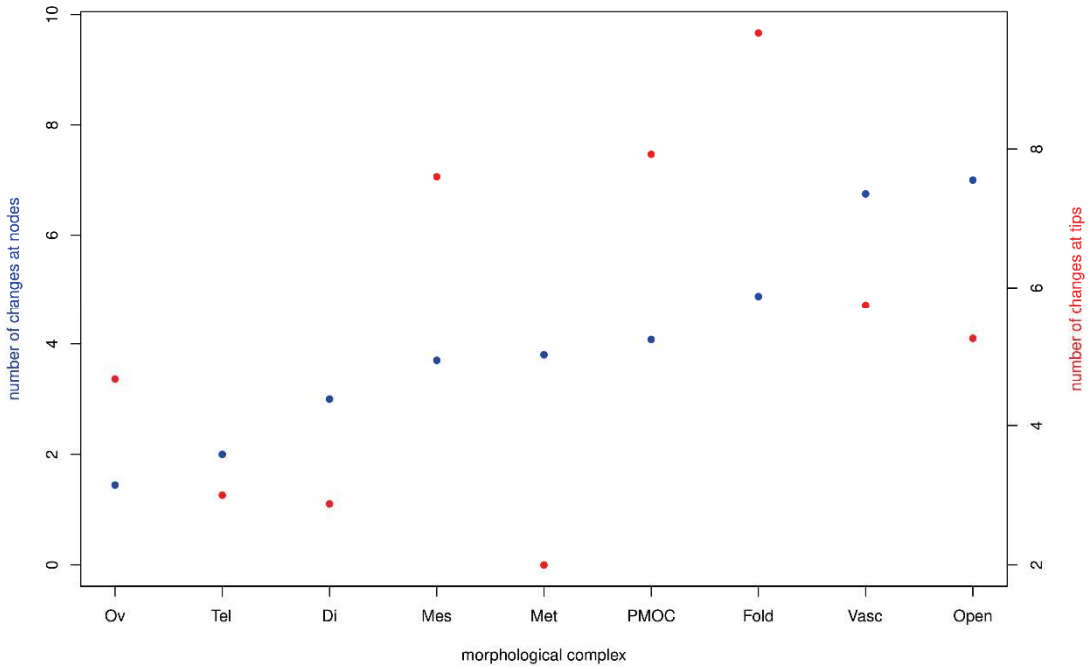

Figure III-13: Number of morphological changes at nodes and at tips for each "global region" of the endocast, averaging the number for all characters of each complex. Groups are ordinated from lowest to highest number of changes at nodes to show if there is a link between the two variables. Abbreviations: Ov-Overall shape; Tel-Telencephalon; Di-Diencephalon; Mes-Mesencephalon; Met-Metencephalon; PMOC-Pons-Medulla Oblongata Continuum; Fold-Neopallial foldings; Vasc-Vascular structure casts; Open-Cranial openings. This stands for the phylogeny with *Palaeophyllophora* as sister-genus to *Hipposideros*. Other cases are figured in the Appendix III-6-2.

There are overall mixed patterns of distribution, with highly varying number of changes that impact the RI and CI values for each character but also for the morphological complexes of characters. Some distribution patterns can however be proposed, only relying on these data and on the character states mapping (Appendix III-7): some characters have little changes and support deep divergences (e.g., character 51), others show a high and general phylogenetic signal, with a high RI, some node changes across, but also some tips changes that quickly lower their CI (e.g., character 19), others show a more restricted phylogenetic signal, with a high RI (>0.5), but with also potential reversions in the supported complex and some in other morphological complexes (e.g., character 47), and others show no phylogenetic signal and seem highly convergent (low RI and CI; e.g., character 71). Such patterns are not exactly determined because each character has is distribution pattern, and metrics like RI, CI, or number of changes only give help to one who wants to describe each character. Such a description will not be done here as it would be tedious; states mappings are provided for each character (Appendix III-8), and only the most noticeable will be further discussed (some of these having been described previously).

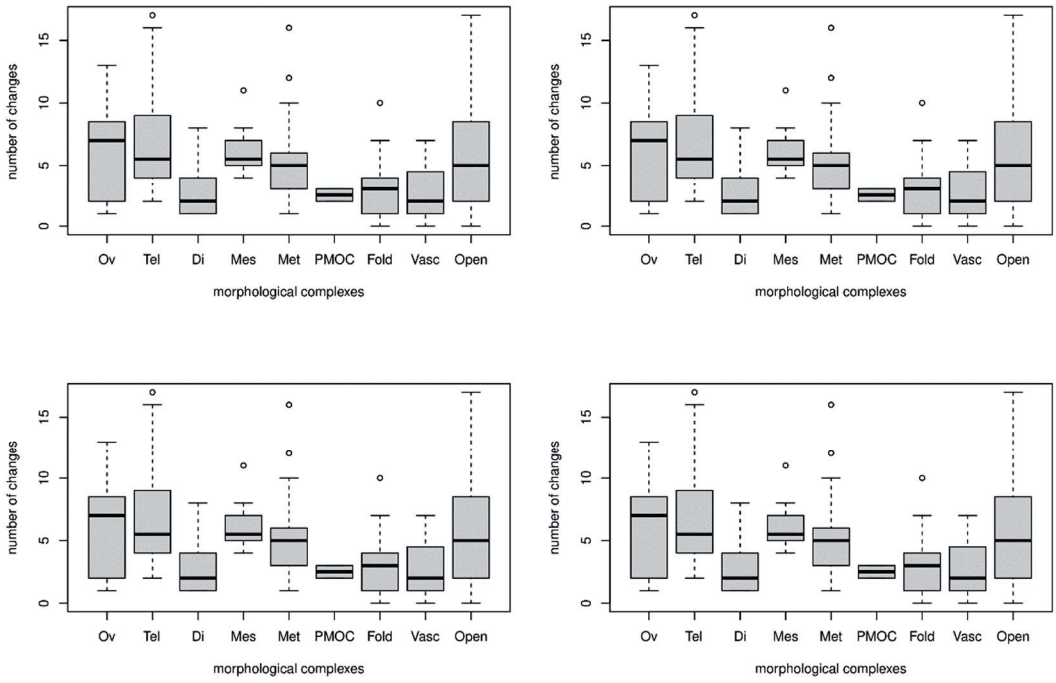

Figure III-14: Distribution of the number of morphological changes for each "global region" of the endocranial cast and for each phylogeny (*Palaeophyllophora* in most apical to most basal position going from left to right and from top to bottom). Abbreviations: Ov-Overall shape; Tel-Telencephalon; Di-Diencephalon; Mes-Mesencephalon; Met-Metencephalon; PMOC-Pons-Medulla Oblongata Continuum; Fold-Neopallial foldings; Vasc-Vascular structure casts; Open-Cranial openings.

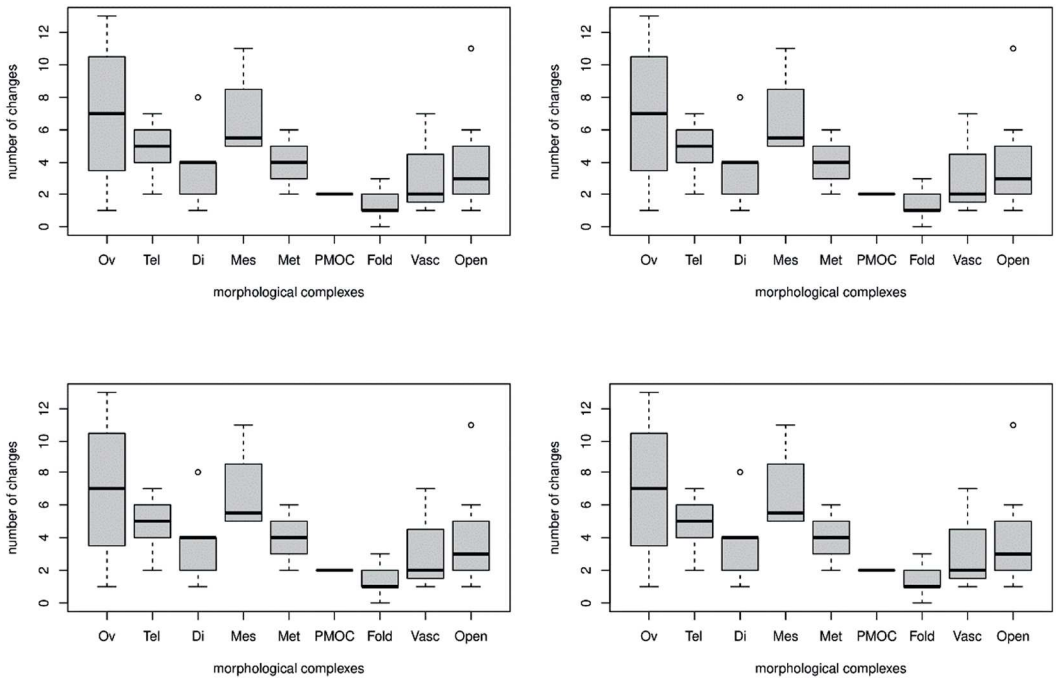

Figure III-15: Distribution of the number of morphological changes at nodes only for each "global region" of the endocranial cast and for each phylogeny (*Palaeophyllophora* in most apical to most basal position going from left to right and from top to bottom). Abbreviations: Ov-Overall shape; Tel-Telencephalon; Di-Diencephalon; Mes-Mesencephalon; Met-Metencephalon; PMOC-Pons-Medulla Oblongata Continuum; Fold-Neopallial foldings; Vasc-Vascular structure casts; Open-Cranial openings.

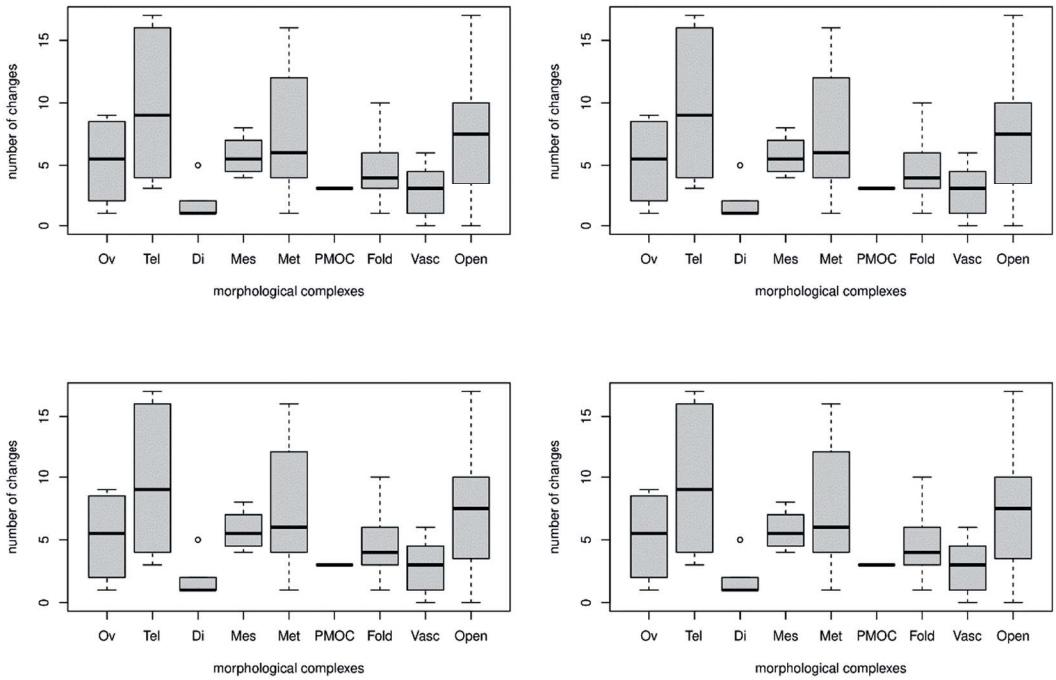

Figure III-16: Distribution of the number of morphological changes at tips only for each "global region" of the endocranial cast and for each phylogeny (*Palaeophyllophora* in most apical to most basal position going from left to right and from top to bottom). Abbreviations: Ov-Overall shape; Tel-Telencephalon; Di-Diencephalon; Mes-Mesencephalon; Met-Metencephalon; PMOC-Pons-Medulla Oblongata Continuum; Fold-Neopallial foldings; Vasc-Vascular structure casts; Open-Cranial openings.

III.1.B.b) Evolution and rates of evolution

Most of the characters (47 with character 24 if *Palaeophyllophora* is the sister-genus to *Hipposideros*, 46 without it otherwise) show a significant slope of their phenotypic evolution (Appendix III-2, Table 1), but only 30 to 34 characters (without characters 19, 20, 35, and 57 if *Palaeophyllophora* is the sister-genus to *Hipposideros*, without character 64 if *Palaeophyllophora* diverges first, and without character 36 if *Palaeophyllophora* diverges before the *Macronycteris* + *Doryrhina* clade) show a significant slope of their rate of evolution (with two times more negative slopes than positive ones, 20 to 22 vs 10 to 12; Appendix III-2, Table 1). Of all these characters, 18 to 19 (with character 24 and without characters 19 and 57 if *Palaeophyllophora* is the sister-genus to *Hipposideros*, and without character 36 if *Palaeophyllophora* diverges earlier than the *Macronycteris* + *Doryrhina* clade) show both significant phenotypic and rate evolution slopes (with a bit more characters with a negative rate slope, 10 to 11 vs 7 to 8; Appendix III-2, Table 1).

Phenotypic evolution slopes (Fig. III-17) are not normally distributed according to Shapiro-Wilk tests (p-values between 0.01 and 0.02, Appendix III-2, Table 3) while those of rate evolution are (Fig. III-18; p-values between 0.5 and 0.6, Appendix III-2, Table 3). I still use non-parametric tests to further explore these evolution slopes, because the normal distribution is not expected while working with morphological characters (which may covariate between them at varying and unpredictable degrees); the mappings and estimations of evolution of each character have been separately done, there are no reasons to expect a normal trend to null evolution rates by considering all characters.

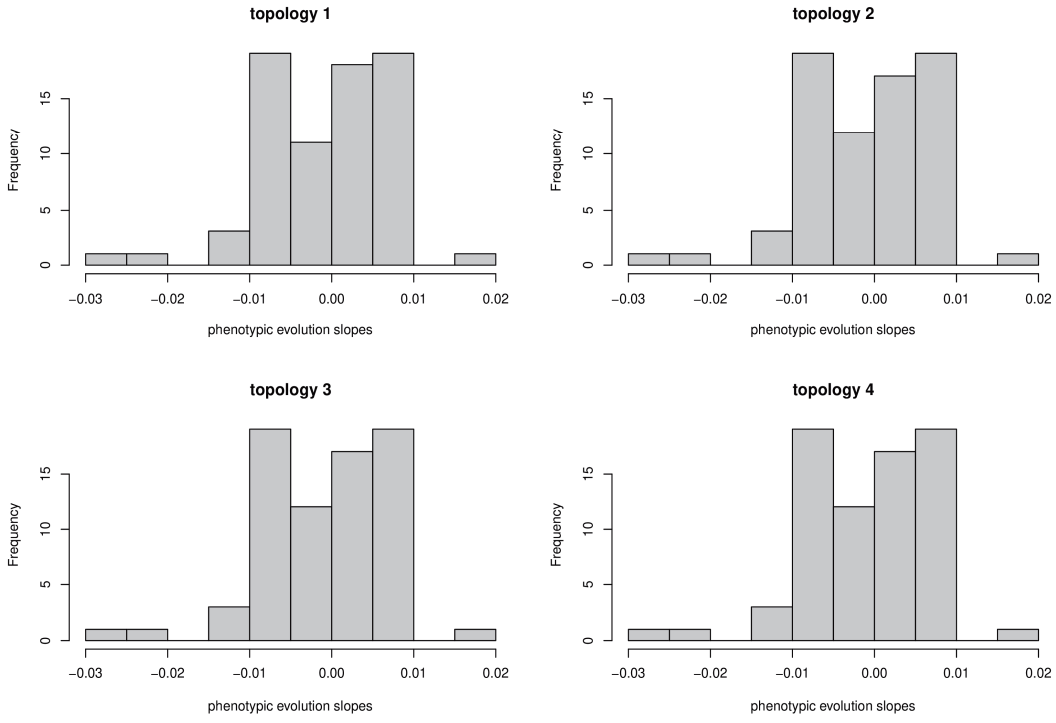

Figure III-17: Distribution of the slope of the temporal trend of each character (i.e., “phenotypic” or “trait” slope) and for each phylogeny. Number of topology indicates an increasingly basal position of *Palaeophyllophora* (i.e., 1-sister-genus to *Hipposideros*, 4-sister-taxon to all other hipposiderids).

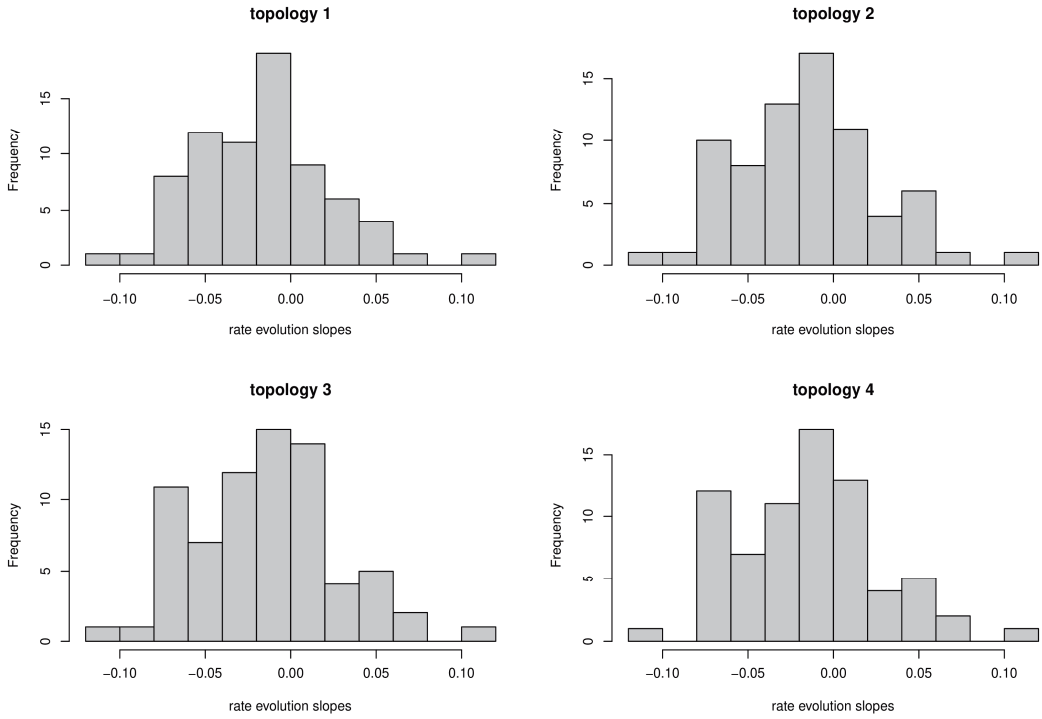

Figure III-18: Distribution of the slope of the temporal trend of the evolutionary rates of each character (i.e., "rate" slope) and for each phylogeny. Number of topology indicates an increasingly basal position of *Palaeophyllophora* (i.e., 1-sister-genus to *Hipposideros*, 4-sister-taxon to all other hipposiderids).

There is no obvious correlation between phenotypic and rate evolution slopes (Fig. III-19; p-values between 0.8 and 0.9, Appendix III-2, Table 3). There is no heterogeneity in phenotypic (Fig. III-20; p-values around 0.1, Appendix III-2, Table 3) and in rate (Fig. III-21; p-values between 0.15 and 0.25, Appendix III-2, Table 3) evolution slopes between morphological complexes, and no morphological complex subset of either the phenotypic or rate evolution slope significantly differs from 0 (p-values between 0.2 and 1; Appendix III-2, Table 3).

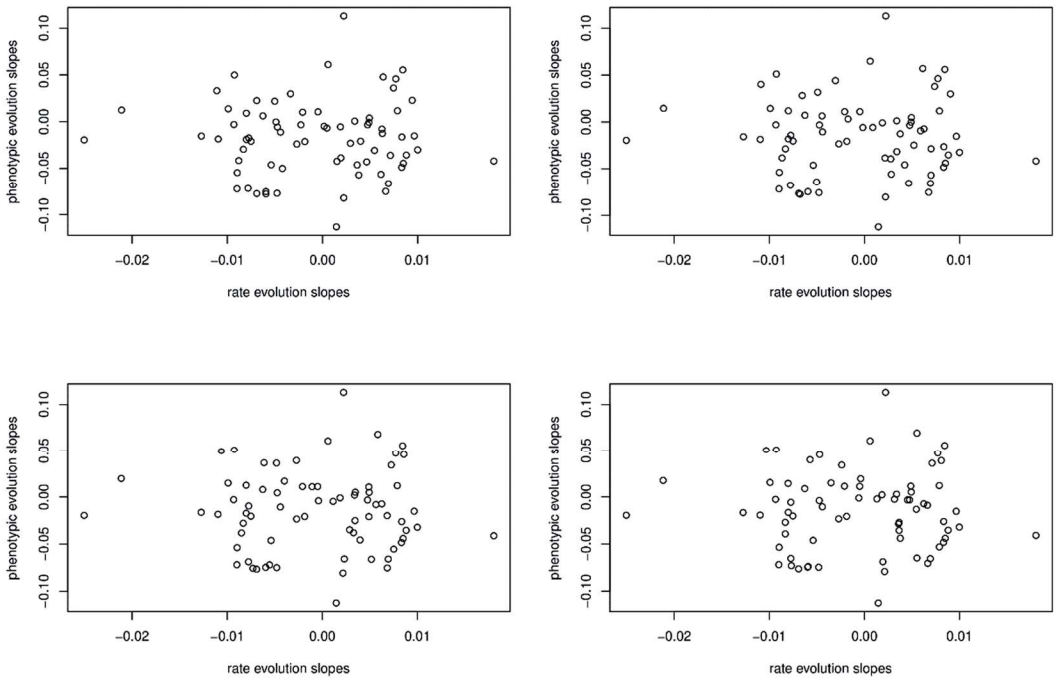

Figure III-19: Biplot of the slope of the temporal trend of both the actual value and the evolutionary rates of each character for each phylogeny (*Palaeophyllophora* in most apical to most basal position going from left to right and from top to bottom).

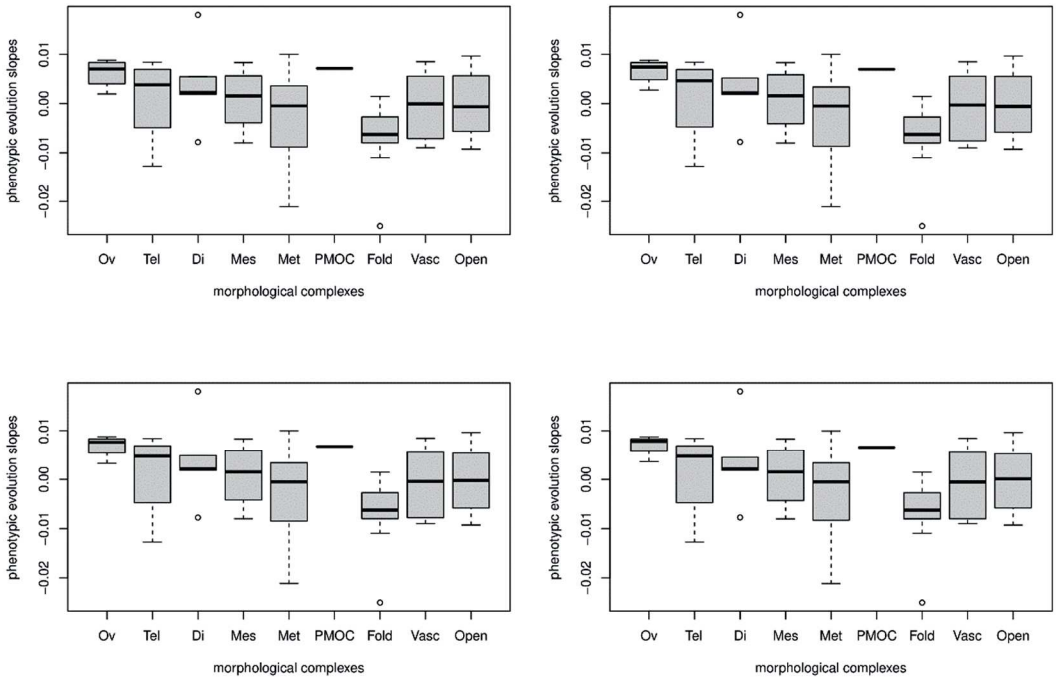

Figure III-20: Distribution of the slope of the temporal trend of the characters (i.e., “phenotypic” or “trait” slope) in each “global region” of the endocranial cast and for each phylogeny (*Palaeophyllophora* in most apical to most basal position going from left to right and from top to bottom). Abbreviations: Ov-Overall shape; Tel-Telencephalon; Di-Diencephalon; Mes-Mesencephalon; Met-Metencephalon; PMOC-Pons-Medulla Oblongata Continuum; Fold-Neopallial foldings; Vasc-Vascular structure casts; Open-Cranial openings.

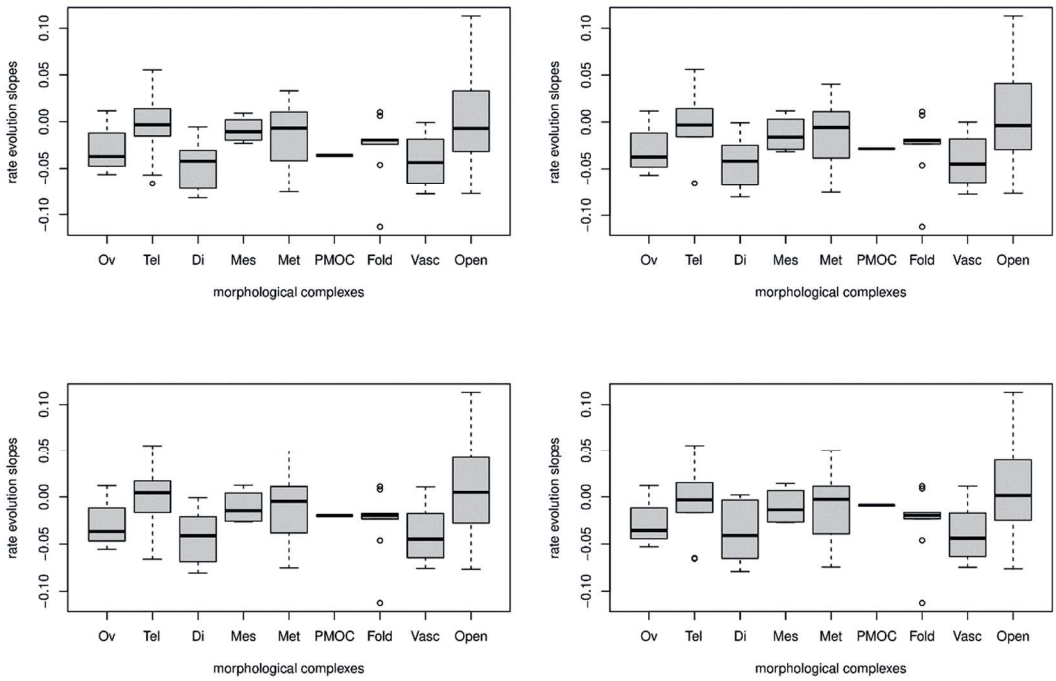

Figure III-21: Distribution of the slope of the temporal trend of the evolutionary rates of the characters (i.e., "rate" slope) in each "global region" of the endocranial cast and for each phylogeny (*Palaeophyllophora* in most apical to most basal position going from left to right and from top to bottom). Abbreviations: Ov-Overall shape; Tel-Telencephalon; Di-Diencephalon; Mes-Mesencephalon; Met-Metencephalon; PMOC-Pons-Medulla Oblongata Continuum; Fold-Neopallial foldings; Vasc-Vascular structure casts; Open-Cranial openings.

III.1.B.c) Covariation with size

A covariation of the states of a given character with the (ranked) size of the coded taxa may indicate a potential allometric cause for the morphological variation of that character. Here, I plotted the states of every character against the ranks of the brain mass of the corresponding taxa (Fig. III-22), tested the correlation between each using Kendall's tau and Pearson's rho and estimated the proportion of variance explained by this relationship R^2 (Appendix III-2, Table 3), and indicated how strong is the link using these three statistics (Appendix III-2, Table 1).

Fifteen of the 73 characters (5, 13-15, 20, 22, 27-28, 30-31, 33, 62, 67, 71-72) are very unlikely to be correlated with brain mass, and 11 (4, 36, 38, 44, 46, 50-52, 54-55, 60) are very likely to be correlated with it. Between these two extreme cases, of the remaining 47 characters, 35 show a very significant (i.e., inferior to 0.01) p-value for the Kendall and Pearson correlation tests with average to low R^2 value (from 10% to 50% of explained variance), 11 show a significant (i.e., less than 0.05) p-value for both tests (most of them still having a low part of explained variance, under 10%), and one shows nearly significant (i.e., less than 0.1) p-values (Appendix III-2, Table 1).

Overall, characters with strong correlation appear to also have a high RI and the reverse. The strong correlation between the (absolute) correlation coefficients (Kendall's tau and Pearson's rho) of each character and the RI (p-values near to 1.10^{-8} for tau and 5.10^{-9} for rho, Appendix III-2, Table 3) is congruent with this trend.

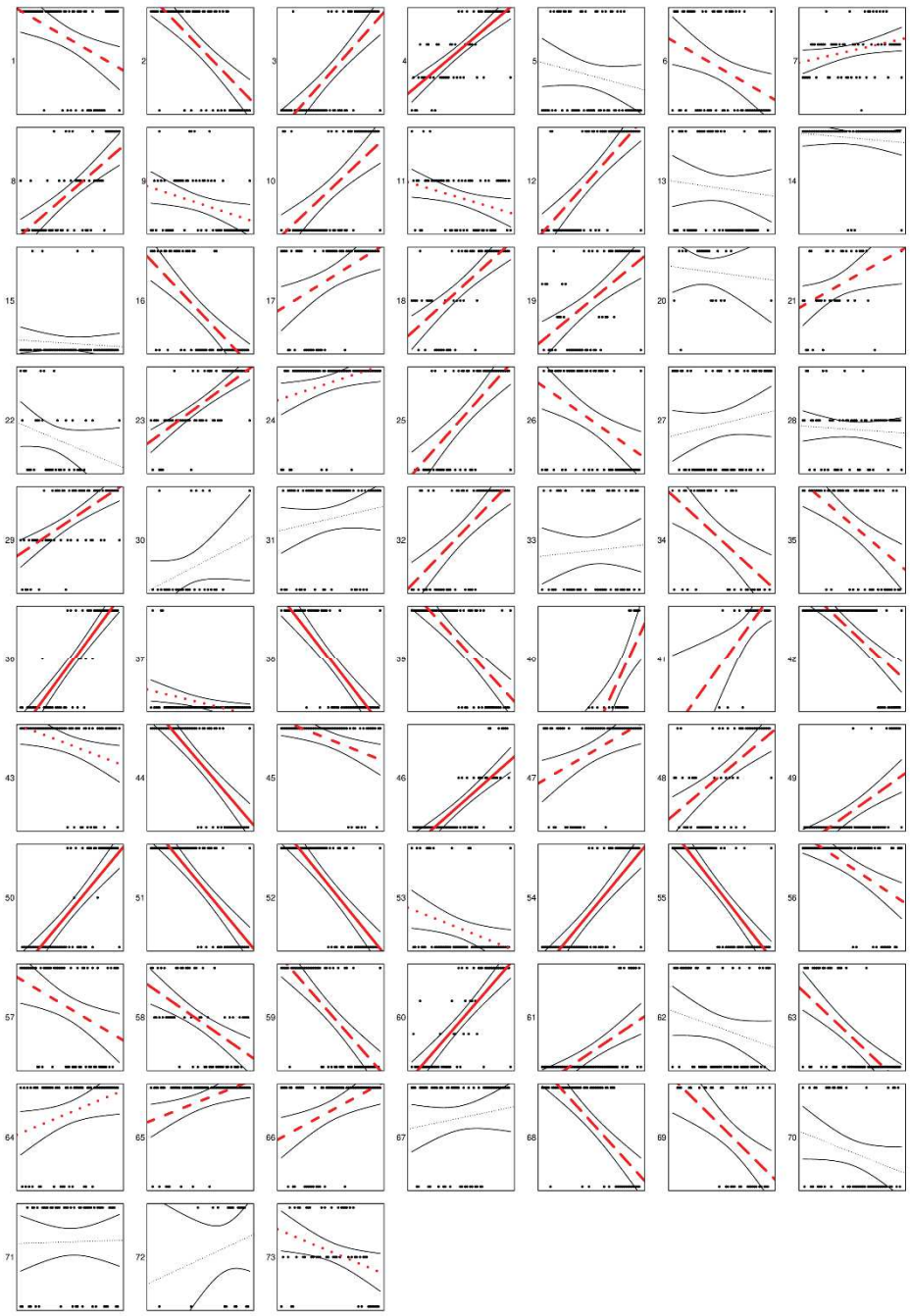

Figure III-22: Biplots of ranked brain mass (x-axis) and states values (y-axis) of each character (black points), the number of the character being on the left of each plot. Superimposed are, for each character, the regression line of the regression between these two variables, and the confidence interval (95%) of this regression around the regression line. The thickness and the color of the line indicates if the regression is significant for a Pearson test (significant if line is thick; otherwise thin) and for a Kendall test (significant if line is red; otherwise black). The longer the dashes of the lines, the higher the adjusted R squared of the regression: continuous line if over 0.5, long dashes if over 0.25, short dashes if over 0.1, dots if under 0.1.

III.1.C) Taxa and deep nodes

III.1.C.a) Sum of morphological changes and rates of evolution

There is a high variation of morphological changes between taxa (i.e., for a given phylogeny), going from no changes to 40-41 for nodes and to 25 for tips (Fig. III-23). Apart from the root, most of the morphological changes occur at familial-level nodes, or to subfamilial well-known nodes. The pteropodid node is the node with the most morphological changes. There are also several morphological changes at the nodes of megadermatids (28-30 morphological changes), rhinopomatids (23-25), and rhinolophids (22-23). There only are one or two changes at the node of hipposiderids, but several internal nodes diverge: the crown *Hipposideros* node has 19 changes, the (*Aselliscus* + *Coelops*) + *Riversleigha* node has 18 changes, and the *Macronycteris*+*Doryrhina* node shows 14 changes. Rhinonycterids are a peculiar case, as the three main nodes of the family show at least 15 changes. Finally, the pteropodines node is the main morphological changes hotspot inside the pteropodid family, with also 15 changes. Several taxa also exhibit numerous changes from their closest hypothetical ancestor: there are several cases in pteropodids (*Sphaerias*, *Megaerops*, *Megaloglossus*, *Eonycteris*, *Casinycteris*, *Nyctimene*, and *Eidolon*) with at least 10 character changes, but there also are in megadermatids (*Cardioderma cor*, 10 changes), rhinolophids (*Rhinolophus luctus, Rhinolophus pearsoni*, and *Rhinolophus rouxii*, with 16, 13, and 10 changes each), rhinonycterids (*Cloeotis* with 18 changes, and *Triaenops* with 16 changes) and in hipposiderids (*Asellia* with 24 changes, *Doryrhina* with 10, *Coelops* with 20, *Aselliscus* with 25, the fossil *Palaeophyllophora oltina* with 12, and *Hipposideros armiger* with 16).

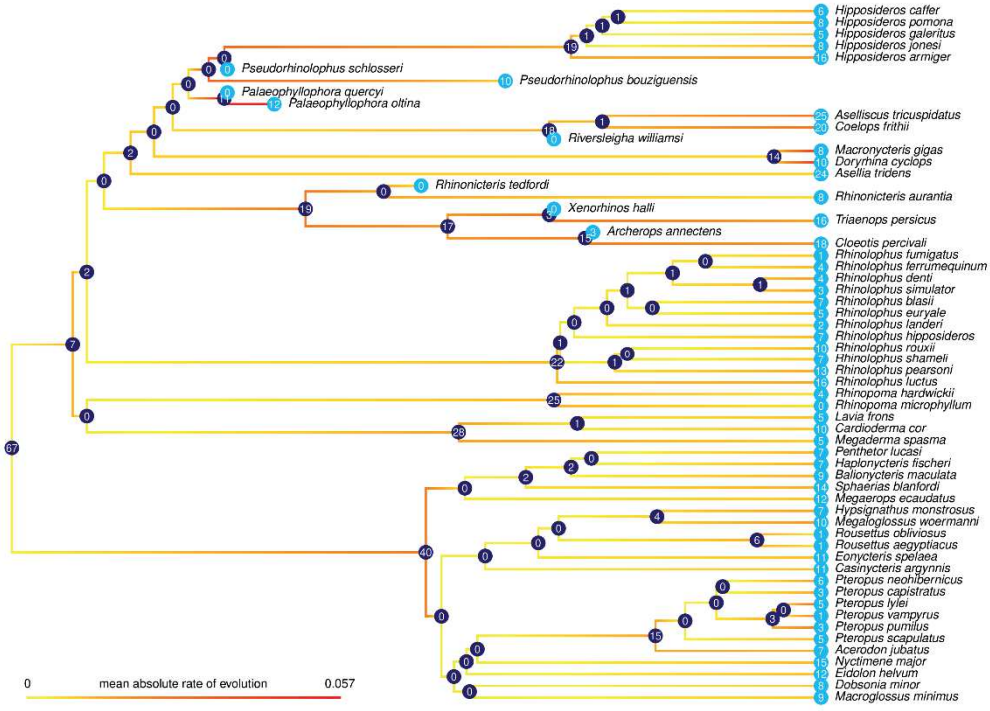

Figure III-23: mapping of the absolute evolutionary rates averaged over all characters for each taxa (color gradient), with the number of morphological changes at each node (marine pastille) and tip (light blue pastille). This stands for the phylogeny with *Palaeophyllophora* as sister-genus to *Hipposideros*. Other cases are figured in the Appendix III-6-3.

This variation of number of morphological changes across taxa parallels, to some extent, the distribution of the average absolute rate of evolution of all characters (Fig. III-23; Appendix III-2, Table 2). Most nodes with a high number of changes also show a quite high average absolute rate, but there also

are nodes with a high average absolute rate and few morphological changes (the rhinolophoid node, that of *Palaeophyllophora* species, and that which groups *Pteropus lylei*, *Pteropus vampyrus*, and *Pteropus pumilus*). Average absolute rate slightly but noticeably changes across phylogenies, especially regarding the deep nodes of hipposiderids: the later *Palaeophyllophora* diverges, the highest the average rate of evolution is for the whole (stem + crown) *Hipposideros* clade. The *Aselliscus*+*Coelops* node also varies in average absolute rate: while it is low if *Palaeophyllophora* diverges later, it is quite high if *Palaeophyllophora* diverges just before it, and a bit less high if *Palaeophyllophora* diverges even sooner. Some terminal branches also show a high, either constant or increasing, average rate of evolution: this is especially the case for three pteropodids (*Pteropus lylei*, *Pteropus vampyrus*, and *Pteropus pumilus*), but also for several hipposiderids (*Macronycteris*, *Doryrhina*, *Aselliscus*, *Coelops*, *Palaeophyllophora oltina*, and *Hipposideros armiger*). Finally, there is again a peculiar pattern in rhinonycterids, where only both *Rhinonicteris* terminal branches show moderate to low average absolute rates. It is also noticeable that, except the rhinonycterid case, most nodes with a high average absolute rate are "isolated": the nodes before and after them show quite lower average absolute rates.

III.1.C.b) Deep nodes rate evolution

The distribution of the aggregated differences in the slope of absolute rate evolution for each "deep node" (Appendix III-2, Table 2; Fig. III-24) shows little difference between each deep node, all seeming centered around a difference (to the general slope) of 0, even if hipposiderids have several low-valued outliers and rhinolophids have several high-valued ones. However, there is a highly significant heterogeneity between deep nodes (p-values between 1.10^{-9} and 2.10^{-8}, Appendix III-2, Table 3). Pteropodids and rhinopomatids are the most diverging nodes from the others, pteropodids having a higher slope difference, while rhinopomatids have a lower slope difference; both highly differ from each other (p-values between 5.10^{-8} and 5.10^{-7}, Appendix III-2, Table 4). Pteropodids further always differ from the whole rhinolophoid node (p-values between 3.10^{-4} and 0.01, Appendix III-2, Table 4), the megadermatid node (p-values between 2.10^{-2} and 4.10^{-2}, Appendix III-2, Table 4), and the rhinonycterid node (p-values between 2.10^{-3} and 8.10^{-3}, Appendix III-2, Table 4). Rhinopomatids further always differ from the "other" rhinolophoid node (i.e., its parent node; p-values between 5.10^{-3} and 1.10^{-2}, Appendix III-2, Table 4) and the rhinolophid node (p-values between 8.10^{-7} and 5.10^{-6}, Appendix III-2, Table 4). Rhinopomatids also may differ from the hipposiderid node, the p-value raising as *Palaeophyllophora* is in an increasingly basal position (p-values between 2.10^{-4} and 0.12, Appendix III-2, Table 4). Pteropodids and rhinopomatids may even further differ from "true" rhinolophoids, but the p-value rises as *Palaeophyllophora* diverges earlier and earlier for pteropodids (from 9.10^{-3} for an apicalmost position of *Palaeophyllophora* to 0.30 for its basalmost position, Appendix III-2, Table 4) and the reverse for rhinopomatids (from 9.10^{-3} for a basalmost position of *Palaeophyllophora* to 0.65 for its apicalmost position, Appendix III-2, Table 4). Rhinolophids differ from the rhinolophoid and the rhinonycterid nodes (p-values between 2.10^{-3} and 0.045 for the former, and between 0.012 and 0.039 for the latter, Appendix III-2, Table 4). As do pteropodids and rhinopomatids, rhinolophid may also differ from 'true rhinolophoids" for an apical position of *Palaeophyllophora* only (p-values from 0.045 to 0.81, Appendix III-2, Table 4).

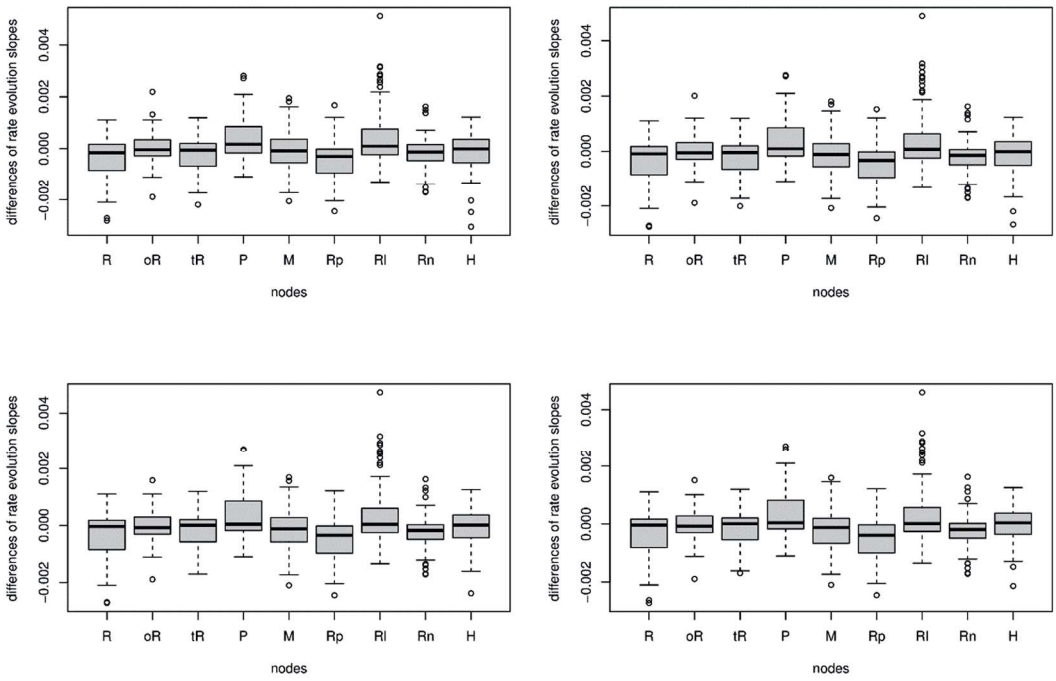

Figure III-24: Distribution of the difference between the slope of the temporal trend of the evolutionary rates of the characters (i.e., "rate" slope) for each considered "deep node" vs. that of the rest of the tree for each phylogeny (*Palaeophyllophora* in most apical to most basal position going from left to right and from top to bottom). Abbreviations: R-Rhinolophoidea; oR-"other" Rhinolophoidea; tR-"true" Rhinolophoidea; P-Pteropodidae; M-Megadermatidae; Rp-Rhinopomatidae; Rl-Rhinolophidae; Rn-Rhinonycteridae; H-Hipposideridae.

The distribution of the aggregated differences in estimated marginal means of absolute rate evolution for each "deep node" (Fig. III-25) shows more differences between deep nodes, both being their general position (no medians close to zero, being either over or under, while they are mostly aligned regarding aggregated differences in slopes, with the exception of rhinopomatids) and their dispersion, which greatly varies among nodes (with high variation for "true" rhinolophoid, rhinolophid, and hipposiderid nodes). There also is a very significant heterogeneity across deep nodes (Appendix III-2, Table 3; p-values between 2.10^{-12} and 9.10^{-12}), but with this time fully consistent pairwise differences across phylogenies. Hipposiderid node is the most diverging, with higher differences in estimated marginal means than the rhinolophoids node (p-values between 9.10^{-7} and 2.10^{-6}, Appendix III-2, Table 4), "other" rhinolophoids node (p-values between 8.10^{-6} and 5.10^{-5}, Appendix III-2, Table 4), pteropodids (p-values between 2.10^{-4} and 7.10^{-4}, Appendix III-2, Table 4), megadermatids (p-values between 1.10^{-3} and 3.10^{-3}, Appendix III-2, Table 4), and rhinopomatids (p-values between 1.10^{-6} and 2.10^{-6}, Appendix III-2, Table 4). The "true" rhinolophoids node also has higher estimated marginal means than the rhinolophids node (p-values between 6.10^{-4} and 1.10^{-3}, Appendix III-2, Table 4), the "other" rhinolophoids node (p-values between 3.10^{-3} and 1.10^{-2}, being slightly significant, Appendix III-2, Table 4), and the rhinopomatids (p-values between 7.10^{-4} and 1.10^{-3}, Appendix III-2, Table 4). Rhinonycterids node also has higher estimated marginal means than the "other" rhinolophoids node (p-values between 5.10^{-3} and 9.10^{-3}, Appendix III-2, Table 4), rhinopomatids (p-values between 4.10^{-4} and 2.10^{-3}, Appendix III-2, Table 4), and rhinolophids (p-values between 5.10^{-4} and 2.10^{-3}, Appendix III-2, Table 4). Rhinolophoids node has higher estimated marginal means than "other" rhinolophoids node (p-values between 0.02 and 0.049, being very slightly different, Appendix III-2, Table 4), and rhinopomatids and rhinolophids nodes (p-values between 5.10^{-3} and 6.10^{-3} for each, Appendix III-2, Table 4). Finally, pteropodids may slightly differ from rhinonycterid as the position of *Palaeophyllophora* gets more basal (p-values between 0.07 and 0.04, Appendix III-2, Table

4) and from “true” rhinolophoids in the reverse scenario (p-values between 0.03 and 0.07, Appendix III-2, Table 4).

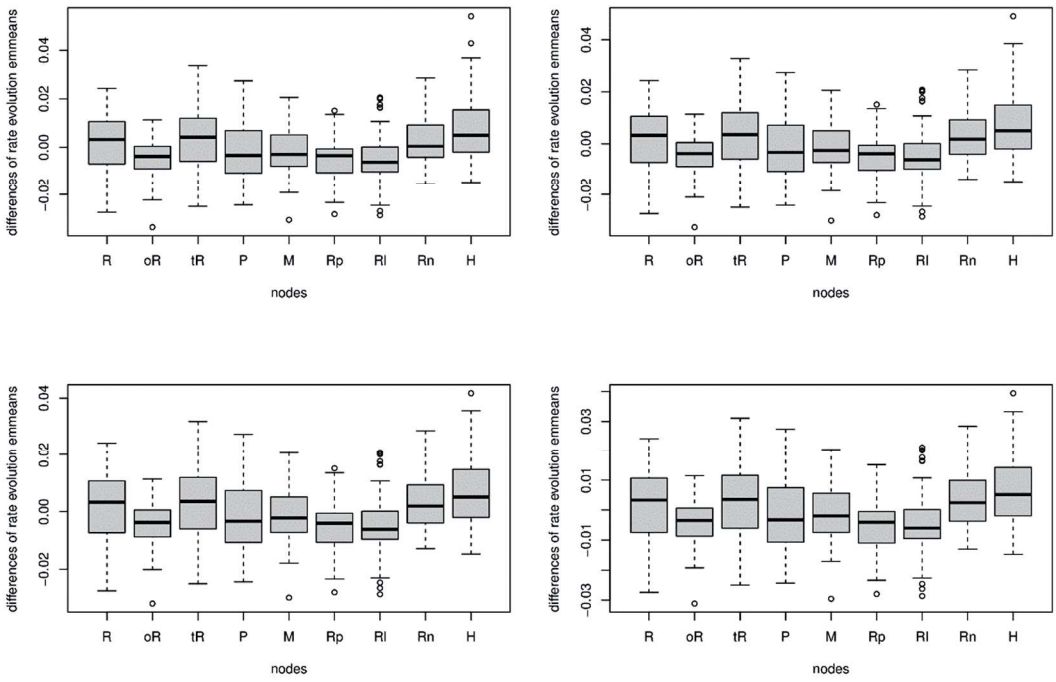

Figure III-25: Distribution of the difference between the average (i.e., estimated marginal mean) of the evolutionary rates of the characters for each considered “deep node” vs. that of the rest of the tree for each phylogeny (*Palaeophyllophora* in most apical to most basal position going from left to right and from top to bottom). Abbreviations: R-Rhinolophoidea; oR-“other” Rhinolophoidea; tR-“true” Rhinolophoidea; P-Pteropodidae; M-Megadermatidae; Rp-Rhinopomatidae; Rl-Rhinolophidae; Rn-Rhinonycteridae; H-Hipposideridae.

III.1.C.c) Deep nodes ancestral character estimates

Ancestral character estimations at the root and at the deepest rhinolophoid nodes (whole rhinolophoids, ‘true’ and ‘other’ rhinolophoids) are quite close to those of the Hipposideridae family. This is probably due to the old stratigraphic age of some hipposiderid fossil species (*Palaeophyllophora* species, *Hipposideros* (*Pseudorhinolophus*) *schlosseri*), as the statistical method for reconstructing ancestral estimates mainly relies on branch lengths.

Only seven characters vary between the root, the deep rhinolophoid nodes, and the hipposiderids. They regard the flexures, potentially the shape of the piriform lobes, the inflation of the caudal colliculi, the thickness of the vermis, the position of the orbitotemporal canal, and the completeness of the transverse sinus cast. The root (the basalmost node) differs the most from the other nodes, with two to five single differences, while the hipposiderids (the apicalmost of these nodes) differ from one to three single differences. Apart from these differences, reconstructed endocasts (Fig. III-26) of these nodes all seem very similar. The other rhinolophoid families are quite different from the rhinolophoid ancestral estimates (and thus from hipposiderids) but also from each other. Also according to Figure III-23, megadermatids seem to be the most morphologically divergent of these families and share the ancestral-most estimations with pteropodids among all other nodes. Yet, pteropodids are still very different from all other nodes, and just a little bit less from megadermatids.

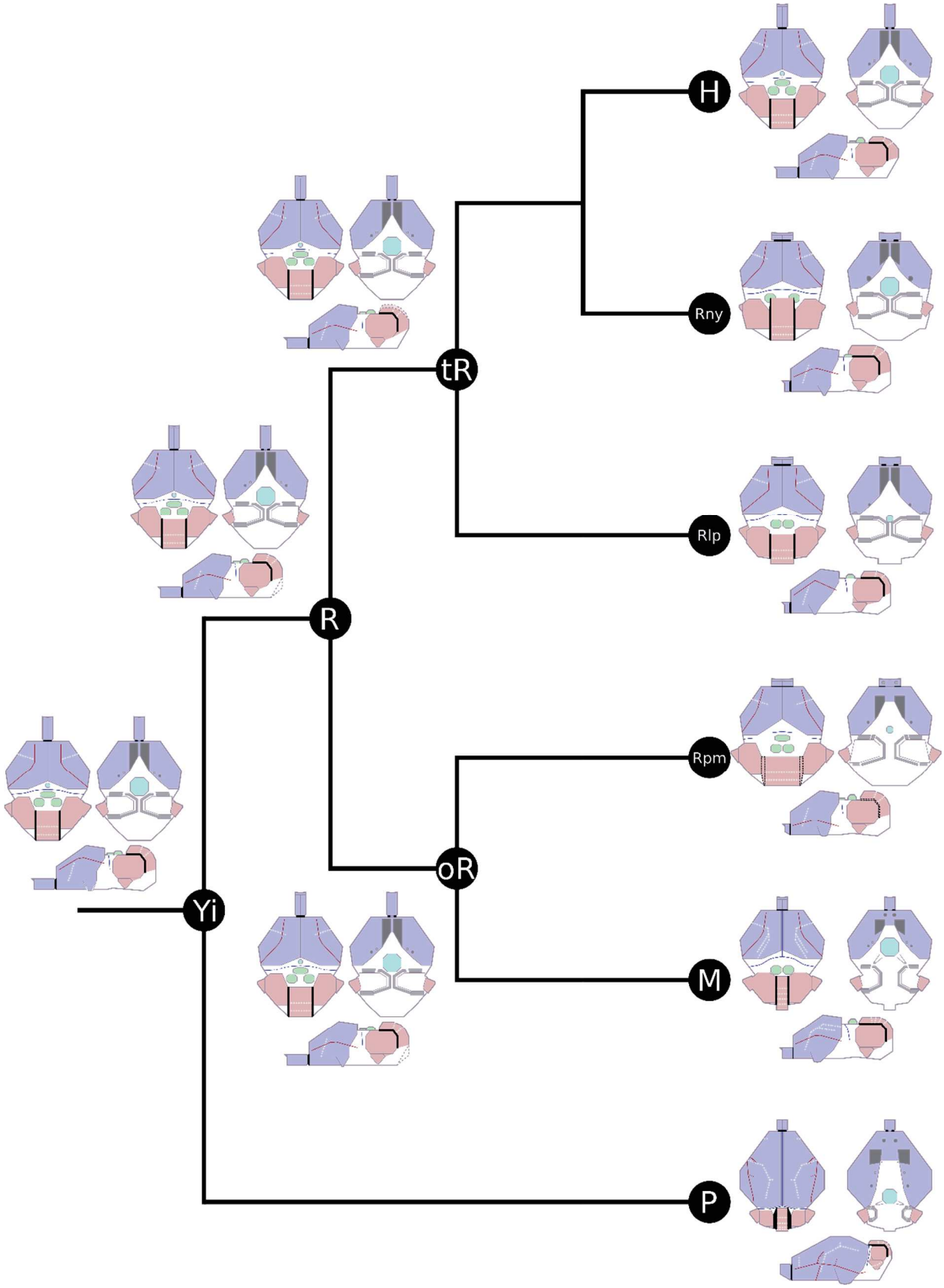

Figure III-26: simplified phylogeny of Yinpterochiroptera with the theoretical ancestral endocasts of “deep nodes” investigated here in dorsal (top left), ventral (top right), and lateral left (bottom) views. From basalmost to apicalmost, nodes are those of Yinpterochiroptera (‘Yi’), then of Rhinolophoidea (‘R), then of “true” and “other” Rhinolophoidea (‘tR’ and ‘oR’), then of sampled families that are Hipposideridae (‘H’), Rhinonycteridae (‘Rny’), Rhinolophidae (‘Rlp’), Rhinopomatidae (‘Rpm’), Megadermatidae (‘M’), and Pteropodidae (‘P’).

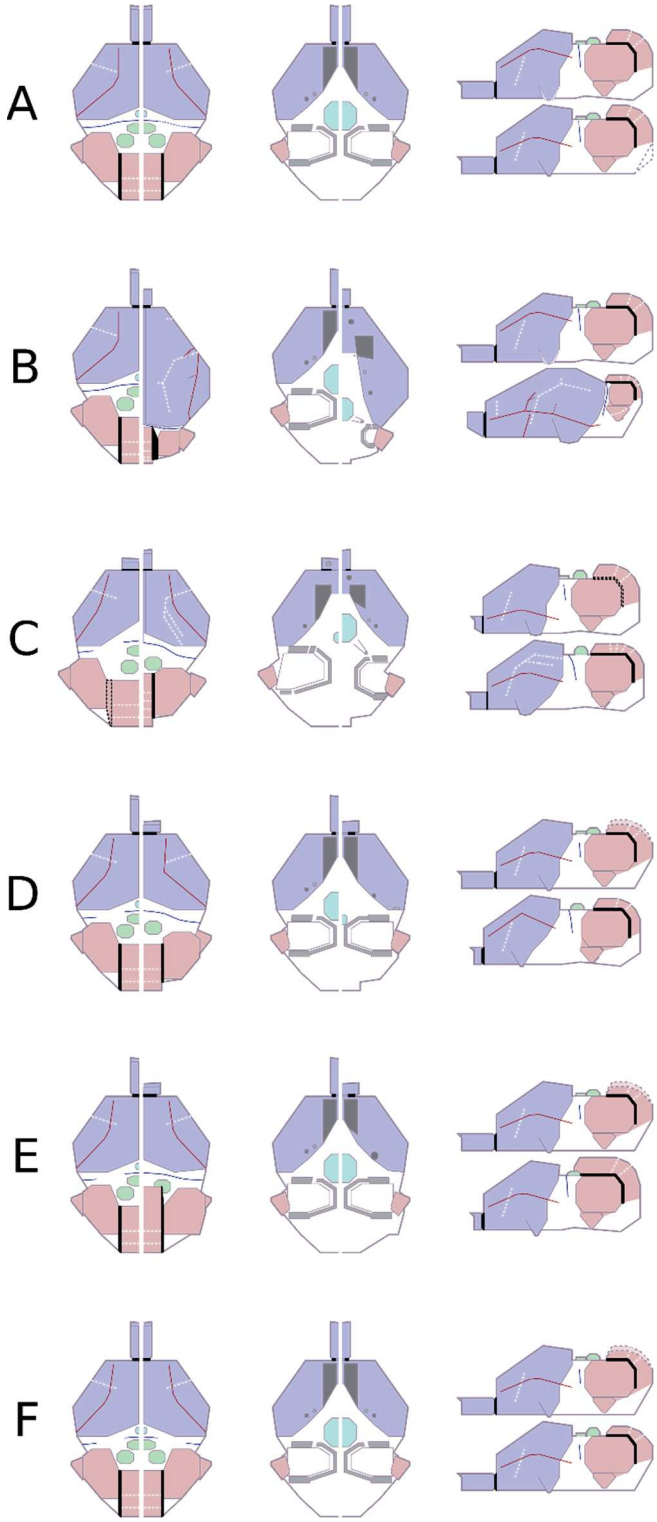

Figure III-27: discussed comparisons of theoretical ancestral endocasts of “deep nodes” investigated here in dorsal (left), ventral (middle) and lateral left (right) views. For lateral views, the first listed taxon is on the top. Comparisons are: A-Yinpterochiroptera vs. Rhinolophoidea; B-Yinpterochiroptera vs. Pteropodidae; C-Rhinopomatidae vs. Megadermatidae; D-“true” Rhinolophoidea vs. Rhinolophidae; E-“true” Rhinolophoidea vs. Rhinonycteridae; F-“true” Rhinolophoidea vs. Hipposideridae.

The pteropodids are morphologically highly divergent from all other taxa (families and deeper nodes; Figs. III-26,27-A,B), with numerous differences (36 with megadermatids, 46 to 51 with other taxa). These differences regard the more expanded cerebrum (which is way bigger than the cerebellum and hides the mesencephalon), with more complex patterns of neopallial sulci and of stapedial artery ramification at the Yinpterochiroptera scale. These changes imply i) a fully covered mesencephalon and a compressed cerebellum, though the vermis is quite folded, ii) the presence of the cast of the superior sagittal sinus, and iii) the presence of numerous endocranial foramina such as the anterior carotid, the anterior pterygoid, and optic foramina.

In 'other' rhinolophoids, rhinopomatids and megadermatids do not particularly resemble each other (Figs. III-26,27-C): there are 33 differences between them, but 28 to 35 and 26 to 37 differences between megadermatids and rhinopomatids (resp.) compared to other rhinolophoid nodes (i.e., families and deepest nodes). The reconstructed rhinopomatid endocast (Fig. III-26) resembles that of basal rhinolophoid nodes, although there are numerous (27 to 28) differences. In general, the reconstructed rhinopomatid endocast also shows some unique characteristics: the cerebellum is larger than the cerebrum, the paramedian fissure is not well delineated, all circum-petrosal apertures are individualized, the jugular foramen is smaller than pyriform window, and the unknown foramen #1 is present. The megadermatid reconstructed endocast does not resemble the more basal rhinolophoid ones, but it is still different from other rhinolophoid family ones by a similar magnitude than is that of rhinopomatids. In megadermatids, the cerebrum is wider relative to the cerebellum than in other rhinolophoids, with a little more complex neopallial sulcal pattern, a thinner and more folded vermis, there is an anterior carotid foramen with a carotid sulcus, a visible superior sagittal sinus cast, and an individualized optic foramen. Most of these features are shared with or similar to the pteropodid conditions, but there still are some features retrieved at more basal rhinolophoid nodes, such as a large hypophysis and exposed caudal colliculi.

There is a comparable number of differences between 'true' rhinolophoids families, with 24 differences between hipposiderids and rhinonycterids, 23 between rhinolophids and rhinonycterids, and 25 between hipposiderids and rhinolophids. There are still fewer differences between 'true' rhinolophoid family ancestral estimated endocasts than between other families (inside 'other' rhinolophoids, or between 'true' rhinolophoids and other families). In 'true' rhinolophoids, rhinonycterids noticeably differ by the high size and the anterior development of their cerebellum, which partially hides the tectum of mesencephalon (Figs. III-26,27-E); rhinolophids (Figs. III-26,27-D) and hipposiderids (Figs. III-26,27-F) also differ by (subtler) differences regarding the delineation of the anterior tectum and the vermis thickness (for instance). Endocranial opening patterns also deserve to be noted: even though the pattern remains simple in each family, all the reconstructions differ (Figs. III-26,27-D,E,F). For the other characters, there are frequently one state shared by two families while another one characterizes the other family; for instance, the hypophysis is similar between hipposiderids and rhinonycterids, the sphenorbital fissure is similar between hipposiderids and rhinolophids, and the olfactory bulbs and the circum-petrosal apertures are similar between rhinonycterids and rhinolophids.

III.2) Discussion

III.2.A) Variation due to phylogenetical uncertainty

The variable position of the genus *Palaeophyllophora* implies slight differences in the reconstruction of the morphological evolution of the endocast anatomy, as there are in general few changes in RI and CI. Six out of the 73 characters show a variation in their mapping, with varying aces and a little variation in the location of morphological changes (which impacts the RI and CI). However, it has to be emphasized that the ancestral reconstructions are roundings of decimal values; here, all changes of states are due to small decimal variation (Appendix III-9).

Thus, if the phylogenetic uncertainty does not have major consequences on the mapping of the morphological characters, these variations still show that the reconstructions at some points of the tree clearly are difficult to resolve and depend on the phylogeny. These irresolutions occur both at the suprafamilial level (regarding the rhinolophoids, "true" rhinolophoids, and "other" rhinolophoids nodes, and the hipposiderids+rhinonycterids node) and at the intrageneric level (regarding the two most apical nodes of the genus *Hipposideros*).

An uncertainty at the suprafamilial level may highlight a complicated evolution between major rhinolophoid taxa: crown rhinolophoid groups exhibit contrasted morphologies, both among and between “true” and “other” rhinolophoids (this is particularly well highlighted by the graphic ancestral endocast reconstructions Figs. III-26,27). It is thus complicated, even more in groups with low extant diversity or with recent diversity explosion, to properly reconstruct such ancient conditions. While the reconstructions are unambiguous for numerous characters, they are still uncertain for some others. Fossil data particularly allow better reconstructing ancient character states, and as much as possible fossil species are needed in order to better constraint the picture of endocast evolution through rhinolophoids.

An intrageneric uncertainty, on the other hand, could clearly be resolved by adding more extant species, as they concern recent groups and shorter branches of the tree. They may also highlight morphological splits between groups of species, but that kind of hypothesis can only be assessed with a more-focused sampling. What can be said here is only that it would be of interest to investigate the morphological variation of the endocast in the genus *Hipposideros*, and especially just before and at the onset of the geographical split between *Hipposideros* species groups that probably occurred during the middle Miocene.

III.2.B) Character distribution, phylogenetic relevance, evolution

As highlighted by orthogonal points of view in the results, there are plenty of evolutionary patterns of anatomical characters, but also of endocranial types of structures. Distribution patterns greatly vary between characters, from structuring characters to randomly distributed ones (Appendix III-7). In general, several characters have a good phylogenetic signal (with half of the characters having a RI over 0.5) but are highly subject to convergence (most of the characters having a CI under 0.2, though this measure is known to decrease with the size of the sample, Archie 1989). There seems to be no variation in the phylogenetic consistency and in the homoplasy sensitivity between the different types of structures: the variation is not significant regarding the RI, and if it is significant for the CI, there is no significant pair. Similarly to the previous RI/CI negative proportionality, some structures seem to have a high variation of RI depending on the characters (mesencephalon, neopallial foldings, cranial openings) and a concurrent reduced variation of CI. However, as there are very few significances, it would clearly be hasty to extrapolate about the phylogenetic properties of these structures.

Regarding the whole number of morphological changes (considering both homologous and homoplasic changes), there again is a wide array of values depending on the characters, both regarding changes at nodes and at tips. If the number of changes at nodes and tips are statistically correlated, it is however difficult to find a pattern. This significance is lost when the complete set of anatomical structures is considered, therefore caution is needed for that point. An heterogeneity is however present in the number of changes at nodes, tips, and both: in general, there is a lower number of changes for the neopallial folding characters compared to those of the telencephalon (at nodes and tips, and at nodes) and of the mesencephalon (at nodes). The low number of changes for neopallial foldings may be due to the characters coding structures only (or mostly) present in pteropodids: seven of the nine characters are presence/absence characters, with numerous cases of full absence in rhinolophoids, thus clearly lowering the number of changes. The relative low variation in neopallial folding characters number of changes should be considered in the light of the type of characters and of the effective sample to which may apply the character variation of each structure.

Generally speaking, there is a wide array of patterns and a large variation among characters but also among general structures. The endocast characters established here are variously relevant phylogenetically: be it at the general structure scale or at the character level, they turn out to always be mixed patterns of distribution. Phylogenetic relevance should be addressed with more focus, character by character. Ecological correlations should be attempted at that level and after controlling for phylogenetic signal.

Half of the characters show a significant slope of evolution rates through time, indicating a variation of the states through time; two-thirds of these show a negative slope, indicating a reduction of the states variation through time (while the phylogeny ramifies), and the other third show a positive slope, with an increase of states variation. A quarter to a third of the characters show both a significant trend of state and rate evolution through time, and among them, the difference reduces between characters with negative or positive rate slope. Among the dozen of characters that increase in state variation through time, most also have a state trend, while only half of the roughly 20 characters that decrease in state variation through time also show a state trend. Having most of the characters that increase in state variation through time also have a state trend may not be very surprising: these characters may have "diversified" through time, starting from a state and changing more and more and with the appearance of new states along the phylogeny. Characters with a reduced variation in states would imply a constrained selection on their states, with two possibles scenarios: a quickly reached optimum (with an initial small variation, but no more variation and the same states maintained) or a very selective trend (with few states at the same time, but going from states to states). Here, characters distribute equally between these two scenarios. All these characters with a significant rate evolution through time also deserve to be investigated in more detail, as they are likely to be related either to diversification (driven by phylogeny or by ecological convergence, among others) or to selection, for instance.

A morphological covariation with size could be related to an allometric relationship, the shape of a structure varying only due to size variation. Here, it appears that most of the morphological characters covary to some extent with size, but also does the RI of these characters. This can be explained by the basal dichotomy in Yinpterochiroptera between rhinolophoids and pteropodids: pteropodids are generally larger than rhinolophoids, even if there also is a size variation among rhinolophoids (megadermatids being larger than most of the other rhinolophoids). Thus, given that the body size itself bears a phylogenetic signal (see Moyers-Arévalo et al. 2020), it is difficult to assess if the covariation with

both size and phylogeny of a given character is due to allometry or phylogeny. This implies ontogenetic investigations, which are far beyond the scope of this study.

III.2.C) The case of the exposed mesencephalic tectum

A peculiar feature of the brain of bats has been previously discussed: the exposure of the tectum of the mesencephalon, and especially the caudal colliculi. During the XXth century, some researchers investigated the role and the evolution of these structures in bats, being an obligatory step during the auditory information process (a specificity of bats, Reep & Bhatnagar 2000). Dechaseaux (1973) summarized that the presence, exposure, and inflation of the caudal colliculi are largely admitted to correspond to a high specialization towards echolocation. Regarding their evolution, Edinger (1964a) exposed previous thoughts stating that the presence of a visible mesencephalic tectum on endocasts was thought to be a primitive stage in mammalian brain evolution; using Mesozoic and Cenozoic mammalian endocasts, she instead proposed that it would in fact be a secondary and maintained exposure through time in bats. Apart from these general considerations, that were crucial in chiropteran (paleo)neurology, there was no significant investigation on the evolution of other brain structures in bats. Only Dechaseaux (1956) shortly compared the brains of fossil and extant bats, generally concluding that there was a trend towards an overlap of the tectum from fossil to extant species that is concurrent with an expansion of the cerebral hemispheres, together with a rhinencephalon reduction. These trends apply from fossil to extant "microchiropteran" bats, and Dechaseaux also says that they are even more marked for megachiropteran ones. Here, the distribution of mesencephalic characters at the Yinpterochiroptera scale allows to discuss a bit more, and with a more robust methodology, the evolution of these structures.

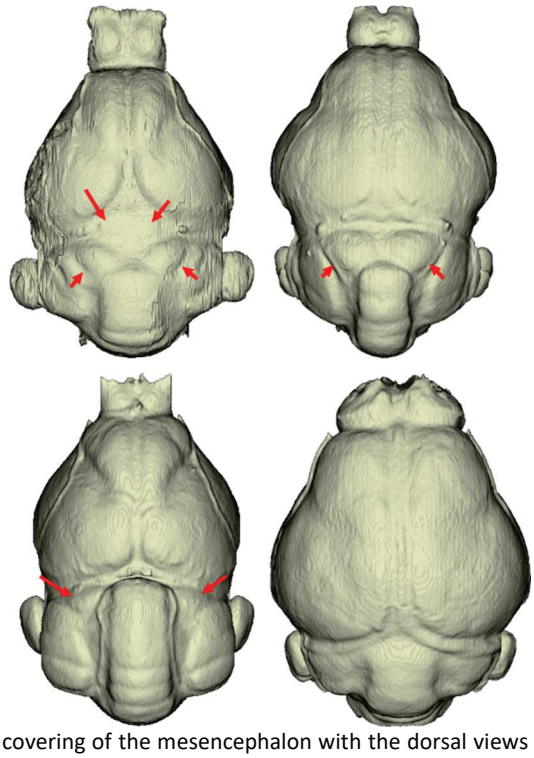

Figure III-29: Examples of variation in the covering of the mesencephalon with the dorsal views of the endocasts of the fossil hipposiderid *Palaeophyllophora oltina* (top left, with all four colliculi visible), the megadermatid *Megaderma spasma* (top right, with only the caudal colliculi visible), the rhinonycterid *Triaenops persicus* (bottom left, with part of the caudal colliculi visible), and the pteropodid *Haplonycteris fischeri* (bottom right, fully covered mesencephalic tectum). Not to scale.

Regarding the mesencephalic tectum itself, character 19 accounts for its relative exposure. This character has a high phylogenetic consistency (RI over 0.9, Appendix III-2, Table 1) and its distribution (Figs. III-27,29) shows a clear pattern, with pteropodids having a fully covered tectum (state 3) and rhinolophoids having ancestrally a fully exposed one (state 0). However, there also are rhinolophoid cases

of clear to full overlap of the tectum, especially in Rhinonycteridae and in the hipposiderid *Coelops frithii*. Apart from these cases, the tectum is fully exposed in megadermatids, rhinopomatids, and rhinolophids (with the exceptions of the megadermatid *Megaderma spasma*, the rhinolophid *Rhinolophus luctus* where it is slightly covered, state 1). In hipposiderids, the tectum is a bit overlapped convergently in the *Macronycteris* + *Doryrhina* clade and in *Hipposideros* sensu stricto. This character is clearly covarying with size, but this can also be due to the actual covariation between phylogeny and size (see previously). There also is a positive trend of evolution of the states of this character (Appendix III-2, Table 1), implying a trend towards a covering of the tectum, which converges with the conclusions of Dechaseaux (1956).

However, other tectum characters (characters 20 to 22, regarding the delineation of rostral colliculi, the inflation of caudal colliculi, and the distance between caudal colliculi) show quite a lower phylogenetic consistency (all RI under 0.6, Appendix III-2, Table 1) and more complicated distributions (Appendix III-8-20,21,22). Of these characters, only character 22 (distance between caudal colliculi) shows a significant trend of decreasing states (i.e., meaning that they become closer) through time. Particularly, character 21 regarding the inflation of caudal colliculi is very blurry: “other” rhinolophoids, half of the rhinolophids, one extant rhinonycterid, one extant hipposiderid, and the two *Pseudorhinolophus* fossil species show highly inflated caudal colliculi, both *Rhinonicteris* species, *Asellia*, and *Macronycteris* show smooth ones, and all other rhinolophoid species show an intermediate condition. The state trend through time is highly not significant (p-values over 0.8, Appendix III-2, Table 1), indicating no trend through time. This means that the inflation of the caudal colliculi does not seem to depend on the phylogeny, or on the tectum exposure, and that there is no temporal trend. Conclusions about the evolution of the mesencephalic tectum in bats must be approached with caution, given that, when looking with a bit more detail than what has been previously done, there also are mixed patterns of evolution of the structures. If a trend in reduction of the mesencephalic exposure may be found here concurrent to what has been proposed by Dechaseaux (1956), a general reduction of exposed dorsal mesencephalic structures is however not retrieved.

Some characters established and scored here may also account for the degree of overlap of the mesencephalic tectum by other structures that are the cerebral hemispheres anteriorly and the vermis and cerebellar hemispheres posteriorly.

Regarding the cerebral hemispheres, characters 9 and 10 indirectly account for their posterior expansion: a mediolaterally oriented posteromedial margin of these hemispheres coupled with a convex outline of their posterior margin translate a posterior expansion, while a diagonally oriented posteromedial margin and a generally flattened posterior margin may translate a lack of expansion. Concurrently with the phylogenetic and temporal trends found for the tectum overlap, there seems to be an expansion of the cerebral hemispheres, but with a dichotomy (Figs. III-26,27-A,B): pteropodids all have expanded cerebral hemispheres, while rhinolophoids have less expanded ones. Especially, the angulation of the posteromedial margin in rhinolophoids starts by an intermediate condition, and then several convergent evolutions towards one or the other extreme states occur. The RIs are however high for both characters (over 0.75) and the temporal state trends are significant and indicate a posterior expansion of the cerebral hemispheres (Appendix III-2, Table 1). This also converges with the conclusions of Dechaseaux (1956), but the concerned taxa for this point and for the tectum overlap are not necessarily the same; only pteropodids show, here, a fully tectum overlap and a posterior cerebral expansion, but rhinonycterids show only the former while several hipposiderid extant species show only the latter (Fig. III-27-D,F).

Regarding the cerebellar structures, character 26 is especially well suited to track the overlap over the mesencephalic tectum: most of the rhinolophoids have cerebellar hemispheres located more anteriorly than the vermis, but in some rhinolophoid cases and in all pteropodids, the vermis extends further anteriorly to those hemispheres. This is what has been established for character 26, and there is a strikingly similar distribution to that of the tectum overlap (Appendix III-8-26): all taxa with an advanced or full overlap of the mesencephalon also have an anteriorly protruding vermis, with the addition of the hipposiderid *Riversleigha williamsi*, whose tectum is fully exposed. This character has a high RI (over 0.8, Appendix III-2, Table 1), a p-value between 5% and 6% (just above the significance level) with a negative slope value (which may indicate a temporal trend toward a presence of that protrusion) but more importantly a significant negative slope of rates through time (Appendix III-2, Table 1). This indicates a reduction of the rate variation through time, with an initial set-up of that anterior protrusion of the vermis (probably at the family-level) and a maintain of that state in groups.

In pteropodids, using endocasts only, it is not possible to determine the relative contribution of the cerebral hemispheres and of cerebellar structures to the mesencephalic tectum overlap; cross-sections of the brain show that both structures cover the tectum (Baron et al. 1996), and it is not possible to know whether the one or the other first started to expand, and neither if this was diachronic between these two structures or not. To gather pteropodid fossil skulls would be utopic, but this could clearly add elements to better solve this question. It is however clear that the tectum overlap is mainly driven by the vermis in rhinonycterids. As already pointed out by Edinger (1964a), the tectum overlap may not only be due to the expansion of the telencephalon, but also to an enlargement of the metencephalon. Rhinonycterids are a case study for that point.

III.2.D) Testing secondary homologies

Several anatomical characters rely on structures whose homology has been discussed in the Nomenclature section using structural and ontogenetic arguments. Such establishments of homologies can be referred to as “primary” homologies (de Pinna 1991). Primary homology hypotheses can further be tested using an evolutionary framework, considering homologous transformations as synapomorphies (de Pinna 1991), i.e., secondary homologies. Here, I particularly look at the distribution of some characters whose first definition is proposed here. The concerned characters regard neopallial foldings (presence or absence of sylvian, its posterior extent, bridge, lateral, infrasylvian, orbital, and intermediate sulci; characters 37, 38, 39, 42, 43, 44, 45, respectively), blood structure casts (presence of middle cerebral artery and superior sagittal sinus casts; characters 51 and 52, respectively), and cranial foramina casts (presence of unknown 1, 2, 3, anterior carotid, and posterior carotid foramina casts, and presence of carotid sulcus; characters 64, 65, 66, 67, 68, 69, respectively).

There are few a priori doubts regarding some of the neopallial foldings: the sylvian, orbital, and lateral sulci have been described before and have been mostly found in megabats (see Baron et al. 1996 for instance). The sylvian sulcus is present in all taxa except three hipposiderid species; its presence is inferred as an ancestral condition (Appendix III-8-37). Similarly, the orbital sulcus is present in all pteropodids with the exception of *Casinycteris argynnis*, so its presence is inferred as a synapomorphy of pteropodids (Appendix III-8-44). The lateral sulcus, however, is here retrieved as being convergent in *Eidolon*, *Nyctimene*, *Dobsonia*, pteropodines, *Eonycteris*, and *Rousettus*; the lateral sulcus could be non-homologous in all these groups (Fig. III-28). However, by looking at the continuous values reconstructed in pteropodids (Appendix III-9-42), it is not fully clear if the lateral sulcus absence is ancestral in pteropodids, with intermediate values between presence and absence. Typically, a larger sample focusing on pteropodids would be needed to better evaluate the homology of the lateral sulcus in that family.

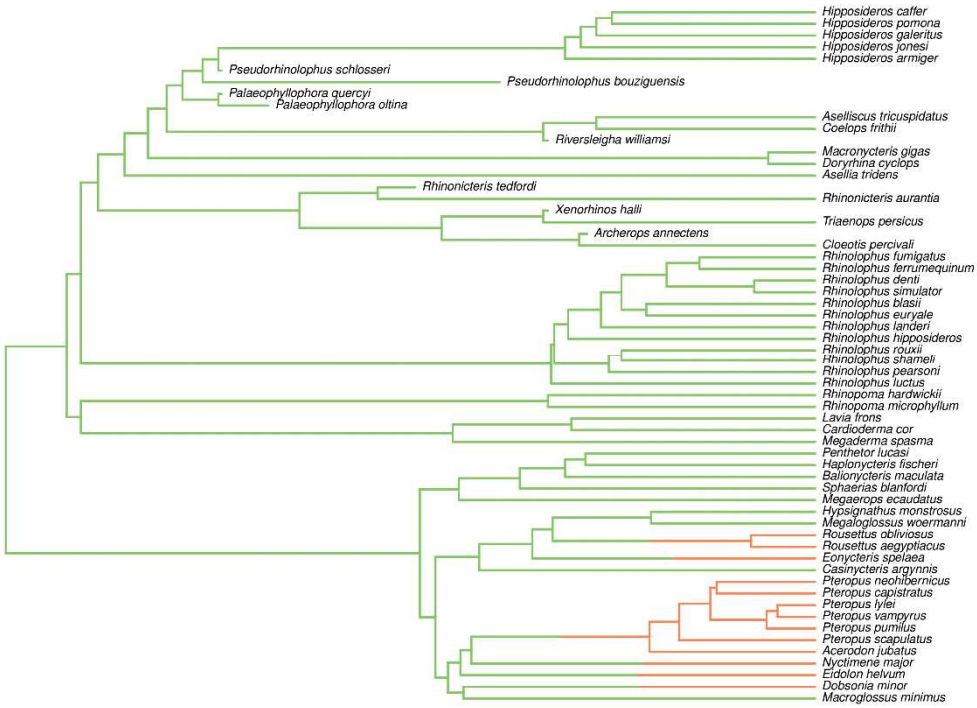

Figure III-28: Discrete mapping of character 42 regarding the presence (orange) or absence (green) of a lateral sulcus. This stands for the phylogeny with *Palaeophyllophora* as sister-genus to *Hipposideros*. Other cases are figured in Appendix III-6-4.

The posterior extension of the sylvian sulcus (its suprasylvian part; Fig. III-30) is shared by all pteropodids and more occasionally by some rhinolophoids (two of the three megadermatids, three rhinolophids, three hipposiderids). Regarding pteropodids, this posterior extension is a familial synapomorphy, and this extension would be homologous in this family; in the rhinolophoid taxa, a posterior extension is also retrieved as being a synapomorphy of megadermatids (with a further reversion for *Cardioderma cor*) and of the *Macronycteris* + *Doryrhina* hipposiderid clade, while it is a local change for the other concerned taxa. This would mean that this extension is not homologous in pteropodids and rhinolophoids, but also within rhinolophoids. Size may explain all these changes: all concerned taxa are medium to large sized (with the exception of two rhinolophids whose brain volume is beyond 500mm^3) and this character correlates well with size (Fig. III-22, Appendix III-2, Table 1). Phylogenetic vs allometric origin of this character should be further explored in rhinolophoids using more large-sized species, while it would be more difficult to test the homology between pteropodids and rhinolophoids using macromorphology only.

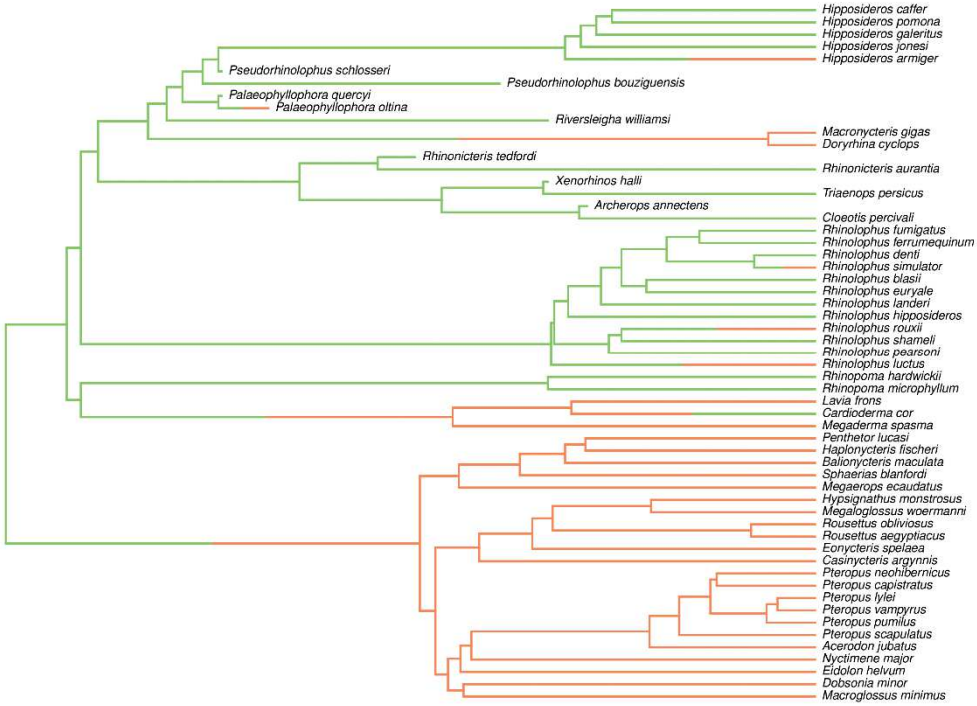

Figure III-30: Discrete mapping of character 38 regarding the presence (orange) or absence (green) of a suprasylvian extension to the sylvian sulcus. This stands for the phylogeny with *Palaeophyllophora* as sister-genus to *Hipposideros*. Other cases are figured in Appendix III-6-5.

Other foldings (bridge, infrasylvian, and intermediate sulci) have been defined here, enhancing the interest to test their homology using phylogenetic comparative methods. The bridge sulcus is retrieved in all pteropodids but two species (*Casinycteris argynnis* and *Pteropus lylei*; Appendix III-8-39); its presence is therefore reconstructed as being a synapomorphy of all pteropodids. A convergent bridge sulcus is also present in the megadermatid *Lavia frons*. However, it is quite difficult to propose the megadermatid and the pteropodid bridge sulci as being homologous, since only *Lavia* exhibits one. The infrasylvian sulcus shows an interesting pattern (Fig. III-31), being a synapomorphy of megadermatids and potentially of cynopterines (a convergent change is proposed for all cynopterines but *Megaerops* and also for *Megaerops* because of the short length before the cynopterine node). Convergent infrasylvian sulci in other pteropodids are found in unrelated species (*Hypsignathus monstrosus*, *Eonycteris spelaea* and *Pteropus neohibernicus*). Considering all these infrasylvian sulci as being homologous is difficult, especially

between megadermatids and pteropodids. Continuous values of reconstructed states (Appendix III-9-43) further show that the values are intermediate at both the megadermatid and pteropodid nodes, that at the megadermatid node being slightly more toward the “present” state. A common causality may be the size, but this character correlates very weakly with size here (Fig. III-22, Appendix III-2, Table 1). Thus, while a larger and more focused pteropodid sample is needed, it can be proposed that the infrasylvian sulci are both homologous at the pteropodid and at the megadermatid scale, whereas it is more difficult to propose a common origin for each. Finally, the intermediate sulcus appears to be fully convergent in the various pteropodid species that exhibit it (Appendix III-8-45): all major pteropodid subgroups have some species showing an intermediate sulcus, but all these cases are reconstructed as being convergent. There is still a little bit of doubt regarding the ancestral condition of pteropodids (Appendix III-9-45): an absent intermediate sulcus is reconstructed, but not being as strict as in rhinolophoids. It is very difficult to conclude about this intermediate sulci, and, as for some other characters, a more focused study on pteropodids may answer to this point.

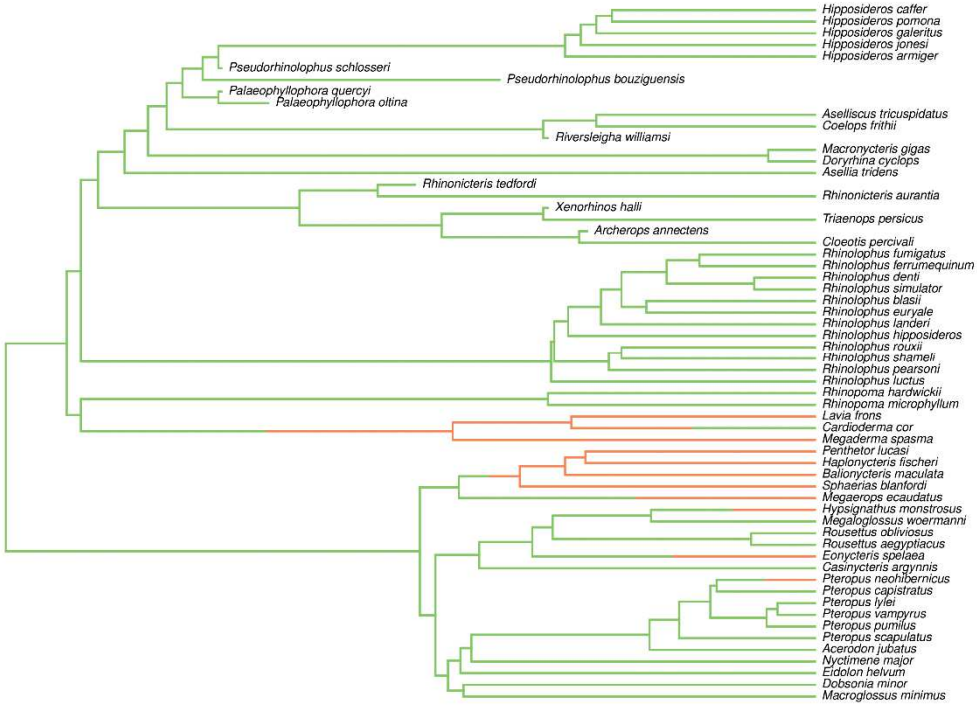

Figure III-31: Discrete mapping of character 43 regarding the presence (orange) or absence (green) of an infrasylvian sulcus. This stands for the phylogeny with *Palaeophyllophora* as sister-genus to *Hipposideros*. Other cases are figured in Appendix III-6-6.

A middle cerebral artery cast is retrieved in all pteropodids and only in pteropodids (Appendix III-8-51). There are thus no real doubts about the homology of that cast. The reason why it is absent in rhinolophoids would however deserve a particular attention by studies dealing with cranial soft structures. The superior sagittal sinus cast is also found in all pteropodids, but also in megadermatids (with the exception of *Cardioderma cor*). This character correlates well with size (Fig. III-22, Appendix III-2, Table 1), thus there may be an allometric reason to expose this cast in large-sized yinpterochiropterans. Once again, dealing with cranial soft tissues may help better explain this distribution and its causes: there are few doubts that the cast of this imprint, in both families, is left by the same structure.

The unknown foramen #1 is present in various rhinolophoid species, of each family with the exception of megadermatids (Appendix III-8-64). The presence of the unknown foramen #1 may be a synapomorphy of rhinopomatids, of non-*Rhinonicteris* rhinonycterids, of an hipposiderid clade (*Riversleigha* + *Aselliscus* + *Coelops*), and would be convergently acquired otherwise. Fossil species especially often show an unknown foramen #1, and if the unknown foramen #1 is reconstructed absent for all yinpterochiropteran bats, there is a bit of uncertainty in all deep nodes of the phylogeny (except for pteropodids) down to the root while dealing with the continuous values (Appendix III-9-64). The unknown foramen #2 shows a somewhat similar pattern of distribution, though its distribution itself is clearly different (Appendix III-8-65): a present unknown foramen #2 is a synapomorphy for non-*Rhinonicteris* rhinonycterids and for the genus *Hipposideros* sensu stricto, while it is convergent in some other species (the hipposiderid *Aselliscus tricuspidatus*, the rhinolophid *Rhinolophus blasii*, the rhinopomatid *Rhinopoma hardwickii*, and the megadermatid *Cardioderma cor*). This time, there is quite less doubt about the reconstructed state at deep nodes (Appendix III-9-65) and these changes appears to really be convergent. The unknown foramen #3, finally, characterizes well the rhinolophids: all rhinolophids exhibit that foramen, in addition to the hipposiderid *Coelops frithii* and the rhinonycterid *Triaenops persicus* (Fig. III-32). The homology of this foramen across Rhinolophidae makes few doubts, while its homology across Rhinolophoidea (i.e., with rhinonycterids and hipposiderids) is more uncertain. Further work is needed to identify properly these three unknown foramina and their soft-tissue correlates, and to see if they may be homologous for all rhinolophoids or not. Especially, the third unknown foramen, present in all rhinolophids, may characterize this family and is of strong interest.

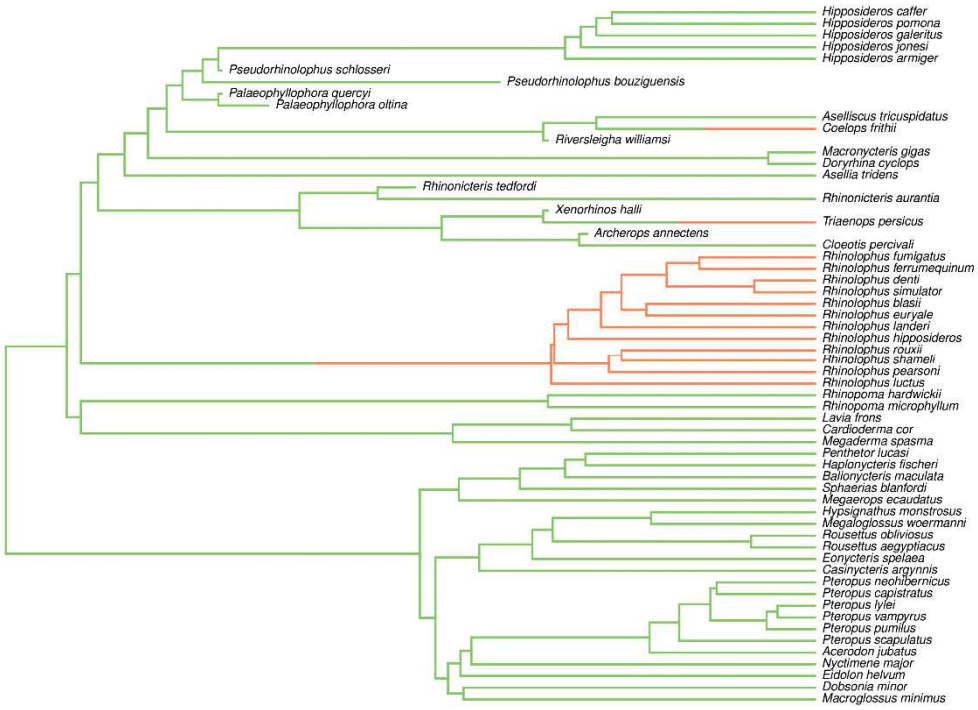

Figure III-32: Discrete mapping of character 66 regarding the presence (orange) or absence (green) of an unknown foramen #2. This stands for the phylogeny with *Palaeophyllophora* as sister-genus to *Hipposideros*. Other cases are figured in Appendix III-6-7.

Other foramina whose homology has been tentatively established at the Yinpterochiroptera scale regard the entrance point of the internal carotid artery into the skull (after sending off the stapedial artery) through a carotid foramen: there may be a carotid canal, with a point of entrance into the skull (which is not visible on an endocast) and a point of entrance into the endocranial cavity (the “anterior”

carotid foramen), or there may be a single entrance foramen (the “posterior”, classical, carotid foramen). There are taxa with an anterior carotid foramen in every sampled yinpterochiropteran family (Appendix III-8-67), but this does not seem to occur often enough to be a large-scaled shared condition: only megadermatids and other lower level clades (*Hipposideros* sensu stricto, *Archerops* + *Cloeotis*, *Riversleigha* + *Aselliscus* + *Coelops*) show a present anterior carotid foramen as being a synapomorphy. The continuous values reconstructed (Appendix III-9-67) show that the pteropodid and rhinolophid nodes do not have values strictly assessing an absence of that foramen, but that is all regarding the “deep nodes”: other ancient nodes are reconstructed without that foramen with more strength. On the other side, the presence of a posterior carotid foramen is synapomorphic for both the Pteropodidae (only four pteropodid species have an anterior rather than a posterior carotid foramen) and the Rhinopomatidae (Fig. III-33). In my sample, there are no other occurrences of that foramen outside these families. Across taxa showing either the anterior or the posterior carotid foramen, the presence of a carotid sulcus just anteriorly to the carotid foramen (no matter which one) is synapomorphic for pteropodids and for megadermatids (these families having as synapomorphy one or the other carotid foramen to be present); such a sulcus is absent in all other rhinolophoid families (Appendix III-8-69). This character correlates well with size (Fig. III-22, Appendix III-2, Table 1). Of these three distributions, some conclusions can be drawn. First, all pteropodid species exhibit a carotid foramen, mostly a posterior one, some species exhibiting an anterior one. As for previous characters, a specific work on a larger sample of pteropodids is needed to better understand that variation. Second, only pteropodids and megadermatids show a carotid sulcus, which can be due to their large size; though maybe not that intuitive, it has to be further explored why the larger size is associated with present and/or more pronounced structures (e.g., see the cases of the posterior extension of the sylvia, or of the presence of a superior sagittal sinus cast). Third, a dedicated work dealing with the internal carotid artery entrance into the skull is needed at the whole Yinpterochiroptera scale, at least, in order to better identify the various structures involved, and to properly assess which ones can be identified on an endocranial cast.

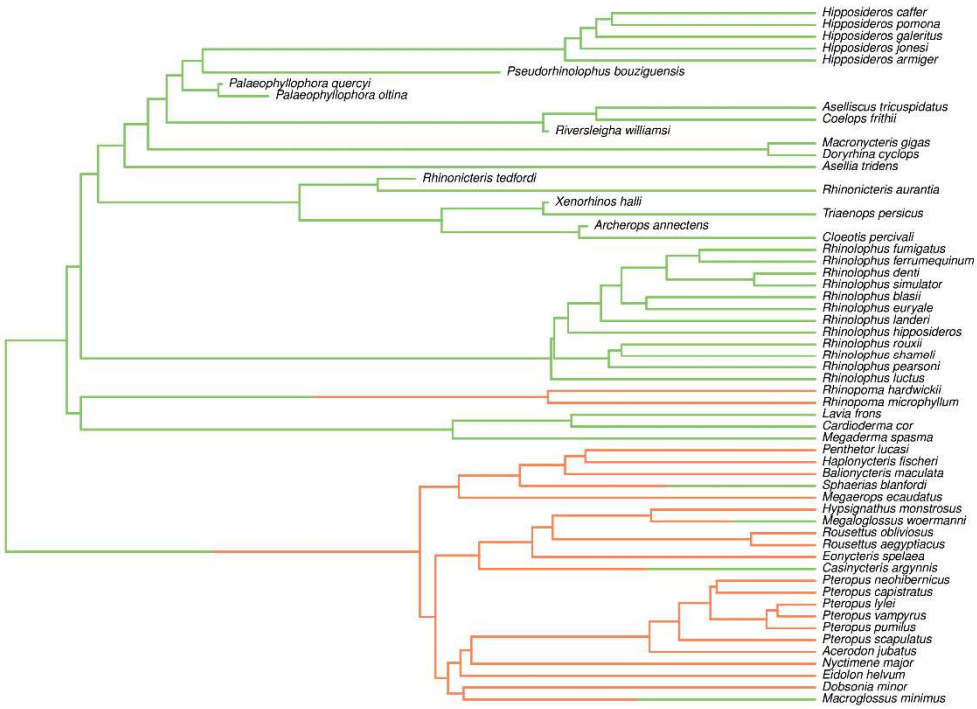

Figure III-33: Discrete mapping of character 68 regarding the presence (orange) or absence (green) of a posterior carotid foramen cast. This stands for the phylogeny with *Palaeophyllophora* as sister-genus to *Hipposideros*. Other cases are figured in Appendix III-6-8.

III.2.E) General morphological evolution across taxa (Figs. III-23,26)

The variation in the number of morphological changes is broad, with more extreme cases at nodes than at tips. Particularly, numerous changes occur at nodes of familial and subfamilial levels, but there are also many terminal taxa showing several morphological changes, within each family. This may indicate that the endocast morphology characterizes subfamilies/families, considering a subordinal morphological variation, which is a quite accurate level. A tip-level morphological variation, which can be here considered as noise, still persists and highlights that endocasts show a general familial to subfamilial conformation together with non-negligible specificities. On one hand, the average absolute evolutionary rates indicate the average evolutionary variation, no matter its direction (towards low or high values, that are states here), and thus inform about the morphological versatility; on the other hand, low average absolute evolutionary evolutionary rates indicate taxa that went through a general morphological stasis. The observations drawn using the number of morphological changes stand by taking into account the average absolute rates: generally, taxa with numerous morphological changes also have a high average absolute evolutionary rate. A noteworthy exception to this regards is the Rhinolophoidea node: few morphological changes are reconstructed at that node, but the average absolute rate is as high as for some other family-level nodes, indicating that there were events at that node. One can suppose that the changes, if they were not enough to change state, were at least frequent and of enough importance. This is not really surprising since its sister taxon is the family Pteropodidae, that underwent several morphological changes of importance: there is an obvious contrast between pteropodid and rhinolophoid morphology.

The endocast morphology generally characterizes high to medium levels of the phylogeny (from the suborder to the subfamily), where morphological conformations can be drawn. Still, noise remains at smaller levels of the phylogeny, highlighting consequent variation in individual lineages. The latter point emphasizes the importance and the interest of dealing with the endocranial morphology at finer levels, with more exhaustive samples: a familial endocast blueprint would not impede the study of endocranial morphological variation at finer phylogenetical level. Deciphering the phylogenetical signal at the tribal and generic level (and, potentially, its variation between families) clearly is of major interest in yinpterochiropteran bats, as soon as an adequate sampling effort is done. Hereafter, I try to characterize suprafamilial to familial nodes, and to provide first steps into the morphological evolution in each family.

III.2.E.a) Early steps of evolution of the endocast: root and rhinolophoids (all, “true”, and “other”)

The superfamily Rhinolophoidea dichotomizes in two clades that each contain three families: the "true" rhinolophoids are the rhinolophids, the rhinonycterids, and the hipposiderids, while the “other” rhinolophoids are the megadermatids, the rhinopomatids, and the craseonycterids (a single specific family not documented here). According to various molecular clock dates (e.g., Teeling et al. 2005, Shi & Rabosky 2015, Amador et al. 2018), congruent with those I find on my sample, the split between these families took place in the beginning of the middle Eocene (~45 Mya). However, the crown diversification of all families (with the exception of rhinonycterids) took place more recently: megadermatids and rhinopomatids diversified around the Paleogene/Neogene boundary (Teeling et al. 2005, Shi & Rabosky 2015, Foley et al. 2015, 2017, Amador et al. 2018), and rhinolophids and the speciose *Hipposideros* genus diversified during the middle Miocene (~15 Mya; Dool et al. 2016, Amador et al. 2018). This means that there is a considerable time gap between the moment when the family originated from the others and the onset of the crown diversification of that family. While the history of each family will be depicted in

the next paragraphs, I will first emphasize on the very first (and short) steps of rhinolophoid diversification, when the rhinolophoid subclades differentiated during the early middle Eocene.

Looking at the reconstructed morphology for the root (i.e., for the whole suborder) and for all, “true”, and “other” rhinolophoids nodes, only few differences distinguish these four clades (Fig. III-26). The ancestral reconstruction for the Yinpterochiroptera in fact strikingly resembles that of rhinolophoids, way more than that of megabats (the sister-taxon to rhinolophoids). The only difference between the estimated ancestral morphologies of Yinpterochiroptera and of Rhinolophoidea (Fig. III-27-A) regards the dorsoventral position of the orbitotemporal canal; there may also be difference regarding the completeness of the transverse sinus cast, but there is an uncertainty for the Rhinolophoidea reconstruction, and some uncertainty at the root regarding the cervical flexure and the width of the piriform lobes (rhinolophoids and pteropodids showing opposite conditions on these points). There are much more striking differences between the Yinpterochiroptera and the Pteropodidae estimated morphologies (Fig. III-27-B) regarding both the general brain organization (covering of the mesencephalic tectum, relative proportions of cerebrum vs cerebellum, number of cerebral and cerebellar foldings, basicranial foramina organization, blood structure casts prominence) and more subtle changes (carotid foramina organization, paraflocculare folding, bundle-like aperture of the olfactory bulbs, size of the sphenorbital fissure). Indeed, all these changes are likely to be linked to the drastic ecological specificities of pteropodids among bats (e.g., relying on vision rather than on audition, fruit and associated floral structures diet, large size; e.g., Baron et al. 1996). While some of these changes can be related to endocranial morphology (e.g., absence of echolocation and hidden mesencephalic tectum, and especially hidden caudal colliculi), it would be largely hazardous to go further. These morphological changes, and their functional consequences, should first be investigated in order to precisely relate morphology, function, and ecology (which has not been done yet).

Pteropodids have significantly higher absolute evolutionary rate slopes than rhinolophoids (Fig. III-24, Appendix III-2, Table 4), meaning that their absolute evolutionary rates increase more with time, with more and more state changes. Rates of evolution are not particularly different between deep rhinolophoid nodes; the only difference is that “true” rhinolophoids absolute evolutionary rates are a bit higher than those of “other” rhinolophoids, meaning that the rates are higher in “true” rhinolophoids (on average), and thus they are generally more likely to state changes (irrespective of time). In general, there are high absolute average rates at the onset of pteropodids and rhinolophoids, associated with numerous morphological differences (as also seen with their reconstructed ancestral morphology), followed by few differences. In rhinolophoids especially, the “true” and “other” rhinolophoid nodes (but also the hipposiderids + rhinonycterids node) are neither associated with high absolute rates nor with high number of morphological changes. A hypothesis explaining this would be that all families also underwent substantial morphological modifications through time, and that the absence of a fossil record deprives one from an accurate estimate of ancestral morphology. In that sense, the fact that the most ancient fossils of the sample are hipposiderid species directly impacts the deep rhinolophoid node reconstructions, that all resemble each other but also these hipposiderid fossils.

III.2.E.b) Megabat endocranial morphology, with the particular case of the highly derived pteropodines

As previously said, pteropodids generally highly differ from rhinolophoids (Figs. III-26,27-A,B). Morphological diversity within Pteropodidae is substantial, but does not follow intra-familial relationships.

The only node with a noticeable number of morphological changes, and a high average absolute rate (Fig. III-23), is that of pteropodines, with the genera *Pteropus* and *Acerodon*. With 15 morphological changes, it is clear that pteropodines morphologically diverge from other pteropodids. Within this subfamily, all species are close morphologically, with one to seven changes on terminal branches, and three changes alone on the latest *Pteropus* nodes (regrouping *P. lylei*, *P. vampyrus*, and *P. pumilus*). Comparatively, sister subfamilies to pteropodines (Nyctimeninae, Eidolinae, Macroglossusinae) show numerous specific changes, but no changes at nodes; and therefore, endocast characters carry a poor phylogenetic signal in this clade.

Among the two other main pteropodid clades (Rousettinae and Cynopterinae), there also is weak morphological support to the deepest nodes, and small support to more recent ones, the most changes occurring along terminal branches. There are still several morphological changes at the onset of the genus *Rousettus*, but a single change for each of the two sampled species. *Rousettus aegyptiacus*, the only echolocating pteropodid bat, shows here no particular morphology compared to its sister taxon. Its peculiar ecology is thus not visible on its endocast morphology.

As represented on the Fig. III-23, there is a high average absolute rate of evolution at the onset of pteropodids, meaning that they initially diverge considerably compared to rhinolophoids. Then, absolute rates are small, and increase progressively through time until present. This is confirmed by the pairwise comparisons of aggregated rate trend slopes through time: pteropodids have a higher slope than the rhinolophoids and their subclades (Fig. III-24, Appendix III-2, Table 4), but it does not reach high absolute rate values among yinpterochiropterans, as their average absolute rates do not differ from that of rhinolophoids (Fig. III-25, Appendix III-2, Table 4).

In general, and with the exception of pteropodines, there is weak support of endocranial morphology to the deep nodes of the pteropodid family. A large part of the morphological changes occur along terminal branches. However, the fact that the two species of *Rousettus* strikingly resemble each other and may indicate that the morphological disparity is present above the intra-generic level. The genus *Pteropus* is quite speciose among pteropodids, but the species sampled here do not differ much, at least less than other pteropodid genera. Based on an enlarged pteropodid sample, it would be worth investigating the precise phylogenetic level(s) where the most morphological variation occurs. Focusing on a subfamily, like that of cynopterines (where some nodes show few, but still some, morphological changes), and compare to other subfamilies, would be of interest. Similarly, within pteropodids, very long branches resulting from small sampling obscure known diversifications, like in the subfamilies closely related to pteropodines. Finally, different phylogenetic hypotheses should also be taken into account to verify if the endocranial morphology may support one or the other of the variously proposed relationships between pteropodid subfamilies.

III.2.E.c) Contrasting the "other" rhinolophoids: endocranial morphology of megadermatids and rhinopomatids

Rhinopomatids and megadermatids do not look alike regarding their endocranial morphology (Fig. III-27-C). Several differences distinguish them, the most striking being the shape of the vermis (long and slender in megadermatids, short and wide in rhinopomatids), the exposure of rostral colliculi in rhinopomatids, the more folded cerebrum and cerebellum in megadermatids, and the different basicranial foramen pattern. Without surprise, a high number of morphological changes characterizes each family (23 or 25 changes in rhinopomatids, 28 or 30 in megadermatids, both cases depending on the position of *Palaeophyllophora* in hipposiderids) and these familial nodes have high average absolute evolutionary rates (Fig. III-23). In each family, there are then different evolutionary scenarios.

The rhinopomatid family is less diversified, with only three species pertaining to a single genus (which though diversified during the late early Miocene, ~ 17 Mya), and the two sampled species do not differ much in endocranial morphology. There are thus low absolute rates along the terminal rhinopomatid branches, after their clear differentiation from the megadermatids. In that way, the absolute evolutionary rate slopes are low in general within rhinopomatids, especially lower than those of the whole "other" rhinolophoids clade (Fig. III-24, Appendix III-2, Table 4), as well as the average absolute rates, at least lower than those of the whole Rhinolophoidea superfamily (Fig. III-25, Appendix III-2, Table 4).

Megadermatids are a bit more diversified than rhinopomatids, with six recognized species pertaining to six genera (some of them also having fossil species). In a different way than for rhinopomatids, megadermatid species sampled here further differ substantially after the Megadermatidae differentiation. The single internal node of my megadermatid subtree yields a single morphological change, and species all have either five (*Lavia*, *Megaderma*) or ten (*Cardioderma*) specific changes (Fig. III-23). In that way, average absolute rates do not decrease that much after the family onset. Absolute evolutionary rates do not really differ from those of the rest of the tree, either in the slope of their temporal trend or in their average value (Figs. III-24,25, Appendix III-2, Table 4).

The rhinopomatid fossil record is quite scarce, therefore more extant taxa would be worth studing, but only one additional extant species exists that could bring further information. Megadermatids, however, have a richer diversity, and more recognized fossil species. It is also quite interesting to note that rhinopomatids and megadermatids crown group ages are comparable (with ~5 My of difference), but there is quite more morphological variation between megadermatid genera than between rhinopomatid species. There is thus, like in pteropodids, an inter-generic rather than an inter-specific morphological variation, and this does not seem to depend on the stratigraphic age of the corresponding taxa. Moreover, megadermatids could be related to the enigmatic family Necromantidae, a single-genus family endemic from the Quercy Phosphorites formation containing three species. Skulls of *Necromantis* have been described and illustrated in the literature (e.g., Revilliod 1920), and both families have been brought together (e.g., Hand et al. 2012), but this has never been formally tested (actually, Megadermatidae is the extant bat family that least differ to necromantids, rather than resembling them). Finally, adding an endocast of *Craseonycteris thonglongyai* could also orient the reconstruction at the "other" rhinolophoids node, or bring a third morphological conformation in that clade.

III.2.E.d) Endocranial morphology of rhinolophids: the genus Rhinolophus

The Rhinolophidae family diverges the first in the "true" rhinolophoids clade, and is nowadays represented by the single (but very speciose) genus *Rhinolophus*. This genus would have diversified in the late early Miocene (around 17 Mya, as for the genus *Rhinopoma*). Some extinct radiations are however known, such as the genera *Vaylatsia* from the Quercy Phosphorites (Maitre 2014) or *Protorhinolophus* from China (Ravel et al. 2016), but no fossil skulls have been documented yet. Thus, the only picture of endocranial evolution of this family relies on its crown group, and a half to two-thirds of the evolutionary history of this family is unavailable. During these ~30 My, several morphological changes occurred and contributed to establish a *Rhinolophus* conformation of the endocast: 22 or 23 (depending on the position of *Palaeophyllophora*) morphological changes distinguish the rhinolophid endocast from the "true" rhinolophoid one, with a high average absolute evolutionary rate at the rhinolophid node (Fig. III-23).

The comparison between the ancestral reconstructions of rhinolophids and of "true" rhinolophoids (Fig. III-27-D) shows numerous differences that are however subtler than in previous comparisons. Some main differences allow a quick characterization of rhinolophids, such as the more dorsally located and more pinched orbitotemporal canal, the double windowed paraflocculi, the small size of the hypophysis cast, or the presence of an unknown foramen #3. There are other differences on every aspects of the endocasts, but they are less striking than in "other" rhinolophoids families for instance. Further documentation of the long branch before the diversification of crown rhinolophids would, for sure, help constraining this fine pattern of endocranial transformation.

In rhinolophids, two main phases of the evolutionary history of endocast morphology can be identified (Fig. III-23). A first phase regards Asian basal rhinolophids, up to the European *Rhinolophus hipposideros*, which all have several specific morphological changes (seven to sixteen). Then is a second phase, for the African clade of rhinolophids, with quite fewer morphological changes (one to seven). In the whole family, there are very few morphological changes occurring at nodes (five changes, ten nodes), while the overwhelming majority of changes occur at terminal branches. However, African rhinolophids seem to be more morphologically constrained than Eurasian ones (the European form being at the boundary between the two phases). This difference between Asian and African species could also be explained by the branch lengths, the African diversification being much more recent than the Asian one. In this sense, the pteropodine diversification is grossly of similar age, and the number of specific morphological changes are comparable in pteropodines and in Asian rhinolophids. Average absolute rates quickly decrease in the deepest rhinolophid nodes, and then increase again for all terminal branches. Rate values and trend slopes are similar to those of the rest of the tree (Figs. III-24,25, Appendix III-2, Table 4), and the evolution of characters (and their changes) in that clade is not strikingly different from the rest of the tree.

Like in pteropodids, there is an onset of the rhinolophid conformation, and then specific changes - the difference being that, in rhinolophids, all species belong to the same genus. However, like in pteropodids, there are conflictual hypotheses regarding the relationships between rhinolophid major clades (Asian, African, European), but also regarding the monophyly of Asian rhinolophids (in the considered hypothesis here, the Asian *Rhinolophus luctus* is basal to the other Asian species). Thus, testing other hypotheses with more details may lead to different results, with potential implications beyond major rhinolophid clades.

III.2.E.e) The contrasted endocranial morphology evolution among rhinonycterid "lineages"

The Rhinonycteridae clade has very recently been raised to the familial rank, rhinonycterids previously being a subtribe of hipposiderids (Foley et al. 2015). It is a little diversified family nowadays (four genera, nine species), but with a rich extinct diversity, comparable to the extant one (six genera among which four extinct, eight species; Wilson et al. 2016, Brown et al. 2019). It also appears that the three extant rhinonycterid species sampled here constitute three "lineages", each having "its" closely-related fossil species.

As for the other families, an important number of morphological changes characterize the family (Fig. III-23), but there are as much changes for the next, intrafamilial, internal node and for the *Archerops* + *Cloeotis* node. Fossil species are generally slightly younger than their pertaining node (that of the "lineage" they belong), having few specific changes. Extant species, on the other hand, underwent more changes. Counterintuitively, there is a reverse proportionality between the number of specific changes of these extant species and the length of their terminal branch: the *Rhinonicteris* node is the oldest terminal node and *Rhinonicteris aurantia* differs the fewest from its fossil sister-species with only eight changes, while *Triaenops* and *Cloeotis* differ by more than fifteen changes. Average absolute evolutionary rates follow this trend, and only terminal *Rhinonicteris* branches tend to relatively low values (though even lower values are easy to find elsewhere in the tree), whereas all other taxa have high values. In this way, rhinonycterids do not have particularly high values of absolute rate trend slopes (Fig. III-24, Appendix III-2, Table 4), but they have high average absolute rate values (Fig. III-25, Appendix III-2, Table 4).

Rhinonycteridae is a quite versatile family, with strong and marked differences between lineages. There are fewer differences between the *Rhinonicteris* species, belonging to the same genus, than in the two other lineages. The clade containing these two lineages is morphologically quite different from *Rhinonicteris*, and the *Archerops* + *Cloeotis* lineage also strongly differs from the *Xenorhinos* + *Triaenops* one. Some morphological changes occur at the onset of the latter lineage, with three morphological changes; it is quite less than the other cases of this family, but this is still high compared to the previously described families - this lineage simply differs less dramatically. The *Archerops* + *Cloeotis* lineage is the more diverging of the three, but the extant species (*Cloeotis percivali*) also differs the most from its fossil sister-taxon (*Archerops annectens*) of the three lineages. Here, and in contrast to the other previously described families, there is a chaotic variation of endocranial morphology for almost all taxa, which is as difficult to explain as the cases of specific-only variation. All fossil species have been found in the Riversleigh Formation, in Australia, thus no geographic separation and local adaptations may be related to the between-lineages variation. Similarly, these lineages do not differ that much in their ecology - and even if they had differed, the only link would be in the fact that changes in morphology would accompany changes in ecology, not much more. Documenting the last extant genus (*Paratriaenops*) and some more extant species should be achievable, as well as integrating some other fossil species for which skulls have been found and described (e.g., *Brachipposideros* in Hand 1993, 1997, and *Brevipalatus* in Hand & Archer 2005). More thorough and extensive analyses in this family may help to disentangle all this morphological variation.

Rhinonycterids also show a quite "extreme" morphology in "true" rhinolophoids in comparison with the reconstructed morphology of that clade (Fig. III-27-E). Particularly, the prominence of the cerebellum is noticeable in this family and is quite unique at the Rhinolophoidea scale. It gets to the point that the mesencephalic tectum is greatly to fully covered, depending on the species. Functional and/or ecological causes for these morphological change should also be investigated, as it tends to parallel to some extent

a pteropodid condition (though, in this family, it is the cerebrum that develops the most and overlaps the mesencephalic tectum).

III.2.E.f) Hipposiderid endocranial morphology evolution

Hipposideridae is a speciose family, with a comparable diversity to that of rhinolophids, both being the two most diversified rhinolophoid families. If most hipposiderid species belong to the genus *Hipposideros*, there are several other extant genera that diverged quite early according to molecular clock dating (e.g., Foley et al. 2015, 2017). The fossil record of this family is particularly rich, with numerous species found in Quercy Phosphorites and Riversleigh formations (e.g., Brown et al. 2019). Here, five fossil species further constrain the evolution of the endocast morphology in different hipposiderid clades: some species as stem *Hipposideros* species (the two *Pseudorhinolophus* species), another (*Riversleigha williamsi*) as a stem of two other genera (*Aselliscus* and *Coelops*), and a genus (*Palaeophyllophora*, with two species) of floating position.

The ancestral reconstructed morphology of the hipposiderid endocast resembles that of the yinpterochiropteran, rhinolophoid, and "true" rhinolophoid reconstruction (Fig. III-27-F): the statistical method used here highly rely on branch lengths as weights for changes, and as the fossil hipposiderid species date from the Eocene to the Miocene, there is a strong constraint on the first nodes of the tree. As also confirmed by Figure III-23, there only is one change at the basal hipposiderid node, being the least differentiated family - by far. Following this node, there are no morphological changes at the other deep nodes of the family; morphological changes occur in the *Palaeophyllophora* genus, for the *Macronycteris* + *Doryrhina* and the *Riversleigha* + *Aselliscus* + *Coelops* clades, and in the *Hipposideros* genus sensu stricto. The following nodes (the *Aselliscus* + *Coelops* node, and the further *Hipposideros* sensu stricto nodes) yield zero or a single morphological change. As a summary, beyond some major nodes establishing the various main hipposiderid clades, the majority of the morphological changes occur along terminal branches. A noteworthy point is that, after the basal *Hipposideros* sensu stricto node where *H. armiger* diverges from the other species, these other species (both from Asia and Africa) generally differ less than in the rest of the family (less than 10 morphological changes along each terminal branch).

Average absolute evolutionary rates follow the distribution of the number of morphological changes, with the exception of the basal nodes of the *Hipposideros* genus sensu lato: absolute rates are particularly high at the nodes where the *Pseudorhinolophus* species diverge, while there are no morphological changes. This may represent changes that may be just not strong enough to result in morphological changes, being precursor modifications to definitive changes occurring along the long branch between the two groups of species. Similarly, absolute rates are higher at the deepest nodes with few to no associated morphological changes, whereas in other parts of the tree, such low number of changes are associated with very low absolute rates (e.g., see in rhinolophids or pteropodids). A similar hypothesis may explain this here: there is basal variation, not enough to make states changes, but just "activating" the morphological versatility that further occur in the family.

In this family, average absolute evolutionary rates are not very low at the onset of the family, there are pulses of rates at various moments depending on the date of the onset of the various hipposiderid clades, and there are generally a high number of morphological changes along terminal branches. It is thus not surprising that trend slopes in Hipposideridae do not differ that much from the rest of the tree (Fig. III-24, Appendix III-2, Table 4). In the same way, one may also expect that hipposiderids stand out compared to the other considered clades regarding the distribution of the average absolute rates (Fig. III-25, Appendix III-2, Table 4), with average rates being significantly higher than five of the eight considered

clades (only absolute rates of “true” rhinolophoids, rhinolophids, and rhinonycterids are not significantly smaller).

A similar summary and similar perspectives to those of rhinonycterids can be drawn regarding hipposiderids, but the sample used here may confirm these a bit more since a richer diversity is considered. Hipposideridae also appears as a quite versatile family regarding the evolution of the endocranial morphology, with morphologically marked clades and marked intergeneric differences. The case of the *Hipposideros* genus is particularly interesting as it has both an extant and an extinct diversity, with recognized fossil subgenera (one of them being represented here: *Pseudorhinolophus*). Hipposiderids may represent a case study for both intra- and intergeneric variation of the endocast morphology. For what may be drawn here, there seems to be a very high intergeneric disparity, whereas further sampling effort may better address the intrageneric variation.

IV) Quantitative evolution

IV.1) Bias of the numeric segmentation vs physical extraction

I extracted all endocranial casts using the same protocol to minimize potential reconstruction biases. I also assess, for my yinpterochiropteran sample, the measurement bias between a digital endocast and a real fresh brain. I first transform endocast volumes into masses using the specific gravity of the chiropteran brain (1.036 mg/mm^3, Baron et al. 1996), then I express the log masses of the brain and olfactory bulbs masses of my chiropteran sample against those also present in the sample of Baron et al. (1996). I only discard *Rhinolophus hipposideros*: the estimated mass is roughly the double of that measured by Baron et al. (1996). I trust the identification of the specimen I scanned and reconstructed, and therefore hypothesize that there may have been a problem with the specimen weighed by Baron et al. (1996). I perform three linear models illustrated by Figure III-34 (but see Appendix III-3, Table 1) using the brain masses, the olfactory bulbs masses, and both. The linear regression with both masses shows the best fit and the lowest p-value; I use the parameters of that model to transform the three variables I use (brain, olfactory bulbs, and paraflocculi log masses).

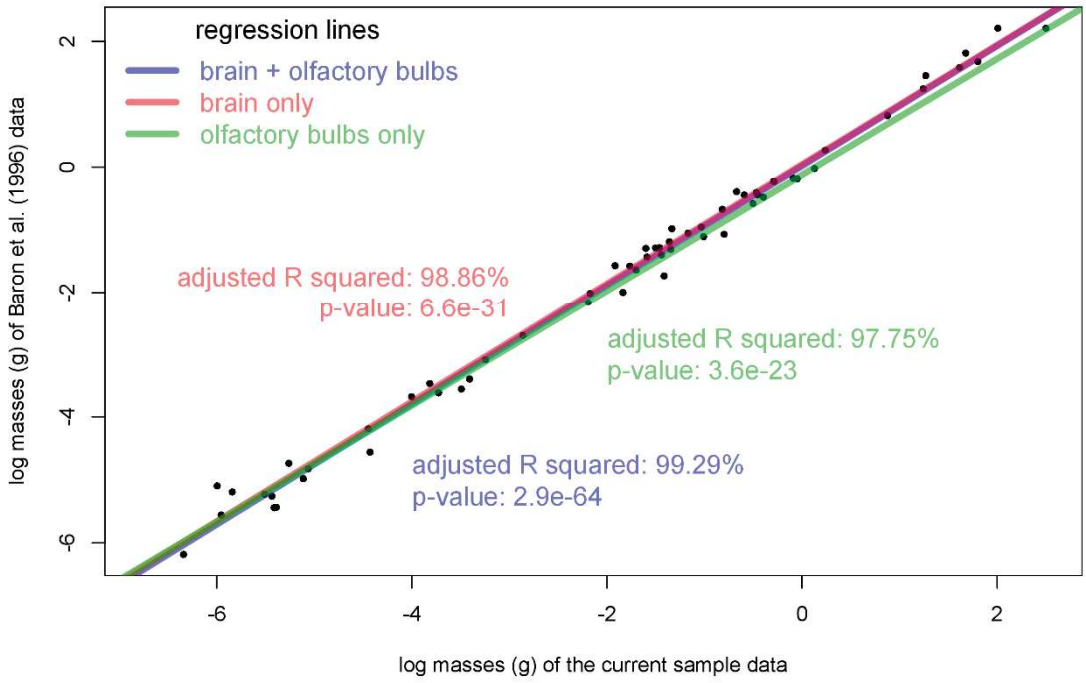

Figure III-34: Numeric extraction bias of endocasts illustrated by comparing log brain and olfactory bulbs masses of yinpterochiropteran species found in both my sample and that of Baron et al. (1996). Regression lines and main statistics depending on which structure is chosen are superimposed to the plot. Notice the higher adjusted R squared and the lower p-value by considering both brain and olfactory bulbs.

IV.2) Total brain mass (Figs. III-35-37)

IV.2.A) Relative brain mass evolution

The brain mass is treated here as the relative brain mass, which is similar to the "encephalization" (see Methods). The distribution of the relative brain mass (Fig. III-35), through residuals of the brain mass relative to the body mass, shows an increase of relative brain mass value from deepest nodes to more apical ones. Of the six families represented here, there is an increase from the root to the node of four families (pteropodids, megadermatids, and rhinolophids whose basal edge switches from negative to positive values, and hipposiderids that undergo such switch along internal nodes), while there is a decrease before the onset of the two other families (rhinopomatids and rhinonycterids). High values are generally found in pteropodids, with several increases but also some decreases (*Hypsignathus monstrosus*, *Pteropus vampyrus*, and the species related to pteropodines, that are *Eidolon helvum*, *Nyctimene major*, and *Acerodon jubatus*). The three megadermatid species all have positive values, the highest one being for *Megaderma spasma*, and in the opposite, the two species of the sister-family Rhinopomatidae both have among the lowest values. In rhinolophids, species show generally slightly positive values, except for *Rhinolophus hipposideros* (with a high relative brain mass) and *Rhinolophus landeri* and *Rhinolophus ferrumequinum* (with respectively low and very low relative brain masses). Patterns are more contrasted in rhinonycterids, where the extant *Rhinonicteris aurantia* and the fossil *Xenorhinos halli* have slightly positive values while the extant *Triaenops persicus* and *Cloeotis percivali* have slightly negative ones and the extinct *Archerops annectens* and *Rhinonicteris tedfordi* have highly negative values. In hipposiderids, grossly, *Hipposideros* species have positive values, with a slightly positive value reconstructed for the node of *Hipposideros* even though only two of the five extant species have high relative brain masses, while other genera have negative values, some being slightly negative (*Hipposideros* [*Pseudorhinolophus*] *schlosseri*, *Aselliscus*, *Doryrhina*, and *Coleops* even have a slightly positive value), and some being highly negative (*Palaeophyllophora*, *Asellia*, *Macronycteris*, *Riversleigha*).

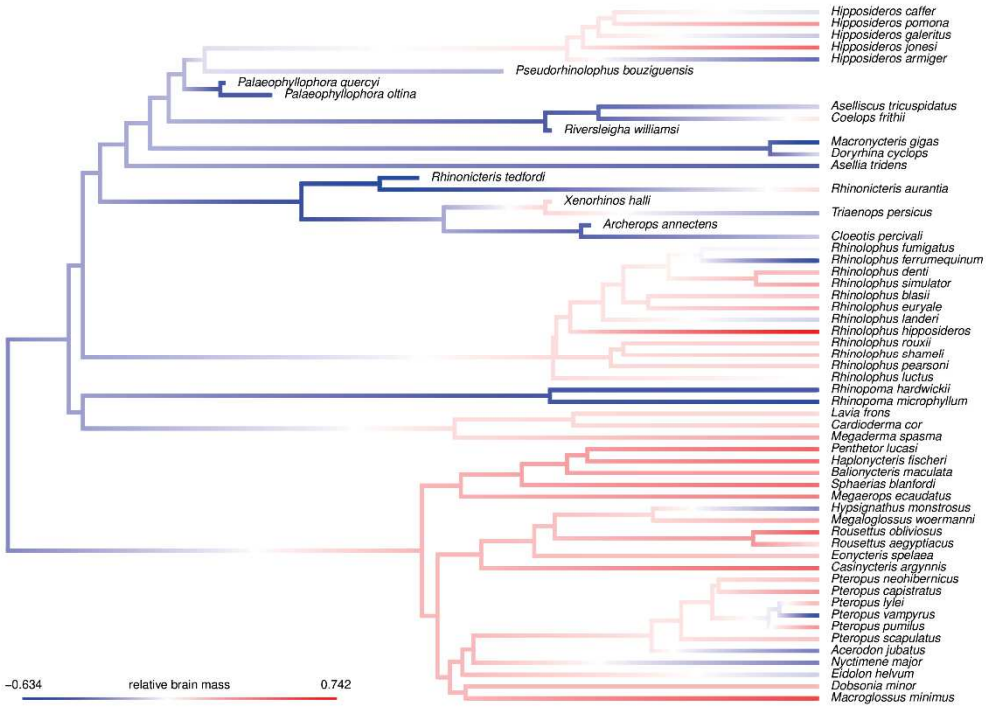

Figure III-35: Mapping of the relative brain mass on the Yinpterochiroptera phylogeny pruned to the sample of this study. This stands for the phylogeny with *Palaeophyllophora* as sister-genus to *Hipposideros*. Other cases are figured in Appendix III-10-1 X.

Evolutionary trends (Fig. III-37; Appendix III-3, Tables 2-4) show a general increase of relative brain mass (p-values at the 10^{-5} to 10^{-6} levels, Appendix III-3, Table 2), with little deviation from the root (~ 0.32 to 0.34 times the standard deviation of relative brain mass values, Appendix III-3, Table 2), but that however does not significantly differ from a Brownian motion regime (p-values between 0.09 and 0.118, Appendix III-3, Table 2). Among major groups (down to the familial level), none shows a clearly different pattern from the general one: there is no decrease of relative brain mass through time in each of these groups, some being very close to a null evolution (especially in rhinopomatids and in pteropodids; Fig. III-37), and some other showing a little steeper slope, representing a slightly accelerated increase of relative brain mass (especially in rhinonycterids; Fig. III-37). Rhinonycterids, but also megadermatids and rhinopomatids, all have a slope that significantly differs from Brownian motion-simulated slopes (Appendix III-3, Table 3). Pairwise comparisons between clades show significant differences between pteropodids and both subclades of rhinolophoids, the latter having a steeper slope through time, and the "true" rhinolophoids slope is steeper than the "other" rhinolophoids one (Appendix III-3, Table 4). Rhinopomatids slope is gentler than that of megadermatids in "other" rhinolophoids, while in "true" rhinolophoids the slope of rhinonycterids is clearly steeper than that of rhinolophids, and a bit even more than that of hipposiderids (Appendix III-3, Table 4). Through the use of estimated marginal means ('emmeans'), pteropodids appear to have a generally higher relative brain mass than rhinolophoids, (p-values at the 10^{-5} level, Appendix III-3, Table 3). 'True' rhinolophoids and three of the five rhinolophoid families (rhinopomatids, rhinonycterids, and hipposiderids) have lower relative brain mass than that of the rest of the yinpterochiropteran tree (p-values around 9.10^{-4}, 4.10^{-4}, 3.10^{-3}, and 3.10^{-3} respectively, Appendix III-3, Table 3) but, except for rhinopomatids, the relative brain mass difference is close to that separating pteropodids and rhinolophoids. Pairwise comparisons further support a difference in relative brain mass between pteropodids and both "true" and "other" rhinolophoids (p-values close to 1.10^{-4} and 0.02 respectively, Appendix III-3, Table 4), with a slightly larger difference with the latter compared to the former (the difference between the two rhinolophoid clades being not significant: p-value of 0.9, Appendix III-3, Table 4). In "other" rhinolophoids, there is a large difference in relative brain mass between megadermatids and rhinopomatids (p-value of 3.10^{-3}, Appendix III-3, Table 4), while in "true" rhinolophoids, only rhinolophids have a larger relative brain mass than the two other families (rhinonycterids and hipposiderids, p-values of 0.01 and 0.03 respectively, Appendix III-3, Table 4), this difference is not significant (p-value close to 0.7, Appendix III-3, Table 4).

IV.2.B) Absolute rates evolution

Absolute rate distribution (Fig. III-36) of relative brain mass also shows a mixed pattern. In all phylogenies, there are numerous taxa and some nodes with highly changing rates. In pteropodids, the basal node of the family has a high absolute rate; this rate is even superior at the basal node of pteropodines, indicating major accelerations of evolution. Within pteropodids, some terminal taxa also show high absolute rates, either in pteropodines (*Pteropus neohibernicus*, *Pteropus pumilus*) or in other subfamilies (*Hypsignathus monstrosus*, *Megaloglossus woermanni*). Cynopterines, to a lesser degree, also have high absolute rates in the deepest nodes of the subfamily. In rhinolophoids, few taxa or nodes show high changing rates. Regarding terminal taxa, high rates occur in rhinolophids (*Rhinolophus luctus*, *Rhinolophus denti*) and hipposiderids (*Palaeophyllophora oltina*, *Macronycteris gigas*, *Doryrhina cyclops*, *Aselliscus tricuspidatus*, and *Hipposideros armiger*). Rhinonycterids demarcate from other families, because all their nodes show high absolute rates, while terminal taxa do not.

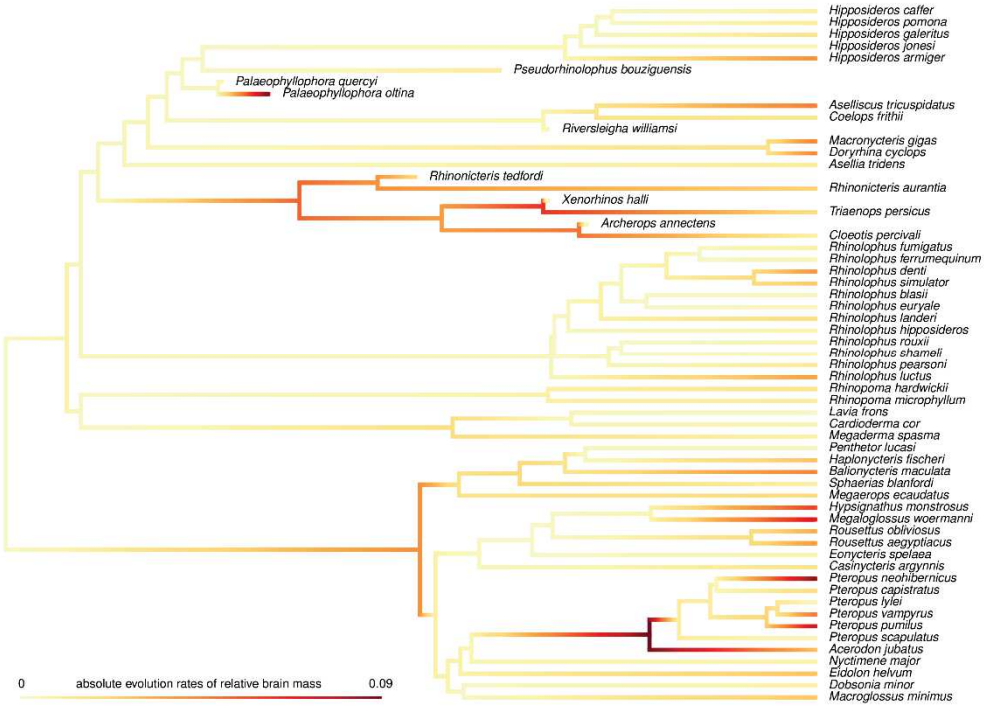

Figure III-36: Mapping of the absolute evolutionary rates of relative brain mass on the Yinpterochiroptera phylogeny pruned to the sample of this study. This stands for the phylogeny with *Palaeophyllophora* as sister-genus to *Hipposideros*. Other cases are figured in Appendix III-10-2.

It appears that absolute rates generally raise through time (Fig. III-37; p-values between the 10^{-5} and the 10^{-6} levels, Appendix III-3, Table 2), meaning that there is a global increase of versatility with time. Even if this general trend increases in range through time four times more than would do a Brownian motion, this difference remains not significant (p-values between 0.29 and 0.46, Appendix III-3, Table 2) and the rate evolution does not differ from a Brownian motion regime. The absolute rate evolution across major clades clearly does not follow, even roughly, the same general trend as for the relative brain mass. Deepest rhinolophoid nodes (all rhinolophoids, “true” and “other” rhinolophoids) have a flatter slope, close to a zero value and lower than the general trend, while pteropodids have a steeper slope, indicating that the slightly raising yinperochiropteran trend of rate changes is mainly driven by pteropodids rather than by rhinolophoids (Fig. III-37). All rhinolophoid families, however, do not show the same general pattern as the superfamily: rhinolophids clearly have increasing absolute rates, with a steeper slope

comparable to that of pteropodids, while rhinonycterids and megadermatids decrease in absolute rate, with a negative slope. These graphical observations are partially supported by pairwise tests of slope differences. Pteropodids differ from whole rhinolophoids with a steeper slope (though the p-values are close to 0.04 and are slightly significant, see Appendix III-3, Table 3), but not from one or the other of the rhinolophoid subclades (p-values close to 0.36 when compared to "other" rhinolophoids, and to 0.11 when compared to "true" rhinolophoids, Appendix III-3, Table 4). In the same way, rhinonycterids slope is clearly lower than that of the rest of the tree (p-values near 0.02, Appendix III-3, Table 3) but neither than that of rhinolophids nor that of hipposiderids (p-values near 0.17 for both, Appendix III-3, Table 4). Other noteworthy results are the very high non-significance of the difference of the absolute rates trend of rhinopomatids compared to the rest of the tree (p-values over 0.99, Appendix III-3, Table 3), as well as the very low difference between both rhinolophoid subclades slopes (p-values over 0.999, Appendix III-3, Table 4). Rhinolophids and rhinonycterids further differ in their absolute rate emmeans for the rest of the tree (p-values near 0.01 and 0.02 respectively, Appendix III-3, Table 3), the rhinonycterids having quite high absolute rates while the rhinolophids have quite low ones (p-values of the difference between both group slopes close to 9.10^{-3}, Appendix III-3, Table 4). A comparison of average absolute rates within versus outside clades highlights three major shifts (Appendix III-3, Table 5). Two of them are increases of absolute rates and are located in the pteropodid families: the nodes from the pteropodid family down to the clade Pteropodinae + *Nyctimene major* have significantly higher absolute rates, as well as the Rousettinae node (the clade with the two *Rousettus* species, *Megaloglossus woermanni*, and *Hypsignathus monstrosus*). The third one is a decrease of absolute rates and regards the two first nodes of the Rhinolophidae, the p-value of the second being slightly lower (p-value up to 0.0045) than the first (p-value up to 0.0081).

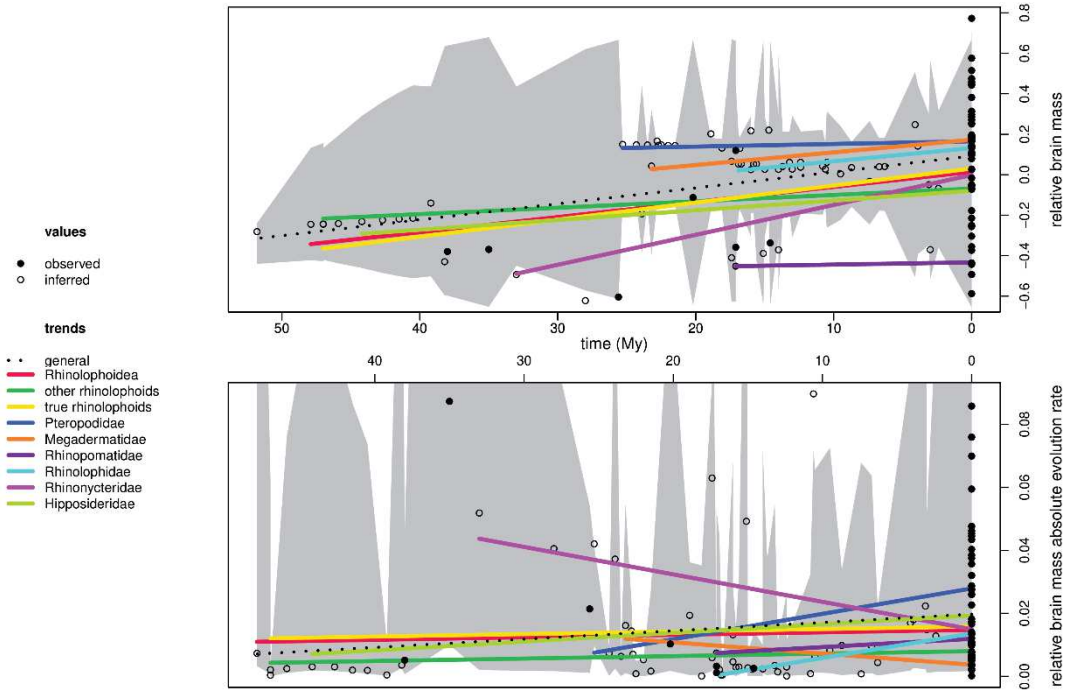

Figure III-37: Temporal trends of relative brain mass (top) and of its absolute evolutionary rates (bottom). The gray background illustrates a simulated variation under a Brownian motion regime. This stands for the phylogeny with *Palaeophyllophora* as sister-genus to *Hipposideros*. Other cases are figured in Appendix III-10-3.

IV.2.C) Group by group evolution

There is a general increase in relative brain mass through time in Yinpterochiroptera (Figs. III-35,37; Appendix III-3, Table 2): a negative relative brain mass is reconstructed as the ancestral condition of the suborder, then is a general increase from the root to the node of most families (pteropodids, megadermatids, rhinolophids, and hipposiderids) and two secondary decreases (before rhinopomatids and rhinonycterids). There are however different patterns depending on the families (see below), and also a mixed pattern of rate variation (Fig. III-36): there are few, but important major variations in rates, together with numerous terminal variations. Together with a general increase in relative brain mass, there is a general increase of absolute rates of brain mass (Fig. III-37), which however may mainly be due to that of pteropodids (whereas the slope of rhinolophoids is flatter). Still, this indicates that yinpterochiropteran taxa in general tend more and more to change in brain mass and to increase in relative brain mass through time; both these global increases however do not differ from a Brownian motion regime (Appendix III-3, Table 2).

There is an increase of the relative brain mass from the root to the megachiropteran node, with an ancestral high (positive) relative brain mass for this family (Fig. III-35). Concurrently is a high absolute evolutionary rate of relative brain mass at the family node (Fig. III-36). Within the family, there are no major changes (no temporal trend with a flatter slope than that of rhinolophoids; Fig. III-37, Appendix III-3, Tables 3-4): despite few taxa decrease towards negative values (Fig. III-35), all pteropodids in average share a high relative brain mass, higher than rhinolophoids (Appendix III-3, Table 4). There are, however, several rate changes across pteropodids. Regarding internal nodes, a major rate change occurs at the Pteropodinae node, while a slighter one occurs at the Cynopterinae node. There are, in addition, some taxa with specific rate accelerations, such as rousettine genera (*Rousettus*, *Hypsignathus*, *Megaloglossus*) or other isolated species in the other subfamilies. All these accelerations, occurring at different times, make the absolute rates trend to increase through time (Fig. III-37), the slope being steeper than all other (significantly steeper than for all other rhinolophoids; Appendix III-3, Table 3), and likely driving the whole Yinpterochiroptera slope, that is steeper than that of rhinolophoids. Average absolute rates however do not demarcate from those of rhinolophoids (Appendix III-3, Tables 3-4). The pteropodid to Pteropodinae + Nyctimeninae nodes show significant shifts in rate evolution regime, towards increased rates, enhancing relative brain mass variation (Appendix III-3, Table 5). The Rousettinae node also stands out in the same way. Regarding the former case, this result may be due to the high nodal values for rates at the Pteropodidae and Pteropodinae nodes (Fig. III-36). The latter observation helps interpreting the location of the significant shifts: there may be in fact two shifts, one at the onset of the family Pteropodidae, and another one close to the onset of the subfamily Pteropodinae (i.e., maybe including sister-subfamilies). The brain mass is here expressed relative to body mass, showing the brain mass independently from an allometric relationship. Still, this does not impede finding a variation in relative brain mass to be linked to the body mass, and this seems to be the case here. Indeed, pteropodids are larger bats than rhinolophoids, and pteropodines are larger bats than other pteropodids (e.g., Moyers-Arévalo et al. 2020). To find shifts in relative brain mass variation at those nodes may imply a further link between brain mass variation and body mass, independent from the allometric link between brain mass value and body mass. In the Rousettinae case, the shift found at the subfamily node can be due to convergent high tip values for these rates (the Rousettinae node having a low absolute rate value, Fig. III-36). Indeed, there are variation of the four concerned species in their relative brain mass, both towards negative and positive values. These changes in relative brain mass do not seem to yield any phylogenetic signal, and so do the absolute rates; the fact that the relative brain mass variation becomes more chaotic however seems to

characterize that clade, yielding a significant shift in rate regime at the subfamilial node.

As described previously, there is a mixed pattern of relative brain evolution before the onset of the rhinolophoid families: during the early first steps of rhinolophid differentiation, there are both increases (before megadermatids, rhinolophids, hipposiderids) and decreases (before rhinopomatids, rhinonycterids) of relative brain mass (Fig. III-35). However, once family-level diversification is achieved, none tends to decrease through time (Fig. III-37), even if patterns still differ. Both "true" and "other" rhinolophoids general slopes are steeper than that of pteropodids (Appendix III-3, Table 4): the relative brain mass is high in value in all pteropodids, and seems to vary in both ways then, while relative brain mass increases before and within each family (maybe with the exception of rhinopomatids). In addition, the slope of "true" rhinolophoids is significantly steeper than that of "other" rhinolophoids (Appendix III-3, Table 4); this is probably due to the rhinopomatid trend, which seems close to a null evolution. Concurrently, the average relative brain mass of "true" rhinolophoids seems higher than that of "other" rhinolophoids, but this difference is slightly not significant. Deep rhinolophoid node rates of evolution of relative brain mass, however, do not show any particular burst: only rhinonycterids show a burst in absolute rates comparable to that of pteropodids (Fig. III-36). Most of the variation occurs in "true" rhinolophoids, at nodes regarding rhinonycterids, and at few tips regarding hipposiderids and rhinolophids. Absolute rates evolution through time is quite flat for deep rhinolophoid nodes the slight increases observed are due to the previously quoted punctual bursts (Fig. III-37). Deep rhinolophoid slopes do not increase enough to distinguish individual trends among rhinolophoid clades (Appendix III-3, Table 4), but still increase enough to prevent supporting a significant difference with pteropodids (Appendix III-3, Table 3). As it can be expected at this high phylogenetic scale, average absolute rates do not demarcate from the rest of the tree (Appendix III-3, Table 3), nor from pteropodids (Appendix III-3, Table 4). There are thus drastic changes between deep rhinolophoid nodes, when familial differentiation occurs, but the familial differences do not seem to follow the phylogenetic relationships (Fig. III-35): in both main rhinolophoid subclades, there are both increases and decreases of relative brain mass. Moreover, after setting that change, there are no changes of comparable magnitude to those occurring before the onset of the families. This picture, drawn using the mapping of the relative brain mass only, needs to be appreciated with caution, due to the long branches before the diversification of three of the five rhinolophoid families (rhinolophids, rhinopomatids, and megadermatids). This is particularly well illustrated considering absolute rates, that represent these changes in relative brain mass (Fig. III-36): the high changes in relative brain mass for the three previously quoted families actually occur over a long time before each familial diversification, with low rates of evolution. This emphasizes the key role of fossil occurrences, that help calibrating the evolution of such variables (and its evolution rates), but this also prevents from drawing too hasty conclusions. There are major changes in rhinolophoid deep nodes leading to familial nodes, but these changes seem to not be driven by phylogenetic relationships, and they took place over a long time span (without "shifts" or "bursts" for families for which it looks like, such as megadermatids, rhinopomatids, or rhinolophids).

"Other" rhinolophoids comprise two highly different families: the "basal" rhinopomatids (small-sized insectivorous bats traditionally considered as plesiomorphic; e.g., Baron et al. 1996, Hulva et al. 2007) and "false vampires" megadermatids (medium-sized carnivorous bats). Regarding the relative brain mass, each of these families show clear, marked, and opposed tendencies (Fig. III-35). Megadermatids have a high, positive, relative brain mass, while rhinopomatids have a low, negative, one; both families significantly differ in average relative brain mass (Appendix III-3, Table 4). Megadermatids also more increased in relative brain mass through time (Fig. III-37, Appendix III-3, Table 4). Trends of both families

are so distinct from each other that they also both differ from a Brownian motion regime (Appendix III-3, Table 3) and from the general trend (megadermatids slope being steeper than the general one, while rhinopomatids slope is flatter, closer to a null evolution; Fig. III-37). Though spectacular, the onset of very negative values in rhinopomatids and very positive values in megadermatids from an intermediate reconstructed "other" rhinolophoids ancestor took place over a long time (over 20 My) and absolute evolution rates are low, though that of megadermatids is a bit higher than that of rhinopomatids (Fig. III-36). Absolute rates evolution in each family is however a bit different: it slightly rises in rhinopomatids (closely paralleling the general trend; Appendix III-3, Table 3), while it decreases in megadermatids. However, the difference between these slopes is not marked enough to assess that they differ (Appendix III-3, Table 4). The only difference between the two "other" rhinolophoid families regards the relative brain mass value (Fig. III-35): rhinopomatids have smaller relative brain masses than megadermatids. The variation and the evolution of that trait do not differ between these two taxa: both the absolute rates (Fig. III-36) and the temporal trends (Fig. III-37) are similar.

The "true" rhinolophoids clade comprises three families: rhinolophids, rhinonycterids, and hipposiderids. All these families have their own evolution of relative brain mass (Fig. III-35). Rhinolophids have slightly positive values of relative brain mass (with the exception of two species that have negative values), whereas negative values are more common in hipposiderids and in rhinonycterids (Appendix III-3, Table 4). In these two families, however, the evolution pattern of relative brain mass is far from straightforward, with numerous reversions or convergences: rhinonycterid species mostly have negative relative brain mass (only *Xenorhinos halli* and *Rhinonicteris aurantia* have slightly positive relative brain masses) with a wide array of ancestral reconstructions, while in hipposiderids, only *Hipposideros* sensu stricto and *Coelops frithii* have positive values (with secondary reversions in *Hipposideros* species). Rhinonycterid ancestral value of relative brain mass is very low, very negative (the lowest of the three family, not far from that of rhinopomatids) but relative brain mass clearly increases through time in this family. In this way, the slope of relative brain mass evolution through time is very raised (Fig. III-37): it is steeper than the general trend and does not follow a Brownian motion regime (Appendix III-3, Table 3). Rhinonycterid slope of relative brain mass evolution is also steeper than those of its closely-related families (Appendix III-3, Table 4): it is slightly significantly higher than that of hipposiderids (a family in which the gradual relative brain mass increase along the successive nodes leading to *Hipposideros* mainly contributes to the general increase of the family), and clearly higher than that of rhinolophids (whose gradual increase throughout the whole family takes place over a shorter time). The drastic changes that rhinonycterid underwent not only impact their relative brain mass evolution slope, but also their absolute rates reconstruction (Fig. III-36): all nodes have high absolute rates, with major changes between rhinonycterid "lineages", whereas tips have lower rates, and less abrupt changes (which not means less absolute changes, as the branches are longer) within rhinonycterid "lineages". Therefore, the absolute rates evolution slope through time of rhinonycterids is negative (Fig. III-37) and significantly differs from the rest of the tree (Appendix III-3, Table 3), though not differing from those of hipposiderids and rhinolophids (Appendix III-3, Table 4). On the other hand, absolute rates are high for all taxa, even if tips have a bit lower rates; average absolute rates are quite high in this family, being higher in average than the average absolute rate of the rest of the tree (Appendix III-3, Table 3). In the two other "true" rhinolophoid families, absolute rate distribution is much more uneven, with generally low values and some high values at some tips (a bit more frequent in hipposiderids; Fig. III-36); evolution slope of their absolute rates are positive (Fig. III-37), with a quite steep slope for rhinolophids (almost as steep as the pteropodid one) but do not significantly differ from the rest of the tree. Average rhinolophid rates are

significantly lower than those of the rest of the tree (Appendix III-3, Table 4); their evolution slope is very steep because the rate of the family node is very low (Figs. III-35,36). A shift towards low rates is also found for this family (Appendix III-3, Table 5), regarding the two most basal nodes (that of the family and that excluding *Rhinolophus luctus*). As a summary, the "true" rhinolophoid clade gathers three families with very contrasted evolution of relative brain mass: it is generally high but slightly varies in rhinolophids, it is very low but raises through time with a chaotic and versatile pattern in rhinonycterids, and it is low with various directions depending on the subclades (increase along the branch leading to *Hipposideros* and *Coelops*, decrease or net stasis in other genera) in hipposiderids, without clear pattern.

IV.2.D) Comparison with "neontological" works

Most works concluded that there is a higher brain mass in phytophagous bats than in non-phytophagous ones, together with a neocortical development (e.g., Stephan & Pirlot 1970, Pirlot & Stephan 1970, Eisenberg & Wilson 1978). Phytophagous bats would have to process more information, especially spatial information, regarding food location in complex environments, and this may be visible both on general brain size, on hippocampus size, and on neocortical development (Eisenberg & Wilson 1978, Safi & Dechmann 2005). Some results (Safi et al. 2005) actually found that phytophagous bats have consistently high relative brain mass because of the high neuronal requirements implied by this diet, whereas, in non-phytophagous bats, relative brain mass would vary depending on the habitat complexity, and thus on the locomotory mode.

Safi et al. (2005) used the work of Norberg & Rayner (1987) on wing morphology and found a correlation between relative wing surface (expressed against body mass) and habitat complexity, and they predicted the latter using the former. By doing so, yinpterochiropteran families can be divided in three main groups: pteropodids have strongly varying relative wing surface (on both sides of the allometrical slope), rhinopomatids have low, negative, relative wing surface (under the allometrical slope) which is linked to their low complex habitat and their fast and low maneuverable flight, and other families (hipposiderids including rhinonycterids, rhinolophids, and megadermatids) have high, positive relative wing surface (over the allometrical slope), linked to their more complex and cluttered habitat, with a slower and more maneuverable flight (though rhinonycterids have both a fast and a highly maneuverable flight according to Benda 2019). Such groupings are not in accordance with my results on relative brain mass.

Pteropodids generally have a higher relative brain mass compared to other bats of my sample, which is congruent with the hypotheses of Safi et al. (2005): they have to process more information due to their diet, and have a generally more encephalized brain. Regarding rhinolophoids, there is no difference between rhinopomatids and other taxa: rhinopomatids have a very low relative brain mass, which may concur with their low complex habitat, but other families are more heterogeneous. For instance, both megadermatids and rhinolophids have higher relative brain mass, whereas hipposiderids and rhinonycterids show a mixed pattern with most taxa having low relative brain mass. Predictions regarding the link between relative brain mass and habitat complexity are here very partially found: pteropodid have a high relative brain mass, but this may actually due to their diet, and rhinopomatids have a low relative brain mass, but other rhinolophoid families seem to vary more in their relative brain mass than in their habitat complexity (as predicted by relative wing area).

Ecological causalities raised by Safi et al. (2005) are somewhat doubtful, at least regarding Yinpterochiroptera, and too vague to really explain the pattern of relative brain mass evolution through this clade. Moreover, the phylogenetic signal of the correlated trait should be investigated first: ecological

characteristics, and their morpho-anatomical implied adaptations, may bear a phylogenetic signal and/or have a different degree of variation across families. Drawing conclusions at such a large phylogenetic scale without being able to explain the causality between the two correlated traits and take this correlation at face value is misleading and methodologically doubtful. Moreover, looking closer at the results of Safi et al. (2005), one can see that, in spite of a significant correlation between log relative wing area and log relative brain mass for all and animalivorous bats, the part of explained variance by the regression is incredibly low (eight percent and 21% of explained variance respectively). This implies that their conclusions are valid for the same percentages of relative brain mass variation, leaving then 92% and 79% of the relative brain mass variation unexplained. They simply cannot declare that "wing area predicts encephalization in bats" (Safi et al. 2005: 284). Proper analyses on relative brain mass evolution, ecological traits, and the putative causality chain between both, should further be investigated. Here, I attempt to draw a first picture of relative brain mass in the most contrasted bat clade.

Following Safi et al. (2005), other works (Niven 2005, Yao et aL. 2012, Smaers et al. 2012, 2021, Thiagavel et al. 2018, Maugoust & Orliac 2021) tried to address relative brain size evolution in a temporal framework. Most of them did not include fossil taxa, some found the "ancestral" bat to be intermediate in body and brain sizes and wing area (Safi et al. 2005, Thiagavel et al. 2018). They thus concluded to a bidirectionnal evolution of relative brain size in bats, with increases or decreases from the bat "ancestor" and extant bat families (Safi et al. 2005, Niven 2005) depending on their ecology (habitat complexity, diet). Recalling ecological correlates, they found a mixed pattern of evolution of relative brain mass in pteropodids, increases between the root and some rhinolophoid families (megadermatids, craseonycterids), and decreases for most other ones (rhinopomatids, rhinolophids, and hipposiderids + rhinonycterids).

Smaers et al. (2012, 2021) instead studied the evolution of the allometric relationship between brain and body size, at the whole order scale. They find a first shift at the onset of bats with a decrease of relative brain mass value (both average body and brain masses decrease, but average brain mass decreases faster than average body mass) and an increase of its variation (both body mass and brain mass decrease in variation, but brain mass variation decreases less than do that of body mass). They also find a shift with the exact reverse pattern in pteropodids, which are larger than other bats. This would mean that bats have a lower and a more varying relative brain mass than their closely related laurasiatherian taxa, and that pteropodids have a higher and less varying relative brain mass than their bat sister-taxa. Extrapolating, there would be a positive correlation between relative brain mass and body size values and a negative correlation between their variations (i.e., the smaller the body mass, the more varying and the smaller the relative brain mass). These findings join the conclusions of previous works: Safi et al. (2005) somewhat find the negative relationship between the variation of both variables (phytophagous, large-sized bats, have consistently high neurological demands and little varying relative brain mass, whereas animalivorous bats vary more in their habitat and have a more varying relative brain mass) and proposed the positive correlation between relative brain mass and body mass values (the phytophagous, large-sized bats, having higher relative brain mass than other bats).

Finally, Yao et al. (2012) and Maugoust & Orliac (2021) briefly addressed brain mass evolution using fossil hipposiderids, and concluded that the brain mass decrease in this family retrieved by Niven (2005) is not found. The present results further support these studies, and give more detail about the points where there was an increase or a decrease of relative brain mass at Yinpterochiroptera scale. Especially, there is an increase in relative brain mass before the onset of all families except rhinopomatids and

rhinonycterids, but including hipposiderids and rhinolophids (both predicted as decrease in relative brain mass). The mixed pattern of pteropodids found by Niven (2005) is not found either: there is an increase of relative brain size before this family, and most pteropodids retain a high relative brain mass. Computation of evolutionary rates also gives more details about the tempo of relative brain mass evolution, and highlights high variation at some nodes (especially the nodes of pteropodids, pteropodines, and all rhinonycterid internal nodes). High relative brain size may correlate with ecological traits, but I have no explanation for these results at the Yinpterochiroptera scale yet. Besides, evolutionary rates of relative brain size may correlate with body size in pteropodids; such confounding effect should be considered first. Therefore, much remains to explain regarding relative brain mass variation and evolution; fossil taxa indubitably provide critical milestones, and modern techniques (both regarding data acquisition and treatment) now allow to better reconstruct step by step trait evolution.

IV.3) Olfactory bulbs mass (Figs. III-38-40)

IV.3.A) Relative olfactory bulbs mass evolution

Olfactory bulbs mass is here treated relative to the brain mass, following Jerison's "law of proper mass" (see Methods). The distribution of the relative olfactory bulbs mass (Fig. III-38), using residuals of the olfactory bulbs mass relative to the brain mass, shows high ancestral values (with a high relative olfactory bulbs mass) decreasing in some major clades, that are the pteropodines, the megadermatids, the rhinopomatids, and the rhinolophids (with the except of two reversions in *Rhinolophus hipposideros* and *Rhinolophus ferrumequinum*). There is also a decrease of relative olfactory bulbs mass in the *Archerops* + *Cloeotis* rhinonycterid clade and in *Rhinonicteris aurantia*. Finally, in hipposiderids, there are multiple convergent decreases: in the *Macronycteris* + *Doryrhina* clade, in the *Riversleigha* + (*Coelops* + *Aselliscus*) clade (with a secondary increase for *Aselliscus* and a more pronounced decrease for *Coelops*), and in extant *Hipposideros* species.

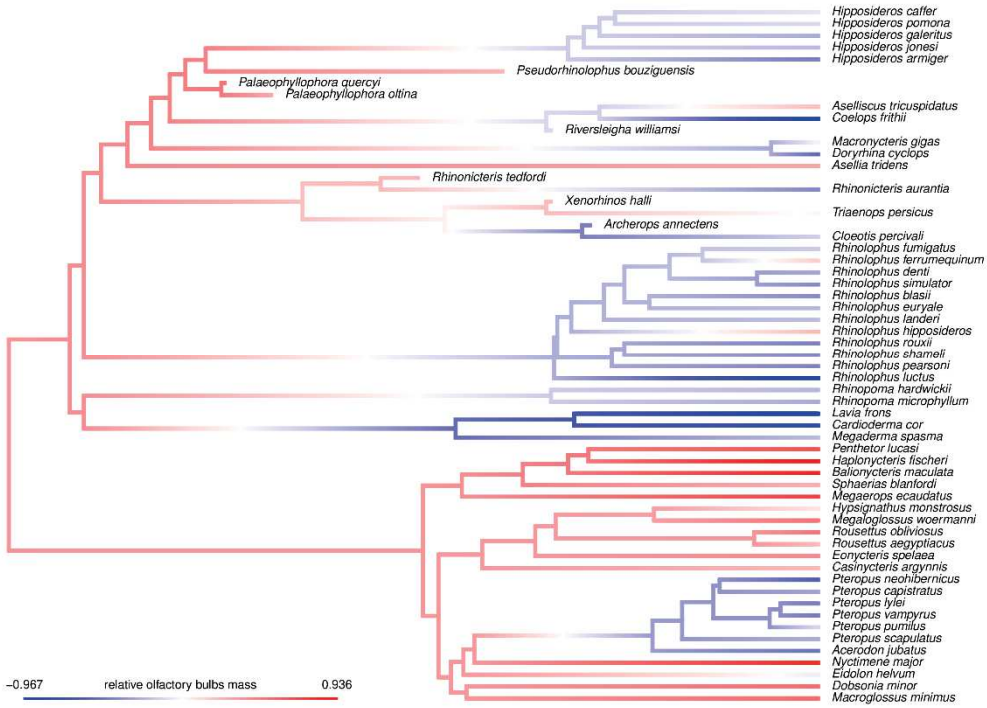

Figure III-38: Mapping of the relative olfactory bulbs mass on the Yinpterochiroptera phylogeny pruned to the sample of this study. This stands for the phylogeny with *Palaeophyllophora* as sister-genus to *Hipposideros*. Other cases are figured in Appendix III-10-4.

The evolutionary slope for the evolution of relative olfactory bulbs (Fig. III-40) mass through time is negative (p-values between 1.10^{-4} and 6.10^{-4}, Appendix III-3, Table 2) at the Yinpterochiroptera scale, with a negative shift of the mean value (~-0.26 to -0.29 times the standard deviation of relative olfactory bulbs mass) that is not significant to distinguish it from a Brownian motion regime (p-values between 0.06 and 0.1, Appendix III-3, Table 2). Deep rhinolophoid nodes, hipposiderids, and rhinonycterids parallel the general trend, while the slope for the four other families is closer to zero, being even very slightly positive in rhinopomatids and rhinolophids. The trends of deep rhinolophoid nodes, hipposiderids, rhinonycterids, but also rhinopomatids are different from a Brownian motion regime (Appendix III-3, Table 3), as well as that of rhinolophids if *Palaeophyllophora* is the basalmost hipposiderid genus (Appendix III-3, Table 3), while the slopes of pteropodids, megadermatids, and rhinolophids (for the other positions of *Palaeophyllophora*) are not significantly different from a Brownian motion regime (as seen on the Fig. III-

40). Concurrently, the pteropodids slope is higher than those of “other” and “true” rhinolophoids, that of the latter being higher than that of the former (Appendix III-3, Table 4). In rhinolophoids, the megadermatid slope is higher than that of rhinopomatids regarding “other” rhinolophoids, and within “true” rhinolophoids, the rhinolophid slope is the higher, followed by that of hipposiderids and that of rhinonycterids (Appendix III-3, Table 4). Relative olfactory bulbs mass is higher in pteropodids than in rhinolophoids according to the Figure III-40 and to the emmeans of each group (p-values at the 10^{-8} level, Appendix III-3, Table 3); in other groups, it is worth noting that megadermatids relative olfactory bulbs mass is clearly lower than that of other yinpterochiropteran bats (Fig. III-40; p-values close to 2.10^{-4}, Appendix III-3, Table 3), as are rhinolophids in a more moderate way (Fig. III-40; p-values close to 2.10^{-3}, Appendix III-3, Table 3. Pairwise emmeans comparisons only support a clear distinction between pteropodids and both the “true” and the “other” rhinolophoid nodes (p-values at the 10^{-6} level for both, Appendix III-3, Table 4); other comparisons are not significant, though the “other” vs “true” rhinolophoids difference has a low p-value (close to 0.06), the latter emmean being slightly higher. A noteworthy result is also the very high p-value of the rhinonycterid/hipposiderid emmeans comparison (p-values > 0.99, Appendix III-3, Table 4).

IV.3.B) Absolute rates evolution

Absolute rate distribution of relative olfactory bulbs mass (Fig. III-39) is very similar to that of brain mass: the rate values are comparable (they seem lower in color on the Figure III-39, but the rate range is doubled compared with that of brain mass), and the same nodes experience rate bursts. The families with extreme relative brain mass absolute evolutionary rates (i.e., pteropodids and rhinonycterids) have comparable "extreme" values regarding relative olfactory bulbs mass absolute evolutionary rates. Some slight differences can still be identified at few nodes: megadermatids have slightly lower rates, whereas rhinolophids and rhinopomatids (at the basal family node), and hipposiderids (at the first deepest nodes of the family) have slightly higher rates. Two terminal rhinolophoid taxa also show particularly high absolute rates, the hipposiderid taxa *Macronycteris gigas* and *Doryrhina cyclops*. The hipposiderids *Coelops frithii* and *Palaeophyllophora oltina* also have high (though not that extreme) absolute rate values.

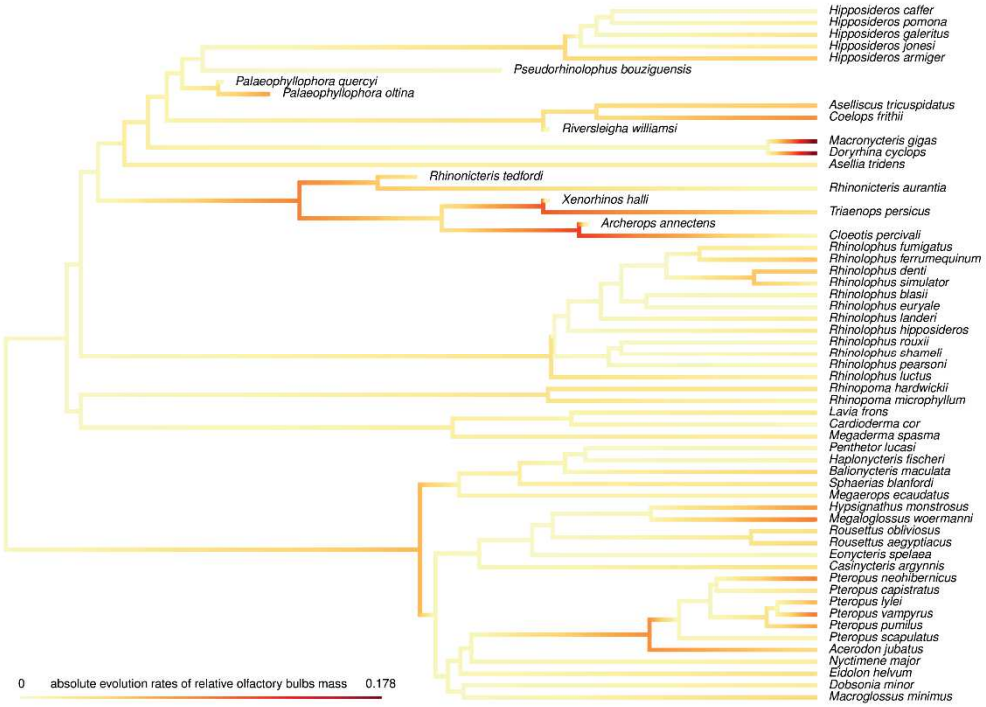

Figure III-39: Mapping of the absolute evolutionary rates of relative olfactory bulbs mass on the Yinpterochiroptera phylogeny pruned to the sample of this study. This stands for the phylogeny with *Palaeophyllophora* as sister-genus to *Hipposideros*. Other cases are figured in Appendix III-10-5.

There is a general increase in absolute rate variation through time (Fig. III-40; p-values between 2.10^{-4} and 1.10^{-3}, Appendix III-3, Table 2) with a threefold absolute rate spread (the range increasing three times more than under a Brownian motion regime), which is however not significant (p-value between 0.2 and 0.5, Appendix III-3, Table 2). The general trend is paralleled by those of deep rhinolophoid nodes and of megadermatids. Hipposiderids, rhinolophids, and pteropodids also have positive slopes, but a bit steeper than the general one (Fig. III-40). Rhinonycterids have a quite negative slope of absolute rate evolution through time, while that of rhinopomatids is only slightly negative. In that way, only the rhinonycterids slope is remarkable enough to differ from the rest of the tree, with a significantly lower slope (p-values around 0.01, Appendix III-3, Table 3). Apart from that clade, no other clade slope stands out in particular, the pteropodid/rhinolophoid difference included. Pairwise slopes comparisons are only significant regarding rhinonycterids and hipposiderids (but with p-values close to 0.03, Appendix III-3,

Table 4); there are no difference between pteropodids and deep rhinolophoid nodes (all p-values > 0.3, Appendix III-3, Table 4), between deep rhinolophoid nodes (p-values > 0.97, Appendix III-3, Table 4) between "other" rhinolophoid families (p-values around 0.98, Appendix III-3, Table 4), nor in other "true" rhinolophoids comparisons (p-values > 0.9999 between rhinolophids and hipposiderids, and p-values around 0.2 between rhinolophids and rhinonycterids; Appendix III-3, Table 4). Absolute rate emmeans do not greatly differ between taxa: only those of rhinolophids and rhinonycterids do, being either significantly lower (p-values around 0.02, Appendix III-3, Table 3) or higher (p-values around 0.04, Appendix III-3, Table 3) than for the rest of the tree. Pairwise comparisons only highlight a difference between rhinolophids and other "true" rhinolophoid families (p-values around 0.02 for both comparisons, Appendix III-3, Table 4), that of rhinolophids being particularly low. There are no other differences, all other p-values being higher than 0.5 (Appendix III-3, Table 4). Shifts towards low absolute rates are found at the rhinolophid node (p-values close to 7.10^{-3}, Appendix III-3, Table 5) and at the following rhinolophid node (i.e., excluding *Rhinolophus luctus*, p-values close to 0.02, Appendix III-3, Table 2), the former (negative) difference being slightly higher. Another shift, toward higher absolute rates, is found at the rhinonycterid + hipposiderid node (p-values > 0.99, Appendix III-3, Table 5).

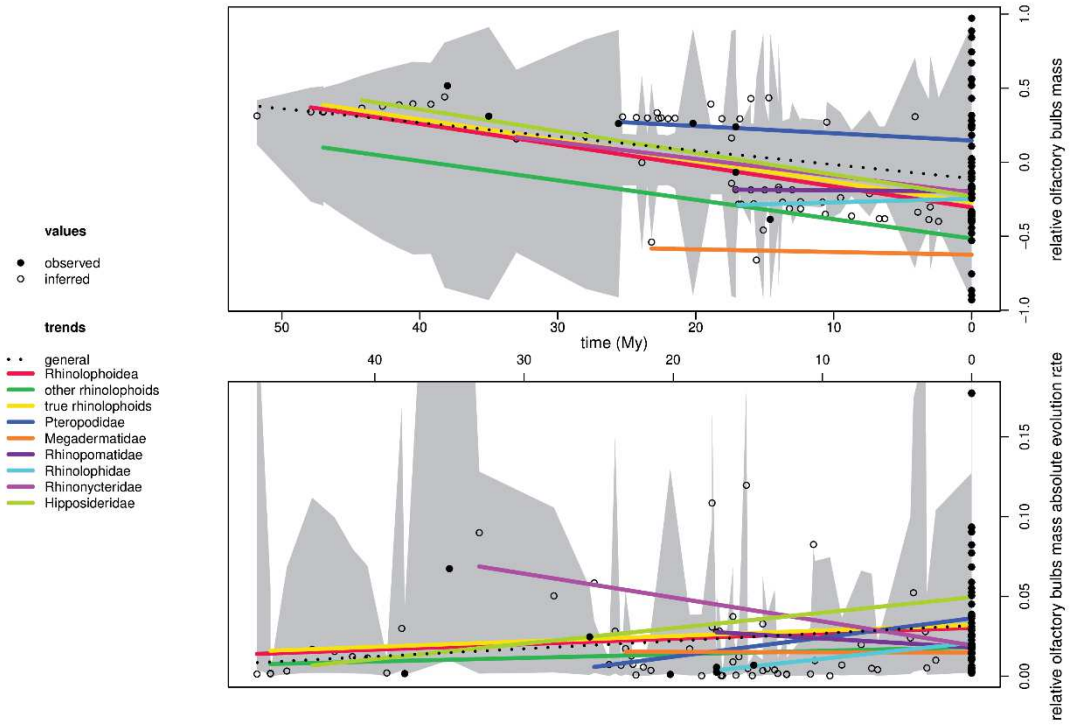

Figure III-40: Temporal trends of relative olfactory bulbs mass (top) and of its absolute evolutionary rates (bottom). The gray background illustrates a simulated variation under a Brownian motion regime. This stands for the phylogeny with *Palaeophyllophora* as sister-genus to *Hipposideros*. Other cases are figured in Appendix III-10-6.

IV.3.C) Group by group evolution

A high, positive relative olfactory bulbs mass is reconstructed for the Yinpterochiroptera suborder (Fig. III-38). There is a very subtle (to null) decrease before Pteropodidae, and a slight increase before rhinolophoid deepest nodes and hipposiderids. Otherwise, there are more pronounced decreases: the smallest regards rhinonycterids, whose familial reconstruction has a positive relative olfactory bulbs mass, but decreases are more severe regarding rhinolophids, rhinopomatids, and even more pronounced for megadermatids. Throughout the tree, there are some later decreases towards negative values in pteropodids (for pteropodines), rhinonycterids (for the *Archerops* + *Cloeotis* clade and for *Rhinonicteris aurantia*), and hipposiderids (all extant genera, except *Asellia* and *Aselliscus*, in a convergent way). There are also rare increases, regarding some pteropodids subfamilies (Nyctimeninae and Cynopterinae, the relative olfactory bulbs mass being even higher), and some rhinolophid and hipposiderid species (two rhinolophids and the hipposiderid genus *Aselliscus*). With these general decreases in several families, the general evolutionary trend of relative olfactory bulbs mass shows a negative slope at the Yinpterochiroptera scale (Fig. III-40), though not differing from a Brownian motion regime (Appendix III-3, Table 2). There is a general increase in absolute rates through time in Yinpterochiroptera (Fig. III-40), though not significantly different from a Brownian motion regime (Appendix III-3, Table 2).

Pteropodids ancestral reconstructed relative olfactory bulbs mass does not differ that much from that of the Yinpterochiroptera node (Fig. III-38). Actually, all pteropodids retain high, positive relative olfactory bulbs mass, with the noticeable exception of Pteropodinae: there is a clear change before the pteropodine node with low, negative relative olfactory bulbs masses shared by all members of that subfamily. Eidoloninae also tend to have slightly negative relative olfactory bulbs mass. On the other hand, Nyctimeninae and Cynopterinae increase in relative olfactory bulbs mass. This generally high relative olfactory bulbs mass makes pteropodids to significantly differ from the rest of the tree (Appendix III-3, Table 3) and especially from the two main rhinolophoid subclades (Appendix III-3, Table 4). However, the negative pteropodines values make the pteropodid slope of relative olfactory bulbs mass evolution slightly negative (Fig. III-40). This slope is still flatter than the general trend (though not significantly differing from a Brownian motion regime; Appendix III-3, Table 3), and especially flatter than those of both major rhinolophoid subclades (Appendix III-3, Table 4). Relative olfactory bulbs mass variation, appreciated through evolution rates (Fig. III-39), shows major changes at the Pteropodidae and Pteropodinae nodes, and more minor changes at the Cynopterinae deepest nodes. In that way, the evolution slope of absolute rates is positive and steep (Fig. III-40), though there are no significant differences against rhinolophoids main clades, both concerning the slope and the average of absolute rates (Appendix III-3, Tables 3-4). Interestingly, no shifts in rate regime are retrieved regarding relative olfactory bulbs mass (Appendix III-3, Table 5), implying that there actually is a higher general (i.e., at Yinpterochiroptera scale) variation pattern regarding olfactory bulbs. Pteropodids are phytophagous bats, and deeply rely on the sense of smell (Bhatnagar & Kallen 1974, Jones et al. 2013) that can be approximated by the relative mass of olfactory bulbs following Jerison's [1973] principle of proper mass. In that way, a stasis of a high relative olfactory bulbs mass is congruent with all these hypotheses.

As for pteropodids, the ancestral reconstructions of the deepest **rhinolophoid** nodes show high, positive, relative olfactory bulbs masses (Fig. III-38), down to the last clades comprising families. Then, between the root and the family onsets, are various patterns, with convergent decreases in "other" rhinolophoids (i.e., before rhinopomatids and megadermatids), in rhinolophids, and a slighter one in rhinonycterids. Then are secondary and/or late variations, mostly towards lower (and often negative)

relative olfactory bulbs mass values, and sometimes towards higher, positive values. The slopes of evolution through time of relative olfactory bulbs mass for deep rhinolophoid nodes follow the general tendency (Fig. III-39), being a bit steeper and then contrary to the general slope they are significantly different from a Brownian motion regime (Appendix III-3, Table 3). This is likely due to the pteropodid contribution to Yinpterochiroptera, the slope of that family being flatter than those of deep rhinolophoid nodes (Appendix III-3, Table 4). Among rhinolophoids, "true" rhinolophoids slope is a little bit less steep than that of "other" rhinolophoids (Appendix III-3, Table 4). As previously described, average relative olfactory bulbs mass for deep rhinolophoid nodes is lower than that of pteropodids (Appendix III-3, Table 4), and linked to the slope comparisons, that of "true" rhinolophoids seems slightly higher than that of "other" rhinolophoids, though this difference is slightly not significant (Appendix III-3, Table 4). The distribution of relative olfactory bulbs mass absolute rates of evolution (Fig. III-40) shows some little but noticeable changes before the onset of some families: rhinopomatids and rhinolophids basal nodes especially show slightly higher absolute rates, and hipposiderid deepest nodes do as well. There are otherwise no changes between the superfamily and the family scales; absolute rate evolutionary trends show a comparable slope and parallel the general trend (Fig. III-39). There are thus no marked differences between these groups and relative to the rest of the tree, both regarding the slope and the average value of their absolute rates (Appendix III-3, Tables 3-4). However, there are some shifts in rate regime (Appendix III-3, Table 5), especially regarding rhinolophids (with a decrease of rate variation) and the rhinonycterids + hipposiderids node (with an increase of rate variation), which is likely due to the slightly higher absolute rates of the deepest hipposiderids nodes. As previously, the spectacular changes in the values of relative olfactory bulbs mass at the suprafamilial level have to be tempered by taking into account the branch lengths.

Regarding relative olfactory bulbs mass (Fig. III-38), both **"other" rhinolophoid** families tend convergently towards low, negative relative olfactory bulbs mass. In that way, evolutionary trends of relative olfactory bulbs mass (Fig. III-40) are almost flat and that of rhinopomatids differs from a Brownian motion regime, as for pteropodids (Appendix III-3, Table 3). The internal evolution is though different in each family: both rhinopomatid species have very similar values, while there is a duality between *Megaderma* (that rises in relative olfactory bulbs mass) and the two other genera (*Cardioderma* and *Lavia* that further drop in relative olfactory bulbs mass). The rise in relative olfactory bulbs mass caused by *Megaderma* probably causes the megadermatid slope to be significantly higher than that of rhinopomatids (Appendix III-3, Table 4), whereas the drops caused by *Cardioderma* and *Lavia* likely cause the average relative olfactory bulbs mass of megadermatids to be much lower than that of the rest of the tree (Appendix III-3, Table 3). Both "other" rhinolophoids families have low absolute rates of relative olfactory bulbs mass evolution (Fig. III-39), but those of megadermatids seem slightly higher; in each family, changes are very marginal and there are no striking values. Absolute rate trends (Fig. III-40) better account for the evolution in each family: the slope of megadermatids is flat, while that of rhinopomatids slightly decreases, implying a reduction of the relative olfactory bulbs mass variation through time. These trends are however neither significantly different against the rest of the tree nor between them (Appendix III-3, Tables 3-4), and there are obviously no shifts in rate regime (Appendix III-3, Table 5).

There are contrasted distributions of relative olfactory bulbs mass in **"true" rhinolophoids** (Fig. III-38). Rhinolophid relative olfactory bulbs mass is negative since the initial diversification of the family, and though there are two slight secondary increases, the average relative olfactory bulbs mass of the family is lower than that of the rest of the tree (Appendix III-3, Table 4). The case is different in the two other families: both the rhinonycterids and hipposiderids have initial positive relative olfactory bulbs mass that

then decreases for some taxa of each family, being in average neither strikingly high nor low relative to the rest of the tree (Appendix III-3, Table 4). In rhinolophids, with the exception of the two secondary increases (*Rhinolophus hipposideros* and *Rhinolophus ferrumequinum*) and of a single further decrease (*Rhinolophus luctus*), there is not much variation of the relative olfactory bulbs mass. The familial trend of evolution thus shows a flat to slightly positive slope (Fig. III-40) that slightly differs from a Brownian motion regime (depending on the phylogeny; Appendix III-3, Table 3). On the other hand, there is much more variation in the two other families. In rhinonycterids, there is a gradual decrease of relative olfactory bulbs mass, with three of the six species having negative values, while in hipposiderids, all extant genera but two also decrease towards negative relative olfactory bulbs masses. Evolutionary trends in both families thus follow the general trend, with a negative slope differing from a Brownian motion regime (Appendix III-3, Table 3) and are both lower than that of rhinolophids (Appendix III-3, Table 4). Regarding absolute rate distributions of relative olfactory bulbs mass (Fig. III-40), rhinolophids absolute rates are very low, lower than the rest of the tree (Appendix III-3, Table 3) and than the two other "true" rhinolophoids families (Appendix III-3, Table 4). A shift in rate regime towards a decrease of relative olfactory bulbs mass variation is retrieved for rhinolophids (for the two deepest rhinolophid nodes; Appendix III-3, Table 5). On the other hand, rhinonycterids still greatly vary, with high nodal rate bursts, but with also higher terminal absolute rate values, implying that average absolute rhinonycterid rates exceed that of the rest of the tree (Appendix III-3, Table 4). Hipposiderids still have an intermediate pattern, varying more than rhinolophids and less than rhinonycterids (though the deepest nodes have slightly higher absolute rates and some tips have very high rates), causing the detection of a shift of rate regime regarding the hipposiderids + rhinonycterids clade (Appendix III-3, Table 5). Rhinonycterids have a very negative slope of absolute rates evolutionary trend (Fig. III-40), quite lower than for the rest of the tree (Appendix III-3, Table 3) and than that of hipposiderids (Appendix III-3, Table 4), while the two other families have positive slopes, slightly steeper than the general trend, and then not particularly differing from the rest of the tree nor between them (Appendix III-3, Tables 3-4). The major discrepancies regard the patterns of evolution of the relative olfactory bulbs mass in each family (Fig. III-38): rhinolophids have a negative, little changing relative olfactory bulbs mass, whereas rhinonycterids gradually, strongly, and following phylogenetic relationships decrease through time regarding that trait; hipposiderids also decrease through time, but in a more convergent way (extant genera and generic assemblages being convergent).

IV.3.D) Comparison with “neontological” works

Bhatnagar & Kallen (1974) demonstrated that the olfactory bulbs mass is a good proxy for olfactory acuity. In this way, they distinguished three main groups with corresponding olfactory bulbs mass and olfactory acuity: insectivorous bats (such as hipposiderids, rhinolophids, rhinonycterids, and rhinopomatids) with small olfactory bulbs, “mixed” feeding bats (i.e., other animalivorous bats, such as megadermatids) with intermediate olfactory bulbs mass, and phytophagous bats (such as pteropodids) with large olfactory bulbs. They however warn that the “bulb-cerebral hemisphere ratio” does not predict olfactory acuity in bats, though it does in birds, because the neocortical development is unrelated to olfactory acuity. Even if they consider only the cerebral hemispheres as the reference of their ratio, their conclusions apply by comparing olfactory bulbs mass to that of the whole brain. Indeed, if pteropodids do have large olfactory bulbs given their size, some other insectivorous bat families do (hipposiderids and rhinonycterids in fossil forms and some extant species); megadermatids should have an intermediate value due to their diet, but they actually have among the lower olfactory bulbs relative masses. In general, the differences visible with the absolute olfactory bulbs size disappear by considering relative olfactory bulbs size. This may concur with the conclusions of Deaner et al. (2007) based on primates: they encourage dealing with absolute rather than relative masses and sizes regarding brain regions. However, one could also ask whether the global size may actually correlate with diet.

Energetic constraints are high in bats, both because of the sustained flight and of the echolocation system. Some authors (Barton et al. 1995, Hutcheon et al. 2002) then proposed a sensory trade-off between vision + olfaction and echolocation in phytophagous and non-phytophagous bats. More recent works regarding the evolution of olfactory receptor genes in bats (Hayden et al. 2010, 2014, Jones et al. 2013) found that these genes were not more pseudogenized in non-phytophagous bats than in phytophagous ones. Actually, the point is that phytophagous bats have more olfactory receptor genes of some gene families, and not that non-phytophagous bats have pseudogenized genes. They expose that the sensory trade-off between vision + olfaction and echolocation in phytophagous and non-phytophagous bats is not supported, given that non-phytophagous bats do not have deprecated olfaction. They argue that olfaction still is an important sense in these, not only for food detection but also for communication (see also Dechmann & Safi 2005). Relative olfactory bulbs mass may also, or only, or not, account for this, while the allometric component would represent the diet.

The absence of trade-off implying olfaction does not totally invalidate the conclusions of Barton et al. (1995), who found “grades” of bats according to both their diet and the global size of their brain and of their olfactory bulbs. As highlighted by Jones & MacLarnon (2004), it is rather being phytophagous that may enable having a larger size than the reverse; results on olfactory gene receptors confirm this trend: phytophagy expands olfactory acuity and may allow being larger-sized, animalivory does not reduce the acuity and/or the size. If the relative olfactory bulbs mass is still linked someway to olfactory acuity, my results may converge toward this: a high relative olfactory bulbs mass is reconstructed as the ancestral condition for Yinpterochiroptera, and may have allowed exploring the two strategies.

IV.4) Paraflocculi mass (Figs. III-41-43)

IV.4.A) Relative paraflocculi mass evolution

As for the olfactory bulbs mass, the paraflocculi mass is expressed here as the relative paraflocculi mass, using the residuals of that mass against the brain mass. The distribution of that relative paraflocculi mass (Fig. III-41) shows high values reconstructed at the deepest nodes of the tree, and only more or less intense decreases in the various families. This is particularly true for pteropodid and rhinolophid basal nodes, where the value is slightly positive, and in rhinonycterids. In the latter family (only represented by *Triaenops* and *Cloeotis*), there is a clear decrease towards a negative value at the rhinonycterid node; thereafter, the decreases continue in *Cloeotis* while it inverts and rises in *Triaenops*. Apart from that case, other negative reconstructed ancestral values are at the subfamilial level. They regard the pteropodine family (in which all taxa hence show negative values), the *Doryrhina* + *Macronycteris* clade (but, as in rhinonycterids, there is one genus in which the decreases continues - *Doryrhina* - and another in which it inverts - *Macronycteris*), the *Aselliscus* + *Coelops* clade, and the *Hipposideros* clade (with however a quick reversion in *Hipposideros armiger*). There also are isolated decreases to a negative value in pteropodids for four terminal taxa (*Hypsignathus*, *Megaloglossus*, *Balionycteris*, and *Haplonycteris*).

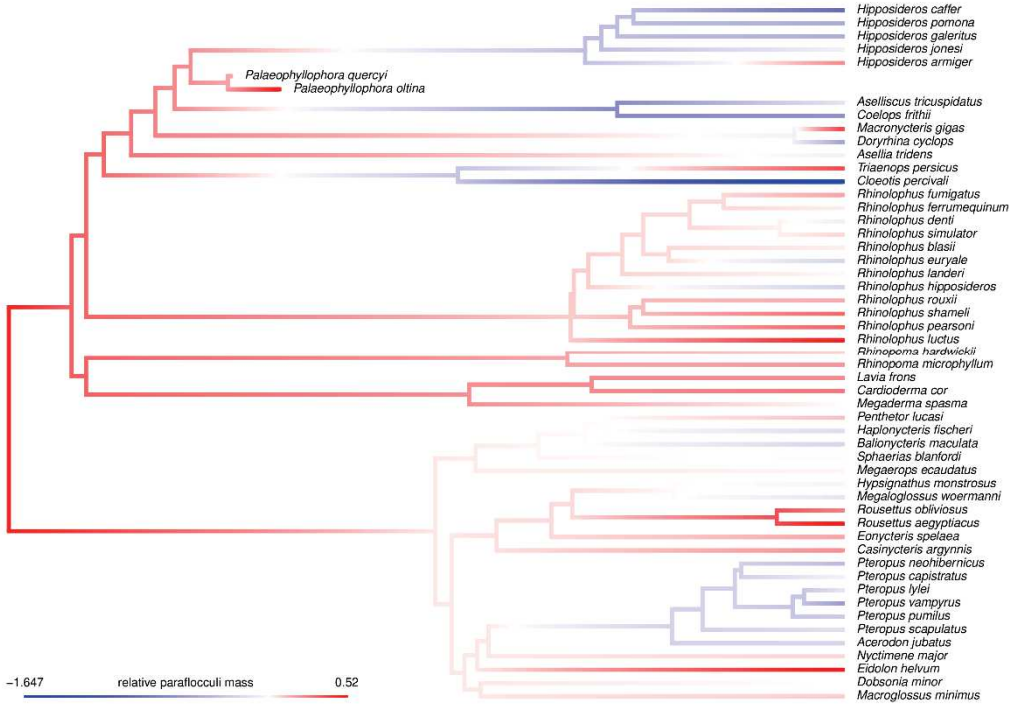

Figure III-41: Mapping of the relative paraflocculi mass on the Yinpterochiroptera phylogeny pruned to the sample of this study. This stands for the phylogeny with *Palaeophyllophora* as sister-genus to *Hipposideros*. Other cases are figured in Appendix III-10-7.

There is a slightly negative and significant slope (Fig. III-43; p-values between 3.10^{-3} and 0.01, Appendix III-3, Table 2), without significant deviation (~-0.18 to -0.21 times the standard deviation of relative paraflocculi mass values, Appendix III-3, Table 2) from a Brownian motion regime (p-values between 0.2 and 0.5, Appendix III-3, Table 2). Several clades follow that trend (rhinolophoids, "true" rhinolophoids, hipposiderids, rhinonycterids) while some other have a flatter, even slightly positive, slope (pteropodids, rhinolophids, "other" rhinolophoids and its composing families megadermatids and rhinopomatids). The slopes that significantly differ from random (i.e., following Brownian motion regime) slopes are those of the second case, which are closer to 0 and/or positive: the slopes of megadermatids,

rhinopomatids, and rhinolophids all are significant (Appendix III-3, Table 3), together with that of hipposiderids, which demarcates from the Brownian regime as being steeper in decreasing. Pteropodids and "other" rhinolophoids slopes are floating near the significant level, both being significant for a basal position of *Palaeophyllophora* in hipposiderids, and the pteropodid slope being also significant if *Palaeophyllophora* diverges just after *Asellia* (Appendix III-3, Table 3). Pairwise comparisons support the graphic observations: pteropodids slope is clearly distinct from that of basal rhinolophoid nodes, the value of the former being higher than those of the latter (Appendix III-3, Table 4). Between deep rhinolophoid nodes, the steepest (negative) slope is that of "true" rhinolophoids, among which rhinolophids are clearly distinct from hipposiderids and rhinonycterids, both having steepest negative slopes (that of hipposiderids being a bit more negative than that of rhinonycterids; Appendix III-3, Table 4). Among "other" rhinolophoids, the rhinopomatid slope is more raised than the megadermatid one, accordingly to the graphic observations (Appendix III-3, Table 4). Pteropodid and rhinolophoid emmeans of the relative paraflocculi mass are clearly overlapping (Fig. III-43; p-value > 0.98, Appendix III-3, Table 3); the three "true" rhinolophoid families are however significantly distinct from the rest of the tree, the relative paraflocculi mass emmean of rhinolophids being higher than that of the rest of the tree (p-values around 0.04, Appendix III-3, Table 3), while those of hipposiderid and rhinonycterid are lower (p-values near 2.10^{-3} and 0.01 respectively, Appendix III-3, Table 3). The relative paraflocculi mass emmean of the "other" rhinolophoids node also float around the significant level, being under it if *Palaeophyllophora* is the sister-taxon to *Hipposideros* (p-value of 0.0498, Appendix III-3, Table 3) and over it otherwise (p-values up to 0.051, Appendix III-3, Table 3); that may imply a higher relative paraflocculi mass for that group, the megadermatids having especially unsignificant but still low p-values (near 0.11, Appendix III-3, Table 3). Pairwise comparisons of emmeans further support the higher emmean of rhinolophids compared to both rhinonycterids (p-values near 2.10^{-3}) and hipposiderids (p-values around 0.01, Appendix III-3, Table 4). Otherwise, the distinction between "true" and "other" rhinolophoids, though not significant, have low p-values (around 0.09, Appendix III-3, Table 4), suggesting a higher relative paraflocculi mass emmean in the latter.

IV.4.B) Absolute rates evolution

Absolute rate distribution (Fig. III-42) of relative paraflocculi mass shows very few extreme values: only *Macronycteris gigas*, *Doryrhina cyclops*, and *Palaeophyllophora oltina* show striking rates. There are also few nodes with even moderate values: only the rhinolophoid, rhinonycterid, and pteropodine nodes stand out. Most of the variation occurs in fact at the terminal tips, especially in pteropodids, with also some cases in rhinolophoids (*Rhinolophus luctus*, *Rhinolophus denti*, *Cloeotis percivali*, *Hipposideros armiger*, and *Hipposideros caffer*).

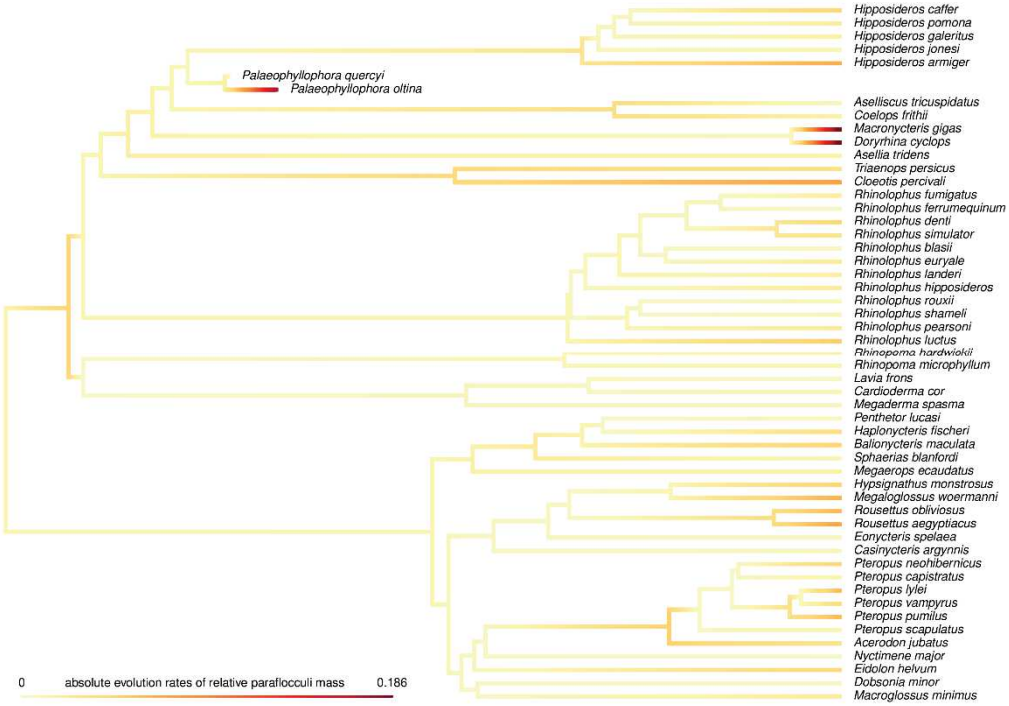

Figure III-42: Mapping of the absolute evolutionary rates of relative paraflocculi mass on the Yinpterochiroptera phylogeny pruned to the sample of this study. This stands for the phylogeny with *Palaeophyllophora* as sister-genus to *Hipposideros*. Other cases are figured in Appendix III-10-8.

Temporal trends of relative paraflocculi mass absolute evolutionary rates (Fig. III-43) clearly converge between all groups. There is too subtle and not significant general increase of rate variation through time (p-values between 0.08 and 0.3, Appendix III-3, Table 2), with however a significantly higher spread of the rate compared to Brownian motion (all p-values under 0.048, Appendix III-3, Table 2). This general, almost flat, trend is followed by all groups, with only some taxa showing a slightly steeper (rhinolophids, pteropodids) or flatter (megadermatids, rhinopomatids) slope. These slopes are however not different enough between them, and none are significant compared to the rest of the tree (all p-values > 0.14, Appendix III-3, Table 3). Moreover, there are absolutely no pairwise differences that can be made between clade slopes, all p-values being over 0.5 (Appendix III-3, Table 4). The absolute rate emmean of hipposiderids stands out, being higher than that of the rest of the tree (p-value close to 3.10^{-3}, Appendix III-3, Table 3) and specifically higher than that of rhinonycterids (p-values near 0.01, Appendix III-3, Table 4). Several nodes show significant shifts of their absolute rates, at a generally high level: both nodes of “true” and “other” rhinolophoid nodes show a shift towards high and low absolute rate values respectively, though the “true” rhinolophoid nodes is very slightly significant (p-value slightly over 0.975, while that of “other” rhinolophoid node is around 8.10^{-3}, Appendix III-3, Table 5). However, the shift toward low rates of the “other” rhinolophoids node is paralleled at the megadermatids node (p-values

near 8.10^{-3}, Appendix III-3, Table 5), with a slightly higher shift in megadermatid, which probably causes that at the "other" rhinolophoids node. Similarly, just following the "true" rhinolophoids node, the second most basal node of rhinolophids (excluding *Rhinolophus luctus*) is also significant towards low absolute rates (p-values around 0.02, Appendix III-3, Table 5), while the hipposiderid + rhinonycterid, the hipposiderid, and the second and third basalmost nodes of hipposiderids (respectively discarding *Asellia* and *Asellia* and the *Macronycteris* + *Doryrhina* clade) all are significant towards high absolute rates, the highest difference being for the second basalmost hipposiderid node while the hipposiderid + rhinonycterid node is the most significant (p-value > 0.999, Appendix III-3, Table 5).

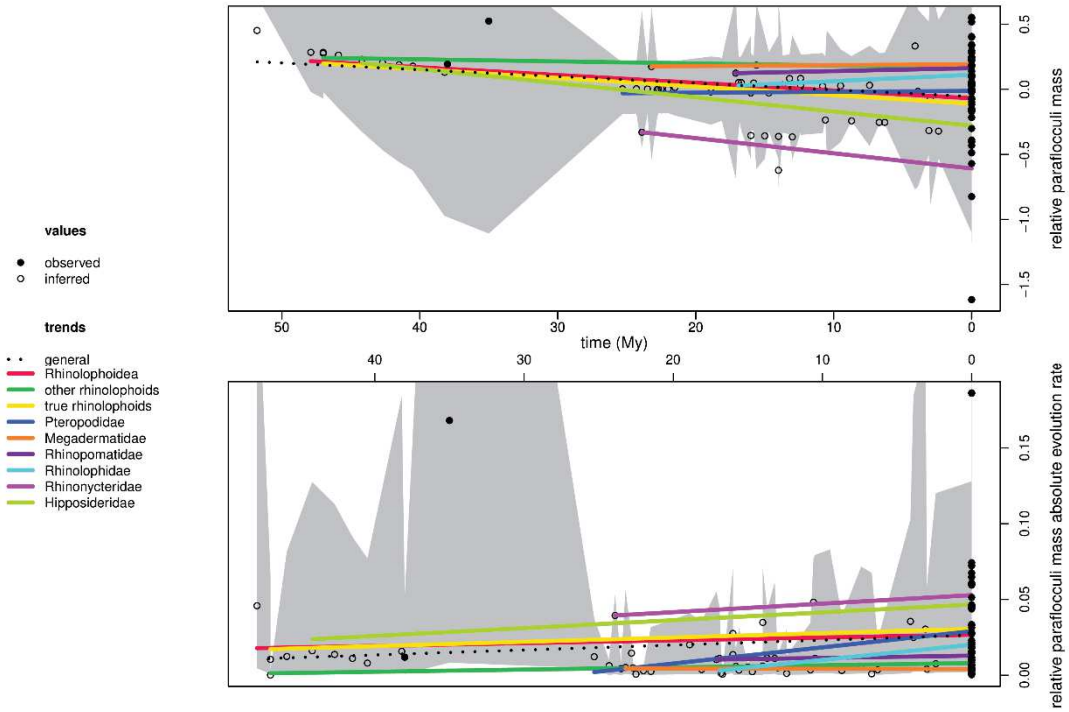

Figure III-43: Temporal trends of relative paraflocculi mass (top) and of its absolute evolutionary rates (bottom). The grey background illustrates a simulated variation under a Brownian motion regime. This stands for the phylogeny with *Palaeophyllophora* as sister-genus to *Hipposideros*. Other cases are figured in Appendix III-10-9.

IV.4.C) Group by group evolution

There are high reconstructed values for the Yinpterochiroptera ancestor (Fig. III-41), with then decreases of varying magnitude depending on the clades (Fig. III-41). There are generally decreases to still positive values between the root and the node of most families; the only exception is the rhinonycterid family, whose ancestral estimate is already a very low, negative value. Pteropodid and rhinolophid ancestral reconstructions are slightly positive, whereas that of both "other" rhinolophoids families and of hipposiderids are still very high values. Then are some intrafamilial further decreases, generally leading to negative values, but also several secondary increases, both cases being found in every family. Only some of these further or secondary changes characterize clades (decrease in pteropodines and *Hipposideros* sensu stricto; increase in rousettines and Asian rhinolophids), most are isolated or convergent. The general trend of relative paraflocculi mass evolution through time is thus a slight decrease (Fig. III-43), the general slope being slightly negative (though significant) and not differing from a Brownian motion regime (Appendix III-3, Table 2). Several yinpterochiropteran subclades follow the generally decreasing trend, but some other groups have an opposite trend, slightly increasing through time. Relative paraflocculi mass changes generally are less striking than for the two other traits, and less leading to sign changes (i.e., positive towards negative values, or the reverse). Occurring on long times, those changes relative to time (i.e., evolution rates) are quite less striking once mapped (Fig. III-42) than for the two other traits (Figs. III-37,43): the only striking rates are located in hipposiderids, for taxa that underwent drastic changes over a short time. Other noticeable, though less abrupt, changes also are present at some nodes (rhinolophoids, rhinonycterids, pteropodines) and at numerous tips (mainly pteropodids, but also some "true" rhinolophoid tips). Very low rates are present in "other" rhinolophoids families, and in pteropodid and rhinolophid deep nodes. The general trend of absolute rate evolution (Fig. III-43) is thus close to stasis: though negative, the general slope is not significant, whereas the rate spread is significantly higher than from a Brownian motion regime (Appendix III-3, Table 2) - this is likely due to the extreme hipposiderid values. Other yinpterochiropteran subclades generally follow this trend, though some groups have slightly steeper or flatter slopes.

The ancestral reconstruction for **pteropodids** is a slightly positive value, as well as for the deepest family nodes (Fig. III-41). Then is a confused pattern across genera: some changes clearly follow the phylogenetic relationships (shared decrease towards negative values in pteropodines, shared slight increase in rousettines terminally dichotomizing in a further increase and in a secondary slight decrease), but most changes are isolated and/or convergent (striking increase in Eidolinae, slight decrease in *Dobsonia minor*, convergent decrease in the cynopterines *Haplonycteris fischeri* and *Balionycteris maculata*). Extant taxa show a wide array of trait values, whereas nodes generally have slightly negative or positive values. The family-level trend of evolution through time of the relative paraflocculi mass (Fig. III-43) is slightly positive, the secondary increases weighting a little bit more the general trend than the slighter decreases. This trend thus does not follow the general decrease through time: it is slightly differing from a Brownian motion regime (Appendix III-3, Table 3) and significantly differing from both "true" and "other" rhinolophoids (with a higher slope; Appendix III-3, Table 4). However, the general stasis (to increase) around slightly positive or negative values in pteropodids implies a null average relative paraflocculi mass for the family; while contrasted against that of rhinolophoids, their is no significant difference (Appendix III-3, Tables 3-4). The variations in relative paraflocculi mass are thus slight in pteropodids, with some slight changes at nodes and a bit less slight changes at nodes. Absolute rate distribution pattern follows this (Fig. III-42): there are very few noticeable taxa presenting high absolute rates. The only striking node is that of pteropodines, that probably underwent the most "violent"

change in pteropodids (from slightly positive values to slightly negative ones). Otherwise, some tips also show marked absolute rates but indicate convergences in the variation pattern; these are the four more derived rousettine species (*Hypsignathus monstrosus* and *Megaloglossus woermanni* that underwent a decrease towards slightly negative values, and both *Rousettus* species that further increased in relative paraflocculi mass), two intermediate cynopterines (*Haplonycteris fischeri* and *Balionycteris maculata*, both experiencing a decrease towards slightly negative values in that subfamily), eidolines (as the single *Eidolon helvum*, that has the one of the highest pteropodid relative paraflocculi mass together with the *Rousettus* species), and some pteropodines (three *Pteropus* species). The more frequent high absolute rates at tips than at nodes yield to a slightly increase slope of absolute rate evolution through time (Fig. III-43), though not significantly differing from the rest of the tree (i.e., the rhinolophoids; Appendix III-3, Table 3): this slope may be the steepest of all yinpterochiropteran subclades, the differences are too tiny to significantly differ from them, and as well do the average absolute rate, as there are very few extreme values (Appendix III-3, Table 4). Pteropodid patterns of relative paraflocculi mass evolution slightly differ from the general trend: there is not a general, slight decrease of that trait, but an oscillation around a null relative paraflocculi mass. Pteropodinae is the clearest pteropodid subclade with a "phylogenetic" trend, decreasing towards slightly negative values. Otherwise, most changes occur along terminal branches, being sometimes convergent (e.g., in cynopterines) to potentially phylogenetic (e.g., in *Rousettus*), and otherwise clearly isolated (e.g., eidolines).

Deep changes in **rhinolophoids** are quite weaker regarding the relative paraflocculi mass (Fig. III-41): there only is one trend to a sign change (before rhinonycterids, with a very marked decrease), otherwise there are very little decreases before each family. Rhinolophoids seem to be more homogeneous: all families (except rhinonycterids) have positive ancestral reconstructed values, with generally parallel decreases in each of the two main rhinolophoid subclades. There however is a marked difference between "other" and "true" rhinolophoids, as only "true" rhinolophoid families each go towards negative values for several taxa; only the megadermatid *Megaderma spasma* goes towards a null relative paraflocculi mass in "other" rhinolophoids. Consequently, temporal trends of relative paraflocculi mass evolution are quite different between each clade (Fig. III-43): that of "other" rhinolophoids clearly do not follows the general trend, with a very slightly negative slope that is slightly significantly different from a Brownian motion regime (Appendix III-3, Table 3), whereas that of "true" rhinolophoids clearly parallels the general trend. Both still have a lower slope than that of pteropodids, and rhinolophoids as a whole do not have an average relative paraflocculi mass differing from that of pteropodids (Appendix III-3, Table 4). The latter comparison of averages relative paraflocculi mass could be explained by the wide array of values in rhinolophoids, and especially in "true" rhinolophoids; "true" and "other" rhinolophoids have very differing ranges of values (as exemplified by their different trends). In that way, "other" rhinolophoids average relative paraflocculi mass floats around the significance level and would be higher than the rest of the tree (Appendix III-3, Table 3), and especially than "true" rhinolophoids (the difference between both clades being slightly not significance; Appendix III-3, Table 4). If there is a slight difference in the average values, there are however much less differences regarding absolute evolutionary rates (Fig. III-42), all deep rhinolophoid node having very low absolute rates. The two nodes with remarkably higher rates are those of Rhinolophoidea (likely caused by a slight decrease from the root) and of Rhinonycteridae (that underwent a more drastic decrease). Due to the higher terminal variation in relative paraflocculi mass in "true" rhinolophoids (with further decreases of relative paraflocculi mass, and some secondary increases), there are more extreme absolute rates at tips in this clade (in each family of this clade); on the other hand, the low variation of relative paraflocculi mass in "other" rhinolophoids

make this clade to only have very low absolute rate values. Trends in the evolution of absolute rates are thus a bit different between both clades (Fig. III-43), "true" rhinolophoids having a slightly steeper slope than "other" rhinolophoids do; both trends still parallel the general trend, not differing from the rest of the tree (Appendix III-3, Table 3), and also without significant difference between them (Appendix III-3, Table 4). There however are some shifts in rate regimes (Appendix III-3, Table 5): there is a general decrease of variation in "other" rhinolophoids and in megadermatids (the latter being more significant than the former, maybe "causing" it), while there is a slightly significant increase in "true" rhinolophoids, followed by both an increase regarding hipposiderids and rhinonycterids and a decrease regarding rhinolophids (but see next paragraphs). As a summary, relative paraflocculi mass is "smoother" than the other traits in deep rhinolophoid nodes, with a clearer pattern of evolution. There are also some discrepancies between the two major rhinolophoid subclades, both regarding their trends, their average relative paraflocculi mass, and their evolution regime: "true" rhinolophoid appear as more versatile, though rhinolophids converge with "other" rhinolophoids in being more constrained.

This time, both **"other" rhinolophoid** families do not follow fully opposite patterns but are in agreement. As already noted, both families have high, positive, relative paraflocculi mass values (Fig. III-41) and do not vary very much (Fig. III-42). Trends of relative paraflocculi mass evolution in both families are similar (Fig. III-43): they slightly increase through time, differing from the general trend and from a Brownian motion regime (Appendix III-3, Table 3). The rhinopomatid slope appears to be slightly steeper than that of megadermatids; given the low variation in both these families, it is not very surprising that this little difference is significant here (Appendix III-3, Table 4). Both families having high relative paraflocculi masses, they do not differ in their average value of this trait (Appendix III-3, Table 4), but both contribute to make the "other" rhinolophoid node to differ from the rest of the tree (Appendix III-3, Table 3). The variation in relative paraflocculi mass being low and constantly low in each family (Fig. III-42), the slope of the absolute rate evolution through time is flat, a bit flatter than the general trend; this difference is however not enough to make them differ from the rest of the tree (Appendix III-3, Table 3). As it can also be expected, there is no significant difference between megadermatid and rhinopomatid rate slopes (Appendix III-3, Table 4). A shift in rate regime is retrieved at the "other" rhinolophoids and megadermatids nodes (Appendix III-3, Table 5); the latter being a little bit more significant, it may "cause" the former. However, though no shift is retrieved for rhinopomatids, they do not differ in their average absolute rates from megadermatids (Appendix III-3, Table 4). The easiest explanation is to consider a shift in rate regimes at the "other" rhinolophoids node, affecting both families in the same way, as consistently retrieved here: both families have high relative paraflocculi masses that do not vary that much in time, in and between families. Fossils documenting one or the other family would be of critical interest to test these conclusions, and to better assess the location of a shift towards a constrained evolution of the relative paraflocculi mass in this rhinolophoid subclade, if retrieved.

The **"true" rhinolophoids** clade is more versatile than "other" rhinolophoids, as it has been previously started to be described. It is in this clade that the inter- and intra-familial variation of relative paraflocculi mass is the highest among the tree (Fig. III-41): rhinolophids ancestral reconstruction is low, though still positive, and there are both further (terminal, thus convergent) decreases and secondary increases, rhinonycterids ancestral state is the only family-level taxon with a negative value, though both the two species used here (the other ones do not having preserved in situ petrosals) have opposite trends, and hipposiderids show a mixture of convergent decreases and increases at the inter-generic level. In rhinolophids, all Asian species secondary tend to high values of relative paraflocculi mass: in that way, the Asian *Rhinolophus luctus* converges with the Asian clade regrouping the other Asian species. The African

Rhinolophus fumigatus and *Rhinolophus simulator* also secondarily converge in an increase of their relative paraflocculi mass, but they do not reach the values of the Asian species. There are also three convergent decreases towards negative values in that family, regarding EurAfrican. In that way, *Rhinolophus hipposideros* clearly follows the trend of the African clade rather than that of the Asian species. Rhinolophid internal nodes generally show the same value, without clear trend between them; considering that extant species have slightly contrasted trends, the family-level trend of relative paraflocculi mass evolution is flatter than the general one, even being slightly increasing (Fig. III-43). In rhinonycterids, after having a negative ancestral relative paraflocculi mass, both remaining species sampled here have very different futures: *Triaenops persicus* secondary highly increases and reaches a very high value, whereas *Cloeotis percivali* further decreases and reaches a very low value (Fig. III-41). The low value of *Cloeotis* being by far lower than the value of *Triaenops* is high, there is a negative slope for the evolutionary trend of the rhinonycterid relative paraflocculi mass (Fig. III-43), being a bit steeper (i.e., more decreasing) than the general trend. Finally, hipposiderids show an interestingly mixed pattern (Fig. III-41): there is a very slight decrease from the root to the family node, the oldest taxa (internal nodes and *Palaeophyllophora* species) still have high relative paraflocculi masses, and then all crown generic group experience marked decreases, all reaching negative relative paraflocculi masses. There are two secondary increases in extant hipposiderid taxa: *Macronycteris gigas* and *Hipposideros armiger* both have high, positive values, but still their pertaining clade (*Macronycteris* + *Doryrhina* clade for the former; *Hipposideros* sensu stricto for the latter) having negative ancestral reconstructions. A clear decrease pattern is thus retrieved for this family through time (Fig. III-43), though there are some marked secondary increases tempering the familial slope. Given the contrasted evolution pattern of relative paraflocculi mass in these three families, it is not surprising that they all differ from each other (Appendix III-3, Table 4): only rhinolophid increase through time, whereas hipposiderids decrease more than rhinonycterids, and the two extreme cases (rhinolophids and hipposiderids) are extreme enough to also differ from a Brownian motion regime (Appendix III-3, Table 3). These three families also differ from the rest of the tree regarding their average relative paraflocculi mass: that of rhinolophids is higher, while those of rhinonycterids and hipposiderids are lower (Appendix III-3, Table 3), and, as for the slopes, the average value for rhinolophids is above those of rhinonycterids and hipposiderids (both being, this time, not significantly different; Appendix III-3, Table 4).

The contrasted patterns for these three families regarding the distribution of relative paraflocculi mass are partly retrieved on the absolute rate distribution (Fig. III-42): rhinolophids have very low absolute rates (with the exception of *Rhinolophus luctus* and *Rhinolophus denti*, both increasing in relative paraflocculi mass), rhinonycterid node has a high rate, and both rhinonycterid species have high rates too (that of *Cloeotis* still exceeding that of *Triaenops*), and hipposiderids show terminal bursts of rates (regarding both species of the *Macronycteris* + *Doryrhina* clade, and *Palaeophyllophora oltina*) or "simply" slightly higher rates for some taxa (the *Aselliscus* + *Coelops* clade, the *Hipposideros* sensu stricto node, and two *Hipposideros* species). In all cases, there are high values at tips rather than at nodes; it is not surprising to find that all these three families have increasing absolute rates through time (Fig. III-43), with comparable slopes, even if the rhinolophid slope is slightly steeper. There are no differences regarding slopes, the differences between them and contrasting to the rest of the tree being too weak (Appendix III-3, Tables 3-4). There are however differences in the average absolute rates regarding these families. Hipposiderids demarcate from the rest of the tree in having strikingly high average absolute rates (Appendix III-3, Table 3) but also especially from rhinolophids (Appendix III-3, Table 4); this is likely due to the three very high rate values in hipposiderids. Rhinonycterids and rhinolophids, otherwise, do not differ

between them or from the rest of the tree: the evolution of their absolute rates, contrary to that of their relative paraflocculi mass, more fits the general framework. There are still some shifts of rate regimes (Appendix III-3, Table 5): there is an acceleration of the relative paraflocculi mass versatility from the "true" rhinolophoid node to the third basalmost hipposiderid node (excluding the *Macronycteris* + *Doryrhina* clade) plus the rhinonycterid node, and there is a deceleration at the second basalmost node of rhinolophids (excluding *Rhinolophus luctus*). Lower rates seem to characterize rhinolophids; *Rhinolophus luctus* may be an exception and/or may pertain to the Asian clade (depending on the phylogenetical results), which could slightly modify the shift location. The other accelerations seem to be caused by both the hipposiderid and rhinonycterid families, as both show very versatile evolution patterns of relative paraflocculi masses; a shift towards an acceleration of the variation of that trait would be unlikely at the "true" rhinolophoid node, but it would make sense at the hipposiderids + rhinonycterids node. However, there also may be a further acceleration in hipposiderids, given the very convergent pattern between crown inter-generic groups; this point would need further focused investigation. The "true" rhinolophoid families are very different, and a dichotomy appears between rhinolophids in one side (with high and few varying relative paraflocculi masses) and rhinonycterids + hipposiderids in another side (with lower and more varying relative paraflocculi masses). In the latter case, the absence of the fossils species that I have been able to use for the two other traits could be harmful: only two rhinonycterid species remain, and the only hipposiderid species form a clade, with no extinct comparison points for the *Hipposideros* genus. Further investigations in both these families are needed, expanding both fossil and extinct samples, in order to better characterize this very varying pattern of relative paraflocculi mass evolution.

IV.5) Cross traits comparison

Phylogenetic mappings of three traits considered here (Figs. III-35,38,41) do not show striking similarities between traits: both relative olfactory bulbs and paraflocculi masses have a high value reconstructed for the whole Yinpterochiroptera clade and then decrease through time, but with different patterns (Figs. III-40,43). On the other hand, relative brain mass is reconstructed as very low at the yinpterochiropteran root, and then increases through time (Fig. III-37). This means that, as a basal condition for that group, the whole brain was little encephalized whereas both olfactory bulbs and paraflocculi were large. Then, proportions inversed with time. Two hypotheses may explain this. First, it could be a physical increased integration of these structures in the brain through time: if the brain expanded, it may have had covered and "integrated" olfactory bulbs and paraflocculi, resulting in apparent lower values of these structures (while part of what was exposed being less and less exposed through time). While this may work for olfactory bulbs (an anatomical character of the morphological section regards the relative independence of the olfactory bulbs cast to the rest of the telencephalon), it is quite unlikely for the paraflocculi. Here, these structures are always well separated from the rest of the brain by a thick stem. The second hypothesis could regard a transfer of the functions primarily held in the olfactory bulbs and paraflocculi to other parts of the brain: especially, neocortical structures are known to assume functions some non-telencephalic structures are specialized for (for instance, mesencephalic rostral colliculi play a role in integration of visual, but there also are fields regarding visual integration in the neocortex likely subordinating some functions initially done by rostral colliculi; Edinger 1964a,b, Zhaoping 2016, Barchini et al. 2018). However, if true, this hypothesis does not stand for all non-telencephalic structures; for instance, caudal colliculi are still highly prominent in rhinolophoids through time (see the dedicated point in the morphological section) and do not appear to "transfer" functions to neocortical structures. A third, but more case-to-case hypothesis could be that the functions associated to the enlargement of olfactory bulbs and of paraflocculi become reduced through time, but, at least for olfactory bulbs, this clearly does not seem to happen in all taxa and cannot be regarded as a general rule.

Tracking the evolutionary rates of these traits through time (Figs. III-36,39,42), there are more striking similarities and differences. The pattern of major changes in relative olfactory bulbs mass in fact strikingly follows that of relative brain mass, and this is clearly highlighted by the distribution of absolute rates (Fig. III-39). The rate values at nodes are comparable, and the same nodes have the particularly high burst in rates: the pteropodids (together with the pteropodines) and the rhinonycterids, with a very similar pattern. There however are slight differences at nodes regarding other groups: megadermatids have a bit lower rates, whereas rhinolophids and rhinopomatids have a bit higher rates at the family node, and hipposiderids have higher rates at the deepest nodes of the family. There also are some tips with particularly high values occurring in pteropodids, similar to the case of relative brain mass rates. On the other hand, the pattern of absolute rates of relative paraflocculi mass evolution completely differs: there are very few changes through time, and they mainly appear at terminal taxa. The patterns of trends for each major clade are also strikingly similar for both relative brain and olfactory bulbs masses (Figs. III-37,40) and clearly contrasts with that of relative paraflocculi mass (Fig. III-43), in which there is a slightly increase through time shared by all groups.

This intriguing shared pattern of changes between the relative brain mass and the relative olfactory bulbs mass would mean that changes in the encephalization of the brain are "automatically" accompanied by changes in the size of the olfactory bulbs. It however has to be noted that changes in trait values are not strictly correlated (Figs. III-35,38), and rhinonycterids illustrate all retrieved cases: relative brain and olfactory bulbs masses decrease before the familial node, both are similar on the branch leading to the *Rhinonicteris* genus, but relative brain mass increases while relative olfactory bulbs mass still decreases between the familial node and the rhinonycterid internal node, then either both increase (before the *Xenorhinos* + *Triaenops* node) or decrease (before the *Archerops* + *Cloeotis* node). Some terminal branches also show scenarios where the relative brain mass decreases while the relative olfactory bulbs mass increases (*Hipposideros caffer*, *Macronycteris gigas*, *Rhinolophus ferrumequinum*, *Rhinolophus landeri*, *Nyctimene major*), but this case is more rare.

The fact that changes in relative brain and olfactory bulbs masses are so closely associated necessarily implies that both structure evolve together to a certain degree. The simplest explanation would be that the whole brain encephalization is due to an increase of olfactory bulbs relative mass, but the fact that the directions of variation are independent refutes this hypothesis and as well as a simple coevolution hypothesis between the two structures; especially, cases with increasing brain encephalization and decreasing olfactory bulbs size are not rare (e.g., megadermatids, Pteropodinae). Conversely, the fact that increasing relative olfactory bulbs mass and decreasing relative brain mass (or the reverse) are not the only patterns also refutes a trade-off hypothesis of olfactory structures. There may thus be interacting processes, at the genetic and/or ontogenetic scales, governing both jointly and independently the relative masses of the brain and of the olfactory bulbs: some processes are common and imply a common variation, governing the fact that there is variation or not, and others are specific to each structure and rather govern the direction of the variation, if there is any.

Comparing relative brain and olfactory bulbs masses variations at the family level (Figs. III-35,38), there is an initial relative brain mass increase before pteropodids, whereas relative olfactory bulbs do not change that much. As previously and separately showed, pteropodids are thought to highly rely on the sense of smell and to process more information to find food than animalivorous bats (e.g., Bhatnagar & Kallen 1974, Safi et al. 2005, Hayden et al. 2014). In that way, an increase of brain encephalization and a stasis of relatively large olfactory bulbs are congruent: the brain becomes more encephalized, and the olfactory bulbs still are large. This however relies on the fact that olfactory bulbs relative size is linked to olfactory acuity, which is not asserted (see previous parts regarding olfactory bulbs). The covariation pattern then changes and varies across pteropodids: relative brain and olfactory bulbs masses variations are of similar direction in both Pteropodinae and Cynopterinae, with a joint variation (both relative masses increases in Cynopterinae and decreases in Pteropodinae), but there is an antagonistic variation in Nyctimeninae (as the single *Nyctimene major* here, where the relative brain mass decreases while the relative olfactory bulbs mass increases). In the case of Nyctimeninae, if relative olfactory bulbs mass is related to olfaction, this pattern may be linked to their particular nose: Nyctimeninae have independent and tube-shaped nostrils that may allow them having sort of a stereo-olfaction and scan their environment using this sense (Hall & Pettigrew 1995). In that case, increased relative olfactory bulbs mass may be related to this peculiarity, while maybe reducing in relative brain mass as a trade-off enhancing olfaction.

In the “other” rhinolophoids clade, there are opposite patterns of the covariation between both relative brain and olfactory bulbs masses variation along the branches leading to both rhinopomatids and megadermatids: there is a joint reduction of relative brain and olfactory bulbs masses before rhinopomatids, whereas it is antagonistic before megadermatids. These two patterns may be further correlated to the ecological specificities of each family, that clearly contrast in their ecology: rhinopomatids live in quite more open habitats than megadermatids and have a very different flight (faster in rhinopomatids, more maneuverable in megadermatids) and different prey hunting strategies (aerial hawking of insects in rhinopomatids, gleaning of small animals in megadermatids) (e.g., Baron et al. 1996, Francis 2019, Horacek 2019). However, taking into account that such covariation patterns also apply to other ecologically different taxa (the pattern before megadermatids is also present before the rhinolophid node, and similar patterns are present along the branch leading to both rhinopomatids and rhinonycterids), the general causes of these patterns must first be investigated before correlating them to the familial ecologies. The “other” rhinolophoid case is a good example of that point, and of the need of a broader phylogenetic context to better consider these patterns.

Major changes also regard the covariation patterns between relative brain and olfactory bulbs masses for “true” rhinolophoid families. Rhinolophids generally follow an antagonistic pattern, where relative brain mass increases and relative olfactory bulbs mass decreases before the family node, and then both do not vary much within the family. As previously exemplified, the rhinonycterids illustrate a wide array of possible patterns. Hipposiderids also present a complex pattern: there is a joint pattern for the deepest family nodes (both traits increase), then are an antagonistic pattern for the genera *Hipposideros* sensu stricto (further increasing in relative brain mass but decreasing in relative olfactory bulbs mass) and *Palaeophyllophora* (reverse case) and a joint pattern for the other clades (with a joint decrease), and then are some particular cases for terminal taxa (joint terminal increase for *Aselliscus*, antagonistic pattern as *Hipposideros* for *Coelops*, antagonistic pattern as *Palaeophyllophora* for *Macronycteris*). Such a variation, in hipposiderids and in rhinonycterids, leads to question the hypothesis of a common constraint implying a joint change, no matter its direction. Indeed, at the Yinpterochiroptera scale, independence seems unlikely: changes are always associated for both traits, but also are static. At the family-level, other considerations may better explain the changes of change patterns, maybe with disconnected constraints on brain and on olfactory bulbs allowing them to increase or decrease in relative mass independently. In rhinonycterids and hipposiderids, there would still be independent pressure acting on both relative masses (toward increase or decrease), but the common constraint (on the fact of covarying or not) would be absent.

IV.6) Contrasting evolutionary patterns with and without fossil taxa

IV.6.A) Traits evolution without fossils

IV.6.A.a) Brain mass (Figs. III-44-46)

By discarding fossils, the reconstructed ancestral relative brain masses clearly change, which drastically affects the global pattern of relative brain mass evolution (Fig. III-44): deepest reconstructions become slightly positive (instead of negative) values, implying a decrease of relative brain mass in four of the six families (rhinopomatids and rhinonycterids, but also rhinolophids and hipposiderids) and an increase in only two families (megadermatids and pteropodids). In the two families where fossils were discarded (rhinonycterids and hipposiderids), the relative brain mass evolution is not totally similar. There is a gradual decrease of relative brain mass in rhinonycterids, while the pattern is more confused with fossils, and in hipposiderids as well, the positive values of the two *Hipposideros* species being convergent. Tracking trends of relative brain mass (Fig. III-46) confirms the visual pattern of mapping: there is a general decrease (p-values close to 3.10^{-3}, Appendix III-3, Table 2) differing from Brownian motion (p-values around 0.03, deviation of ~-0.21 times the standard deviation of relative brain mass values) paralleled by all major groups (Fig. III-46; Appendix III-3, Table 3). Moreover, the pattern of differences between clades also changes a bit: the slope of pteropodids is slightly higher than that of "other" rhinolophoids, and the slope of rhinonycterids is way smaller than that of hipposiderids, and even more than that of rhinolophids (Appendix III-3, Table 4). Pairwise comparisons of relative brain mass emmeans remain similar, even though that of rhinolophids is no more significantly different from those of hipposiderids and rhinonycterids (p-values near 0.99 and 0.35 respectively, Appendix III-3, Table 4).

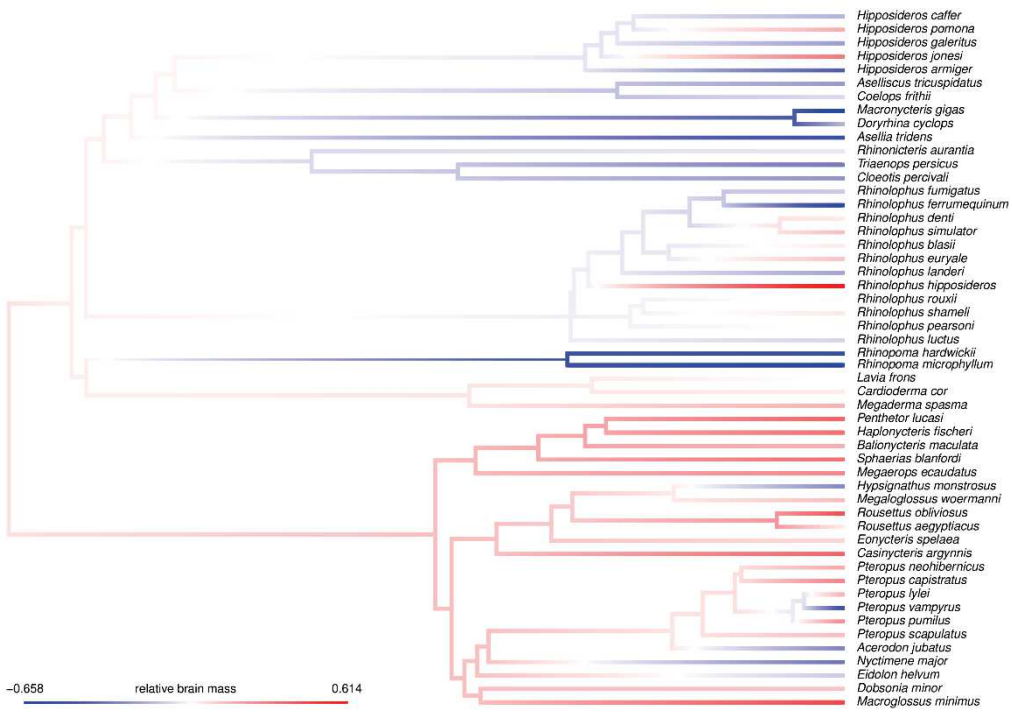

Figure III-44: Mapping of the relative brain mass on the Yinpterochiroptera phylogeny pruned to the sample of this study without fossil species. This stands for the phylogeny with *Palaeophyllophora* as sister-genus to *Hipposideros*. Other cases are figured in Appendix III-10-10.

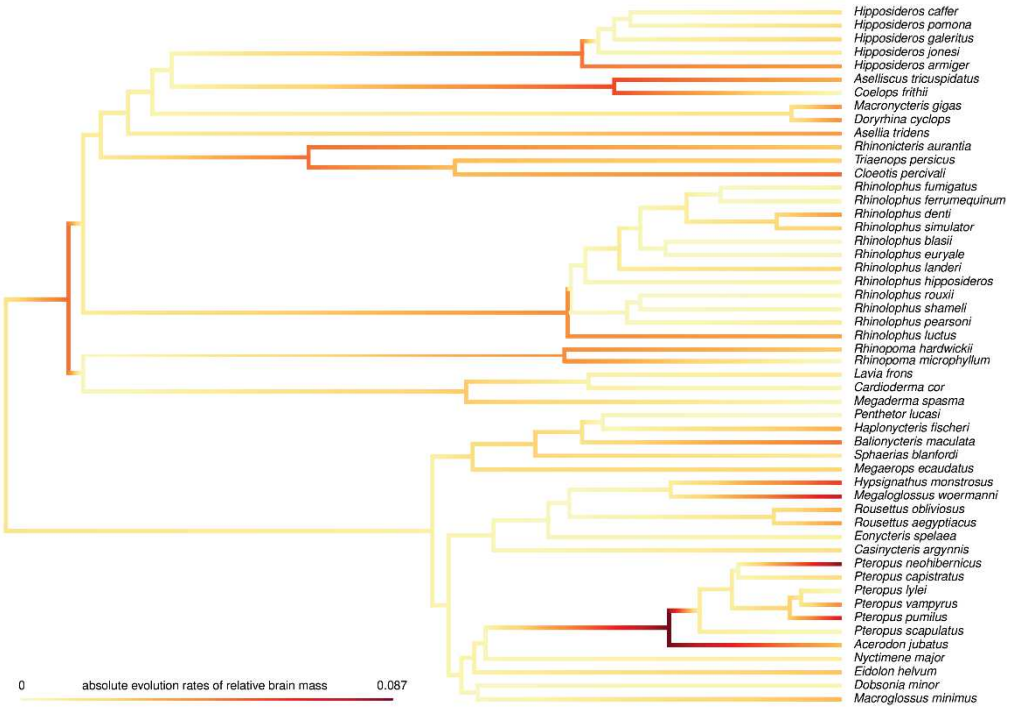

Figure III-45: Mapping of the absolute evolutionary rates of relative brain mass on the Yinpterochiroptera phylogeny pruned to the sample of this study without fossil species. This stands for the phylogeny with *Palaeophyllophora* as sister-genus to *Hipposideros*. Other cases are figured in Appendix III-10-11.

The distribution of absolute evolution rates of relative brain mass (Fig. III-44) clearly changes. There is no basal pteropodid burst anymore, while there is a basal acceleration in rhinolophoids. Rhinolophoid families in general show basal accelerations: rhinonycterids retain a similar pattern, but the most noticeable change cocerns the basal nodes of rhinolophids, rhinopomatids, and (to a lesser extent) megadermatids. Among terminal taxa, those showing terminal accelerations with fossils still do without, the major change being that rhinonycterid tips have higher absolute rates than with fossils. Evolutionary trends pattern of absolute rates (Fig. III-46) is similar, though the general increase is lower and slightly not significant (p-value between 0.07 and 0.3, Appendix III-3, Table 2). All major clades retain the same pattern of absolute rate evolution, even though the values of the slope slightly differ, with the exception of rhinopomatids whose slope inverts in sign, being clearly decreasing without fossils, affecting the slope of "other" rhinolophoids in the same way but not with the same magnitude (slightly negative slope). The slope of whole rhinolophoids is also noticeable as being very close to zero, indicating a global stasis of rate variation, but that overshadows more complex (and opposite) patterns. Pteropodids slope is higher than that of rhinolophoids as with fossils (p-value close to 7.10^{-3}, Appendix III-3, Table 3), as well as that of rhinonycterid, the difference between the slope of the latter group compared to the rest of the tree being not significant anymore. Otherwise, no pairwise slope comparison becomes significant. Rhinolophid rate emmean is still different from all others, being lower (p-values of 0.01, Appendix III-3, Table 3), while that of rhinonycterid remains only slightly significant (p-values between 0.046 and 0.051, Appendix III-3, Table 3); the difference between the emmeans of both groups however remains significant (p-values close to 0.03, Appendix III-3, Table 4). The significant shifts toward an increase of absolute rates retrieved between the pteropodid node and the node before that of pteropodines are not all found without fossils; only the two nodes before Pteropodinae remain significant (with the highest difference for the node Pteropodinae + *Nyctimene major*). The shift at the node of Rousettinae remains, however, significant (p-

value > 0.98, Appendix III-3, Table 5). The rhinolophid node also remains significant in a decrease of absolute rates, while this is the third and not the second basalmost rhinolophid node that is also significant (Appendix III-3, Table 5).

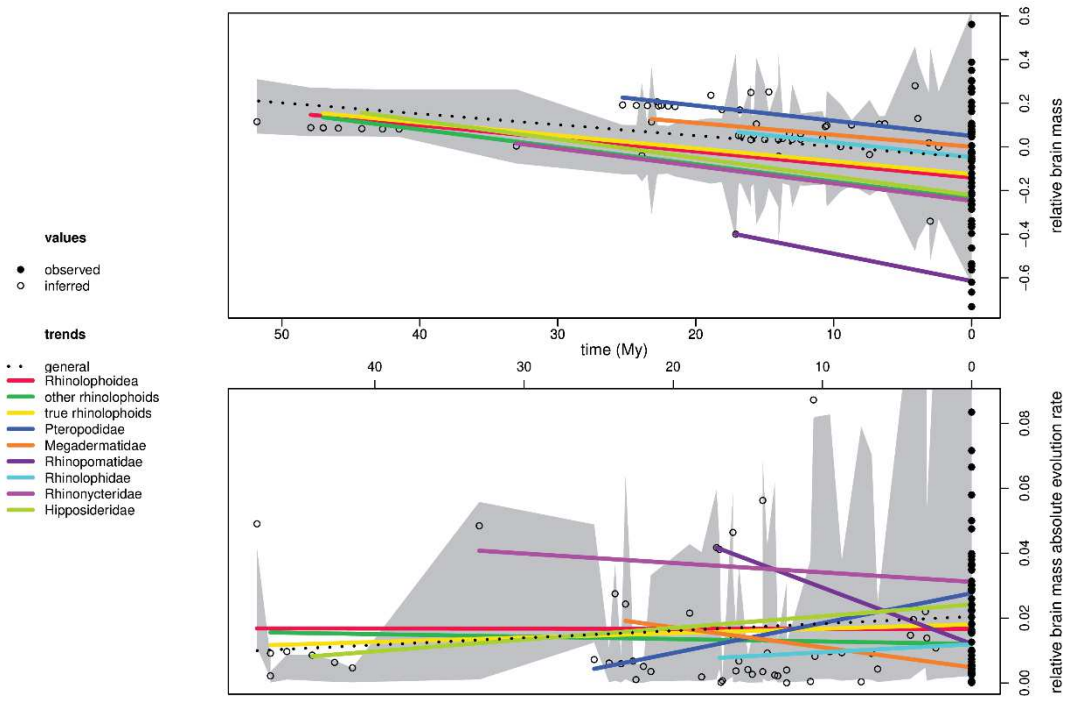

Figure III-46: Temporal trends of relative brain mass (top) and of its absolute evolutionary rates (bottom) without fossil species. The grey background illustrates a simulated variation under a Brownian motion regime. This stands for the phylogeny with *Palaeophyllophora* as sister-genus to *Hipposideros*. Other cases are figured in Appendix III-10-12.

IV.6.A.b) Olfactory bulbs mass (Figs. III-47-49)

Without fossils, the pattern of relative olfactory bulbs mass distribution (Fig. III-47) fully stands and is exactly similar to that with fossils. The pattern of evolutionary trend of the relative olfactory bulbs mass (Fig. III-49) is also very similar with and without fossils, with a slightly more negative slope (p-values close to 4.10^{-4}, Appendix III-3, Table 2) whose deviation from Brownian motion is comparable but significant (~-0.25 times the standard deviation of relative olfactory bulbs mass, Appendix III-3, Table 2). It is noticeable that all clades, with no exception, follow the general trend (Fig. III-49): as with relative brain mass, all clades are lower than Brownian motion slopes (Appendix III-3, Table 3), and slope pairwise comparisons yield the same ordinations (Appendix III-3, Table 4). The same stands for emmeans of each group: that of pteropodids is above that of rhinolophoids (p-values at the 10^{-6} level, Appendix III-3, Table 3) that of megadermatids is clearly beyond the other (p-values close to 3.10^{-3}, Appendix III-3, Table 3), and that of rhinolophids is slightly lower than the rest of the tree (p-values close to 0.04, Appendix III-3, Table 3). As with fossils, only pteropodids and basal rhinolophoid nodes differ in their emmeans (p-values at the 10^{-5} level, Appendix III-3, Table 4), and the same observations can be made for the other pairwise comparisons (p-values close to 0.08 between “other” and “true” rhinolophoids, p-values close to 0.99 between hipposiderids and rhinonycterids, the two families concerned by the exclusion of fossil values; Appendix III-3, Table 4).

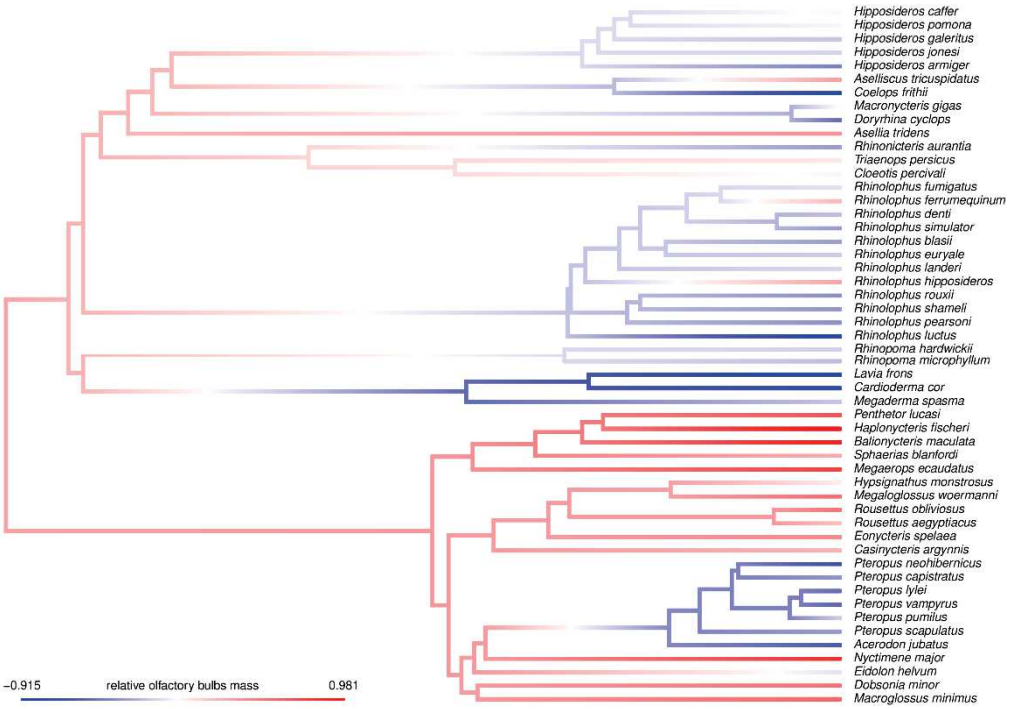

Figure III-47: Mapping of the relative olfactory bulbs mass on the Yinpterochiroptera phylogeny pruned to the sample of this study without fossil species. This stands for the phylogeny with *Palaeophyllophora* as sister-genus to *Hipposideros*. Other cases are figured in Appendix III-10-13.

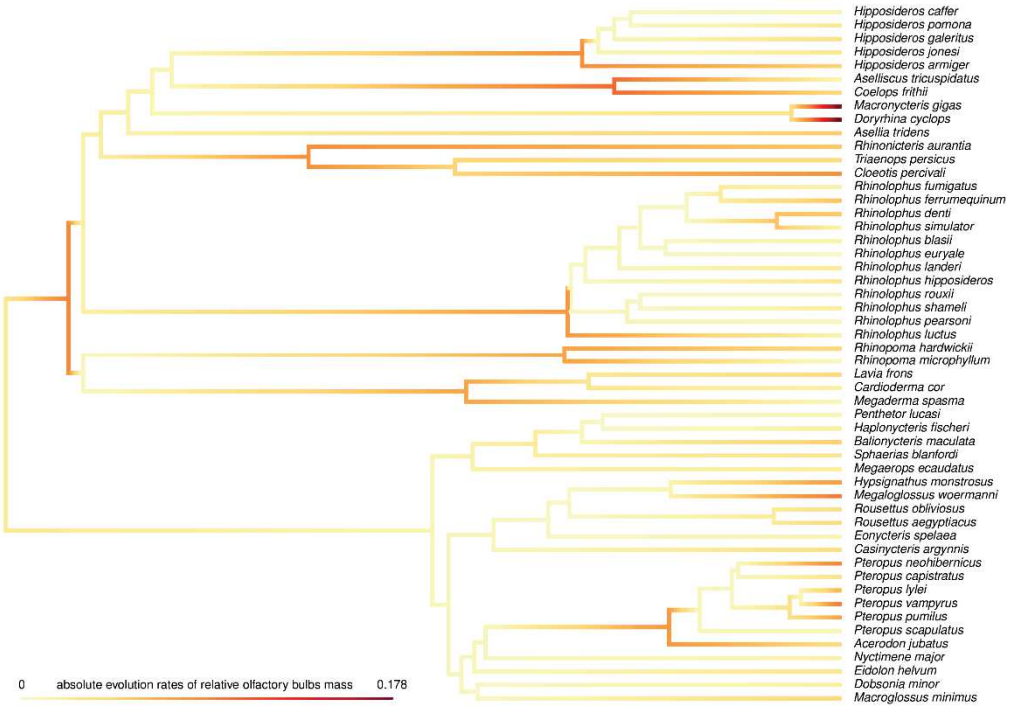

Figure III-48: Mapping of the absolute evolutionary rates of relative olfactory bulbs mass on the Yinpterochiroptera phylogeny pruned to the sample of this study without fossil species. This stands for the phylogeny with *Palaeophyllophora* as sister-genus to *Hipposideros*. Other cases are figured in Appendix III-10-14.

Discarding fossil taxa clearly changes the distribution of rates across the tree (Fig. III-48), though the pattern strikingly resembles that of relative brain mass absolute evolutionary rates. In that way, there also are rhinolophoid rate accelerations (at the superfamily and family nodes), while the initial burst of pteropodids found with fossils is absent without fossils. In the latter family, this is however the only major change: all other rate accelerations found with fossils are retrieved without. Terminal accelerations found in rhinolophoids with fossils also persist without; as with the case of relative brain mass, the only major changes regard rhinonycterid tips whose absolute rates are higher without fossils. The pattern of absolute rate variation through time differs a bit when fossils are absent (Fig. III-49): the general slope is a bit flatter and slightly not significant (p-values between 0.05 and 0.08, Appendix III-3, Table 2), and only the "true" rhinolophoids and the rhinolophids nodes clearly parallel it. The "other" rhinolophoids node, as well as the two families in that clade, have a negative slope, but it is much closer to zero. In a similar way, the slope of whole rhinolophoids slightly rises, but is quite flat. Pteropodids and hipposiderids have a steeper slope, while other families (rhinopomatids, megadermatids, and rhinonycterids) have a negative slope, of varying magnitude (decreasing respectively). Pteropodids and rhinolophoids have significantly different slopes (p-values close to 0.03, Appendix III-3, Table 3), but this is the only significance among nodes; the rhinonycterid slope, much flatter than with fossils, is no longer significant (p-values > 0.1, Appendix III-3, Table 3). As with fossils, there are no significant pairwise slope comparisons, the rhinonycterid being particularly concerned by the absence of fossil values; it is however worth noting that the p-values for the pairwise comparisons between pteropodid and deep rhinolophoid slopes, though clearly not significant, are lower than previously (p-values around 0.2, Appendix III-3, Table 4). Rhinolophids, but also hipposiderids, show significantly different absolute rate emmeans compared to the rest of the tree, that of rhinolophids still being lower (p-values of 0.02, Appendix III-3, Table 3) and that of hipposiderids being higher (p-values of 0.02, Appendix III-3, Table 3). The rhinonycterid absolute rate emmean is clearly higher than that of the rest of the tree, but this difference floats around the significant level: it is under it (p-value of 0.047, Appendix III-3, Table 3) for a longer branch of *Hipposideros* and of the *Aselliscus* + *Coelops* clade (due do the basal position of *Palaeophyllophora*, the node between these two clades is older than in other hypotheses), while it is slightly over it otherwise (up to 0.052, Appendix III-3, Table 3). The same significant taxonomic differences appear there, the rhinolophid absolute rate emmean being lower than that of hipposiderids (p-values close to 0.02, Appendix III-3, Table 4) and that of rhinonycterids (p-values near 0.04, Appendix III-3, Table 4). Previously detected shifts in absolute rates are also found, with even some more shifts without fossils. The second basalmost rhinolophid node (discarding Asian rhinolophids) becomes significant toward a decrease of absolute rates too (p-values slightly under 0.025, Appendix III-3, Table 5), the absolute rate difference at that node being less significant but larger than those of the two more apical rhinolophid nodes (p-values < 0.001 for both, Appendix III-3, Table 5). Similarly, the hipposiderid + rhinonycterid node is still highly significant (p-values > 0.999, Appendix III-3, Table 5), but the hipposiderid node becomes significant too (p-values > 0.99, Appendix III-3, Table 5), as well as the hipposiderid node discarding *Asellia tridens* (p-values > 0.99, Appendix III-3, Table 5) and the following basal hipposiderid node, discarding the *Macronycteris* + *Doryrhina* clade (p-value of 0.62 for deeper *Hipposideros* + (*Aselliscus* + *Coelops*) node, p-values > 0.99 otherwise, Appendix III-3, Table 5); among these nodes, only the apicalmost one keeps the higher absolute rate difference (contrary to the rhinolophid condition).

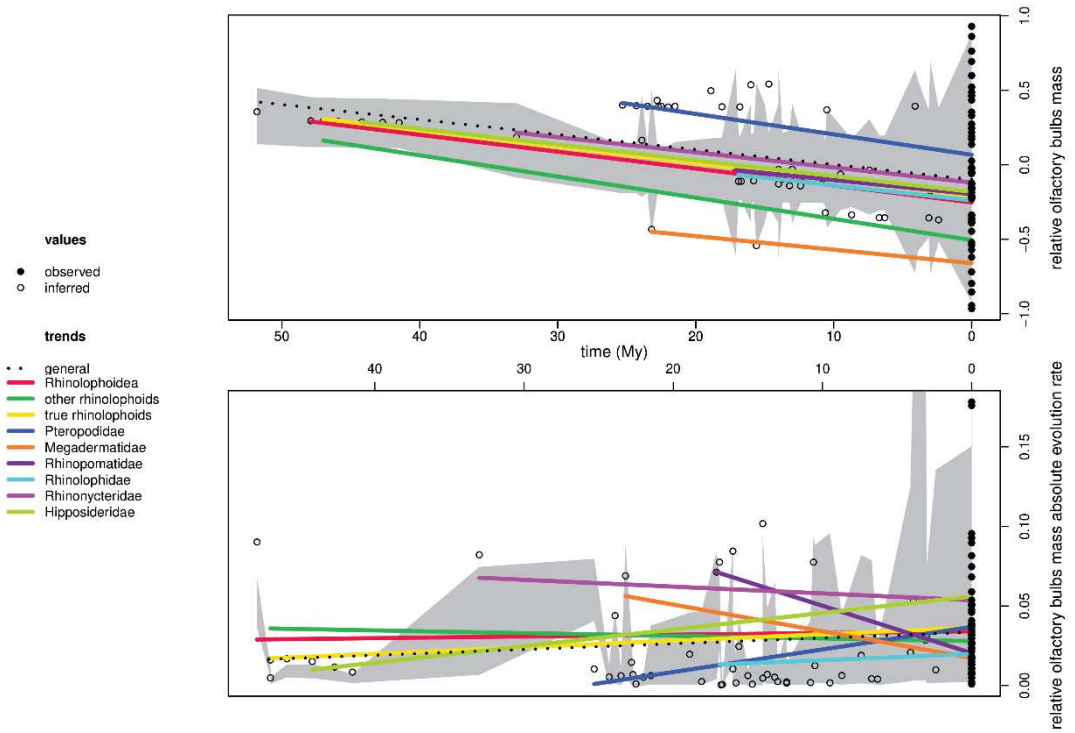

Figure III-49: Temporal trends of relative olfactory bulbs mass (top) and of its absolute evolutionary rates (bottom) without fossil species. The grey background illustrates a simulated variation under a Brownian motion regime. This stands for the phylogeny with *Palaeophyllophora* as sister-genus to *Hipposideros*. Other cases are figured in Appendix III-10-15.

IV.6.A.c) Paraflocculi mass (Figs. III-50-52)

Discarding fossils here only discards the *Palaeophyllophora* species, as no other fossil endocast preserves the paraflocculi. The distribution of the relative paraflocculi mass (Fig. III-50) is thus similar, but it differs in the fact that the ancestral reconstruction values are lower, still positive. This leads to increases in relative paraflocculi mass in some families (megadermatids, rhinopomatids, rhinolophids) with a stasis in hipposiderids. Temporal evolution of relative paraflocculi mass (Fig. III-52) concurs with the previous observation: the general slope is a bit steeper, closer to 0, and not significant (p-values around 0.057, Appendix III-3, Table 2), with a smaller but significant deviation of the mean from Brownian motion (~-0.14 times the standard deviation of relative paraflocculi mass values). The slopes of deep rhinolophoid nodes and hipposiderids parallel the general, flatter trend, and it is worth noting that all other slopes (regarding the other five families) become negative, and most of them significantly differ from the Brownian motion regime (Appendix III-3, Table 3), but with several changes: megadermatid, rhinopomatid, and rhinolophid slopes remain significant, as well as that of "other" rhinolophoids (that is significant with fossils only if *Palaeophyllophora* is the basal most hipposiderid genus), those of hipposiderids and pteropodids become not significant while those of rhinolophoid and "true" rhinolophoid become significant, and that of rhinonycterids is floating around the significant level (Appendix III-3, Table 3). Without fossils, all pairwise slope comparisons remain significant. The slope of "other" rhinolophoids remains flatter than that of "true" rhinolophoids", but both are now flatter than that of pteropodids (all being decreasing, but the pteropodid slope was positive with fossils). Otherwise, all slopes now decreasing, the hierarchy are maintained: the slope of rhinopomatids remains steeper than that of megadermatids, and the slope of rhinolophids remains flatter than that of hipposiderids and even more than that of rhinonycterids (Appendix III-3, Table 4). Regarding relative paraflocculi mass emmeans, there are no changes but removing fossils: the three "true" rhinolophoid families are still distinguished

from the rest of the tree, rhinolophids having a larger average relative paraflocculi mass (p-values around 3.10^{-3} for rhinolophids) while hipposiderids and rhinonycteris have a smaller one (p-values around 6.10^{-4} for rhinonycterids and 6.10^{-3} for hipposiderids, Appendix III-3, Table 3), and rhinolophids still distinguish themselves from hipposiderids and rhinonycterids in pairwise comparisons, having a higher average relative paraflocculi mass (p-values close to 1.10^{-4} compared to rhinonycterids and to 6.10^{-4} compared to hipposiderids, Appendix III-3, Table 4).

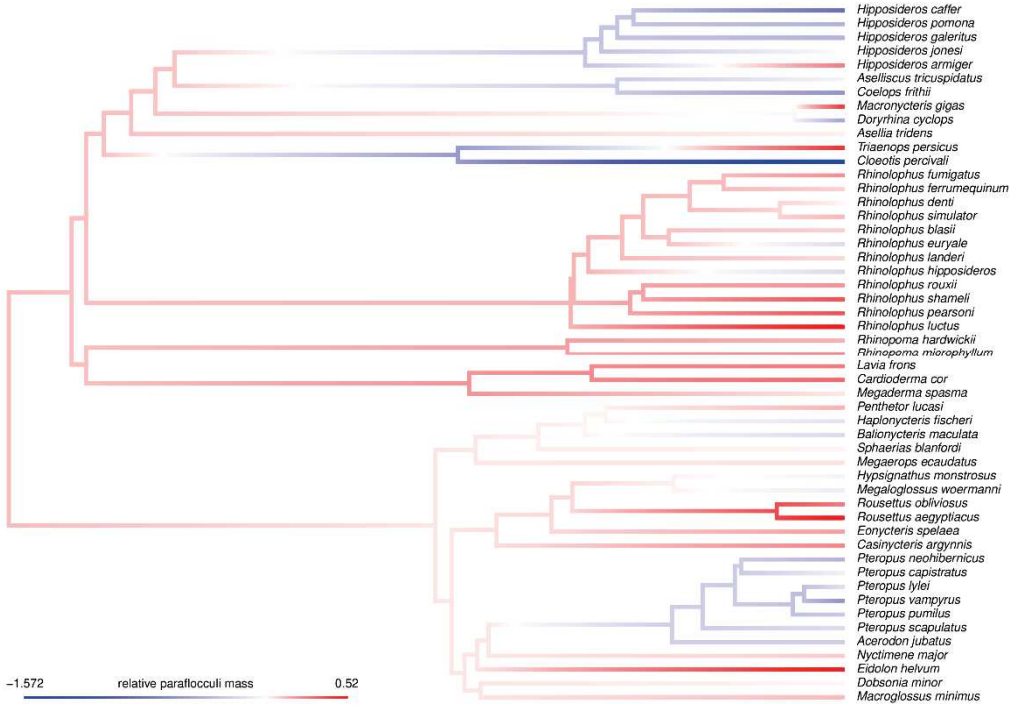

Figure III-50: Mapping of the relative paraflocculi mass on the Yinpterochiroptera phylogeny pruned to the sample of this study without fossil species. This stands for the phylogeny with *Palaeophyllophora* as sister-genus to *Hipposideros*. Other cases are figured in Appendix III-10-16.

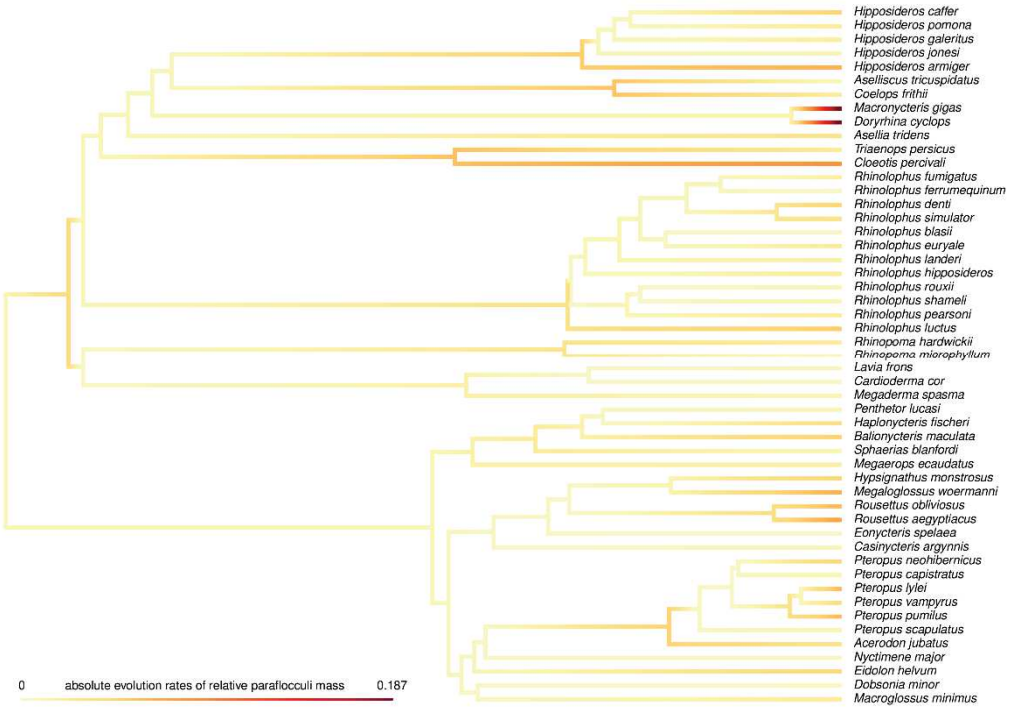

Figure III-51: Mapping of the absolute evolutionary rates of relative paraflocculi mass on the Yinpterochiroptera phylogeny pruned to the sample of this study without fossil species. This stands for the phylogeny with *Palaeophyllophora* as sister-genus to *Hipposideros*. Other cases are figured in Appendix III-10-17.

As for the mapping of the relative paraflocculi mass, removing the fossils does not change the distribution of its absolute evolutionary rates (Fig. III-51). However, the temporal trends noticeably change (Fig. III-52): if the pteropodids slope does not change, all others vary. The general trend is slightly steeper and becomes significant (p-values between 2.10^{-3} and 5.10^{-3}, Appendix III-3, Table 2), and a bit more so are the slopes of rhinolophoid, “true" rhinolophoid, and hipposiderid nodes, while the other slopes are lower, some becoming flatter (“other” rhinolophoids, rhinolophids) or even negative (rhinonycterids, rhinopomatids, megadermatids). These changes are however too slight to make the node slopes significant relatively to a Brownian motion regime (all p-values > 0.12, the lowest being around 0.14 for hipposiderids, Appendix III-3, Table 3) nor to distinguish clades from each other (all p-values > 0.4, Appendix III-3, Table 4). In a parallel way, hipposiderid absolute rates emmean is significantly higher than that of the rest of the tree (p-value around 4.10^{-3}, Appendix III-3, Table 3) and specifically higher than that of rhinolophids (p-values around 0.1, Appendix III-3, Table 4). There are no major variations regarding the shifts towards low absolute rates: that occurring at the “other” rhinolophoids node becomes not significant (but that of megadermatids still is, p-values of both being around 0.05 and 0.02 respectively, Appendix III-3, Table 5), and there is a supplementary shift at the rhinolophid node (p-values around 0.02, Appendix III-3, Table 5) but is lower in support and in shift to that of the second basalmost rhinolophid node. On the other hand, all the shifts towards high absolute rates occurring from the hipposiderid + rhinonycterid node to the hipposiderid except *Asellia tridens* and *Macronycteris* + *Doryrhina* clade remain significant, the basalmost of these being the most significant (p-values > 0.999, Appendix III-3, Table 5), while that of hipposiderids but *Asellia tridens* shows the largest absolute rate difference.

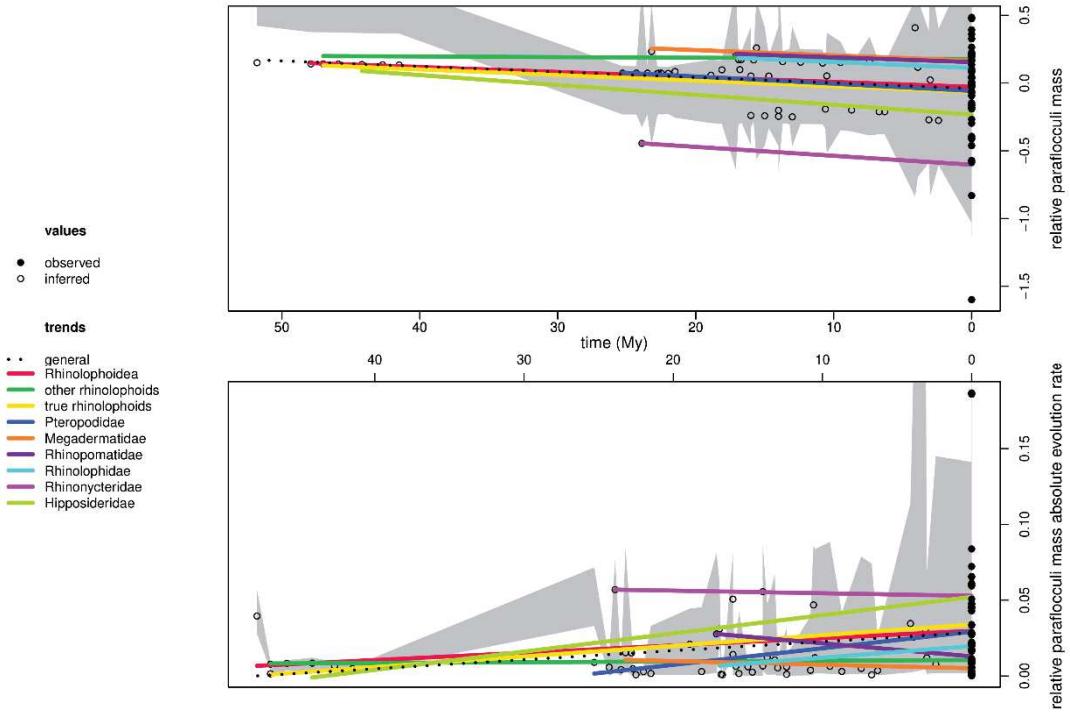

Figure III-52: Temporal trends of relative paraflocculi mass (top) and of its absolute evolutionary rates (bottom) without fossil species. The grey background illustrates a simulated variation under a Brownian motion regime. This stands for the phylogeny with *Palaeophyllophora* as sister-genus to *Hipposideros*. Other cases are figured in Appendix III-10-18.

IV.6.B) Reconstruction parameters comparisons

In addition to the comparison of reconstructions with and without fossils (i.e., previous parts), I directly compare the different values obtained for the same taxa, with and without fossils. All values regarding ancestral reconstructions (for nodes), absolute evolutionary rates (for all taxa), and absolute rate differences (between within and outside a clade, for all nodes up to half of the sample) are computed against each other (i.e., with vs without fossils) for each trait and regarding the first phylogeny only (with *Palaeophyllophora* as the sister-genus to *Hipposideros*; Fig. III-53 and Appendix III-10-19 for the other phylogenies). On these biplots, the "deep nodes" of interest (i.e., all, "true", and "other" rhinolophoids nodes plus all family-level nodes) are highlighted using the same colors as previously (i.e., in Figs. III-37,40,43) and the root is indicated as a black-bordered white small square, and the significant shifts in rate regime are indicated by varying symbols (depending if the absolute rate difference is significant with and/or without fossils). In a case when fossil taxa values do not modify the evolutionary pattern of the three traits, the same value is expected with or without fossils; the line of best fit if evolutionary patterns are equal with or without fossils is thus a y = x line, that is added to the biplots, and the more a point drift from this line, the more it is affected by the presence/absence of fossil taxa values. Lines at x = y = 0 are also drawn for ancestral reconstructions, in order to see sign inversions (in the top left and bottom right areas). Finally, the calculation of an adjusted R squared using this line of best fit as a reference affords an idea about the strength of the relationship between values with and without fossils: the more robust a relationship is, the less impact fossils have.

Regarding the ancestral estimations of all traits (i.e., relative masses), there are some points obviously separated from the theoretical line: the nodes of families with fossils (hipposiderids and rhinonycterids regarding brain and olfactory bulbs masses) are far from the line, as well as their close nodes (i.e., the deepest nodes of the tree). This is particularly true for relative brain and paraflocculi masses, while it is

clearly less striking for relative olfactory bulbs mass. There are sign inversions only regarding the relative brain mass, with deep nodes (root, deep rhinolophoid nodes, hipposiderid node) having negative values with fossils and positive values without them, and with some other nodes including that of rhinolophids having positive values with fossils and negative values without them. The adjusted R squared is very low (even slightly negative) for relative brain mass, as numerous points are far from the line; it is positive for the two other traits, being higher for relative olfactory bulbs mass (all points are aligned along the theoretical line, though several show an offset, either above or under the line) than for relative paraflocculi mass (more points being far from the theoretical line).

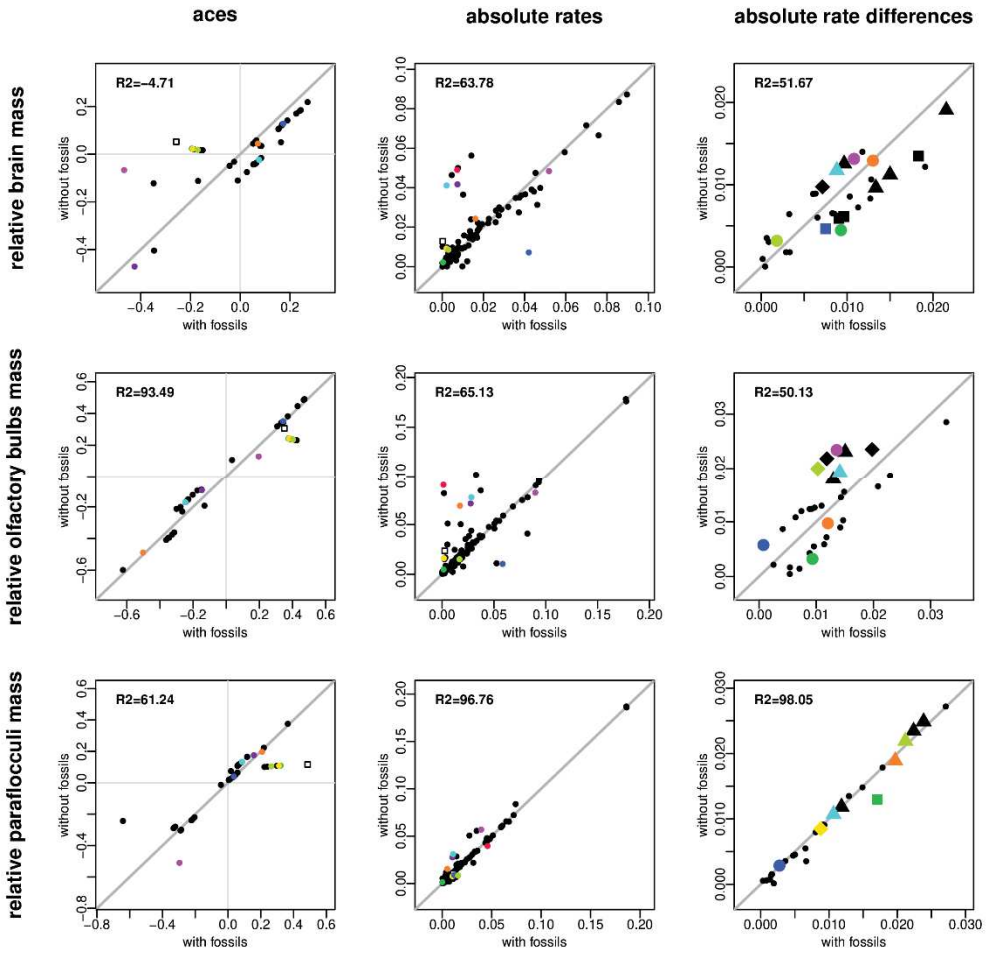

Figure III-53: Comparisons of ancestral reconstruction (for nodes), absolute evolutionary rates (for all taxa), and differences between within and outside taxa average absolute rates (for all nodes up to half of the tree) for each trait studied here. Superimposed are the theoretical line of identical fit by considering fossils or not (thick light gray line) and the adjusted R squared explained by this y = x relationship. For nodal reconstructions, plot area is separated by lines at zero values in order to see the sign changes in reconstruction (top left and bottom right areas of the plot). Note that here, a negative adjusted R squared indicates a particularly poor fit (worse than a horizontal line). This stands for the phylogeny with *Palaeophyllophora* as sister-genus to *Hipposideros*. Other cases are figured in Appendix III-10-19.

Regarding the absolute evolutionary rates (considering the evolution of relative masses, thus taking the effect of the predictor during the rate calculation), there are also major discrepancies between analyses with and without fossil taxa. The plots regarding the absolute rate estimates also have more points than the others because rates are also calculated for extant taxa, not only for nodes. In both the brain and the olfactory bulbs, numerous points are quite far from the theoretical line, and the adjusted R squared is not very high. The furthest "deep nodes" from the line are the rhinolophoids (the furthest point) and the rhinolophid, rhinopomatid, megadermatid, and pteropodid points (all at a similar distance). Hipposiderids, rhinonycterids, and "true" and "other" rhinolophoid points are quite closer to the line. Rates are thus similarly estimated for these groups with or without fossils, but the latter seem to highly impact other groups that do not include fossils. It is also worth noting that in the case of points far from the line, there are two cases: for some points, absolute rates are estimated to be close to zero with fossils but to be higher without fossils (e.g., rhinolophoids, megadermatids, rhinolophids, rhinopomatids) and for other points, it is the reverse, with high absolute rates only by considering fossil taxa (e.g., pteropodids). Regarding points close to the line, there also are two cases: for some points (e.g., rhinonycterids), absolute rates are always high, while for most points (e.g., hipposiderids, "true" and "other" rhinolophoid nodes), absolute rates are always low. For paraflocculi mass, the adjusted R squared is quite higher than for brain and olfactory bulbs mass; this corresponds to the visual imprint of the plot, where fewer values are less far from the line. Most of the considered "deep nodes" always have low absolute rates, but some families (rhinonycterids, rhinolophids, rhinopomatids) have slightly higher absolute rates by discarding fossils than by including them.

In the case of absolute rate differences between within vs outside considered clades, the pattern is a bit different: for both the brain and olfactory bulbs masses, the adjusted R squared are not very high, and most points are located on both sides of the theoretical line, while the adjusted R squared is very high with almost all points on the line for the paraflocculi mass. The adjusted R squared is even slightly lower for olfactory bulbs mass than for brain mass, probably because there are some points further from the line than for brain mass. This means that, in these two cases, rate difference values are rarely similar, whereas most of the absolute rates and of the ancestral estimates are. On the other hand, regarding paraflocculi mass, there are few different absolute rate differences by considering fossil taxa or not. It also has to be kept in mind that, though these differences may vary depending on the presence of fossil taxa or not, only a few have been found to be significantly different from a random distribution. Regarding brain mass, four shifts have been only found to be significant using fossil data (square symbol, especially one regarding pteropodids), one is significant only without fossils (lozenge symbol), and five are found with or without fossils (especially one regarding rhinolophids). All these significant shifts are displaced from the theoretical line, seven being under the theoretical line (lower value without fossils than with them), while three are above it. Regarding olfactory bulbs mass, three shifts are significant without fossils (especially one regarding hipposiderids), and three are significant with or without fossils (especially one for rhinolophids), which is a quite higher ratio than for brain mass. As for brain mass, these shifts are not on the theoretical line; differing from the brain mass, all are above that line, with a greater value in rate differences without than with fossils. Finally, regarding paraflocculi mass, one shift is significant only with fossils (for "other" rhinolophoids), two are significant only without fossils (regarding "true" rhinolophoids and rhinolophids), and five are significant in both cases (especially two regarding hipposiderids and megadermatids). In all cases except that significant only with fossils, the rate differences are similar with and without fossil taxa.

Another way to investigate the impact of the inclusion of fossils is to look at the evolutionary trends, regarding the evolution through time of both the trait (relative masses) and its absolute evolutionary rates. Here, I look at the pairwise differences between taxonomic groups of the parameters of these trends. I compared "deep nodes" that are comparable (i.e., that are at the same taxonomic level and/or sister-taxa) both with and without fossils; it is a key point to know if differences in groups evolutionary trend depends on the sampling of fossil taxa. I thus contrasted the taxonomic differences in the evolutionary trend slope and in the emmeans for both the trait and its absolute rates (with *Palaeophyllophora* as the sister-genus to *Hipposideros*; Fig. III-54 and Appendix III-10-20 for the other phylogenies). As previously, a y = x theoretical line is plotted, lines at x = y = 0 are drawn to assess sign inversions (in top left and bottom right areas), and an adjusted R squared based on this equation is calculated in order to better account for the offset of taxonomic differences.

At first glance, almost all pairwise taxonomic differences highly diverge from the theoretical line. All pairwise differences between taxa for the slope of the evolutionary trend are significant for each trait (i.e., relative brain, olfactory bulbs, and paraflocculi masses). Moreover, there is no distribution of pairwise taxonomic slope difference for each trait that would fit the theoretical line (very low adjusted R squared, even negative for relative brain and paraflocculi masses). In addition, numerous taxonomic differences change in their sign depending on the presence of fossil taxa; given that they all are significant, this implies important changes in the reconstructed evolutionary patterns of groups depending on the trait. This is particularly true regarding relative brain and paraflocculi masses evolution; changes are slighter regarding relative olfactory bulbs mass evolution, still with offsets, but not of the level of the two other traits. This adjusted R squared for relative olfactory bulbs mass is low, but not as low (still positive) as for the two other variables. Sign inversions especially regard the differences between "true" rhinolophoid families (hipposiderids, rhinonycterids, and rhinolophids) regard both the relative brain mass evolution (with fossils, the slope of the evolutionary trend of the relative brain mass is higher for rhinonycterids than for the other two families, while it is lower without them) and the relative paraflocculi mass evolution (rhinolophids slope is higher than those of rhinonycterids and hipposiderids with fossils, while it is close - against hipposiderids - to lower - against rhinonycterids - without them). The hipposiderid/rhinonycterid difference for relative paraflocculi mass is the only to fall on the theoretical line for that variable; this is noteworthy, as the two other "true" rhinolophoid taxonomic differences are very far from that line. In the other main rhinolophoid clade, the "other" rhinolophoids, the megadermatid vs rhinopomatid difference also changes in sign regarding the relative paraflocculi mass (megadermatids have a clearly higher slope value without fossils, while rhinopomatids do with fossils), while it is the further from the line regarding relative olfactory bulbs mass (though not inverting, the megadermatid slope is much higher than that of rhinopomatids without fossils). Pairwise differences between the two main rhinolophoid clades and pteropodids fall near the theoretical line and are distributed around a null difference; they sometimes change in sign, generally regarding pteropodids, for both the relative brain mass (higher slope for pteropodids than "other" rhinolophoids with fossils, but lower without them) and the relative paraflocculi mass (pteropodid slope higher than that of both major rhinolophoid clades without fossils, while it is lower with fossils), but there is also a taxonomic difference between main rhinolophoid clades that nearly inverts regarding relative paraflocculi mass (slopes are close between the major rhinolophoid clades without fossils, while that of "true" rhinolophoids is higher with them).

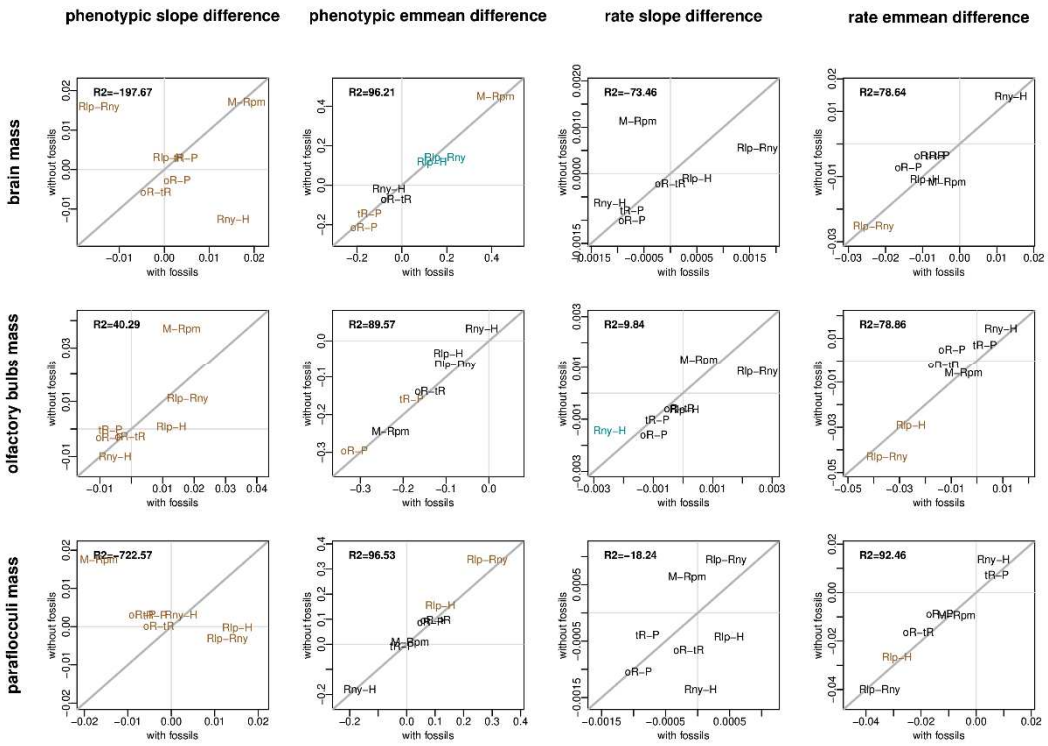

Figure III-54: Comparisons of relevant pairwise taxonomic differences between temporal trend slope/average (i.e., estimated marginal mean, or "emmean") of each value/evolutionary rate of each trait studied here. The color of the pairwise taxonomic comparisons indicate their significance: brown-significant with and without fossils, blue green-significant only with fossils, pink- significant only without fossils, black-not significant. Superimposed are the theoretical line of identical fit by considering fossils or not (thick light gray line) and the adjusted R squared explained by this y = x relationship. Plot area is separated by lines at zero values in order to see the sign changes (top left and bottom right areas of the plot). Note that here, a negative adjusted R squared indicates a particularly poor fit (worse than a horizontal line). This stands for the phylogeny with *Palaeophyllophora* as sister-genus to *Hipposideros*. Other cases are figured in Appendix III-10-20.

Average trait values comparisons strikingly vary less than the evolution slopes do: all adjusted R squared values are high (for relative olfactory bulbs mass) to very high (for relative brain and paraflocculi masses), few taxonomic differences diverge from the theoretical line. In addition, quite fewer taxonomic differences are significant. There is only one slight sign change, hipposiderids having an average relative olfactory bulbs mass higher than that of rhinonycterids with fossils, while it is the reverse without them. There is a difference depending on the sampling of fossil taxa in the significance of pairwise taxonomic differences only for average relative brain mass: rhinolophids have a higher average relative brain mass than the two other "true" rhinolophoid families, the value is similar with or without fossils, but this difference is only significant with fossils. Rhinolophids also have a significantly higher relative paraflocculi mass than the two other "true" rhinolophoid families, but neither the value of the difference nor its significance vary depending on the presence of fossils. The other significant taxonomic differences contrast pteropodids to the two main rhinolophoid clades for average relative brain and olfactory bulb masses, and megadermatids to rhinopomatids for average relative brain mass only; all are close to the theoretical line.

Similarly to the evolutionary trend of the trait, the slopes of the evolutionary trend of the evolutionary rates of the trait are quite dispersed, and fits to the theoretical line are low. Again, the most striking variation regards relative brain and paraflocculi masses absolute rates evolution (with a negative adjusted R squared), though in a not as extreme way as for trait slope taxonomic difference, whereas absolute rate evolution slopes of relative olfactory bulbs mass fit a bit more the theoretical line (low, but still positive adjusted R squared). This time, however, less taxonomic differences change in sign: the slopes of rhinopomatid and rhinolophid evolution rate of relative brain and paraflocculi masses are higher than those of megadermatids and hipposiderids (respectively) with fossils and lower without them, the slope of rhinonycterid evolution rate of relative paraflocculi mass is slightly higher than that of hipposiderids with fossils, while it is clearly lower without them, and that of “true” rhinolophoids is higher than that of “other” rhinolophids for relative olfactory bulbs mass with fossils, but lower without them. Some other taxonomic differences strikingly differ with or without fossils, though not changing in sign: the rhinonycterid slope of evolution rate of relative brain and olfactory bulbs masses is lower than that of rhinolophids with fossils, and as well as that of hipposiderids regarding relative olfactory bulbs mass only, and almost all taxonomic differences are far from the theoretical line regarding relative paraflocculi mass. Contrary to the slopes of trait evolution, only one taxonomic difference is significant regarding the slopes of trait rates evolution (rhinonycterid vs hipposiderid difference regarding relative olfactory bulbs mass), and only with fossils. Then, though there are some striking variations in the taxonomic differences, they have to be taken into account with much more caution than those of trait evolution slopes.

Similarly to the average traits, the average values of their absolute rates fit much more the theoretical line than the evolution slope of these rates. They however diverge a bit more from that line than the average trait values, the adjusted R squared being not as high. Some taxonomic differences are significant, but they are few; they only concern taxonomic differences between rhinolophids and other “true” rhinolophoid families (against rhinonycterids for relative brain mass, hipposiderids for relative paraflocculi mass, and both for relative olfactory bulbs mass). In addition, as for average trait values, there is only one inversion in the difference signs (pteropodids have higher average rate of relative olfactory bulbs mass evolution than “other” rhinolophoids with fossils, while it is lower without them). The few taxonomic differences that slightly diverge from the theoretical line also regard “true” rhinolophoid, contrasting rhinonycterids to the two other families (average rhinonycterid rate of relative olfactory bulbs and paraflocculi mass evolution being slightly less higher than those of rhinolophids and hipposiderids with fossils). Some other taxonomic differences involving the “other” rhinolophoid node also are slightly above the line (with a slightly more positive difference), contrasting to both “true” rhinolophoids and pteropodids for relative brain and olfactory bulbs masses. All deviations are still slight, and only one significant difference does not fall on the theoretical line, without sign change.

IV.6.C) Discussion

The phylogenetic comparative method used here outputs several variables that characterize each trait evolution through time, and especially their evolutionary rates. From these rates, the ancestral character estimates are calculated. Both these variables are then expressed against time (taking absolute values for the evolutionary rates), and both trends through time for different group can be compared using the slope of the trend and the estimated marginal mean of the variable (i.e., a way to give a central tendency). Rates can also be compared within against outside a given clade. All these comparisons are indicators of how a trait evolves, and especially how does the trait and the trait variation change through time and across taxa. Most studies dealing with brain (and sub-units) mass in bats only deal with extant taxa, whereas I include some fossil species in my sample. I here first emphasize how the difference in evolution of these traits can be characterized by accounting for fossil species or not, and then discuss these implications relative to those raised by previous studies (next section).

Ancestral estimations of trait values is perhaps the most demonstrative statistical output to observe the impact of the inclusion of fossil taxa or not by comparing the trait mappings and the biplot of the ancestral estimations. Here, relative brain mass shows the most differences in ancestral estimates with and without fossils: especially, deep tree nodes (root and deep rhinolophoid nodes) and the hipposiderid node have negative values and some nodes including that of rhinolophids have positive values by considering fossils, but these signs invert by discarding fossils (Fig. III-53). This is particularly striking by comparing the mappings of that trait (Figs. III-35,44), and this has major implications because the scenarios between the root and each family node also invert depending on the sampling of fossil taxa (with numerous decreases reconstructed without fossils, and only increases before pteropodids and megadermatids). This also has implications for the families to which the fossil taxa belong, and especially for rhinonycterids, whose evolution pattern is heterogeneous with fossil taxa, but quite more gradual without them. Regarding the two other traits, the changes are more anecdotal: there are some points diverging from the theoretical line for relative paraflocculi mass, as for relative brain mass, but without sign changes (Fig. III-53) and the mappings are very comparable (Figs. III-41,50); the distribution on the phylogenies are even more similar regarding relative olfactory bulbs mass (Figs. III-38,47), and the ancestral estimates are also very close by considering fossils or not (Fig. III-53, with a very high fit to the theoretical line.

Comparisons between “deep nodes”, both regarding their evolutionary trend slope and the average value of the traits, further show contrasted behaviour regarding the inclusion of fossil taxa: in general, slopes vary much, whereas average values do not. This is not a surprising result: adding or removing some species is more or less likely to affect clade slopes if these values do not fit the “extant only” evolutionary trend, whereas regarding average trait values, the effect of extreme values may be tempered. There are especially inversions in slope signs for relative brain mass evolution (Figs. III-37,46), all groups much more following the general (decreasing) trend without fossils; there also are some (but less) sign changes for relative paraflocculi mass evolution (Figs. III-43,52), while there are no sign changes for relative olfactory bulbs mass evolution (Figs. III-40,49). In all cases, removing fossils causes a much better fit of all clade trends to the general trend; this point is also expected, as all observed values are at time 0, then no observed value in the past can disrupt the general trend and all converge by going back in the time. Taxonomic slope differences are also affected by the absence of fossils (Fig. III-53): there are also some sign changes in the taxonomic slope difference for relative brain and paraflocculi masses, mainly affecting “true” rhinolophoid families (fossils belong to two out of the three families), but also between the distant

"other" rhinolophoid families, and between deep rhinolophoid nodes (though the differences in the latter case are slight) regarding relative paraflocculi mass. Though also substantially varying, there is no sign change for relative olfactory bulbs mass. Average trait values, however, little vary: few taxonomic differences differ following the presence or absence of fossils (Fig. III-54) and there are few changes in the taxonomic difference significances and in the hierarchy between clades (Appendix III-3, Tables 3-4). The only exception is the case of the difference between rhinolophids and other "true" rhinolophoid families, that only are significant by taking into account fossil taxa. The absence of significance without fossils may be linked to the lower sample size of both hipposiderids and rhinonycterids: the differences are similar with or without fossils, thus fossil taxa are likely to follow the general relative brain mass range, and maybe their presence weights these differences enough to make them significant.

As a summary regarding trait evolution, some key points can be raised. First, the relative brain mass is clearly the most affected trait by the absence of fossils: it is the only variable for which there are inversions of ancestral estimates, all trend slopes before and within the onset of major clades further inverting in sign. The relative paraflocculi mass is also clearly affected, but to a lesser degree: there are several trend slopes sign inversions, but they only regard relative paraflocculi mass evolution in the major clades, not before them. The relative olfactory bulbs mass is almost unchanged: though there is some variation, it is quite lower than for the two other traits, and the distribution, the slopes, and the ancestral estimates are very similar with or without fossils. Fossil species then highly deviate from expectations based on extant taxa only regarding their relative brain mass; they also substantially deviate regarding their relative paraflocculi mass, but almost not regarding their olfactory bulbs mass. Such a pattern of varying adequacy between neontological and paleontological reconstructions on a structure and some of its sub-structures then shows that all these parts evolve differently. The second point is that the number of fossil taxa may obviously play a key role in the differences between reconstructions using these fossils or not, but this is not guaranteed at all: relative olfactory bulbs mass evolution is the less varying, though there are as many fossils available for relative brain mass evolution, and quite less for relative paraflocculi evolution (only two species of the *Palaeophyllophora* genus). The impact of fossil taxa appears as impossible to predict, even by considering functionally "similar" structures (all are nervous structures of the brain cavity, at least), because of the previously quoted variations in the adequacy of neontological vs paleontological reconstructions.

Complementary to the comparisons of trait evolution with or without fossils are the comparisons of trait rates evolution. Here, absolute rates are used as the goal is to locate changes, not to look at their sign - trait evolution already indicates this. By contrasting these absolute rates for each trait, there is this time a very high fit for relative paraflocculi mass, and a lower and similar fit for both relative brain and olfactory bulbs masses (Fig. III-53). Interestingly, the repartition of the absolute rates deviations around the theoretical line is very similar for relative brain and olfactory bulbs masses, recalling the joint variation that seems to occur between these two traits (see previous sections). It is especially important to note that several "deep nodes" drastically vary in their absolute rate value depending on the presence of fossils (see also the Figs. III-36,39,45,48 to compare rate mappings for both traits), both regarding the whole Rhinolophoidea node, some rhinolophoid familial nodes, and some other inter-generic nodes also substantially vary. It is also interesting to note that the nodes of the two families with fossil species fall near the theoretical line, and with different values (rhinonycterid node always has high rates, while hipposiderid node always has low rates). This contrasts with the relative paraflocculi mass rates, which are estimated much more similarly with or without fossils (see also Figs. III-42,51), major clades often having low rate values. These variation however have a low impact on the comparisons of average

absolute rate differences between clades: all taxonomic differences are roughly distributed around the theoretical line, there are no significant sign inversions across traits (there is one for relative olfactory bulbs mass average rates, but the taxonomic difference is not significant).

Differences between “deep nodes” and the rests of the tree however more often vary, especially regarding relative brain and olfactory bulbs mass rates, the rate differences (interpreted as shifts in rate regimes; Fig. III-53, Appendix III-3, Table 5) for these two variables following the theoretical line but frequently being either under or over it, with a regular gap. Significant shifts always do not fall on the line; taking fossil differences as a reference; the exclusion of fossils tends to underestimate shifts for relative brain mass and to overestimate them for relative olfactory bulbs mass. There also are a notable amount of shifts depending on the presence or not of fossil shifts: in all three traits, generally only half of the significant shifts are found to be significant in both cases. The discrepancies between including or not fossils for several nodes highly impacts the slope of the absolute rates evolution through time for all traits: there is a loose fit of the taxonomic slope differences to the theoretical line (Fig. III-54), and slopes in each clade also quite vary (Figs. III-37,40,43,46,49,52). The significance of clade slopes varies for relative brain and olfactory bulbs mass rates (Appendix III-3, Table 3), some differing from all other only while discarding fossils (rhinolophoids and pteropodids slope of relative olfactory bulbs mass rate evolution), others only while considering fossils (rhinonycterids slopes of relative brain and olfactory bulbs mass evolutions). Taxonomic slope differences also vary considerably (Fig. III-54, Appendix III-3, Table 4): there are frequent sign inversions, especially regarding relative brain and paraflocculi masses rates, though almost all taxonomic differences are not significant. A single taxonomic difference is significant, but only with fossil taxa, and it falls not very close to the theoretical line.

Regarding trait rates evolution, there is a consequent impact of the presence or absence of fossil taxa. First, the reconstructed values clearly differ, especially for several deep nodes, from the root down to the family-level, even with high discrepancies at the inter-generic level in families. In turn, these offsets cause noticeable differences of evolutionary trend slopes and in the detection of shifts in rate regimes. There are slighter variations of average absolute rates for clades: as for trait evolution, it is likely that the effect caused by the presence/absence of fossil taxa are tempered by the mass effect of the clades. Second, traits are not affected the same way for the trait rates as for the trait values: here, relative brain and olfactory bulbs masses show very similar distribution pattern and similar discrepancies of the absolute rates with or without fossil taxa, indicating joint constraints for both structures. Relative paraflocculi mass varies less, with the exception of the rate evolutionary trend slopes differences (though none are significant), which may mean that the quantity of fossil taxa could impact the reconstruction of the trait rates rather than the trait itself.

V) Conclusions

This third chapter, framed at the Yinpterochiroptera scale, builds on an unprecedented sample of 52 modern and 8 fossil taxa and aims at approaching the global endocranial evolution in this wide chiropteran clade through the study of both qualitative and quantitative morphological traits and to assess the impact of fossil inclusion on ancestral character reconstructions.

A set of 73 anatomical characters first sets the basis to determine the phylogenetic relevance of endocast morphology and therefore the potential to identify fossil species based on endocasts. Phylogenetic ridge regression method allowed to track the evolution of each anatomical character in a phylogenetic context and to provide an illustrated picture of morphological reconstructions at successive nodes within Yinpterochiroptera. Endocranial morphological characters show a wide array of distribution, regardless of the endocranial region. Some characters are also apparently under selection, with either a temporally static or moving optimum.

The exposure of the mesencephalic tectum, one of the brain features that focused attention in bats, appears to carry phylogenetic signal. Other characters, however, show a more blurry pattern, highlighting that cursory evaluation and comparisons of endocranial morphology have to be deepened. Comparative yinpterochiropteran endocranial anatomy also has to be refined, both regarding soft tissues correlates and ontogeny. Regarding taxa evolution, the present results highlight that rhinolophoids as a whole strikingly differ from pteropodids, and that rhinolophoid families differ from each other.

The first attempt of morphological reconstruction of endocranial morphology of deep rhinolophoid nodes presented here mainly relies on the inclusion of hipposiderid (and rhinonycterid, to a lesser degree) fossils. The reconstruction of the endocranial morphological evolution at deep rhinolophoid nodes needs now to be strengthen by adding fossils older than the crown family diversifications.

Regarding quantitative characters, the results retrieved regarding relative brain mass evolution contradict previous works based on extant taxa: there is a general increase in brain mass through time, on branches leading to most modern families. Ecological correlates of relative brain mass have not been statistically verified here, but do not seem to fit relative brain mass evolution that much. Olfactory bulbs and paraflocculi relative masses generally decrease through time, with few changes regarding paraflocculi. Surprisingly, changes in olfactory bulbs relative mass, almost only occur concurrently to relative brain mass changes. Yet, various correlation patterns between the two traits are observed depending on the taxa. Such a variation in covariation patterns of change, together with traits evolution, raise the question of the processes underlying the variation of relative brain and olfactory bulbs masses through time, and of the selection process that may apply to them. Olfactory bulbs relative mass may be linked to olfaction, but it is quite more uncertain regarding the relative brain mass. Fields to investigate regard the degree of inter- and intra-generic variation, since the inter-generic level is generally the smallest resolution achieved here (except known speciose genera).

Conclusions about ecological correlates remain very limited for now. Both regarding morphological and quantitative neurological traits, further studies comparing brain and ecology should first look properly at the evolutionary history of ecological traits of interest, then at the evolution of neuronal traits, then compare both, and nuance conclusions depending on the available anatomo-functional knowledge allowing to talk about covariation as causality. Ecology and phylogeny seem to be related to each other to a certain degree; being able to compare ancestrally reconstructed values of both ecological and neuronal traits may clearly enhance our understanding of brain evolution in these bats.

The present results also emphasize the key role of fossil taxa and the impact of their phylogenetic

position. Endocranial morphology has almost not been put into an evolutionary context in previous works, and the impact of the inclusions of fossils has not been undertaken. They however, for sure, bring dramatically crucial information to constrain the picture of endocranial evolution. Documenting all extant families would be necessary to have the best assessment of endocranial morphology through time, close to and within crown taxa. Relative brain mass evolution has been tackled by some previous works, and the present results already contradict parts of their conclusions; furthermore, the inclusion of fossils induces crucial changes in evolutionary scenarios and emphasizes the limitations of neontology-based reconstructions.

Part Four

A stem bat endocast helps addressing endocranial evolution in Chiroptera

I) Introduction

The evolutionary history of the mammalian order Chiroptera is marked by the acquisition of spectacular morpho-anatomical changes leading to a unique combination of ecological traits among mammals. Bats are indeed the only mammals capable of active flight, and share with cetacean artiodactyls the ability to echolocate (e.g., Freeman 2000, Teeling et al. 2000, Teeling 2009). The phenotypical manifestations of these two ecological traits are plentiful, both regarding soft-tissues and the skeleton (e.g., Simmons & Geisler 1998, Freeman 2000, Amador et al. 2019). Further specializations occur in some bat clades as exemplified by Phyllostomidae: the various subfamilies of that taxon exhibit a wide array of diets (e.g., phytophagy, piscivory, sanguivory) and related morpho-anatomical adaptations (e.g., Baker et al. 2012, Dumont et al. 2012, Santana et al. 2012). Dealing with bats, important evolutionary questions addressed in the literature generally regard secondarily specialized taxa. But, at the mammalian scale, a key question regards the sequence of acquisition leading to the full bat condition. Some works (see Anderson & Ruxton 2020 for a review) tried to address the question of the acquisition of the two main distinctive traits, active flight and echolocation. The fact that all extant bats are able to fly suggests that active flight was shared by "ancestral" bats (e.g., Smith 1970, Simmons & Geisler 1998, Simmons et al. 2008). This is less clear regarding echolocation: species of the family Pteropodidae, or "megabats", nested in the suborder Yinpterochiroptera, are unable to echolocate. Today, two equally parsimonious hypotheses exist (e.g., Anderson & Ruxton 2020): either the echolocation has been acquired once, before the hypothetical common ancestor of all living bats, and then secondarily lost in pteropodids, or the echolocation was acquired twice, once in Yangochiroptera (a "microbat" suborder composed of three superfamilies) and once in Rhinolophoidea (the sister-taxon to Pteropodidae in Yinpterochiroptera). Fossil bats belonging to the wastebasket group "Eochiroptera", a stem assemblage to the crown group of Chiroptera, are therefore of critical interest to answer this problem. Though some works proposed a common acquisition of echolocation (based on debatable anatomical arguments; Simmons & Geisler 1998, Simmons et al. 2008, 2010, Veselka et al. 2010) and almost closed the debate, the recent work of Nojiri et al. (2021) dealing with ontogeny of the hearing apparatus instead suggested a convergent acquisition of echolocation.

The brain is the integrating center of all incoming information received by the body, and answers to these signals by motor responses. In the case of bats, echolocation and active flight, relying on auditory and balance information processing and on active (i.e., motor) actions, are expected to deeply transform the brain. Addressing the evolution of the brain may therefore bring critical clues to understand the evolutionary history of bats. The best way to constrain an evolutionary scenario based on extant taxa is to include fossils in the picture, reducing this way the array of possible stories. Brains of fossil taxa are obviously impossible to gather; however, the external surface of the bat brain reflects well on the inner face of the braincase (Orlov 1961, Dechaseaux 1962, Kochetkova 1978). By reconstructing the mold of the braincase of bats, one is therefore able to depict the external aspect of the brain, including fossil species. Endocranial casts of bats are known since the beginning of the XXth century (Dechaseaux 1956, 1962, 1970, 1973, Edinger 1926, 1929, 1961, 1964a, b), but have been only little studied at that time (Dechaseaux 1962, 1973, Edinger 1964a). With the recent generalization of µCT-scanning techniques, non destructive access to internal anatomical structures has become widespread; more and more fossil endocranial casts of vertebrates have therefore been described (e.g., Radinsky 1978, 1981, Macrini et al. 2006, Orliac et al. 2012, Clement et al. 2015, Balanoff & Bever 2017). Most XXIth century studies of bat brain evolution (e.g., Safi et al. 2005, Niven 2005, Smaers et al. 2012) however only used extant taxa and

proposed, for instance, that bats experienced a general decrease of relative brain size (i.e., the amount of brain in excess after allometric needs, also known as encephalization) except in phytophagous bats (pteropodids and some phyllostomids). Some recent studies (Yao et al. 2012, Maugoust & Orliac 2021) including few fossils contradicted these results, suggesting a more complex history and emphasizing the crucial role of fossils. However, the latter studies only dealt with fossil representatives of the extant family Hipposideridae.

Here, I describe the first eochiropteran endocranial cast and I reconstruct for the first time the evolutionary history of the main brain characteristics at the Chiroptera scale using the deepest calibration point available. To do so, I use a recently developed phylogenetic comparative method that highly relies on fossil information, and I discuss both the morphological evolution of the visible features of the endocranial cast and the evolution of quantitative traits, including encephalization. I especially look after the phylogenetic relevance of discrete anatomical characters at a broader scale than previously done (Part Three), I aim to precise the evolution of the exposure of the mesencephalic tectum (the main morphological discussed feature throughout the literature), and I try to compare the ancestral reconstructed endocranial morphology of superfamilial bat clades. Regarding quantitative traits, I characterize the evolution of brain encephalization through time (which has mostly been discussed using extant taxa only) but also of relative olfactory bulbs and paraflocculi masses. I also compare the evolution of these variables, as a covariation between changes in relative brain and olfactory bulbs masses has been found in Yinpterochiroptera (Part Three).

II) Material & Methods

II.1) Taxa and specimens

I document here the endocranial cast of the specimen UM VIE250 attributed to the a new eochiropteran species currently under study (Hand et al. in prep). This species, hereafter named as the 'Vielase bat' was discovered in the Vielase locality, in the Quercy Phosphorites Formation (southwestern France). The fauna of this site, described by Legendre et al. (1992), is correlated to the MP10/MP11 European standard-level (i.e., the boundary between the early and the middle Eocene, 49 Mya). The locality has been further numerically dated to 50.97 ± 0.124 My by Escarguel (1999) using rodent lineages. This eochiropteran species is retrieved basally to the crown chiropteran clade (Hand et al. in prep). This makes this endocranial cast the oldest and the most basal of chiropterans.

Most of the cranial braincase is preserved without deformation, but the left posteroventral portion is broken: the left petrosal is missing, and the dorsal and left edges of the foramen magnum are missing. The cranium is only partly filled with sediment that has been virtually removed. The following description relies on the nomenclature established by Maugoust & Orliac 2021 and further emended in Part Two.

The complete list of the specimens used, with the curation places and the µCT-scanning details are provided in Table 1 (see also Appendix 1 for more details on this table). Of these specimens, several scans (42) have been downloaded from the Morphosource (Boyer et al. 2017) repository of Shi et al. (2018), and the scans of the other specimens (35) were performed using the µ-CT facilities of the MRI platform in the ISEM. I performed the segmentation of all specimens with the exception of most of that of *Palaeophyllophora quercyi*.

II.2) 3D Data acquisition

A single endocranial cast documents each species; all information about curation places and µCT-scanning procedure are given in the Table 1 (general Material & Methods part). For the specimen of the 'Vielase bat', the left posteroventral half is missing. Therefore, brain, olfactory bulbs, and paraflocculi volumes have been computed by doubling the volume of the left half only.

II.3) Phylogenetic framework

In order to take into account the endocranial disparity from the order to the family levels, I try to document both as many chiropteran families as possible and as many deep chiropteran nodes as possible. For all but five families, the sample documents one species per family. I chose the basal-most species whose skull has been digitized by Shi et al. (2018). The five families not documented here are the rhinolophoid family Craseonycteridae, the emballonuroid or noctilionoid family Myzopodidae, the noctilionoid families Mystacinidae and Furipteridae, and the vespertilionoid family Cistugidae. All these families have a poor specific diversity with either one (Craseonycteridae) or two (Myzopodidae, Mystacinidae, Furipteridae, Cistugidae) recognized species (Burgin et al. 2018, Arroyo-Cabrales 2019, Goodman 2019, Kingston & Soisook 2019, Ruedi 2019, Toth 2019). Sixteen of the 21 extant chiropteran families are therefore represented in the present sample, documented by 26 species.

There are five "main" bat clades that are the family Pteropodidae and the superfamilies Rhinolophoidea, Emballonuroidea, Noctilionoidea, and Vespertilionoidea. Here, I often designate these clades as being the "main bat clades/groups", or the "bat superfamilies" (even if Pteropodidae is a family, though it was formerly the Megachiroptera suborder…). Relationships between these chiropteran groups follow the results of Amador et al. (2018), congruent with some previous reference studies at least at the ordinal scale (Meredith et al. 2011, Shi & Rabosky 2015). Especially, a relationship between noctilionoid and emballonuroid bats is supported in the three previously quoted references, whereas older works supported a closer relationship between noctilionoids and vespertilionoids (Jones et al. 2002, Teeling et al. 2005) or emballonuroids and vespertilionoids (Agnarsson et al. 2011). Within each main bat clade, I try as much as possible to follow superfamily-level works, or at least to use them to confirm the broader-scaled results of Amador et al. (2018). Regarding emballonuroids, two families are present in my sample (nycterids and emballonurids); the family Myzopodidae may belong to this superfamily or to noctilionoids, but this problem does not affect my sample, because it does not include a myzopodid species. Regarding noctilionoids, I follow the latest noctilionoid-scale phylogeny of Rojas et al. (2016): both the relationships between taxa and the node datations derive from their work. Regarding vespertilionoids, I follow the relationships between families found by Amador et al. (2018), also retrieved by Shi & Rabosky (2015) at the Chiroptera scale, and by Lack & Van den Bussche (2010) at the Vespertilionoidea scale.

Among the five families with more than one taxa are the yinpterochiropteran families Pteropodidae and Hipposideridae. I sampled more than one pteropodid species because it is the third most diverse chiropteran family (Burgin et al. 2018); I selected three species in order to document the three main pteropodid groups (see the Methodology section of Part Three). I sampled more than one hipposiderid species because I dated (cf. Part Three) the deepest nodes of this family from the Eocene. The retained species are *Asellia tridens*, the basalmost species of the family, *Doryrhina cyclops* and *Hipposideros armiger*. I did not retain the hipposiderid fossil taxa I documented in Part Three because i) their phylogenetic position is debated and ii) I prefer to keep a similar sampling methodology for both yinpterochiropterans and yangochiropterans.

I sample more than one species in the yangochiropteran families Emballonuridae, Phyllostomidae, and Vespertilionidae. Emballonurid diversity is not very high (54 species according to Burgin et al. 2018 and Bonnacorso 2019) but deepest nodes of this family found by molecular analyses are quite old (around 40-50 Mya, see Amador et al. 2018 for comparisons). These ages are likely due to the rich emballonurid fossil record: species pertaining to the crown Emballonuridae are retrieved since the early Eocene (Ravel et al. 2016, Brown et al. 2019). Due to these deep differences, emballonurid relationships are rather well resolved (see Amador et al. 2018), with three main distinguished clades. I sample one extant species in each, using the phylogeny and the node ages found by Amador et al. (2018). Phyllostomids are quite diversified nowadays (217 species and second most diverse chiropteran family, Solari et al. 2019) but they are particularly highly disparate in their morphology and in their ecology (e.g., Stockwell 2001, Baker et al. 2012, Dumont et al. 2012, Santana et al. 2012). There are some disagreements between analyses about the very first clades to diverge in phyllostomids; as for the whole Noctilionoidea family, I follow the results of Rojas et al. (2016), which are a little bit divergent from those of Amador et al. (2018). Vespertilionidae is the most diverse chiropteran family (496 species, Moratelli et al. 2019), with several well-identified subfamilies. The crown group of this family however represents a recent radiation: the root of the crown vespertilionids is the only node dated before 30 Mya by molecular analyses (Lack & Van den Bussche 2010, Amador et al. 2018). In spite of a massive specific diversity, I therefore only document the basalmost node of the crown vespertilionids, which distinguishes Vespertilioninae (the genus *Scotophilus* being found as the more basal one by Lack & Van den Bussche [2010] and Amador et al. [2018]) and the other subfamilies, the basalmost one being the Kerivoulinae (with the sole genus *Kerivoula*).

I use the software dateFBD (Didier & Laurin 2020) to perform the dating of the deepest chiropteran nodes, that are the node distinguishing the crown chiropterans from the 'Vielase bat' and the node distinguishing the two chiropteran suborders Yinpterochiroptera and Yangochiroptera (the ages of the successive nodes in each being already known thanks to molecular studies). As an input, I take the age interval of Escarguel (1999) for the 'Vielase bat', and for both suborders I consider a range between the age of the whole Chiroptera order and that of the considered suborder using the estimates of Amador et al. (2018). The other parameters of the software are the same as those used for the yinpterochiropteran datation of Part Three (see Methodology of that chapter), and the commands to run these analyses plus the output figures are given in Appendix IV-0. As previously, I retain only the ages of maximal posterior probability. The time-calibrated phylogeny of my sample is provided in Figure IV-1.

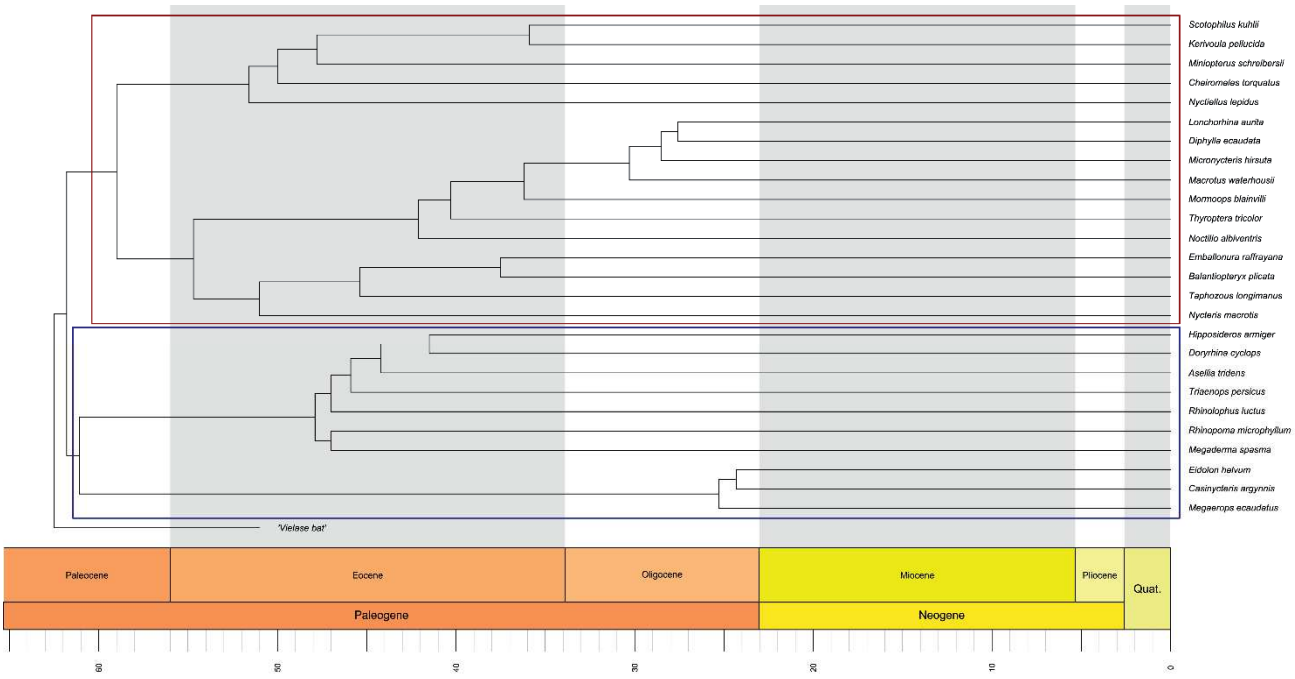

Figure IV-1: Time-calibrated phylogeny of the chiropteran sample considered in this part. The blue rectangle represents Yinpterochiroptera, and the red one represents Yangochiroptera.

II.4) Anatomical characters

The anatomical characters used in Part Three are considered here. Some of them are modified to take into account the morphological variation at the global Chiroptera scale. The characters modified are listed below. Modifications are underlined while regarding reformulations, and in bold while regarding addition of states. Examples and/or details are provided as in Part Three only while adding states or for substantial reformulations of states. Unless otherwise indicated here or in the Anatomical characters section of Part Three, all characters have been scored using the plates illustrated by Figure IV-2 (for yangochiropteran species) and Figure IV-3 (for the eochiropteran 'Vielase bat').

3. Relative rough proportions of cerebrum vs cerebellum: cerebrum close to larger than cerebellum (0); cerebrum way larger than cerebellum (1). I replace the "close to or a bit larger than" by "close to larger" because actually cerebrum is generally bigger than cerebellum. The point is to decide if it is larger or very much larger. This character has been established in yinpterochiropteran bats to distinguish two endocast conformations, the one belonging to the state one being a very much bigger cerebrum than the cerebellum. In yangochiropteran bats, there are some taxa with an obviously bigger cerebrum too (the noctilionid *Noctilio albiventris*, the phyllostomids *Diphylla ecaudata*, *Macrotus waterhousii*, and *Micronycteris hirsuta*, the thyropterid *Thyroptera tricolor*, the molossid *Cheiromeles torquatus*, and the vespertilionids *Kerivoula pellucida* and *Scotophilus kuhlii*), but in a different conformation than for pteropodids: here, the cerebellum is still prominent, being shorter but taller and wider. I do not want to further modify or divide the state one; together with character 4 (regarding the relative width of the cerebrum and of the cerebellum), taxa with much smaller cerebellum (in length, width, and height) and those with smaller because compressed cerebellum (shorter, but wider and taller) are distinguished.

8. Olfactory bulbs, length vs width: **much wider than long (0);** wider than long (1); roughly as long as wide (2); clearly longer than wide (3). Most yangochiropteran bats have olfactory bulbs that are way wider than long; those that are not are three of the four phyllostomids (*Diphylla ecaudata*, *Macrotus waterhousii*, and *Micronycteris hirsuta*) and the natalid *Nyctiellus lepidus*. I add this state to take this into account as there are no such "extreme" cases in yinpterochiropteran bats. To be scored as state 0, the two olfactory bulbs considered together have to be clearly reduced in length, much more than twice as wide as long.

10. Cerebral hemispheres, shape of their posterior margin in dorsal view: mainly made of straight lines (0); curved and convex (1). Previous formulation of the states was "rather flat" and "clearly convex" for states zero and one; there however are some outlines made of two straight lines with an angle, which could be coded by both states. I modify these states to better distinguish these conditions: posterior margin can be made of straight lines, with or without clear angle between them if there are more than one, or clearly curved and convex.

13. Piriform lobes, ventral protrusion: **extreme (0)**; moderate (1); low to absent (2). There are many yangochiropteran bats with highly protruding piriform lobes ventrally (the emballonurid *Taphozous longimanus*, the mormoopid *Mormoops blainvilli*, the notilionid *Noctilio albiventris*, the phyllostomid *Diphylla ecaudata*, the thyropterid *Thyroptera tricolor*, the miniopterid *Miniopterus schreibersii*), while that of other yangochiropterans (the emballonurids *Balantiopteryx plicata* and *Emballonura raffrayana*, the phyllostomid *Micronycteris hirsuta*, the molossid *Cheiromeles torquatus*, the natalid *Nyctiellus lepidus*, and the vespertilionids *Kerivoula pellucida* and *Scotophilus kuhlii*) and yinpterochiropterans (see examples in Part Three) are clearly protruding but not as much. I therefore also reformulate the state one (former state zero) from "present" to "moderate", and the state two (former state one) to include a "low"

protrusion, when it is not clear if there is no protrusion or a very small one.

47. Orbitotemporal canal, shape of the dorsal convexity: sharp (0); rounded (1).

49. Orbitotemporal canal, anteroposterior position of the anterior opening: close or anterior to the circular fissure (0); close to the sylvia and/or to the middle cerebral artery cast (1). In some taxa (the emballonurids *Emballonura raffrayana* and *Taphozous longimanus*, the molossid *Cheiromeles torquatus*, or the eochiropteran 'Vielase bat'), the orbitotemporal canal ends posteriorly but there is no middle cerebral artery cast; since this cast and the sylvian sulcus are located in the same area, I add this precision. I let the precision of the middle cerebral artery cast, as the orbitotemporal canal seems to blend with it in pteropodids (but see Anatomical characters section of Part Three).

51. Middle cerebral artery, cast: present (0); absent (1). There is no modification on this character or on its states, but I want to explain state zero with the sampling at the chiropteran scale. In one yangochiropteran species of my sample (the phyllostomid *Diphylla ecaudata*), a middle cerebral artery cast is present in a similar shape to that of pteropodids, with a continuous bulge. In some other species (the mormoopid *Mormoops blainvilli*, the phyllostomids *Lonchorhina aurita*, *Macrotus waterhousii* and *Micronycteris hirsuta*), it is also present as a succession of foramina and/or of bulges that also mark the pathway of this artery, though not as clear as the previous condition. Both cases fit state zero of this character; only endocasts with absolutely no mark of the cast of this artery belong to state one.

58. Sphenorbital fissure, global elongation: **very small, wider than long (0)**; small, roughly as long as wide (1); moderate, longer than wide (2); high, much longer than wide (3). There is a particular case (the phyllostomid *Diphylla ecaudata*) in which the sphenorbital fissure is of greater width than length, by far. As this does not exists in yinpterochiropteran bats, I add a state to take this variation into account.

60. Sphenorbital fissure, width of the gap between them (= of the sphenorbital bridge): very thin, sphenorbital fissures almost in contact (0); thin, sphenorbital fissures close but clearly not in contact (1); average, as wide as the half to the full width of each fissure (2); wide, as wide as the hypophysis (3). There are cases (the emballonurid *Taphozous longimanus*, the nycterid *Nycteris macrotis*, the phyllostomids *Lonchorhina aurita* and *Micronycteris hirsuta*, the thyropterid *Thyroptera tricolor*) where the sphenorbital fissures are more separated than the condition to fit state one, but less than for state three. I therefore modify the state to better characterize state two: the gap between sphenorbital fissures has to be from the half to the full width of each fissure.

61. Oval foramen, shape: circular to ovoid (0); very much anteroposteriorly elongated (1). The state one characterizes the oval foramen of most pteropodids, but there are cases of oval foramen that are both ovoid and anteroposteriorly elongated (the emballonurids *Balantiopteryx plicata* and *Emballonura raffrayana*, the phyllostomid *Macrotus waterhousii*). I modify this to really distinguish both cases; ovoid oval foramen, no matter its elongation, belongs to state zero, and it has to be clearly elongated anteroposteriorly and of more irregular shape to belong to state one.

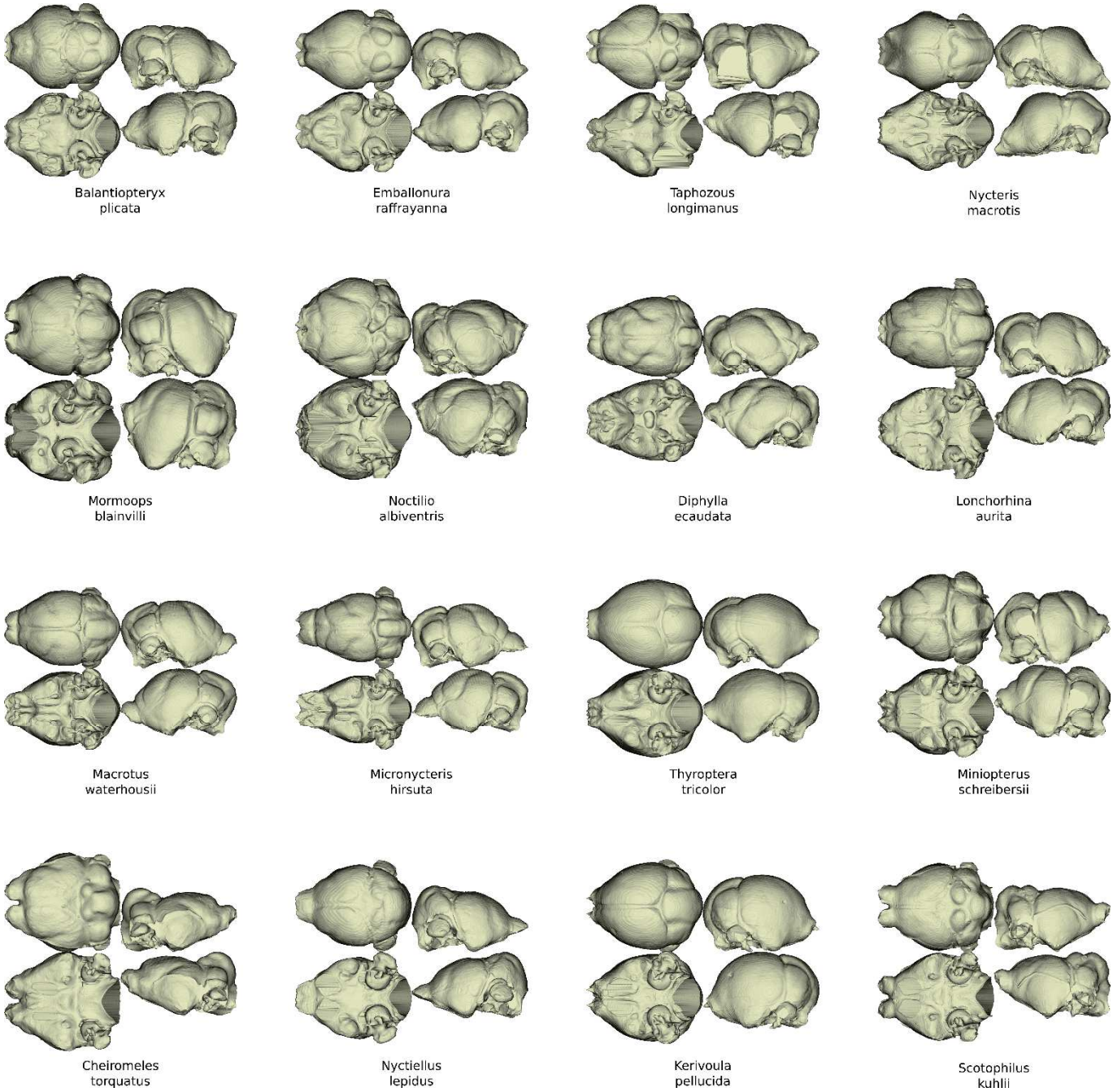

Figure IV-2: Anatomical plate of the comparative yangochiropteran sample used here. For each species are dorsal (top left), ventral (bottom left), lateral right (top right) and lateral left (bottom right) views.

II.5) Quantitative data

Body mass estimates for extant taxa have been calculated using the datasets of Baron et al. (1996) and Jones et al. (2009). For the eochiropteran 'Vielase bat', a body mass of 18.94g has been estimated by Hand et al. (in prep) using dental equations of Gunnell et al. (2009). Other quantitative variables used here are the masses of the brain, of the olfactory bulbs, and of the paraflocculi.

II.6) Statistical treatment

The scripts used for the statistical treatment of this part are provided in the Appendix IV-1. I follow the statistical treatment detailed in Part Two.

In both the qualitative and quantitative data treatment, I consider as “deep nodes” to investigate the sampled superfamilies or likewise clades (Vespertilionoidea, Noctilionoidea, Emballonuroidea, Rhinolophoidea, and Pteropodidae), the two suborders they belong to (Yangochiroptera and Yinpterochiroptera) and the crown group of the order Chiroptera (that I frequently only name “Chiroptera”). The reconstructed general trends, on their side, account for the whole Chiroptera order evolution.

As previously explained, my sample effort was put in an equivalent way in both Yangochiroptera and Yinpterochiroptera. I however addressed endocranial evolution at the Yinpterochiroptera scale using a much broader (and representative) sample (Part Three). Therefore, to be sure my yinpterochiropteran subsampling does not impact the reconstructions of deep bat nodes, I keep all nodal values reconstructed in Part Three up to the superfamily level. The reduced sampling of extant yinpterochiropteran species only serves to give an idea about the effect of sampling few taxa: intra-familial reconstructions obtained here can be compared to those based on a more representative sample of Part Three.

The only difference with the general statistical treatment previously exposed (see Part Two) is that I do not test a covariation between morphological character states and brain size. I consider that the current sample is too limited compared with the considered phylogenetic scale to properly assess a potential covariation. In Part Three, while dealing with Yinpterochiroptera, this may stand as I sampled more than 10% of the extant diversity and several fossil taxa. The conclusions, in this part, are furthermore tentative and deserve further exhaustive work. At the Chiroptera scale, with less than 2% of the extant specific diversity, I find this too presumptuous.

III) Description of the endocranial cast of the 'Vielase bat'

III.1) Overall shape

Despite the broken part, the incredible 3D preservation of the specimen UM VIE250 allows access to endocranial structures with similar detail as for extant species. Due to the break on the left side, the total volume was estimated by duplicating the volume of the right half of the endocast. With this method, the estimated total volume is of 245.0 mm^3. The global shape is hexagonal discarding the olfactory bulbs and the right paraflocculus, longer than wide, with an anteroposterior asymmetry: the anterior half (i.e., telencephalon and diencephalon) is visually longer and more angular than the posterior one (i.e., metencephalon and myelencephalon), the posterior outline being curved in dorsal view (Fig. IV-3-a,b). The maximal width is reached at the level of the paraflocculi, which protrude laterally; discarding them, the cerebrum is clearly wider than the cerebellum. The brain is lissencephalic, with a single shallow sulcus on each cerebral hemisphere (Fig. IV-3-a,b,e,f). The imprint left by the right petrosal promontorium (Fig. IV-3-c,d,e,f) is slightly tilted dorsally compared to the general rhombencephalon plane. In lateral view (Fig. IV-3-e,f), the overall endocast is quite longer than high, and it increases in height posteriorwards. The rhombencephalon seems anteroposteriorly compressed, with sort of a triangular shape (Fig. IV-3-e,f): it is higher and longer dorsally, and shorter ventrally, the foramen magnum forming most of the posterior side of this triangle. This foramen magnum opens posteriorly, a bit tilted ventrally; a cervical flexure can not be measured as the dorsal border of this aperture is missing (Appendix IV-2, Fig. 1). Prosencephalon and rhombencephalon are almost aligned, with a cephalic flexure of 178°.

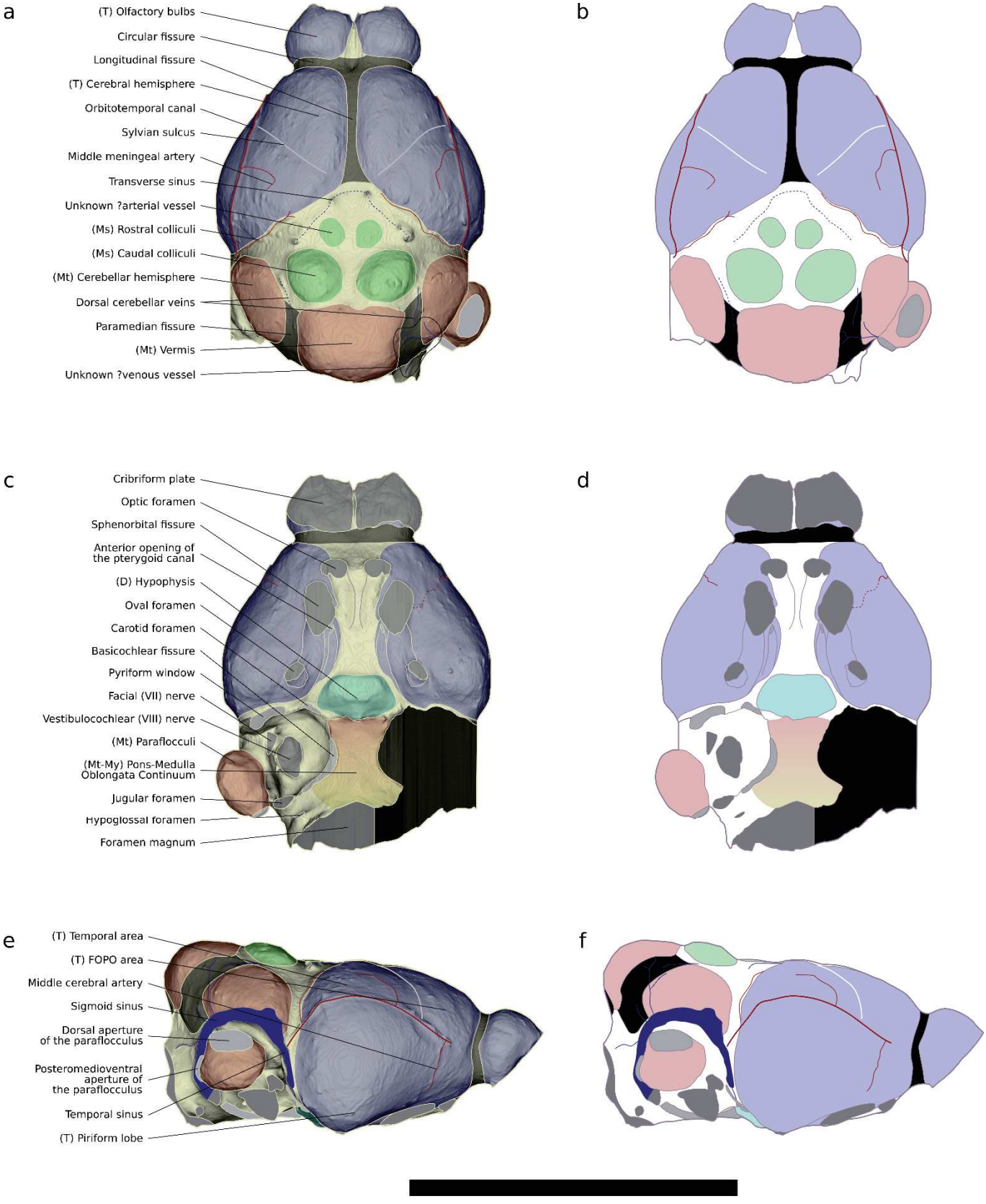

Figure IV-3: Endocranial cast of the cranium of the 'Vielase bat' UM-VIE250 in dorsal (a-b), ventral (c-d), and lateral right (e-f) views. Left figures (a,c,e) illustrate the endocranial cast with superimposed semi-translucent limits of the structures. Right figures (b,d,f) illustrate only the limits of the structures. Brain regions are: blue/T-telencephalon, light blue/D-diencephalon, green/Ms-mesencephalon, red/Mt-metencephalon, yellow/My-myelencephalon.

III.2) Telencephalon

Dorsally (Fig. IV-3-a,b), the olfactory bulbs are short, slightly wider than long. They are trapezoidal in shape, being narrower anteriorly. They are clearly distinguishable from each other, but linked over almost all their length. They are well separated from the rest of the telencephalon by a strongly marked circular fissure of constant width and of general dorsoventral orientation in lateral view (Fig. IV-3-e,f). In lateral view, it appears that these bulbs are made of a single bulge. The cribriform plate of the ethmoid is quite raised dorsally. This gives to the olfactory bulbs a triangular shape in lateral view, with a ventral point. There does not seem to be an anterodorsal bundle of nerves exiting the olfactory bulbs; anterior openings seem to be perforations of the cribriform plate (Fig. IV-3-c,d,e,f). Olfactory bulbs have a volume estimated to 8.8mm^3, representing 3.6% of the total endocast volume.

Cerebral hemispheres have a bean shape in dorsal view (Fig. IV-3-a,b), with an angular lateral edge and a more curved medial one. They do not contact each other, a marked and broad longitudinal fissure separating them. Posteromedial corners are very obtuse, curved, and located near the midpoint of the whole hemisphere length. Posterior edges of both hemispheres thus substantially diverge. Laterally (Fig. IV-3-e,f), there is no marked difference in dorsal inflation of an anterior and a posterior part; the whole dorsal edge is continuous, slightly curved. There is however a large and salient piriform lobe (the whole posterior half of the hemisphere protrudes ventrally), the ventral tip being wide and rounded.

A dorsal limit to the piriform lobe is difficult to locate laterally (Fig. IV-3-e,f), because the rhinal fissure is almost impossible to locate. There may be a very slight depression running along the hemisphere, grossly at the half of its height, but it is quite shallow; there also is such a shallow groove located very ventrally. A limit between the paleocortex and the neocortex is therefore impossible to draw with certainty.

Each hemisphere bears a marked, broad and shallow, neopallial sulcus. Dorsally (Fig. IV-3-a,b), this sulcus is diagonally oriented, perpendicular to the anterior part of the hemisphere's lateral edge. This sulcus marks the hemisphere surface starting from its posteromedial corner, then going anterolaterally and finishing by being confounded with the anterior part of the orbitotemporal canal. In lateral view (Fig. IV-3-e,f), this sulcus is still decipherable ventrally to the orbitotemporal canal, but it is less marked - on that section, it is dorsoventrally oriented, going slightly anterodorsally towards the orbitotemporal canal. On its more recognizable section (i.e., over the orbitotemproal canal), it goes posterodorsally from the orbitotemporal canal, and notches the continuous dorsal outline of the hemisphere. Given its shape, location, and given that it is the only decipherable sulcus on these hemispheres, it is interpreted as a sylvian sulcus. Though almost crossing all of the hemisphere height, there is no posterior extension of the sylvia: there is no clear bending in dorsal view (Fig. IV-3-a,b) with a marked change of orientation. The presence of this marked sylvia further allows distinguishing an anterior area and a posterior area of the neopallium. Given the theoretical organizations proposed in Part Two, these parts may correspond to the fronto-orbito-parieto-occipital ("FOPO") area and the temporal areas respectively. However, the fact that the medial end of the sylvian sulcus is here located quite anteriorly may rather imply that the posterior part comprises both the occipital and temporal areas.

III.3) Diencephalon

Dorsally (Fig. IV-3-a,b), no epiphysis cast is decipherable. Ventrally (Fig. IV-3-c,d) is a marked hypophysis cast. It is located at the level of the posterior end of the cerebral hemispheres, and is quite much wider than long. This cast is ellipsoidal in shape, though there are three short posterior "projections": one goes posteriorwards from the middle of the posterior border of the cast, and two go posterolaterally starting to the posterolateral edges of the cast.

III.4) Mesencephalon

The tectum of the mesencephalon is fully visible (Fig. IV-3-a,b), and all four colliculi are distinguishable. The rostral colliculi do not protrude at all and consist in slight bulges of similar extent on both sides of the sagittal plane. Not much more detail can be observed on these colliculi, as they are barely visible. Caudal colliculi, on the other hand, do protrude dorsally. They are easy to delineate, and are of ovoid shape, pointing anterolaterally. In both cases (i.e., rostral and caudal colliculi), there is a clear and wide separation between the colliculi. Rostral colliculi are difficult to see in lateral view (Fig. IV-3-e,f), as other vascular structures lateral to them protrude more. Caudal colliculi, on the other hand, are easy to locate. They are protruding dorsally, but not in a tremendous way: their dorsal top reaches that of the cerebellar vermis.

III.5) Metencephalon

In dorsal view (Fig. IV-3-a,b), the metencephalon is visible as the cerebellum. It is the widest point of the endocast, but this is due to the lateral protrusion of the paraflocculi - without them, the cerebellum is slenderer than the cerebrum. On both the vermis and the cerebellar hemispheres, no grooves are visible, and thus no cerebellar fissure or sulcus can be identified - as a corollary, cerebellar lobules cannot be distinguished and identified.

The cerebellar vermis, medially, is wider than the cerebellar hemispheres lying on both sides of it. The vermis is short and wide, being almost twice as wide as long; its length is comparable to that of both caudal colliculi. In lateral view (Fig. IV-3-e,f), the vermis is slightly longer than high. The shape of its external outline is like a rounded angle; its dorsal surface is horizontal, and its occipital surface is vertical. All in all, it forms sort of a rounded angle, the posterodorsal angle of the whole endocast.

The vermis is separated from the cerebellar hemispheres by shallow and broad paramedian fissures (Fig. IV-3-a,b). Both cerebellar hemispheres are positioned quite anteriorly to the vermis, anteroposteriorly overlapping the caudal colliculi on almost their whole length. Cerebellar hemispheres are longer than the vermis, but clearly slenderer (width near the half of the vermis width). Both hemispheres are not parallel: they diverge from each other anteriorly. Together with the shallow paramedian fissure and a posteriorly non-protruding vermis, this gives a curved shape to the posterior outline of the cerebellum (and of the endocast). In lateral view (Fig. IV-3-e,f), the cerebellar hemispheres are longer than high, with a well-demaracated anterior border.

Only the right paraflocculus could be reconstructed, due to the missing left petrosal. The paraflocculus is linked to the rest of the cerebellum almost on its whole length (Fig. IV-3-c,d). It is globular in shape, a little bit flattened dorsally (Fig. IV-3-e,f). It has two openings, one is a posteromedioventral opening, and the other opens laterodorsally, likely communicating with the sigmoid sinus dorsally. There is no ventral parafloccular fossa, no lateral paraflocculus sulcus, and a very slight imprint of the lateral semicircular canal in ventral view (Fig. IV-3-c,d). Doubling the volume of the right paraflocculus, both paraflocculi would have a volume of 6.0mm^3, accounting for 2.4% of the total endocast volume.

Ventrally (Fig. IV-3-c,d), the metencephalon and the myelencephalon both contribute to the pons-medulla oblongata continuum. There is no mark indicating a separation between both structures. The whole continuum is short and wide between the petrosal casts: it is approximatively twice as long as wide, and almost as wide as the hypophysis, located just anteriorly to it.

III.6) Cranial nerve exit casts (Fig. IV-3-c,d)

As previously described, the openings beneath the olfactory bulbs all seem to be perforations of the cribriform plate, without exit of a supplementary nerve bundle (see also Fig. IV-3-e,f).

The optic nerve (II) exits through a well defined optic foramen, large and sub-circular in shape. The optic canal is also visible on a short portion, posteriorly to the optic foramen. The optic chiasm is however not visible: the optic canals are not marked long enough posteriorly to decipher it. Both optic foramina are located under the cerebral hemispheres, far from the circular fissure, and are well separated from each other.

Oculomotor (III), trochlear (IV), abducens (VI), and trigeminal as its ophthalmic branch (V1) nerves all exit in the sphenorbital fissure. No round foramen is present; the maxillary branch (V2) of the trigeminal nerve thus has to also open in that fissure. The sphenorbital fissures are located just posteriorly to the optic foramina, but the gap between them is wider than that between optic foramina; there is a wide sphenorbital bridge, almost as wide as the hypophysis, very close in width to that of the pons-medulla oblongata continuum. They are longer than wide (approx. two times), and slightly divergent anteriorly. Following these fissures posteriorly are, for each, a bulge corresponding to the nerve pathway before exiting the endocranium through the sphenorbital fissure. These bulges, from the sphenorbital fissure, go posteriorwards then bend and diverge from each other until the end of the cerebral hemispheres.

Medially to the bending of these bulges are the oval foramina, through which the mandibular branch of the trigeminal nerve (V3) exits the brain. Their epithet correctly defines them: these foramina are oval, elongated diagonally, and they converge anteriorly. It is worth noting that these foramina are smaller than the optic foramina. A short ridge follows the anteromedial angle of both oval foramina, even bending lateralwards in the case of the right oval foramen.

The facial (VII) and vestibulocochlear (VIII) nerves are separated, and orthogonal in their orientation: the facial nerve goes laterally, and the vestibulocochlear nerve goes ventralwards, though a little bit anteriorwards (Fig. IV-3-e,f).

The glossopharyngeal (IX), vagus (X), and accessory (XI) nerves exit through the jugular foramen. It is located posteriorly to the petrosal cast, mediolaterally between the vestibulocochlear nerve cast and the paraflocculus. This foramen is short, but wide; it is of comparable size to the optic foramen, shorter and wider, and comparable in its size and shape to the pyriform window.

The hypoglossal nerve (XII) exits through the eponymous foramen. It is located a little bit posteromedially to the jugular foramen, opening anteroventrally (Fig. IV-3-e,f). This foramen is small and mediolaterally elongated. It lies at the middle of the condyloid fossa, between the jugular foramen and the foramen magnum, but a little bit closer to the latter.

III.7) Other braincase opening casts (Fig. IV-3-c,d)

Anteriorly, few other foramina than those for cranial nerves exit are observed. None of the three unknown foramina defined in the Part Two are retrieved in the *Vielasia* endocast. The caudal alisphenoid canal foramen is not present between the sphenorbital fissure and the oval foramen, and it is difficult to determinate whether it is coalescent with the oval foramen or not. There however are anterior openings of the pterygoid canal, located medially to the posteromedial corner of each sphenorbital fissure. There is also, following posterior to each anterior opening of the pterygoid canal, a noticeable mark that parallels medially the one following the sphenorbital fissure, but ends roughly at the anteroposterior level of the oval foramen. The the pterygoid nerve, exiting through the anterior opening of the pterygoid canal, is thus quite thick.

Other openings are found around the petrosal cast. There is an identifiable pyriform window, anteromedial to the petrosal cast. This window is short, but quite wide, half as wide as the petrosal cast. It is medially followed by a thin aperture along the medial half of the petrosal cast anterior border. At the anteromedial corner of that cast, the aperture widens a little bit, maybe being the mark of a (posterior) carotid foramen. Continuing posteriorly, along the medial border of the petrosal cast, is the basicochlear fissure. It is a wide fissure, especially in the posterior half of the petrosal cast medial border. Overall, the whole continuation between the pyriform window and the marked part of the basicochlear fissure is a bit blurry, with variations in thickness, and it is difficult to determine 1) if there is a carotid foramen and 2) if all these structures really are in continuity. Observations on the skull (Appendix IV-2, Fig. 2) show that the petrosal connects the basisphenoid and the basioccipital; there is therefore no coalescence between apertures surrounding the petrosal, also including the jugular foramen.

The foramen magnum is partly preserved, with the ventral and right borders only. It seems clearly wider than long in ventral view (Fig. IV-3-c,d); this is not surprising as it is oriented dorsoventrally rather than anteroposteriorly (see general remarks), so it looks short in ventral view. An occipital view (Appendix IV-2, Fig. 1) shows that it probably is a little bit wider than high, with an ovoid shape. Its ventral margin (Fig. IV-3-c,d) is rounded, with a blunt and wide anterior angle of this margin. Due to its partial preservation, no more can be said regarding its morphology.

III.8) Vascular imprints

The most marked vascular imprint is the orbitotemporal canal (Fig. IV-3-a,b,e,f). In lateral view (Fig. IV-3-e,f), it is located on the dorsal half of the cerebral hemisphere, though not that dorsally located; in dorsal view (Fig. IV-3-a,b), it is still quite laterally located. It is straight in dorsal view (Fig. IV-3-a,b), and widely convex dorsally in lateral view (Fig. IV-3-e,f). Posteriorly, it connects to other vascular imprints that dorsolaterally surround the petrosal, extending a little bit further posteriorly than the cerebral hemisphere. Anteriorly, it finishes well before (posteriorly to) the circular fissure. On both the left and right canals, a subtle dorsal ramification is present. The ramification originates between the sylvian sulcus and the top of the orbitotemporal canal. Then, this ramification extends dorsally to dorsoposteriorly, paralleling the sylvia over a short distance (Fig. IV-3-a,b); it then bends posteroventrally and ends (Fig. IV-3-e,f). It may further continue posteroventrally and join the orbitotemporal canal just posteriorly to its dorsal top, but the surface is too irregular to see a clear continuity. It is the clearest of the ramifications of ramification-like structures connected the orbitotemporal canal, and it is present on both sides; I interpret it as being the middle meningeal artery. There is also a shorter, and more anteriorly located, ramification on the right orbitotemporal canal, but it is difficult to interpret it differently than a meaningeal ramus. There is also another, long, ramification on each canal. Each ramification joins the

canal just anteriorly before the canal itself ends posteriorly (Fig. IV-3-e,f), and goes anterodorsally from the junction, following the posterior border of the cerebral hemisphere on a variable length (half of the posterior border of the left cerebral hemisphere, almost the whole posterior border of the right one; Fig. IV-3-a,b). Such a posteriorly located ramification of the orbitotemporal canal is unknown to my knowledge, and may be another main meningeal artery; it is marked, present on both sides, and quite long, and I found it unlikely to be a "simple" meningeal ramus.

On both sides, a vessel-like imprint is present ventrally to the anterior extremity of the orbitotemporal canal casts (Fig. IV-3-e,f, see also Fig. IV-3-c,d). It is dorsoventrally oriented, and connects dorsally or merges with the anterior end of the orbitotemporal canal. Ventrally, the imprint extends continuously at halfway towards the anterior extremity of the sphenorbital fissure; after that point (Fig. IV-3-c,d), it seems to continue towards the middle of the sphenorbital fissure, but in a discontinuous way. This structure may be interpreted as the imprint of the middle cerebral artery, but it is quite less marked and thinner than the orbitotemporal cast, which may seem surprising since it is an important arterial vessel of the braincase. No ophthalmic ramus or artery can be seen here.

There is no cast of the longitudinal sinus between the cerebral hemispheres (Fig. IV-3-a,b). There however is the cast of a transverse sinus, especially visible as running along the anterior part of the mesencephalic tectum. It is never continuous and consists of punctual connections with the dorsal cranial roof (two located laterally to the rostral colliculi, two located anterior to each of them) and of bulges linking each anterior and lateral spots; it is therefore not very difficult to track. Its lateral extensions (i.e., laterally to the mesencephalic tectum) are, however, not decipherable. Traces of a dorsal cerebellar vein are visible on both sides, between the vermis and the cerebellar hemispheres. The right one is a continuous ridge, medially to the medial border of the right cerebellar hemisphere. The left one consists of two spots located at the levels of the anterior and posterior ends of the right one, but without continuity between them. For both, there however are no anterior extensions.

Vascular structure imprints surrounding the petrosal are only visible on the right side, as only the right petrosal has been preserved (Fig. IV-3-e,f). There is a continuous imprint, probably filled by different sinuses. This imprints anteriorly starts as a slender mark dorsolaterally extending from the pyriform window (Fig. IV-3-c,d). It then goes dorsally, slightly posteriorly, and quickly widens (Fig. IV-3-e,f). It surrounds the anterior, dorsal, and posterior petrosal borders, then ending in the jugular foramen (i.e., being coalescent with it). The slender anterior part, dorsoventrally oriented and connecting the pyriform window, could be the communicant sinus. In its continuity, the wider dorsoventrally oriented part is identified here as the cast of the temporal sinus; the orbitotemporal canal ends in it, at its half. The dorsal (anteroposteriorly oriented) and posterior (dorsoventrally oriented) parts are identified as the sigmoid sinus cast. Both sinus casts are confluent. The sigmoid sinus is thicker than the temporal sinus, and only narrows (being as wide as the temporal sinus) just before joining the jugular foramen. There are several short ramifications of the sigmoid sinus around its posterodorsal corner, but they are not identifiable: all go posterodorsally, but they vary in length, thickness, and some further dichotomize. The knowledge of bat endocranial veins is too limited to propose individual identifications for now.

IV) Morphological evolution

IV.1) Character support to the topology, evolution, and sampling implications

IV.1.A) Consistency and Retention Indexes (Fig. IV-4)

The consistency and retention indexes calculated at the tree level are of 0.167 and 0.110 respectively (Appendix IV-3, Table 1). These very low values are better appreciated while looking at the distribution of both indexes for each character (Fig. IV-4, top panels; Appendix IV-3, Table 1) and for each morphological complex (Fig. IV-4, bottom panels; Appendix IV-3, Table 1).

Regarding the retention index (Fig. IV-4, left panels), almost half of the characters have a barely positive value, and most of the morphological complexes are centered around the 0 value. This implies that there are several characters with distributions implying more changes than the maximal number of reconstruction using the parsimony method - character 56 ('Anterior opening of the pterygoid canal'), with a RI of -8, has been removed from the data used to generate Figure IV-4 in order to not shrink the rest of the distribution. Only the characters of mesencephalic structures, of the Pons-Medulla Oblongata Continuum, and of the neopallial foldings do not have characters with a negative RI. On the other hand, overall shape characters never have a positive RI.

It is mathematically impossible to have negative values of the consistency index (Fig. IV-4, right panels). Still, most characters have very low values: no character has a CI over 0.5, and most characters have a CI below 0.3. For this index, all morphological complexes are not centered on the same values; especially, characters of the Diencephalon, of the Pons-Medulla Oblongata Continum, of the neopallial foldings, and of the cranial openings are a little bit shifted toward higher values (with a median around a CI of 0.2, except for the Pons-Medulla Oblongata Continuum character which has a CI of 0.5), whereas other groups median is below 0.2 and generally around or below 0.15.

There is also a substantial variation of each morphological complex distribution of the values of both indexes. For instance, characters describing the Telencephalon and the vascular structure casts have a highly varying RI, whereas those describing the Mesencephalon and the cranial apertures have reduced spread. Vascular structure casts character have again highly varying CI, together with diencephalic characters, whereas telencephalic and metencephalic characters show a reduced variation. In spite of these apparent discrepancies, there is no significant heterogeneity between morphological complexes in the CI and in the RI (p-values of 0.39 and 0.53 respectively, Appendix IV-3, Table 3). The previously described differences therefore have to be considered with caution.

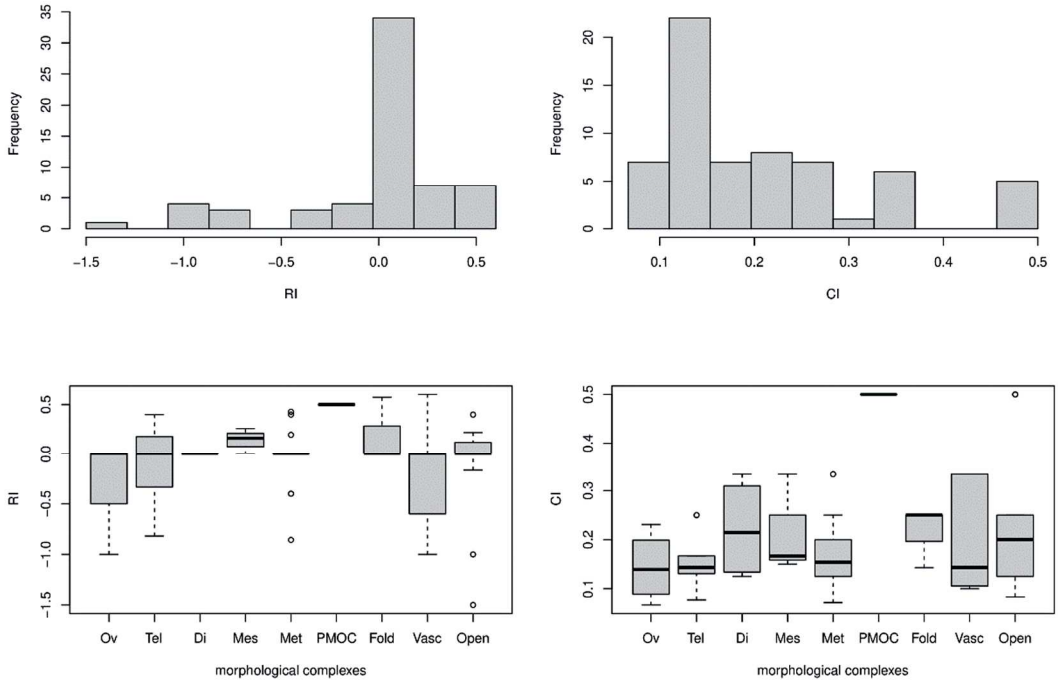

Figure IV-4: Distribution of the retention index (RI, left) and of the consistency index (CI, right) across all characters (histograms, top) and across morphological complexes (boxplots, bottom). Autapomorphic and constant characters have been removed, together with the character 56 (RI of -8) for graphical purposes. Abbreviations: Ov-Overall shape; Tel-Telencephalon; Di-Diencephalon; Mes-Mesencephalon; Met-Metencephalon; PMOC-Pons-Medulla Oblongata Continuum; Fold-Neopallial foldings; Vasc-Vascular structure casts; Open-Cranial openings.

IV.1.B) Number of changes (Fig. IV-5)

For each character, there are at most three morphological changes occurring at internal nodes, whereas there is up to 21 morphological changes at tips for a single character - this does not mean that 21 tips do change, there can be several changes for a tip for a given multistate character. The number of changes at nodes and at tips seem decoupled (Fig. IV-5, top left panel): independently from the number of changes at nodes, there is a high variation of the number of changes at tips. However, the few characters with more than one change at nodes all have more than five changes at tips, indicating a potential positive relationship between the number of changes at nodes and at tips. Of the ten concerned characters, seven have three or four states; this link between number of changes at tips and nodes may be explained by the number of *possible* changes (i.e., the number of states). The correlation test between the number of changes at tips and at nodes is significant (p-value of 3.10^{-4}, Appendix IV-3, Table 3), which may support the previous observations; the test however does not indicate the sign of the correlation, which is likely due to the number of character states.

Treating the number of morphological changes at tips and/or at nodes given the morphological complexes (Fig. IV-5, top right and bottom panels), a mixed pattern appears. Simply averaging the number of changes at nodes and tips for these groups, all of them show a low average number of changes at nodes, but more varying average number of changes at tips. The characters describing the neopallial foldings and the Pons-Medulla Oblongata Continuum vary little (less than four changes at tips), whereas those describing the overall shape of the endocast, the Telencephalon, and the Mesencephalon highly vary (more than ten changes at tips). This time, there is no correlation between the number of changes at nodes and tips (p-value of 0.34, Appendix IV-3, Table 3).

The previous observations regarding the number of changes at tips given the morphological complexes can also be seen on the boxplots showing the variation of the number of changes at tips in each morphological complex (Fig. IV-5, bottom right panel). Character groups show a heterogeneous variation only regarding the number of changes at tips (p-value of 2.10^{-3}, Appendix IV-3, Table 3), whereas there is no heterogeneity for changes at nodes and when considering both tips and nodes (p-values of 0.25 and 0.07 respectively, Appendix IV-3, Table 3). Pairwise comparisons show that the characters describing neopallial foldings change less at tips than do those describing the overall shape of the endocast, the Telencephalon, and the Mesencephalon (p-values of 3.10^{-2}, 3.10^{-2}, and 2.10^{-3} respectively, Appendix IV-3, Table 4). There is no other significant pairwise comparison; one can regard these groups as being the most extreme in their number of changes at tips, as also illustrated by the average number of changes (Fig. IV-5, top right panel).

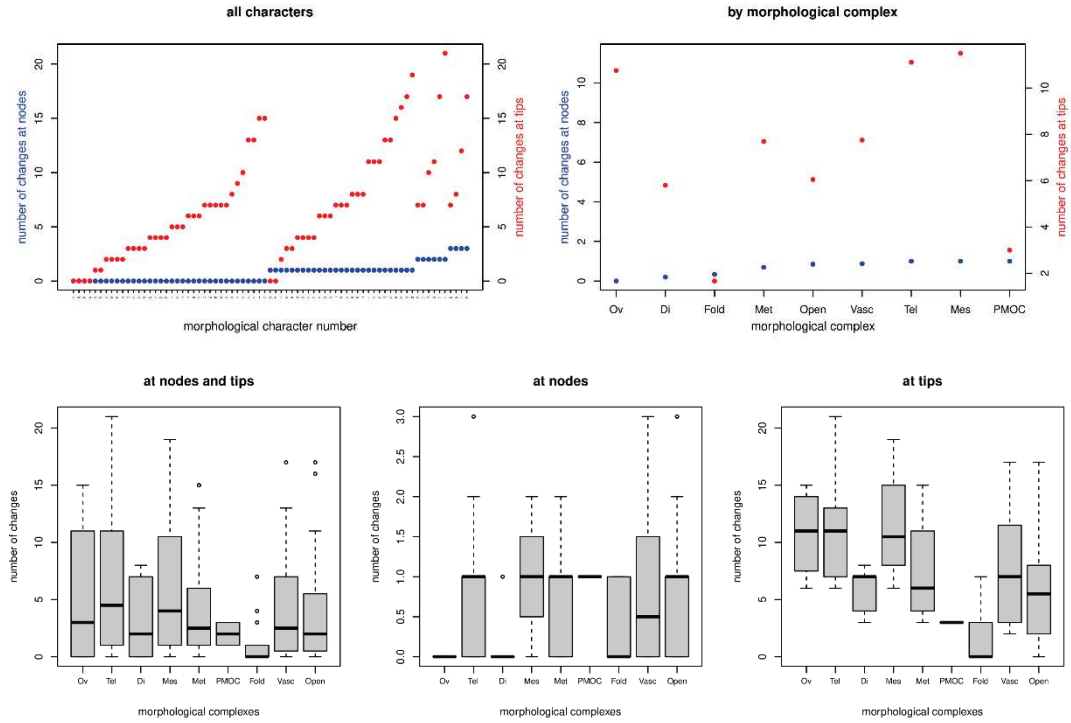

Figure IV-5: Distribution of the number of morphological changes at nodes and/or at tips. Top: number of morphological changes at tips and number of morphological changes at nodes ordered given the number of morphological changes at nodes; top left for each morphological character, top right averaged for each morphological morphological complex. Bottom: number of morphological changes at nodes and/or at tips (left both, middle at nodes, right at tips) across morphological complexes. Abbreviations: Ov-Overall shape; Tel-Telencephalon; Di-Diencephalon; Mes-Mesencephalon; Met-Metencephalon; PMOC-Pons-Medulla Oblongata Continuum; Fold-Neopallial foldings; Vasc-Vascular structure casts; Open-Cranial openings.

IV.1.C) Discussion on the phylogenetical relevance of endocranial characters at the Chiroptera scale

The main observation drawn from the previous results is that there is much more variation at tips than at nodes concurrently with very low consistency and retention indexes. This indicates that the characters, distributed according to the chosen PCM, are not following the phylogenetic relationships and may instead be convergent. There is generally no discrepancy between morphological complexes regarding their CI and RI or their number of changes, with the exception of the characters of the neopallial foldings that vary very little at tips, and of the characters of overall, telencephalic, and mesencephalic features that highly vary at tips. Maybe the most important point supporting the general low phylogenetic

consistency is that most of the characters and of the morphological complexes are centered around a zero value of the retention index (Fig. IV-4, left panels). It is also interesting to note that the previously quoted morphological complexes that vary very little or very much at tips do not differ that much by looking at their RI and CI. Similar results at the Yinpterochiroptera scale (Part Three), working on the same anatomical characters (see state modifications in the Material & Methods section), showed much more variation at nodes (way more comparable to the variation at tips), and retention indexes centered around 0.5, with grossly half of the characters having a RI equal or superior to 0.5. The fact that the same characters vary that much in their distribution (and, therefore, in the way they change along the phylogeny) using the same PCM, but with a different sample, shows the drastic impact of taxonomic sampling on character state distribution.

Two hypotheses can be proposed: either the endocranial characters (as they are defined here) are much more relevant at the Yinpterochiroptera than at the Chiroptera scale, or the difference in the sampling is responsible of these differences. The first hypothesis seems unlikely to me: the morphological disparity observed at the Yinpterochiroptera (with megabats and some “microbats”) scale would already encompass the potential morphological disparity present at the whole Chiroptera scale. The PCM used here heavily relies on the branch lengths, and therefore heavily benefits from the inclusion of deep taxa, by “breaking” potential long branches. In the present chiropteran sample, there are generally long branches between superfamilial and familial nodes, especially in Yangochiroptera. In the PCM used here, long branches much more tolerate changes than short ones, therefore changes are firstly reconstructed on long branches rather than on short ones. This may explain the very high number of changes at tips that generally represent families or infrafamilial clades.

With this PCM, to get a better consistency between phylogenetic relationships and endocranial characters, and therefore more adequate ancestral reconstructions, one would need to “break” the long branches. There are two non-exclusive solutions to sort out this. The first is to consider punctual fossil occurrences. In the present sample, old node reconstructions are heavily impacted by the values of the eochiropteran ‘Vielase bat’ and of old yinpterochiropteran families. By adding old fossils to some branches, changes could be constrained on the deepest nodes if the fossils have a similar morphology to their extant representatives. The second solution is to expand the sample of extant species; while this may segment branches at the family-level, this procedure cannot go deeper in time than the root age of the considered clade. An example is the case of pteropodids: the root age of this family is estimated at the end of the Oligocene, and a long branch persists between the root of this family and the root of Yinpterochiroptera, where numerous changes can take place. In terms of sampling cost, the first solution is clearly time-saving: extrapolating, adding a single fossil taxa may refine the reconstruction of the characters evolution. Future directions should then expand this sample with some fossil occurrences (some skulls are known for emballonurids, vespertilionids, molossids; Revilliod 1920, Brown et al. 2019), consider larger sample of extant groups and/or work at a lower phylogenetical level (a first stepping stone is the work on Yinpterochiroptera in Part Three).

IV.1.D) Characters temporal trends and interpretation of absolute rate trends sign

The distribution of the temporal trend slopes of the characters ('traits') and of their absolute evolutionary rates ('absolute trait rates') are provided in Figure IV-6 (top left and top center panels) and in Appendix IV-3, Table 1. Temporal trend slopes of the characters are distributed around a 0 value (normality test p-value of 0.24, Appendix IV-3, Table 3), with however a secondary peak in positive values. Temporal trend slopes of absolute evolutionary rates of the characters are not centered around zero, most of them are positive, and the distribution is skewed toward positive values, being non-normal (p-value of 4.10^{-6}, Appendix IV-3, Table 3). The interaction between evolutionary trends slopes of a character and its absolute evolutionary rates (Fig. IV-6, top right panel) shows sort of a random distribution, with absolutely no link between the two (p-value of 0.98, Appendix IV-3, Table 3).

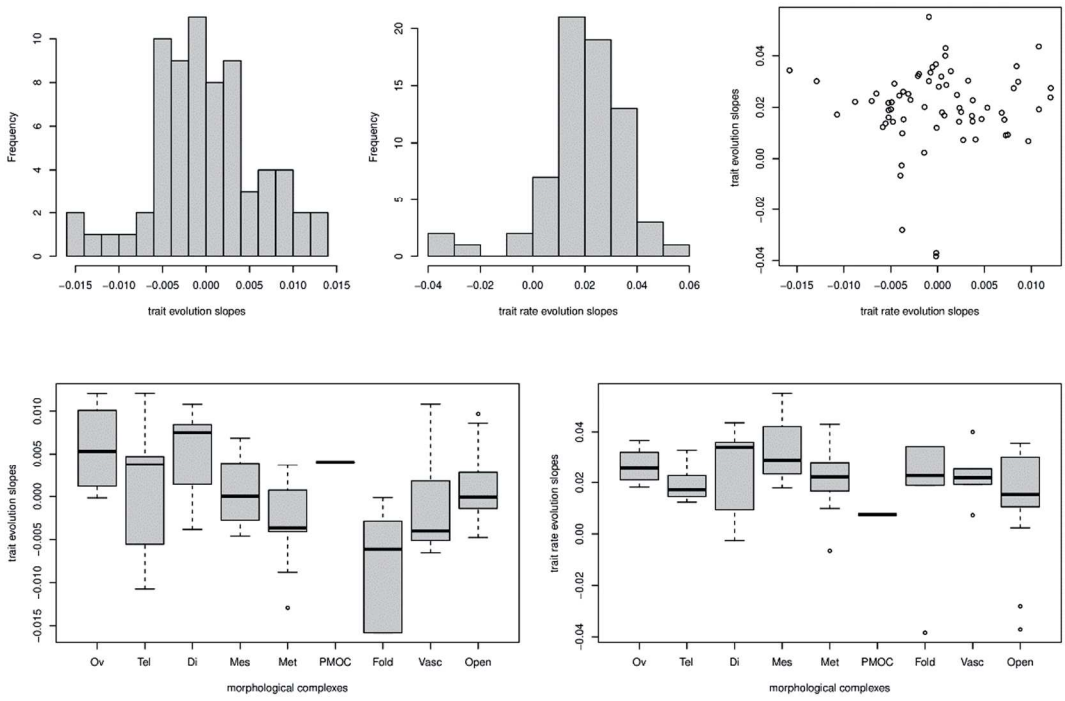

Figure IV-6: Distribution and interaction of the temporal trend slopes of morphological characters ('trait') and of their absolute evolutionary rates ('trait rate'). Top: distribution and interaction for each morphological character; top left distribution of trait slopes, top middle distribution of trait rate slopes, top right interaction of trait and trait rate slopes. Bottom: distribution in all morphological complexes; left distribution of trait slopes, right distribution of trait rate slopes. Abbreviations: Ov-Overall shape; Tel-Telencephalon; Di-Diencephalon; Mes-Mesencephalon; Met-Metencephalon; PMOC-Pons-Medulla Oblongata Continuum; Fold-Neopallial foldings; Vasc-Vascular structure casts; Open-Cranial openings.

Distribution of trait and absolute trait rate slopes in each morphological complex are provided in Figure IV-6 (bottom panels) and in Appendix IV-3, Table 1. There is a clear heterogeneity among groups regarding trait slopes (p-value of 2.10^{-2}, Appendix IV-3, Table 3) but not regarding absolute trait rate slopes (p-value of 0.49, Appendix IV-3, Table 3). In both cases, groups are not all distributed in a homogeneous way around a particular value. But while all repartitions overlap regarding absolute trait rate slopes, there are genuine discrepancies regarding trait slopes. No pairwise difference is significant, but two are near the 5% risk level: in both cases, neopallial foldings characters slopes generally have lower values than characters slopes of either the Diencephalon or the overall endocast shape (p-value around 8% in both cases, Appendix IV-3, Table 4). These groups may be regarded as the most extreme cases of trait slope variation. Finally, there is no morphological complex in which the repartition of either trait or absolute trait rate slope significantly differs from zero (all p-values over 0.2, Appendix IV-3, Table 3): even though some groups only have positive values (e.g., overall shape characters only have positive trait and absolute trait rate slopes; Fig. IV-6, bottom panels), there are too few values to statistically assess the shift from a zero value.

Beyond the values of the trait and absolute trait rate slopes, to discuss their significance is mandatory. Near half of the characters show a significant slope (i.e., to a zero value) either of the trait or of the absolute trait rates evolution through time (31 and 26 respectively). This tempers the observations regarding slope distributions (Fig. IV-6, top left and top center panels): trait slopes are centered around zero but nearly half are significant, whereas absolute trait rate slopes are shifted towards positive values but are a little bit less significant. Of the significant trait slopes, half are increasing and half are decreasing; this is not that surprising since it simply informs about the evolution towards state 0 or towards the maximal state, and one rather should consider the proportion of significant trait slopes, no matter their sign. Regarding significant absolute trait rate slopes, all have positive values, which is not surprising given the general distribution shifted towards positive values (see Fig. IV-6, top center panel), and indicates that states tend to vary more through time. Both trait and absolute trait rate slope are significant for ten characters. Among those, six have a positive trait slope, and four have a negative one, close to the half/half proportion of significant trait slopes.

Overall, there is a slightly inverted location of the variation compared with the Yinpterochiroptera scale study: in the latter, absolute trait rate slopes vary more, and some that are significant are negative, whereas here, there are more discrepancies in trait slopes, and all absolute trait rate slopes are positive. Particularly, the latter point has to be considered in the light of the repartition of characters that has been described and discussed in the previous section. Indeed, the characters have a convergent distribution rather than following phylogenetic relationships. In that way, with the overwhelming majority of changes occurring at tips, it is not surprising to find that there is an increase of the variation through time: there are more and more taxa with time (i.e., whether they are nodes or tips), and with convergent changes, there are more and more changes in recent taxa. So while the sign of the significant absolute trait rate slopes enabled to propose biological hypotheses regarding their sign in Yinpterochiroptera (Part Three), they have to be regarded with more caution at the Chiroptera scale, and in the light of the previously discussed points concerning the sampling and the PCM used here. While a negative absolute trait rate slope can be biologically interpreted, a positive one should thus be first faced with the character distribution and the potential biases induced by long phylogenetical branches between taxa.

IV.2) Evolution of endocranial morphology in Chiroptera

IV.2.A) General overview of morphological variation

Average absolute rates over all characters are mapped together with the number of morphological changes for each taxa in Figure IV-7. Striking is the number of changes at tips: most tips have morphological changes for more than 20 characters (even for at least 30 in pteropodids, megadermatids, and nycterids), whereas some extant yangochiropteran taxa have changes concerning between 10 and 20 characters (phyllostomid and vespertilionid species). There are few nodes with morphological changes: these are the rhinolophoid node (mainly impacted by the hipposiderids, the only rhinolophoid family without individual morphological changes), the Emballonuroidea and Emballonurinae (with one change), the Vespertilionidae (two changes), and several noctilionoid internal nodes (Noctilionoidea, Phyllostomidae + Mormoopidae, Phyllostomidae, and Phyllostomidae without Macrotinae clades, with two to ten changes).

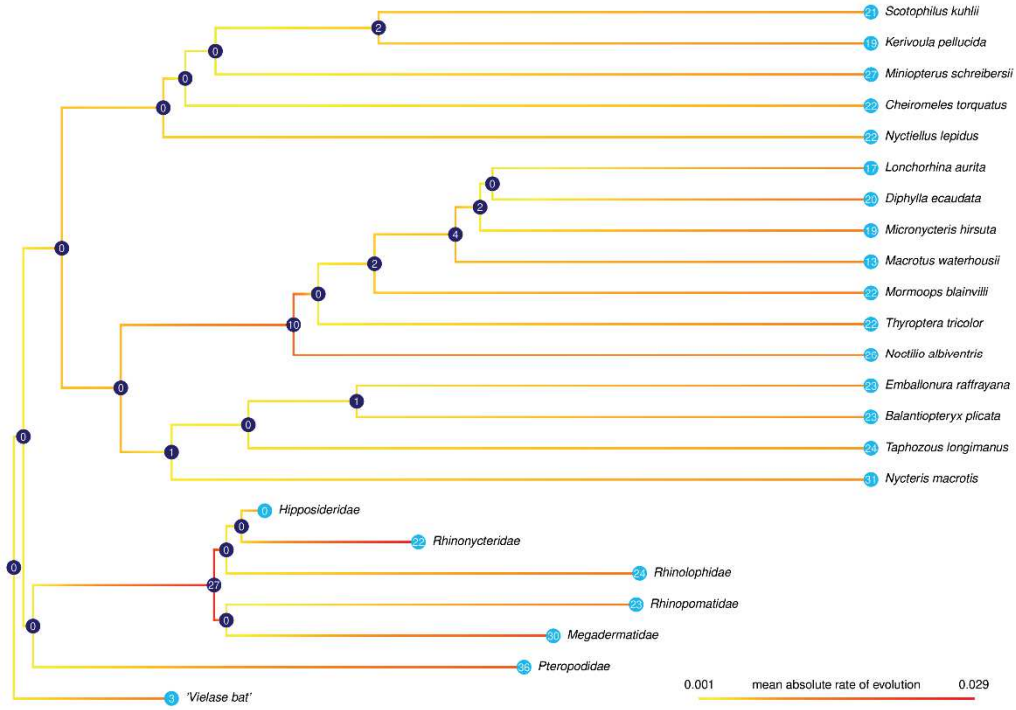

Figure IV-7: mapping of the absolute evolutionary rates averaged over all characters for each taxa (color gradient), with the number of morphological changes at each node (marine pastille) and tip (light blue pastille).

Average absolute rates follow this pattern, with all terminal branches increasing in absolute rate through time. There are also high absolute rates at nodes with changes, but some nodes without changes have moderate average absolute rates: these are the Vespertilionoidea and the Emballonuroidea + Noctilionoidea, and the Yangochiroptera nodes. This may indicate that there are incipient changes at these nodes established later, at the superfamilial to familial nodes. One may also suspect that some changes would be located at these nodes by more constraining changes on the deep taxa of the phylogeny (by incorporating fossils and/or expanding extant taxa samples).

In spite of the apparent limitations regarding the phylogenetic signal of endocranial characters at the Chiroptera scale (with the present sample), some main bat clades exhibit non-negligible morphological support. A main example is the case of noctilionoids: the root node of the superfamily has changes on ten characters, and several successive deep nodes also have some changes (especially that of phyllostomids,

with changes for four characters). The PCM used here may sometimes rest a little bit too heavily on fossil taxa values for the reconstruction of "surrounding" taxa (there are no changes at the deepest chiropteran nodes, and few changes at nodes on the whole tree) and reconstruct too many individual, parallel changes; it becomes caricatural regarding rhinolophoid deepest nodes, fully dependent on the hipposiderids. Still, some changes occur along short branches rather than along longer ones in yangochiropterans; this indicates that there are strong morphological trends (i.e., stronger than the optimization of the PCM) in large-scale clades.

IV.2.B) Evolution of the exposure of the mesencephalic tectum

The repartition of the characters linked to the exposure of the mesencephalic tectum have been discussed at the Yinpterochiroptera scale, contrasting rhinolophoid and pteropodid trends (Part Three). There are however some variation in yangochiropterans too, with cases of varying exposure of the tectum (Fig. IV-8).

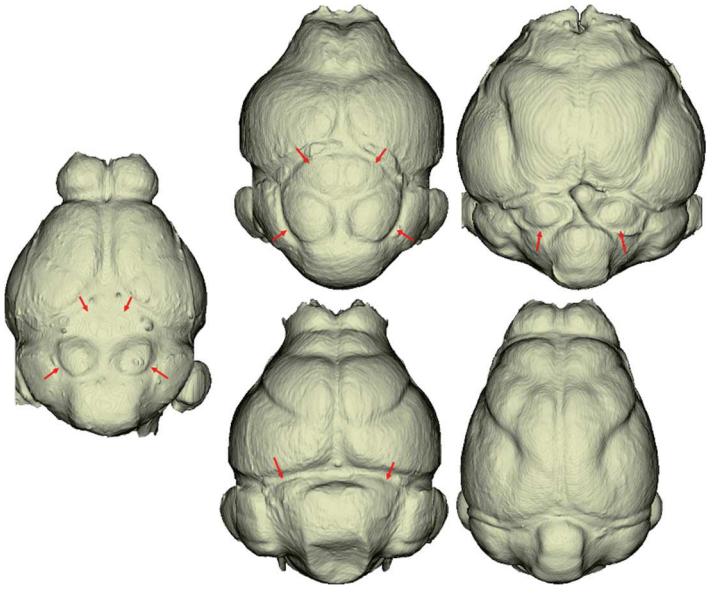

Figure IV-8: Overview of the mesencephalic exposure (indicated by red arrows) with dorsal view of the endocasts of the fossil eochiropteran 'Vielase bat' (left, with fully exposed mesencephalic tectum, individualized caudal colliculi, and rostral colliculi more difficult to decipher), the emballonurid *Balantiopteryx plicata* (top center, with both the rostral and the caudal colliculi visible), the noctilionid *Noctilio albiventris* (top right, with only caudal colliculi individualized), the miniopterid *Miniopterus schreibersii* (bottom center, with the caudal colliculi partly covered), and the phyllostomid *Diphylla ecaudata* (bottom right, with a fully covered mesencephalic tectum).

The main character accounting for the exposure is the character 19. It has positive CI and RI (0.15 and 0.26 respectively, Appendix IV-3, Table 2), a positive, significant slope, indicating a reduction of the exposure through time, whereas the absolute rate slope is not significant. The mapping of this character (Appendix IV-5, Fig. 19) is rather clear: a full exposure is widely present, with punctual covering of varying magnitude (full in pteropodids and a vespertilionid, advanced in rhinonycterids and in the miniopterid), and a shared increasing covering in noctilionoids (partial covering as a basal condition, then advanced or full covering in non-noctilionid species). The variable exposure of the mesencephalic tectum are synapomorphies in pteropodids, rhinonycterids, and noctilionids, but there also are some isolated covering (in *Kerivoula pellucida* and *Miniopterus schreibersii*, but also in the hipposiderid *Coelops frithii*, see Part Three).

Numerous clades therefore show exposed rostral colliculi, with a varying and rather convergent level of delineation of them (character 20, Appendix IV-5, Fig. 20): rostral colliculi are easily seen in some emballonurids, barely decipherable in vespertilionoids (vespertilionids, natalids), emballonuroids (some emballonurids), and rhinolophoids (rhinopomatids), and not visible at all in the same superfamilies (in

megadermatids, rhinolophids, nycterids, and molossids). Recalling the data of Baron et al. (1996), Reep & Bhatnagar (2000) stated that presence of well-developed rostral colliculi would characterize gleaning bats (some vespertilionids, nycterids, megadermatids, some phyllostomids, potentially natalids and thyropterids). The anterior part of the mesencephalic tectum (where are the rostral colliculi) is exposed in most of these taxa (not in thyropterids, not tested here in the concerned phyllostomids). The degree of delineation of the rostral colliculi, however, does not distinguish ecological groups of gleaning bats; they are supposed to have large rostral colliculi, but these structures are only clearly decipherable in some groups.

Regarding caudal colliculi, their degree of inflation (character 21) and the distance between them (character 22) are also greatly convergent traits (Appendix IV-5, Figs. 21,22): the three states of both characters are found in rhinolophoids, emballonuroids, and vespertilionoids, whereas they are reconstructed as being low and well separated in all noctilionoids (though not at the noctilionoid node, with a convergence between phyllostomids and noctilionids). Dechaseaux (1956) also described the distance between caudal colliculi, noting a trend through time for an increasing gap between them, which is not found here (Appendix IV-3, Table 2).

The three previous characters still do not have negative RI values (between 0 and 0.17, Appendix IV-3, Table 2), but these values remain lower than that for the character accounting for the global exposure. As already exemplified in yinpterochiropteran bats (Part Three), the variation of the covering of the mesencephalic tectum has to be interpreted without haste: the general covering may follow the phylogeny quite well, there is still a subtler variation in the morphology of colliculi in species with a similar covering. The conclusions of Dechaseaux (1956), who proposed a general trend toward a covering of the tectum trough time, are somewhat retrieved here: this applies to some bat taxa, but not all, and to varying degrees if dealing with the differentiation of the colliculi. For the latter point, finer works should investigate the functional implications of their varying protrusion; very first works of that type led Dechaseaux (1973) to associate the degree of hypertrophy of the caudal colliculi to the ability to echolocate (not to the degree of sophistication of echolocation).

Characters associated with the covering of the mesencephalic tectum regard the posterior expansion of the cerebral hemispheres (characters 9 and 10; Appendix IV-5, Figs. 9,10) and the anterior expansion of the vermis (character 26; Appendix IV-5, Fig. 26). The cerebral characters have low RI (-0.18 and 0, Appendix IV-3, Table 2) and show very varying distributions. Character 9, which accounts for the angle of the posterior border of the cerebral hemisphere (the more diagonal it is, the less expanded are the hemispheres), shows several convergences and parallelisms, with a temporal trend toward an increasing mediolaterally oriented posterior border (significant negative slope, Appendix IV-3, Table 2), meaning a posterior expansion of the hemisphere. Character 10 is more simple, accounting for the shape of the posterior border with two states (made of straight lines or curved, posteriorly convex, also indicating a posterior expansion of the hemisphere), and its distribution is only made of convergences, without temporal trend (Appendix IV-3, Table 2). A similar pattern is found for the distribution of character 26, that accounts for the degree of anterior protrusion of the vermis; this character has however a higher RI (0.4, Appendix IV-3, Table 2) due to the fact that an anterior protrusion of the vermis is shared by all non-noctilionids noctilionoids. In Yinpterochiroptera, occurrences of a covering of the mesencephalic tectum are likely to be due to different structures (cerebrum in pteropodids, cerebellum in rhinonycterids; Part Three). At the Chiroptera scale, the other (phylogenetic) case of tectum covering in phyllostomids largely joins that of pteropodids, with at least contribution of both the cerebrum and of the cerebellum. In both

taxa, the cerebrum is way bigger than the cerebellum (see distribution of character 3 accounting for this point, Appendix IV-5, Fig. 3), and the cerebrum may play a more important role in the tectum covering than do the cerebellum. The confidence in the relative proportions of cerebrum and cerebellum has however to be taken with caution, since most vespertilionoids also have way bigger cerebrum than cerebellum without covering of the tectum: the only species with a fully covered tectum, *Kerivoula pellucida*, is also the only species with a cerebrum slightly larger than the cerebellum.

IV.2.C) Morphological evolution at main deep nodes of Chiroptera

Figure IV-7 shows average absolute rates for each taxon, and therefore can inform about local changes in average rate regime of evolution of the morphological characters. A complementary way to determine if the main deep chiropteran nodes differ between each other is to look at the values of the averages (using estimated marginal means) of the absolute rates and their temporal trend slopes, for each clade and for each character. Expressing the difference between rate slopes and average values of the considered clade vs the rest of the three, this results in the two boxplots provided in Figure IV-9, and this both informs about the central trend and the variation of rate slopes and averages for all the considered clades. There are obvious visual differences in both cases. First, yinpterochiropteran bats seem to have higher rate slopes and average values, whereas yangochiropterans have lower ones. The distribution of average rate values of yinpterochiropterans seems skewed toward high differences (only upper outliers), whereas that of yangochiropteran bats seems skewed toward low ones (only lower outliers). Second, rhinolophoids and yangochiropteran superfamilies are all aligned for rate slope differences, with generally slightly positive differences, whereas rhinolophoids seem to clearly have higher average rates than all other three superfamilies, that all remain on the same level. There is also a broader variation of rate slope differences in rhinolophoids compared to that of other superfamilies.

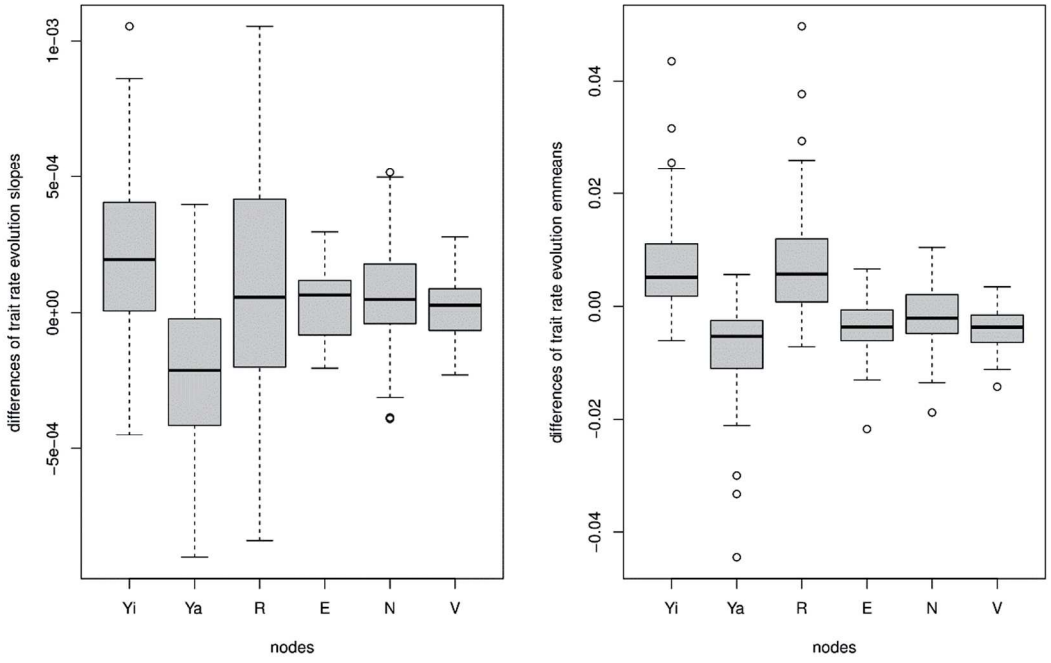

Figure IV-9: Distribution of the difference between the slope of the temporal trend (left) and the average (i.e., estimated marginal means, right) of the evolutionary rates of the characters for each considered "deep node" vs. that of the rest of the tree for each phylogeny. Abbreviations: Yi- Yinpterochiroptera; Ya- Yangochiroptera; R- Rhinolophoidea; E- Emballonuroidea; N- Noctilionoidea; V- Vespertilionoidea.

Both variables (trait slopes and averages) are significantly heterogeneous (p-values of 3.10^{-12} and 9.10^{-35}, respectively; Appendix IV-3, Table 3), which is not very surprising. Then are several significant pairwise comparisons for rate slopes, and even more for trait average values (Appendix IV-3, Table 4). Regarding trait slopes, Yinpterochiroptera distribution is over that of yangochiropterans (p-value of 5.10^{-13}), confirming that slopes are higher in the former than in the later. All superfamilies also differ from Yangochiroptera (p-values between 6.10^{-4} and 6.10^{-7}), having higher rate slopes. Only vespertilionoids have significantly lower rate slopes than yinpterochiropterans (p-value of 5.10^{-3}); this indicates that, among the four superfamilies and even if there are no significant differences between them, vespertilionoids is the clade that tends to have slightly lower rate slopes. Yinpterochiroptera also have higher average rate values than Yangochiroptera (p-value of 3.10^{-21}), and due to tightened distributions of average rate differences (whereas they are wider for rate slope differences, Fig. IV-9), more differences appear to be significant regarding the four superfamilies. The first point is that these superfamilies do not all differ from Yangochiroptera: only do the noctilionoids (p-value of 2.10^{-3}) and rhinolophoids (p-value of 1.10^{-18}), in both cases with higher average rates. The second point is that yinpterochiropterans and rhinolophoids have higher average rates than the three other yangochiropteran superfamilies (p-values between 3.10^{-8} and 1.10^{-15} for Yinpterochiroptera and between 1.10^{-6} and 2.10^{-13} for rhinolophoids): yinpterochiropterans and especially rhinolophoids have higher average rates than yangochiropterans, both at the subordinal and superfamilial scales.

In spite of parallel increases in rates for most tips that are visible on Figure IV-7, and despite the local high absolute average rate for noctilionoids, yinpterochiropteran bat therefore seem to have a higher and a more increasing character state variation through time than yangochiropterans. Figure IV-7 also shows close number of morphological changes at tips in both yinpterochiropterans and yangochiropterans; the only difference is that these changes are known to likely occur at the family level in Yinpterochiroptera (cf. Part Three), whereas this remains to be assessed for Yangochiroptera. This difference in tip ages for both suborders may explain this discrepancy between the apparent similar evolution in character state variation (and, subsequently, in number of morphological changes) for both suborders and the differences in temporal trends through time. However, the difference in average rates depends less on time; this may be rather linked to the fact that Yinpterochiroptera comprise two very distinct subclades (Pteropodidae, or megabats, and “microbat” Rhinolophoidea), whereas all Yangochiroptera superfamilies are “microbat” ones.

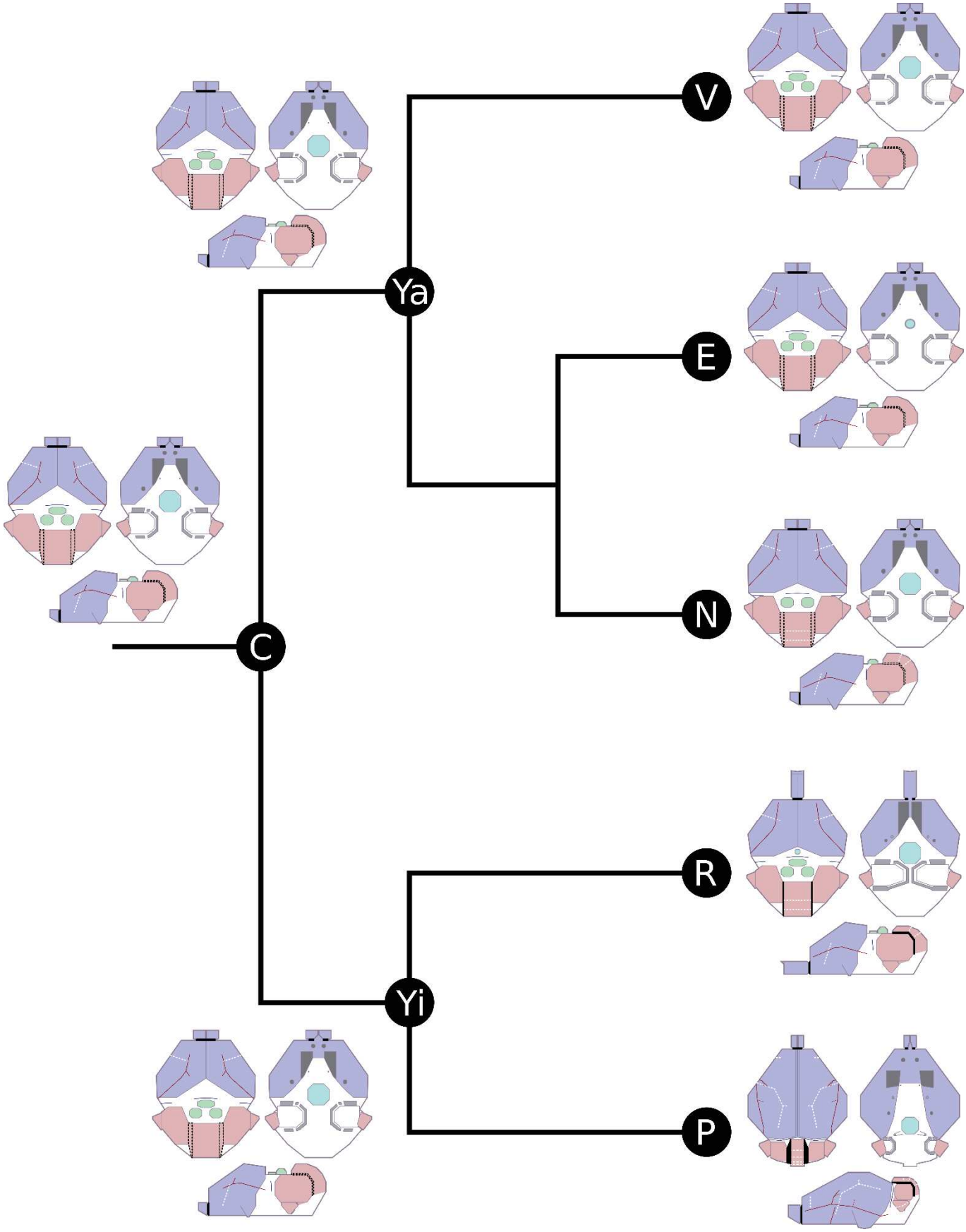

Figure IV-10: simplified phylogeny of Chiroptera with the theoretical ancestral endocasts of “deep nodes” investigated here in dorsal (top left), ventral (top right), and lateral left (bottom) views. From basalmost to apicalmost, nodes are those of crown Chiroptera (‘C’), then of Yangochiroptera (‘Ya’), Yinpterochiroptera (‘Yi’), then of of sampled superfamilies that are Vespertilionoidea (‘V’), Emballonuroidea (‘E’), Noctilionoidea (‘N’), Rhinolophoidea (‘R’), and Pteropodidae (‘P’).

Figure IV-10 illustrates the reconstructed ancestral states for the main deep chiropteran clades studied here, that are, the root of the crown Chiroptera order, both crown Chiroptera suborders, and the four bat superfamilies plus Pteropodidae. The high difference between rhinolophoids and pteropodids discussed previously is even more striking considering the hypothetical ancestral endocast morphology: there are considerable changes between the two clades (but see Part Three for more details). Among Yangochiroptera, the noctilionoids differ the most, but this is not as striking: there are some slight changes, regarding the piriform lobes, the exposure of the mesencephalic tectum, the foldings of the cerebellar vermis, the orbitotemporal canal, and the foramina surrounding the petrosal cast. There are otherwise little to no difference between the two other yangochiropteran superfamilies and the previous, more basal reconstructions. To characterize the ancestral morphology of the endocast for the three yangochiropteran superfamilies, it is therefore needed to consider better the discrepancies between them and to address better the evolution of endocranial morphology between the suborder Yangochiroptera and the three superfamilies. Inclusion of fossil taxa may critically revise the reconstruction proposed here, especially in Yangochiroptera. There are known cranial remains of emballonuroids (the emballonurid *Vespertiliavus* from Quercy Phosphorites, SW France) and of vespertilionoids (the molossid *Nyctinomus stehlini* from miocene Limagne basin, central France). The fossil genus *Stehlinia*, also known from Quercy Phosphorites, has been tentatively proposed as being a highly derived paleochiropterygid (an eochiropteran family) or a highly plesiomorphic vespertilionid (see Smith et al. 2012); in both cases, this taxon would constitute a key milestone in bat endocranial evolution, but its phylogenetic position remains to be ascertained.

IV.2.D) Contrasting stem and crown bats (Fig. IV-11)

The small number of changes between most of the main deep chiropteran nodes may be due to the PCM technique used here, which maximizes the information obtained thanks to old occurrences and penalizes large changes over short time spans. Still, there are some differences between the endocast of the eochiropteran 'Vielase bat' and the reconstruction for the crown Chiroptera order. The 'Vielase bat' dates from approximately 50 My, which is 10 to 15 My younger than some deep nodes of the crown chiropteran group (Chiroptera crown group, both suborders, and the clade Noctilionoidea + Emballonuroidea). This gap in time allows the used PCM here to reconstruct changes that are autapomorphic to *Vielasia*, if there is too much agreement between crown chiropteran taxa. This is the case of the gross ratio of olfactory bulbs dimensions (character 8), the thickness of the vermis as seen in lateral view (character 28), and the width between the sphenorbital fissure casts (character 60). There are therefore only three characters that change, which is few compared to the total number of characters (73). However, the states exhibited by the 'Vielase bat' for these characters, and those reconstructed for the Chiroptera node, are already interesting.

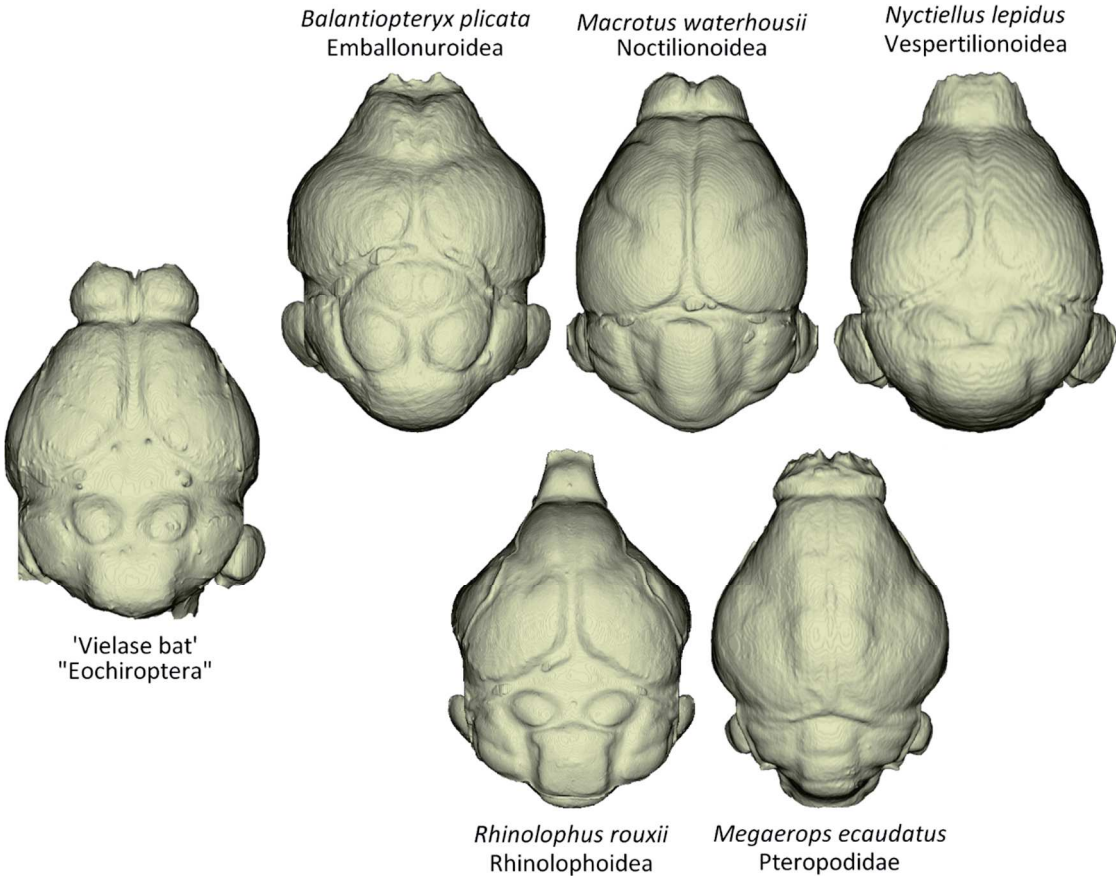

Figure IV-11: Overview of the endocranial morphology with dorsal views of the eochiropteran 'Vielase bat' (left) and of one species per major chiropteran group (i.e., the four superfamilies and the pteropodid family), with yangochiropteran to the top and yinpterochiropteran to the bottom.

For the gross ratio of olfactory bulbs dimensions (Appendix IV-5, Fig. 8), the 'Vielase bat' exhibits a configuration retrieved in most yangochiropteran bats (only three of the four phyllostomids plus the natalid species have a different state) of very compressed olfactory bulbs, being much wider than long. In Yinpterochiroptera, the olfactory bulbs are reconstructed as being either much longer than wide (in rhinolophoids) or roughly as long as wide (for pteropodids). For this case, the 'Vielase bat' rather exhibits a yangochiropteran condition. It is also interesting to note that this character is unlikely to be related to the relative olfactory bulbs mass (Fig. IV-13): *Vielasia* together with pteropodids and some other taxa have high, positive relative olfactory bulbs mass, whereas most extant "microbat" taxa have low, negative ones. Shape and relative size of the olfactory bulbs would therefore be decoupled, and the reasons to the variation in shape of these structures may not be linked to olfaction.

The vermis, in lateral view, is thick (i.e., dorsally protruding) in the 'Vielase bat', while it is less in most chiropteran taxa (Appendix IV-5, Fig. 28); a thick vermis is retrieved in some taxa of all four superfamilies (hipposiderids, rhinonycterids, molossids, miniopterids, phyllostomids, and emballonurids). The fact that the 'Vielase bat' convergently shares this rare state with extant taxa of all superfamilies would deserve further investigation. Especially, rhinonycterids generally have a thick vermis, and this is the only known chiropteran case of familial consistency for that trait - apart from rhinonycterids, thick vermis is not observed often, and there are isolated cases in Yinpterochiroptera. The cerebellum is involved in motor functions and in equilibrium information process (e.g., Paulin 1993); deciphering the meaning of a dorsally protruding vermis is therefore of major interest, and all the more if it is a rarely found morphology across bats.

Finally, the 'Vielase bat' has widely separated sphenorbital fissures, whereas they are less apart in crown chiropterans (Appendix IV-5, Fig. 60). This character state is also retrieved, less frequently than for the previous character, among crown taxa: there are occurrences in "microbat" emballonurids and phyllostomids but also in megabats. Sphenorbital fissures are very close to each other in some rhinolophoid families (the three "true" rhinolophoid ones: hipposiderids, rhinonycterids, rhinolophids), and the widespread states are a thin (but marked) or a moderate gap between them. The distribution of this character state is here retrieved as convergent; it would be worth investigating the biological grounds for this convergence, because it concerns highly diverging extant taxa (both in "microbats" and in megabats) and because it is a pathway for several cranial nerves and for some major blood vessels. This could also be a plesiomorphy for bats, with a temporal trend toward a decrease of the gap between sphenorbital fissures (extreme cases would be "true" rhinolophoids), and with some extant taxa retaining widely separated sphenorbital fissures (and, as previously, the reason why this would be retained would be interesting to study).

V) Quantitative evolution

V.1) Bias of the numeric segmentation vs physical extraction at the Chiroptera scale (Fig. IV-12)

I extracted all endocasts following the same protocol in order to minimize potential reconstruction biases. The bias of measurement between a digital endocast and a real fresh brain is also assessed here. After transforming endocast volumes into masses using the specific gravity of the chiropteran brain (1.036 mg/mm^3, Baron et al. 1996), I express the log masses of the brain and olfactory bulbs masses of my chiropteran sample against those also present in the sample of Baron et al. (1996). I do not only include the taxa present in the current analyses, but also the yinpterochiropteran taxa present in the analyses of Part Three; I still discard *Rhinolophus hipposideros*. I perform three linear models (Fig. IV-12; Appendix IV-4, Table 1) using the brain masses, the olfactory bulbs masses, and both. The linear regression with both masses shows the best fit and the lowest p-value; I use the parameters of that model to transform the three variables I use (brain, olfactory bulbs, and paraflocculi log masses).

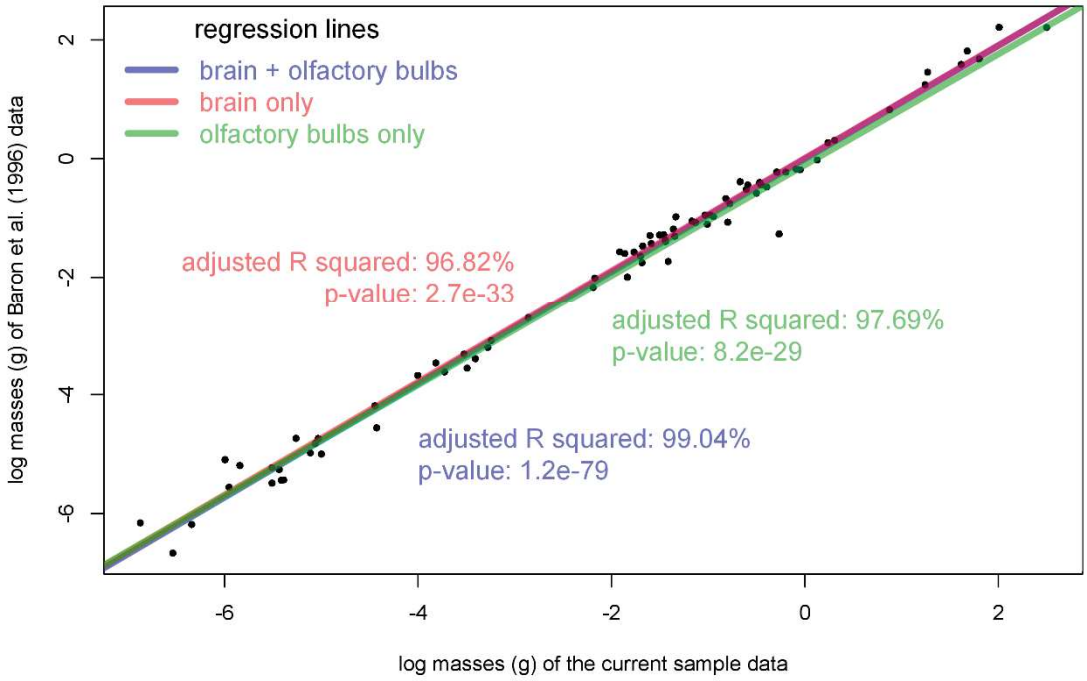

Figure IV-12: Numeric extraction bias of endocasts illustrated by comparing log brain and olfactory bulbs masses of chiropteran species found in both my sample and that of Baron et al. (1996). Regression lines and main statistics depending on which structure is chosen are superimposed to the plot. Notice the higher adjusted R squared and the lower p-value by considering both brain and olfactory bulbs.

V.2) Total brain mass (Fig. IV-13)

The distribution of the relative brain mass (Fig. IV-13), using residuals of the log brain vs log body masses linear relationship, shows a general pattern of increase, but with mixed trends. There is an increase from the deepest nodes of the phylogeny to all superfamilial nodes with the exception of vespertilionoids (cf. relative brain mass mapping). Within all groups, there are further increases in relative brain mass through time (cf. relative brain mass temporal trends). These two increasing phases result in the general increase at the Chiroptera scale (p-value of 8.10^{-6}, Appendix IV-4, Table 2), not differing from a Brownian motion regime (p-value of 0.345, Appendix IV-4, Table 2). The way each group increases in relative brain mass towards modern times however varies: there is a very slight increase in rhinolophoids, a very high increase in emballonuroids, whereas vespertilionoids, pteropodids, noctilionoids, and both yinpterochiropterans and yangochiropterans roughly follow the general trend. Particularly, rhinolophoids and yinpterochiropterans as a whole have a flatter slope than that simulated under a Brownian motion regime, whereas emballonuroids but also noctilionoids have a higher one (Appendix IV-4, Table 3). All pairwise comparisons tested between groups are significant. First, the yangochiropteran slope is higher than the yinpterochiropteran one (Appendix IV-4, Table 4), which is not surprising looking at the trends (Fig. IV-13). Between subclades of both suborders (i.e., "microbat" superfamilies plus pteropodids), a hierarchy can be drawn: emballonuroids have the highest slope, then follow the noctilionoids, the pteropodids, the vespertilionoids, and the rhinolophids have the flattest slope. It is also interesting to point out that most groups are distributed around the global trend in terms of relative brain mass average value, with the exception of vespertilionoids and of pteropodids. Vespertilionoids appear to have significantly lower average relative brain mass than the rest of the tree (p-value of 4.10^{-4}, Appendix IV-4, Table 3), which is expected by looking at their relative brain mass mapping. Their average relative brain mass is specifically lower than those of pteropodids and noctilionoids (p-values of 4.10^{-6} and 3.10^{-3} respectively, Appendix IV-4, Table 4). Pteropodids, on the other hand, have a significant higher average relative brain mass against all other compared groups (p-value of 6.10^{-5} against the rest of the tree, all p-values between 4.10^{-2} and 4.10^{-6} against other superfamilies, Appendix IV-4, Tables 3-4).

The pattern of absolute rates distribution (Fig. IV-13) shows a "quiet" evolution, with very few "hotspots" of change of relative brain mass. The taxa that show main variations are the Pteropodidae family, the Rhinolophoidea and Noctilionoidea superfamilies, and some terminal taxa such as all three pteropodids, but also one phyllostomid (*Diphylla ecaudata*), the natalid (*Nyctiellus lepidus*), and the molossid (*Cheiromeles torquatus*) species. There is a general increase through time of relative brain mass absolute rates (Fig. IV-13; p-value of 8.10^{-5}, Appendix IV-4, Table 2), but it is probably caused by the previously quoted taxa and their age: there are some nodes with high absolute rates, and a little bit more tips with also high absolute rates. None of the tested group slopes differ from that of the rest of the tree (all p-values over 0.27, Appendix IV-4, Table 3), but there are still different patterns. Especially, pteropodids slightly decrease in absolute rates through time, and vespertilionoid slope is the steepest (Fig. IV-13). Yinpterochiropterans have slightly significant higher average absolute rates (p-value of 0.048, Appendix IV-4, Table 3) than the rest of the tree, but this is not significant against yangochiropterans specifically (p-value of 0.115, Appendix IV-4, Table 4); the eochiropteran *Vielasia* therefore contributes to significantly distinguish the yinpterochiropterans from Yangochiroptera + *Vielasia*. The pteropodids case is different, and their singularity probably drives the almost significance of yinpterochiropterans against other bats. They slightly decrease, but this is only due to the very high value at the family node, not to low values at the tips. Indeed, pteropodids have both higher average absolute rates than all other chiropteran main clades (p-value of 3.10^{-5} against the rest of the tree, p-values between 3.10^{-3} and 5.10^{-}

[4] against other superfamilies, Appendix IV-4, Tables 3-4) and different, higher rate regime (p-value over 0.99, Appendix IV-4, Table 5). This likely influence another shift found in yinpterochiropterans (pteropodid shift value being the double of that of yinpterochiropterans, Appendix IV-4, Table 5).

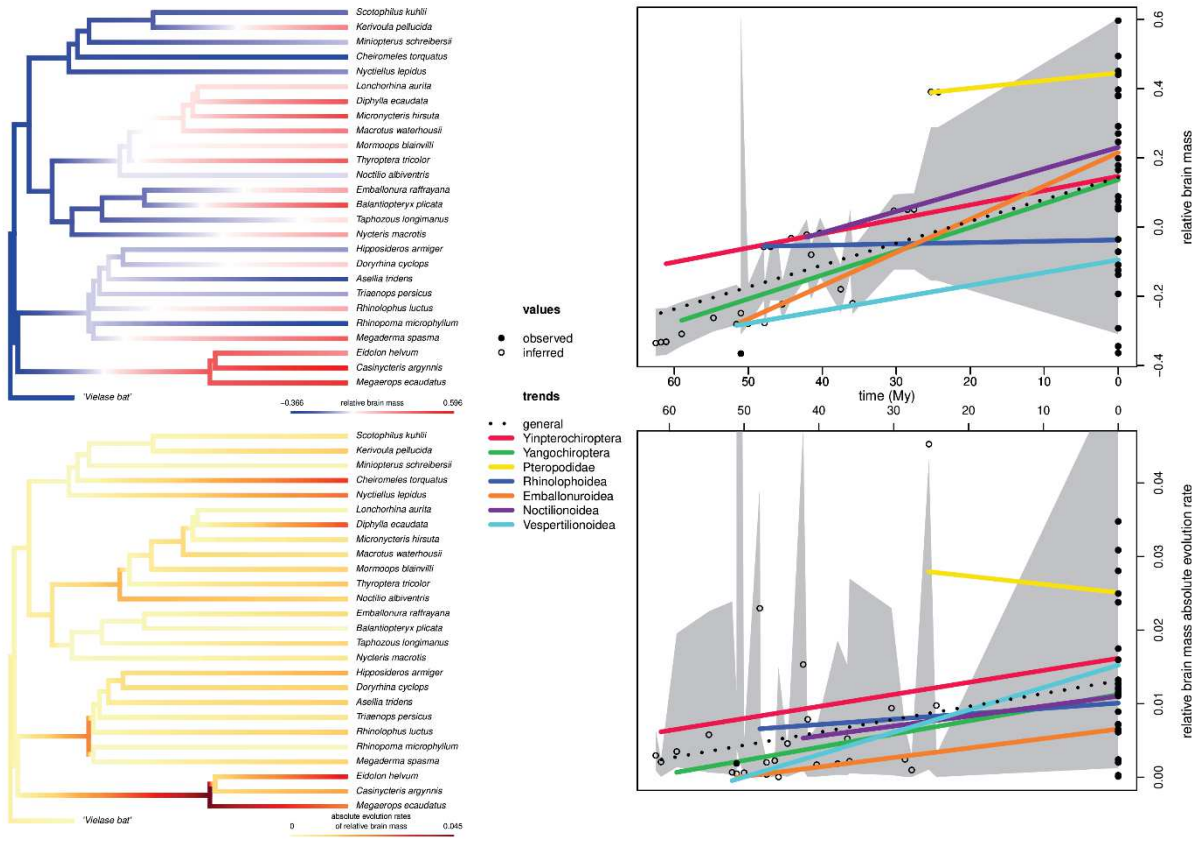

Figure IV-13: Evolution of relative brain mass in Chiroptera. Left: mappings on the Chiroptera phylogeny pruned to the present sample. Right: temporal trends, the gray background illustrating a simulated variation under a Brownian motion regime. Top: relative brain mass. Bottom: absolute rates of evolution of relative brain mass. Legend in the center applies for figures on the right.

Pteropodids show the highest average relative brain mass of all bats, with an increase towards the onset of the family and a further increase within the family. They also vary more than other bats, and there may be a tendency to a slight decrease of this variation through time. There is also an increase between the root and the superfamily Rhinolophoidea (i.e., the other yinpterochiropteran clade), which is enough to make this node have a high absolute rate of evolution. Following this increase, there is however a kind of a stasis through time in this superfamily, mainly due to different trends among families. Compared to other bats, relative brain mass values of rhinolophoids are low with little variation. There is also an increase from the root to the basal nodes of the Noctilionoidea, a yangochiropteran superfamily; similar to rhinolophoids, there is a high absolute rate at the root of the superfamily. In this clade, the only decrease in time in relative brain mass seems to regard noctilionids; otherwise, there is an increase in all other sampled families. Noctilionoids therefore have a high average relative brain mass, though this is not significant. If all noctilionoid families (except noctilionids) increase in relative brain mass in time (and so does the whole superfamily), there are however no tremendous variation of relative brain size, with a uniform pattern for the whole superfamily. The two other yangochiropteran superfamilies, Emballonuroidea and Vespertilionoidea, have a very low ancestral relative brain mass. Patterns within each superfamily then differ: there is a convergent and homogeneous (i.e., with not very much rate variation) increase of relative brain mass in emballonuroids, with average values compared to other bats, while there is a slighter and more heterogeneous increase in vespertilionoids, having low values

compared with other bats. Branches are short between superfamilies and between suborders, and no major change has been reconstructed along them. The relative brain mass of the eochiropteran 'Vielase bat' is very low, and the deepest crown bat nodes have similar very low values; such low values still persist at the root of two superfamilies, and also within some extant families (e.g., rhinopomatids, molossids).

There is an undeniable pattern of increase of relative brain mass in bats which is even clearer when fossil taxa are included; there is also a clear increase of the relative brain mass variation through time. There are however distinct patterns that are decipherable here, at least at the superfamilial and familial levels. Previous authors (e.g., Stephan & Pirlot 1970, Hutcheon et al. 2002, Safi et al. 2005) suggested that phytophagous bats (i.e., pteropodids and some phyllostomids) have a higher relative brain mass due to their diet, directly or indirectly (processing of geographical information to gather food, processing of information about the habitat complexity, etc). Safi et al. (2005) and Niven (2005) proposed patterns of increase or decrease (depending on the families) from the ancestor of bats; their conclusions are generally not supported by my results. Habitat complexity, expressed by “wing area[,] predicts encephalization in [insectivorous] bats”, whereas encephalization is “consistently high" in phytophagous bats (i.e., pteropodids and some phyllostomids) according to Safi et al. (2005: 284). Pteropodids are a particular case in bats, and this also stands regarding their general brain encephalization; they have a high and highly varying encephalization of the brain. How pteropodid specificities are due to their diet remains to be addressed. Regarding phyllostomids, the present sample is composed of sanguivore (*Diphylla ecaudata*), insectivore (*Lonchorhina aurita*, *Micronycteris hirsuta*) and mixed insectivore-frugivore (*Macrotus waterhousii*) species. Following Safi et al. (2005) hypothesis, only the latter should show an increase in relative brain size, which is clearly not the case here: all noctilionoids have high relative brain mass and increase through time (with the exception of the noctilionid species). There are also some complex patterns across other insectivorous bats, with varying heterogeneity between families within a given superfamily, and a variation of the differences between families in superfamilies.

Phylogenetic patterns, and especially phylogenetic signal, of the whole brain encephalization have only been superficially addressed in the literature. Similarly, ecological traits have not been mapped over order-scale phylogenies. Though, both kind of traits have been correlated and tentatively explained by previous works. Starting with brain encephalization, my results highlight that the impact of phylogenetic signal should first be explored and understood, since there are variations following phylogenetical relationships. The same statement could be drawn by looking at ecological traits: groups of specialized ecology can be clades, and the variation of the ecological traits linked to this specialization could therefore be also characterized by phylogeny (the best example regards pteropodids). Since it is risky to explain whether the phylogeny or the ecology drive the other, one should first investigate then eliminate the confounding influence of phylogeny, and of the ecological traits following it, before contrasting ecology and anatomy.

V.3) Olfactory bulbs mass (Fig. IV-13)

The mapping of the relative olfactory bulbs mass on the chiropteran phylogeny shows a highly convergent pattern of decreases in time (Fig. IV-13), with high, positive ancestral values whereas most of the extant tips have negative values. There is a slight decrease from the root to each main chiropteran clade, and a more pronounced decrease within all these clades with the exception of pteropodids. The general decreasing trend at the Chiroptera scale is significant (p-value of 7.10^{-9}, Appendix IV-4, Table 2), and slightly do not differ from a Brownian motion regime (p-value of 0.1, Appendix IV-4, Table 2). Most subclades parallel the general trend, with two exceptions: emballonuroid slope is steeper (i.e., more decreasing) than the general trend, whereas that of pteropodids is flatter. All subclades except Yinpterochiroptera however have a significant slope against those simulated under a Brownian motion regime (Appendix IV-4, Table 3). Pairwise comparisons between subclades are all significant and, as for the relative brain mass, there is a hierarchy between groups (Appendix IV-4, Table 4). First, the slope of yangochiropterans is steeper than that of yinpterochiropterans. Second, the flatter slope is for pteropodids, and increasingly steeper slopes are for vespertilionoids, noctilionoids, rhinolophoids, and emballonuroids. Together with the extinct eochiropteran 'Vielase bat', some extant tips retain positive relative olfactory bulbs mass: all three pteropodids, but also an hipposiderid (*Asellia tridens*), some phyllostomids (*Micronycteris hirsuta* and *Diphylla ecaudata*), and a natalid (*Nyctiellus lepidus*). The fact that all pteropodids still have high values make them to significantly differ from other bats in average relative olfactory bulbs mass (p-value of 4.10^{-4} against the rest of the tree, p-values between 3.10^{-2} and 5.10^{-4} against other superfamilies, with only the difference against Vespertilionoidea being not significant; Appendix IV-4, Tables 3-4). Emballonuroids also differ from the other bats, but by having lower average relative olfactory bulbs mass (p-value of 1.10^{-2} against the rest of the tree, Appendix IV-4, Table 3). Otherwise, the other supefamilies (Rhinolophoidea, Noctilionoidea, Vespertilionoidea) have similar average values, as well as do the two chiropteran suborders (Appendix IV-4, Tables 3-4).

The variation in relative olfactory bulbs mass is a more chaotic through time and through clades (Fig. IV-13). There are some nodes with distinguishable absolute rates (very high for pteropodids, high for hipposiderids, high for Yangochiroptera and deep subclades), but especially several tips with quite high rates (pteropdids plus approximately half of the yangochiropteran species). There is no clear structure in the mapping of these rates, and there is not more structure in their temporal trends. There is a general increase of absolute rates through time (p-value of 7.10^{-4}, Appendix IV-4, Table 2), which can be easily understood as there are more tips than nodes with high values. There however are high discrepancies between main bat clades: none distinguish from the rest (all p-values over 0.07, Appendix IV-4, Table 3) or from same-level other clades (p-values over 0.29 for pairwise comparisons, Appendix IV-4, Table 4), and there are no shift in rate regime (all p-values between 0.03 and 0.94 while they have to be lower than 0.025 or higher than 0.975, Appendix IV-4, Table 5). Only graphical results can help to slightly distinguish trends (Fig. IV-13): yangochiropteran clades have slightly steeper slopes (that of noctilionoid being clearly steeper than the general trend), while yinpterochiropteran clades have flatter slopes, slightly increasing for rhinolophoids and slightly decreasing for pteropodids. All differences being not significant, this comparison has low support; still, it is interesting to note the difference between both bat suborders. It is also worth noting that all clades have similar absolute rate ranges of values; only rhinolophoids distinguish from the other bats by having slightly lower average absolute rates (p-value of 0.04, Appendix IV-4, Table 3). Absolute rates of relative olfactory bulbs mass evolution thus do not seem characteristic of peculiar clades (maybe with the exception of pteropodids) but to characterize tips of the sample (i.e., at the family-level at most).

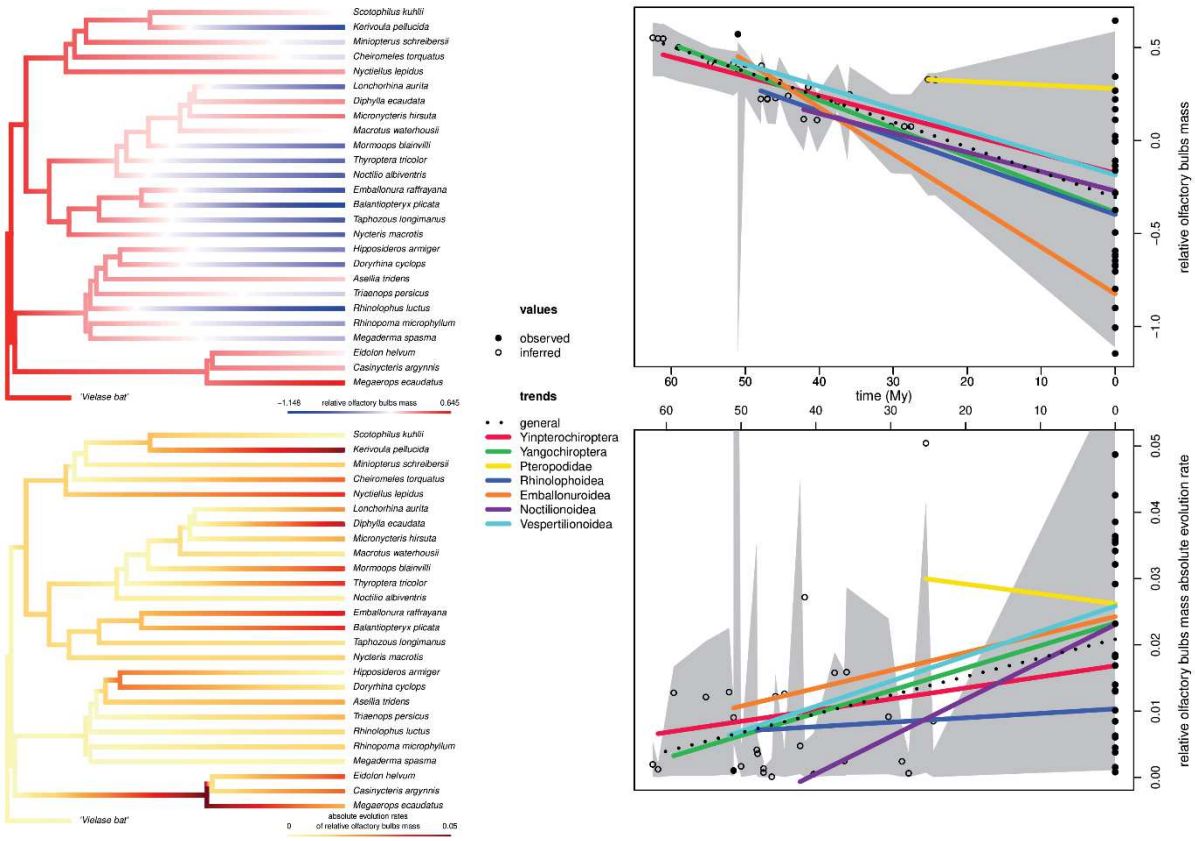

Figure IV-14: Evolution of relative olfactory bulbs mass in Chiroptera. Left: mappings on the Chiroptera phylogeny pruned to the present sample. Right: temporal trends, the gray background illustrating a simulated variation under a Brownian motion regime. Top: relative olfactory bulbs mass. Bottom: absolute rates of evolution of relative olfactory bulbs mass. Legend in the center applies for figures on the right.

Pteropodids have their own evolution pattern of relative olfactory bulbs mass: they have enlarged olfactory bulbs compared to their brain size, which is a familial characteristic, and this trait changes only little over time after the onset of the family. Other clades and taxa underwent a convergent decrease of relative olfactory bulbs mass over time (which can be regarded as a poor phylogenetic signal). These decreases are highly variable in their magnitude, with therefore different patterns of variation for main bat clades. Yangochiropteran clades may vary a little bit more than yinpterochiropteran ones do, with a slight variation at the deepest nodes and a high variation at most tips. Across Yangochiroptera, emballonuroids underwent a drastic decrease of relative olfactory bulbs mass through time, whereas there may be a little bit more variation with time (i.e., toward nowadays) in noctilionoids. Yinpterochiropteran subclades contrast, as there is a slight increase in rates for rhinolophoids and a slight decrease for pteropodids; the whole suborder trend is an increase, but this may mainly be driven by the difference in average rates between these two groups.

High relative olfactory bulbs mass in pteropodids is consistent with their diet, megabats being phytophagous, and this result supports previous studies (e.g., Bhatnagar & Kallen 1974, Hutcheon et al. 2002). These works actually suggested that a high relative olfactory bulbs mass is generally present in phytophagous bats, not only pteropodids. Here, the only (partly) frugivore species of my sample, *Macrotus waterhousii*, has a low (close to zero) relative olfactory bulbs mass, whereas some closely-related species have large olfactory bulbs relative to their brain (the insectivore *Micronycteris hirsuta* and the sanguivore *Diphylla ecaudata*). Similarly, the natalid *Nyctiellus lepidus* and the hipposiderid *Asellia tridens* have high relative olfactory bulbs masses, and are not phytophagous (Tejedor 2011, Monadjem

et al. 2019). If Bhatnagar & Kallen (1974) proposed the volume of the olfactory bulbs as a predictor of the olfactory acuity, it is however unsure regarding the volume of the olfactory bulbs cavity. My results especially show that bats with high relative olfactory bulbs are not always phytophagous, as suggested in Part Three. To determine which ecological inferences can be drawn using relative olfactory bulbs mass is therefore critical to better interpret the variations of the latter.

V.4) Paraflocculi mass (Fig. IV-14)

Evolution of relative paraflocculi mass across bats is a bit disparate (Fig. IV-14). Indeed, there are both node-level and tip-level variations, with both increases and decreases. Overall, values reconstructed at the deepest nodes of the Chiroptera order are high (so is the relative paraflocculi mass of the eochiropteran 'Vielase bat'), but not the highest values found on the tree. All chiropteran superfamilies are basally reconstructed with a positive relative paraflocculi mass, while pteropodids have a basal negative one. Anyway, there is a slight (for superfamilies) or a more drastic (for pteropodids) decrease of relative paraflocculi mass from the root to these main bat clades. Within each are more contrasted patterns, that still contribute to a general decreasing trend for the whole order (p-value of 1.10^{-3}, Appendix IV-4, Table 2) significantly differing from a Brownian motion regime (p-value of 0.037, Appendix IV-4, Table 2). All clades except pteropodids parallel the general trend. Several main bat clades have temporal slope significantly differing from a Brownian motion regime; only the two suborders (Yinpterochiroptera and Yangochiroptera) and the superfamily Rhinolophoidea have non-significant slopes (Appendix IV-4, Table 3). All pairwise comparisons between groups are significant (Appendix IV-4, Table 4). In that way, the yangochiropteran slope is slightly higher than the yinpterochiropteran one. The pteropodid slope, positive, is above all others, and there is a hierarchy in slopes between bat superfamilies (emballonuroids have the steepest slope, then follow the vespertilionoid, rhinolophoid, and noctilionoid slopes that are less and less steep). It is however worth noting that this superfamily-level consideration hides some patterns visible on the trait mapping (Fig. IV-14). First, in pteropodids, the increase through time is likely to be mostly driven by *Eidolon helvum*, that has a very high relative paraflocculi mass. Second, there are convergent decreases in rhinolophoids (in rhinolophids and megadermatids), emballonuroids, and vespertilionoids. Third, there are convergent decreases in the two basalmost noctilionoid taxa (the noctilionid *Noctilio albiventris* and the thyropterid *Thyroptera tricolor*), but then is an increase towards the node of Phyllostomidae and for phyllostomid taxa. An increase is also present in some rhinolophoid taxa (the rhinonycterid *Triaenops persicus* and the rhinolophid *Rhinolophus luctus*).

The distribution of absolute rates of relative paraflocculi mass evolution is as heterogeneous as for the trait itself (Fig. IV-14). There are some nodes with a high variation (Pteropodidae, Rhinolophoidea, Vespertilionoidea, Noctilionoidea) as well as some tips (e.g., the pteropodid *Eidolon helum*, the thyropterid *Thyroptera tricolor*, the phyllostomid *Diphylla ecaudata*). This makes the general trend to be increasing through time (p-value of 4.10^{-3}, Appendix IV-4, Table 2), but there are highly different patterns depending on the groups. In Yangochiroptera, the whole suborder slope and those of two superfamilies (Noctilionoidea and Vespertilionoidea) parallel the general slope, whereas that of emballonuroids is a little bit flatter. In Yinpterochiropterans, there are two opposite trends: there is a decrease in absolute rates through time for rhinolophoids, whereas there is a striking increase in pteropodids. This makes the whole yinpterochiropteran slope to be only slightly increasing. Being the only group with a decreasing slope, rhinolophoid distinguish from all other bat clades (p-value of 2.10^{-2}, Appendix IV-4, Table 3), even though they do not significantly differ from other clades in pairwise comparisons (Appendix IV-4, Table 4). Apart from that group, there are no significant difference (Appendix IV-4, Tables 3-4), and this is

somewhat logical as all slope grossly parallel the general trend. Pteropodids are still distinct from the other clades regarding the average absolute rates, that are significantly higher than those of the rest of the tree (p-value of 2.10^{-2}, Appendix IV-4, Table 3), but not enough to be significant in pairwise comparisons (Appendix IV-4, Table 4). Two shifts in rate regime are found for the Yinpterochiroptera and for the Pteropodidae clades (Appendix IV-4, Table 5); the shift difference for pteropodids is twice as big as that of yinpterochiropterans, and probably causes it.

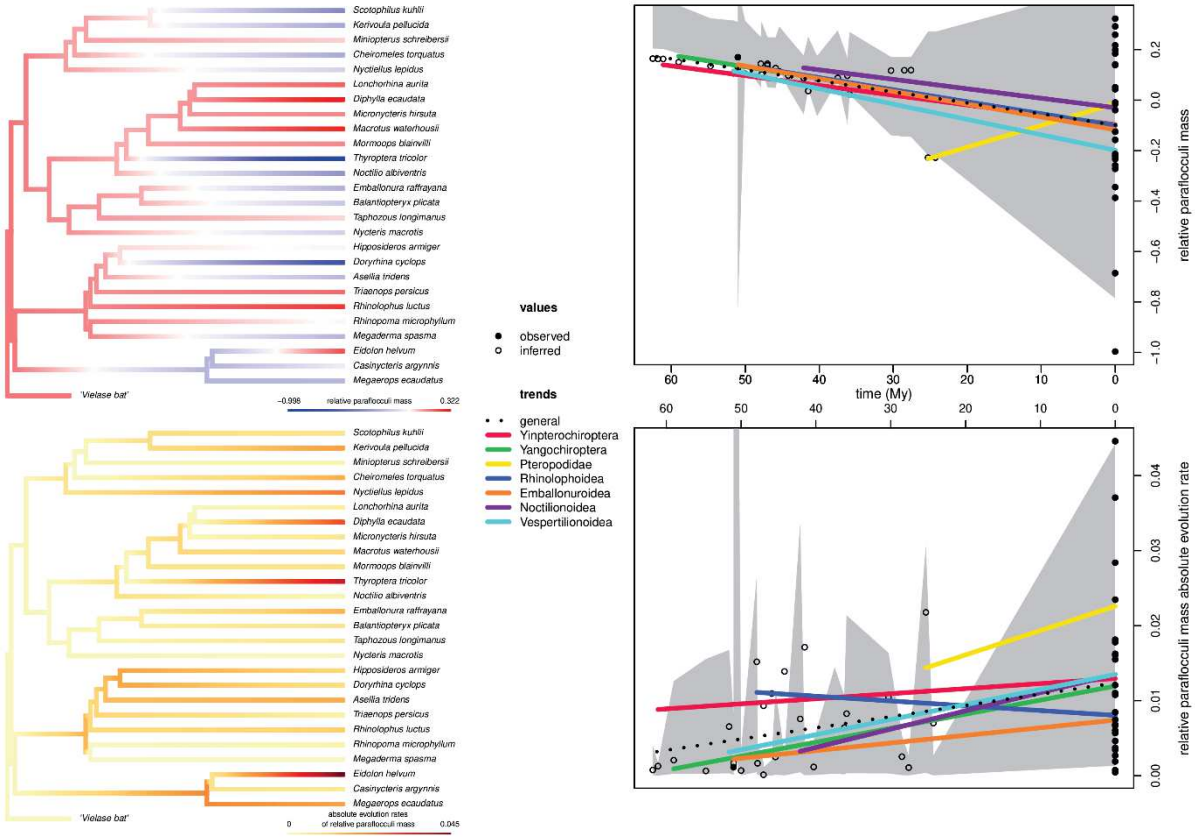

Figure IV-14: Evolution of relative paraflocculi mass in Chiroptera. Left: mappings on the Chiroptera phylogeny pruned to the present sample. Right: temporal trends, the gray background illustrating a simulated variation under a Brownian motion regime. Top: relative paraflocculi mass. Bottom: absolute rates of evolution of relative paraflocculi mass. Legend in the center applies for figures on the right.

Pteropodids stand out from the rest of the clades: it is the only main bat clade with a basal negative relative paraflocculi mass, it is also the only main bat clade with an increase of relative paraflocculi mass through time, and they differ from the other bats in their variation of that trait, with a shift in rate regime. However, the striking value of *Eidolon helvum* cautions too hasty conclusions and may explain a large part of all these results. In that way, the previous more focused work at the Yinpterochiroptera scale (Part Three) indicates a shallow increase through time of relative paraflocculi mass, and a gentle increase of absolute rates through time. Otherwise, there is a clear distinction between yinpterochiropteran subclades (pteropodids and rhinolophoids), both having opposite pattern on trait and trait rates evolution through time: the root value for each clade is negative and positive, then the trait and its rates increase and decrease (respectively). In Yangochiroptera, superfamilies are more homogeneous regarding relative paraflocculi mass evolution, both on the trait value and on its evolutionary rates. However, there are distinct patterns down to the family-level that worth be noted and would require further investigation. This is particularly the case for the secondary increases on the branches leading to and within phyllostomids + mormoopids, as well as in some rhinolophoid families (though this point has been already explored previously).

Paraflocculi are thought to be linked to motor function, equilibrium, and gaze stabilization (e.g., Kawano et al. 1996, Reep & Bhatnagar 2000, Rambold et al. 2002), and are likely to be of great interest for flying mammals. If their relative volume is linked to these functional aspects (which fully remains to be tested), there may be a covariation between relative paraflocculi mass and flight types (that involve, among other functions, those quoted for paraflocculi). Such covariations have been extensively used in rodents (e.g., Bertrand et al. 2017, 2018), but Ferreira-Cardoso et al. (2017) demonstrated the absence of ecological signal in the size of the paraflocculi. Here, species with high relative paraflocculi masses are of varying ecology: there are sanguivore (*Diphylla*), phytophagous (*Eidolon*), and insectivorous (e.g., *Triaenops*, *Miniopterus*) species, being for instance gleaners (*Micronycteris*) or slow (e.g., *Rhinolophus*) to fast (e.g., *Taphozous*) aerial hawkers. Simple explanations such as diet, habitat, or flight type are therefore insufficient to explain the distribution of high relative paraflocculi mass. As for the other traits, there is a crucial need to know exactly what is the functional impact of the relative size of paraflocculi, and how this may be linked to ecological traits.

V.5) Cross traits comparison

Regarding the evolution of the three traits considered here (Figs. IV-13-14), some similar observations can be drawn at the Chiroptera scale and at the Yinpterochiroptera scale (Part Three). First, the mappings of the traits are not parallel, and the main common point is that the relative olfactory bulbs and paraflocculi masses are reconstructed as high and positive, in deepest chiropteran nodes (they are also high in the eochiropteran 'Vielase bat') and then decrease over time, whereas relative brain mass is reconstructed as basally low and subsequently increases. Despite the wider frame, it is difficult to go beyond the hypotheses exposed in Part Three regarding this inverted proportionality through time: there could have been a physical integration of the olfactory bulbs and of the paraflocculi to an expanding brain, or a transfer of functions of these regions to the neopallium, or these structures may have lost in functionality. A last hypothesis could be that there is no particular link between these relative masses, which may be supported by the fact that there are various trends and associations among bat clades; to test this would need to precisely know the functions associated with the variation in relative olfactory bulbs and paraflocculi masses.

The similarities in absolute evolutionary rates mappings (Figs. IV-13-14) found at the Yinpterochiroptera scale between evolution rates of relative brain and olfactory bulbs masses are not found at the Chiroptera scale. Actually, there is a consistency between temporal trends of the absolute rates of these two traits in both yinpterochiropteran subclades, the Pteropodidae and the Rhinolophoidea: in both cases, pteropodids have high rates and slightly decrease in rates through time, whereas rhinolophoids have low rates and they even more slightly increase through time. This does not stand for yangochiropteran superfamilies that vary more in average value and in temporal trend of their rates. Thus, though less striking on the mappings, there may still be a covariation between relative brain and olfactory bulbs mass rates, but only concerning Yinpterochiroptera. This observation that the rates of both traits are clearly less linked in Yangochiroptera helps to constrain the focus of further studies addressing this point. The fact that this is less marked in Yinpterochiroptera with a reduced sample also indicates that this covariation and its variation between yinpterochiropteran subclades should be addressed at most at the super-familial scale, and at lower levels depending on the cases (but see Part Three). Relative paraflocculi mass evolutionary rates do not covary with the rates of one or the other of the two relative masses, neither in yinpterochiropterans nor in yangochiropterans.

As a general observation, there are poor links between relative masses and ecological traits in my sample. The phytophagous species are assumed to have larger brain and olfactory bulbs; the main discussed point is a putative covariation between relative brain and olfactory bulbs masses, and diet. This is not supported here, as many animalivorous species have large relative brain and/or olfactory bulbs masses as well. A covariation with flight type is also difficult to see. This would impact the relative brain and paraflocculi masses, but species of highly varying flight have similar values of one and/or the other trait. As already expressed in the previous sections, relating ecological and neural traits should first consist in a detection of the covariation with phylogeny (for both kind of traits), then be assessed by eco-functional studies, and finally traits could be expressed one against the other.

Regarding main bat clades, some points can be raised.

First, evolution of all traits and of their rates in yinpterochiropterans seems to be less disturbed and more steady than in yangochiropterans: trends slope are always flatter in the former suborder than in the second. This however may hide an averaging of two opposite, or at least contrasted, trends in rhinolophoids and in pteropodids, which is a frequent thing: only the trends of both groups regarding relative brain mass evolution through time is similar. Yangochiropteran more tilted slopes highlight very varying trends among yangochiropteran superfamilies, not a common trend between them.

The second main point precisely regards the yangochiropteran superfamily Emballonuroidea: the most striking point regarding this clade is that the slope of the temporal trend of any trait is always extreme, being either the highest or the lowest of all compared superfamilies. Emballonuroid relative brain mass raises more than any other clade, and the relative olfactory bulbs and paraflocculi masses decrease more than the other clades (only pteropodid slope of relative paraflocculi mass evolution is steeper). Paradoxically, the slopes of the temporal trend of the trait rates are more stable: only that of relative olfactory bulbs mass rates is as steep as the other. There is therefore a marked evolution between the root and the tips in this superfamily; this deserves further work including more cranial remains already known in the fossil record (Brown et al. 2019).

The third main point regards the noctilionoid superfamily, and especially the phyllostomids. It is a well-studied family, quite diversified nowadays (217 species according to Solari et al. 2019), but they are especially disparate in their ecology, and their associated morpho-anatomical adaptations (e.g., Stockwell 2001, Baker et al. 2012, Dumont et al. 2012, Santana et al. 2012). The present sample is limited and do not consider all the ecological variation of this family; yet, some trends are already noticeable. The most striking points are that the species of this family have high (i.e., positive) relative brain and paraflocculi masses. An increase for relative brain mass is not surprising (most clades experience it), whereas the high relative brain mass values at tips but also at nodes make them to stand out with pteropodids (another highly derived family). The secondary increase in relative paraflocculi mass, and the very high values throughout the whole family (actually even extending to the phyllostomids + mormoopids clade) are more striking among bats; only some rhinolophoid clades have also high and increasing relative paraflocculi masses (rhinolophids and rhinonycterids). It is not very surprising that this family is distinct from the others regarding the evolution of relative neural tissue masses, but this confirms the potential and the interest in studying these traits in this family. Links between anatomy and ecology have been proposed in this family, but they either concern external features (e.g., Dumont et al. 2012, Santana et al. 2012)) or neural structures but without proper evolutionary framework (McDaniel 1976, but also large scale studies discussing about phyllostomids such as Hutcheon et al. 2002 and Safi & Dechmann 2005). Thorough proper studies on neural tissue masses would surely bring information regarding the evolution of this multifaceted family.

VI) Conclusions

The endocranial cast of an eochiropteran species is described here in details for the first time. This endocast, virtually extracted from an incredibly well preserved skull, is almost complete: only lacks a posteroventral half. The morphology of this 50 My old taxon is not unique or outlandish and falls within the broad morphological variation found in the crown Chiroptera clade. As a corollary, a key point is that, as for many other bats, this taxon exhibits an exposed mesencephalic tectum with protruding caudal colliculi, a hallmark of echolocation. This supports the hypothesis of an early acquisition of echolocation in bats and of a secondary loss in megabats. Quantitative variables used here (body, brain, olfactory bulbs, and paraflocculi masses) can also be scored for this species. Together, these two points allow for including this taxon as a basalmost constrain for the reconstruction of endocranial evolution in bats.

Anatomical characters describing the endocast morphology mostly seem to bear a weak phylogenetic signal at the Chiroptera scale: they have low parsimony indexes (CI, RI) values, and the overwhelming majority of changes take place at terminal tips rather than at nodes. This contrasts with previous results at the Yinpterochiroptera scale (cf. Part Three) that found a moderate to good congruence between anatomical characters distribution and phylogenetical relationships. The strong difference in phylogenetic relevance may be due to a difference in the sampling strategy, the latter being induced by a difference in the systematic level of study. Indeed, this work aims to decipher endocranial evolution between the ordinal and suprafamilial levels; sampling effort was put at the familial level. This implies several long branches between taxa, allowing to the PCM used here to favor much convergent changes over a long time rather than few shared changes over a short time. In that way, reconstructed evolutionary rates are always high for terminal taxa.

Still, there are nodes with high rates and numerous morphological changes. Rhinolophoid and noctilionoid superfamilies are particularly divergent. For the former, this may be due to the inputted reconstructions obtained at the Yinpterochiroptera scale. For the latter, it reveals a “too” strong phylogenetic signal for some characters, “forcing” the PCM to reconstruct changes deep in time. Some morphological changes are noticeable: the exposure of the mesencephalic tectum tends to reduce with time (confirming previous works), but with convergent trends regarding the specific morphology of rostral and caudal colliculi, and with different trends of structures overlapping the tectum. The eochiropteran 'Vielase bat' also slightly differs from the ancestral reconstruction of the crown Chiroptera clade, and the differing points deserve further investigation, maybe with different evolutionary scenarios for each.

Evolution of relative brain mass has been previously proposed for bats based on extant taxa only. A previous study at the Yinpterochiroptera scale (see Part Three) proved the importance of fossil calibrations in such evolutionary reconstructions, with highly diverging results. By applying similar methods at the Chiroptera level, I also found diverging results from previous neontological studies. Especially, relative brain size increased through time in crown bats, with therefore distinct patterns among superfamilies and families. Interestingly, high values in both relative olfactory bulbs and paraflocculi masses are reconstructed as a basal condition in bats, both traits therefore decreasing with time (while relative brain mass, ancestrally reconstructed as negative, increases).

The present results overturn putative ecological causalities of diet on quantitative neural traits; especially, several animalivorous bats are as highly encephalized as the phytophagous bats (i.e., Pteropodidae and some Phyllostomidae). Relative olfactory bulbs mass may better covary with diet, but a link between relative (and not absolute) olfactory bulbs mass and olfaction acuity remains to be asserted. Relative paraflocculi mass evolution, on the other hand, does not seem to covary with flight types, and the exact eco-functionality of relative parafloccular mass also remains to be proven. It is therefore needed to independently study the evolution (and the phylogenetic signal) of both neuro-anatomical and ecological traits in first, then to compare the evolution of both (anatomo-functional studies of neurological traits being crucial to convert covariations in causalities).

The covariation between evolutionary rates of relative brain and olfactory bulbs masses found at the Yinpterochiroptera scale (Part Three) is weakly retrieved here, and only in the latter clade - not in Yangochiroptera. Distinct patterns among bat superfamilies are also found. In Yinpterochiroptera, there is a contrasted, generally opposed, evolution between pteropodids and rhinolophoids; this is not surprising, and leads to a flat average for the whole suborder. In Yangochiroptera, emballonuroids always show the most brutal evolution through time of the three tested traits (the general trends being exaggerated), whereas noctilionoids both join pteropodids with particularly high relative brain mass and are characterized by a general (except noctilionids) maintain of a high relative paraflocculi mass.

As a perspective regarding both qualitative and quantitative treats, it appears to be crucial to “break” some long branches while working at the ordinal scale. One should therefore either focus at a lower systematic level (morphological resolution is already way better at the subordinal level) or add fossil representatives of extant clades to better constrain deep-time reconstructions. For the latter point, cranial remains of fossil taxa are known in emballonuroids (the emballonurid genus *Vespertiliavus*) and in vespertilionoids (the molossid species *Nyctinomus stehlini*, the potentially vespertilionid genus *Stehlinia*). This would clearly enhance and refine the first results presented here about the evolution of the chiropteran endocast.

A particular clade to stand out is the superfamily Noctilionoidea, which is incredibly diverse, both talking about species account and morpho-ecological pecularities (especially in the family Phyllostomidae). Noctilionoidea is the yangochiropteran clade with the highest number of morphological changes reconstructed here, and it also exhibits particularities regarding quantitative traits. This taxon may then reveal as an ideal sandbox to test eco-neurological correlations. The lack of documentation of endocranial morphology for old (i.e., ante-Quaternary) and/or early diverging noctilionoids clearly impedes for confirming basalmost reconstructions. Therefore, dealing with Yangochiroptera as a whole and including emballonuroid and vespertilionoid fossil species may help: this would both better inform about the evolution of neurological traits in Yangochiroptera deepest nodes and propose more confident ancestral reconstructions for Noctilionoidea.

General conclusions and perspectives

I) Conclusions

The aim of this thesis is to contribute to fill a knowledge gap about bat brain evolution using "fossil brains". Indeed, paleoneurological knowledge of bats is stuck in the XXth century with old concepts: only short descriptions of natural endocranial casts are available (no works since the review of Dechaseaux 1973), the systematic framework of Chiroptera changed in the beginning of the XXIth century (from a duality Micro-/Megachiroptera to a duality Yinptero-/Yangochiroptera, e.g., Teeling et al. 2002), and no phylogenetic comparative method has been used to describe the evolutionary history of the bat brain yet. On the other side, comparative neurobiology of bats either focuses on internal structures or takes large shortcuts: knowledge of the bat brain expanded but many works have been undertaken regarding micromorphology of the brain (i.e., inner morpho-anatomy) without an evolutionary framework (e.g., the massive atlas of Baron et al. 1996), or try to explain causality chains between gross neural traits and ecology whilst lacking most of the intermediate links (e.g., Safi et al. 2005). Here, I try to start filling in the gap between comparative neurobiological and paleoneurological knowledges, and I draw first hypotheses about general brain evolution in bats by using both extant and extinct species.

As a first preliminary step, I try to evaluate the potential and the limits of the current knowledge in bat paleoneurology. This is done by describing some endocranial casts belonging to one bat family, the Hipposideridae, a case study to begin with for investigating fossil bat endocasts. I first provide a largely revised nomenclature of the endocranial cast anatomy in bats, based on the observations made on the fossil sample. This nomenclature obviously deserves further comparisons and a broader sampling to be generalizable at the Chiroptera scale, but it is a first step towards recoupling paleoneurology, comparative neurobiology, and comparative anatomy in bats. Besides, it confirms that the external organization of endocranial soft tissues (mostly involving the brain) do reflect on the inner surface of the braincase. Using that nomenclature, I describe and compare the endocasts of the four species sampled, and I further compare these fossil taxa to the sole illustration of the brain of an extant hipposiderid species present in the literature (Baron et al. 1996). This anatomical work provides first clues about the morphological variation present within a family, and allows for discussing potential evolutionary and temporal trends. Especially, morphology appears to be conservative in Hipposideridae, and this may relate to a conservative ecology in this family. However, thorough comparisons highlight differences at the generic level that may be explained either by phylogeny or by time (i.e., "evolutionary grades"). I also use common volume measurements for describing quantitative evolution of the brain, in order to be able to compare the endocasts I describe to other studies. I especially find that there are no apparent changes in the encephalization (calculated using the encephalization quotient) through time in this family, contradicting previous neontological studies (e.g., Safi et al. 2005, Niven 2005) and supporting the unique, yet only quantitative, previous paleontological study (Yao et al. 2012). I also find that the fossil hipposiderids fall within or near the hipposiderid morphospaces while regressing logarithms of olfactory bulbs and paraflocculi masses against the log brain mass. Altogether, quantitative results suggest that there are no major functional/ecological discrepancy between fossil and extant hipposiderid taxa, further supporting a relative monotony of main brain characteristics in this family. Considering both the morphology and the measurements of the brain, little changes seem to have occurred during hipposiderid evolutionary history. Some finer morphological variation is however important to note and to further investigate. I emphasize the role of fossils in the description of brain evolution in a given clade, as fossils are key milestones to constrain evolutionary scenarios.

This very first work encourages further digging in and solving the methodological gaps that persist and that impede proper analyses of brain evolution. As previously expressed (see first part of the Introduction), several limits of modern paleoneurology remain to be considered and addressed. This Part Two is therefore an intermediate part: I express the rationales I use and the literature I can summarize and interpret, before applying all the methods described to bat case studies.

The first limit I try to address regards the large gap now existing between our understanding of bat paleoneurology, comparative neurobiology, and comparative anatomy. Indeed, qualitative paleoneurological studies in bats stopped in the 1970's (Dechaseaux 1970, 1973) and have never thoroughly and precisely described the bat natural endocranial casts; interpretation of endocasts correlates regarding actual brain structures have not been discussed. Comparative neurobiology of bats knowledge, on the other hand, clearly expanded during the end of the XXth century, but without broader integration of cerebral morphology, and no detailed comparison to other mammals (which is especially critical for assessing the homologies of the few neopallial foldings present in various bats). Finally, comparative anatomy of the bat skull (for non-neural soft tissues or bones) has been very little studied, even though the latest works on osseous structures are rich and provided discussion about structure homologies (e.g., Wible & Davis 2000, Giannini et al. 2006). I therefore tentatively emend and expand the nomenclatural work I performed in the case of hipposiderids endocasts (Part One). This aims to stand for the whole Chiroptera order, with therefore several hypotheses and proposed homologies to be generalizable for all bats.

The second major issue of modern paleoneurology concerns the metrics used to describe the quantitative evolution of "fossil brains" and their statistical treatment. I first discuss the rationale of these commonly used metrics, and the potential errors made by some of the previous works. Especially, the EQ is flawed, and one should not perform statistical treatment using ratios or regression residuals. I therefore propose to work directly with absolute neural masses, and to use statistical treatment that can further express them relative to other masses (i.e., compare brain mass to body mass, and compare brain part mass to brain mass). I also quickly discuss the currently existing phylogenetic comparative methods, and try to highlight their advantages and their drawbacks. The inclusion of fossil species is crucial, therefore I also describe and compare the current available implementations of these various methods. I finally chose a statistical method (phylogenetic ridge regression, Castiglione et al. 2018) built to include fossil occurrences, that relies neither on (strict) parsimony nor than on optimality, but that rather aims to reconstruct trait evolution at the branch level, putting the (obligatory) incertitude of the reconstruction to the lowest phylogenetical level possible. Using this method and its implementation, I also expose the statistical treatment I perform and its aims, both on qualitative and on quantitative data. I therefore intend to assess the phylogenetic relevance and the evolution of anatomical characters, to reconstruct and to discuss morphological evolution across clades, and finally to describe and to compare the evolution of relative neural masses (both their value and their variation).

The first case regards a clade (the suborder Yinpterochiroptera) whose daughter-taxa are among the most contrasted among mammalian orders: the "microbat" superfamily Rhinolophoidea, and the megabat family Pteropodidae. Part One only aimed to decipher potential and limits and give an idea of the incoming task to adequately address endocranial evolution in bats; in Part Three, I therefore aim higher and I substantially increase the sampling effort. For Yinpterochiroptera, I gather a sample of extant species representing one eighth of the current specific diversity, with an inter-tribal to intra-generic resolution (depending on the families systematics). I include the four previously described fossil hipposiderid taxa, and I add four other fossil species that help better address endocranial evolution in Hipposideridae and in its sister-family, the Rhinonycteridae. There are no fossil occurrences in the other considered families, but this is due to a lack of (known) cranial remains. I therefore still consider the Yinpterochiroptera suborder, the deepest nodes being (at least partially) constrained by the only currently available fossil occurrences of the whole suborder. I define 73 anatomical characters (using the anatomical nomenclature established in Part Two) to describe the endocranial variation from the subordinal (i.e., comparing whole rhinolophoids to pteropodids) to (at least) the intrafamilial levels. I follow the statistical protocol described in Part Two, adding to it two parts. The first one regards the variation implied by the given phylogenies, the place of the hipposiderid genus *Palaeophyllophora* remaining uncertain among Hipposideridae. The second one aims to compare "neontological" (i.e., discarding the fossil sample used) and "paleontological" analyses regarding quantitative neural traits (the only neural traits whose evolution has been described in the literature).

I find a wide array in the distribution of the anatomical characters states on the considered phylogeny, with patterns varying greatly. Characters generally have substantial phylogenetic signal, but vary much; it has however to be noted that this variation does not depend of the general structures (i.e., brain parts, cranial openings, vascular structure marks etc.). Some characters also seem to evolve under selection, with cases of stasis and cases of moving optimum over time. Tracking the evolution of the dorsal exposure of the Mesencephalon is also of interest in the Yinpterochiroptera clade, that contrasts echolocating and non-echolocating bats. The general exposure follows the phylogeny, and the degree of exposure diminishes with time, supporting earlier works (e.g., Dechaseaux 1956). Distribution of the other characters describing the mesencephalic morphology is however more difficult to interpret. The distributions of characters that regard the structures whose homology has been tentatively proposed in Part Two confirm the homology for some cases, and suggest full convergences in others. As a general rule, these homologies have obviously to be further investigated. I also reconstruct the evolution of the endocranial morphology among major yinpterochiropteran taxa (families and other biologically meaningful suprafamilial clades). Pteropodids are obviously highly divergent from rhinolophoids, but there are also family-level conformations of the endocranial morphology among rhinolophoids.

The results regarding relative neural masses including fossils generally contradict previous "neontological" works. First, there is an increase through time of the relative brain mass, and most familial node values are higher than that of the Yinpterochiroptera node. This contradicts previous neontological works that suggested a decrease with time (Safi et al. 2005, Thiagavel et al. 2018). In general, there are major differences by considering fossil taxa or not, mostly regarding temporal trends of relative neural masses evolution. This is of critical importance, because conclusions drastically differ with or without fossils. Relative olfactory bulbs and paraflocculi masses decrease with time, with therefore a general opposite pattern to that of relative brain mass. An interesting pattern is an apparent covariation of the absolute rates of evolution of the relative brain and olfactory bulbs masses: when the relative brain mass changes, the relative olfactory bulbs mass also does. However, the direction of the changes are not linked,

and all possible cases of concurrence and of divergence are retrieved. Ecological correlates that have been assessed in the literature (sometimes, treated as causes) are found to little correspond to the results retrieved here. This is especially true regarding relative brain mass, putatively covarying with types of animalivorous bats and consistently high in frugivorous bats (i.e., pteropodids in the context of Yinpterochiroptera). This pattern is not retrieved here. On the other hand, relative olfactory bulbs mass may better covary with diet types.

The second case of study is the whole Chiroptera order (Part Four). This widening of the phylogenetic scale of study diminishes the resolution of the sample; I therefore describe trends of brain evolution of suprafamilial clades. Together with the ancestral values reconstructed for yinpterochiropteran families in Part Three, the analyses performed in Part Four benefit from the inclusion of the endocranial cast of an eochiropteran taxa. For the first time, the inner morphology of the braincase is described for a bat species outside to the crown Chiroptera order. The striking fact about this endocast is that it resembles to a typical modern bat's. Especially, the mesencephalic tectum is widely exposed, with salient caudal colliculi, hallmark of the echolocation. This endocast therefore supports the hypotheses of a Chiroptera acquisition/Pteropodidae secondary loss of echolocating ability in bats.

The distributions of the anatomical characters are less congruent with the phylogenetic relationships than they were for Yinpterochiroptera. This is likely due to the sampling strategy: the phylogeny is mostly composed of long branches toward families, allowing the used PCM to reconstruct numerous convergent changes over a long time rather than few changes over a short time. Still, some nodes stand out by having several morphological changes, indicating that the phylogenetic signal of the anatomical characters is probably strong. This is especially the case of the Noctilionoidea superfamily, and of the successive nodes of this superfamily down to the family level. At the Chiroptera scale and considering the morphology of an eochiropteran taxon, the exposure of the mesencephalic tectum appears to reduce with time, and trends vary much more regarding both the morphology of particular mesencephalic structures and the structures thought to progressively cover the mesencephalic tectum. This supports the previous observations at the Yinpterochiroptera scale, and highlights a complex evolution of the Mesencephalon in bats.

The trends in relative brain mass evolution arising from neontological works, already questioned by one work including fossils (Yao et al. 2012), are furthermore battered by the results of Parts One and Three. All of these studies have however been performed at a familial level (Yao et al. 2012, Part One) or a subordinal level (Part Three), and only considering extant representatives of persisting clades. Here, studying the whole Chiroptera order plus an eochiropteran taxon, I support the previous hypotheses that 1) fossil taxa are crucial for reconstructing the evolutionary history of the relative brain mass because 2) there it generally increased through time at the bat scale. As in Yinpterochiroptera (Part Three), there is a decrease with time of relative olfactory bulbs and paraflocculi masses, and the reverse proportionality between the temporal trends of relative brain mass and relative olfactory bulbs and paraflocculi masses remains to be investigated. The covariation of changes between relative brain and olfactory bulbs masses found in Yinpterochiroptera (Part Three) is not retrieved at the Chiroptera scale, and weakly persists in the quoted suborder by considering the whole order. Trends in yangochiropteran superfamilies also appear: emballonuroids experienced the most drastic changes with time (in all relative masses), while noctilionoids have a very high relative brain mass and maintained a high relative paraflocculi mass. Yangochiropteran clades deserve further particular attention regarding their endocranial evolution.

II) Perspectives

A first path that remains to pave concerns the correspondence between the soft tissues and the imprints they leave on the inner surface of the braincase. I attempt here to recognize as many structures as possible, but I am limited by the scarcity of works dealing with bony homologies, brain macromorphology, and vascular structures identification. Modern techniques such as diceCT (Clement et al. 2015, Anderson & Maga 2015, Gignac et al. 2016) for instance allow for a better digitization of anatomical structures: not only the bone but also the soft tissues can be contrasted and reconstructed together. This involves strict protocols (Hedrick et al. 2018), but has already been widely attempted with success in mammalian taxa (e.g., Carlisle et al. 2017, Nasrullah et al. 2018, Regnault et al. 2020) including bats on different problem (e.g., Smith et al. 2021 on venous networks in the nasal cavity, Sohn et al. 2021 on rhinolophid genital organs). A first, sorely needed result using these non-invasive methods would be to clarify the structure of bony and soft tissued structures of the skull in bats. Obviously, this involves comparing highly different species, in order to discuss the correspondences between structures. Then, extracting both the endocranial cast and the soft-tissue structures could both inform about qualitative approximations (i.e., which structures can be identified or not) and quantitative biases (i.e., regarding the actual vs the estimated volumes of the brain and its regions).

The way the endocranial morphology has been comprehended here is a pioneering and tentative method to better depict morphological evolution with time in an evolutionary framework. The decision to parse endocranial morphology into characters and states, and to assume them to be continuous in a quantitative-designed PCM (i.e., phylogenetic ridge regression) is debatable. Other methods exist, such as the geometric morphometric methods (GMM) that aim to account for morphological variation using quantitative compartmentalization of the morphology and subsequent statistical methods. GMM start to apply on endocranial casts and some studies already provided interesting results (e.g., Ahrens 2014, Segall et al. 2021, Weisbecker et al. 2021). Both approaches differ in their rationale, the way they are performed, and their limitations. Both should actually be attempted, and subsequently may be compared. The point I want to raise is that the treatment of the morphological information about the bat endocranium undertaken here is one way of investigation. It represents a first step of statistical investigation of the evolution of the endocranial morphology.

The PCM used here is suited for quantitative traits, and regarding that point, the way the relative neural masses evolution is approached here is less “experimental” than the evolution of endocranial morphology. There are already promising results regarding brain size variation with time and throughout phylogenies in cetaceans (Serio et al. 2019, McCurry et al. 2021) and in primates (Sansalone et al. 2020). These traits have also been much more investigated in bats than the morphology (since there is no equivalent works for morphology). Further investigations should then concentrate on the ecological correlates with neural traits often too hastily made in the literature. Several studies in bats putatively demonstrated links between diet and/or habitat complexity and relative brain and olfactory bulbs size. However, these correlations do not seem to stand in the results of this thesis. Moreover, causalities are often confused with correlations. No works clearly demonstrated the whole chain of causality between the considered ecological and neural traits, which are the two extreme points of this chain. If works such as those published previously or done here give ideas about these causalities, anatomical, functional, and ethological works are needed prior to assess the causalities. These works are mandatory in order to investigate the evolution of the ecological traits and/or to draw paleobiological inferences by mean of neural traits.

Fossils appear to be critical to constrain evolutionary hypotheses of trait evolution. This is even clearer in the case of bats and of neural traits: the results including fossils obtained here are categorical, and the results obtained by considering only extant bats are likely to lead to erroneous conclusions. The PCM used here is suited to deal with fossil occurrences, which is not that frequent among the available and conceptually up-to-date PCM's. Phylogenetic ridge regression is however not free of defects. The fact that it only relies on branch length is an advantage because it emancipates from the parsimony and optimality criteria and does not need an a-priori evolutionary model, "feeding" as much as possible on the provided data. This point can turn out to be a disadvantage: changes are more likely to occur on long branches of a phylogeny than on shorter ones, and this may lead to a high number of convergent changes if there are several long branches. This counterpoint therefore implies potentially uninterpretable reconstructions, which happens here (sometimes in the morphological evolution section of Part Three, more frequently in the same section of Part Four). It can be however easily solved by modifying the sample. The major improvement to the work and to the analyses presented here, if dealing with the same methodology, would be to increase the sample size with the aim of "breaking" the long branches of the phylogeny and better figure out the evolution of the tested traits. This can be addressed by adding extant taxa, but more efficiently by adding fossil occurrences. This is possible at the Chiroptera scale, since skulls of fossil taxa are documented in Emballonuroidea (Paleogene emballonurid genus *Vespertiliavus*) and Vespertilionoidea (e.g., the Miocene molossid *Nyctinomus stehlini*), with the additional case of a taxon that may belong either to Vespertilionoidea or to an eochiropteran taxon (Paleogene genus *Stehlinia*). Changing the systematic level of study may also help to better constrain the evolution of the brain for the whole Chiroptera order. This is demonstrated here for Yinpterochiroptera, but this would surely also stand for Yangochiroptera, or even at the superfamilial level in these groups.

As a summary, further directions consists in 1) an expanded knowledge of the comparative anatomy of the bat head, 2) a more exhaustive consideration of the causalities between neural and eco-functional traits, 3) the inclusion of fossil taxa and/or different phylogenetic scales of study, and 4) the comparison with other approaches dealing with endocranial evolution.

Literature cited

Agnarsson I, Zambrana-Torrelio CM, Flores-Saldana NP, May-Collado LJ (2011) A time-calibrated species-level phylogeny of bats (Chiroptera, Mammalia). PLoS Curr 3: RRN1212. https://doi.org/10.1371/currents.RRN1212

Ahrens HE (2014) Morphometric study of phylogenetic and ecologic signals in procyonid (Mammalia: Carnivora) endocasts. Anat Rec 297(12): 2318–2330. https://doi.org/10.1002/ar.22996

Akaike H (1973) Information Theory and an Extension of the Maximum Likelihood Principle. In: Petrov BN, Caski F (eds) Proceeding of the Second International Symposium on Information Theory. Akademiai Kiado, Budapest, pp 267–281

Akaike H (1974) A new look at the statistical model identification. IEEE Trans Automat Contr 19(6): 716–723. https://doi.org/10.1109/TAC.1974.1100705

Alatorre Warren JL, Ponce de León MS, Hopkins WD, Zollikofer CPE (2019) Evidence for independent brain and neurocranial reorganization during hominin evolution. Proc Natl Acad Sci 116(44): 22115–22121. https://doi.org/10.1073/pnas.1905071116

Almeida FC, Giannini NP, Desalle R, Simmons NB (2011) Evolutionary relationships of the old world fruit bats (Chiroptera, Pteropodidae): Another star phylogeny? BMC Evol Biol 11: 281. https://doi.org/10.1186/1471-2148-11-281

Almeida FC, Giannini NP, Simmons NB, Helgen KM (2014) Each flying fox on its own branch: A phylogenetic tree for Pteropus and related genera (Chiroptera: Pteropodidae). Mol Phylogenet Evol 77(1): 83–95. https://doi.org/10.1016/j.ympev.2014.03.009

Almeida FC, Giannini NP, Simmons NB (2016) The Evolutionary History of the African Fruit Bats (Chiroptera: Pteropodidae). Acta Chiropterologica 18(1): 73–90. https://doi.org/10.3161/15081109ACC2016.18.1.003

Almeida FC, Simmons NB, Giannini NP (2020) A Species-Level Phylogeny of Old World Fruit Bats with a New Higher-Level Classification of the Family Pteropodidae. Am Museum Novit 2020(3950): 1–24. https://doi.org/10.1206/3950.1

Amador LI, Moyers Arévalo RL, Almeida FC, Catalano SA, Giannini NP (2018) Bat Systematics in the Light of Unconstrained Analyses of a Comprehensive Molecular Supermatrix. J Mamm Evol 25(1): 37–70. https://doi.org/10.1007/s10914-016-9363-8

Amador LI, Simmons NB, Giannini NP (2019) Aerodynamic reconstruction of the primitive fossil bat Onychonycteris finneyi (Mammalia: Chiroptera). Biol Lett 15(3): 10–14. https://doi.org/10.1098/rsbl.2018.0857

Amador LI, Almeida FC, Giannini NP (2020) Evolution of Traditional Aerodynamic Variables in Bats (Mammalia: Chiroptera) within a Comprehensive Phylogenetic Framework. J Mamm Evol 27(3): 549–561. https://doi.org/10.1007/s10914-019-09475-8

Anderson DR, Burnham KP, White GC (1998) Comparison of Akaike information criterion and consistent Akaike information criterion for model selection and statistical inference from capture-recapture studies. J Appl Stat 25(2): 263–282. https://doi.org/10.1080/02664769823250

Anderson R, Maga AM (2015) A Novel Procedure for Rapid Imaging of Adult Mouse Brains with MicroCT Using Iodine-Based Contrast. PLoS One 10(11): e0142974. https://doi.org/10.1371/journal.pone.0142974

Anderson SC, Ruxton GD (2020) The evolution of flight in bats: a novel hypothesis. Mamm Rev 50(4): 426–439. https://doi.org/10.1111/mam.12211

Anthony R, Grzybowski J de (1930) Le Neopallium des Equidés: Etude du Développement de ses Plissements. J Anat 64(Pt 2): 147–69

Anthony R, Grzybowski J de (1934) Le Neopallium du Boeuf. Etude de son Développement et Interprétation de

ses Plissements. J Anat 68(Pt 4): 558–70

Anthony R (ed) (1928) Leçons sur le cerveau. Librairie Octave Doin-Gaston Doin et Cie, Paris, 359 p

Archer M, Arena DA, Bassarova M, et al (2006) Current status of species-level representation in faunas from selected fossil localities in the riversleigh world heritage area, northwestern queensland. Alcheringa 30(4): 1–17. https://doi.org/10.1080/03115510609506851

Arena DA, Travouillon KJ, Beck RMD, Black KH, Gillespie AK, Myers TJ, Archer M, Hand SJ (2016) Mammalian lineages and the biostratigraphy and biochronology of Cenozoic faunas from the Riversleigh World Heritage Area, Australia. Lethaia 49(1): 43–60. https://doi.org/10.1111/let.12131

Arroyo-Cabrales J (2019) Family Furipteridae (Smoky Bat and Thumbless Bat). In: Wilson DE, Mittermeier RA (eds) Handbook of the Mammals of the World – Volume 9 Bats. Lynx Edicions, Barcelona, pp 412–417

Averianov A, Danilov I, Jin J, Wang Y (2017) A new amynodontid from the Eocene of South China and phylogeny of Amynodontidae (Perissodactyla: Rhinocerotoidea). J Syst Palaeontol 15(11): 927–945. https://doi.org/10.1080/14772019.2016.1256914

Baker RJ, Bininda-Emonds ORP, Mantilla-Meluk H, Porter CA, Van Den Bussche RA (2012) Molecular time scale of diversification of feeding strategy and morphology in New World Leaf-Nosed Bats (Phyllostomidae): a phylogenetic perspective. In: Gunnell GF, Simmons NB (eds) Evolutionary History of Bats. Cambridge University Press, Cambridge, pp 385–409

Balanoff AM, Bever GS, Ikejiri T (2010) The Braincase of Apatosaurus (Dinosauria: Sauropoda) Based on Computed Tomography of a New Specimen with Comments on Variation and Evolution in Sauropod Neuroanatomy. Am Museum Novit 2010(3677): 1–32. https://doi.org/10.1206/591.1

Balanoff AM, Bever GS (2017) 1.10 The Role of Endocasts in the Study of Brain Evolution. In: Kaas JH (ed) Evolution of Nervous Systems, 2nd edn. Academic Press, Oxford, pp 223–241

Barchini J, Shi X, Chen H, Cang J (2018) Bidirectional encoding of motion contrast in the mouse superior colliculus. Elife 7: e35261. https://doi.org/10.7554/ELIFE.35261.001

Baron G, Stephan H, Frahm HD (eds) (1996) Comparative neurobiology in Chiroptera. Birkhäuser Verlag, Basel, 1596 p

Barone R, Bortolami R (eds) (2004) Anatomie comparée des mammifères domestiques : Tome 6, Neurologie I, Système nerveux central. Vigot, Paris, 652 p

Barron DH (1950) An experimental analysis of some factors involved in the development of the fissure pattern of the cerebral cortex. J Exp Zool 113(3): 553–581. https://doi.org/10.1002/jez.1401130304

Barton RA, Purvis A, Harvey PH (1995) Evolutionary radiation of visual and olfactory brain systems in primates, bats and insectivores. Philos Trans R Soc London Ser B Biol Sci 348(1326): 381–392. https://doi.org/10.1098/RSTB.1995.0076

Bauer DF (1972) Constructing confidence sets using rank statistics. J Am Stat Assoc 67(339): 687–690. https://doi.org/10.1080/01621459.1972.10481279

Beaulieu JM, O'Meara BC (2016) Detecting hidden diversification shifts in models of trait-dependent speciation and extinction. Syst Biol 65(4): 583–601. https://doi.org/10.1093/sysbio/syw022

Becker D, Antoine P-O, Engesser B, Hiard F, Hostettler B, Menkveld-Gfeller U, Mennecart B, Scherler L, Berger JP (2010) Late Aquitanian mammals from Engehalde (Molasse Basin, Canton Bern, Switzerland). Ann Paleontol 96(3): 95–116. https://doi.org/10.1016/j.annpal.2011.03.001

Benda P (2019) Family Rhinonycteridae (Trident Bats). In: Wilson DE, Mittermeier RA (eds) Handbook of the Mammals of the World – Volume 9 Bats. Lynx Edicions, Barcelona, pp 194–209

Benda P, Kasso M, Nicolas V, Pleurdeau D, Stoetzel E, Workalemahu S, Bekele A, Denys C (2019) New data on bats from Dire Dawa region, eastern Ethiopia, with the first record of Rhinopoma microphyllum in the country. J Nat Hist 53(41–42): 2579–2591. https://doi.org/10.1080/00222933.2019.1705416

Benoit J, Crumpton N, Mérigeaud S, Tabuce R (2013) A Memory Already like an Elephant's? The Advanced Brain Morphology of the Last Common Ancestor of Afrotheria (Mammalia). Brain Behav Evol 81(3): 154–169. https://doi.org/10.1159/000348481

Bertrand OC, Silcox MT (2016) First virtual endocasts of a fossil rodent: Ischyromys typus (Ischyromyidae, Oligocene) and brain evolution in rodents. J Vertebr Paleontol 36(3): e1095762. https://doi.org/10.1080/02724634.2016.1095762

Bertrand OC, Amador-Mughal F, Silcox MT (2017) Virtual endocast of the early Oligocene Cedromus wilsoni (Cedromurinae) and brain evolution in squirrels. J Anat 230(1): 128–151. https://doi.org/10.1111/joa.12537

Bertrand OC, Amador-Mughal F, Lang MM, Silcox MT (2018) Virtual endocasts of fossil Sciuroidea: brain size reduction in the evolution of fossoriality. Palaeontology 61(6): 919–948. https://doi.org/10.1111/pala.12378

Bertrand OC, Püschel HP, Schwab JA, Silcox MT, Brusatte SL (2021) The impact of locomotion on the brain evolution of squirrels and close relatives. Commun Biol 4(1): 1–15. https://doi.org/10.1038/s42003-021-01887-8

Bhatnagar KP, Kallen FC (1974) Cribriform Plate of Ethmoid, Olfactory Bulb and Olfactory Acuity in Forty Species of Bats. J Morphol 142: 71–90

Bhatnagar KP (2008) The brain of the common vampire bat, Desmodus rotundus murinus (Wagner, 1840): A cytoarchitectural atlas. Brazilian J Biol 68(3): 583–599. https://doi.org/10.1590/S1519-69842008000300017

Blomberg SP, Rathnayake SI, Moreau CM (2020) Beyond Brownian Motion and the Ornstein-Uhlenbeck Process: Stochastic Diffusion Models for the Evolution of Quantitative Characters. Am Nat 195(2): 145–165. https://doi.org/10.1086/706339

Blumenbach JF (ed) (1779) Handbuch der Naturgeschichte, 1st edn. Johann Christian Dieterich, Göttingen, 448 p

Bonnacorso F (2019) Family Emballonuridae (Sheath-tailed Bats). In: Wilson DE, Mittermeier RA (eds) Handbook of the Mammals of the World – Volume 9 Bats. Lynx Edicions, Barcelona, pp 334–373

Boyer DM, Gunnell GF, Kaufman S, McGeary TM (2017) Morphosource: Archiving and Sharing 3-D Digital Specimen Data. Paleontol Soc Pap 22: 157–181. https://doi.org/10.1017/scs.2017.13

Boyko JD, Beaulieu JM (2021) Generalized hidden Markov models for phylogenetic comparative datasets. Methods Ecol Evol 12(3): 468–478. https://doi.org/10.1111/2041-210X.13534

Bravais A (1846) Analyse mathématique sur les probabilités des erreurs de situation d'un point. Mémoires présentés par divers savants à l'Académie royale des sciences de l'Institut de France 9: 255–332

Brown EE, Cashmore DD, Simmons NB, Butler RJ (2019) Quantifying the completeness of the bat fossil record. Palaeontology 62(5): 757–776. https://doi.org/10.1111/pala.12426

Buchanan GD, Arata AA (1969) Cranial vasculature of a neotropical fruit-eating bat, Artibeus lituratus. Anat Anz 124(3): 314–325

Buchholtz EA, Seyfarth E-A (2001) The Study of "Fossil Brains": Tilly Edinger (1897–1967) and the Beginnings of Paleoneurology. Bioscience 51(8): 674–682. https://doi.org/10.1641/0006-3568(2001)051[0674:TSOFBT]2.0.CO;2

Buchler ER (1976) The use of echolocation by the wandering shrew (Sorex vagrans). Anim Behav 24(4): 858–873. https://doi.org/10.1016/S0003-3472(76)80016-4

Bugge J (1974) The Cephalic Arterial System in Insectivores, Primates, Rodents and Lagomorphs, with Special Reference to the Systematic Classification. Acta Anat (Basel) 87(62): 1–159. https://doi.org/10.1159/isbn.978-3-8055-8706-8

Burgin CJ, Colella JP, Kahn PL, Upham NS (2018) How many species of mammals are there? J Mammal 99(1): 1–14. https://doi.org/10.1093/jmammal/gyx147

Bussche RA Van Den, Lack JB (2013) Bat Molecular Phylogenetics: Past, Present, and Future Directions. In: Adams

RA, Pedersen SC (eds) Bat Evolution, Ecology, and Conservation. Springer, New York, NY, pp 111–128

Butler AB (2000) Chordate evolution and the origin of craniates: An old brain in a new head. Anat Rec 261(3): 111–125. https://doi.org/10.1002/1097-0185(20000615)261:3<111::AID-AR6>3.0.CO;2-F

Butler PM (1948) On the Evolution of the Skull and Teeth in the Erinaceidae, with Special Reference to Fossil Material in the British Museum. Proc Zool Soc London 118(2): 446–500. https://doi.org/10.1111/j.1096-3642.1948.tb00389.x

Carlisle A, Selwood L, Hinds LA, Saunders N, Habgood M, Mardon K, Weisbecker V (2017) Testing hypotheses of developmental constraints on mammalian brain partition evolution, using marsupials. Sci Reports 2017 71 7(1): 1–13. https://doi.org/10.1038/s41598-017-02726-9

Cartmill M, MacPhee RDE (1980) Tupaiid Affinities: The Evidence of the Carotid Arteries and Cranial Skeleton. In: Luckett WP (ed) Comparative Biology and Evolutionary Relationships of Tree Shrews. Springer, Boston, MA, pp 95–132

Castiglione S, Tesone G, Piccolo M, Melchionna M, Mondanaro A, Serio C, Di Febbraro M, Raia P (2018) A new method for testing evolutionary rate variation and shifts in phenotypic evolution. Methods Ecol Evol 9(4): 974–983. https://doi.org/10.1111/2041-210X.12954

Castiglione S, Serio C, Mondanaro A, Di Febbraro M, Profico A, Girardi G, Raia P (2019) Simultaneous detection of macroevolutionary patterns in phenotypic means and rate of change with and within phylogenetic trees including extinct species. PLoS One 14(1): 1–13. https://doi.org/10.1371/journal.pone.0210101

Cavalli-Sforza LL, Edwards AW (1967) Phylogenetic analysis. Models and estimation procedures. Am J Hum Genet 19(3 Pt 1): 233–257

Chai S, Tian R, Rong X, Li G, Chen B, Ren W, Xu S, Yang G (2020) Evidence of Echolocation in the Common Shrew from Molecular Convergence with Other Echolocating Mammals. Zool Stud 59: e4. https://doi.org/10.6620/ZS.2020.59-4

Cheung N, McNab AA (2003) Venous anatomy of the orbit. Investig Ophthalmol Vis Sci 44(3): 988–995. https://doi.org/10.1167/iovs.02-0865

Chira AM, Thomas GH (2016) The impact of rate heterogeneity on inference of phylogenetic models of trait evolution. J Evol Biol 29(12): 2502–2518. https://doi.org/10.1111/JEB.12979

Cleland TA, Linster C (2019) Central olfactory structures. Handb Clin Neurol 164: 79–96. https://doi.org/10.1016/B978-0-444-63855-7.00006-X

Clement AM, Nysjö J, Strand R, Ahlberg PE (2015) Brain – Endocast Relationship in the Australian Lungfish, Neoceratodus forsteri, Elucidated from Tomographic Data (Sarcopterygii: Dipnoi). PLoS One 10(10): e0141277. https://doi.org/10.1371/journal.pone.0141277

Coleman MN, Boyer DM (2011) Relationships between the expression of the stapedial artery and the size of the obturator foramen in euarchontans: Functional and phylogenetic implications. J Hum Evol 60(1): 106–116. https://doi.org/10.1016/j.jhevol.2010.09.006

Croux C, Dehon C, Croux C, Dehon C (2010) Influence functions of the Spearman and Kendall correlation measures. Stat Methods Appl 19: 497–515. https://doi.org/10.1007/s10260-010-0142-z

Csorba G, Hutson A, Rossiter S, Burgin C (2019) Family Rhinolophidae (Horseshoe Bats). In: Wilson DE, Mittermeier RA (eds) Handbook of the Mammals of the World – Volume 9 Bats. Lynx Edicions, Barcelona, pp 260–332

Csűrös M (2008) Ancestral Reconstruction by Asymmetric Wagner Parsimony over Continuous Characters and Squared Parsimony over Distributions. In: Nelson CE, Vialette S (eds) RECOMB Workshop on Comparative Genomics. Springer, Paris, pp 72–86

Cunningham CW, Omland KE, Oakley TH (1998) Reconstructing ancestral character states: A critical reappraisal. Trends Ecol Evol 13(9): 361–366. https://doi.org/10.1016/S0169-5347(98)01382-2

Currie TE, Meade A (2014) Keeping Yourself Updated: Bayesian Approaches in Phylogenetic Comparative Methods with a Focus on Markov Chain Models of Discrete Character Evolution. In: Modern Phylogenetic Comparative Methods and Their Application in Evolutionary Biology. Springer Berlin Heidelberg, Berlin, Heidelberg, pp 263–286

Cutcliffe JR, Harder HG (2009) The perpetual search for parsimony: Enhancing the epistemological and practical utility of qualitative research findings. Int J Nurs Stud 46(10): 1401–1410. https://doi.org/10.1016/j.ijnurstu.2009.05.005

Cuthbertson RS, Maddin HC, Holmes RB, Anderson JS (2015) The Braincase and Endosseous Labyrinth of Plioplatecarpus peckensis (Mosasauridae, Plioplatecarpinae), With Functional Implications for Locomotor Behavior. https://doi.org/10.1002/ar.23180

Cuvier G (ed) (1822) Recherches sur les ossemens fossiles, 3rd edn. G. Dufour et E. D'Ocagne, Paris, 412 p

Czarnecki RT, Kallen FC (1980) Craniofacial, occlusal, and masticatory anatomy in bats. Anat Rec 198(1): 87–105. https://doi.org/10.1002/ar.1091980107

Davies KT, Maryanto I, Rossiter SJ (2013) Evolutionary origins of ultrasonic hearing and laryngeal echolocation in bats inferred from morphological analyses of the inner ear. Front Zool 10(2): 1–15. https://doi.org/10.1186/1742-9994-10-2

de Pinna MCC (1991) Concepts and tests of homology in the cladistic paradigm. Cladistics 7(4): 367–394. https://doi.org/10.1111/j.1096-0031.1991.tb00045.x

Deaner RO, Isler K, Burkart J, van Schaik C (2007) Overall Brain Size, and Not Encephalization Quotient, Best Predicts Cognitive Ability across Non-Human Primates. Brain Behav Evol 70(2): 115–124. https://doi.org/10.1159/000102973

Dechaseaux C (1956) L'encéphale des mammifères volants. Colloq Int du Cent Natl la Rech Sci 80: 51–58

Dechaseaux C (1962) Cerveaux d'animaux disparus. Masson et Cie, Paris, 148 p

Dechaseaux C (1970) Récents résultats en paléoneurologie. Bull Académie Société Lorraines des Sci 9(1): 223–232

Dechaseaux C (1973) Essais de paléoneurologie. Ann Paléontologie 59: 8–132

Dechmann DKN, Safi K (2005) Studying communication in bats. Cogn Brain, Behav IX(3): 479–496

Dechmann DKN, Safi K (2009) Comparative studies of brain evolution: A critical insight from the Chiroptera. Biol Rev 84(1): 161–172. https://doi.org/10.1111/j.1469-185X.2008.00067.x

Demos TC, Webala PW, Goodman SM, Kerbis Peterhans JC, Bartonjo M, Patterson BD (2019) Molecular phylogenetics of the African horseshoe bats (Chiroptera: Rhinolophidae): expanded geographic and taxonomic sampling of the Afrotropics. BMC Evol Biol 19(1): 1–14. https://doi.org/10.1186/s12862-019-1485-1

Diamond MK (1991a) Homologies of the meningeal-orbital arteries of humans: a reappraisal. J Anat 178: 223–41

Diamond MK (1991b) Homologies of the stapedial artery in humans, with a reconstruction of the primitive stapedial artery configuration of euprimates. Am J Phys Anthropol 84(4): 433–462. https://doi.org/10.1002/ajpa.1330840408

Diamond MK (1992) Homology and evolution of the orbitotemporal venous sinuses of humans. Am J Phys Anthropol 88(2): 211–244. https://doi.org/10.1002/ajpa.1330880209

Díaz-Uriarte R, Garland T (1996) Testing Hypotheses of Correlated Evolution Using Phylogenetically Independent Contrasts: Sensitivity to Deviations from Brownian Motion. Syst Biol 45(1): 27–47. https://doi.org/10.1093/sysbio/45.1.27

Didier G (2017) Time-Dependent-Asymmetric-Linear-Parsimonious Ancestral State Reconstruction. Bull Math Biol 79(10): 2334–2355. https://doi.org/10.1007/s11538-017-0332-z

Didier G, Chabrol O, Laurin M (2019) Parsimony-based test for identifying changes in evolutionary trends for

quantitative characters: implications for the origin of the amniotic egg. Cladistics 35(5): 576–599. https://doi.org/10.1111/cla.12371

Didier G, Laurin M (2020) Exact Distribution of Divergence Times from Fossil Ages and Tree Topologies. Syst Biol 69(6): 1068–1087. https://doi.org/10.1093/sysbio/syaa021

Didier G, Laurin M (2021) Distributions of extinction times from fossil ages and tree topologies: the example of some mid-Permian synapsid extinctions. Preprint. https://doi.org/10.1101/2021.06.11.448028

Dilenge D, Ascherl GF (1980) Variations of the ophthalmic and middle meningeal arteries: Relation to the embryonic stapedial artery. Am J Neuroradiol 1(1): 45–53

Dinno A (2017) dunn.test: Dunn's Test of Multiple Comparisons Using Rank Sums. V 1.3.5

Dobson GE (1875) Conspectus of the suborders, families, and genera of Chiroptera arranged according to their natural affinities. Ann Mag Nat Hist Fourth Ser 16: 345–357. https://doi.org/10.1080/00222937508681865

Dool SE, Puechmaille SJ, Foley NM, Allegrini B, Bastian A, Mutumi GL, Maluleke TG, Odendaal LJ, Teeling EC, Jacobs DS (2016) Nuclear introns outperform mitochondrial DNA in inter-specific phylogenetic reconstruction: Lessons from horseshoe bats (Rhinolophidae: Chiroptera). Mol Phylogenet Evol 97: 196–212. https://doi.org/10.1016/j.ympev.2016.01.003

Dow RS (1942) The Evolution and Anatomy of the Cerebellum. Biol Rev 17(3): 179–220. https://doi.org/10.1111/j.1469-185X.1942.tb00437.x

Dräseke J (1903) Das Gehirn der Chiropteren. Eur Neurol 13(1): 448–463. https://doi.org/10.1159/000219478

Dubois E (1897) Sur le rapport du poids de l'encéphale avec la grandeur du corps chez les mammifères. Bull la Société d'anthropologie Paris 8(1): 337–376. https://doi.org/10.3406/bmsap.1897.5705

Ducrocq S, Jaeger J-J, Sigé B (1993) Un mégachiroptère dans l´Eocène supérieur de Thaïlande. Incidence dans la discussion phylogénique du groupe. N Jb Geol Paläont Mh 9: 561–575

Dumoncel J, Subsol G, Durrleman S, Bertrand A, Jager E, Oettlé AC, Lockhat Z, Suleman FE, Beaudet A (2021) Are endocasts reliable proxies for brains? A 3D quantitative comparison of the extant human brain and endocast. J Anat 238(2): 480–488. https://doi.org/10.1111/joa.13318

Dumont ER, Dávalos LM, Goldberg A, Santana SE, Rex K, Voigt CC (2012) Morphological innovation, diversification and invasion of a new adaptive zone. Proc R Soc B Biol Sci 279(1734): 1797–1805. https://doi.org/10.1098/rspb.2011.2005

Dunn OJ (1964) Multiple Comparisons Using Rank Sums. Technometrics 6(3): 241. https://doi.org/10.2307/1266041

Early CM, Iwaniuk AN, Ridgely RC, Witmer LM (2020) Endocast structures are reliable proxies for the sizes of corresponding regions of the brain in extant birds. J Anat 237(6): 1162–1176. https://doi.org/10.1111/joa.13285

Eastman JM, Alfaro ME, Joyce P, Hipp AL, Harmon LJ (2011) A Novel comparative method for identifying shifts in the rate of character evolution on trees. Evolution 65(12): 3578–3589. https://doi.org/10.1111/j.1558-5646.2011.01401.x

Edinger T (1926) Fossile Fledermausgehirne. Senckenbergiana 8(1): 1–6

Edinger T (1929) Die fossilen Gehirne. Ergeb Anat Entwicklungsgesch 28: 1–249

Edinger T (1941) The brain of Pterodactylus. Am J Sci 239(9): 665–682

Edinger T (1949) Paleoneurology vs comparative brain anatomy. Confin Neurol 9: 5–24

Edinger T (1963) Meanings of Midbrain Exposure, Past and Present. In: XVI International Congress of Zoology. pp 225–228

Edinger T (1964b) Recent Advances in Paleoneurology. Prog Brain Res 6: 147–160.

https://doi.org/10.1016/S0079-6123(08)63721-8

Edinger T (1964a) Midbrain Exposure and Overlap in Mammals. Am Zool 4(1): 5–19. https://doi.org/10.2307/3881308

Eisenberg JF, Wilson DE (1978) Relative Brain Size and Feeding Strategies in the Chiroptera. Evolution 32(4): 740. https://doi.org/10.2307/2407489

Ekdale EG (2013) Comparative Anatomy of the Bony Labyrinth (Inner Ear) of Placental Mammals. PLoS One 8(6): e66624. https://doi.org/10.1371/journal.pone.0066624

Ekman S, Andersen HL, Wedin M (2008) The limitations of ancestral state reconstruction and the evolution of the ascus in the lecanorales (Lichenized Ascomycota). Syst Biol 57(1): 141–156. https://doi.org/10.1080/10635150801910451

Escarguel G (1999) Les rongeurs de l'Eocène inférieur et moyen d'Europe Occidentale. Systématique, Phylogénie, Biochronologie et Paélobiogéographie des niveaux-repères MP7 à MP14. Palaeoverlebrata 28(2–4): 89–351

Evans HE, Lahunta A de (eds) (2012) Miller's Anatomy of the Dog, 4th edn. Elsevier Saunders, St. Louis, Missouri, 872 p

Ezekiel M (1929) The Application of the Theory of Error to Multiple and Curvilinear Correlation. J Am Stat Assoc 24(165A): 99–104. https://doi.org/10.1080/01621459.1929.10506278

Fabbri M, Mongiardino Koch N, Pritchard AC, Hanson M, Hoffman E, Bever GS, Balanoff AM, Morris ZS, Field DJ, Camacho J, Rowe TB, Norell MA, Smith RM, Abzhanov A, Bhullar B-AS (2017) The skull roof tracks the brain during the evolution and development of reptiles including birds. Nat Ecol Evol 1(10): 1543–1550. https://doi.org/10.1038/s41559-017-0288-2

Farris JS (1989a) The Retention Index and Homoplasy Excess. Syst Zool 38(4): 406. https://doi.org/10.2307/2992406

Farris JS (1989b) The Retention Index and the Rescaled Consistency Index. Cladistics 5(4): 417–419. https://doi.org/10.1111/j.1096-0031.1989.tb00573.x

Felsenstein J (1983) Parsimony in systematics: biological and statistical issues. Annu Rev Ecol Syst 14: 313–333. https://doi.org/10.1146/annurev.es.14.110183.001525

Felsenstein J (1985) Phylogenies and the comparative method. Am Nat 125(1): 1–15

Ferreira-Cardoso S, Araújo R, Martins NE, Martins GG, Walsh S, Martins RMS, Kardjilov N, Manke I, Hilger A, Castanhinha R (2017) Floccular fossa size is not a reliable proxy of ecology and behaviour in vertebrates. Sci Rep 7(1): 2005. https://doi.org/10.1038/s41598-017-01981-0

Fisher SRA (1970) Statistical Methods for Research Workers, 14th edn. Oliver and Boyd, Edinburgh, 362 p

Fitch WM (1971) Toward defining the course of evolution: Minimum change for a specific tree topology. Syst Biol 20(4): 406–416. https://doi.org/10.1093/sysbio/20.4.406

FitzJohn RG (2012) Diversitree : comparative phylogenetic analyses of diversification in R. Methods Ecol Evol 3(6): 1084–1092. https://doi.org/10.1111/j.2041-210X.2012.00234.x

Foley NM, Thong VD, Soisook P, Goodman SM, Armstrong KN, Jacobs DS, Puechmaille SJ, Teeling EC (2015) How and Why Overcome the Impediments to Resolution: Lessons from rhinolophid and hipposiderid Bats. Mol Biol Evol 32(2): 313–333. https://doi.org/10.1093/molbev/msu329

Foley NM, Goodman SM, Whelan C V., Puechmaille SJ, Teeling E (2017) Towards Navigating the Minotaur's Labyrinth: Cryptic Diversity and Taxonomic Revision within the Speciose Genus Hipposideros (Hipposideridae). Acta Chiropterologica 19(1): 1–18. https://doi.org/10.3161/15081109ACC2017.19.1.001

Folinsbee KE, Evans DC, Fröbisch J, Brooks DR, Tsuji LA (2015) Quantitative Approaches to Phylogenetics. In: Henke W, Tattersall I (eds) Handbook of Paleoanthropology. Springer, Berlin, pp 257–294

Francis CM (2019) Family Megadermatidae (False-vampire Bats). In: Wilson DE, Mittermeier RA (eds) Handbook

of the Mammals of the World – Volume 9 Bats. Lynx Edicions, Barcelona, pp 182–193

Freckleton RP (2002) On the misuse of residuals in ecology: Regression of residuals vs. multiple regression. J Anim Ecol 71(3): 542–545. https://doi.org/10.1046/j.1365-2656.2002.00618.x

Freckleton RP (2009) The seven deadly sins of comparative analysis. J Evol Biol 22(7): 1367–1375. https://doi.org/10.1111/j.1420-9101.2009.01757.x

Freeman PW (2000) Macroevolution in Microchiroptera: Recoupling morphology and ecology with phylogeny. Evol Ecol Res 2(3): 317–335

Galton F (1877) Typical laws of heredity. Nature 15(388): 492–495. https://doi.org/10.1038/015492A0

Gannon PJ, Eden AR, Laitman JT (1988) The subarcuate fossa and cerebellum of extant primates: Comparative study of a skull-brain interface. Am J Phys Anthropol 77(2): 143–164. https://doi.org/10.1002/ajpa.1330770202

Garcia KE, Kroenke CD, Bayly P V. (2018) Mechanics of cortical folding: stress, growth and stability. Philos Trans R Soc B Biol Sci 373(1759): 20170321. https://doi.org/10.1098/rstb.2017.0321

Garland T (1992) Rate Tests for Phenotypic Evolution Using Phylogenetically Independent Contrasts. Am Nat 140(3): 509–519. https://doi.org/10.1086/285424

Getz GE (2014) History of Neurobiology. In: Getz GE (ed) Applied Biological Psychology. Springer Publishing Company, New York, NY, pp 1–12

Giannini NP, Wible JR, Simmons NB (2006) On the Cranial Osteology of Chiroptera. I. Pteropus (Megachiroptera: Pteropodidae). Bull Am Museum Nat Hist 2006(295): 1–134. https://doi.org/10.1206/0003-0090(2006)295[0001:OTCOOC]2.0.CO;2

Giannini NP, Gunnell GF, Habersetzer J, Simmons NB (2012) Early evolution of body size in bats. In: Gunnell GF, Simmons NB (eds) Evolutionary History of Bats. Cambridge University Press, Cambridge, pp 530–555

Giannini NP, Cakenberghe V Van, Burgin CJ, Tsang S, Lavery T, Hintsche S, Bonaccorso F, Almeida FC, O'Toole B (2019) Family Pteropodidae (Old World Fruit Bats). In: Wilson DE, Mittermeier RA (eds) Handbook of the Mammals of the World – Volume 9 Bats. Lynx Edicions, Barcelona, pp 16–162

Giffin EB (1990) Gross spinal anatomy and limb use in living and fossil reptiles. Paleobiology 16(4): 448–458. https://doi.org/10.1017/S0094837300010186

Gignac PM, Kley NJ, Clarke JA, et al (2016) Diffusible iodine-based contrast-enhanced computed tomography (diceCT): an emerging tool for rapid, high-resolution, 3-D imaging of metazoan soft tissues. J Anat 228: 889–909. https://doi.org/10.1111/joa.12449

Goloboff PA, Torres A, Arias JS (2018) Weighted parsimony outperforms other methods of phylogenetic inference under models appropriate for morphology. Cladistics 34(4): 407–437. https://doi.org/10.1111/cla.12205

Goloboff PA, Pittman M, Pol D, Xu X (2019) Morphological data sets fit a common mechanism much more poorly than DNA sequences and call into question the Mkv model. Syst Biol 68(3): 494–504. https://doi.org/10.1093/sysbio/syy077

Goodman SM (2019) Family Myzopodidae (Madagascar Sucker-footed Bats). In: Wilson DE, Mittermeier RA (eds) Handbook of the Mammals of the World – Volume 9 Bats. Lynx Edicions, Barcelona, pp 388–393

Gould E, Negus NC, Novick A (1964) Evidence for echolocation in shrews. J Exp Zool 156(1): 19–37. https://doi.org/10.1002/JEZ.1401560103

Gould E (1965) Evidence for Echolocation in the Tenrecidae of Madagascar. Source Proc Am Philos Soc 109(6): 352–360

Grafen A (1989) The Phylogenetic Regression. Philos Trans R Soc B Biol Sci 326(1233): 119–157. https://doi.org/10.1098/rstb.1989.0106

Grosser O (1901) Zur Anatomie und Entwickelungsgeschichte des Gefässsystemes der Chiropteren. Anat Hefte

17(2): 203–424. https://doi.org/10.1007/BF02301074

Gunnell GF, Worsham SR, Seiffert ER, Simons EL (2009) Vampyravus orientalis schlosser (Chiroptera) from the early oligocene (Rupelian), fayum, Egypt body mass, humeral morphology and affinities. Acta Chiropterologica 11(2): 271–278. https://doi.org/10.3161/150811009X485512

Hackethal H (1981) Die bedeutung hirnmorphologischer Merkmale für die taxonomie der placentalen säuger. Mitt. Zool. Mus. Berlin 57(2): 233–340. https://doi.org/10.1002/mmnz.19810570204

Hall L, Pettigrew JE (1995) The bat with the stereo nose. Aust Nat Hist 24: 26–28

Hand SJ (1993) First skull of a species of Hipposideros (Brachipposideros) (Microchiroptera: Hipposideridae), from Australian Miocene sediments. Mem Queensl Museum 33(1): 179–192

Hand SJ (1997) Hipposideros bernardsigei, a new hipposiderid (Mammalia: Microchiroptera) from the Australian Miocene and a reconsideration of the monophyly of related species groups. Münchner Geowiss Abh 34: 73–92

Hand SJ (1998a) Riversleigha williamsi gen. et sp. nov., a large Miocene hipposiderid (microchiroptera) from Riversleigh, Queensland. Alcheringa An Australas J Palaeontol 22(3): 259–276. https://doi.org/10.1080/03115519808619204

Hand SJ (1998b) Xenorhinos , a new genus of Old World leaf-nosed bats (Microchiroptera: Hipposideridae) from the Australian Miocene. J Vertebr Paleontol 18(2): 430–439. https://doi.org/10.1080/02724634.1998.10011070

Hand SJ, Kirsch JAW (2003) Archerops, a new annectent hipposiderid genus (Mammalia : Microchiroptera) from the Australian Miocene. J Paleontol 77(6): 1139–1151. https://doi.org/10.1666/0022-3360(2003)077<1139:AANAHG>2.0.CO;2

Hand SJ, Archer M (2005) A new hipposiderid genus (Microchiroptera) from an early Miocene bat community in Australia. Palaeontology 48(2): 371–383. https://doi.org/10.1111/j.1475-4983.2005.00444.x

Hand SJ, Sigé B, Maitre E (2012) Necromantis Weithofer, 1887, large carnivorous Middle and Late Eocene bats from the French Quercy Phosphorites: New data and unresolved relationships. In: Gunnell GF, Simmons NB (eds) Evolutionary History of Bats: Fossils, Molecules and Morphology. Cambridge University Press, Cambridge, pp 210–251

Hansen TF (1997) Stabilizing selection and the comparative analysis of adaptation. Evolution 51(5): 1341–1351. https://doi.org/10.1111/j.1558-5646.1997.tb01457.x

Harvey PH, Purvis A (1991) Comparative methods for explaining adaptations. Nature 351(6328): 619–624. https://doi.org/10.1038/351619a0

Hassanin A, Bonillo C, Tshikung D, Pongombo Shongo C, Pourrut X, Kadjo B, Nakouné E, Tu VT, Prié V, Goodman SM (2020) Phylogeny of African fruit bats (Chiroptera, Pteropodidae) based on complete mitochondrial genomes. J Zool Syst Evol Res 58(4): 1395–1410. https://doi.org/10.1111/jzs.12373

Hayden S, Bekaert M, Crider TA, Mariani S, Murphy WJ, Teeling EC (2010) Ecological adaptation determines functional mammalian olfactory subgenomes. Genome Res 20(1): 1–9. https://doi.org/10.1101/gr.099416.109

Hayden S, Bekaert M, Goodbla A, Murphy WJ, Dávalos LM, Teeling EC (2014) A Cluster of Olfactory Receptor Genes Linked to Frugivory in Bats. Mol Biol Evol 31(4): 917–927. https://doi.org/10.1093/MOLBEV/MSU043

Hayreh SS, Dass R (1962) The ophthalmic artery: I. Origin and intra-cranial and intra-canalicular course. Br J Ophthalmol 46(2): 65–98. https://doi.org/10.1136/bjo.46.2.65

He K, Liu Q, Xu DM, Qi FY, Bai J, He SW, Chen P, Zhou X, Cai WZ, Chen ZZ, Liu Z, Jiang XL, Shi P (2021) Echolocation in soft-furred tree mice. Science(80-) 372(6548): 1–10. https://doi.org/10.1126/science.aay1513

Heath TA, Huelsenbeck JP, Stadler T (2014) The fossilized birth-death process for coherent calibration of divergence-time estimates. Proc Natl Acad Sci 111(29): E2957–E2966.

https://doi.org/10.1073/pnas.1319091111

Hedrick BP, Yohe L, Vander Linden A, Dávalos LM, Sears K, Sadier A, Rossiter SJ, Davies KTJ, Dumont ER (2018) Assessing Soft-Tissue Shrinkage Estimates in Museum Specimens Imaged With Diffusible Iodine-Based Contrast-Enhanced Computed Tomography (diceCT). Microsc Microanal 24(3): 284–291. https://doi.org/10.1017/S1431927618000399

Hegedus SA, Shackelford RT (1965) A comparative-anatomical study of the craniocervical venous systems in mammals, with special reference to the dog: Relationship of anatomy to measurements of cerebral blood flow. Am J Anat 116(2): 375–386. https://doi.org/10.1002/aja.1001160204

Henson OWJ (1970) 2 The Central Nervous System. In: Wimsatt WA (ed) Biology of Bats: Volume 2. Academic Press, New York, NY, p 57

Herculano-Houzel S (2012) The remarkable, yet not extraordinary, human brain as a scaled-up primate brain and its associated cost. Proc Natl Acad Sci 109(SUPPL.1): 10661–10668. https://doi.org/10.1073/pnas.1201895109

Herculano-Houzel S, da Cunha FB, Reed JL, Kaswera-Kyamakya C, Gilissen E, Manger PR (2020) Microchiropterans have a diminutive cerebral cortex, not an enlarged cerebellum, compared to megachiropterans and other mammals. J Comp Neurol 528(17): 2978–2993. https://doi.org/10.1002/cne.24985

Hitier M, Zhang M, Labrousse M, Barbier C, Patron V, Moreau S (2013) Persistent stapedial arteries in human: From phylogeny to surgical consequences. Surg. Radiol. Anat. 35:883–891

Holland BR, Ketelaar-Jones S, O'Mara AR, Woodhams MD, Jordan GJ (2020) Accuracy of ancestral state reconstruction for non-neutral traits. Sci Rep 10(1): 7644. https://doi.org/10.1038/s41598-020-64647-4

Holland LZ (2015) The origin and evolution of chordate nervous systems. Philos Trans R Soc B Biol Sci 370(1684): 20150048. https://doi.org/10.1098/rstb.2015.0048

Holland LZ, Carvalho JE, Escriva H, Laudet V, Schubert M, Shimeld SM, Yu J-K (2013) Evolution of bilaterian central nervous systems: a single origin? Evodevo 4(1): 27. https://doi.org/10.1186/2041-9139-4-27

Hollander M, A. Wolfe D, Chicken E (eds) (2015) Nonparametric Statistical Methods. John Wiley & Sons, Inc., Hoboken, New Jersey, 819 p

Horáček I (2019) Family Rhinopomatidae (Mouse-tailed Bats). In: Wilson DE, Mittermeier RA (eds) Handbook of the Mammals of the World – Volume 9 Bats. Lynx Edicions, Barcelona, pp 164–177

Hulva P, Horáček I, Benda P (2007) Molecules, morphometrics and new fossils provide an integrated view of the evolutionary history of Rhinopomatidae (Mammalia: Chiroptera). BMC Evol Biol 7(1). https://doi.org/10.1186/1471-2148-7-165

Hunt G, Bell MA, Travis MP (2008) Evolution toward a new adaptive optimum: Phenotypic evolution in a fossil stickleback lineage. Evolution 62(3): 700–710. https://doi.org/10.1111/j.1558-5646.2007.00310.x

Hutcheon JM, Kirsch JAW, Garland Jr T (2002) A Comparative Analysis of Brain Size in Relation to Foraging Ecology and Phylogeny in the Chiroptera. Brain Behav Evol 60(3): 165–180. https://doi.org/10.1159/000065938

Inkscape Project (2018) Inkscape. V 0.92.3

Jerison HJ (1973) Evolution of the Brain and Intelligence. Academic Press, New York, 482 p

Jolicoeur P, Pirlot P, Baron G, Stephan H (1984) Brain Structure and Correlation Patterns in Insectivora, Chiroptera, and Primates. Syst Biol 33(1): 14–29. https://doi.org/10.1093/sysbio/33.1.14

Jones G, Teeling EC, Rossiter SJ (2013) From the ultrasonic to the infrared: molecular evolution and the sensory biology of bats. Front Physiol 4(117): 1–16. https://doi.org/10.3389/fphys.2013.00117

Jones KE, Purvis A, MacLarnon A, Bininda-Emonds ORP, Simmons NB (2002) A phylogenetic supertree of the bats (Mammalia: Chiroptera). Biol Rev Camb Philos Soc 77(2): 223–259. https://doi.org/10.1017/S1464793101005899

Jones KE, MacLarnon AM (2004) Affording Larger Brains: Testing Hypotheses of Mammalian Brain Evolution on Bats. Am Nat 164(1): E20–E31. https://doi.org/10.1590/S1808-185120181701178599

Jones KE, Bielby J, Cardillo M, et al (2009) PanTHERIA: a species-level database of life history, ecology, and geography of extant and recently extinct mammals. Ecology 90(9): 2648–2648. https://doi.org/10.1890/08-1494.1

Joy JB, Liang RH, McCloskey RM, Nguyen T, Poon AFY (2016) Ancestral Reconstruction. PLoS Comput Biol 12(7): e1004763. https://doi.org/10.1371/journal.pcbi.1004763

Kallen FC, Gans C (1972) Mastication in the little brown bat, Myotis lucifugus. J Morphol 136(4): 385–420. https://doi.org/10.1002/jmor.1051360402

Kallen FC (1977) The cardiovascular system of bats: Structure and function. In: Wimsatt WA (ed) Biology of Bats: Volume 3. Academic Press, New York, NY, pp 289–483

Kaňuch P, Aghová T, Meheretu Y, Šumbera R, Bryja J (2015) New discoveries on the ecology and echolocation of the heart-nosed bat Cardioderma cor with a contribution to the phylogeny of megadermatidae. African Zool 50(1): 53–57. https://doi.org/10.1080/15627020.2015.1021711

Kardong K V. (ed) (2012) Vertebrates: Comparative Anatomy, Function, Evolution, 6th edn. McGraw-Hill, New York, 794 p

Kawano K, Takemura A, Inoue Y, Kitama T, Kobayashi Y, Mustari MJ (1996) Visual inputs to cerebellar ventral paraflocculus during ocular following responses. Prog Brain Res 112: 415–422. https://doi.org/10.1016/s0079-6123(08)63346-4

Kendall M, Gibbons JD (eds) (1990) Rank Correlation Methods, 5th edn. Oxford University Press, N, 260 p

Kimchi T, Reshef M, Terkel J (2005) Evidence for the use of reflected self-generated seismic waves for spatial orientation in a blind subterranean mammal. J Exp Biol 208(4): 647–659. https://doi.org/10.1242/jeb.01396

Kingston T, Soisook P (2019) Family Craseonycteridae (Hog-nosed Bat). In: Wilson DE, Mittermeier RA (eds) Handbook of the Mammals of the World – Volume 9 Bats. Lynx Edicions, Barcelona, pp 178–181

Kluge AG, Farris JS (1969) Quantitative Phyletics and the Evolution of Anurans. Syst Biol 18(1): 1–32. https://doi.org/10.1093/sysbio/18.1.1

Kobayashi Y, Matsui T, Ogihara N (2018) Inferring Cortical Subdivisions Based on Skull Morphology. In: Bruner E, Ogihara N, Tanabe HC (eds) Digital Endocasts. Springer Japan, Tokyo, pp 33–46

Kochetkova VI (1978) Foreword. In: Kochetkova VI, Jerison HJ, Jerison I (eds) Paleoneurology. V. H. Winston & Sons, Washington, D.C., pp 1–11

Kratsch C, McHardy AC (2014) RidgeRace: ridge regression for continuous ancestral character estimation on phylogenetic trees. Bioinformatics 30(17): i527–i533. https://doi.org/10.1093/bioinformatics/btu477

Kreft G (1997) The Work of Ludwig Edinger and His Neurology Institute. In: Korf H-W, Usadel K-H (eds) Neuroendocrinology. Springer, Berlin, pp 407–423

Kruskal WH, Wallis WA (1952) Use of Ranks in One-Criterion Variance Analysis. J Am Stat Assoc 47(260): 583–621. https://doi.org/10.1080/01621459.1952.10483441

Kuchinka J (2018) Internal Ophthalmic Arteries Within the Brain-Base Arterial System in Guinea Pig. Anat Rec 301(5): 887–891. https://doi.org/10.1002/ar.23737

Lack JB, Van Den Bussche RA (2010) Identifying the confounding factors in resolving phylogenetic relationships in Vespertilionidae. J Mammal 91(6): 1435–1448. https://doi.org/10.1644/09-MAMM-A-354.1

Langley JN (1883) The Structure of the Dog's Brain. J Physiol 4(4–5): 248–326. https://doi.org/10.1113/jphysiol.1883.sp000130

Larsell O, Dow RS (1935) The development of the cerebellum in the bat (Corynorhinus sp.) and certain other mammals. J Comp Neurol 62(2): 443–468. https://doi.org/10.1002/cne.900620210

Lashley KS (1949) Persistent Problems in the Evolution of Mind. Q Rev Biol 24(1): 28–42. https://doi.org/10.1086/396806

Lavery TH, Leung LK-P, Seddon JM (2014) Molecular phylogeny of hipposiderid bats (Chiroptera: Hipposideridae) from Solomon Islands and Cape York Peninsula, Australia. Zool Scr 43(5): 429–442. https://doi.org/10.1111/zsc.12068

Lebrun R (2018) MorphoDig, an open-source 3D freeware dedicated to biology. V 1.5.3

Lee MSY, Jago JB, García-Bellido DC, Edgecombe GD, Gehling JG, Paterson JR (2011) Modern optics in exceptionally preserved eyes of Early Cambrian arthropods from Australia. Nature 474(7353): 631–634. https://doi.org/10.1038/nature10097

Legendre S, Marandat B, Sigé B, Crochet J-Y, Godinot M, Hartenberger J-L, Sudre J, Vianey-Liaud M, Muratet B, Astruc JG (1992) La faune de mammifères de Vielase (phosphorites du Quercy, Sud de la France): preuve paléontologique d'une karstification du Quercy dès l'Eocène inférieur. Neues Jahrb für Geol und Paläontologie - Monatshefte (7): 414–428

Lewis PO (2001) A likelihood approach to estimating phylogeny from discrete morphological character data. Syst Biol 50(6): 913–925. https://doi.org/10.1080/106351501753462876

Lundeen IK, Kirk EC (2019) Internal nasal morphology of the Eocene primate Rooneyia viejaensis and extant Euarchonta: Using µCT scan data to understand and infer patterns of nasal fossa evolution in primates. J Hum Evol 132: 137–173. https://doi.org/10.1016/J.JHEVOL.2019.04.009

Luo Z-X, Ruf I, Schultz JA, Martin T (2011) Fossil evidence on evolution of inner ear cochlea in Jurassic mammals. Proc R Soc B Biol Sci 278(1702): 28–34. https://doi.org/10.1098/rspb.2010.1148

Lyras GA (2009) The evolution of the brain in Canidae (Mammalia: Carnivora). Scr Geol (139): 1–93

MacLarnon A (1996) The evolution of the spinal cord in primates: evidence from the foramen magnum and the vertebral canal. J Hum Evol 30(2): 121–138. https://doi.org/10.1006/JHEV.1996.0009

Macrini TE, Rowe TB, Archer M (2006) Description of a cranial endocast from a fossil platypus,Obdurodon dicksoni (Monotremata, Ornithorhynchidae), and the relevance of endocranial characters to monotreme monophyly. J Morphol 267(8): 1000–1015. https://doi.org/10.1002/jmor.10452

Macrini TE, De Muizon C, Cifelli RL, Rowe TB (2007) Digital cranial endocast of Pucadelphys andinus, a Paleocene metatherian. J Vertebr Paleontol 27(1): 99–107. https://doi.org/10.1671/0272-4634(2007)27[99:DCEOPA]2.0.CO;2

Maddison WP (1990) A method for testing the correlated evolution of two binary characters: are gains or losses concentrated on certain branches of a phylogenetic tree? Evolution 44(3): 539–557. https://doi.org/10.1111/j.1558-5646.1990.tb05937.x

Maddison WP (1991) Squared-Change Parsimony Reconstructions of Ancestral States for Continuous-Valued Characters on a Phylogenetic Tree. Syst Zool 40(3): 304–314

Maddison WP, Midford PE, Otto SP (2007) Estimating a binary character's effect on speciation and extinction. Syst Biol 56(5): 701–710. https://doi.org/10.1080/10635150701607033

Maitre E (2014) Western European middle Eocene to early Oligocene Chiroptera: systematics, phylogeny and palaeoecology based on new material from the Quercy (France). Swiss J Palaeontol 133(2): 141–242. https://doi.org/10.1007/s13358-014-0069-3

Mann G (1961) Bulbus olfactorius accessorius in chiroptera. J Comp Neurol 116(2): 135–144. https://doi.org/10.1002/cne.901160204

Mann G (1963) Phylogeny and cortical evolution in Chiroptera. Evolution 17(4): 589–591. https://doi.org/10.1055/s-2008-1067919

Mann HB, Whitney DR (1947) On a Test of Whether one of Two Random Variables is Stochastically Larger than the Other. Ann Math Stat 18(1): 50–60. https://doi.org/10.1214/aoms/1177730491

Martin RD (ed) (1990) Primate Origins and Evolution: a Phylogenetic Reconstruction. Chapman and Hall, London, 840 p

Martínez G, Dozo MT, Vera B, Cerdeño E (2019) Paleoneurology, auditory region, and associated soft tissue inference in the late Oligocene notoungulates Mendozahippus fierensis and Gualta cuyana (Toxodontia) from central-western Argentina. J Vertebr Paleontol 39(6): 1–19. https://doi.org/10.1080/02724634.2019.1725531

Martinez Q, Clavel J, Esselstyn JA, Achmadi AS, Grohé C, Pirot N, Fabre PH (2020) Convergent evolution of olfactory and thermoregulatory capacities in small amphibious mammals. Proc Natl Acad Sci U S A 117(16): 8958–8965. https://doi.org/10.1073/pnas.1917836117

Martins EP, Hansen TF (1996) The statistical analysis of interspecific data: a review and evaluation of phylogenetic comparative methods. In: Martins EP (ed) Phylogenies and the comparative method in animal behaviour. Oxford University Press, New York, NY, pp 22–75

Martins EP, Hansen TF (1997) Phylogenies and the Comparative Method: A General Approach to Incorporating Phylogenetic Information into the Analysis of Interspecific Data. Naturalist 149(4): 646–667

Maugoust J (2021) ULT - Useful Little Things in R. V 1.3

Maugoust J, Orliac MJ (2021) Endocranial Cast Anatomy of the Extinct Hipposiderid Bats Palaeophyllophora and Hipposideros (Pseudorhinolophus) (Mammalia: Chiroptera). J Mamm Evol 28(3): 679–706. https://doi.org/10.1007/s10914-020-09522-9

Mccurry MR, Marx FG, Evans AR, Park T, Pyenson ND, Kohno N, Castiglione S, Fitzgerald EMG (2021) Brain size evolution in whales and dolphins: new data from fossil mysticetes. Biol J Linn Soc 133(4): 990–998. https://doi.org/10.1093/biolinnean/blab054

McDaniel VR (1976) Brain Anatomy. In: Baker RJ, Knox Jones Jr. J, Carter DC (eds) Biology of Bats of the New World Family Phyllostomidae. Part I. Texas Tech Press, Lubbock, Texas, pp 147–200

McGuire LP, Ratcliffe JM (2011) Light enough to travel: Migratory bats have smaller brains, but not larger hippocampi, than sedentary species. Biol Lett 7(2): 233–236. https://doi.org/10.1098/rsbl.2010.0744

Meredith RW, Janecka JE, Gatesy J, et al (2011) Impacts of the Cretaceous Terrestrial Revolution and KPg Extinction on Mammal Diversification. Science 334(6055): 521–524. https://doi.org/10.1126/science.1211028

Monadjem A, Soisook P, Thong VD, Kingston T (2019) Family Hipposideridae (Old World Leaf-nosed Bats). In: Wilson DE, Mittermeier RA (eds) Handbook of the Mammals of the World – Volume 9 Bats. Lynx Edicions, Barcelona, pp 210–258

Moratelli R, Burgin CJ, Cláudio V, Novaes R, López-Baucells A, Haslauer R (2019) Family Vespertilionidae (Vesper Bats). In: Wilson DE, Mittermeier RA (eds) Handbook of the Mammals of the World – Volume 9 Bats. Lynx Edicions, Barcelona, pp 716–981

Mourlam MJ, Orliac MJ (2017) Infrasonic and Ultrasonic Hearing Evolved after the Emergence of Modern Whales. Curr Biol 27(12): 1776–1781.e9. https://doi.org/10.1016/j.cub.2017.04.061

Moyers Arévalo RL, Amador LI, Almeida FC, Giannini NP (2020) Evolution of Body Mass in Bats: Insights from a Large Supermatrix Phylogeny. J Mamm Evol 27(1): 123–138. https://doi.org/10.1007/s10914-018-9447-8

Muizon de C, Billet G, Argot C, Ladevèze S, Goussard F (2015) Alcidedorbignya inopinata, a basal pantodont (Placentalia, Mammalia) from the early Palaeocene of Bolivia: Anatomy, phylogeny and palaeobiology. Geodiversitas 37(4): 397–631. https://doi.org/10.5252/g2015n4a1

Murrill RI, Wallace DT (1971) A method for making an endocranial cast through the foramen magnum of an intact skull. Am J Phys Anthropol 34(3): 441–446. https://doi.org/10.1002/ajpa.1330340315

Narayan RK, Ghosh SK (2021) Analysis of variations in morphological characteristics of orbito-meningeal foramen: An anatomical study with clinical implications. Transl Res Anat 24: 100108.

https://doi.org/10.1016/j.tria.2020.100108

Narushima H, Hanazawa M (1997) A more efficient algorithm for MPR problems in phylogeny. Discret Appl Math 80(2–3): 231–238. https://doi.org/10.1016/S0166-218X(97)00088-7

Nasrullah Q, Renfree MB, Evans AR (2018) Three-dimensional mammalian tooth development using diceCT. Arch Oral Biol 85: 183–191. https://doi.org/10.1016/J.ARCHORALBIO.2017.10.018

Nomina Anatomica Veterinaria (2017) International Committee on Veterinary Gross Anatomical Nomenclature (I.C.V.G.A.N.), 6th edn. The Editorial Committee with permission of the World Association of Veterinary Anatomists (W.A.V.A.), Hanover (Germany), Ghent (Belgium), Columbia, MO (USA), Rio de Janeiro (Brazil), 160 p

Neuweiler G (2000) Central nervous system. In: Neuweiler G (ed) The Biology of Bats. Oxford University Press, New York, pp 117–139

Neuwirth E (2014) RColorBrewer: ColorBrewer Palettes. 1.1-2

Ni X, Flynn JJ, Wyss AR, Zhang C (2019) Cranial endocast of a stem platyrrhine primate and ancestral brain conditions in anthropoids. Sci Adv 5(8): eaav7913. https://doi.org/10.1126/sciadv.aav7913

Nieuwenhuys R (1998) Morphogenesis and General Structure. In: Nieuwenhuys R, ten Donkelaar HJ, Nicholson C (eds) The Central Nervous System of Vertebrates. Springer Berlin Heidelberg, Berlin, Heidelberg, pp 159–228

Niven JE (2005) Brain Evolution: Getting Better All the Time? Curr Biol 15(16): R624–R626. https://doi.org/10.1016/j.cub.2005.08.007

Nojiri T, Wilson LAB, López-Aguirre C, Tu VT, Kuratani S, Ito K, Higashiyama H, Son NT, Fukui D, Sadier A, Sears KE, Endo H, Kamihori S, Koyabu D (2021) Embryonic evidence uncovers convergent origins of laryngeal echolocation in bats. Curr Biol 31(7): 1353–1365.e3. https://doi.org/10.1016/j.cub.2020.12.043

Norberg UML, Rayner J (1987) Ecological morphology and flight in bats (Mammalia; Chiroptera): wing adaptations, flight performance, foraging strategy and echolocation. Philos Trans R Soc London B, Biol Sci 316(1179): 335–427. https://doi.org/10.1098/rstb.1987.0030

Northcutt RG (2001) Changing views of brain evolution. Brain Res Bull 55(6): 663–674. https://doi.org/10.1016/S0361-9230(01)00560-3

O'Leary MA (2010) An Anatomical and Phylogenetic Study of the Osteology of the Petrosal of Extant and Extinct Artiodactylans (Mammalia) and Relatives. Bull Am Museum Nat Hist 2010(335): 1–206. https://doi.org/10.1206/335.1

O'Meara BC, Ané C, Sanderson MJ, Wainwright PC (2006) Testing for different rates of continuous trait evolution using likelihood. Evolution 60(5): 922–923. https://doi.org/10.1111/j.0014-3820.2006.tb01171.x

Ogle DH, Wheeler P, Dinno A (2019) FSA: Fisheries Stock Analysis. V 0.8.26

Oken L (ed) (1819) Isis, oder Encyclopädische Zeitung. Brockhaus, Jena, 1864 p

Omland KE (1999) The assumptions and challenges of ancestral state reconstructions. Syst Biol 48(3): 604–611. https://doi.org/10.1080/106351599260175

Orliac MJ, Argot C, Gilissen E (2012) Digital Cranial Endocast of Hyopsodus (Mammalia, "Condylarthra"): A Case of Paleogene Terrestrial Echolocation? PLoS One 7(2): e30000. https://doi.org/10.1371/journal.pone.0030000

Orliac MJ, Gilissen E (2012) Virtual endocranial cast of earliest Eocene Diacodexis (Artiodactyla, Mammalia) and morphological diversity of early artiodactyl brains. Proc R Soc B Biol Sci 279(1743): 3670–3677. https://doi.org/10.1098/rspb.2012.1156

Orliac MJ, Ladevèze S, Gingerich PD, Lebrun R, Smith T (2014) Endocranial morphology of Palaeocene Plesiadapis tricuspidens and evolution of the early primate brain. Proc R Soc B Biol Sci 281(1781). https://doi.org/10.1098/rspb.2013.2792

Orlov YA (ed) (1961) В мире древних животных (In the ancient animal kingdom). Publishing House of the

Academy of Sciences of the USSR, Moscow, 192 p

Palermo EC (2013) Anatomy of the periorbital region. Surg Cosmet Dermatol 5(3): 245–256

Paradis E, Claude J, Strimmer K (2004) APE: Analyses of Phylogenetics and Evolution in R language. Bioinformatics 20(2): 289–290. https://doi.org/10.1093/bioinformatics/btg412

Patterson BD, Webala PW, Lavery TH, Agwanda BR, Goodman SM, Kerbis Peterhans JC, Demos TC (2020) Evolutionary relationships and population genetics of the Afrotropical leaf-nosed bats (Chiroptera, Hipposideridae). Zookeys 929: 117–161. https://doi.org/10.3897/zookeys.929.50240

Paulin MG (1993) The Role of the Cerebellum in Motor Control and Perception. Brain Behav Evol 41(1): 39–50. https://doi.org/10.1159/000113822

Pearson K (1895) VII. Note on regression and inheritance in the case of two parents. Proc R Soc London 58(350): 240–242. https://doi.org/10.1098/RSPL.1895.0041

Pennell MW, Harmon LJ (2013) An integrative view of phylogenetic comparative methods: connections to population genetics, community ecology, and paleobiology. Ann N Y Acad Sci 1289(1): 90–105. https://doi.org/10.1111/NYAS.12157

Pennell MW, Eastman JM, Slater GJ, Brown JW, Uyeda JC, FitzJohn RG, Alfaro ME, Harmon LJ (2014) geiger v2.0: an expanded suite of methods for fitting macroevolutionary models to phylogenetic trees. Bioinformatics 30(15): 2216–2218. https://doi.org/10.1093/BIOINFORMATICS/BTU181

Pennell MW, FitzJohn RG, Cornwell WK, Harmon LJ (2015) Model Adequacy and the Macroevolution of Angiosperm Functional Traits. https://doi.org/101086/682022 186(2): E33–E50. https://doi.org/10.1086/682022

Pettigrew JD, Jamieson BG, Robson SK, Hall LS, McAnally KI, Cooper HM (1989) Phylogenetic relations between microbats, megabats and primates (Mammalia: Chiroptera and Primates). Philos Trans R Soc Lond B Biol Sci 325(1229): 489–559. https://doi.org/10.1098/rstb.1989.0102

Pigache RM (1970) The Anatomy of “Paleocortex.” Springer-Verlag, Berlin, Heidelberg, 66 p

Pilleri G, Gihr M, Kraus C (1984) Cephalization in rodents with particular reference to the Canadian beaver (Castor canadensis). In: Pilleri G (ed) Investigations on Beavers. Brain Anatomy Institute, Bern, pp 11–102

Pirlot P, Stephan H (1970) Encephalization in Chiroptera. Can J Zool 48(3): 433–444. https://doi.org/10.1139/z70-075

Pirlot P, Jolicoeur P (1982) Correlations between major brain regions in chiroptera. Brain Behav Evol 20(3–4): 172–181. https://doi.org/10.1159/000121589

Pitnick S, Jones KE, Wilkinson GS (2006) Mating system and brain size in bats. Proc R Soc B Biol Sci 273(1587): 719–724. https://doi.org/10.1098/rspb.2005.3367

Profico A, Piras P, Buzi C, Di Vincenzo F, Lattarini F, Melchionna M, Veneziano A, Raia P, Manzi G (2017) The evolution of cranial base and face in Cercopithecoidea and Hominoidea: Modularity and morphological integration. Am J Primatol 79(12): 1–12. https://doi.org/10.1002/ajp.22721

R Core Team (2020) R: A Language and Environment for Statistical Computing. V 4.0.2

Radinsky LB (1978) Evolution of Brain Size in Carnivores and Ungulates. Am Nat 112(987): 815–831. https://doi.org/10.1086/283325

Radinsky LB (1981) Brain Evolution in Extinct South American Ungulates. Brain Behav Evol 18(4): 169–187. https://doi.org/10.1159/000121785

Radtke-Schuller S, Fenzl T, Peremans H, Schuller G, Firzlaff U (2020) Cyto- and myeloarchitectural brain atlas of the pale spear-nosed bat (Phyllostomus discolor) in CT Aided Stereotaxic Coordinates. Brain Struct Funct 225(8): 2509–2520. https://doi.org/10.1007/s00429-020-02138-y

Raghavan R, Lawton W, Ranjan SR, Viswanathan RR (1997) A continuum mechanics-based model for cortical

growth. J Theor Biol 187(2): 285–296. https://doi.org/10.1006/jtbi.1997.0450

Rambold H, Churchland A, Selig Y, Jasmin L, Lisberger SG (2002) Partial Ablations of the Flocculus and Ventral Paraflocculus in Monkeys Cause Linked Deficits in Smooth Pursuit Eye Movements and Adaptive Modification of the VOR. J Neurophysiol 87(2): 912–924. https://doi.org/10.1152/jn.00768.2000

Ramdarshan A, Orliac MJ (2016) Endocranial morphology of Microchoerus erinaceus (Euprimates, Tarsiiformes) and early evolution of the Euprimates brain. Am J Phys Anthropol 159(1): 5–16. https://doi.org/10.1002/ajpa.22868

Ratcliffe JM, Fenton MB, Shettleworth SJ (2006) Behavioral flexibility positively correlated with relative brain volume in predatory bats. Brain Behav Evol 67(3): 165–176. https://doi.org/10.1159/000090980

Ravel A, Orliac MJ (2015) The inner ear morphology of the 'condylarthran' Hyopsodus lepidus. Hist Biol 27(8): 957–969. https://doi.org/10.1080/08912963.2014.915823

Ravel A, Adaci M, Bensalah M, Charruault A-L, Essid EM, Ammar HK, Marzougui W, Mahboubi M, Mebrouk F, Merzeraud G, Vianey-Liaud M, Tabuce R, Marivaux L (2016) Origine et radiation initiale des chauves-souris modernes : nouvelles découvertes dans l'Éocène d'Afrique du Nord. Geodiversitas 38(3): 355–434. https://doi.org/10.5252/g2016n3a3

Reep RL, Bhatnagar KP (2000) Brain ontogeny and ecomorphology in bats. In: Adams RA, Pedersen SC (eds) Ontogeny, Functional Ecology, and Evolution of Bats. Cambridge University Press, New York, pp 93–136

Regnault S, Fahn-Lai P, Norris RM, Pierce SE Shoulder Muscle Architecture in the Echidna (Monotremata: Tachyglossus aculeatus) Indicates Conserved Functional Properties. https://doi.org/10.1007/s10914-020-09498-6

Reinhard KR, Miller ME, Evans HE (1962) The craniovertebral veins and sinuses of the dog. Am J Anat 111(1): 67–87. https://doi.org/10.1002/aja.1001110106

Revell LJ (2012) phytools: an R package for phylogenetic comparative biology (and other things). Methods Ecol Evol 3(2): 217–223. https://doi.org/10.1111/J.2041-210X.2011.00169.X

Revilliod P (1917) Contribution à l'étude des Chiroptères des terrains tertiaires (1ère partie). Mémoires la Société Paléontologique Suisse 43: 1–60

Revilliod P (1920) Contribution à l'étude des Chiroptères des terrains tertiaires (2ème partie). Mémoires la Société Paléontologique Suisse 44: 61–130

Richtsmeier JT, Flaherty K (2013) Hand in glove: brain and skull in development and dysmorphogenesis. Acta Neuropathol 125(4): 469–489. https://doi.org/10.1007/s00401-013-1104-y

Robertson A (ed) (1828) Conversations on Anatomy, Physiology, and Surgery. Volume 2. Towar & Hogan, Philadelphia, 467 p

Rohlf FJ (2001) Comparative methods for the analysis of continuous variables: Geometric interpretations. Evolution 55(11): 2143–2160. https://doi.org/10.1111/j.0014-3820.2001.tb00731.x

Rojas D, Warsi OM, Dávalos LM (2016) Bats (Chiroptera: Noctilionoidea) Challenge a Recent Origin of Extant Neotropical Diversity. Syst Biol 65(3): 432–448. https://doi.org/10.1093/SYSBIO/SYW011

Ross CF, Ravosa MJ (1993) Basicranial flexion, relative brain size, and facial kyphosis in nonhuman primates. Am J Phys Anthropol 91(3): 305–324. https://doi.org/10.1002/ajpa.1330910306

Rougier GW, Wible JR, Hopson JA (1992) Reconstruction of the cranial vessels in the Early Cretaceous mammal Vincelestes Neuquenianus: Implications for the evolution of the mammalian cranial vascular system. J Vertebr Paleontol 12(2): 188–216. https://doi.org/10.1080/02724634.1992.10011449

Rowe TB, Macrini TE, Luo Z-X (2011) Fossil Evidence on Origin of the Mammalian Brain. Science 332(6032): 955–957. https://doi.org/10.1126/science.1203117

Royer-Carenzi M, Didier G (2016) A comparison of ancestral state reconstruction methods for quantitative

characters. J Theor Biol 404: 126–142. https://doi.org/10.1016/j.jtbi.2016.05.029

Royston P (1995) Remark AS R94: A Remark on Algorithm AS 181: The W-test for Normality. Appl Stat 44(4): 547. https://doi.org/10.2307/2986146

RStudio Team (2016) RStudio: Integrated Development Environment for R. V 1.1.453

Ruedi M (2019) Family Cistugidae (Wing-gland Bats). In: Wilson DE, Mittermeier RA (eds) Handbook of the Mammals of the World – Volume 9 Bats. Lynx Edicions, Barcelona, pp 710–715

Safi K, Dechmann DKN (2005) Adaptation of brain regions to habitat complexity : a comparative analysis in bats (Chiroptera). Proc R Soc B 272: 179–186

Safi K, Seid MA, Dechmann DKN (2005) Bigger is not always better: when brains get smaller. Biol Lett 1(3): 283–286. https://doi.org/10.1098/rsbl.2005.0333

Sansalone G, Bertè DF, Maiorino L, Pandolfi L (2015) Evolutionary trends and stasis in carnassial teeth of European Pleistocene wolf Canis lupus (Mammalia, Canidae). Quat Sci Rev 110: 36–48. https://doi.org/10.1016/j.quascirev.2014.12.009

Sansalone G, Allen K, Ledogar JA, Ledogar S, Mitchell DR, Profico A, Castiglione S, Melchionna M, Serio C, Mondanaro A, Raia P, Wroe S (2020) Variation in the strength of allometry drives rates of evolution in primate brain shape. Proc R Soc B Biol Sci 287(1930). https://doi.org/10.1098/rspb.2020.0807

Sansom RS, Choate PG, Keating JN, Randle E (2018) Parsimony, not Bayesian analysis, recovers more stratigraphically congruent phylogenetic trees. Biol Lett 14(6): 20180263. https://doi.org/10.1098/rsbl.2018.0263

Santana SE, Grosse IR, Dumont ER (2012) Dietary hardness, loading behavior, and the evolution of skull form in bats. Evolution 66(8): 2587–2598. https://doi.org/10.1111/j.1558-5646.2012.01615.x

Scalia F, Rasweiler IV JJ, Scalia J, Orman R, Stewart M (eds) (2013) Forebrain Atlas of the Short-tailed Fruit Bat, Carollia perspicillata. Springer, New York, NY, 65 p

Schauberger P, Walker A (2020) openxlsx: Read, Write and Edit xlsx Files. V 4.2.3

Schlosser G (2017) From so simple a beginning –What amphioxus can teach us about placode evolution. Int J Dev Biol 61(10–12): 633–648. https://doi.org/10.1387/ijdb.170127gs

Schluter D, Price T, Mooers A, Ludwig D (1997) Likelihood of ancestor states in adaptive radiation. Evolution 51(6): 1699–1711. https://doi.org/10.1111/j.1558-5646.1997.tb05095.x

Schneider CA, Rasband WS, Eliceiri KW (2012) NIH Image to ImageJ: 25 years of image analysis. Nat Methods 9(7): 671–675. https://doi.org/10.1038/nmeth.2089

Schneider R (1957) Morphologische Untersuchungen am Gehirn der Chiroptera (Mammalia). Abhandlungen der Senckenbergischen Naturforschenden Gesellschaft 495:1–92

Schneider R (1966) Das Gehirn von Rousettus Aegyptiacus (E. GEOFFROY 1810) (Megachiroptera, Chiroptera, Mammalia). Ein mit Hilfe mehrerer Schnittserien erstellter Atlas. Abhandlungen der Senckenbergischen Naturforschenden Gesellschaft 513: 1–160

Segall M, Cornette R, Rasmussen AR, Raxworthy CJ (2021) Inside the head of snakes: influence of size, phylogeny, and sensory ecology on endocranium morphology. Brain Struct Funct 226(7): 2401–2415. https://doi.org/10.1007/s00429-021-02340-6

Serio C, Castiglione S, Tesone G, Piccolo M, Melchionna M, Mondanaro A, Di Febbraro M, Raia P (2019) Macroevolution of Toothed Whales Exceptional Relative Brain Size. Evol Biol 46(4): 332–342. https://doi.org/10.1007/s11692-019-09485-7

Shapiro SS, Wilk MB (1965) An analysis of variance test for normality (complete samples). Biometrika 52(3–4): 591–611. https://doi.org/10.1093/biomet/52.3-4.591

Shi JJ, Rabosky DL (2015) Speciation dynamics during the global radiation of extant bats. Evolution 69(6): 1528–

1545. https://doi.org/10.1111/evo.12681

Shi JJ, Westeen EP, Rabosky DL (2018) Digitizing extant bat diversity : An open-access repository of 3D μ CT-scanned skulls for research and education. PLoS One 13(9): 1–13. https://doi.org/10.5061/dryad.f5df5nk.Funding

Sigé B (1968) Les Chiroptères du Miocène inférieur de Bouzigues. 1- Etude systématique. Palaeovertebrata 1(3): 65–133. https://doi.org/10.18563/pv.1.3.65-133

Sigé B, Crochet J-Y, Sudre J, Aguilar J-P, Escarguel G (1997) Nouveaux sites d'âges variés dans les remplissages karstiques du Miocène inférieur de Bouzigues (Hérault, Sud de la France). Geobios 30(Supplement 1): 477–483. https://doi.org/10.1016/S0016-6995(97)80054-X

Silbergleit R, Quint DJ, Mehta BA, Patel SC, Metes JJ, Noujaim SE (2000) The persistent stapedial artery. Am J Neuroradiol 21(3): 572–577

Simmons NB, Geisler JH (1998) Phylogenetic relationships of Icaronycteris, Archaeonycteris, Hassianycteris, and Palaeochiropteryx to extant bat lineages, with comments on the evolution of echolocation and foraging strategies in Microchiroptera. Bull Am Museum Nat Hist 1998(235): 1–182

Simmons NB (2000) Bat phylogeny: an evolutionary context for comparative studies. In: Adams RA, Pedersen SC (eds) Ontogeny, Functional Ecology, and Evolution of Bats. Cambridge University Press, pp 9–58

Simmons NB (2005) Chiroptera. In: Rose KD, Archibald JD (eds) The Rise of Placental Mammals. John Hopkins University Press, Baltimore, pp 159–174

Simmons NB, Seymour KL, Habersetzer J, Gunnell GF (2008) Primitive Early Eocene bat from Wyoming and the evolution of flight and echolocation. Nature 451(7180): 818–821. https://doi.org/10.1038/nature06549

Simmons NB, Seymour KL, Habersetzer J, Gunnell GF (2010) Inferring echolocation in ancient bats. Nature 466(7309): 8–9. https://doi.org/10.1038/nature09219

Slater GJ, Price SA, Santini F, Alfaro ME (2010) Diversity versus disparity and the radiation of modern cetaceans. Proc R Soc B Biol Sci 277(1697): 3097–3104. https://doi.org/10.1098/rspb.2010.0408

Smaers JB, Mongle CS, Kandler A (2016) A multiple variance Brownian motion framework for estimating variable rates and inferring ancestral states. Biol J Linn Soc 118(1): 78–94. https://doi.org/10.1111/BIJ.12765

Smaers JB, Dechmann DKN, Goswami A, Soligo C, Safi K (2012) Comparative analyses of evolutionary rates reveal different pathways to encephalization in bats, carnivorans, and primates. Proc Natl Acad Sci 109(44): 18006–18011. https://doi.org/10.1073/pnas.1212181109

Smaers JB, Mongle CS (2017) On the accuracy and theoretical underpinnings of the multiple variance Brownian motion approach for estimating variable rates and inferring ancestral states. Biol J Linn Soc 121(1): 229–238. https://doi.org/10.1093/BIOLINNEAN/BLX003

Smaers JB, Rothman RS, Hudson DR, et al (2021) The evolution of mammalian brain size. Sci Adv 7(18): eabe2101. https://doi.org/10.1126/sciadv.abe2101

Smith BB (1925) Forecasting the Acreage of Cotton. J Am Stat Assoc 20(149): 31–47. https://doi.org/10.2307/2277432

Smith BB (ed) (1926) Correlation Theory and Method Applied to Agricultural Research. U.S. Department of Agriculture, Bureau of Agricultural Economics, Washington, D.C., 101 p

Smith GE (1902a) On the Homologies of the Cerebral Sulci. J Anat Physiol 36(Pt 3): 309–319

Smith GE (1902b) The Primary Subdivision of the Mammalian Cerebellum. J Anat Physiol 36(Pt 4): 381–5

Smith GE (1903) On the Morphology of the Brain in the Mammalia, with Special Reference to that of the Lemurs, Recent and Extinct. Trans Linn Soc London 2nd Ser Zool 8(10): 319–432. https://doi.org/10.1111/j.1096-3642.1903.tb00497.x

Smith JD (1970) Comments on flight and the evolution of bats. In: Hecht MK, Goody PC, Hecht BM (eds) Major

Patterns in Vertebrate Evolution. Springer US, Boston, MA, pp 427–437

Smith JD (1976) Chiropteran evolution. In: Baker RJ, Knox Jones Jr. J, Carter DC (eds) Biology of the Bats of the New World Family Phyllostomidae, Part I. Texas Tech Press, Lubbock, Texas, pp 49–69

Smith RJ (1993) Logarithmic transformation bias in allometry. Am J Phys Anthropol 90(2): 215–228. https://doi.org/10.1002/ajpa.1330900208

Smith T, Habersetzer J, Simmons NB, Gunnell GF (2012) Systematics and paleobiogeography of early bats. In: Gunnell GF, Simmons NB (eds) Evolutionary History of Bats. Cambridge University Press, Cambridge, pp 23–66

Smith TD, DeLeon VB, Eiting TP, Corbin HM, Bhatnagar KP, Santana SE (2021) Venous networks in the upper airways of bats: A histological and <scp>diceCT</scp> study. Anat Rec Special Issue: 1–21. https://doi.org/10.1002/ar.24762

Sohn JH, Fukui D, Nojiri T, Minowa K, Kimura J, Koyabu D (2020) Three-Dimensional and Histological Observations on Male Genital Organs of Greater Horseshoe Bat, Rhinolophus ferrumequinum. J Mamm Evol 28(2): 559–571. https://doi.org/10.1007/S10914-020-09525-6

Soisook P, Prajakjitr A, Karapan S, Francis CM, Bates PJJ (2015) A new genus and species of false vampire (Chiroptera: Megadermatidae) from peninsular Thailand. Zootaxa 3931(4): 528. https://doi.org/10.11646/zootaxa.3931.4.4

Solari S, Medellín RA, Rodríguez-Herrera B, Dumont E, Burneo S, Tavares V da C, Garbino GST, Camacho MA, Saá DGT, Lim BK, Arroyo-Cabrales J, Rodríguez-Durán A, Aguirre LF, Tschapka M, Espinosa-Martínez D V. (2019) Family Phyllostomidae (New World Leaf-Nosed Bats). In: Wilson DE, Mittermeier RA (eds) Handbook of the Mammals of the World – Volume 9 Bats. Lynx Edicions, Barcelona, pp 444–583

Spoor F, Zonneveld F (1998) Comparative review of the human bony labyrinth. Am J Phys Anthropol Suppl 27: 211–251. https://doi.org/10.1002/(SICI)1096-8644(1998)107:27+<211::AID-AJPA8>3.0.CO;2-V

Standring S (ed) (2016) Gray's Anatomy, 41th edn. Elsevier Health Sciences, London, 1584 p

Steel M, Penny D (2000) Parsimony, likelihood, and the role of models in molecular phylogenetics. Mol. Biol. Evol. 17:839–850

Stephan H, Bauchot R (1959) Le cerveau de Galemys pyrenaicus Geoffroy, 1811 (Insectivora, Talpidae) et ses modifications dans l'adaptation à la vie aquatique. Mammalia 23(1): 1–18. https://doi.org/10.1515/mamm.1959.23.1.1

Stephan H, Pirlot P (1970) Volumetric Comparisons of Brain Structures in Bats. J Zool Syst Evol Res 8(1): 200–236. https://doi.org/10.1111/j.1439-0469.1970.tb00876.x

Stephan H, Nelson JE, Frahm HD (1981) Brain size comparison in Chiroptera. J Zool Syst Evol Res 19(3): 195–222. https://doi.org/10.1111/j.1439-0469.1981.tb00239.x

Steven DH (1964) The distribution of external and internal ophthalmic arteries in the ox. J Anat 98(3): 429–435

Stockwell EF (2001) Morphology and flight manoeuvrability in New World leaf-nosed bats (Chiroptera: Phyllostomidae). J Zool 254(4): 505–514. https://doi.org/10.1017/S0952836901001005

Strausfeld NJ, Ma X, Edgecombe GD, Fortey RA, Land MF, Liu Y, Cong P, Hou X (2016) Arthropod eyes: The early Cambrian fossil record and divergent evolution of visual systems. Arthropod Struct Dev 45(2): 152–172. https://doi.org/10.1016/J.ASD.2015.07.005

"Student" (1908) The probable error of a mean. Biometrika 6(1): 1–25. https://doi.org/10.1093/biomet/6.1.1

Swofford DL, Maddison WP (1987) Reconstructing ancestral character states under Wagner parsimony. Math Biosci 87(2): 199–229. https://doi.org/10.1016/0025-5564(87)90074-5

Tandler J (1899) Zur vergleichenden Anatomie der Kopfarterien bei den Mammalia. Denkschriften der Kaiserlichen Akademie der Wissenschaften, Mathematisch-Naturwissenschaftliche Klasse 67: 677–784

Teeling EC, Madsen O, Van Den Bussche RA, De Jong WW, Stanhope MJ, Springer MS (2002) Microbat paraphyly and the convergent evolution of a key innovation in old world rhinolophoid microbats. Proc Natl Acad Sci U S A 99(3): 1431–1436. https://doi.org/10.1073/pnas.022477199

Tejedor A (2011) Systematics of Funnel-Eared Bats (Chiroptera: Natalidae). Bull Am Museum Nat Hist 2011(353): 1–140. https://doi.org/10.1206/636.1

Thiagavel J, Cechetto C, Santana SE, Jakobsen L, Warrant EJ, Ratcliffe JM (2018) Auditory opportunity and visual constraint enabled the evolution of echolocation in bats. Nat Commun 9(1). https://doi.org/10.1038/s41467-017-02532-x

Tomasi TE (1979) Echolocation by the Short-Tailed Shrew Blarina brevicauda. J Mammal 60(4): 751–759. https://doi.org/10.2307/1380190

Toth C (2019) Family Mystacinidae (New Zealand Short-tailed Bats). In: Wilson DE, Mittermeier RA (eds) Handbook of the Mammals of the World – Volume 9 Bats. Lynx Edicions, Barcelona, pp 394–403

van Dongen PAM (1998) Brain Size in Vertebrates. In: Nieuwenhuys R, ten Donkelaar HJ, Nicholson C (eds) The Central Nervous System of Vertebrates. Springer Berlin Heidelberg, Berlin, Heidelberg, pp 2099–2134

Van Valen L (1979) The evolution of bats. Evol Theory 4(3): 103–121

Veselka N, McErlain DD, Holdsworth DW, Eger JL, Chhem RK, Mason MJ, Brain KL, Faure PA, Fenton MB (2010) A bony connection signals laryngeal echolocation in bats. Nature 463(7283): 939–942. https://doi.org/10.1038/nature08737

Voeten DFAE, Reich T, Araújo R, Scheyer TM (2018) Synchrotron microtomography of a Nothosaurus marchicus skull informs on nothosaurian physiology and neurosensory adaptations in early Sauropterygia. PLoS One 13(1): e0188509. https://doi.org/10.1371/JOURNAL.PONE.0188509

Voogd J, Nieuwenhuys R, van Dongen PAM, ten Donkelaar HJ (1998) Mammals. In: Nieuwenhuys R, ten Donkelaar HJ, Nicholson C (eds) The Central Nervous System of Vertebrates. Springer Berlin Heidelberg, Berlin, Heidelberg, pp 1637–2097

Washburn SL (1947) The relation of the temporal muscle to the form of the skull. Anat Rec 99(3): 239–248. https://doi.org/10.1002/ar.1090990303

Washington SD, Hamaide J, Jeurissen B, van Steenkiste G, Huysmans T, Sijbers J, Deleye S, Kanwal JS, De Groof G, Liang S, Van Audekerke J, Wenstrup JJ, Van der Linden A, Radtke-Schuller S, Verhoye M (2018) A three-dimensional digital neurological atlas of the mustached bat (Pteronotus parnellii). Neuroimage 183: 300–313. https://doi.org/10.1016/j.neuroimage.2018.08.013

Watanabe A, Gignac PM, Balanoff AM, Green TL, Kley NJ, Norell MA (2019) Are endocasts good proxies for brain size and shape in archosaurs throughout ontogeny? J Anat 234(3): 291–305. https://doi.org/10.1111/joa.12918

Watanabe A, Balanoff AM, Gignac PM, Gold MEL, Norell MA (2021) Novel neuroanatomical integration and scaling define avian brain shape evolution and development. Elife 10: 2021.04.20.440700. https://doi.org/10.7554/eLife.68809

Webster AJ, Purvis A (2002) Testing the accuracy of methods for reconstructing ancestral states of continuous characters. Proc R Soc London Ser B Biol Sci 269(1487): 143–149. https://doi.org/10.1098/rspb.2001.1873

Weisbecker V, Rowe TB, Wroe S, Macrini TE, Garland KLS, Travouillon KJ, Black K, Archer M, Hand SJ, Berlin JC, Beck RMD, Ladevèze S, Sharp AC, Mardon K, Sherratt E (2021) Global elongation and high shape flexibility as an evolutionary hypothesis of accommodating mammalian brains into skulls. Evolution: evo.14163. https://doi.org/10.1111/evo.14163

Welch BL (1947) The generalisation of student's problems when several different population variances are involved. Biometrika 34(1–2): 28–35. https://doi.org/10.1093/biomet/34.1-2.28

Welker W (1990) Why Does Cerebral Cortex Fissure and Fold? In: Jones EG, Peters A (eds) Cerebral Cortex:

Volume 8B: Comparative structure and evolution of cerebral cortex, Part 2. Plenum Press, New York, pp 3–136

Wenger Y, Galliot B (2013) Punctuated Emergences of Genetic and Phenotypic Innovations in Eumetazoan, Bilaterian, Euteleostome, and Hominidae Ancestors. Genome Biol Evol 5(10): 1949–1968. https://doi.org/10.1093/GBE/EVT142

Weppe R, Blondel C, Vianey-Liaud M, Pélissié T, Orliac MJ (2020) A new Cainotherioidea (Mammalia, Artiodactyla) from Palembert (Quercy, SW France): Phylogenetic relationships and evolutionary history of the dental pattern of Cainotheriidae. Palaeontol Electron 23(3): 1–20. https://doi.org/10.26879/1081

Wible JR (1983) The internal carotid artery in early Eutherians. Acta Palaeontol Pol 28(1): 281–293

Wible JR (1987) The eutherian stapedial artery: character analysis and implications for superordinal relationships. Zool J Linn Soc 91(2): 107–135. https://doi.org/10.1111/j.1096-3642.1987.tb01725.x

Wible JR (1993) Cranial circulation and relationships of the Colugo Cynocephalus (Dermoptera, Mammalia). Am Museum Novit (3072): 27

Wible JR, Zeller U (1994) Cranial circulation of the pen-tailed tree shrew Ptilocercus lowii and relationships of Scandentia. J Mamm Evol 2(4): 209–230. https://doi.org/10.1007/BF01464275

Wible JR, Davis DL (2000) Ontogeny of the chiropteran basicranium, with reference to the Indian false vampire bat, Megaderma lyra. In: Adams RA, Pedersen SC (eds) Ontogeny, Functional Ecology, and Evolution of Bats. Cambridge University Press, New York, pp 214–246

Wible JR (2010) Petrosal anatomy of the nine-banded armadillo, Dasypus novemcinctus Linnaeus, 1758 (Mammalia, Xenarthra, Dasypodidae). Ann Carnegie Museum 79(1): 1–28. https://doi.org/10.2992/007.079.0101

Wible JR (2011) On the treeshrew skull (Mammalia, Placentalia, Scandentia). Ann Carnegie Museum 79(3): 149–230. https://doi.org/10.2992/007.079.0301

Wible JR (2012) The Ear Region of the Aardvark, Orycteropus afer (Pallas, 1766) (Mammalia, Placentalia, Tubulidentata). Ann Carnegie Museum 80(2): 115–146. https://doi.org/10.2992/007.080.0202

Wilcoxon F (1945) Individual Comparisons by Ranking Methods. Biometrics Bull 1(6): 80. https://doi.org/10.2307/3001968

Wilson DE, Mittermeier RA (eds) (2019) Handbook of the Mammals of the World – Volume 9 Bats. Lynx Edicions, Barcelona, 1008 p

Wilson LAB, Hand SJ, López-Aguirre C, Archer M, Black KH, Beck RMD, Armstrong KN, Wroe S (2016) Cranial shape variation and phylogenetic relationships of extinct and extant Old World leaf-nosed bats. Alcheringa An Australas J Palaeontol 40(4): 509–524. https://doi.org/10.1080/03115518.2016.1196434

Witmer LM, Ridgely RC, Dufeau DL, Semones MC (2008) Using CT to Peer into the Past: 3D Visualization of the Brain and Ear Regions of Birds, Crocodiles, and Nonavian Dinosaurs. In: Endo H, Frey R (eds) Anatomical Imaging. Springer Japan, Tokyo, pp 67–87

Woodhead J, Hand SJ, Archer M, Graham I, Sniderman K, Arena DA, Black KH, Godthelp H, Creaser P, Price E (2016) Developing a radiometrically-dated chronologic sequence for Neogene biotic change in Australia, from the Riversleigh World Heritage Area of Queensland. Gondwana Res 29(1): 153–167. https://doi.org/10.1016/j.gr.2014.10.004

Wright S (1921) Correlation aud Causation. J Agric Res 20: 557–585

Yao L, Brown J-P, Stampanoni M, Marone F, Isler K, Martin RD (2012) Evolutionary Change in the Brain Size of Bats. Brain Behav Evol 80(1): 15–25. https://doi.org/10.1159/000338324

Young GC (2008) Early Evolution of the Vertebrate Eye—Fossil Evidence. Evol Educ Outreach 1(4): 427–438. https://doi.org/10.1007/s12052-008-0087-y

Zhaoping L (2016) From the optic tectum to the primary visual cortex: migration through evolution of the saliency map for exogenous attentional guidance. Curr Opin Neurobiol 40: 94–102. https://doi.org/10.1016/J.CONB.2016.06.017

Appendices

All appendices are stored as a .zip archive file that is available following this link: https://sharedby.blomp.com/H0p5LL

This archive is protected by a password that can be requested to the author by e-mail (scholar email jacob.maugoust@umontpellier.fr to be preferentially used, otherwise personal email jmaugoust@free.fr if scholar email is deprecated).

Remerciements

Je remercie en premier lieu ma mère, qui a bien voulu m'abonner quand j'avais une dizaine d'années à une collection de cartes et de fiches - ce genre de collection qui coûte 2€ la première fois, puis grimpe vite - et dont un des premiers "cadeaux" était le DVD de "Sur la Terre des Dinosaures" de la BBC. Ce film a été un déclic pour moi. Je me fichais pas mal des dinosaures en eux-mêmes ; ce qui me passionnait de voir, c'était les changements entre bestioles selon les moments, les adaptations au milieu etc. Par la suite, j'ai découvert successivement les deux autres volets de la trilogie "Sur la Terre de…". D'abord, "Sur la Terre des Géants", focalisant sur le Paléozoïque, que j'ai dévoré dès qu'il est sorti. Ce film était incroyable : on voyait les *Haikouichthys* se "transformer" petit à petit, développant des nageoires, puis des pattes etc. J'ai dévoré "Sur la Terre des Monstres Disparus", et j'ai découvert un aperçu de l'histoire évolutive des mammifères. C'est peut-être un biais empathique et/ou phylogénétique, mais j'ai alors su que je voulais étudier les mammifères. J'ai rapidement communiqué à mes parents mes désirs futurs de paléontologie, que tous deux ont immédiatement supporté et compris. J'ai ensuite découvert les parcours possibles et j'ai tracé mon avenir : bac scientifique, licence à Montpellier, master paléontologie à Poitiers et Montpellier, puis thèse. J'ai cadré mon futur jusqu'à mes 25 ans, et ma famille en général (plus directement mes parents) m'ont accompagné dans ce petit périple, toujours en m'encourageant et en mettant à disposition les moyens nécessaires pour que j'y arrive. Donc pour commencer, merci à mes parents Suzanne et Bernard, merci à ma famille en général (Ilana, Nicolas, Hélène, Philippe, mais aussi mon parrain Pierre, sa femme Roselyne, ma marraine Charlotte, et son mari 'Benny'). Et un peu merci à la BBC aussi d'avoir fait ces trois films.

Viennent ensuite des personnes que j'ai rencontrées et qui m'ont toujours soutenu, directement ou indirectement. Je n'ai gardé que peu de liens avec ma scolarité anté-bac, donc ça se limite à deux personnes. Chronologiquement vient d'abord mon bro Rémi, que j'ai rencontré en seconde, que j'ai vu et à qui j'ai parlé de manière variable durant les années, mais qui a toujours été là et qui l'est toujours. Il a lui aussi réussi dans son chemin pour devenir archi-ingé (quel BG), sans oublier de m'aider. Quand il était en licence à Montpellier, pour me servir de taxi pour des corvées quotidiennes. Pour me déménager à Poitiers. Pour m'avoir, tout récemment, déménagé en banlieue toulousaine. Et pour m'héberger actuellement, petit chômeur en bout de thèse que je suis. Et pour s'être intéressé à quelque chose qui lui est bien lointain. Donc merci pour tout ça. Est arrivée ensuite Gabrielle, en terminale, celle qui partage ma vie, sans qui tout prend un teint plus fade, et qui m'épaule en permanence. Cela fait donc huit ans qu'elle me supporte, qu'elle m'améliore, qu'elle m'encourage, et qu'elle me rend heureux. S'il y a un CDI que je devais signer, ce serait celui là.

A l'université, j'ai mieux découvert ce qu'était la biologie et la géologie, ainsi que la paléontologie, par petites touches, sans jamais que mon intérêt s'effrite. Donc d'abord, merci aux enseignants qui ont su faire perdurer la flamme qui m'animait avant d'entrer à la face, en L1 Sylvain en amphi et Fabrice en TP (qui m'a d'ailleurs conseillé le parcours à choisir en licence), puis Pierre-Olivier et Guillaume en L3. Après cela, le master a été assez particulier (le contexte, l'éloignement des proches, un tout autre niveau scolaire requis), mais la promo du master était incroyable, les deux années ont été vraiment top. Surtout le M1 : à Poitiers, il faut se serrer les coudes et bien s'entendre, sinon c'est l'ennui assuré.

J'ai pu m'y faire un binôme, Romain, dont je n'arrive pas à me dépêtrer puisqu'il a réussi à me suivre en thèse. Il est limité (il supporte l'OL), mais il est gentil. On s'est bien serré les coudes et encouragé dès le M1, on a fait notre stage d'entre-deux entre le M1 et le M2 ensemble, le M2 quasiment ensemble, et là il a fallu bien s'entraider et se pousser vers le haut pour décrocher le graal (du point de vue d'un étudiant). Donc bon merci pour tout ce qui concerne le taf et tout ce qui ne le concerne pas, ça a été mon partenaire d'aventure pendant cinq ans, ça s'oubliera pas et je pourrai bien venir l'embêter (restons poli) quand lui aussi finira sa thèse !

J'ai aussi pu rencontrer deux personnes qui ont façonné les prémisses de ma carrière de paléontologue (en espérant que carrière il y ait). D'abord Pierre-Olivier, qui m'a tout doucement fait entrer "dans le game", et ce fut un réel plaisir. D'abord en L3, puis avec force encouragements dès le M1. Et ensuite Maëva, qui nous a encadrés Romain et moi pendant le stage de M2, puis qui a décidé de poursuivre le délire un bon trois ans en plus. Professionnellement et personnellement, elle m'a beaucoup appris et fait grandir en quelques années ; pour ces deux points, je lui suis donc infiniment reconnaissant. J'espère pouvoir un jour lui rendre la pareille d'une manière ou d'une autre si j'arrive à m'établir dans la recherche. Par plaisir, plus que par "dette".

Et puis il y a aussi les personnes qui ont gravité autour à partir du moment où j'ai été à l'ISEM de plus en plus longtemps. Je pense d'abord, bien évidemment, à l'équipe de paléonto - les enseignants-chercheurs à qui j'ai eu affaire en premier lieu, et les chercheurs par la suite - qui fournit un cadre de travail vraiment idéal (en tout cas, avec ce qu'il est possible de faire). J'ai une grande appréhension de ce que peut être une autre équipe, je vois difficilement comment faire mieux. Spéciale dédicace à Lolo, voisin de bureau (de face puis mitoyen) et collègue d'heures très matinales. Merci à lui puis à Lionel pour la gestion ô combien démocratique et participative de l'équipe. Il y a également les autres étudiants, les collègues d'infortune, avec qui j'ai pu échanger de manière variable. Notamment Alex, lors d'un stage Pôle Emploi, que j'ai pu traumatiser de concert avec Romain (on a pris de ses nouvelles, il va bien). Désormais camarade de thèse, mais également cogneur invétéré en sports de raquettes, et d'une gentillesse sans faille (et notamment tout récemment pour également m'aider à déménager, quitte à y sacrifier une demi nuit). Et puis les autres avec qui j'ai pu plus ou moins discuter de choses plus ou moins en rapport avec la paléonto, avec Mickaël (qui a essuyé pour nous les plâtres de l'encadrement en thèse de Maëva), Quentin, Manon et Narla pour les doctorants en paléonto, Amira, Arthur, Nathan pour les doctorants d'autres thématiques, Quentin, Sérgio et Rémi pour les compets de baby-foot, et j'en oublie probablement…

Enfin, de manière plus formelle merci à l'ISEM en général, qu'il s'agisse de l'ensemble du RDC du bâtiment 22, de la direction, des plateaux techniques, des services administratifs, et de tous ceux, de manière générale, qui oeuvrent pour que de jeunes étudiants tels que je l'ai été puissent s'épanouir complètement et avoir une aussi belle première expérience de la recherche. Merci également aux personnes présentes lors de mes comités de thèse (notamment Franck Guy, Seb Puechmaille pour ses conseils, et Brigitte par deux fois), à ceux qui m'ont accueilli à bras ouvert dans les collections (énorme merci à Emmanuel GIlissen, beaucoup de discussions en plus des collections, et beaucoup d'autres à venir j'espère; merci à Loïc Costeur pour son hospitalité dans le bunker bâlois, merci à Jean-Marc Pons du MNHN, à Aude Bergeret à Montauban), à ceux qui coordonnent les fouilles dans les Quercy d'où bon nombre de mes spécimens proviennent (en tête de gondole, Thierry Pélissié et Gilles Escarguel, récemment largement épaulés par Maëva). Je remercie aussi la plate-forme MRI, pour son micro-tomographe présent à l'ISEM, et plus particulièrement Renaud qui en a la charge. Enfin, toute ma gratitude va aux membres de mon jury pour avoir accepté d'en faire part; merci à Sue Hand et Guillaume Billet d'avoir accepté de rapporter ma thèse (merci également pour tous les échanges en amont que l'on a pu avoir), et merci également à Ted Macrini, John Wible, et Emmanuel Douzery. Et mes sincères excuses à ceux que j'ai pu oublier.

Abstract

The brain is the integrative center of all incoming and outgoing signals of the body. As such, the study of the brain may help to infer the paleobiology of extinct species and to discuss the evolutionary history of eco-functional traits. Bats are outstanding by two extreme traits: active flight and echolocation. Actually, the megabats Pteropodidae are unable to echolocate. In the current phylogenetic framework, this family is sister-taxon to a “microbat” clade. Questions therefore regard the sequence of acquisition of the echolocation (common acquisition for bats and secondary loss in megabats, or convergent acquisitions between “microbat” clades) and of the active flight (flight or echolocation first, or concurrent acquisition of both). Evolution of brain and endocranial characteristics have little been studied in bats. Chiropteran “fossil brains”, accessible as casts of the endocranial cavity (‘endocasts’), have been described during the first half of the XXth century, but with limited techniques; no recent work tackled the question of the evolution of the brain morphology in bats. Recent studies rather focus on the brain mass with extant taxa, proposing a general reduction of the bat brain mass through time. The aim of this thesis is therefore to study the bat endocranial cast using modern techniques, both qualitatively and quantitatively. The study of four fossil endocasts of the family Hipposideridae allows to evaluate the potentialities of the study of the endocranial cast in bats. A first nomenclature of the morphology of the endocast is provided. These comparisons, together with analyses of the encephalization quotient variation through time and of the relative masses of the olfactory bulbs and of the paraflocculi, suggest a general conservatism of brain morphology and size in Hipposideridae. The second part of this thesis aims to generalize the endocast nomenclature to the whole Chiroptera order, the quantitative metrics commonly used in modern paleoneurology are also described and discussed. I propose to use a recently developed phylogenetic comparative method designed to benefit from fossil taxa inclusion. The third part focus on Yinpterochiroptera, dichotomy between a “microbats” Rhinolophoidea, and megabats Pteropodidae. I define discrete anatomical characters of the endocast, and find them moderately congruent with the phylogenetic framework, with potential cases of selection through time. Reconstruction of the evolution of the endocranial shape in the major yinpterochiropteran clades, highlights major differences between rhinolophoids and pteropodids and between rhinolophoid families. Analyses of the evolution of relative neural masses drastically change when fossils are included. A general increase of relative brain size is found, contradicting neontological scenarios; on the other hand, olfactory bulbs and paraflocculi relative masses decrease with time. Previously proposed ecological correlates to these relative neural masses are weakly supported, suggesting more complexity than a direct causality. The fourth part regards the whole Chiroptera order level. I describe the first endocranial cast of a stem bat species; it is a typical bat in its morphology, supporting the hypothesis of a common acquisition of echolocation in bats. Its inclusion to the ordinal picture generally confirms hypotheses proposed in the third part, both regarding morphological and relative neural masses evolution. As a general summary, this work constitutes a first step towards bats endocasts study. The correspondences between the endocast morphology and the disposition of soft tissues in the braincase remain to be assessed, other methodologies can be applied (and compared), and inclusion of other fossil taxa should greatly enhance the very first picture of the evolution of the bat brain proposed here.

Keywords

Brain – Mammalia – Phylogeny – µCT-scan – Paleobiology

Résumé

Le cerveau est le centre d'intégration de tous les signaux entrants et sortants du corps. Son étude peut aider à déduire la paléobiologie des espèces éteintes et à discuter de l'histoire évolutive des traits éco-fonctionnels. Les chauves-souris présentent deux adaptations extrêmes : le vol actif et l'écholocalisation. En réalité, les mégachiroptères (Pteropodidae) sont incapables d'écholocalisation. Cette famille est pourtant le groupe frère d'un clade de "microchiroptères" (écholocalisatrices). Des questions se posent donc sur la séquence d'acquisition de l'écholocalisation (commune chez les chauves-souris et perte secondaire chez les mégachiroptères, ou convergentes entre clades "microchiroptères") et du vol actif. L'évolution des caractéristiques cérébrales et endocrâniennes a été peu étudiée dans cet ordre. Des "cerveaux fossiles" de chiroptères, moulages de la cavité endocrânienne, ont été décrits au cours du XXe siècle, mais aucun travail récent n'a étudié l'évolution de la morphologie du cerveau chez ce groupe. Les études récentes se concentrent plutôt sur la masse cérébrale des taxons actuels, et proposent une réduction générale de la masse cérébrale des chauves-souris au cours du temps. L'objectif de cette thèse est d'étudier le moulage endocrânien des chauves-souris à l'aide de techniques modernes, tant sur le plan qualitatif que quantitatif. Une première étude du moulage endocrânien de quatre Hipposideridae fossiles permet d'évaluer les potentialités du moulage endocrânien chez les chauves-souris et de fournir une première nomenclature révisée. Ces comparaisons, ainsi que les analyses de la variation du quotient d'encéphalisation au cours du temps et des masses relatives des bulbes olfactifs et des paraflocculi, suggèrent un conservatisme général de la morphologie et de la taille du cerveau chez les Hipposideridae. La deuxième partie généralise la nomenclature de la morphologie des moulages endocrâniens à l'ordre des chiroptères et propose d'utiliser une méthode comparative phylogénétique récente, conçue pour l'inclusion de taxons fossiles. La troisième partie focalise sur les Yinpterochiroptera. Des caractères anatomiques discrets endocrâniens sont définis et s'avèrent modérément congruents avec la phylogénie. L'évolution de la forme endocrânienne des principaux clades yinptérochiroptères met en évidence des différences majeures entre les rhinolophoïdes et les ptéropodidés et entre les familles de rhinolophoïdes. Les résultats des analyses de l'évolution des masses neurales relatives changent radicalement lorsque les fossiles sont inclus. Une augmentation générale de la taille relative du cerveau au cours du temps est trouvée, ce qui contredit les scénarios néontologiques ; alors que les masses relatives des bulbes olfactifs et des paraflocculi diminuent. Les corrélations écologiques précédemment proposées sont faiblement soutenues. La dernière partie traite de l'ordre entier des chiroptères et décrit le premier moulage endocrânien connu d'une espèce "souche" de chauve-souris ; son moulage endocrânien est typique de l'ordre, soutenant l'hypothèse d'une acquisition commune de l'écholocalisation. Son inclusion dans le contexte ordinal confirme les hypothèses proposées dans la 3eme partie, pour l'évolution morphologique et les masses neurales relatives. Ce travail constitue un premier pas vers l'étude des moulages endocrâniens de chauves-souris. Les correspondances entre moulages endocrâniens et tissus mous restent à évaluer et l'inclusion d'autres taxons fossiles devrait grandement améliorer la toute première image de l'évolution du cerveau des chauves-souris proposée ici.

Mots-clés

Cerveau – Mammalian – Phylogénie – µCT-scan – Paléobiologie